Power Systems

Sumedha Rajakaruna
Farhad Shahnia
Arindam Ghosh *Editors*

Plug In Electric Vehicles in Smart Grids

Integration Techniques

Springer

Power Systems

More information about this series at http://www.springer.com/series/4622

Sumedha Rajakaruna · Farhad Shahnia
Arindam Ghosh
Editors

Plug In Electric Vehicles in Smart Grids

Integration Techniques

Springer

Editors
Sumedha Rajakaruna
Electrical and Computer Engineering
Curtin University
Perth, WA
Australia

Arindam Ghosh
Electrical and Computer Engineering
Curtin University
Perth, WA
Australia

Farhad Shahnia
Electrical and Computer Engineering
Curtin University
Perth, WA
Australia

ISSN 1612-1287 ISSN 1860-4676 (electronic)
Power Systems
ISBN 978-981-287-298-2 ISBN 978-981-287-299-9 (eBook)
DOI 10.1007/978-981-287-299-9

Library of Congress Control Number: 2014957146

Springer Singapore Heidelberg New York Dordrecht London

Printed on acid-free paper

Springer Science+Business Media Singapore Pte Ltd. is part of Springer Science+Business Media (www.springer.com)

Preface

Plug in Electric Vehicles (PEVs) use energy storages usually in the form of battery banks that are designed to be recharged using utility grid power. One category of PEVs are Electric Vehicles (EVs) without an Internal-Combustion (IC) engine where the energy stored in the battery bank is the only source of power to drive the vehicle. These are also referred to as Battery Electric Vehicles (BEVs). The second category of PEVs, which is more commercialized than the EVs, is the Plug in Hybrid Electric Vehicles (PHEVs) where the role of energy storage is to supplement the power produced by the IC engine. These two types of PEVs are predicted to dominate the automobile market by 2030. Widespread adoption of PEVs allows the world to reduce carbon emissions in transportation needs significantly. Therefore, it is vital to the success of a collective global effort in meeting the climate energy targets and to reduce the dependence on increasingly scarce fossil fuels. However, significant challenges are thrust upon utility grid operators on how best to integrate the PEVs into smart grids.

This book covers the recent research advancements in the area of integration techniques, infrastructure needs, and effects on power systems related to the anticipated high deployment of PEVs in smart grids. The topics that are covered in this book include the concept of dynamic wireless power transfer for EVs to increase their range and reduce the size of battery bank, PEV parking lots and their planning, management, and control in a smart grid environment, using a scaled-down test bed and advanced cosimulator to evaluate PEV coordination strategies, exploring the cyber security issues of the smart grid with significant PEV penetrations, applying the probabilistic PEV charging model in a distribution grid to evaluate the PEV impacts, V2G and photovoltaics for peak demand reduction in urban regions, PEV impact on power system steady state voltage stability, coordinated wind–PEV energy dispatching approaches in the V2G context, modeling

the effects of voltage unbalances due to PEV penetration, and using PEVs to implement ancillary services in smart distribution grids. Hence, this book introduces many new strategies proposed recently by researchers around the world to integrate PEVs in smart grids and to evaluate their impact on system performance and reliability. The book is aimed at engineers, system planners, researchers, and graduate students interested in the latest developments in this field of research.

Contents

Reviewers

Andrés Arturo Romero, Universidad Nacional de San Juan, Argentina
Alexander Schuller, Karlsruhe Institute of Technology, Germany
Wencong Su, University of Michigan, USA
Behnam Mohammadi-Ivatloo, University of Tabriz, Iran
Mahinda Vilathgamuwa, Queensland University of Technology, Australia
Mahmud Fotuhi-Firuzabad, Sharif University of Technology, Iran
Pavan Balram, Chalmers University of Technology, Sweden
Ona Egbue, University of Minnesota, USA
Enrique Romero-Cadaval, Universidad de Extremadura, Spain
Preetham Goli, University of Houston, USA
N. Mithulananthan, University of Queensland, Australia
Ahmed M.A. Haidar, University of Wollongong, Australia
Pol Olivella-Rosell, Universitat Politècnica de Catalunya-BarcelonaTech., Spain
Hussein T. Mouftah, University of Ottawa, Canada
Alireza Soroudi, University College Dublin, Ireland
Ricardo Rüther, Universidade Federal de Santa Catarina, Brazil
Sajjad Abedi, Texas Tech University, USA
Ona Egbue, University of Minnesota, USA

Chapter 1
Overview of Plug-in Electric Vehicle Technologies

K. Ramalingam and C.S. Indulkar

Abstract The Plug-in Electric Vehicles (PEVs) are the Battery Electric Vehicles (BEVs) and Plug-in Hybrid Electric Vehicles (PHEVs). PEVs will dominate the transportation in the personal mobility mode and in the automobile market by 2030. Widespread adoption of PEVs brings potential, social and economic benefits. The focus on promoting use of electric vehicles in road transportation is very essential to meet the climate change targets and manage the ever hiking prices of fast depleting fossil fuels. However, there are lots of uncertainties in the market about the acceptability of PEVs by customers due to the capital and operation costs and inadequate infrastructure for charging systems. The penetration level in the market is not encouraging, in spite of incentives offered by Governments. Manufacturers are also not sure of the market, even though predictions are strong and attractive. Major manufacturers, however, are already ready with their plans to introduce electric vehicles to mass market. The use of PEVs has both technological and market issues and impacts. Series of research works have been reported to address the issues related to technologies and its impacts on political, economic, environmental, infrastructural and market potential aspects. Works dealing with suitable infrastructure such as charging stations and use of smart grids are reported. These steps are aimed to bring down the capital and operational costs that are comparable to the costing of conventional transport vehicles. The penetration level of PEVs in transportation will accordingly increase and keep the climate targets met and conserve fossil fuels for use in other economic segments. An overview on these issues is presented in this chapter.

Keywords Plug-in electric vehicles · Charging stations · Impacts · Smart grids · Infrastructure incentives

C. S. Indulkar—Former Professor, IIT Delhi

K. Ramalingam (✉)
Airports Authority of India, Delhi, India
e-mail: drramalingamk@gmail.com

C.S. Indulkar
Indian Institute of Technology, Delhi, India
e-mail: indulkar@ieee.org

S. Rajakaruna et al. (eds.), *Plug In Electric Vehicles in Smart Grids*,
Power Systems, DOI 10.1007/978-981-287-299-9_1

1.1 Introduction

The objectives of the introductory chapter are to overview the history and development of Plug-in Electric Vehicles (PEVs), understand the issues in promoting and supporting penetration of PEVs, new vehicle technology, and associated infrastructure issues. The ongoing mitigation strategies and impacts are reviewed with regulatory frame works, standards and policies for public education and creation of a new potential business market and its issues for growth trends.

The electric vehicle was first developed in 1830s by a number of inventors. These early electric vehicles ran on ordinary non-rechargeable batteries and far outsold gasoline cars for decades. The Ford Motor Company in 1910s began to mass produce the Model T gasoline car. Henry Ford chose gasoline power over electricity and steam because gasoline cars could travel much further between refueling. Furthermore, electric cars were vulnerable to breaking down, and mechanics were few then. The assembly-line-produced Model T with gasoline saw runaway sales in America. Renewed interest in the electric vehicle began in the 1960s and 1970s with aims to reduce air pollution and vulnerability to rising oil prices. A combination of public and private investment spurred the beginning of mass production of electric vehicles in the late 1990s and throughout the 2000s.

The GM EV1 was the "first" EV in the 90s before the Nissan Leaf and the other vehicles came up in the U.S, followed by Ford, Toyota, and Honda rolling out models. Nissan sold over 10,000 of the Leaf within the first year of rollout. The Tesla Model S, luxury Battery Electric Vehicles (BEVs), received "Car of the Year" award in 2012. Pike Research projects that PEVs will account for 0.8 % of U.S. car sales by 2017. The market for PEVs is more developed, but has yet to reach rapid deployment. Hybrids vehicles have been retrofitted for plug-in capability, since they were introduced in the early 2000s. The Chevy Volt was the first Extended Range Electric Vehicle (EREV) in the market, but it was soon followed by Toyota and Ford models in 2011 and 2012. The Volt topped with 92 % Consumer Reports' Owner Satisfaction Survey in 2012.

Calef and Goble studied [1] the vehicle technology and reported that California had one of the largest concentrations of electric and hybrid-electric vehicles in the world. Consumer behavior is to evaluate the true value of hybrids vehicles for the benefits of lower emissions and increased fuel economy, offset the costs of prices rise and increased technological complexity. Lave and MacLean [2] compares the lifetime costs of a Toyota Prius and most successful Toyota Corolla. The authors conclude that hybrids would be unable to sell themselves on fuel efficiency alone. Recent advancements in hybrid technology combined with the rapid rise of gas prices have narrowed the gap between the savings and purchase premium associated with Plug-in Electric Vehicles.

Greene [3] studied the relationship between vehicle size and fuel costs and the inverse relationship between a vehicle's size and its fuel-efficiency. A more recent study by Greene et al. [4] found that increases in overall fuel efficiency were due to general technological improvement. Santini et al. [5] found that fuel-efficiency has been the most important attribute in purchase decision. The introduction of the Toyota Prius to the US market was based on costs and benefits, such as fuel savings, lowered performance, purchase price premium, and expected battery life. Kayser's [6] study found that with the rapid increase in gasoline prices, households lowered total gasoline consumption without lowering total miles traveled.

Certainly, the existing economic literature on fuel efficiency and hybrid vehicles offers valuable insights into possible challenges and opportunities for automakers hoping to penetrate the market. The policymakers are looking to encourage environmentally-friendly purchasing patterns. The hybrid sector of the automobile industry is moving forward with new models being introduced by major manufacturers. With the ongoing rise in gasoline prices, and ever-expanding government incentives for electric vehicles, rapid diversification of available hybrid makes and models are produced.

The new vehicle technology in transportation segment is evolving with time. The Plug-in–Electric Vehicles technology has been found acceptable, and is promoted vigorously by states for its positive environmental impacts and climate change challenges. The technology is promoted equally by private players for its growing penetration and acceptance by public with promising business potential and opportunities.

Pike Research group projects that the PEVs in the United States will move to 1 million marks by 2018. The concentrated number of PEVs in an area might affect the grid. Utilities are becoming concerned about the energy load due to rise in PEVs that are connected to the grid.

Khan and Kockelman [7] noted that the high load demands by PEVs on the grid might be an obstacle to growth of the PEVs industry and its manufacturers. PEVs are attractive to end-users and less of a concern for energy suppliers in terms of load balancing. Using smart grid technologies, energy suppliers could create new approaches that would balance charging schedules, avoid harmful and costly spikes and offset existing peak demand. By using solutions that can help schedule and spread out vehicle charging times to off-peak hours and days, including pricing incentives that encourage PEV owners to charge their vehicles during hours of low demand, utilities could balance the grid load, keep costs down and avoid having to activate unclean peak-generation resources. The novel concept is basically to create an optimal charge schedule based on the vehicle data and grid data. Fast charging of PEVs and new kinds of PEV batteries that use cloud-based communications to utility companies are some solutions under consideration. Batteries provide the majority of interaction between the vehicle and the grid, so their development will be pivotal to building a grid infrastructure. Kempton and Letedetre [8] presented electric vehicles as a new power source to electric utilities. The PEVs are also used in Power Sector for stabilising the smart grid system using V2G technologies.

Adoption of PEVs has high-level benefits in three core areas:

- *Energy security*. Electricity is almost exclusively derived from domestic resources. While reducing petroleum imports and leading to the nation's energy independence, PEVs can contribute significantly to a balanced portfolio of domestically produced electrical energy.
- *A cleaner environment*. PEVs produce zero tail-pipe emissions, and research shows that they also produce less total carbon dioxide (CO_2). The ongoing trend of increased electricity generation from renewable sources promises benefits of reduced emissions.
- *Creating a stronger economy*. PEVs and associated infrastructure have positive impacts on the local and national economies by creating new job opportunities in countries manufacturing PEVs. The use of PEVs provides less expensive transportation options in countries, where the PEVs are imported.

Battery charging infrastructure for PEVs and regulatory policies to operate charging stations by utility network systems are matters of concern to promote penetration of PEVs. PEV charging stations are situated in locations at businesses, retail stores, colleges, workplaces, parks and libraries. The charging stations:

- *Offer simple and affordable pricing*. Off-peak hourly charging is cheaper for public and workplace charging with credit cards is simple in US. However, the billing system is not that simple, where the charging infrastructure at public charging station is yet to develop in countries like Europe.
- *Provide convenience*. Public charging station supports level 2 rebates for majority of cars charging at home.
- *Reduce total* CO_2 *with renewable energy*. Charging network is powered by renewable energy resource and thus reduces CO_2 emissions.
- *Sell direct to local auto dealers*. Prepaid cards for 12 months of unlimited public charging are provided directly to dealers to promote a 1-year-free deal to their customers.
- *Attract transportation electrification customers*. A wide net is provided by including vehicle charging for car-share programs, workplace locations, multi-family properties and commercial fleets.
- *Capture funds outside of existing budgets*. PEV-related grants by several others to fund public charging stations on time and on budget keep the utility competitive for future grants.
- *Engage the community*. Spread the Marketing and communications campaign for its Plug-in everywhere network.
- *Plan for the future*. To be proactive with its PEV program,
  - Expedite a broader consensus and develop best practices around PEV and Electric Vehicle Support Equipment (EVSE) deployments.
  - Minimize the potential for localized grid impacts of increased PEV adoption through education and outreach to stakeholders.

– Develop a PEV and EVSE infrastructures model with objectives to represent a new and potentially significant opportunity to increase electric service revenue and to shape the load curves.

Alternative business models as below are deployed to support the PEV/EVSE industry and ecosystem:

- EVSE installation codes, ordinances and regulatory permissions.
- EVSE interoperability road map*, including integration* issues for utilities and public charging providers with multiple technologies, devices, systems and applications.
- Workplace and multi-family housing. These are unique challenges and demands created while supporting EVSE infrastructure within the market segments.
- Marketing communications plan for communicating and educating parties for the successful implementation and adoption of PEVs and EVSEs.

Charging station technologies are advancing rapidly with faster charging capabilities, increased communications, improved controls and lower capital costs. Electric vehicles support fuel independence, cleaner air, and economic growth. The technologies, economics, and support for clean energy have created a new market opportunity. Power utilities are uniquely positioned to embrace and foster this opportunity. However, significant issues on infrastructure requirement must be addressed without delay. The adoption and roll out of PEVs can accelerate with continued collaboration around EVSE infrastructure, utilities, vendors and their collective customers, and play a key role in the world economy and environment.

The environmental benefits of plug-in electric vehicles increase, if they are powered by electricity from 'green' sources such as solar, wind or small-scale hydroelectricity. PEVs use about 40–60 % less petroleum than conventional vehicles. PEVs typically emit less greenhouse gas emissions than conventional vehicles. Over these benefits, all out efforts, led by US, are on with regional plans to promote PEVs the world over to tide over the climate challenges and to secure the fast depleting fossil-fuel energy resources for future generation.

The contents of the chapter are from well researched and published papers and research study reports. It is presented in a comprehensive structure for clear understanding of PEVs by Policy makers, Economists, Transport technologists, Universities, Researchers, Automobile Business Centres, Environmentalists, PEVs manufacturers, Power Utility managers, Road Transport planners and Electric Vehicle users.

The chapter is structured in subsequent sections to overview the world scenario on penetration of Electric vehicles in Sect. 1.2, overview of PEV technologies, PEV systems, Impacts and Standards in Sect. 1.3, technical issues on PEV implementation in Sect. 1.4, manufacturing and marketing issues in Sect. 1.5, market forecasts in Sect. 1.6, promotional programmes and incentives to promote use of PEVs in Sect. 1.7 and finally concluded with the chapter summary in Sect. 1.8.

1.2 World Scenario on PEVs Penetration

The Nissan Leaf is the world's best-selling, highway-capable electric car, with global sales of 100,000 units by January 2014. [9] Several countries publish their statistics and have purchase incentives schemes in place for the more general category of plug-in electric Vehicles (PEVs).

As of December 2013, there were over 400,000 plug-in electric passenger cars and utility vans in the world, led by the United States with a stock of over 170,000 highway-capable plug-in electric cars. Due to its population size, Norway is the country with the highest market penetration per capita in the world, also the country with the largest plug-in electric segment market share of new car sales. In March 2014, Norway became the first country where plug-in electric vehicle is one percent of the registered passenger cars. Estonia is the first country that completed the deployment of a PEV charging network with nationwide coverage, with fast chargers available along highways at minimum distances of 40–60 km.

Table 1.1 presents the top countries according to market share of total new car sales as of March 2014 for each of the following electric-drive segments: plug-in electric vehicle (PEV), battery electric vehicle (BEV), and plug-in hybrid electric vehicle (PHEV).

Norway tops PEV market share of 6.10 % and BEV market share of 5.75 % respectively, while Netherlands tops PHEV market share of 4.72 %. The lowest market shares are of Denmark with 0.29 % in PEV, United States and Denmark with 0.28 % in BEV and Switzerland, France and United Kingdom with 0.05 % in PHEV respectively.

Table 1.2 presents plug-in electric vehicle stock, market penetration per capita and PEV market share of new car sales for the six countries as of December 2013 with the largest plug-in electric-drive fleets.

Table 1.1 Top ten countries of PEVs market shares as of March 2014

Country	PEV market share (%)	Country	BEV market share (%)	Country	PHEV market share (%)
Norway	6.10	Norway	5.75	Netherlands	4.72
Netherlands	5.55	Netherlands	0.83	Swedan	0.41
Iceland	0.94	France	0.79	Japan	0.40
Japan	0.91	Estonia	0.73	Norway	0.34
France	0.83	Iceland	0.69	United States	0.31
Estonia	0.73	Japan	0.51	Iceland	0.25
Swedan	0.71	Switzerland	0.39	Finland	0.13
United States	0.60	Swedan	0.30	United Kingdom	0.05
Switzerland	0.44	Denmark	0.28	France	0.05
Denmark	0.29	United States	0.28	Switzerland	0.05

Table 1.2 Top six countries as on December 2013 on PEV fleet, Population and sales market share

Country	PEV fleet	Population	PEV market share (%)
United States	172,000	320,050,716	0.62
Japan	74,124	127,143,577	0.85
China	38,592	1,385,566,537	0.08
Netherlands	28,673	16,759,229	5.37
France	28,560	64,291,280	0.65
Norway	20,486	5,042,671	5.60

Table 1.3 Comparison of ownership costs as in 2013

Vehicle	Operating mode (powertrain)	Total ownership cost in US average ($)
Nissan leaf SV	All-electric BEV	37,288
Chevrolet volt	Plug-in hybrid	44,176
Average conventional	Gasoline	44,949
Average hybrid	Gasoline-electric hybrid	44,325

The six major countries with the largest plug-in electric-drive fleets are United States, Japan, China, Netherlands, France and Norway. Norway tops 5.60 %, China has 0.08 % and United States has 0.62 % of PEV market share as on 2013.

According to a published study by the Electric Power Research Institute, the total cost of ownership in US dollar average, as on 2013, given in Table 1.3, shows that the Nissan Leaf SV is substantially lower than that of comparable conventional and hybrid vehicles. The cost accounts to the manufacturer's retail price, taxes, credits, destination charge, electric charging station, fuel cost, maintenance cost, and additional cost due to the use of a gasoline vehicle for trips beyond the range of the Leaf.

1.3 Technology

1.3.1 PEV Technologies [10–12]

A Plug-in Electric Vehicle (PEV) uses electric energy from a battery as its primary power source. The use of PEVs reduces or eliminates the need for gasoline or diesel. The cars and trucks have batteries to supply the energy needed and these will need to plug-into recharge. There are several types of plug-in electric vehicles, each with different features. The types of Plug-in-Electric Vehicles include Battery Electric Vehicles (BEVs) and Plug-in Hybrid Electric Vehicles (PHEVs). Other types of electric drive vehicles are Photovoltaic electric vehicles (PVEVs) and Fuel cell electric vehicles (FCVs).

A **Battery Electric Vehicle** (BEV) is fully electric. The vehicle is completely powered by the on-board battery. The initial models of BEVs are expected to go up to 100 miles on a full charge. The batteries will then be plugged-into a power source to recharge.

An **Extended Range Electric Vehicle** (EREV) is similar to BEVs, but it may have an on-board gasoline fuelled generator to provide additional energy, when the batteries are low. These may have up to about 50 miles range on the initial battery energy, and the on board generator may allow the car to travel significantly further before recharging again.

A **Plug-in Hybrid Electric Vehicle** (PHEV) has both an electric motor and a typical gasoline or diesel engine to power the car. The electric and gasoline drives are controlled by the onboard computer to give the car power to get very efficient overall mileage. These cars have an on-board battery to support the electric motor and will be plugged-into fully recharge the battery. The batteries also use the regenerated energy from the braking and deceleration and recycle it through the battery to power the vehicle. When the plug-in battery is depleted, the car reverts to the standard hybrid operation. A plug-in-hybrid electric vehicle is designed with types of configurations such as series-hybrid, parallel-hybrid, or combined series-parallel hybrid [13, 14].

- **Series-Hybrid** Only the electric motor provides power to drive the wheels. Sources of electrical energy are either the battery pack (or ultra-capacitors) or a generator powered by a thermal engine. Such vehicles are also called as Extended-Range Electric Vehicles.
- **Parallel-Hybrid** Both the electric motor and fossil powered engine provides power in parallel to the same transmission.
- **Power split or series/parallel hybrid** combines the advantages of both parallel and series hybrid concepts. This allows running the vehicle in an optimal way by using the electric motors only, or both the IC Engine and the electric motors together, depending on the driving conditions.

The state-of-charge (SOC) is the index in percentage of the nominal energy capacity of the battery remaining in the battery, which determines the energy mode to drive. The technological advantage of PEVs is the capability of driving in different energy modes. Two basic modes are possible; charge depleting operation mode (CD), powered only by the energy stored in the battery. This is suitable for urban driving. The other mode is charge sustaining mode (CS), where the battery is recharged over a driving profile to maintain the SOC level. The two modes can be combined depending on the driving range to reap the full advantage of PEVs. In such cases, the discharge cycle will influence the energy demand over the distance travelled and the environmental performance. The feasibility of CS mode depends on the driving distance and the availability of charging facilities from the grid. The driving behavior and the energy management mode will influence the actual distance travelled.

The range of plug-in electric vehicles will vary by manufacturer, vehicle model, outdoor temperature and driving terrain. Initial models go up to 100 miles on all

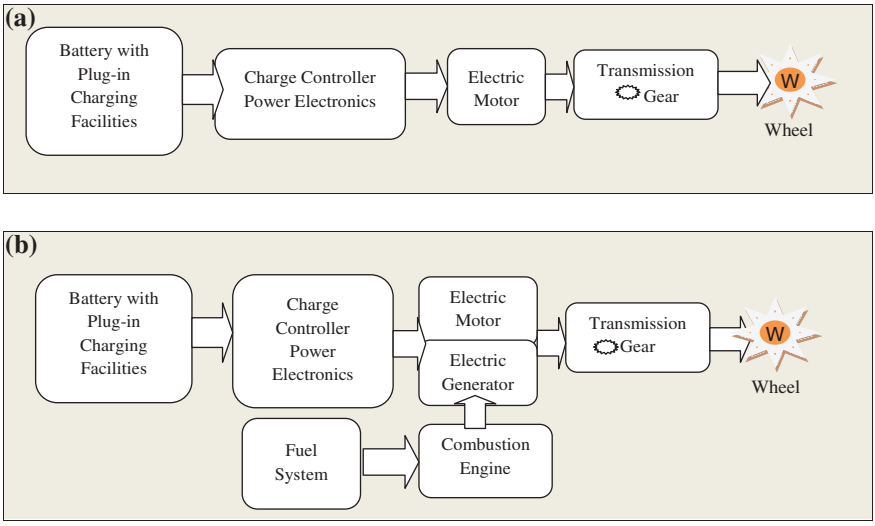

Fig. 1.1 PEVs drive train configurations. **a** all-electric vehicle drivetrain (BEVs), **b** plug-in hybrid electric vehicle drivetrain (PHEVs)

electric range, and certain, extended range models may get up to 50 miles on the battery electric range.

Figure 1.1 shows the basic drive train configuration of (a) BEVs and (b) PHEVs

1.3.2 PEV Systems [14, 15]

The vehicle powered by fossil fuels is an internal combustion engine (ICE) to burn the fossil fuel to power the vehicle. PEVs use a different source of energy viz. electricity. The PEVs system has the following components of the drive train.

- **Electric Motors** This device converts the electrical energy stored in a battery to mechanical energy, thus propelling the vehicle forward or backward by AC or DC motor.
- **Electric Generators** The generator converts mechanical energy to electrical energy. In some vehicles the two functions are combined into a single device by motor-generator.
- **Inverters** Battery packs invariably supply DC current. The AC motor in a PEV is coupled with the battery pack using an inverter. The inverter converts the DC from the battery to AC and powers the AC motor.
- **Chargers** A charger works in conjunction with a generator. It converts the AC electrical output from the generator into DC and charges the battery pack. These devices are usually fitted with a control mechanism by a charge controller to optimize the charging process, which prolongs the life of the battery.

- **Large Battery Packs** Battery packs store the energy that is required to power a PEV. The variants of electric vehicles use different types of battery packs- lead acid, NiMH, Li-ion. Of these systems, the Li-ion battery pack will be the dominant battery pack in all future PEVs. Battery packs attribute heavily to the significant price difference between normal vehicles and PEVs.

These vehicles have two modes of operations namely,

- An all-electric mode, where the vehicle operates like the all-electric vehicles (BEVs)
- A blended mode, where the vehicle uses the battery pack to a large extent, but still relies on the fossil fuelled engine for supplemental power (PHEVs)

Figure 1.2 shows the Plug-in Electrical Charging System components for PEVs. The Electric Vehicle Support equipment (EVSE) include 120 V/240 V AC plug-in, Control device, Charging cable cord, Connector and Coupler. Each vehicle has inlet point to Charger that connects to Battery pack.

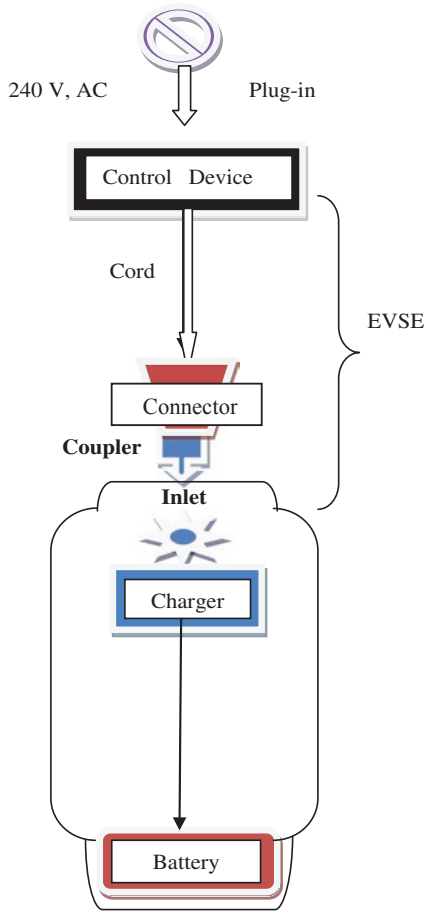

Fig. 1.2 Plug-in electrical charging system

1.3.3 Impacts [16, 17]

The use of PEVs in distribution level network for charging has technical impacts in distribution power network. The impacts vary with the vehicle penetration levels, charging pattern, fleet charging profile, distribution network power losses, integration of PEVs at the transformer levels, vehicle driving pattern, and demand response (DR) strategy to reduce peak loads, driving distance, battery sizes, and tariffs. Researchers are continuing on these issues and strategies are being looked upon to mitigate the impacts. Widespread use of PEVs with new vehicle technology has a positive impact on environment and economy. It helps for clean transportation and energy independence. PEVs are environmentally friendly, as they reduce emission of gases, such as carbon dioxide, nitrogen oxides and sulphur oxides.

The National Renewable Energy Laboratory (NREL) [16, 18] reports that large–scale development of PEVs has limited negative impacts on the electric power generation requirement. PEVs displacing half of the total vehicles on the road in US by 2050 will require only 8 % increase in electricity generation and an increase of 4 % in generation capacity. In addition, there is considerable reduction in GHG emissions from conventional vehicles and reduced fuel use in transportation segment. The average penetration rates in USA for PEVs are 16 % annually, as per the reported case studies.

Other impacts on power grid due to increased penetration of PEVs are: Increase in additional power load in the grid for charging PEVs in uncontrolled scenario, where the consumer behavior and charging timings are unpredictable. However, off-peak charging of PEVs improves the load curve for electric utilities. Therefore, the use of high penetration PEVs should be properly optimized under different charging scenarios and technologies.

The charging scenarios are either controlled or uncontrolled. Certain strategies are required to manage charging behavior to limit the daily charging peak. The charge management method are tariff rates such as real time pricing (RTP) under Time of Use (TOU) tariff and Controlled charging from Smart grid under critical peak pricing (CPP) tariff. With PEV battery capacity range from 2 to 17 kW, the energy requirement will be 5–40 kWh on slow charging.

The power demand of the charger is a function of voltage and current of the charger. The battery capacity determines the charging time, and is inversely proportional to the state of charge (SOC) of the battery. The electric load curve in power system network depends on the percentage of PEVs penetration and the charging strategies.

The charging station has single phase AC/DC conversion devices. DC distribution with super-capacitor energy storage device supplies power to the battery, when the power demand for the charger exceeds the average demand of the grid. A 230 KVA Transformer is required for every 50 parking spaces, and accordingly, infrastructure for charging station and system integration of BEVs to the grid operation is needed.

Demand Response (DR) is another dynamic benefit to the grid by interrupting the PEVs demand on peak hours. The Plug-in bidirectional vehicle-to-grid system (V2G) batteries in smart grid charging become distributed storage systems for the electrical grid. The energy supplied to the grid is priced that pays back the additional cost of V2G batteries in PEVs. The distributed storage would make the grid more stable, secure and resilient by frequency regulation and spinning reserve as backup capacity within the distribution system. V2G system allows greater penetration of wind and solar resources into the grid. V2G promises prominent application in the global transition to the emerging green and sustainable energy economy. Kempton and Tomic [19] presented details on Vehicle-to-Grid (V2G) Power fundamentals. Kempton and Tomic [20] discussed Vehicle-to-Grid Power implementation for stabilizing grid by supporting large scale renewable energy resources.

A large scale penetration of PEVs will impact different aspects of the power system grid:

- The average operating temperature of transformers will increase under the additional load of charging PEVs. This could shorten their life, thus adding costs to the electricity grid.
- There will be potential power supply shortage, if the aggregated battery charging profile includes the on-peak period.
- The batteries should be storing electricity from the lowest carbon emitting sources, namely nuclear energy and renewable energy. But, the challenge is then to make the two demand and supply load curves coincide.

The battery load curve depends on the time for recharging and charging power. The new PEVs fleet impacts the electricity transport and generation capacity. The electricity grid operators require innovative management methods to tackle the issues.

These concerns make the operators of the electricity grid deploy new techniques to monitor, and remotely control the electricity demand. This is actually already one of the roles of electricity grid operators in demand side energy management. Beyond such a mono-directional power flow management from the electricity grid to the vehicle battery, more integration methods are being explored and envisioned to make this in the two directions. These innovations are also being considered in the framework of research and development efforts towards a smart and reliable grid, as needed by the growing role of distributed energy resources, including intermittent renewable energy resources.

The utilities should know the location of PEVs that are plugged-in their distribution networks. If a customer adds a charging station at their home, the utility may not determine the adequacy of the transformer capacity and the mode of collection of additional expenditure for up-gradation of the electrical system to meet the additional load due to sudden charging by PEVs cluster at a time. As a mitigation strategy, most utilities are developing PEV charging permit requirements.

A good network and asset model, with accurate and up-to-date data about line and transformer capacity will be the key fo further development. Advanced analytics, including implementation of advanced distribution management systems (DMS) will be critical to this solution. Coupled with intelligent line and transformer sensors, DMS can help operators to understand the operations in real-time and smarter meters could be a huge benefit, to more effectively manage the network. The utility has to plan for an advanced metering infrastructure (AMI) and integrated system model (ISM) to manage the changing distribution environment.

Service providers will also need tools to manage PEV charging loads, incentivizing consumers to charge PEVs in a more diversified pattern. Utility has to invest on smart meters and line sensors, and real-time monitoring process to understand the extent of the problem. Charging station should have facilities that communicate with PEVs and determine battery storage status, then transfer that information to the utility DMS. This would enable the utility to either proceed with charging the PEV, cycle the charge, or schedule the charge for later. The idea is to charge only the PEVs with near depleted battery power, when the utility is having a peak energy event.

The PEVs will have an impact on utilities with greater emphasis in some specific locations within their service territories. Along with their potential environmental and commercial benefits, PEVs will bring localized distribution problems. The load data of PEVs and its locations are used by the tools to analyze their impacts. Providing incentives for network-friendly charging patterns will be the key to both consumers and utilities realizing the potential of electric vehicles

Smart meters would track electricity use in real time. A smart charger, which include a charger that runs on a timer, could ensure that the plug-in batteries are charged only when the electricity is at its cheapest, saving money to consumers. Moreover, utilities could temporarily turn off chargers in thousands of homes or businesses to keep the grid safe during peak hour demand.

High penetration of PEVs in electric grid has specific impacts on distribution network systems. They are [16]:

- **Phase imbalance** Lower percentage of PEVs using single phase charging results in larger variation in current imbalance, but the lower total load reduces the voltage imbalance. However, when higher numbers of PEVs are charging, then the diversity increases and so lowers the current imbalance and keeps the voltage imbalance within limits.
- **Power Quality issues** PEVs charger works in low voltage and converts AC–DC and supplies through DC/DC converter. These processes produce harmonics distortion in the distribution system. The non-linear elements such as inverters and battery chargers increase voltage distortion and current harmonics significantly in the power system. Harmonic currents cause excessive neutral current and transformer hotspots. Battery chargers for PEVs form harmonic producing

loads significantly and produce harmful effects in distribution system and residential electrical appliances. New designs of chargers are being considered in the market to control harmonics with low TDH of 30 % against the present 60–70 % TDH.

- **Transformer degradation and failures** The transformers are designed for typical load patterns. When PEVs are deployed, the load pattern will change and the power system may not be capable of handling the new load pattern and the additional load demand. The PEVs load may have significant impact on the transformer and reduce the life of the transformer or increase its failures. A study reports that additional PEV loads have increased the transformer failure ratio by 0.02 % per year and reduced the life of the transformer by 69 %, for peak hour level 2 charging scenario. The change in load shape altered by PEVs and its timing increase the heating and cause insulation failure of the transformer. Harmonic distortion, load distortion, increased temperature and higher penetration rate of PEVs in a transformer and charging characteristics degrade the transformer life span by 40 % per year.
- **Circuit Breakers and Fuse Blow-outs** The harmonic distortion affects the interruption capability of circuit breaker. High harmonic current on fuse behavior has thermal effects and dissimilar current distribution that derate the factors of interruption and extend the arcing period in fuse blowout.

1.3.4 Standards [21, 22]

Standards are being developed for PEV charging devices, communications and installations by Electric Power Research Institute, which is playing a leading role. Standards for devices are being developed by the Society of Automotive Engineers (SAE) for vehicles, and Underwriters Laboratories (UL) and the Canadian Standards Association (CSA) for the charging stations. SAE standard J1772 “Electric Vehicle and Plug in Hybrid Electric Vehicle Conductive Charge Coupler” defines the standard plug/connector for electric vehicles for Level 1 and Level 2 charging. Installation standards for PEV charging are being defined in the CSA Canadian Electrical Code and the US National Electrical Code for US perspective. ISO 15118 presents general standards. Communication standards are also under development. PEV charging will require smart chargers that are readily integrated into Smart Grids infrastructures, with two-way communication capabilities to allow information exchange between the vehicle user and the grid. Therefore, Smart Grid communication standards and technologies for home area networks (HAN) are being considered and will play a significant role in the design and development of PEV charging interfaces.

Two internationally recognized organizations work together in the development of new standards for the electric vehicle industry. The IEEE Standards Association (IEEE-SA) and SAE International have been working to develop vehicular technology related to the smart grid. IEEE-SA has more than 100 standards and standards-in-development relevant to the Smart Grid, including those named in the U.S. National Institute of Standards and Technology (NIST) Framework and Roadmap for Smart

Grid Interoperability Standards. SAE has standards relating to plug-in electric vehicles, vehicle-to-grid communications and power, and the Smart Grid. A number of research initiatives are ongoing by FirstEnergy, Electric Power Research Institute (EPRI) and others to ensure that the vehicle technology is compatible with the electric grid.

The industry standard SAE J1772 has defined battery charging levels. Three methods are followed to recharge the battery. The US Electric Power Research Institute (EPRI) defines three charge levels:

- The level 1 method uses the US standard 120 VAC, 15A or 20A branch circuit, used in the residential and commercial buildings. This delivers 1.44 kW maximum power. This method requires a new dedicated circuit for the user to avoid overload. This is the most immediate solution.
- The level 2 method is based on a 240 VAC, single phase, branch circuit with up to 40A, requiring a dedicated circuit. Under 15A, the maximum charge power would be 3.3 kW. This method could be implemented for both residential and public charging.
- The level 3 is the method suitable for fast charging through public facilities, based on 480 VAC, three-phase circuit, and enabling 60–150 kW charging power. This option implies a number of specific safety precautions. Level 3 chargers may recharge the battery up to 80 % of capacity in a short time.

Level 2 methods would be enough to ensure a "rich" charging infrastructure. In addition to these charging facilities, options are also currently being envisaged to make the charging even faster and, also save the driver to charge the battery himself. Such option consists in changing the discharged battery packs by charged battery packs. However, this case requires an important infrastructure to store, monitor, and recharge batteries.

The industry has a standard connector specification for the US for Level 1 and Level 2 charging. A specific plug, referred to as a J1772 connector is used. The connector is same for all plug-in passenger vehicles using Level 1 or Level 2 charging. The time required to recharge vary significantly and depend on the model vehicle, the size of battery and the amount of energy needed by the car at the plugged-in time. A typical full recharge for a Volt or a Leaf may take 8 h or more, if plugged into a Level 1 supply and 4–6 h, if plugged into a Level 2 supply. Tariff rates are different for different levels of charging. It supports the efficient charging of plug-in vehicles at home. These will provide a price incentive to charge in the off-peak times.

1.4 Technical Issues

1.4.1 Batteries [12–15]

Storage Technologies Storage technology is lagging behind other critical PEV technologies. While research expenditure on battery technologies is on the rise, it is still small when compared to other critical automobile and mobility related R&D spending. The United States Advanced Battery Consortium (USABC) has

focused on research in advanced battery technology for BEVs and hybrids. The Matrix Battery Technology is developed. The Matrix Battery Technology relies upon a special configuration of combined series and parallel cells that can perform optimally even if an individual cell becomes dysfunctional. This critical ability helps manufacturers address reliability issues while bringing down costs. Employing a mass of small cells (the matrix concept) reduces overall temperature of the system by diffusing heat faster. The unique construction of the matrix battery system allows for calling up and reshaping permitting versatility and reuse. This salient feature will provide manufacturers great flexibility and scope to address specific battery needs, as BEV specifications are frequently subject to alteration. The Matrix battery concept can help optimize BEV performance to match vehicle dynamics.

Hydrogen gas is increasingly recognized as an important fuel and energy storage sector of the future. The overall demand for hydrogen as a fuel is projected to grow. Traditionally, hydrogen energy market has been centered on the petroleum refinery and chemical manufacturing sectors. However, use of hydrogen has grown for the power-to-gas market combined with its use in the fuel cell sector. The increasing availability of distributed electrolysis, low off-peak electricity prices, and cheap natural gas will improve the economics of the hydrogen market as an important commercial commodity. Navigant Research forecasts that global demand for hydrogen from the power-to-power, power-to-transport, and power-to-gas sectors will reach 3.5 billion kg annually by 2030.

Looking beyond Lithium While government allocates more funds for research for advancing battery technologies, the automobile giants are not dedicating on research comparatively to the resources-money, manpower and time in this vital area. Toyota is working on a magnesium-sulphur combination over lithium, which ranks high in longer storage hours, weight, reliability and life. Lithium's energy density is a hindrance for successful applications both in automobiles and electronics devices. The new magnesium-sulfur batteries, likely to be on production by 2020 by Toyota, may have an edge in this regard, if tests meet critical parameters, particularly on costs and battery life.

Battery performance The battery performance and cost are essential factors in the development of BEVs. The key performance parameters of batteries are: Energy, Power, Lifetime, Safety and cost. Batteries make up roughly one-third of the cost of today's electric vehicles. Unique assembly lines for BEV batteries lead to higher manufacturing costs. Furthermore, electric vehicles require batteries with both high endurance and power, and there is often a trade-off between these capacities. Lithium- ion batteries are the most commonly used batteries for vehicle applications. However, they are also expensive. A lithium-ion battery with average range of 60–80 miles costs more than the price differential between BEVs and traditional vehicles.

The United States Advanced Battery Consortium has set a target of 150$/kWh for advanced electric vehicle batteries. However, it is difficult to set a hard price, because changes in other cost factors of components also influence the total cost.

The battery prices are falling rapidly. Higher production volumes in recent years have pushed down battery prices.

Energy The energy storage capacity (kWh) is important to decide on the distance to travel and mass of the battery pack (kg/l). The high energy storage capacity depends both on high specific energy (kWh/kg) and energy density (Wh/l). The typical energy storage requirements are 6–50 kWh.

Power The peak battery power (W) depends on the range on charge depleting mode, energy management and the total weight of the vehicle. The peak power generally remains constant.

Lifetime The factors affecting the lifetime of the battery are:

- Ability of the battery to withstand degradation over time, generally, 10–15 years. Life cycle depends on the energy mode of operation.
- Should meet safety standards and thermal management requirements.
- Fast recharge time is necessary, but it reduces the battery life.
- Life cycle issues are availability of lithium resource and recycling.
- Influence of vehicle mass. The electricity consumption (Wh/km) increases linearly with the vehicle mass, 6–7 Wh/km for every 100 kg of vehicle mass added.

Nickel Metal Hydride (NiMH) batteries are the typical batteries used currently by manufacturers in mass-produced BEVs. However, NiMH batteries have reached their maximum potential. Car makers are moving to lithium-ion batteries, especially due to higher energy density and low self-discharge rate. It meets the energy storage requirements not only for PHEVs, but also for BEVs in the short to medium term.

Battery disposal The batteries for electric vehicles are recycled after their useful life. While recycling batteries, a small percentage of the poisonous battery metals, especially lead and cadmium would leak into the environment, and that affects human health and ecosystem. But, recent battery technology development has avoided use of lead acid and nickel cadmium in batteries. The most recent battery versions are Lithium-ion and nickel-metal hydride batteries, which have no serious threat to the environment. However, there is the need for an efficient recycling system for used batteries. Several manufacturers have started their own recycling scheme for hybrid batteries, partly as a consequence of "product after life responsibility" and also to recycle metals into new batteries. Public infrastructure for recycling batteries and all other electric parts of PHEVs, or mandating life cycle management from manufacturers, is a long-term requirement for hybridization.

Battery costs The cost of Lithium-ion batteries includes material cost, manufacturing cost, and other costs for R&D, marketing, and transportation. Lithium-ion battery costs are lower than NiMH batteries but the range of 600–700$/kWh is seen more realistic in the short to medium term. The high production volumes of Lithium-ion battery could significantly decline the cost.

Battery Characteristics The key parameters of the batteries used in different types of electric vehicles are:

- all electric range (10–200 miles),
- material either Lithium-ion or NiMH,
- total capacity (kWh) (1–60 kWh),
- specific energy (Wh/kg), (46–160),
- energy density (Wh/I) (200–600), It is the ratio of the total energy (Wh) to the mass of the pack (kg/Volume l).
- peak power (kW) (27–100),
- specific power (W/kg),(500–1,500),
- battery pack weight (kg), (29–500),
- life in years (10–15),
- deep cycle life numbers (>2,500), and
- specific cost ($/kWh).

A full energy performance of PEV implies quantifying both the fuel and the electricity consumptions over the considered distance driven.The final energy consumption will depend on the distance travelled and will be influenced by both the charging pattern and the driving behavior.

Lithium supply security Current technology for plug-in vehicle is based on the lithium-ion battery and electric motor. Lithium, heavy metals and other rare elements such as neodymium, boron and cobalt are used for the batteries and power train of PEVs. The demand for these materials is expected to grow significantly due to the incoming market entrance of plug-in electric vehicles. Some of the largest world reserves of lithium and other rare metals are found in China and South America throughout the Andes mountain chain. Chile was the leading lithium metal producer, followed by Australia, China, and Argentina and US brine pools in Nevada. Nearly, half the world's known lithium reserves, about 5.4 million tons, are located in Bolivia deserts. Other important reserves are located in Chile, China, and Brazil. Rare earth elements used in batteries, mostly, are located in China, and that controls the world market for these elements.

Hazard to pedestrians Electric-drive cars at low speeds produce less roadway noise as compared to vehicles propelled by internal combustion engines. The visually impaired people consider the noise of combustion engines a helpful aid while crossing streets. In that sense, plug-in electric cars and hybrids with low noise could pose an unexpected hazard to road users. Vehicles operating in electric mode at below 30 km/h speed can be particularly hard to hear for all types of road users including the visually impaired. At higher speeds, the sound created by tire friction and the air displaced by the vehicle make sufficient audible noise. Japan, U.S. and the European Union have legislations to regulate the minimum level of sound for plug-in electric vehicles, so that visually impaired people and other pedestrians can hear them coming and detect the direction of vehicle approaching. Most of the plug-in electric cars make warning noises by using a speaker system.

Battery swapping A different approach to resolve the problems of range anxiety and lack of recharging infrastructure for electric vehicles was developed by Better Place. Its business model considers that electric cars are built and sold separately from the battery pack. As customers are not allowed to purchase battery packs, they must lease them from Better Place, which will deploy a network of battery swapping stations thus expanding BEVs range and allowing long distance trips. Subscribed users pay a per-distance fee to cover battery pack leasing, charging and swap infrastructure, the cost of sustainable electricity, and other costs. Better Place has signed agreement for deployment in Australia, Denmark, Israel, Canada, California, and Hawaii.

The first modern commercial deployment of the battery swapping model was implemented in Israel and Denmark by Better Place. The development of charging and swapping infrastructure costs high investment. Tesla Motors designed its Model S to allow fast battery swapping, which takes just over 90s. The first stations are planned to be deployed in California, San Francisco and Los Angeles, which will be followed by the Washington, DC to Boston corridor.

1.4.2 Smart Charging Infrastructure [12, 13, 22–24]

A novel load management solution is necessary for coordinating the charging of multiple plug-in electric vehicles (PEVs) in a smart grid system. Utilities are becoming concerned about the potential stresses, performance degradations and overloads that may occur in distribution systems with multiple domestic PEV charging activities. Uncontrolled and random PEV charging can cause increased power losses, overloads and voltage fluctuations, which are all detrimental to the reliability and security of newly developing smart grids. Therefore, a real-time smart load management (RT-SLM) control strategy is developed for the coordination of PEV charging based on real-time and minimization of total cost of generating the energy plus the associated grid energy losses. The approach reduces generation cost by incorporating time-varying market energy prices and PEV owner-preferred charging time zones based on priority selection. The RT-SLM algorithm appropriately considers random plug-in of PEVs and utilizes the maximum sensitivities selection (MSS) optimization. This approach enables PEVs to begin charging as soon as possible considering priority-charging time zones, while complying with network operation criteria such as losses, generation limits, and voltage profile.

The diffusion of Plug-in Electric Vehicles (PEVs) is expected to increase considerably over the next few years. Ad-hoc charging systems interacting in real-time with smart grids will be needed increasingly to overcome the severe overload problems in electric distribution grids caused by the huge demand for energy to charge a large number of vehicles. These systems will have to implement the scheduling of the charging process on the basis of negotiation phases between the user and the electric utility, in which information about fares, amount of required energy and maximum time available for completing the charging before user drive-off, are exchanged. The adoption of a variable charging rate is a very promising solution to fully exploit the

distribution grid capacity, allowing higher customer satisfaction and utility financial profits with respect to fixed charging rate.

Successful integration of plug-in electric vehicles into the power system is a major challenge for the future smart grid, such as charging and control strategies of PEVs, vehicle-to-grid (V2G) technology, and several application domains, such as wind energy integration, frequency regulation, design of parking areas and participation in electricity markets.

DC Fast Charging Equipment The battery electric vehicle (BEV) industry is gearing up for the spread of direct current (DC) fast charging technology, which promises drastic reductions in the battery charging time. A new connector that combines alternating current (AC) and DC fast charging in one unit, based on a standard developed by the Society of Automotive Engineers, is now in competition with an earlier system, known as CHAdeMO, that was developed by Japanese automakers and the Tokyo Electric Power Company.

Vendors report that DC fast charging can reduce the time to a full charge on a standard BEV from the 6–8 h range to less than an hour. The benefits of fast charging, however, go beyond simply the time of charge to include additional benefits such as reducing the size and cost of the onboard battery. Pike Research forecasts that shipments of DC fast charging units will accelerate rapidly over the decade at a compound annual rate of 40.6 %.

The fast charging infrastructure for Electric Vehicles has become a completely new social infrastructure. Figure 1.3 shows the charging infrastructure system.

The California PEV collaborative report has recommended standard guidelines for vehicle accessibility to EVSE stations, vehicle parking and signage to locate the charging stations. The BEV parking facilities should meet the same standards as required for normal vehicles. The charging sites will be accessible to the designated curb side parking spots owned either by public or private for public charging.

Curbside Charging Stations Charging stations that are installed in curbside, allowing access to vehicles from street traffic public-right-of-way is called curbside charging. The recommended standards for Curbside charging stations are:

- The location should be immediately prior to the intersection in the direction of the vehicle travel Public Charging Station.
- The Vehicle shall access the EVSE from either perpendicular or diagonal to the charging station depending on the width of the road.
- Accessible aisle to EVSE will be with a minimum width of 3 ft.
- Sidewalk clearance of minimum 4 ft of unobstructed space for pedestrian movement between the EVSE and the built in obstruction
- Charger clearance: EVSE should be with minimum 2 ft from the curb
- Charger protection: EVSE must be protected with guards poste for vehicles approaching either perpendicular or diagonal access from the curb
- Equipment with the Retractable cord is advised
- The Charging station should have adequate lighting to operate EVSE and proper Signs to locate the Station and with contact address for informing problems with the equipment.

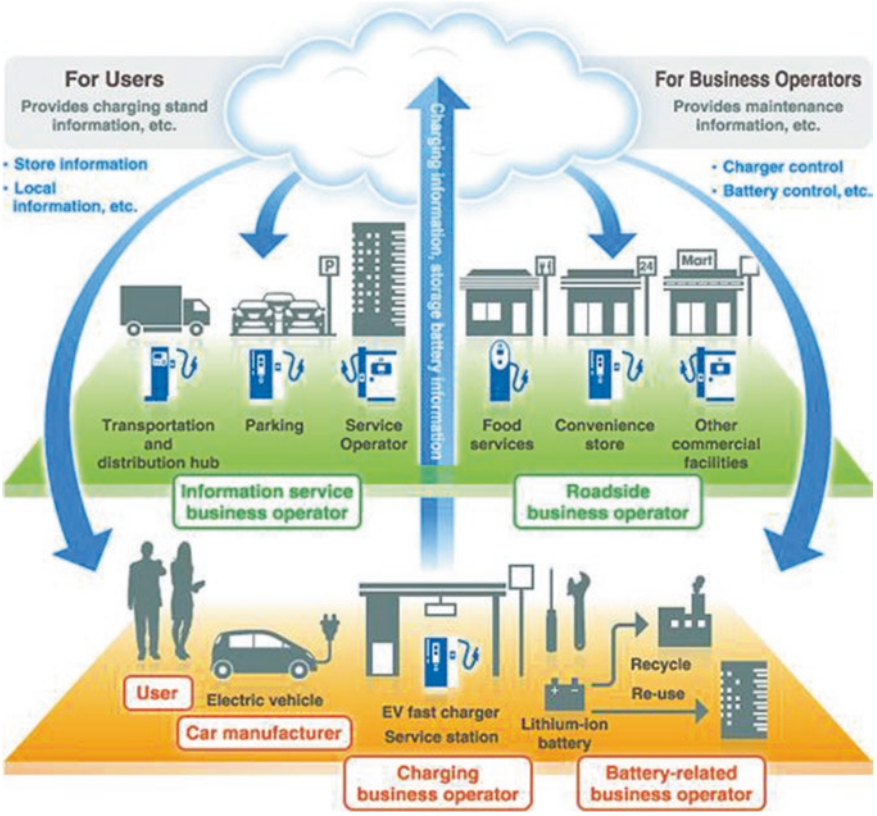

Fig. 1.3 Smart charging infrastructure

Off-street Charging Stations Charging stations that are located not in the public-right-of–way such as designated fuelling or parking spots are considered Off-street charging. The recommended standards for Off-street charging stations are:

- The location for EVSE should be in accordance with the requirement for accessible parking spots.
- The vehicle should approach the charger on a perpendicular or diagonal to the EVSE. Accessible aisle to EVSE is with a minimum width of 3 ft, and the total width of the station space is 12 ft.
- Van-accessible aisle to EVSE should be with a minimum width of 8 ft and the total width of charging station space should be 17 ft.
- Accessible EVSE area should be minimum 30 × 48 in.
- Sidewalk clearance of minimum 4 ft of unobstructed space for pedestrian movement between the EVSE and the built in obstruction
- Charger clearance: EVSE should be with minimum 2 ft from the curb
- Charger protection: EVSE must be protected with guards posts on the side from which the vehicle will be approaching.

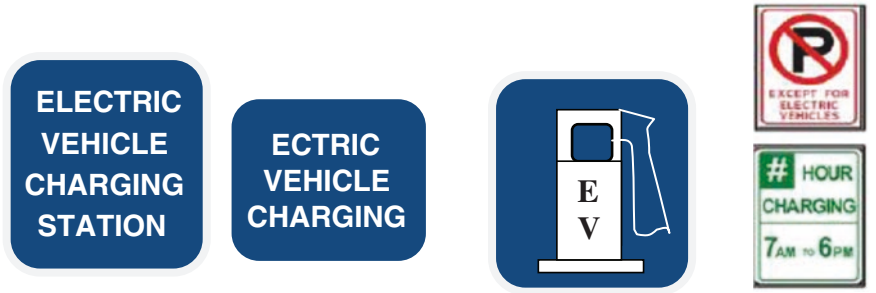

G66-21 (CA) D9-11 bP D9-11 b Regulatory Signage

Fig. 1.4 Standards for signage for BEVs charging station

- Height of EVSE should not be more than 4 ft. From the surface area.
- Equipment with the Retractable cord is advised
- The Charging station should have adequate lighting to operate EVSE and proper Signs to locate the Station and with contact address for informing problems with the equipment.

All general service signs must have white letters, arrows, symbols and borders on a blue background. Standard sizes are also specified for signage. Figure 1.4 shows the currently approved general service signs and regulatory signs specifically related to electric vehicles charging stations.

The charging station sites sizes are:

- Site and sizing for G66-21 (CA) are: Charging station—12″ × 12″ or 18″ × 18″. Conventional Road—24″ × 24″
- Site and sizing for D9-11 bP are: Freeway—30″ × 24″, Expressway 30″ × 24″ and Conventional Road—24″ × 18″
- Site and sizing for D9-11 b are: Freeway—30″ × 30″, Expressway 30″ × 30″ and Conventional Road—24″ × 24″

1.4.3 Integration of PEVs to Electric Grid [22, 25]

In an integrated smart system, the electric vehicle with ‘vehicle to grid’ (V2G) system is capable to send power to the electric grid generally. An automobile with V2G is referred as ‘mobile energy’ or ‘smart charging’. With the V2G technology, the parked car could supply electricity to the grid. The main benefits are: Profitable grid management, especially for ancillary services (A/S). A/S support the stable operation of the electric system, and consist in on-line generators synchronized to the grid to keep frequency and voltage steady, ready to be increased/decreased instantly (2–3 min) via automatic generation control (AGC) and spinning reserves.

A smart grid has to cope with the large scale integration of Distributed Energy Resources (DER), Intelligent and Controllable Loads and Electric Vehicles. The increasing number of electric vehicles brings an extensive amount of distributed and fast-response battery storage capacity, thus paving the way for new chances for Renewable Energy Systems integration.

The integration of Electric Vehicles in electric power systems poses challenges on technical, economic, policy and regulatory issues that should be managed with new architectures, concepts, algorithms, and procedures. PEVs offer an uncommon opportunity to address energy security, air quality, climate change and economic growth. However, market growth is uncertain due to policy, economics and technical challenges and easy adoption of PEVs nationwide. United States, Centre for climate and Energy Solutions and the PEV Dialogue group have the following recommendations to promote adoption of PEVs.

- Regulatory Frame work to foster innovation to increase PEV value without compromising the reliability of the electric grid.
- Public and private investments in Charging infrastructure.
- Facilitate PEV roll outs for easy purchase.
- Consumer education on PEV technology.

Next-generation transmission and distribution infrastructure will handle bidirectional energy flows, allowing for distributed generation (DG), such as from photovoltaic panels, fuel cells, charging to/from the batteries of electric cars, wind turbines, pumped hydroelectric power, and other sources. Classic grids were designed for one-way flow of electricity, but if a local sub-network generates more power than it is consuming, the reverse flow can raise safety and reliability issues. A smart grid with integrated PEVs improves voltage level and operates the grid in stand-alone mode also.

Communications and metering technologies inform smart devices, during the high cost peak usage periods, to reduce demand. The utility companies have the ability to reduce consumption by communicating to devices directly and prevent system overloads. A utility could reduce the usage of a group of electric vehicle charging stations or shifting temperature set points of air conditioners in a city. 'Peak curtailment or peak leveling' is possible with smart devices. Prices of electricity are increased during high demand periods, and decreased during low demand periods. Consumers and businesses will tend to consume less during high demand periods, if consumers are aware of the high price premium for using electricity at peak periods. This could make trade-offs such as cycling on/off air conditioners.

The overall effect of smart grid is a signal that awards energy efficiency and energy consumption that is sensitive to the time-varying limitations of the supply. At the domestic level, appliances with a degree of energy storage or thermal mass will play the market and minimize energy cost by adapting demand to the lower-cost energy support periods under the dual-tariff energy pricing policy.

Demand response (DR) support allows generators and loads to interact in real time, coordinating demand to flatten spikes. Eliminating the fraction of demand that

occurs in these spikes eliminates the cost of adding reserve generators, cuts wear and tear and extends the life of equipment, and allows users to cut their energy bills by allowing low priority devices to use energy, only when it is the cheapest.

The utilities meet the demand and succeed or fail to varying degrees, such as brownout, rolling blackout and uncontrolled blackout. The total amount of power demand by the users can have a very wide probability distribution, which requires spare generating plants in standby mode to respond to the rapidly changing power usage. This one-way flow of information is expensive; the last 10 % of generating capacity may be required as little as 1 % of the time, and brownouts and outages can be costly to consumers. Use of robust two-way communications, advanced sensors, and distributed computing technology will improve the efficiency, reliability and safety of power delivery. It also opens up the potential for entirely new services such as fire monitoring and alarms that can shut off power, make phone calls to emergency services. The benefits associated with the smart grid include:

- More efficient transmission of electricity
- Quicker restoration of electricity after power disturbances
- Reduced operations and management costs for utilities, and ultimately lower power costs for consumers
- Reduced peak demand, which will also help lower electricity rates
- Increased integration of large-scale renewable energy systems
- Better integration of customer-owner power generation systems, including renewable energy systems
- Improved security

Figure 1.5 shows a smart grid with a charging station for PEVs.

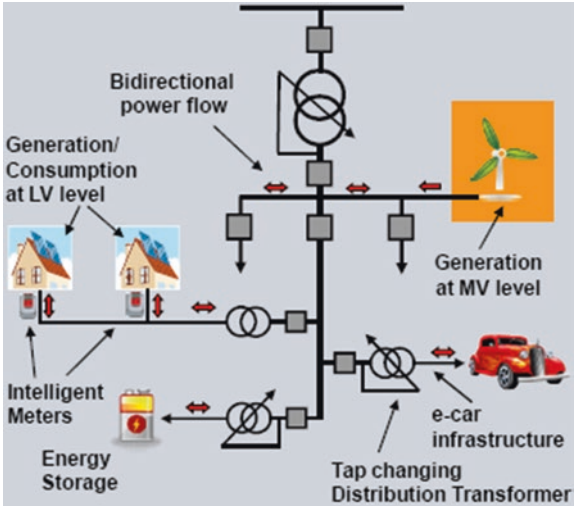

Fig. 1.5 A smart grid showing charging station for PEVs

1.5 Manufacturing and Markets Issues

The major global PEV car manufacturers are collaborating or partnering with major battery manufacturers. They have been planning to produce improved PEVs. The active global players are: Toyota, Japan with Panasonic for Prius model, General Motors with LG Chem for Chevy Volt model, Volkswagen with Sanyo for Golf Town model, Ford with JCI-saft, Nissan with NEC Japan for Leaf model, Chrysler with A123-Systems for Dodge Circuit model, Mitsubishi with GS Yuasa for i-MiEV model, BYD Auto with BYD for F3DM model, Tata Motors, India with Electro-vaya for Indica EV model, Tesla Motors with Multiple for Roadster model, Peugeot with Mitsubishi, and Daimler with Tesla for Smart EV model. Other manufacturers are BMW for i3 sedan model, Fisker for karma sedan model, and Honda for Honda Accord model. REVA Electric Car Company Private Ltd, India has released REVA-i model for distribution in UK, Greece, Cyprus, Norway, Iceland, Spain and Germany.

PEVs connect many Industries. There are opportunities to automotive industries, electricity utilities, Vehicle charging company, battery manufacturers and all levels of Government and most importantly consumers. Governments are driven to adopt PEVs in the transport sector to increase the fuel economy standards, meeting the local air quality standards, energy security and compulsion to reach the target of climate change.

The market challenges are high initial cost of PEVs due to high battery costs, limited drive range, high charging time and limited charging infrastructure at private and public locations. Other challenges are lack of consumer education and acceptance, smart grid integration and lack of familiarity to PEVs. Solutions to these challenges are actively being considered by states to address these issues and to promote PEVs.

In addition to plug-in cars, manufacturers are making light trucks in many styles and configurations for business use. There are several light truck models, like the Ford Transit Connect, the Navistar eStar, Smith Electric and Bright Electric vehicles and others either available or soon to be available. Table 1.4 shows the list of major global PEVs car manufacturers.

Table 1.4 Major global manufacturers [23]

Model	Battery partner	Vehicle type
Toyota	Panasonic	PHEV
GM/Chevy volt	LG chem/compact power	PHEV
Volkswagen/golf twin drive	Sanyo; unannounced	PHEV
Ford	JCI-saft	PHEV
Nissan/leaf	NEC	EV
Chrysler/dodge circuit EV	A123-systems	EV
Mitsubishi/i-MiEV	GS Yuasa	EV
BYD auto/F3DM	BYD	PHEV
Tata motors/indica EV	Electro-vaya	EV
Tesla motors/roadster; model S	Multiple	EV; EV
Peugeot	Mitsubishi	EV
Daimler/smart EV	Tesla	EV

Pike Research reports [15] that 210,000 PEVs will be sold around the world, with over 36 new models. Other predictions are that capital investments will shift from vehicles to battery components. Research continues on nano-scale components and activated carbon that could make PEVs more cost effective and marketable. Market for e-bike will grow faster world over. 48 V batteries will be used against 12 V batteries. Slow charging vehicles will be preferred on tariff consideration than fast charging vehicles. Battery swapping model will reduce initial price of PEVs.

Market penetration of PEV would largely depend on the price of oil, which is the significant factor for users to switch-over to PEVs and public policies from regulatory bodies. The following are the regulatory bodies, which are responsible for policies for regulation of electric vehicles in transportation segment.

- World Electric Vehicle Association (WEVA)
- Electric Drive Transportation Association (EDTA)
- Electric Vehicle Association of Asia Pacific (EVAAP)
- European Association for Battery, Hybrid and Fuel Cell Vehicles (AVERE)

1.6 Electric Vehicle Market Forecasts

The major PEVs markets [9, 11, 15, 26] are in North America, Western Europe, and Asia Pacific with compound annual growth rate of 23.7 % through 2023, according to Navigant research report. Outside of the United States, the largest urban markets will be Tokyo and Paris, with PEV sales in 2023 of nearly 49,000 and 25,000 vehicles, respectively. The report, "Electric Vehicle Geographic Forecasts", predicts that the market opportunity for PEVs is in North America, Europe and Asia Pacific. The select PEV markets in Europe are London, England; Paris, France; Berlin, Germany; Amsterdam, Netherlands; and Oslo, Norway and in Asia Pacific are Tokyo, Japan; Seoul, South Korea; Sydney, Australia; Hong Kong; and Singapore, extend through 2023. Market predictions and expectations are inherently uncertain and actual results may differ materially. Various published research reports predict PEVs annual growth projections of 16–20 %.

Figure 1.6 shows the region wise projected PEV sales World Market 2012–2020 as published by Pike Research report, 2012.

The fast-growing market for electric vehicles has become an important part of the global automotive industry. Governments worldwide are keen to increase penetrations of PEVs due to the environmental, economic, and energy security benefits. As such, government incentives to spur growth in PEV development have been fundamental to growing plug-in electric vehicle (PEV) penetration within vehicle market.

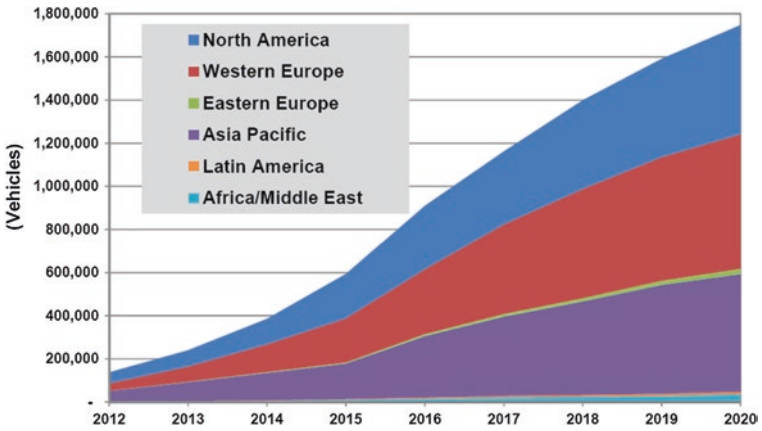

Fig. 1.6 PEVs sale world market predicted for 2012–2020 (*Source* Pike Research, 2012)

1.7 Promotional Programs on PEVs

1.7.1 Government Programs [22, 27, 28]

Several national and local Governments around the world have promotional programs in Canada, China, Europe, India, Japan and United States to promote adoption of PEVs. The programs include incentives by way of rebate for purchasing new BEVs. Canada has provision of green colored license plate, which entitles PEVs owners to use Government. charging stations and parking spots in addition to priority lane for driving. The Chinese Government. provides subsidies directly to the automakers for each PEVs sale, and also provides annual tax exemption and subsidy for purchase of new electric vehicles.

Europe provides tax exemption for new PEVs as incentive and charges carbon-di-oxide related taxes as disincentive for passenger cars. Some states in Europe provide 30 % income tax rebate on purchase price and tax deduction up to 40 % on investment on external recharging station infrastructure, exemption from road taxes, tax breaks, annual bonuses, exemption from first registration taxes, free parking in public parking spaces, exemption from annual circulation taxes, exemption from all non-recurring vehicle fees, weight allowance for PEVs in vehicle-weight based tax system and waiver of import tax for Electric vehicles. UK provides Plug-in car grant and plug-in van grant up to 25 % of the cost of PEVs meeting the specified vehicle criterion. UK supports plugged-in Places for providing match funding to public private partners for installation of BEVs charging infrastructure in lead places. All PEVs are eligible for 100 % discount on London congestion charges. Greener Vehicle Discount (GVD) and Ultra Low Emission Discount (ULED) schemes are also operative for BEVs in UK.

In India, the Government provides 20 % subsidy of ex-factory price of PEVs and exemptions on road taxes, VAT and registration charges. There would be customs/excise duty reduction, which currently stands at 5 % for lithium- ion batteries and other parts, which are used in the manufacture of PEVs. The government has also announced the setting up of a National Mission for Hybrid and Electric Vehicles to encourage manufacture and sale of these vehicles.

Japanese Government provides subsidies up to 50 % on clean energy vehicles and provides tax deduction and exemptions on environment friendly vehicles based on stipulated parameters that meet the environmental performance criterion. New next generation vehicles are exempted from both the acquisition tax and the tonnage tax, and 50 % reduction of the annual automobile tax.

US Government grants tax credits on PEVs purchase. It provides tax credit up to 50 % of the cost of buying and installing home-based charging station. The tax credit has been made as rebate per PEV purchase from funds through Clean Vehicle Rebate Program (CVRP). Some states also provide incentives by exempting sales tax and excise tax. Other facilities are free charging of electric vehicles in public charging stations and work place charging stations. PEVs are offered preferred parking spots in public parking spaces. Employers provide rebates for purchasing electric vehicles and granting quick permissions for installation of Charging stations and EVSE permits. State employees are encouraged with reduced interest rates on vehicle loans for purchasing reduced emission vehicles. Some states offer federal tax credits for electric vehicle purchases and for charging station installations. The incentives vary with respect to vehicle size and type, battery performance parameters and subject to limitations and eligibility requirements.

1.7.2 Types of Incentives [22, 27–29]

The various types of incentives offered by states in US are to promote plug-in electric vehicles use by stakeholders such as consumers, business centres and Government entities for purchase of PEVs or for installations of EVSE charging stations. These incentives are to reduce the initial purchase cost and improved operational advantages for switch-over to PEVs.

Incentives to customers The incentives for PEVs purchase are rebates, reduction of sales and use tax and income tax credit to make the purchase price for the consumer affordable. Rebate facilities and vehicle excise tax exemption are available to individuals, business and Government vehicles purchase. Loans and grants are available to non-profit entities or private businesses to purchase PEVs, install EVSEs or engage in activities to promote PEVs to offset the cost of purchase price. Licence tax exemption or reduced vehicle registration fees are also available. Reduced or exempted personal property tax or exemption from premium insurance charges on vehicles are some of the incentives offered by Government to PEV consumers on purchase.

Incentives to manufacturers and sales of PEVs The practicing incentives by some States are: PEVs manufacturer tax credit or exemptions from regulations on certain aspects of PEVs manufacturing industry. Driving experience incentives include facilities to drive on high occupancy Vehicle lanes, toll fee reduction, waiver of emission testing, exemption from vehicle emission inspections, exemption from parking fees at priority parking spots with special license plate to enjoy such offers by PEVs owners.

Incentives for EVSE Charging Infrastructure Incentives for EVSE purchase, installations and fueling are income tax credit for EVSE purchase and installation, Energy tax credit, purchase rebate for EVSE system, loans and grants for EVSE purchase and installation, PEV infrastructure and Battery tax exemptions, exemption of electricity from Transportation Fuel Tax, free charging to state owned facilities, free parking of state owned EVSE stations are some of the incentives to reduce the PEV purchase cost.

Incentives to private and public fleet Owners Incentives to PEV use in private and public fleets are purchase vouchers to fleets, stars designation for public recognition and marketing opportunities to fleet PEVs. Other incentives are special funding from states for technical training, safety programmes, workforce training for vehicle maintenance or educational initiatives on PEVs.

Incentives to promote V2G technology Incentives to promote Vehicle to Grid (V2G) technology development are: grants to universities for research and development in V2G technology, V2G energy credit to PEV drivers, grants for car sharing organizations for transition to use PEVs, Time of Use (TOU) tariff to encourage off-peak charging of PEVs, exemption of charge providers from regulations as utilities, which is applicable to electricity suppliers, sharing of PEV registration information with Utilities to promote planning and reliability of electricity distribution system.

Incentives to Administrative promotions for PEVs Some states establish PEV/EVSE infrastructure advisory council to plan and integrate PEVs into state transportation network.

These incentive programs may be followed by other countries also very soon, as they are also keen to use electric vehicles with focus to meet climate change targets and the large benefits on use of PEVs.

1.8 Summary

This chapter presents an overview of the broad variety of all kinds of Electric Vehicles; more specifically of Plug-in Electric Vehicles (PEVs). The new vehicle technology has evolved with time since 1830, when the first electric vehicle was developed. Historically, interest in the electric vehicle began in the 1960s and 70s with aims to reduce air pollution and to combat the rising oil prices to operate oil-fired conventional transport vehicles. PEVs include Battery Electric Vehicles

(BEVs) and Plug-in-Hybrid Electric Vehicles (PHEVs). The PEV technology was accepted over time for use in personal and public transport mobility. Series of research works were reported to address various issues related to technical, political, economical and environmental aspects to improve the penetration level of adopting use of Plug-in Electric Vehicles. It has been reported that the use of PEVs has been advocated largely by developed and developing countries in view of its large potential benefits on energy security, environmental protection, clean pollution free climate, and economic benefits for countries manufacturing PEVs in consideration of depleting and costly oil fired engines used in transportation segment.

The top countries that manufacture BEVs and PHEVs are Norway, Netherlands, Iceland, Japan, France, Estonia, Sweden, United States, Switzerland and Denmark. Norway topped the penetration level of 5.6 % and Netherlands with 5.37 %, whereas US had reported penetration of 0.62 %, and China had the lowest penetration level of 0.08 % as on 2013.

A comprehensive overview of PEV technology and the impacts and issues on development of the new vehicle technology are presented. The PEV drive-train configurations with various components that make the PEVs are discussed. The issues, on positive impacts on adoption of PEVs and issues related to technical aspects in the development of technology in terms of bringing down the cost of the vehicle, negative impacts on use of PEVs in electric power system and the specific reference to integration of PEVs in smart grid system by using V2G technology to connect and supply power to smart grid, are discussed Details are given about the development of standards for PEV charging devices and communications and installations standards for integrating PEVs to smart grid system The various technical issues in promoting faster adoption of PEVs in respects of charging stations, infrastructure installations, development of cost-effective quality batteries and its characteristics for use in PEVs are presented. It is reported that there is need to building the infrastructure for PEVs, and to address issues pertaining to policies on pricing, regulations to vehicle integration, building smart electric grid, manufacturing safe components such as batteries and electrical components, building battery charging installations, operational infrastructure including manpower development, funding for infrastructure building and policies on regulation of services of the new technology. The adoption of PEVs connects many industries. It is brought out that there are opportunities and issues related to manufacturers, electric utilities, vehicle charging companies, battery manufacturers and all levels of Governments and most importantly the vehicle users. The manufacturing and market issues of major global manufacturers of PEVs in terms of regulatory policies and trained manpower deployment are discussed. The market forecasts for electric vehicles have been referenced. ‘Electric Vehicle Geographic Forecasts’ predicts that the market opportunity for PEVs is in North America, Europe and Asia Pacific with growth projected at 16–20 %.

The adoption of PEVs as a new technology in an established automotive industry is challenging. Many countries are working on these issues so that the PEVs are adopted faster in transportation. However, the adoption to PEVs is slow and sluggish, since the initial purchase cost is high due to high battery cost and lack of public awareness on the new transport vehicle. There are key challenges to mitigate issues related to customers, manufacturers, marketing setups, public recognition and

regulations, power system related issues on Electric Vehicle Service Equipment for battery charging stations. The various Government programmes and types of incentives for promoting adoption of PEVs by many countries and major manufacturers in the world are comprehensively summed up. Such promotional incentives to all stake holders will ensure that the initial purchase price is affordable. Operational concessions and incentives are also considered by different states to ensure faster adoption of PEVs. Many manufacturers have announced launching of different models with an aim to reduce the cost of initial purchase and promote adoption of PEVs and avail the cheap operational cost benefits and the best social and environmental benefits.

Different range of PEV models and vehicles are available in the market to choose by consumers. The consumers and leading automotive makers rate the PEVs use as very high. Independent Research Institutes, on regular study on the technology, have predicted high growth and adoption of PEVs between 2020 and 2050. PEVs have increased triple in population in the first third year of the market and tends to grow. Battery costs are on the track to decline by 50 % in 2020. Several models are competitive in the market and grow year-on-year with momentum with Government supports. However, the challenges too remain active. Technology level is yet to be adopted. Public policy goals associated with the technology and energy security are needed. A scalable and viable business model for public charging infrastructure has yet to fully emerge. Consumers are unsure and have misunderstandings on PEVs use. Investment on R&D of battery technology is required with aggressive goals set by policy makers.

A lot many countries are yet to focus on use of electric vehicles. A wide range of facts and information on PEVs have been presented in this chapter and will be useful, in view of the compelling reasons to meet environmental and climatic targets for manufacturers, knowledge learners and researchers, business promoters and Government policy makers to learn, plan, manufacture and promote use of PEVs faster in countries that are yet to focus on this technology.

References

1. Calef D, Goble R (2007) The allure of technology: how France and California promoted electric and hybrid vehicles to reduce urban air pollution. Policy Sci 40(1):1–34
2. Lave LB, MacLean HL (2002) An environmental-economic evaluation of hybrid electric vehicles: Toyota's Prius vs. its conventional internal combustion engine Corolla. Transp Res 7(2):155–162
3. Greene DL (1998) Why CAFÉ worked. Energy Policy 26(8):595–613
4. Greene DL, Patterson PD, Singh M, Li J (2005) Feebates, rebates and gas-guzzler taxes: a study of incentives for increased fuel economy. Energy Policy 33(6):757–775
5. Santini DJ, PatttersonPD, Vyas AD (1999) The importance of vehicle costs, fuel prices, and fuel efficiency to HEV market success. In: Proceedings from 79th annual meeting of the transportation research board, Washington, DC
6. Kayser HA (2000) Gasoline demand and car choice: estimating gasoline demand using household information. Energy Econ 22:331–348
7. Khan M, Kockelman KM (2012) Predicting the market potential of plug-in electric vehicles using multiday GPS data. Energy Policy 46:225–233

8. Kempton W, Letendre S (1997) Electric vehicles as a new power source for electric utilities. Transp Res Part D 2(3):157–175
9. Electric Vehicle Transportation Center (2014) Report on electric vehicle sales and future projections. University of Central Florida
10. Nemry F, Leduc G, Muñoz A (2009) Plug-in hybrid and battery-electric vehicles: state of the research and development and comparative analysis of energy and cost efficiency, JRC Technical Notes JRC 54699 © European Communities
11. Electric vehicles: potential, technology and government initiatives—a report, Energy Alternative India (EAI). http://www.eai.in/ref/ct/ev/ev.html
12. Plug-in electric vehicles: literature review, center for climate and energy solutions. http://www.c2es.org/initiatives/pev, http://www.c2es.org/docUploads/PEV-action-plan.pdf. July 2011
13. Plug-in electric vehicle handbook for consumers, EERE Information Center 1-877-EERE-INFO (1-877-337-3463) www.eere.energy.gov/informationcenter, US Department of Energy. http://www.electricdrive.org/index.php?ht=d/sp/i/20952/pid/20952. Sept 2011
14. Hybrid electric vehicles: an overview of current technology and its application in developing and transitional countries—UNEP-hev_report, 2009. http://www.unep.org/transport/pcfv/PDF/HEV_Report.pdf
15. Plug-in electric vehicles. battery electric and plug-in hybrid electric vehicles: OEM strategies, demand drivers, technology issues, key industry players, and global market forecasts—Pike Research Report published 2012. http://www.navigantresearch.com/wp-content/uploads/2012/06/PEV-12-Executive-Summary.pdf
16. Liu R, Dow L, Liu E (2011) A survey of PEV impacts on electric utilities. In: IEEE PEs innovative smart grid technologies conference, CA USA, Jan 2011
17. Kintner-Meyer M, Schneider K, Pratt R (2007) Impacts assessment of plug-in hybrid vehicles on electric utilities and regional US power grids part 1: technical analysis. Pac Northwest Natl Lab pp.1–20. https://www.ferc.gov/about/com-mem/5-24-07-technical-analy-wellinghoff.pdf
18. Brooker A, Thomton M, Rugh J (2010) Technology improvement pathways to cost-effective vehicle electrification. In: Conference paper NREL/CP-540-47454, Feb 2010
19. Kempton W, Tomic J (2005) Vehicle-to-Grid Power fundamentals: calculating capacity and net revenue. J Power Sources 144(1):268–279
20. Kempton W, Tomic J (2005) Vehicle-to-grid power implementation; from stabilizing the grid to supporting large-scale renewable energy. J Power Sources 144(1):280–294
21. Towards an ontario action plan for plug-in-electric vehicles (PEVs) Waterloo Institute for Sustainable Energy, University of Waterloo, Waterloo, May 2010. http://normandmousseau.com/documents/Canizares-2.pdf
22. Greater charlotte plug-in-electric vehicle (PEV) readiness plan, clean cities, US Department of Energy, Version 1.1, Feb 2013. http://www.advancedenergy.org/portal/ncpev/docs/GreaterCharlottePEVReadinessPlan-Version1.1-February2013.pdf
23. Shuaib K, Zhang L, Gaouda A, Abdel-Hafez M (2012) A PEV charging service model for smart grids. Energies 5:4665–4682. doi:10.3390/en5114665
24. Accessibility and signage report by California PEV Collaborative, May 2012. http://www.evcollaborative.org/sites/all/themes/pev/files/PEV_Accessibility_120827.pdf
25. An action plan to integrate plug-in electric vehicles with the US electric grid, Mar 2012. http://www.c2es.org/docUploads/PEV-action-plan.pdf
26. EV market outlook, state of the plug-in electric vehicle market, July 2013. https://www.pwc.com/en_IL/il/energy-cleantech/assets/ec_state_of_pev_market_final.pdf
27. Plug in electric vehicle (PEV) incentives analysis and options for North Carolina, NC State University, US Department of Energy, Nov 2012. http://nccleantech.ncsu.edu/wp-content/uploads/FINAL-PEV-INCENTIVE-PAPER-v5.pdf
28. Menu of plug-in electric vehicle incentives, US Department of Energy, Mar 2013. http://www.transportationandclimate.org/sites/default/files/Menu of Plug-In EV Incentives_Final.pdf
29. A summary of accomplishments and recommendations, the Washington plug-in electric vehicle task force, Feb 2013. http://www.commerce.wa.gov/Documents/PEV-Task-Force-Gov-Rpt-2013.pdf

Chapter 2
Wireless Power Transfer (WPT) for Electric Vehicles (EVs)—Present and Future Trends

D.M. Vilathgamuwa and J.P.K. Sampath

Abstract 100 year old gasoline engine technology vehicles have now become one of the major contributors of greenhouse gases. Plug-in Electric Vehicles (PEVs) have been proposed to achieve environmental friendly transportation. Even though the PEV usage is currently increasing, a technology breakthrough would be required to overcome battery related drawbacks. Although battery technology is evolving, drawbacks inherited with batteries such as; cost, size, weight, slower charging characteristic and low energy density would still be dominating constrains for development of EVs. Furthermore, PEVs have not been accepted as preferred choice by many consumers due to charging related issues. To address battery related limitations, the concept of dynamic Wireless Power Transfer (WPT) enabled EVs have been proposed in which EV is being charged while it is in motion. WPT enabled infrastructure has to be employed to achieve dynamic EV charging concept. The weight of the battery pack can be reduced as the required energy storage is lower if the vehicle can be powered wirelessly while driving. Stationary WPT charging where EV is charged wirelessly when it is stopped, is simpler than dynamic WPT in terms of design complexity. However, stationary WPT does not increase vehicle range compared to wired-PEVs. State-of-art WPT technology for future transportation is discussed in this chapter. Analysis of the WPT system and its performance indices are introduced. Modelling the WPT system using different methods such as equivalent circuit theory, two port network theory and coupled mode theory is described illustrating their own merits in Sect. 2.3. Both stationary and dynamic WPT for EV applications are illustrated in Sect. 2.4. Design challenges and optimization directions are analysed in Sect. 2.5. Adaptive tuning techniques such as adaptive impedance matching and

D.M. Vilathgamuwa (✉)
School of Electrical Engineering and Computer Science,
Queensland University of Technology, Brisbane, Australia
e-mail: mahinda.vilathgamuwa@qut.edu.au

J.P.K. Sampath
School of Electrical and Electronic Engineering,
Nanyang Technological University, Singapore, Singapore
e-mail: prasadku001@e.ntu.edu.sg

S. Rajakaruna et al. (eds.), *Plug In Electric Vehicles in Smart Grids*,
Power Systems, DOI 10.1007/978-981-287-299-9_2

frequency tuning are also discussed. A case study for optimizing resonator design is presented in Sect. 2.6. Achievements by the research community is introduced highlighting directions for future research.

Keywords Wireless power transfer · Electric vehicles · Dynamic EV charging · Stationary EV charging

2.1 Introduction

PEVs have been proposed as the prospective mode of transportation to address environment, energy and many other issues. In spite of receiving many government subsidy and tax incentives, EVs have not become an attractive solution to consumers. Major drawback of EV is with the energy storage technology. Short comings of today's battery technology includes cost, size, weight, slower charging and low energy density. For example, energy density of commercial Lithium-Ion complete battery pack is around 100 Wh/kg [1]. This value is much smaller than that of gasoline engine. It would be infeasible to achieve range of a gasoline vehicle from a pure PEV with current battery technology. Long charging times and mechanical hassles with charging cables are main drawbacks of present PEV technology that impede the widespread proliferation of PEVs.

WPT technology can be used as a solution in eliminating many charging hazards and drawbacks related to cables. The concept of dynamic WPT enabled EVs, which means the EV could be charged while moving in a road will increase the effective driving range while reducing the volume of battery storage. Not only from the consumer perspective, but also from sustainable energy point of view WPT enabled EVs are greatly beneficial. For example, the concept of Vehicle-to-Grid [2] to enrich distributed energy generation model can be brought into next stage with WPT facilitated EVs [3]. Some futuristic concepts of motor/capacitor/WPT EVs have been proposed where EV is continuously charged and possible to run forever without batteries [4].

WPT technology is improving significantly covering aspects such as RF technology, near-field energy transfer, energy conversion and management, energy storage elements, novel materials and fabrication techniques EMC/EMI considerations. However, WPT is yet to fully mature in terms of power transfer efficiency, range, and power rating. Extensive research studies that have been carried out presently would bring the world closer to the futuristic concept of motor/capacitor/WPT EVs.

2.2 Basics of WPT Technology

WPT is the transmission of electrical power from the power source to an electrical load without the use of physical connectors. History of WPT began with the formulation of Maxwell's equations in 1862. Maxwell described phenomena of radio

waves in his equations. Later, in 1884 Henry Poynting illustrated electromagnetic waves as an energy flow and is used in his Poynting theorem. Nikola Tesla investigated the principle of WPT at the end of the 19th century [5]. Tesla's experiment was not exploited to a commercial level because of its seemingly unsafe nature, low efficiency, and financial constraints. After Tesla's initial experiments, electromagnetic waves are used for wireless communications and remote sensing applications.

With the advent of advanced semiconductor technologies, Tesla's proposition has now become a reality. The wireless nature of this transmission makes it useful in environments where implementation of physical connectors can be inconvenient, hazardous or impossible, particularly in EVs.

2.2.1 Wireless Energy Transfer Methods

Wireless power transfer methods encompass technologies such as Laser, photoelectric, radio waves (RF), microwaves, inductive coupling and magnetic resonance coupling. These technologies can be broadly categorized based on underlying mechanism, transmission range, and power rating. Based on the power transfer distance wireless energy transfer methods can be categorized into two types; near field and far field. If transfer distance is longer than the wavelength of electromagnetic wave, it is categorized in to far field technique. Laser, photoelectric, RF, microwave can be considered as far field energy transfer methods. Inductive coupling and magnetic resonance coupling based methods are regarded as near field approaches. Even though far field techniques have transmission range up to several kilometres, they suffer from the trade-off between directionality and efficiency. Frequency range of far field approaches are typically very high (GHz range) compared to near field (kHz–MHz). Inductively coupled near field approaches can be used to transmit high power efficiently in very near range (up to several centimetres). Efficiency of such systems deteriorates exponentially with the distance. The non-radiative WPT system demonstrated in 2007 by MIT [6] based on magnetic resonance coupling can be used in mid-range application with an acceptable efficiency. This MIT experiment has gained accentuating attention from the research community because many real world applications require longer transmission range.

2.2.2 Inductive Coupling Versus Magnetic Resonance Coupling

Traditional inductive power transfer (IPT) systems based on inductive coupling resulting from the Faraday's law of induction and Ampere's circuital law. The integrated magnetic field due to current carrying loop (transmitting coil) is defined by the Ampere's circuital law. According to Faraday's law of induction, time-varying

magnetic field induces electric field in receiving coil. Initial configurations of IPT systems used inductor in series with the coil [7]. This is analogues to loosely coupled transformer. Later, IPT based topologies are adopted with capacitor compensation [8]. Conversely, magnetic resonance technology originally used with self-resonance coils which resonates with its self-inductance and parasitic capacitance [6]. An external lumped capacitor is added to build the resonance coils when parasitic capacitance of coils are inadequate to make resonance at frequency of interest in later studies [9, 10]. Frequency selection for IPT based designs are limited to several kilohertz while magnetic resonance based systems can operate in frequencies up to a few Megahertz. Typical IPT schemes are limited to a few centimeters whereas magnetic resonance WPT can be used with larger range.

2.3 Modelling the WPT System

Modeling the WPT system is crucial in designing WPT system for EVs. Simplicity and the accuracy of the model are important. The modeling methodology needs to provide guide lines in the selection of system performance indices and design parameters.

The block diagram in Fig. 2.1a shows typical two resonator WPT system powered using high frequency (HF) power source. HF source can either be an inverter or combination of a power amplifier (PA) and a signal generator (SG). PA and SG based setups are commonly used in laboratory prototyping, but PA and SG combination has to be replaced with a high frequency inverter in real world implementation. Receiver resonator is connected to the load through a battery chargering circuity. In EV charging applications battery is connected through a rectifier and regulator circuit. Load impedance consists of the impedance of the charging circuit. Battery load can be approximated to a resistive AC load [11].

Equivalent source resistance represents output impedance of the power source. In case of PA and SG combination, source impedance is typically 50 Ω. But in power converter based designs this value is much smaller than 50 Ω. Therefore, source resistance must be chosen with careful attention in the design process based on the type of the source.

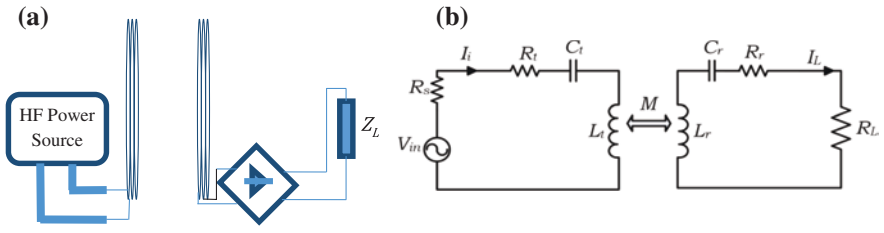

Fig. 2.1 **a** Two resonator WPT system. **b** The equivalent circuit

2.3.1 Equivalent Circuit Theory

As electrical lengths (ratio of cable lengths to operating wavelength) of cables and coils are very short, the system can be analysed in lumped parameter model. Lumped parameter circuit model is shown in Fig. 2.1b. Two types of resonant coils have been used in WPT; self-resonators and LC resonators. Self-resonators resonate with the self-inductance of coil and parasitic capacitance between turns, whereas LC type has an externally added lumped capacitor. Self-resonators have the advantage of low loss, but realization at low frequencies is challenging because the typical parasitic capacitance is very low. LC type is more controllable during the design process. Compensation capacitor of the LC resonator can either be Parallel (P) or Series (S) to the coil. Series compensation inherits voltage source characteristic while parallel compensation has current source characteristic. Based on the transmitting and the receiving resonator capacitor compensation, four topologies; Series–Series (SS), Series–Parallel (SP), Parallel–Series (PS), and Parallel–Parallel (PP) can be realized. If parallel compensation is used at either side, the capacitance value depends on the coupling coefficient, which is a variable in a moving load application. Therefore SS compensation is preferred for EV applications.

Using Kirchhoff's voltage law, Eq. (2.1) can be obtained.

$$\begin{aligned} &\begin{bmatrix} Z_t + R_s & j\omega M \\ j\omega M & Z_r + R_L \end{bmatrix} \begin{bmatrix} I_i \\ I_L \end{bmatrix} = \begin{bmatrix} V_i \\ 0 \end{bmatrix} \\ &Z_{t,r} = R_{t,r} + j\omega L_{t,r} + \frac{1}{j\omega C_{t,r}} \\ &M = k\sqrt{L_t L_r} \end{aligned} \tag{2.1}$$

where V_i is the driving voltage applied on the transmitter resonator at carrier frequency ω, and Z_t and Z_r are the self-impedances of transmitter and receiver resonators respectively. These impedances are made up of $L_{t,r}$, $C_{t,r}$ and $R_{t,r}$ which are inductance, capacitance and resistance of the coils respectively. Capacitance includes both distributed capacitance of the coil and externally added lumped capacitance. The mutual inductance (M) between the transmitter and the receiver can be expressed in terms of coupling coefficient (k) and coil inductances.

Output power at the load and Power Transfer Efficiency (PTE) can be calculated as,

$$\begin{aligned} \mathrm{P_{out}} &= |I_\mathrm{L}|^2 \mathrm{R}_L \\ PTE &= \frac{|I_L|^2 R_L}{|I_i|^2 (R_t) + |I_L|^2 (R_L + R_r)} \\ I_i &= \frac{(R_L + Z_r) V_s}{(Z_t + R_s)(R_L + Z_r) + (\omega M)^2} \\ I_L &= \frac{(j\omega M) V_s}{(Z_t + R_s)(R_L + Z_r) + (\omega M)^2} \end{aligned} \tag{2.2}$$

At the resonance condition, reactive impedance of the coil becomes zero. Resonance frequencies of the transmitter and receiver coil becomes,

$$X_{t,r} = j\omega_{t,r}L_{t,r} + \frac{1}{j\omega_{t,r}C_{t,r}} = 0$$
$$\omega_{t,r} = \frac{1}{\sqrt{L_{t,r}C_{t,r}}} \tag{2.3}$$

Equivalent circuit method allows us to determine element parameters such as currents and voltage across coils, compensation capacitors. Therefore it is essential to use equivalent circuit based analysis to estimate component ratings in designing high power WPT system. Detailed analysis of design parameters and performance indices based on equivalent circuit is presented in Sect. 2.5.1.

2.3.2 Two Port Network Theory

Measurement of scattering parameters (S-parameter) is easier compared to voltage and current measurements in laboratory prototyping. In particular, S-parameter measurement is suitable at the initial stage of the design. S-parameter analysis of WPT system can be done using two port network modeling as shown in Fig. 2.2.

Using the definitions of two port network theory impedance parameter matrix (Z parameter matrix) and scattering parameter matrix (S parameter matrix) can be given as follows,

$$\begin{bmatrix} V_1 \\ V_2 \end{bmatrix} = \begin{bmatrix} Z_{11} & Z_{12} \\ Z_{21} & Z_{22} \end{bmatrix} \begin{bmatrix} I_1 \\ -I_2 \end{bmatrix}$$
$$\begin{bmatrix} b_1 \\ b_2 \end{bmatrix} = \begin{bmatrix} S_{11} & S_{12} \\ S_{21} & S_{22} \end{bmatrix} \begin{bmatrix} a_1 \\ a_2 \end{bmatrix} \tag{2.4}$$

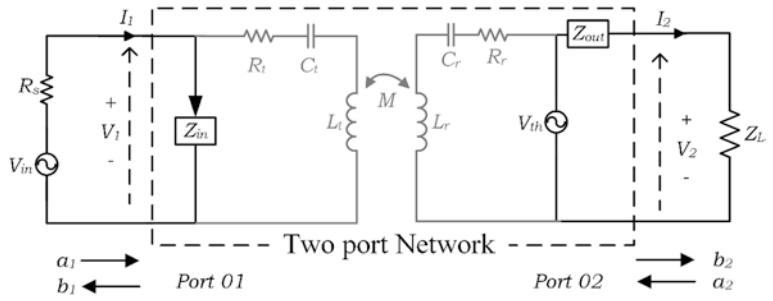

Fig. 2.2 Two port network modelling of the WPT system

Input and output impedances can be calculated using Z parameters;

$$\begin{aligned} Z_{in} &= \frac{V_1}{I_1} = Z_{11} - \frac{Z_{21}Z_{12}}{Z_{22}+Z_L} \\ V_{th} &= \frac{Z_{21}}{Z_{22}+Z_L}V_{in} \\ Z_{out} &= \frac{V_{th}}{I_{SC}} = Z_{22} - \frac{Z_{12}Z_{21}}{Z_{11}+Z_s} \\ R_{in} &= real(Z_{in}),\ R_L = real(Z_L) \end{aligned} \tag{2.5}$$

Input power, output power and the efficiency become,

$$\begin{aligned} P_{in} &= |I_1|^2 R_{in} = \frac{|V_{in}|^2}{|R_s+Z_{in}|^2}R_{in} \\ P_{out} &= |I_2|^2 R_L = \frac{|V_{th}|^2}{|Z_{out}+R_L|^2}R_L = \frac{|Z_{21}|^2|V_{in}|^2}{|(Z_{in}+Z_s)(Z_{22}+Z_L)|^2}R_L \\ PTE &= \frac{P_{out}}{P_{in}} = \frac{|Z_{21}|^2}{|Z_L+Z_{22}|^2}\frac{R_L}{R_{in}} \end{aligned} \tag{2.6}$$

S-parameters are convenient as they can be easily measured in laboratory experiments. Z parameters can be obtained by using the following conversion,

$$\begin{bmatrix} Z_{11} & Z_{12} \\ Z_{21} & Z_{22} \end{bmatrix} = \frac{Z_0}{\Delta}\begin{bmatrix} (1+S_{11})(1-S_{22})+S_{12}S_{21} & 2S_{12} \\ 2S_{21} & (1-S_{11})(1+S_{22})+S_{12}S_{21} \end{bmatrix} \tag{2.7}$$

where $\Delta = (1-S_{11})(1-S_{22}) - S_{12}S_{21}$.

When the source and load impedances are matched with characteristic impedance (Z_0) of the system ($R_s = Z_L = Z_0$), normalized output power (NOP) and PTE become,

$$\begin{aligned} NOP &= \frac{P_{out}}{|V_{in}|^2/(4Z_0)} = |S_{12}|^2 \\ PTE &= \frac{|S_{12}|^2}{1-|S_{11}|^2} \end{aligned} \tag{2.8}$$

S-parameters can be measured connecting network analyzer to transmitting and receiving resonators. Power electronic converter or power amplifier is not needed in these experiments. S-parameter based analysis and measurement are recommended at the initial stage of the design process. Frequency characteristic of performance indices can be determined using this method at lower power level. It must be noted that source impedance is typically 50 Ω in network analyzer measurements. However, source impedance is much smaller if a power converter is used.

2.3.3 Coupled Mode Theory

Coupled mode theory (CMT) analyses energy exchange between resonant objects in time domain [12]. CMT analysis of WPT system is used to obtain more insight understanding of resonator behavior.

$$\begin{aligned}\frac{da_1(t)}{dt} &= -(j\omega + \Gamma_1)a_1(t) + jKa_2(t) + V_{in}(t)\\ \frac{da_2(t)}{dt} &= -(j\omega + \Gamma_2 + \Gamma_L)a_2(t) + jKa_1(t)\end{aligned} \tag{2.9}$$

where $a_{1,2}$ are time varying field amplitudes of two resonant objects (transmitting and receiving resonators) and ω is the eigen frequency. $\Gamma_{1,2}$ are intrinsic decay rates (or resonance widths) of sending and receiving coils due to losses, and Γ_L is the resonance width of the load. Resonance widths are inversely proportional to resistances in equivalent circuit approach. $V_{in}(t)$ is the excitation signal applied to sending coil. K is the coupling rate between resonators.

In steady sate and pure sinusoidal excitation signal ($F_s(t) = A_s e^{-j\omega t}$), resulting field amplitudes are $a_1(t) = A_1 e^{-j\omega t}$ and $a_2(t) = A_2 e^{-j\omega t}$. Average power absorbed by the transmitting resonator and the power delivered to receiving resonator are $P_1 = 2\Gamma_1|A_1|^2$ and $P_2 = 2\Gamma_2|A_2|^2$ respectively. Input power from the source $P_{in} = P_1 + P_2 + P_{out}$ [13]. Output power delivered to the load and power transfer efficiency can be expressed as,

$$\begin{aligned}P_{out} &= 2\Gamma_L|A_2|^2\\ PTE &= \frac{1}{1 + \frac{\Gamma_2}{\Gamma_L} + \left[1 + \frac{\Gamma_1\Gamma_2}{K^2}\left(1 + \frac{\Gamma_L}{\Gamma_2}\right)^2\right]}\end{aligned} \tag{2.10}$$

CMT is applicable for designs with high quality factor and low coupling coefficient.

2.4 WPT for EV Charging

WPT for EV charging has many advantages compared to wired-PEV charging. Inconveniences in wired PEV charging process are major impediments in gaining interest of consumers. Due to industrial requirements and advancements in technology, power transfer distance in WPT systems has increased from several millimeters to several centimeters. Although number of researchers working on the WPT technology, still there are numerous challenges to overcome in bringing it to commercial level. Acceptable power transfer efficiency at high transfer range, increasing power level, misalignment tolerance and safety considerations are major technical challenges. Demonstrated research works show promises that the WPT can be brought in to commercial level with a reasonable cost [14].

Stationary EV charging for PEVs and dynamic EV charging for moving vehicles have been studied and demonstrated in the literature. Although both stationary and dynamic WPT for EVs have been undergoing from laboratory demonstrations, to bring them to large scale commercialization, still there is significant work needs to be done on performance optimization, standardization, cost effectiveness and safety considerations. Charging process should be automated as much as possible.

2.4.1 Stationary WPT for EV Charging

Stationary WPT can replace the charging cable for PEVs. WPT system is activated when vehicle reaches to the charging area. Figure 2.3 illustrates typical stationary WPT platform for EV charging. High frequency power inverter converts low frequency utility power to high frequency AC power. Resonance electromagnetic field generated in the transmitting resonator transfers power to the receiving resonator. Received power at the secondary resonator is rectified to charge the battery pack. Power converters used for the WPT can mainly categorized in to two types, namely indirect power converters and direct power converters. Utility power is first converted to DC and then invert to high frequency AC power in indirect conversion method. Energy conversion undergoes two conversion stages AC-DC-AC in indirect method. Alternatively, direct conversion method converts energy directly from low frequency mains to high frequency in a single stage [15, 16]. The charging system can be implemented in urban areas such as parking lots and bus stops.

Stationary WPT for EV charging has better market acceptance and lower implementation cost compared to dynamic WPT. A few WPT enabled EVs have been introduced to market including "Leaf" by Nissan Motor Co., "2014 Volt" by Chevrolet, "Qualcomm HaloIPT" by Qualcomm Co., and "PUGLESS" by Evatran Co. Some of the commercial pilot projects have been successfully demonstrated recently. Automotive manufacturers such as Delphi, Magna, Maxwell and Panasonic have been working on developing WPT systems. The development kit, WiT-3,300 released by WiTricity Corporation is capable of delivering 3.3 kW power over

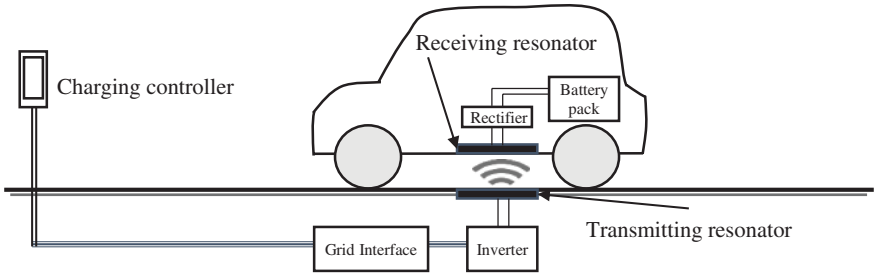

Fig. 2.3 Stationary WPT for EV

18 cm with 90 % efficiency. Size of WiT-3,300 transmitter and receiver resonators of are 50×50 cm [17]. University of Auckland has achieved 5 kW stationary IPT system with 90 % efficiency over 20 cm distance using 75 cm size coil design [18].

Stationary WPT solutions for EV charging has to be designed shifting the system complexity more towards the transmitting side infrastructure and keeping the vehicle component as simple as possible. Although mechanical and electrical hazards with plugged-in charger can be eliminated using stationary WPT for EV charging, driving range and slower charging time will still be a dominant issue.

2.4.2 Dynamic WPT for EV Charging

From the vehicle viewpoint, dynamic WPT enabled infrastructure where EVs can be charged continuously while in motion, theoretically solve the EV battery problem with unlimited driving range. However, employment of such system is reliant on the infrastructure development, which in turn limited by its cost. In addition, amount of the energy gained through WPT depends on the power level of the system, vehicle speed and duration that vehicle travel within the WPT enabled zone.

Dynamic EV charging approaches can be mainly categorized into two types based on transmitter array design; single transmitter track and segmented transmitter coil array. First type consists of a substantially long transmitter track connected to a power source. The receiver is noticeably smaller than the length of the track. Segmented coil array based designs have multiple coils connected to high frequency power sources as shown in Fig. 2.4a.

Transmitter track based systems are easier to control as the track is powered from a single source. Coupling coefficient along the track is nearly constant when the vehicle moves along the track. The transmitter track can be few meters to several tens of meters long. But this type of design suffers from several drawbacks. Firstly, the electromagnetic field emitted within the uncoupled region has to be suppressed to eliminate harmful exposure. Secondly, the compensation capacitor has to be distributed along the track to compensate large inductance. This brings additional constrain in construction. Thirdly, coupling coefficient is fairly low because of the smaller transmitter region covered by the receiver resulting lower efficiency. Usually ferromagnetic materials have been used to guide the magnetic flux and increase the efficiency. Relative range of track based systems are much smaller than unity.

On the other hand, segmented coil array eliminates field exposure and requirement for distributed compensation while lowering coupling issues. However, it introduces some other design challenges. It is necessary to track the receiver position and switch the appropriate power source as the load moves along the array. In addition, separation between transmitter coils needs to be carefully optimized. When coils are placed too apart, efficiency reduces steeply when the receiver moves away from the transmitter and power transfer will not be continuous. However, coils cannot be kept too close to each other due to two reasons. Firstly, negative mutual inductance between adjacent transmitter coils are significant generating negative

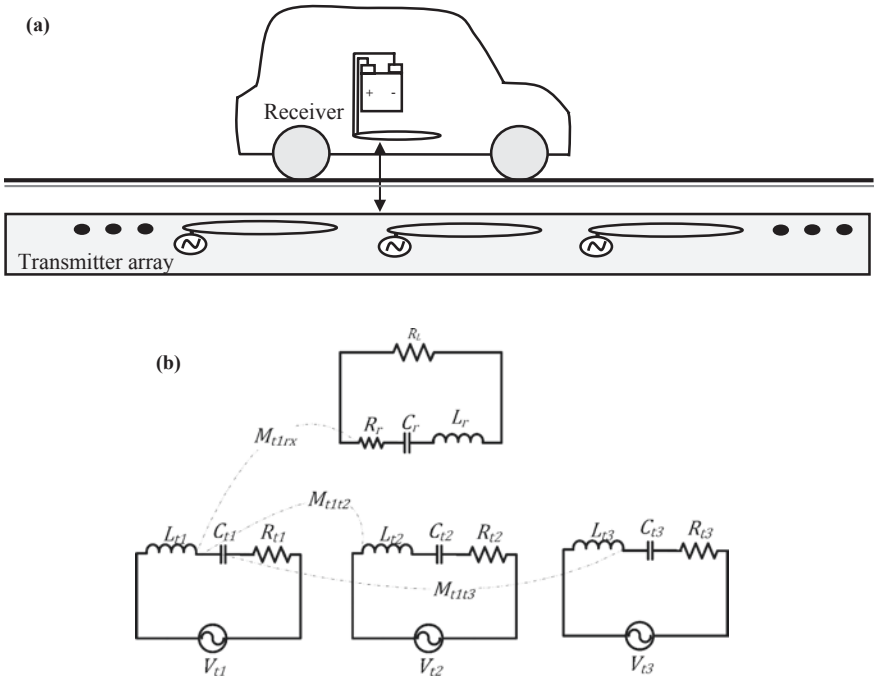

Fig. 2.4 **a** Dynamic EV charging with segmented coil array. **b** Equivalent circuit considering three nearby transmitters are powered simultaneously

current stress. Secondly, design cost will be increased with many transmitters in a given length of the track. Connecting source converters to multiple coils is also a design issue. Several transmitter coils can be connected to a single power converter in parallel, or there can be a converter connected to each coil. In both cases system complexity in terms of controlling the power flow is higher. Analysis of segmented coil based design can be carried out to derive most optimal design. Figure 2.4b shows equivalent circuit considering three nearby transmitters are powered simultaneously. Equation (2.11) can be used to study the system performance.

$$\begin{bmatrix} Z_{t_1} & X_{t_1t_2} & X_{t_1t_3} & X_{t_1r} \\ X_{t_2t_1} & Z_{t_2} & X_{t_2t_3} & X_{t_3r} \\ X_{t_3t_1} & X_{t_3t_2} & Z_{t_3} & X_{t_3r} \\ X_{rt_1} & X_{rt_2} & X_{rt_3} & (Z_r + R_L) \end{bmatrix} \begin{bmatrix} I_{t_1} \\ I_{t_2} \\ I_{t_3} \\ I_r \end{bmatrix} = \begin{bmatrix} V_{t_1} \\ V_{t_2} \\ V_{t_3} \\ 0 \end{bmatrix} \tag{2.11}$$

$$P_{out} = |I_r|^2 R_L$$

$$PTE = \frac{P_{out}}{P_{in}} = \frac{|I_r|^2 R_L}{\left|I_{t_1}\right|^2 R_{t_1} + \left|I_{t_2}\right|^2 R_{t_2} + \left|I_{t_3}\right|^2 R_{t_3} + |I_r|^2 (R_L + R_r)}$$

$Z_m = R_m + j(\omega L_m - 1/\omega C_m), (m = t_{1,2,3}, r)$ are the self-impedances of transmitter and receiver coils where $L_m, C_m,$ and R_m are inductance, capacitance and parasitic

resistance of the coil. Capacitance includes both distributed capacitance and externally added capacitance. $X_{mn} = X_{nm} = j\omega M_{mn} = j\omega M_{nm} (m = t_{1,2,3}, r)$ where $M_{mn} = M_{nm}$ is mutual inductance between mth coil and nth coil. ω is the operating frequency of the source. Subscripts $t_{1,2,3}$ represent three nearest transmitter coils to the receiver coil (represented by subscript r).

Some of the notable achievements in designing dynamic EV charging platforms can be identified as follows. UC Berkeley has conducted a test as a proof-of-concept of a dynamic WPT system for EV based on IPT in late 70s' [7]. They transferred a 60 kW of power through 7.6 cm distance to a passenger bus along 213 m long track. Due to limited semiconductor technologies, operating frequency of Berkeley system was 400 Hz and their efficiency was only 60 %. From there, researchers and industry have improved the performance of the dynamic EV charging systems. Korea Advanced Institute of Science and Technology (KAIST) is a leading research contributor in dynamic EV charging. The online electric vehicle (OLEV) centre of KAIST has demonstrated a transmitter track based roadway powered EV system. The OLEV has achieved 20 kW power transfer over 20 cm at 83 % efficiency with the use of Shaped Magnetic Field in Resonance (SMFIR) technology. SMFIR consists of current carrying transmitter rails of 5–60 m long and pickup module of 80 cm [19]. The relative transfer distance of KAIST-OLEV is still much smaller than unity. Oakridge National Lab (ORNL) has successfully demonstrated WPT system for moving EV using segmented coil array. ORNL has transferred 2 kW over 10 cm using 33 cm diameter coils with a maximum efficiency about 85 % [20]. But the efficiency of their setup tends to drop drastically with misalignment.

2.5 Design Challenges and Optimization Candidates

2.5.1 Analysis of WPT System

System performance indices can be analyzed using all three modeling approaches presented in Sect. 2.3. In this section we analyze performance indices for power transfer efficiency and transferred power with respect to design parameters. Equivalent circuit approach is chosen for the analysis. The efficiency term is not uniformly applied by the researchers in the literature. Both maximum power transfer operation and maximum efficiency condition are used as design goals. The maximum power transfer refers to the condition where maximum power is drawn from the source. The maximum power transfer occurs when the source impedance and the input impedance seen by the source are matched. Conversely, objective of the maximum efficiency operation is to optimize energy efficiency in the power transfer process.

As it can be seen in Fig. 2.5, the maximum PTE always occurs at the resonance frequency (f_0) for a two-coil system. Besides PTE declines with the coupling

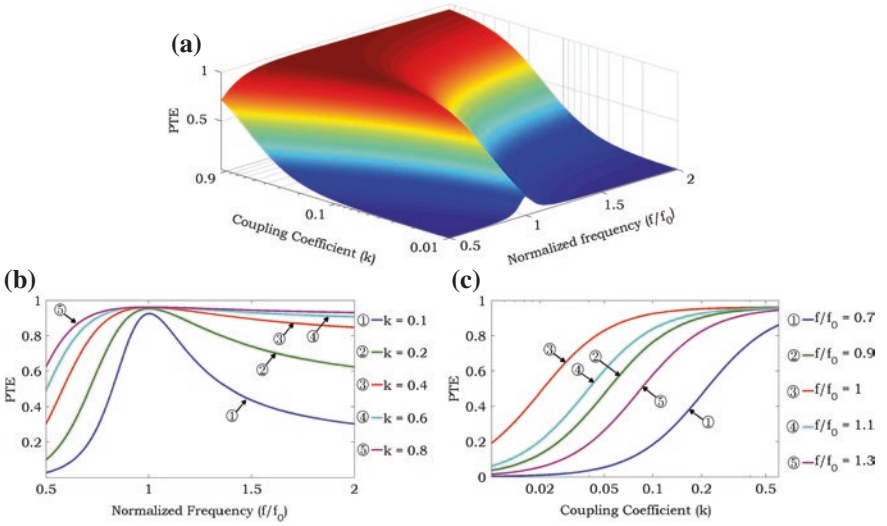

Fig. 2.5 **a** Power transfer efficiency (PTE) variation with respect to frequency (f) and coupling co-efficient (k). **b** PTE versus frequency. **c** PTE versus coupling coefficient. Frequency is normalized to resonance frequency (f_0)

coefficient between transmitter and receiver. On the other hand, output power is not always the maximum at the resonance frequency. When electromagnetic coupling between two coils is higher (strongly coupled), frequency at which maximum power transfer occurs is split. Transferred power to the load ($|S_{21}|^2$ or *NOP*) shows double peak behavior with respect to the frequency as can be seen in Fig. 2.6. This frequency splitting phenomenon [21] has led to various adaptive controlling efforts to maximize the power transfer, including frequency tuning [21, 22], impedance matching [23–25] and coupling manipulation [21, 26]. The point where the frequency splitting ends is referred to as the critical coupling point. Beyond the critical coupling point the transferred power to the load drops exponentially with increasing coil separation.

Both the transferred power to the load and the input to output efficiency have been used as the figure of merit in the literature. *NOP* can also be computed by modeling the system as two port network and using transfer scattering parameter, $|S_{21}|^2$ at impedance matched condition. It also should be noted that the maximum efficiency point shifts away from the resonance frequency in multi coil telemetry [9]. Based on the application, decision regarding optimization effort must be made between the transferable power and the efficiency. For low power applications where the importance of losses is not significant, the maximum power transfer operation is the main consideration. Energy efficiency is also a vital factor in high power applications.

At resonance condition, where $\omega_0 = 1/\sqrt{L_t C_t} = 1/\sqrt{L_r C_r}$ the power output and the efficiency can be expressed as,

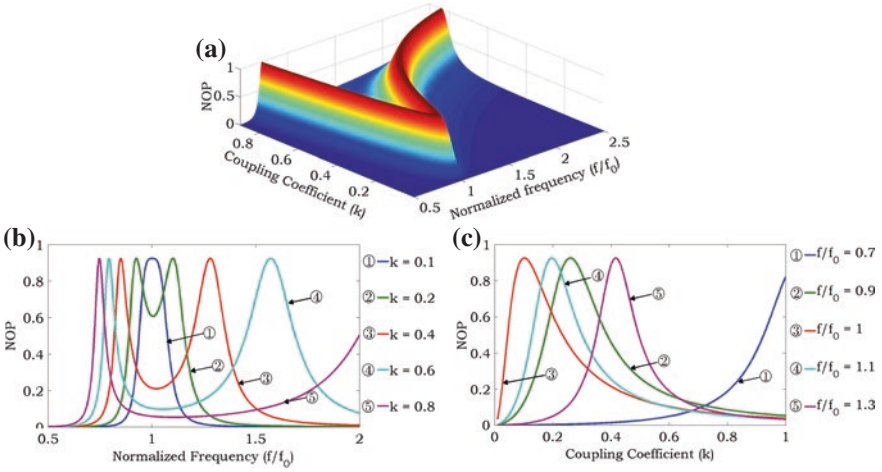

Fig. 2.6 **a** Normalized output power (*NOP*) variation with respect to frequency (*f*) and coupling co-efficient (*k*). **b** *NOP* versus frequency. **c** *NOP* versus coupling coefficient. Frequency is normalized to resonance frequency (f_0)

$$
\begin{aligned}
P_{out,\omega_0} &= \frac{V_i^2 R_L (\omega_0 M)^2}{\left((R_s + R_t)(R_L + R_r) + (\omega_0 M)^2\right)^2} \\
\mathrm{PTE}_{\omega_0} &= \frac{R_L (\omega_0 M)^2}{\left((R_s + R_t)(R_L + R_r) + (\omega_0 M)^2\right)(R_L + R_r)}
\end{aligned}
\tag{2.12}
$$

Both PTE and the output power at the resonance depend on the value of load resistance as depicted in Fig. 2.7. Equation 2.13 gives values of load resistance for both maximum efficiency and maximum output power operating conditions. Impedance matching network can be used to make equivalent load resistance to its optimal value. Figure 2.8 shows the variation of optimal load resistance with respect to coupling coefficient.

$$
\begin{aligned}
R_{L,PTE\_max} &= \sqrt{\frac{(\omega_0 M)^2 R_r}{(R_s + R_t)} + R_r^2} \\
R_{L(max\_Pout)} &= \frac{(\omega M)^2}{(R_s + R_t)} + R_r
\end{aligned}
\tag{2.13}
$$

2.5.2 *Designing the Figure-of-Merit of the System*

Both PTE and transferred power cannot be optimized simultaneously. If transferred power is chosen as the first optimization goal, the maximum achievable efficiency can

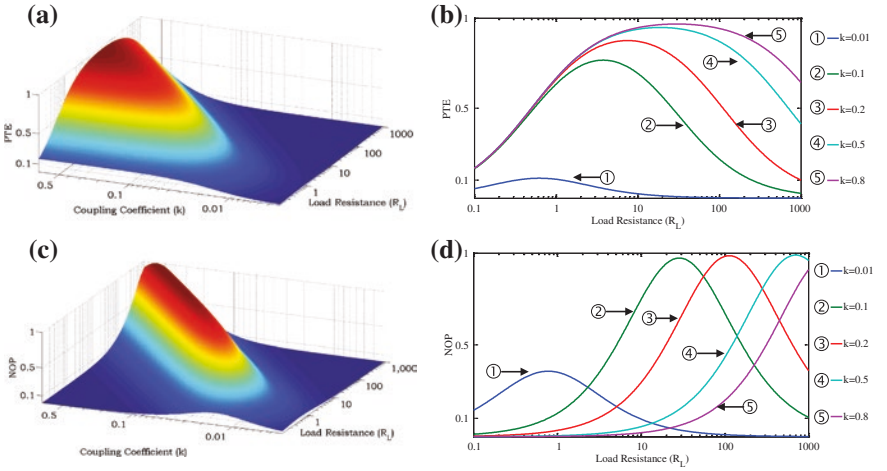

Fig. 2.7 **a**, **b** Power transfer efficiency (PTE), **c**, **d** Normalized output power (*NOP*) variation with respect to load resistance (R_L) and coupling co-efficient (k)

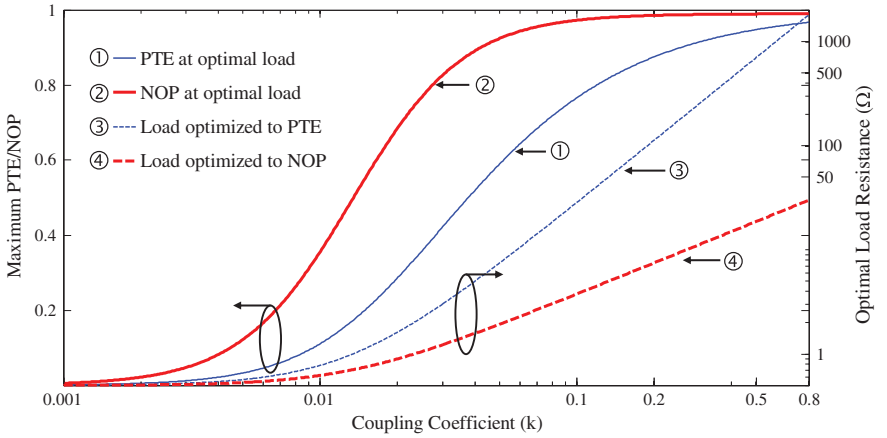

Fig. 2.8 Effect of load resistance on the power transfer efficiency (PTE) and normalized output power (NOP)

be limited. Which is not desirable for EV applications. On the other hand, if the first focus is on improving the efficiency of the system, other techniques such as adaptive impedance matching can be used to improve the transferred power. Therefore, it is recommended to focus on improving the efficiency in initial design stages.

2.5.2.1 Optimizing Power Transfer Efficiency

Maximum achievable efficiency when load resistance is optimized to $R_{L,PTE}$ can be expressed as [10, 27];

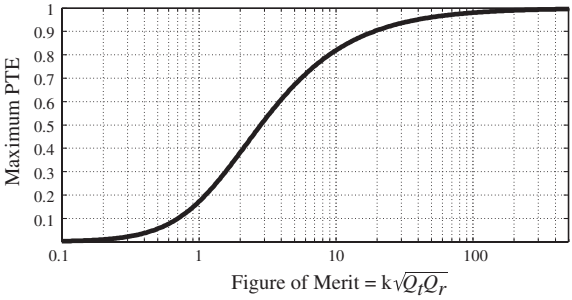

Fig. 2.9 Maximum achievable efficiency as a function of figure-of-merit (FOM), $k\sqrt{Q_t Q_r}$

$$\text{PTE}_{opt} = \frac{k^2 Q_t Q_r}{\left(1 + \sqrt{1 + k^2 Q_t Q_r}\right)^2} \tag{2.14}$$

where $Q_{t,r} = \frac{\omega_0 L_{t,r}}{R_{t,r}}$ are unload quality factors of the transmitter and the receiver coils. As can be seen from Fig. 2.9, the maximum efficiency depends on the quality factors of the resonators, and the coupling coefficient between resonators. In order to achieve acceptable efficiency in a lager relative distance, (i.e. low coupling co-efficient) it is required to have resonator coils with high quality factor. Therefore, the operating frequency must be high enough and the AC resistance of resonators should be low. However, higher frequency operation leads to an increase in the complexity of the power electronic circuits. In initial demonstration done by MIT, team has achieved 40 % efficiency between sending and receiving resonators in 2 m distance [6].

2.5.2.2 Optimizing Transferred Power

Transferred power is also important to be considered because it determines VA ratings, thus the component ratings, especially ratings of the series capacitor and power converter switches. Transferred power becomes maximum when the maximum power is drawn from the source. This happens when the source impedance matches the input impedance of the coil system. Input impedance of the coil is varied with the coupling coefficient variation and operating frequency. When operating at self-resonance frequency, the maximum power transfer occurs at a particular coefficient value referred to as critical coupling point. Value of the critical coupling can be derived as in (2.15). Coupling coefficient equals to critical coupling at a particular distance. But in dynamic EV charging WPT distance and the coupling coefficient are continuously varying. Therefore, operating at critical coupling point is not desirable.

$$k_{critical} = \sqrt{\frac{(R_s + R_t)(R_L + R_r)}{\omega_0^2 L_t L_r}} = \sqrt{\frac{1}{Q_T Q_R}} \tag{2.15}$$

where Q_T and Q_R are loaded quality factors in transmitter and receiver resonators.

When operating out of critical coupling point, the reactive power of a transmitter can be 50 times larger than the transmitted active power [28]. Therefore, voltage and current in the coils can be very high without a proper design optimization. This high current could affect power rating of power converter switches and compensation capacitor. Voltage across the series capacitor and the inductor coil at the resonance operation can be expressed as in Eq. (2.16). The output power can be increased by increasing the voltage applied on the transmitter resonator, but it will also increase required capacitor rating. With high quality factor resonators (typically 400–1,000) this increase will be more significant.

.

$$\mathrm{V}_{c_{t,r}} = V_{t,r} Q_{t,r} \tag{2.16}$$

Adaptive impedance matching networks can be used to match the source impedance to input impedance of WPT network [23–25]. Unlike PA based laboratory prototyping where source impedance is 50 Ω, in power converter based designs the source impedance can be a very small value. Therefore, the matching network should be capable of bringing input impedance of the WPT system close to source impedance.

2.5.3 Power Transfer Distance and Misalignment Tolerance

As identified in previous sections system performance is largely dependent on the electromagnetic coupling coefficient which has linear relationship with mutual inductance. In this section we analyze mutual inductance variation with respect to relative position of the receiver. Calculations are presented for a multi turn circular coil. Mutual inductance between circular resonators can be calculated using filament method [29] by modelling coil as a set of filamentary circular coils. Mutual inductance between misaligned filamentary circular coils with parallel axes shown in Fig. 2.10a can be computed using Eqs. (2.17), (2.18) and (2.19) [30, 31].

$$\begin{aligned} M &= \frac{\mu_0}{\pi}\sqrt{r_t r_r}\int_0^{\pi} \frac{\left(1-\frac{y_{tr}}{r_r}\cos\phi\right)\Phi(m)}{\sqrt{V^3}}d\phi \\ a &= \frac{r_r}{r_t}, b = \frac{z_{tr}}{r_t}; m^2 = \frac{4aV}{\left((1+aV)^2+b^2\right)} \\ V &= \sqrt{1+\frac{y_{tr}^2}{r_r^2}-2\frac{y_{tr}}{r_r}\cos\phi}; \Phi(k) = \left(\frac{2}{m}-m\right)K(m) - \frac{2}{m}E(m) \end{aligned} \tag{2.17}$$

Complete Elliptic Integrals,

$$K(m) = \int_0^{\pi/2} \frac{1}{\sqrt{\left(1-m^2 sin^2\gamma\right)}}d\gamma; E(m) = \int_0^{\pi/2} \sqrt{\left(1-m^2 sin^2\gamma\right)}d\gamma$$

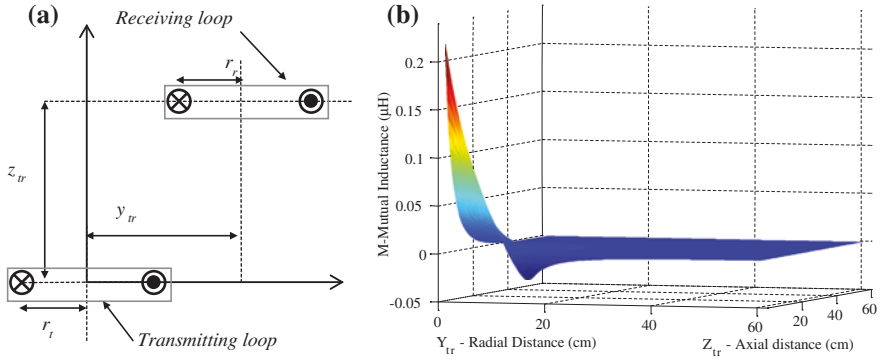

Fig. 2.10 **a** Filamentary circular coil arrangement. **b** Mutual inductance with respect to radial and lateral misalignment for elementary circular loops

Equation (2.17) becomes singular when $z_{tr} \neq 0$ and $r_r = y_{tr}$. In that case Eq. (2.18) needs to be used [30].

$$
\begin{aligned}
M &= \frac{\mu_0}{2\pi} r_t \int_0^{\pi} \sqrt{\left((1+aV)^2 + b^2\right)}\,\psi(m)\,d\phi \\
a &= \frac{r_r}{r_t}, b = \frac{z_{tr}}{r_t}, m^2 = \frac{4aV}{\left((1+aV)^2 + b^2\right)} \\
V &= 2\sin\left(\frac{\phi}{2}\right) \text{ and } \psi(k) = \left(1 - \frac{m^2}{2}\right)K(m) - E(m)
\end{aligned}
\tag{2.18}
$$

The total mutual inductance between two multi turn coils will be,

$$
M_{tot} = \sum_{i=1}^{N_t} \sum_{j=1}^{N_r} M_{ij} \tag{2.19}
$$

where N_t and N_r are total number of turns in transmitter and receiver windings, and M_{ij} is mutual inductance between ith transmitter and jth receiver turns.

Mutual inductance for circular elementary coils with 890 mm radius is depicted in Fig. 2.10b. Mutual inductance reduces steeply with the increase of radial distance. For a given displacement, higher mutual inductance can be achieved by using larger coil size. Therefore, by increasing the dimensions higher efficiency can be achieved for a given distance. But this is not a good engineering approach. It would be appropriate if highest possible efficiency is achieved with minimum dimensions and cost. Therefore, power transfer distances need to be analysed by normalizing them to the coil dimension. A term relative range can be defined using the maximum dimension of transmitter and receiver as Eq. (2.20). In case of circular transmitter and receiver, relative range becomes geometric mean of radii.

$$
d_{relative} = \frac{\sqrt{(D_t D_r)}}{2} \tag{2.20}
$$

where D_t and D_r are maximum dimensions of transmitter and receiver coils.

It can be seen from Fig. 2.10b that mutual inductance drops to a negative value when axial distance is low. In case a transmitter array is used for dynamic EV charging, this negative mutual inductance causes a negative current stress on the adjacent transmitter reducing the efficiency of the system. If transmitter coils are kept very close to each other this negative mutual coupling can be even more significant.

2.5.4 Operating Frequency Selection

Operating frequency selection of the design has to be carried out with a number of technical and regulatory constraints. Considering maximum achievable efficiency for a WPT system in Eq. (2.14), highest possible quality factor is desirable. There are three options available in increasing quality factor; increasing inductance or frequency, and decreasing resistance. AC resistance increases with the increase of frequency due to skin effect losses. Usually inductance of a coil is determined by its shape and is independent on the operating frequency. Therefore, there is an optimum frequency for a given design type for highest possible quality factor. Typically, this optimum frequency is in MHz range for most designs. However, design of high power EV WPT system in MHz range frequencies is still beyond today's semiconductor technologies. Therefore, upper limit of the operating frequency is restricted by device constrains. There have been successful attempts to use frequencies ranges from 10 to 150 kHz for EV applications [32, 33]. With the advent of modern semiconductor technologies such as wide band gap devices, frequency limit of the devices are increasing rapidly. Therefore, cost effective, high power near MHz WPT for EV applications is not very far away.

2.5.5 Adaptive Tuning Methods

2.5.5.1 Adaptive Impedance Matching

Operating at maximum transferred power condition is important with regard to component rating. At a particular distance where coupling coefficient equals to critical coupling, transferred power becomes maximum. But in dynamic EV charging, WPT distance, thus the coupling coefficient is continuously varying. Adaptive impedance matching (AIM) network between source and the transmitter coils (Fig. 2.11) can be used in such a scenario [23–25]. On the other hand, the equivalent load impedance is dependent on the state of charge of the EV battery, which is varying with the charging. Adaptive impedance matching network can be used between receiver coil and EV battery charger to make equivalent load impedance to its optimal value.

Matching networks should be capable of adaptively changing the impedance of the network. Input impedance seen by the source has to be maintained at matched

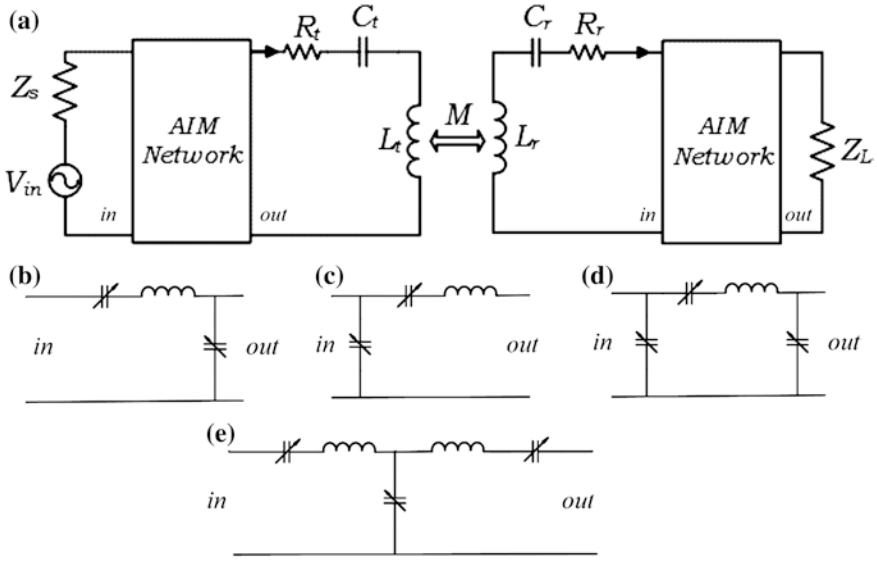

Fig. 2.11 **a** Transmitter and receiver side adaptive impedance matching (AIM). **b** L-type. **c** Inverted-L type. **d** Π type and **e** T-type matching networks

condition under dynamic changes in WPT system. Usually, a switched capacitor bank along with an inductor is used to change the impedance [23–25]. Current controlled inductor which has been used to control micro-inverter [34] can also be used as a variable inductor for the matching network. Based on the component arrangement of the matching network impedance, matching networks can be categorised into L-type, inverted L-type, T-type and Π-type. These matching networks are illustrated in Fig. 2.11. L-type and inverted L-type matching networks are simple but design freedom is higher in complicated T and Π types. Resistive losses in the components also become significant in complex matching networks with number of switching devices. Therefore, choice of matching network has to be carried out based on the design constrains such as coupling variation, number of components and switching devices.

2.5.5.2 Adaptive Frequency Tuning

Frequencies where maximum power transfer occurs at higher coupling coefficients can be determined by the Eq. (2.21). These two frequencies are known as electric resonance (f_e) and magnetic resonance (f_m) frequencies. It can be seen that both these frequencies are varying with the coupling coefficient. If the system operating frequency can be tuned to either of these frequencies maximum power transfer operation can be maintained. There have been attempts to use variable frequency techniques to adaptively tune frequency of power converters to maximum power

transfer condition [21, 22]. It must be noted that such frequency tuning approaches have to be used with compromised efficiency.

$$f_m = \frac{\omega_0}{2\pi\sqrt{1+k}}$$
$$f_e = \frac{\omega_0}{2\pi\sqrt{1-k}} \tag{2.21}$$

2.5.6 Optimization of Resonator Design

Typical resonators used for stationary EV charging are in the form of a pad shape and built with the use of ferromagnetic materials in general. Such resonator coils with ferrite materials can be identified as two types based on the magnetic field distribution; double-sided and single sided. Magnetic flux propagate in both sides of the resonator in double sided resonator types [35]. This type of design needs additional shielding to prevent eddy current generated in EV chassis. Therefore, double sided resonator coil is not the optimal choice due to high shielding losses. Single sided resonator coils have a ferrite layer below the coil guiding the flux towards receiver [18, 36, 37]. Circular unipolar pad [36] and rectangular double D (DD) [18] shaped coil designs have achieved enhanced coupling in both radial and axial separations.

Resonator types used for dynamic WPT can be categorised based on the transmitter configuration. Transmitter track type configurations have long wires embedded in ferrite to shape the magnetic field. U-shape, W-shape and I-shape ferrite cores have also been used in this types of designs [32, 38]. One of the major challenges in transmitter track design is that receiver coil only covers a small part of the track resulting in a very poor coupling as identified in previous sections. When it comes to segmented transmitter array, coil design is similar to stationary EV charging. However, in dynamic charging coupling deterioration against lateral displacement is more significant than stationary charging case.

2.6 Optimization of Resonator Design

The coils play an imperative role in WPT design stages. For WPT coils, there are two performance indices: quality factor and electromagnetic coupling between transmitter and receiver. The quality factor can be improved by decreasing the AC resistance (skin and proximity losses) of the coil while maintaining high inductance. But, enhancement of the electromagnetic coupling is severely limited by the misalignment and distance between coils which cannot be compromised due to most application constrains. Instead, coupling variation can be optimized by choosing appropriate coil structure for a particular position displacement profile.

There have been a number of studies which addressed the losses related to resonators. Several optimized resonator designs have been proposed. For example, [39] presents a detailed optimization process for double layer printed

spiral coil. The authors have illustrated design procedure for optimal choice of number of turns, track width and turns separation. Reference [40] presents multi turn surface spiral for low AC resistance. But these designs can only be used in limited power levels as they are constructed in PCBs. Furthermore, substrate losses play considerable role in AC resistance. In order to address the issue of coupling deterioration with misalignment, inserting a negative current loop is considered in [41]. Although this approach reduces the coupling variation, it also reduces overall coupling due to its negative magnetic flux.

2.6.1 AC Resistance, Self-inductance and Parasitic Capacitance

Modeling WPT coils can be done using either analytical or simulation methods. For rectangular or circular coil shapes analytical optimization can be carried out using equations. But for complicated coil shapes with ferromagnetic materials, finite element analysis based simulations have to be carried out. AC resistance, inductance and parasitic capacitance of a circular multi-turn coil is discussed in this section.

Usually Litz wires are adopted to reduce the skin effect resistance of coil designs. AC resistance of circular Litz wire winding with N number of turns can be calculated using Eq. (2.22) [42, 43].

$$R_{ac} = R_{dc}\left(1 + \frac{f^2}{f_h^2}\right),\ f_h = \frac{2\sqrt{2}}{\pi r_s^2 \mu_0 \sigma \sqrt{N N_s \eta_a \beta}} \tag{2.22}$$

where R_{dc}, r_s, N_s and β represent the dc resistance of the coil, radius of each single strand number of strands per bunch and the area efficiency of the coil. The dc resistance is dependent on the manufacturing methods and type of the litz wire, usually available in the datasheet. The value of η_a is the area efficiency of the coil dependent on the height and width of the coil (Refer Fig. 2 in [43]).

Self-inductance of a multi-turn coil with N_t coaxial turns N_l concentric layers can be calculated using circular loop approximation as in Eq. (2.23).

$$\begin{aligned} L(R,r) &= \mu_0 R\left(\ln\frac{8R}{r} - 2\right) \\ L_{self} &= N_t \sum_{i=1}^{N_l} L(R_i, r) + \sum_{i=1}^{N_l}\sum_{j=1}^{N_l}\sum_{k=1}^{N_t}\sum_{l=1}^{N_t} M_{ikjl}\left(1-\delta_{ij}\right)(1-\delta_{kl}) \end{aligned} \tag{2.23}$$

where $\delta_{ij}(or\ \delta_{kl}) = 1$ for $i = j$ $(or\ k = l)$ and $\delta_{ij}(or\ \delta_{kl}) = 0$ otherwise. $L(R, r)$ is inductance of a circular loop with radius R formed using radius r wire. M_{ikjl} is the mutual inductance between two circular turns, ith layer kth turn and jth layer lth turn.

In general, self-capacitance of the coils used for WPT in kHz range is not significant compared to inductive reactance. But with the increase of the frequency, capacitive reactance also needs to be taken into account for accurate modelling. This stray capacitance between turns needs to be taken into account in designing the value of the lumped capacitor. Self-capacitance of a multi layered coil considered previously can be obtained using Eq. (2.24) [43].

$$
\begin{aligned}
C_{self} &= \frac{1}{(N_t N_l)^2}\left[C_b N_l (N_t - 1) + C_m \sum_{i=1}^{N_t} (2i-1)^2 (N_l - 1)\right] \\
C_b &= \epsilon_0 \epsilon_r \int_0^{\pi/4} \frac{\pi D_i r_0}{\varsigma + \epsilon_r r(1 - \cos\theta)} \\
C_m &= \epsilon_0 \epsilon_r \int_0^{\pi/4} \frac{\pi D_i r_0}{\varsigma + \epsilon_r r(1 - \cos\theta) + 0.5\epsilon_r h}
\end{aligned}
\tag{2.24}
$$

C_b is parasitic capacitance between two nearby turns in the same layer, and C_m is that of nearby turns in adjacent layers. D_i, r, ς, ε_r, h are the average diameter of the coil, wire radius, thickness and relative permittivity insulation and separation between two layers respectively. Quality factor of the coil can be determined based on the inductance and the resistance calculations.

2.6.2 Optimization of Resonator Design Parameters

In this section a case study of optimization process of a multi turn helical coil design is presented. The shape of the coil and design parameters are illustrated in Fig. 2.12. Number of layers (N_l), Number of turns (N_t), separation between layers (S_l) and separation between turns (S_t) are considered for the optimization process. A single turn with multiple layers results in a planar spiral coil shape whereas a single layer with multiple turns results in a helical shaped coil. Outermost radius (r_o) is kept at 9 cm and maximum height of the coil is restricted to 5 cm because most applications have to be designed within a given footprint area. The radius of the wire is fixed at 1 mm. AC resistance, inductance and quality factor are analysed using finite element analysis software Ansoft Maxwell® 2D. Each turn is approximated as a circular current loop in 2-D simulation as shown in Fig. 2.12b.

In order to analyse the effect of N_l and S_l, we choose single turn coil which represents a planar spiral. Simulation results presented in Fig. 2.13 show quality factor variation with respect to S_l and N_l. Both S_l and N_l affect AC resistance and inductance which ultimately determines the quality factor. It can be observed that both number of layers and separation have to be optimised to achieve a high quality factor. With the number of layers, coil inductance increases and consequently it affects the quality factor. In contrast, the physical effect of higher N_l increases the

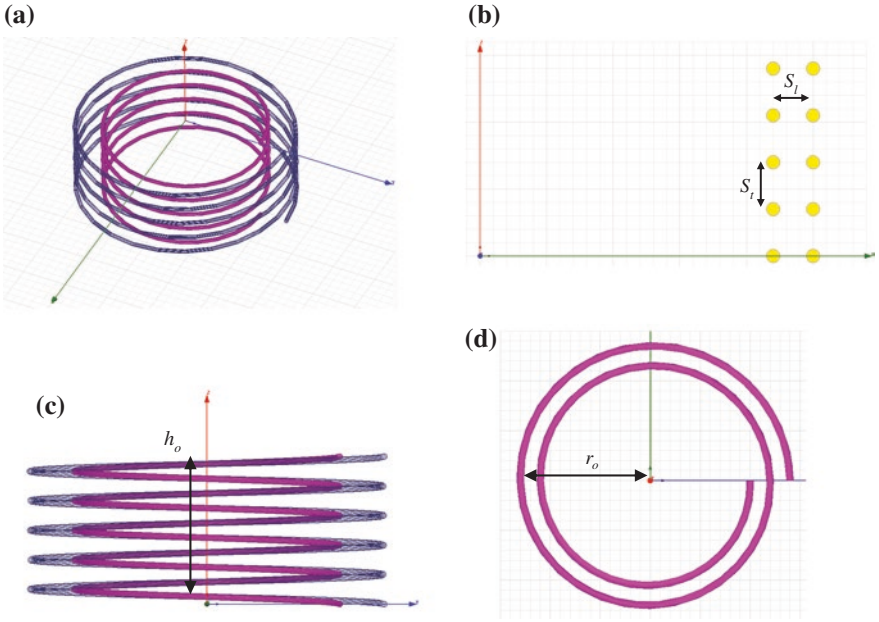

Fig. 2.12 Multi layered helical coil with two layers and 5 turns **a** 3-D view, **b** 2-D approximation, **c** side view, **d** top view

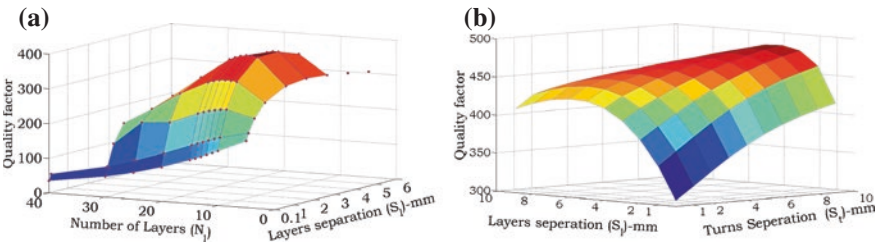

Fig. 2.13 **a** Quality factor versus number of layers and separation between layers at 1 MHz for planar spiral coil ($N_l = 1$). **b** Quality factor versus separation between layers and separation between turns at 1 MHz for multi layered spiral coil. (number of layers—5 and number of turns—3)

spiral coil length, thus the resistance, causing detrimental impact on the quality factor. On the other hand, lower S_l increases coil inductance as layers are confined to outer radius. However, when layers are very close to each other with low S_l, proximity losses are increased resulting a high AC resistance. This explains the steep dip in quality factor found in Fig. 2.13a for low S_l. The effect of the proximity losses with closer turns is more significant in higher frequencies. Therefore, separation between turns is a crucial design parameter with WPT operating at high frequency. Therefore, tightly wound coils with very small separation are not recommended for obtaining highest possible quality factor for WPT applications.

Next, impact of S_l and S_t is analysed for choosing a coil with 5-layes and 3-turns. Figure 2.13b shows quality factor variation with respect to S_l and S_t. Similar to planar spiral case, both lower and higher extremes of S_l results in a low quality factor. Previous explanation holds for this observation as well. Conversely, it can be seen that quality factor increases with S_t. Inductance of the coil is less dependent on S_t, because loop radius is independent of S_t. Larger turns separation reduces the proximity effect losses, leading to higher quality factor. This incremental effect of quality factor is less significant at higher S_t because influence of the proximity effect resistance becomes negligible. Increase of S_t is also limited by the coil height. It must also be noted that our circular current loop approximation becomes invalid at very high S_t.

Therefore, we next analyse the effect of number of layers and number of turns with a substantial separation between turns and layers (chosen as 3 mm). Results presented in Fig. 2.14a show that highest possible number of turns within the chosen footprint volume results in the best quality factors. Design with two layers shows the maximum quality factor with these parameters.

Figure 2.14b presents the quality factor variation of two layered coil with respect to separation between layers and turns. The maximum possible number of turns is chosen for the analysis. 11 number of turns with 3 mm turn separation result in best quality factor of 582. The maximum quality factors that can be obtained using planer spiral (at $N_t = 11$ and $S_t = 3$ mm) and helical (at $N_l = 12$ and $S_l = 2$ mm) coils are 400 and 530 respectively.

Based on the above analysis we can suggest recommendations for designing high quality factor coils for the WPT applications. Firstly, tightly wound coils with low separation between turns/layers is not recommended because proximity effect losses dominates the AC resistance. Secondly, multi layered helical coil can be used to increase the quality factor. Performance of multi layered helix is better than both planar spiral and the single layered helix. Third, design guideline for the multi layered helix can be derived as; 1. Choosing substantial value of separation between turns/layers, 2. Maximum possible turns with the given footprint area, 3. Optimizing the number of layers with the selected design.

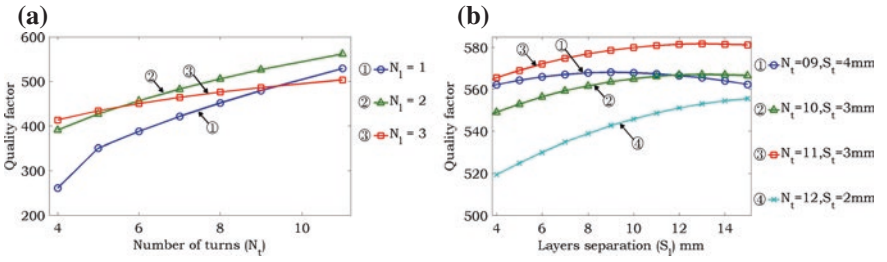

Fig. 2.14 **a** Quality factor vs number of turns and number of layers at 1 MHz for multi layered helical coil (separation between layers and separation between turns equals to 3 mm). **b** Quality factor vs separation between layers and number of turns with two layers

2.7 Future Directions and Trends

Dynamic WPT enabled EV charging is the ultimate objective of the current research activities. Dynamic WPT enabled infrastructure would allow power delivery while EV is in motion. Future EV equipped with such technology would not carry a large amount of energy storage.

However, substantial amount of research work has to be carried out to bring current technology to achieve such a scenario. Major design challenges are increasing the WPT range with acceptable efficiency level. Design and optimization of resonators plays a major role in improving the system performance in extended range. With the advent of modern semiconductor technologies such as wide band gap devices, frequency limit of the high power WPT system has been increasing in a rapid manner. Therefore, cost effective, high power, near MHz WPT would be next step of the WPT for EV charging. Ferromagnetic materials used for magnetic field shaping in kHz frequencies is not appropriate for high frequency applications. Materials amenable for near MHz WPT resonators have to be investigated for future solutions. Resonator arrangements such as use of repeaters or meta materials need to be investigated for EV applications. Tuning approaches such as adaptive impedance matching and frequency tuning techniques will have to be implemented to maintain system performance in dynamic moving conditions. Furthermore, investigations of appropriate matching networks have to be carried out. In addition, design of high frequency power converters for future WPT application would be another challenging aspect of future research. Reducing conduction and switching losses in power conversion is a vital factor in improving the efficiency. Direct power conversion topologies such as matrix converters can be identified as a potential direction for future WPT applications.

2.8 Conclusions

WPT technology for EV battery charging is discussed in this chapter. Efficiency, transferred power, range and misalignment tolerance are identified as the performance indices. A detailed analysis of WPT system is presented highlighting the contributions by the research community. Modeling methods and their own merits are presented. WPT methods for EV charging are elaborated with design challenges. Dynamic WPT for EV is identified as the next generation of transportation electrification. Recommendations for WPT coil designs are presented with case study.

References

1. Etacheri V, Marom R, Elazari R, Salitra G, Aurbach D (2011) Challenges in the development of advanced Li-ion batteries: a review. Energy Environ Sci 4:3243–3262
2. Madawala UK, Schweizer P, Haerri VV (2008) Living and mobility—a novel multipurpose in-house grid interface with plug in hybrid blue angle. Paper presented at the IEEE international conference on sustainable energy technologies, 2008

3. Madawala UK, Thrimawithana DJ (2011) A bidirectional inductive power interface for electric vehicles in V2G systems. IEEE Trans Ind Electron 58:789–4796
4. Hori Y (2013) Looking at cars 100 years in the future. Paper presented at the IEEE international conference on mechatronics (ICM), 2013
5. Tesla N (1914) Apparatus for transmitting electrical energy. US patent 1,119,732, December 1914
6. Kurs A, Karalis A, Moffatt R, Joannopoulos JD, Fisher P, Soljačić M (2007) Wireless power transfer via strongly coupled magnetic resonances. Science 317:83–86
7. Eghtesadi M (1990) Inductive power transfer to an electric vehicle-analytical model. Paper presented at the 40th IEEE vehicular technology conference, 1990
8. Madawala UK, Stichbury J, Walker S (2004) Contactless power transfer with two-way communication. Paper presented at the 30th annual conference of IEEE Industrial Electronics Society, 2004
9. Chi KL, Zhong WX, Hui SYR (2012) Effects of magnetic coupling of nonadjacent resonators on wireless power domino-resonator systems. IEEE Trans Power Electron 27:1905–1916
10. Chih-Jung C, Tah-Hsiung C, Chih-Lung L, Zeui-Chown J (2010) A study of loosely coupled coils for wireless power transfer. IEEE Trans Circuits Syst II : Eexpress Briefs 57:536–540
11. Chang-Yu H, Boys JT, Covic GA, Budhia M (2009) Practical considerations for designing IPT system for EV battery charging. Paper presented at the IEEE vehicle power and propulsion conference, 2009
12. Haus H, Huang WP (1991) Coupled-mode theory. Proc IEEE 79:1505–1518
13. Karalis A, Joannopoulos JD, Soljačić M (2008) Efficient wireless non-radiative mid-range energy transfer. Ann Phys 323:34–48
14. Seung-Hwan L, Lorenz RD (2011) A design methodology for multi-kW, large air-gap, MHz frequency, wireless power transfer systems. Paper presented at the IEEE energy conversion congress and exposition (ECCE), 2011
15. Thrimawithana DJ, Madawala UK (2010) A novel matrix converter based bi-directional IPT power interface for V2G applications. Paper presented at the IEEE international energy conference and exhibition (EnergyCon), 2010
16. Nguyen Xuan B, Vilathgamuwa DM, Madawala UK (2014) A sic-based matrix converter topology for inductive power transfer system. IEEE Trans Power Electron 29:4029–4038
17. WiTricity (2014) WiT-3300 Deployment Kit. http://www.witricity.com/assets/WiT-3300_data_sheet.pdf. Accessed 10 July 2014
18. Budhia M, Boys JT, Covic GA, Chang-Yu H (2013) Development of a single-sided flux magnetic coupler for electric vehicle IPT charging systems. IEEE Trans Ind Electron 60:318–328
19. Jiseong K, Jonghoon K, Sunkyu K, Hongseok K, In-Soo S, Nam Pyo S et al (2013) Coil design and shielding methods for a magnetic resonant wireless power transfer system. Proc IEEE 101:1332–1342
20. Onar OC, Miller JM, Campbell SL, Coomer C, White CP Seiber LE (2013) A novel wireless power transfer for in-motion EV/PHEV charging. Paper presented at the twenty-eighth annual IEEE applied power electronics conference and exposition (APEC), 2013
21. Sample AP, Meyer DA, Smith JR (2011) Analysis, experimental results, and range adaptation of magnetically coupled resonators for wireless power transfer. IEEE Trans Ind Electron 58:544–554
22. Kim NY, Kim KY, Choi J, Kim CW (2012) Adaptive frequency with power-level tracking system for efficient magnetic resonance wireless power transfer. Electron Lett 48:452–454
23. Beh T, Kato M, Imura T, Oh S, Hori Y (2013) Automated impedance matching system for robust wireless power transfer via magnetic resonance coupling. IEEE Trans Ind Electron 60:3689–3698
24. Kusaka K, Itoh JI (2012) Proposal of switched-mode matching circuit in power supply for wireless power transfer using magnetic resonance coupling. Paper presented at the twenty-seventh annual IEEE applied power electronics conference and exposition (APEC), 2012
25. Waters BH, Sample AP, Smith JR (2012) Adaptive impedance matching for magnetically coupled resonators. PIERS Proc 694–701
26. Thuc Phi D, Jong-Wook L (2011) Experimental results of high-efficiency resonant coupling wireless power transfer using a variable coupling method. IEEE Microwave Wirel Compon Lett 21:442–444

27. Xue RF, Cheng KW, Je M (2013) High-efficiency wireless power transfer for biomedical implants by optimal resonant load transformation. IEEE Trans Circuits Syst I Reg Papers 60:867–874
28. Seung-Hwan L, Lorenz RD (2011) Development and validation of model for 95 %-efficiency 220 W wireless power transfer over a 30 cm air gap. IEEE Trans Ind Appl 47:2495–2504
29. Babic SI, Akyel C (2008) Calculating mutual inductance between circular coils with inclined axes in air. IEEE Trans Mag 44:1743–1750
30. Akyel C, Babic SI, Mahmoudi M-M (2009) Mutual inductance calculation for noncoaxial circular air coils with parallel axes. Prog Electromagnet Res 91:287–301
31. Grover FW (1964) Inductance calculations. Dover, New York
32. Byeong-Mun S, Kratz R, Gurol S (2002) Contactless inductive power pickup system for Maglev application. Paper presented at the 37th IAS industry applications conference, 2002
33. Mecke R, Rathge C (2004) High frequency resonant inverter for contactless energy transmission over large air gap. Paper presented at the IEEE 35th annual power electronics specialists conference, 2004
34. Nayanasiri DR, Vilathgamuwa DM, Maskell DL (2013) Current-controlled resonant circuit based photovoltaic micro-inverter with half-wave cyclo converter. Paper presented at the IEEE industry applications society annual meeting, 2013
35. Budhia M, Covic G, Boys J (2010) A new IPT magnetic coupler for electric vehicle charging systems. Paper presented at the IEEE 36th annual conference of industrial electronics society, 2010
36. Budhia M, Covic GA, Boys JT (2011) Design and optimization of circular magnetic structures for lumped inductive power transfer systems. IEEE Trans Power Electron 26:3096–3108
37. Jaegue S, Seungyong S, Yangsu K, Seungyoung A, Seokhwan L, Guho J et al (2014) Design and implementation of shaped magnetic-resonance-based wireless power transfer system for roadway-powered moving electric vehicles. IEEE Trans Ind Electron 61:1179–1192
38. Sungwoo L, Jin H, Changbyung P, Nam-Sup C, Gyu-Hyeoung C, Chun-Taek R (2010) On-line electric vehicle using inductive power transfer system. Paper presented at the 2010 IEEE energy conversion congress and exposition (ECCE), 2010
39. Kainan C, Zhengming Z (2013) Analysis of the double-layer printed spiral coil for wireless power transfer. IEEE J Sel Top Power Electron 1:114–121
40. Lee S-H, Lorenz RD (2013) Surface spiral coil design methodologies for high efficiency, high power, low flux density, large air-gap wireless power transfer systems. Paper presented in the 28th Annual IEEE applied power electronics conference and exposition (APEC), 2013
41. Wang-Sang L, Wang-Ik S, Kyoung-Sub O, Jong-Won Y (2013) Contactless energy transfer systems using antiparallel resonant loops. IEEE Trans Ind Electron 60:350–359
42. Ram RAK, Mirabbasi S, Mu C (2011) Design and optimization of resonance-based efficient wireless power delivery systems for biomedical implants. IEEE Trans Biomed Circuits Syst 5:48–63
43. Yang Z, Wentai L, Basham E (2007) Inductor modeling in wireless links for implantable electronics. IEEE Trans Mag 43:3851–3860

Chapter 3
Planning, Control, and Management Strategies for Parking Lots for PEVs

Wencong Su, Jianhui Wang and Zechun Hu

Abstract Plug-in electric vehicles (PEVs), as a major component of Smart Grid technologies, can achieve high energy efficiency, reduce carbon emissions, spur high-technology innovation, and ensure a reliable energy supply. An ever-increasing number of PEVs will radically change the traditional views of the power and transportation industries, the social environment, and the business world. The electrification of transportation brings both opportunities and challenges to existing critical infrastructures. This book chapter takes the position that the successful rollout of PEVs depends highly on the affordability, availability, and quality of the associated services that the nation's critical infrastructures can provide (e.g., a PEV charging facility at a parking lot). There is an urgent need to accelerate the design, development, and deployment of cost-effective, reliable, and customer-friendly PEV charging infrastructures. This chapter presents a comprehensive overview of the planning, control, and management aspects of PEV parking lots in a Smart Grid environment.

Keywords Smart grid · Plug-in electric vehicle (PEV) · Parking lot · Parking deck

W. Su (✉)
Department of Electrical and Computer Engineering, University of Michigan-Dearborn, Dearborn 48128, MI, USA
e-mail: wencong@umich.edu

J. Wang
Center for Energy, Environmental, and Economic Systems Analysis, Decision and Information Sciences Division, Argonne National Laboratory, Argonne 60439, IL, USA
e-mail: Jianhui.wang@anl.gov

Z. Hu
Department of Electrical and Computer Engineering, Tsinghua University, Beijing, China
e-mail: zechhu@tsinghua.edu.cn

S. Rajakaruna et al. (eds.), *Plug In Electric Vehicles in Smart Grids*, Power Systems, DOI 10.1007/978-981-287-299-9_3

3.1 Introduction

Transportation systems that move people, goods, and services in societies worldwide pose unprecedented environmental, economic, and social challenges, particularly in response to the growing urgency to conserve energy and cut back on carbon emissions and pollution [1]. Advances in transportation electrification not only offer great promise with regard to addressing these stubborn problems, they also have the potential to revolutionize future transportation systems [2–4]. The massive deployment of PEVs would also enable a more sustainable transportation system because energy would be received from renewable sources, which would dramatically increase energy efficiency and improve the existing environment [5–7]. In the last decade, all around the world, efforts to boost the use of electric-drive transportation technologies have accelerated because of their low-pollution emissions, energy independence, low operating cost, high performance, flexible fueling, and high fuel economy. PEVs, a subcategory of electric vehicles (EVs), have drawn increased attention because their owners have the luxury of choosing when and where to "plug in" (similar to how consumers choose how and when to recharge their electronic devices like cell phones).

The U.S. Government has put a lot of effort into accelerating the introduction and penetration of advanced electric drive vehicles in the market. The U.S. Department of Energy (DOE) projects that about 1 million PEVs will be on the road by 2015. At this penetration rate, PEVs would account for 2.5 % of all new vehicle sales in 2015 [8]. The Electric Power Research Institute (EPRI), using a moderate penetration scenario, has projected that 62 % of the entire U.S. vehicle fleet will consist of PEVs by 2050 [9]. If one believes that the early-1900s infrastructure boom was the engine that powered U.S. economic growth 80 years ago, then one could assume that a similar and even more powerful development of transportation electrification could accomplish even more in the next several decades. According to several forecasts [10], a strong growth in PEV sales is expected globally, as shown in Fig. 3.1. In Asia, China, which is the world's largest automotive market, has made the electrification of transportation a central part of its national strategic plan and has identified clean-energy cars as one of the three key investment areas for the years 2011–2015 [11]. China aims to achieve cumulative sales of 500,000 PEVs by 2015. In February 2014, China's Finance Ministry decided to extend the subsidy program for new buyers of PEVs after the current subsidy regime expires in 2015, in order to achieve a goal of 5 million PEV adoptions by 2020. In addition, the Chinese government has initiated two national plans, "Ten Cities and Thousand Units" and "Demonstration Cities for New Energy Vehicle Adoption", to promote the penetration of PEVs both in the public transportation (e.g., bus and taxi) sector and private purchase across more than 25 cities [12]. In Japan, the number of PEVs has been the second largest in the world, after the U.S. [13]. According to the Navigant research report [14, 15], annual light-duty PEV sales in the Greater Tokyo Area will surpass those in the Los Angeles metropolitan area in 2020. The Greater Tokyo Area is expected to become the city with largest market penetration (approximately 260,000 PEVs and 2.3 % of the vehicle fleet) in the world by

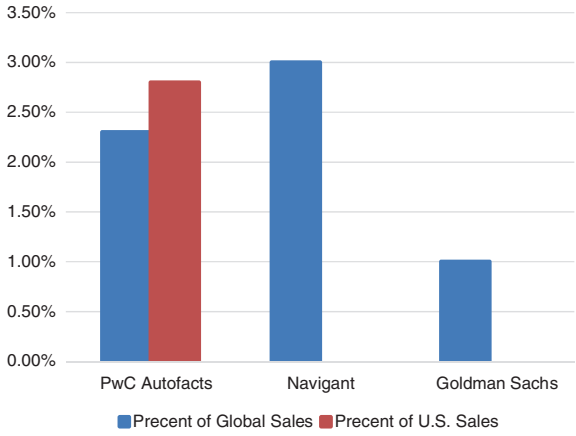

Fig. 3.1 PEV sales projection, 2020 [10] *Source* PwC Autofacts, Navigant, and Goldman Sachs

2023. In the UK., since 2006, more than 10,000 PEVs had been registered through February 2014, including all-EVs, commercial vans, and plug-in hybrids [16]. As of November 2013, the British government had pledged 400 million pounds to support the deployment of PEVs in the next 5 years [17]. That funding has been and will be allocated for research and development (R&D) and infrastructure, such as public charging points and charging stations. There were about 5,000 public charging points in the UK. as of November 2013. By April 2014, the country had become the leader in deploying quick charging (i.e., fast charging) in Europe, with 211 charging stations available across the country [18].

An ever-increasing number of PEVs will radically change the traditional views of the power industry [19], transportation industry [20], social environment [21], and business world [22, 23]. The electrification of transportation brings both opportunities and challenges to existing critical infrastructures. The successful rollout of the electrification of transportation depends highly on the affordability, availability, and quality of the associated services that our nation's critical infrastructures can provide. Unfortunately, the existing critical infrastructure does not meet the growing need for electric capacity and demands for transportation during the 21st century, which is an ominous sign of a looming economic crisis. Emerging technologies (e.g., the Smart Grid [24, 25] and intelligent transportation systems [26]) cannot make much of a difference if the fundamental infrastructure is not ready for them yet.

One big issue PEV drivers face is how, when, and where to recharge their cars or trucks. The PEV charging facility is part of an infrastructure that is critical in accommodating and supporting the successful rollout of PEVs. Depending on the location of a charging facility, the planning, control, and management strategies associated with it can be categorized into one of two groups: home charging or public charging. This chapter presents a comprehensive overview of the planning, control, and management aspects of public charging facilities (e.g., PEV parking lots) in a Smart Grid environment. The

chapter is structured as follows: Sect. 3.2 is an introduction on state-of-the-art PEV charging facilities at parking lots. Section 3.3 investigates long-term planning for PEV parking lots in terms of opportunities, challenges, and solutions. Section 3.4 describes control and management strategies for PEV parking lots. Section 3.5 summarizes this chapter and discusses future research trends.

3.2 PEV Charging Facility

This section provides a brief overview of PEV charging facilities. Their power consumption, installation requirements, safety issues, estimated costs, and communication and computing requirements have to be considered in order to determine planning, control, and management strategies for PEV parking lots.

The charging infrastructure is critical with regard to accommodating and supporting a successful rollout of PEVs. A recent Massachusetts Institute of Technology (MIT) report concludes that it appears to be a bigger challenge to create a nationwide infrastructure for PEVs than it is to produce affordable batteries to power the cars [27]. PEV charging stations can be installed at homes (e.g., in both single-family and multi-family residential situations), workplaces, private fleet facilities, and public facilities (e.g., parking decks and lots).

In North America, all PEVs produced must comply with the Society of Automotive Engineers (SAE) J1772 standard [28]. SAE J1772 gives the general requirements for EV conductive charge systems for use in North America, and it defines a common architecture for those systems, covering both operational requirements and the functional and dimensional requirements for the vehicle inlet and mating connector.

Tables 3.1 and 3.2 summarize the vehicle-to-grid communication standard and the vehicle-to-grid energy transfer standard in North America, respectively [30].

It is important to mention that the standard charging level for PEVs varies depending on location (e.g., North America, Europe, Asia). Figure 3.2 [29] summarizes the PEV charging standard around the world. For example, Europe connectors must follow the International Electrotechnical Commission (IEC) 62196 standard. In early 2013, the European Commission announced that the “Type 2” plug developed by the German company Mennekes will be the common standard for charging PEVs across the European Union. The rival CHAdeMO standard is supported by Japanese automakers like Nissan and Mitsubishi. IEC 61851 has been adopted in China. There are slight differences in the terminology used in these standards. For example, the IEC standard refers to “modes” or “types” while the SAE standard refers to “levels,” but they are all virtually the same. China also promotes to standardize the design and operation of battery-swapping station after dozens of pilot projects in operation.

Table 3.1 Vehicle-to-grid communication standard for North America, 2011 [29]

SAE J	Title	Scope	Status
SAE J2847/1	Communication between PEV and the utility grid	Identifies the communication medium and criteria for the PEV to connect to the utility for level 1 and level 2 alternating current (AC) energy transfer	Published November 2013
SAE J2847/2	Communication between PEV and off-board DC chargers	Identifies additional messages for direct current (DC) energy transfer to the PEV. The specification supports DC energy transfer via forward power flow (FPF) from grid to vehicle	Published August 2012
SAE J2847/3	Communication between PEV and the utility grid for reverse power flow	Identifies additional messages for DC energy transfer to the PEV. The specification supports DC energy transfer via DC reverse power flow (RPF) from vehicle to grid	Published December 2013
SAE J2847/4	Diagnostic communication for PEVs	Establishes the communication requirements for diagnostics between PEVs and the EV supply equipment (EVSE) for charge or discharge sessions	Work in process
SAE J2847/5	Communication between plug-in vehicles and their customers	Establishes communication requirements between PEVs and their customers for charge or discharge sessions	Work in process
SAE J2836/1	Use cases for communication between PEVs and the utility grid	Identifies the equipment (system elements) and interactions to support grid-optimized AC or DC energy transfer for plug-in vehicles, as described in SAE J2847/1. Key system elements include the vehicle's rechargeable energy storage system (RESS), power conversion equipment (charger and/or inverter), utility meter, etc	Published April 2010
SAE J2836/2	Use cases for communication between PEV and EVSE	Establishes use cases for communication between PEVs and the off-board charger, for energy transfer, and for other applications. J2836/2 use cases must be supported by SAE J2847/2	Published September 2011
SAE J2836/3	Use cases for communication between PEV and the utility grid for reverse power flow	Establishes use cases for communication between PEVs and the public electric power grid, a home branch circuit, or an isolated micro grid, for reverse energy transfer and other applications	Published January 2011

(continued)

Table 3.1 (continued)

SAE J	Title	Scope	Status
SAE J2836/4	Use cases for diagnostic communication for PEVs	Provides general information required for diagnostics and include the detailed messages to provide accurate information to the customer and/or service personnel so they can identify the source of the issue and help resolve it	Work in process
SAE J2836/5	Use cases for communication between PEVs and their customers	Describes how the customer will be able to interact with the PEV as it charges and discharges. Identifies information and controls for each session, including status, updates, and potential changes	Work in process
SAE J2931	Electric vehicle supply equipment (EVSE) communication model	Establishes the digital communication requirements for the EVSE as it interfaces with a home area network (HAN), an energy management system (EMS), or the utility grid systems. Provides a knowledge base that addresses the communication medium's functional performance and characteristics. Is intended to complement J1772 while addressing the digital communication requirements associated with Smart Grid interoperability	Published September 2012
SAE J2931/2	Inband signaling communication for PEVs	Establishes the requirements for physical layer communications using in-band signaling between PEVs and the EVSE. Enables onward communications via an EVSE bridging device to the utility smart meter or HAN. This onward communication is known as Frequency Shift Keying (FSK) and is similar to Power Line Carrier (PLC), but uses the J1772 control pilot circuit	Work in process
SAE J2344	Use cases for communication between PEV and the utility grid	Gives technical guidelines on the safety of EVs during normal operations and charging. To be considered when designing EVs having a gross vehicle weight rating of 4,563 kg (10,000 lb) or less for use on public roads	Published March 2010

Table 3.2 Vehicle-to-grid energy transfer standard (North America, 2011) [29]

SAE J	Title	Scope	Status
SAE J2293/1	Energy transfer system for electric vehicles—part 1: functional requirements and system architectures	Describes the total EV energy transfer system (ETS) and allocates requirements to the EV or EVSE for the various system architectures	Published July 2008
SAE J2293/2	Energy transfer system for electric vehicles—part 2: functional requirements and system architectures	Describes the SAE J1850-compliant communication network between the PEV and EVSE for this application (ETS network)	Published July 2008
SAE J2785	Determination of the maximum available power from a rechargeable energy storage system on a hybrid electric vehicle	Describes a test procedure for rating the peak power of the RESS used in the combustion engine of a hybrid electric vehicle (HEV)	Published April 2007
SAE J1711	Recommended practice for measuring the exhaust emissions and fuel economy of hybrid electric vehicles	Sets recommended practices for measuring the exhaust emissions and fuel economy of HEVs, including PHEVs	Published June 2010
SAE J2841	Definition of the utility factor for plug-in hybrid electric vehicles using national household travel survey data	Describes the equation for calculating the total fuel and energy consumption rates of a PHEV	Published September 2010
SAE J2344	Guidelines for electric vehicle safety	Gives technical guidelines on the safety of EVs during normal operations and charging. To be considered when designing EVs having a gross vehicle weight rating of 4,563 kg (10,000 lb) or less for use on public roads	Published March 2010

Table 3.3 illustrates the North American standard PEV charging level, assuming a 90 % overall energy efficiency. Both AC Level 1 and 2 charging stations convert the utility's AC power into DC power through the vehicle's on-board chargers. At the other end of spectrum, the DC Level 1 and 2 charging stations provide electricity from AC to DC through an off-board charger, so DC power is delivered directly to the vehicle. The charging times can range from a few minutes (min) to 20 hours (h), based on the level of charging stations, type of battery, battery capacity, remaining battery state-of-charge, and many other factors. Table 3.4 compares the typical charging times of a variety of PEVs.

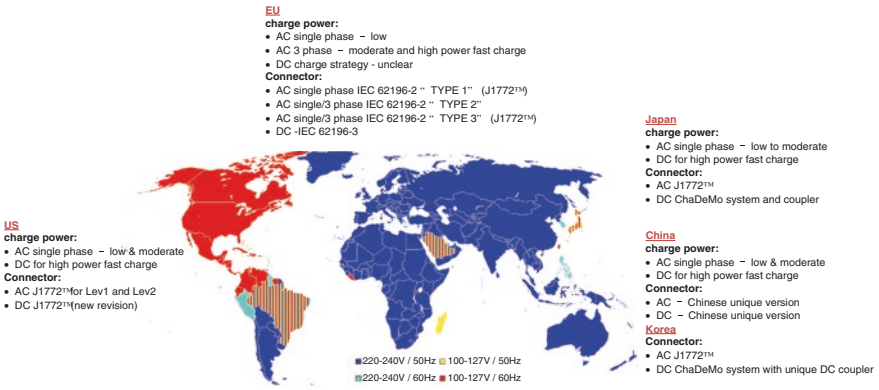

Fig. 3.2 Regional PEV charging standard and strategies [29]

Table 3.3 Charge method electrical ratings for North America from standard SAE J1772

Charging method	Normal supply voltage (V)	Maximum current (Amps-continuous)	Rated power (kVA)	Phase
AC level 1	120	12	1.44	Single
	120	16	1.92	Single
AC level 2	208	Up to 80	16.6	Single
	240	Up to 80	19.2	Single
DC level 1	200–500 maximum	80	Up to 40	Three
DC level 2	200–500 maximum	200	Up to 100	Three

Table 3.4 Typical charging time

EV configuration	Battery size (kWh)	120 V and 12 A	240 V and 32 A	480 V and 100 A
PHEV-10	4	3 h 5 min	35 min	Not applicable
PHEV-20	8	6 h 10 min	1 h 10 min	Not applicable
PHEV-40	16	12 h 20 min	2 h 20 min	22 min
BEV	24	18 h 30 min	3 h 30 min	33 min
PHEV bus	50	Not applicable	7 h 17 min	1 h 9 min

AC Level 1 charging uses a standard 120-V single-phase outlet for a three-prong connection, which is the most common U.S. grounded household outlet. Typical current ratings for these receptacles are between 15 and 20 amps (A). One end of the cord is a standard, three-prong household plug (NEMA 5–15 connector), and the other is a J1772 standard connector. Depending on the battery type and capacity, it can take 3–20 h to fully recharge a PEV battery. AC Level 1 charging provides approximate 3–4 miles of range per hour (h) of charging time. Since the standard electrical outlets are available almost everywhere and the charging time is relatively long, AC Level 1 charging is particularly suitable for overnight charging.

AC Level 2 is typically described as the "primary" and "standard" method for both private and public charging facilities. It specifies a single-phase branch circuit with typical voltage ratings from 208 V AC (commercial application) to 240 V AC (residential application). According to the SAE J1772 standard, Level 2 charging allows for maximum current up to 80 A of AC with a 100-A circuit breaker. A more typical peak current would be 32 A of AC with a branch circuit breaker rated at 40 A. This provides approximately 7.68 kW with a 240 V AC circuit. AC Level 2 charging adds about 15–20 miles of range per hour of charging time. Figure 3.3 shows the AC Level 2 charging schematic [30].

DC Level charging is a higher-voltage, fast-rate DC charging for commercial and public applications. It is intended to perform in a manner similar to what is offered at a commercial gasoline service station, in that recharge is rapid [30]. By significantly reducing the charging time, DC level charging would enable

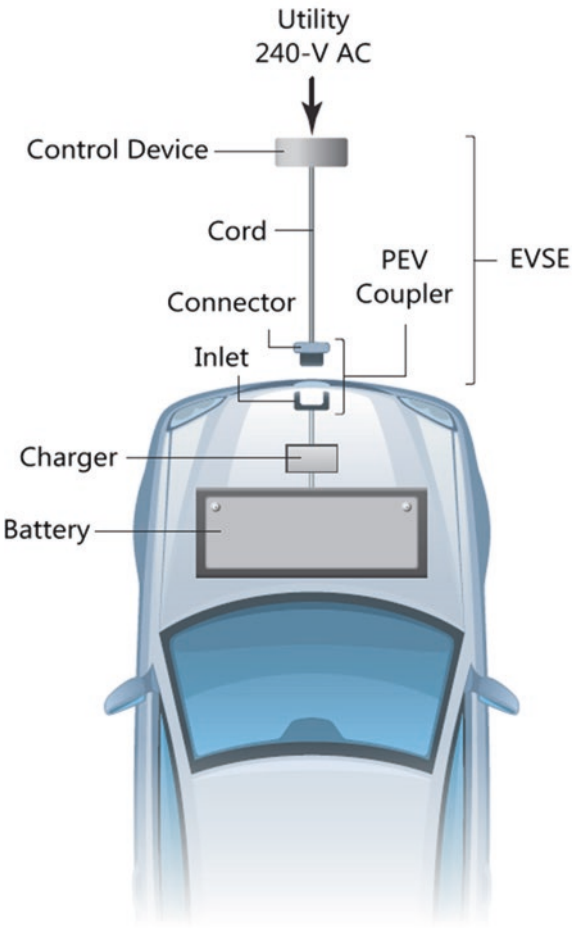

Fig. 3.3 AC level 2 charging schematic [30]

long–distance travel. The maximum current specified is 400 A. The off-board charger is serviced by a three-phase circuit at 208, 480, or 600 V AC. DC level charging can add more than 40 miles of range to a PEV per hour of charging time. Figure 3.4 shows the DC level charging schematic [30].

References [30, 31] give the detailed charging scenarios for single attached or detached garages, carports, multi-family dwellings, commercial fleets, public charging stations, and curbside chargers in terms of power consumption, estimated cost, installation requirements, and safety issues. Most PEV charging is expected to take place in public charging facilities. Several studies compare the charging infrastructure in detail [32].

In addition to AC and DC Level charging, there are two alternative charging methods: inductive charging and battery swapping. These two methods are discussed in the remainder of this section.

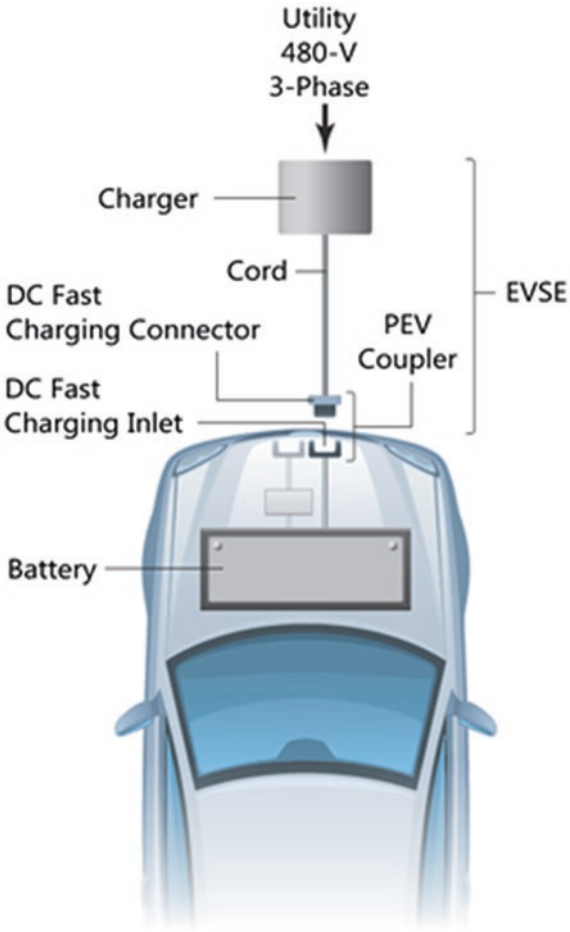

Fig. 3.4 DC level charging schematic [30]

Inductive charging (also known as wireless charging) uses an electromagnetic field to transfer electricity to a PEV without a cord, wire, or plug. As a consequence, the potential of wireless charging technology can be seen well in higher-power applications (e.g., battery chargers for PEVs). Plugging and unplugging an outdoor high-power connector can be a safety concern in certain weather conditions and when insulation is worn. Wireless chargers make charging more convenient, a feature that is especially useful in harsh environments. Wireless Power Transfer (WPT) technology can address many issues related to the cost, driving range, and battery life of PEVs. When energy is wirelessly transferred to PEVs, charging becomes easier. WPT has the potential to greatly increase the convenience of PEV charging, so drivers might more readily take advantage of every available opportunity to charge their PEVs. If a stationary WPT system were used, the drivers would just need to park their cars and leave. If a dynamic WPT system were used (which means the EV could be powered while driving), the PEV range would be unlimited. Furthermore, the battery capacity of a dynamic wirelessly charged EV could be reduced to 20 % or less of that of a regular PEV, which would reduce the cost of EVs to an amount comparable to the cost of gasoline-powered cars. DOE has been sponsoring all major research institutes and vehicle suppliers to push making the wireless charger marketable for several years. However, the main disadvantages of the state-of-the-art inductive charging technology are low overall efficiency and high power losses. To date, a typical commercial PEV inductive charger can deliver high power at an efficiency of about 86 % (6.6 kW of power delivery from a 7.68–kW power draw). Recently, in research at the University of Michigan–Dearborn, a 200–mm distance, 8–kW WPT system with DC-to-DC efficiency as high as 96.5 % was achieved [33]. Although WPT can be a key solution to the problems associated with a large deployment of EVs, the question is how to make the WPT efficient and effective at a reasonable cost. Many interesting projects have been done by using many innovative circuit topologies and system analysis [34–38]. With regard to its functional aspects, WPT is ready for PEVs in both stationary and dynamic applications. However, to make WPT available for large-scale deployment, much work still needs to be done. For example, WPT heavily relies on the precise alignment of the receiving coil on the car with the transmitting coil under the pavement to maintain effective and efficient energy transfer. The flexibility of the car path makes it impossible for a driver to follow the transmitting path. Figure 3.5 [39] shows the inductive charging (wireless charging) schematic. The associated inductive charging standard, SAE J2954, is currently under development.

Battery swapping is a method by which drivers can replace their “dead” batteries (in which the PEV battery’s state of charge is below a certain level) with fresh batteries at a battery swapping station (BSS). The method has been proposed and researched in recent years. This type of method is not strange; it has been used with other electric appliances, such as cell phones, clocks, and electronic toys. Most of them are at a very low voltage level (1–5 V), while the PEV batteries have voltage levels in the hundreds. The aspect of this method that is most attractive to customers is that batteries can be changed quickly, which can save drivers a lot

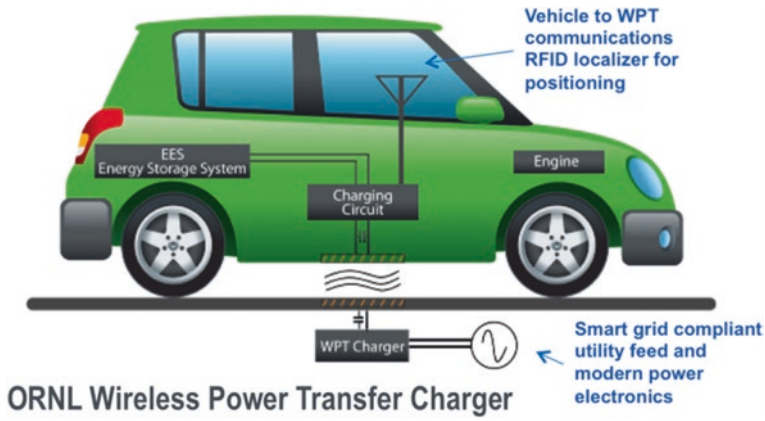

Fig. 3.5 Inductive charging (wireless charging) Schematic [39]

of time. For example, Tesla, which is a famous electric car maker, swaps a battery in 90s [40]. References [41, 42] point out some other important benefits of BSSs, as follows. First, in general, because batteries are collected and managed in centralized locations, it is easier and more convenient to maintain and manage them, which means longer battery lives and less cost to management. Second, centralized charging gives stations a chance to avoid the grid's peak demand times and to charge batteries at valley times. This saves lots of money in running PEVs. Because of these advantages, many countries attach great importance to BSS projects, such as the BSS for the Beijing Olympic Games, Shanghai World Expo EV BSS, Guangzhou University City EV BSS in China [41], and the world's first BSS for taxis in Tokyo [42]. However, there are also many disadvantages associated with BSSs. Reference [43] points out that the construction investment is very high, the battery management system is not good enough to ensure the of batteries' safety, and the high demand for a monitor and robot system is a big challenge to engineers. Customers also have some hesitation with regard to BBSs. In response to a survey in 2011, 62 % of the people chose to charge their batteries, and only 38 % wanted to use BBSs [44]. Many researchers are now looking for optimal BBS methods. Reference [45] discusses using neural networks to predict the load demand of a BSS. Reference [46] discusses optimal planning for the BSS's charging schedule. In the end, the technical challenges of battery swapping can be summarized as follows: (1) the upfront investment in battery packs is huge; (2) standardization is difficult; (3) swapping stations require a lot of financial investment, space, and manpower; and (4) safety and reliability are a big concern. Figure 3.6 illustrates the principal of battery swapping [47].

On the other hand, other infrastructure services (e.g., communication and information networks) will play a primary role in supporting the electrification of transportation. A DOE report [48] gives an extensive overview of the Smart Grid benefits and communication needs. One section addresses the specific challenges

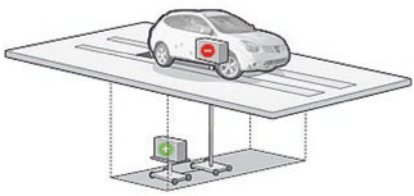

2. Remove the dead battery

A conveyor moves the car over a robotic arm. A latch opens and drops the spent battery onto the arm, which then lowers itself into the bay.

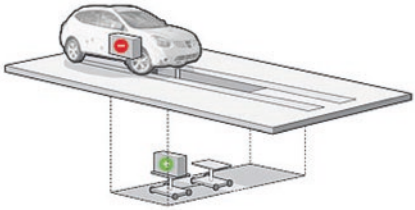

1. Drive in

The driver swipes a card to activate the system and then drives into the change station.

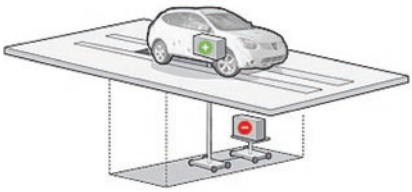

3. Install the fresh battery

Another robotic arm with a fresh battery moves into position and rises to insert the new battery into the car. The depleted battery is recharged and placed in a queue for another customer.

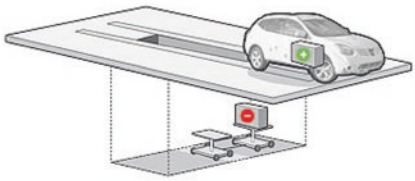

4. Drive out

After a quick test, the car rolls off the conveyor belt, and the customer drives away.

Fig. 3.6 Swapping station work schematic [47]

and opportunities presented by PEVs. In order to make rates or programs specifically available to customers with PHEVs and PEVs, utilities must offer them special services. The services include being able to (1) enroll, register, and initially set up communications between a vehicle user and the utility or an alternative energy supplier (one-time setup); (2) repeatedly reestablish communications for each PEV charging session (repeat communications and rebinding); (3) provide PEV charging (and other) status information to customer information channels (e.g., web and display devices); and (4) correctly bill PEV customers according to their selected rates or programs [49]. Like in-home charging, public charging will need to match supply and demand; unlike in-home charging, public charging may have to do this very quickly and accurately, since vehicle owners will likely want to avoid a long delay once their vehicle is plugged in [48]. It is estimated that the bandwidth for both load balancing and billing purposes will be between 9.6 and 56 kbs [48]. A variety of communication protocols can achieve reliable two-way

communication networks. Since PEVs can be recharged at various locations (e.g., municipal parking decks and office parking lots), it is critical to maintain the compatibility of communication technologies. The communication infrastructure for the Smart Grid has been recently been investigated in References [50, 51].

In addition to certain bandwidth, reliability, and power consumption requirements, security issues need to be considered when different wireless communication technologies are being applied [24]. For example, wireless billing security is viewed as a major concern of PEV users. The actual vehicle's location needs to be kept confidential for user privacy. Another security issue is unauthorized transactions by a third party or hacker. In general, security in the communication network at public charging facilities for PEVs is of critical importance [52]. Recently, based on different perspectives, a number of papers have investigated security-related issues in the communication networks of the charging infrastructure.

- *Vulnerabilities Analysis*: Traditional power grid communications have relied predominantly on wired communication to provide reliable and predictable monitoring and control. However, the data transmission in wireless networks is inherently public, which presents a unique security threat at the physical layer. A lot of work has been done recently to identify the threats and vulnerabilities of wireless technologies and to summarize their security performance [53]. Alcaraz and Lopez [54] reviewed several wireless communication standards and analyzed their security. They identified a set of threats and potential attacks in their routing protocols and provided recommendations and countermeasures to help the industry protect its infrastructure. Lu et al. [55] categorized the goals of potential attacks against the Smart Grid communication networks into three types: network availability, data integrity, and information privacy. They then qualitatively analyzed the impact and feasibility of the three types of attacks.
- *Prevention*: Cryptography is the main scheme for preventing malicious attacks in the communication network. HomePlug and Zigbee use the 128-bit advanced encryption standard (AES) to secure data transmitted across the physical network. AES encryption is a 128-bit fixed-length block cipher, standardized in 2002 by the National Institute of Standards and Technology (NIST) [56]. Improvements for HomePlug security are proposed in Reference [57]. Cellular data are more likely to be at particular risk. The current security protocol used in 3-G networks is KASUMI, which is an A5/3 block cipher. Alternative proposals for more secure cellular data encoding schemes have been proposed in the GSM (global system for mobile communication) network. One is the Rijndael-based algorithm, which is similar to AES [58].
- *Detection*: In order to avoid unauthorized transactions, charging facilities must be able to detect attempts by intruders to gain unauthorized access to the communication network. In general, intrusion detection for Smart Grid communications falls mainly into the cybersecurity field of supervisory control and data acquisition (SCADA) and power systems and has been well studied in the literature [59, 60].

- *Client Privacy*: In PEV charging scenarios, the vehicles usually contribute data on their location, identity, usage patterns, etc.; payment information; and information on the charging station to process these data. The main privacy concern is handling clients' personal information [61]. For example, EV charging reveals the PEV's location and distance traveled.

3.3 Long-Term Planning for PEV Parking Lots

This section looks at the long-term planning for the PEV parking infrastructure (e.g., parking lots). Despite the benefits contributed by PEVs, there are significant economic and social challenges associated with developing an electric transportation system [62–65]. First, PEVs are still substantially more expensive than gasoline and hybrid vehicles. The savings in the cost of fuel (given current gasoline prices) does not justify the higher upfront cost to purchase the PEV at the current level. Federal and state government subsidies, based on the grounds that EVs are cleaner and hence offer more social benefits than gasoline vehicles, are being offered to offset their higher purchase cost [66–69]. Similar subsidies were offered for hybrid vehicles when they were initially introduced to the market, and their impacts were studied. The second impediment to consumer adoption of PEVs is its small driving range per charge, which leads to range anxiety. A well-developed and well-planned charging infrastructure could help alleviate range anxiety and increase EV sales [70–72].

It is important to note that the adoption of PEVs may complicate the understanding and design of interdependent critical infrastructure systems. Therefore, these multidisciplinary complexities must be addressed to determine the optimal sizes and locations of PEV parking lots. For example, PEVs, being transportation tools and electricity carriers, can be charged anywhere and anytime, which creates more spatial and temporal uncertainty. In addition to engineering considerations, the choice of locations for new PEV charging stations may be subject to local policies and regulations, financial incentives, and public interests.

Figure 3.7 is a flowchart of the general process for installing EVSE at a public PEV charging facility [30]. The whole planning process for commercial PEV parking lots, as compared with that for residential installations, may require more permit approvals and documentation from a variety of agencies. To be successful, the long-term planning for parking decks for PEVs needs to consider issues posed by utilities, governing authorities, enthusiasts, original equipment manufacturers, business owners, contractors, and approving authorities throughout the process. Considerations for commercial PEV parking lots include, but are not limited to, the building code, zoning requirements, community or design guidelines, parking and signage requirements, and electrical source and metering.

To date, there is no such well-established integrated planning tool that one can rely on. All the multidisciplinary challenges and opportunities of the long-term planning strategies must be addressed. Moreover, a well-justified business model

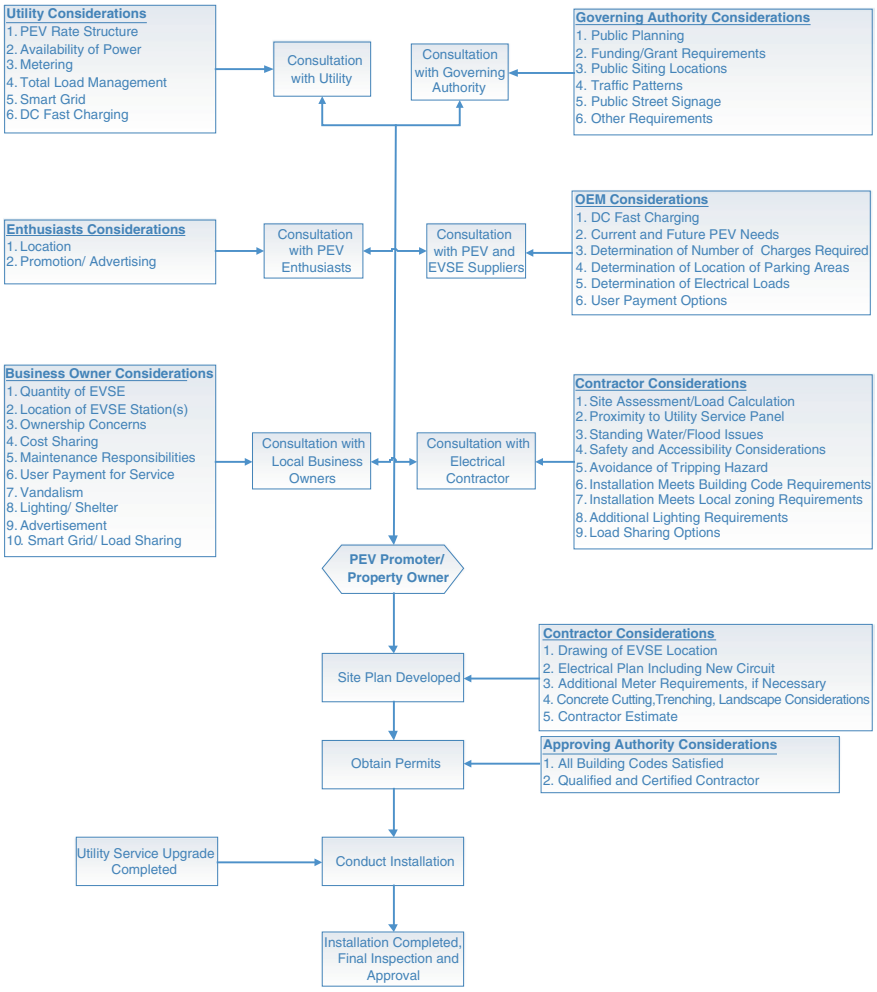

Fig. 3.7 General process for installing EVSE at a public facility [30]

on which the long-term planning of PEV parking lots should depend has not been constructed yet. The PEV driver's choices regarding activity location, route, and departure time affect the vehicle's charging demand over space and time. Figure 3.8 illustrates the PEV charging load with both spatial and temporal uncertainties [73, 74]. For example, several charging events are possible at different locations and times for the traveler activities indicated in yellow, such as at the home garage (before 8:30 AM), at university campus parking lots (9:30 AM–5:00 PM), at the grocery store (5:30–7:00 PM), and at the gym (7:30–9:00 PM). There are also several charging events possible at different locations and times for the traveler activities indicated in red, such as at the home garage (before 6:00 AM), at the office building parking lots (8:00 AM–5:00 PM), at the shopping center (5:30–6:30 PM),

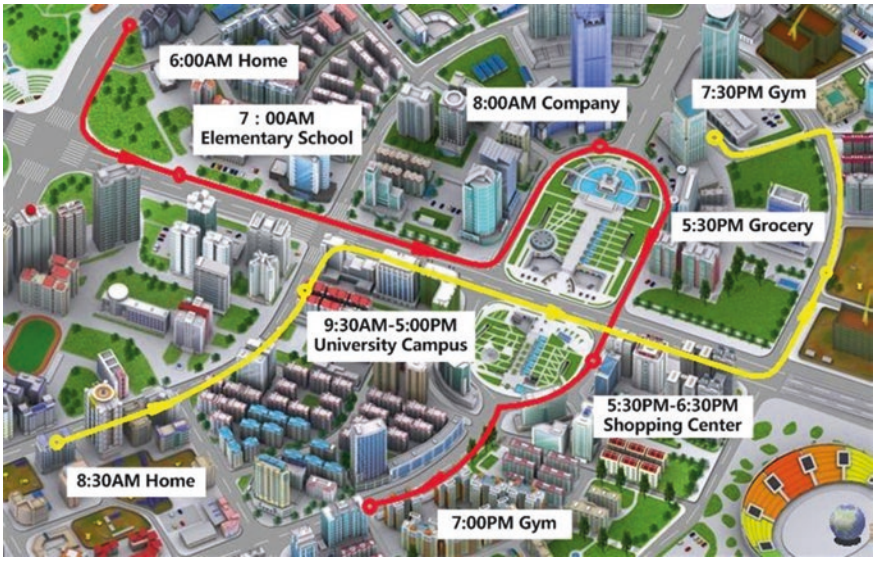

Fig. 3.8 Illustrated PEV charging with temporal and spatial uncertainties [73, 74]

and at the gym (7:00–9:00 PM). It is very challenging to predict such complex behaviors for a large number of PEV drivers in a complex network.

Among all the engineering considerations, power systems and transportation systems are the two most important aspects to consider when planning PEV charging facilities. In essence, PEVs and charging infrastructures (like parking lots) interconnect a power grid system and a charging infrastructure. For example, the emerging PEVs will change the temporal and spatial patterns of traffic in the transportation networks, which essentially will lead to an uncertain charging load to the power grid systems. On the other hand, due to their inherent interdependence with each other, the decisions made regarding power systems will, in turn, affect the traffic pattern results. For instance, commercial charging station capacities and prices will be significant factors in causing drivers to choose particular routes and change their behavior. In conclusion, the need to develop an interdisciplinary approach for investigating the impact of PEV charging on highly interdependent electric transportation systems is urgent.

In our recent work [20, 75–77], our intent has been to establish an integrated framework for planning a PEV charging facility that considers multidisciplinary complexities (e.g., driving behavior, route and departure time choice, charging station location, engineering, policy, economic, environment, technology, and social impacts). Our ultimate goal is to advance the fundamental knowledge base in order to model and simulate the interdependency of the transportation network and the electricity distribution infrastructure that will be created by a large-scale penetration of PEVs in metropolitan areas. We will accomplish the overall objective by (1) modeling the spatio-temporal traffic demand of PEVs using a traffic simulator, (2)

quantifying the spatio-temporal profile of the PEV charging load on the electricity distribution network as a function of the transportation network operation, and (3) exploring the system impacts of the spatio-temporal electricity charging load under various charging schemes. Our initial work is designed to develop a micro-level analysis tool for planning PEV charging facilities incorporating spatial and temporal information. The complete power system is modeled in EPRI's open source Distribution System Simulator (OpenDSS) [78], which is dedicated to the advanced analysis of distribution systems. OpenDSS is a multi-phase simulation tool that supports both frequency and time-domain analysis for electric utility distribution systems. OpenDSS can perform sequential power flows over successive time intervals (e.g., 20 min) over a specified overall period. This OpenDSS capability allows for direct consideration of variations of PEV load patterns and daily and seasonal conventional load variations [79]. Given that PEV parking lots are ideal places for installing on-site renewable energy generators, OpenDSS provides a platform to evaluate the combination of PEV charging and use of a renewable energy resource such as solar or wind. Moreover, many OpenDSS built-in functions can be used directly. For example, the "Autoadd" feature in OpenDSS can help in determining the optimal placement of charging stations. More specifically, it searches each available bus for a location that results in the greatest improvement per unit.

Several vehicle databases in the public domain are available for extracting information on driving behavior and traffic patterns at either a national level or an individual vehicle level, without considering a real-world transportation network at the city or regional level. Among them, the National Household Travel Survey (NHTS) from the U.S. Department of Transportation has data that have been used extensively to estimate PEV driving behavior and traffic patterns [80]. This dataset is created for use in gaining a detailed perspective on driving habits. However, it is not ideal to devise a detailed city-level or regional-level model of driving habits by analyzing such an extremely large dataset.

Given the situation just mentioned, one can deduce that a detailed city or regional transportation network modeling and simulation tool is needed badly. It would predict traffic dynamics and network flow patterns by solving how to assign time-varying travelers/vehicles to a congested, time-varying network, under time-dependent user equilibrium (UE) conditions or under time-dependent system optimal (SO) conditions. Since the planners will focus on distribution-level power analysis, the transportation modeling and simulation tool will have to capture the dynamics of individual travelers/vehicles (e.g., driving from home to a public charging station after work) rather than of aggregate travel demand. Therefore, in order to model the PEVs' travel activities in the transportation networks, we need to integrate an activity-based, travel-demand model with a simulation-based dynamic traffic assignment model [81, 82] to explicitly model the travel choices of each PEV driver with regard to activity location, activity duration, departure time, and route. The results from the integrated modeling and simulation of the transportation network will provide, for each individual PEV, the battery state of charge, duration at a location, and routing plan. With regard to integrating activity-based travel-demand models and dynamic network models to find effective

supply-and-demand management and operational strategies to mitigate traffic congestion, research is still ongoing. The strategies will employ emerging advanced intelligent transportation system (ITS) techniques (e.g., the provision of advanced traveler information, advanced traffic management systems).

To be more specific, the planners are particularly interested in the dimensions associated with the following four choices made by each individual PEV driver:

- *Activity location:* The activity location chosen depends on characteristics related to the trip's purpose, attributes related to traveling from the current location to the available destination locations (e.g., travel time and cost), and characteristics related to the activity location itself (e.g., charging facility and scheme). This choice also depends on the PEV's driving range and its battery's current state of charge. With the large-scale penetration of PEVs into the marketplace, price-based factors (e.g., PEV charging cost, which varies with the geographical location) can also have an impact on the congestion pattern in the transportation system. In addition, the model can define a rule or assign a task (e.g., if the battery state of charge drops below 20 %) to each vehicle to determine when to recharge. Since the integrated model can provide both static and animated graphical simulation results through its intuitive graphical user interface (GUI), it is also an ideal tool to achieve the real-time simulation and monitoring.
- *Activity duration:* The choice of activity duration at a location depends on characteristics related to the trip's general purpose. The PEV traveler also has to depend on the charging time needed to allow him/her to make his/her the next trips.
- *Departure time:* The choice of when to depart from a location depends on the preferred arrival time at the destination or the preferred departure time at the origin and on the time it takes to travel from the origin to the destination. The PEV traveler also needs to consider the charging scheme at the origin and destination locations, such as the charging price and scheme in his/her utility function.
- *Route:* The route chosen depends on assumptions made by the traveler. In general, a traveler will choose the path that requires the least amount of travel time. A PEV driver might instead consider choosing the path that involves the least energy consumption or the path that takes the least travel time with driving range constraints.

This integrated modeling and simulation of the transportation networks will provide data on detailed, spatio-temporal, PEV travel activities that consider traffic flow dynamics.

Once the spatio-temporal PEV traffic demand is determined by the integrated PEV activity-based demand and dynamic network equilibrium model, we will explore three charging schemes to meet the required electricity load. Figure 3.9 illustrates the interdependency mapping between the transportation network and the power distribution system based on GPS information. For the distribution system, the bus coordinates where the charging spots are located and clustered into user-defined nodes and zones on the transportation network. The charging load locations can be collected from published parking infrastructure data by the PEV charger manufacturer [83–85]. Alternatively, one can assume the charging stations are at generic locations (e.g., office building, highway exit, shopping center), which can be situated at links on transportation networks.

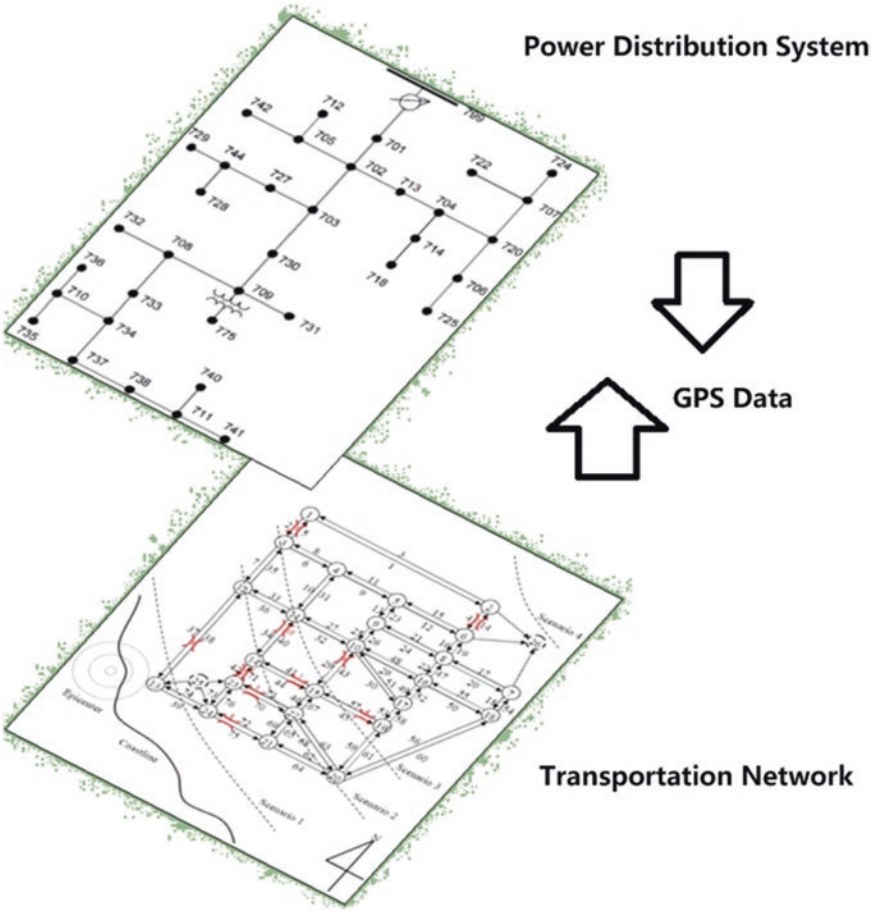

Fig. 3.9 Illustrated interdependency mapping between the transportation network and the power distribution system based on GPS information

As detailed in previous sections, there are various PEV charging levels. From a planning perspective, we may also use the co-modeling and simulation platform to make the best choice on the basis of a variety of charging scenarios or schemes, such as:

1. *Uncontrolled charging:* This charging process starts immediately by using the maximum charging power when a PEV arrives.
2. *Constrained charging:* Assuming the total charging time is known, the required charging power is equally distributed over the entire parking period.
3. *Smart charging:* Assuming the expected departure time for each vehicle is known, this charging process finds the relatively low-price time intervals for charging the PEV when it is parked and decides how and when to charge the PEV.

We can apply both deterministic and stochastic analytical approaches for planning PEV parking decks. A deterministic analysis covers both system and component levels. The former analysis is intended to assess the system-wide PEV impact, while the latter focuses on the impacts of PEC charging on individual power system components (e.g., distribution transformer and power line). Here are a few examples:

1. Deterministic analysis
    1.1. System-level analysis under different scenarios
        1.1.1. Peak day/hour: Distribution system power losses
        1.1.2. Peak day/hour: Extent to which PEV charging load demand adversely affects system voltage regulation
        1.1.3. Peak day/hour: Bus voltage profile
        1.1.4. Peak demand correlation between transportation and power distribution networks
        1.1.5. Average trip distance and charging time
        1.1.6. Vehicle driving patterns
    1.2. Component-level analysis (ability of component and asset class to supply PEV charging load) under different scenarios
        1.2.1. Thermal loading with different types of baseloads (e.g., airport, residential, and business): Extents to which a component's normal and emergency ratings are exceeded
        1.2.2. Vehicle density at any location
2. Stochastic analysis
    2.1. Impact likelihood: Determined through stochastic simulations (Monte Carlo) over a full day/week/year
    2.2. Results: Are Gathered from each stochastic set and aggregated across various asset classes and voltage levels to form general conclusions about likely impacts on the distribution system

The real-world operational conditions of PEV charging can be categorized in many ways, such as:

1. Power system scenarios
    1.1. PEV penetration level
    1.2. Weekday, weekend, holiday
    1.3. Charging level and control scheme
    1.4. Uncontrolled charging (e.g., start charging as soon as vehicle arrives)
    1.5. Constraint charging (e.g., allocate charging load evenly over parking time)
    1.6. Smart charging (e.g., base charging on time of use, real-time price)

2. Transportation scenarios

   2.1. Price based (e.g., add toll at the selected road)
   2.2. Time based (e.g., use flexible working hours)
   2.3. Control based (e.g., employ signal controls and ramp metering)

Figure 3.10 presents an analytical framework for coupling the modeling and simulation of power systems and transportation networks [73]. This coupling framework can facilitate the process of planning for the deployment of new PEV charging facilities. It is important to note that the objectives from a power system perspective can conflict with those from a transportation perspective. For example, it might make more sense to deploy new charging stations at a certain parking facility that is visited frequently by PEV owners. However, it could be very costly to upgrade the required electric system (e.g., by installing new dedicated branch circuits and metering devices). Another example is that the power grid operators may prefer to have the additional load caused by PEV charging to be connected to a certain distribution feeder with a light baseload, since the cost of providing electricity to these locations is much lower.

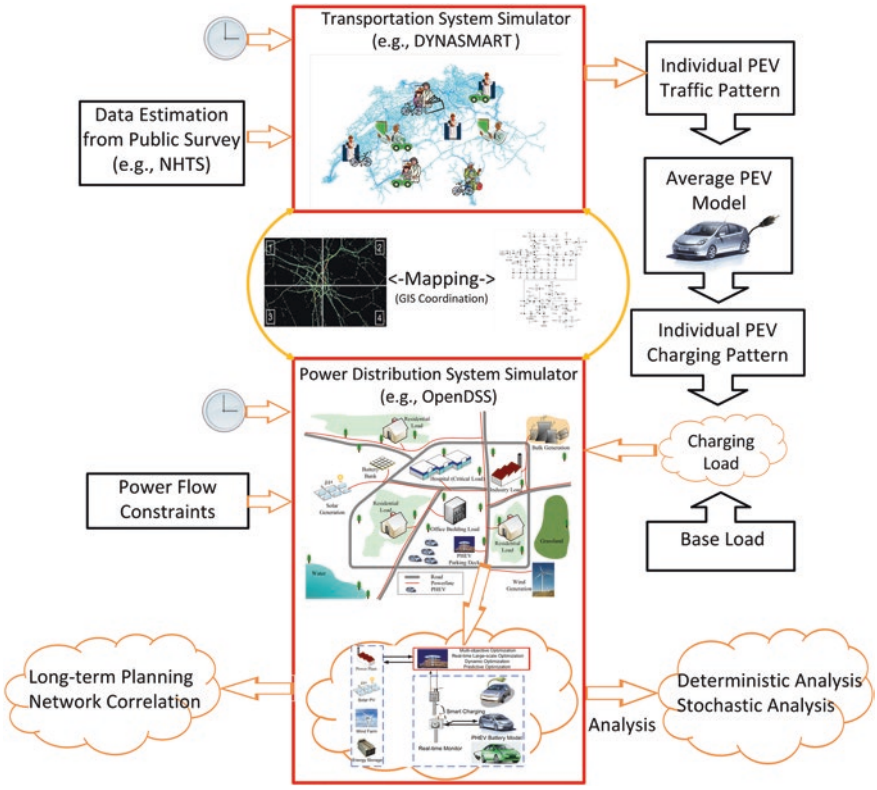

Fig. 3.10 Co-modeling and simulation framework [73]

However, it may sacrifice the convenience of the PEV parking locations. In short, there is no universal solution that maximizes all the objectives from different perspectives. The need for future research and investigations related to the long-term planning of PEV parking lots is still great. Due to the lack of real-world PEV data (e.g., start time, initial battery state of charge, customer preferences), most current work focuses on theoretical studies. In past few years, DOE has continued to collect and analyze data on more than thousands of PEVs and charging stations deployed through Transportation Electrification Initiative funded by the American Recovery and Reinvestment Act. By the end of 2013, this initiative had deployed more than 18,000 charging points in residential, commercial, and public locations, supporting over 11,000 PEVs. The effort has revealed important information on how drivers use their PEVs and use the charging infrastructure under real-world scenarios, which has proven to be invaluable to stakeholders as they plan for the mass deployment of millions of PEVs in the coming years.

At the early development stage of PEV lots, free charging accounted for a large portion of the total number of installed charging stations [86, 87], with a goal of promoting public awareness of PEVs. However, this kind of "free lunch" cannot last forever. Here we will briefly explore a potential economic model of PEV parking lots, covering ownership, investment plans, and cost recovery mechanisms. PEV charging stations in a public parking facility might have split ownership. For example, one entity might own the parking infrastructure (e.g., a university might own the parking lot) and another entity (perhaps a private investor) might own the charging stations and associated equipment. There might even be a combination of owners. For example, utilities might own and operate the smart metering infrastructure and the power line that connects with the transformers. The general business model is not clearly defined yet.

3.4 Control and Management of PEV Parking Lots

This section investigates aspects of control and management associated with the economical operation of PEV parking lots. If parking lot control and management are not carried out properly, the large numbers of PEVs parked there might degrade the power system's stability and reliability. For instance, several hundred PEVs might arrive at parking lots in a short period of time (e.g., during the early morning hours when people arrive at work). Under AC Level 2, the hourly charging load of a PEV is approximately equivalent to the energy use of an average household. At this level, multiple PEV charging loads connected to one feeder at peak time could cause a serious transformer overload during such a short time period.

There are more than 250 million vehicles in the U.S. today. PEVs are assumed to account for 10 % of the entire vehicle fleet. Their charging level is 10 kW. Based on these data, 250 GW of generating capacity is needed to support the charging load of the PEVs at peak times. The total U.S. generating capacity is

roughly 1,000 GW. If regulated wisely, PEVs could serve as distributed energy storage to relieve the peak demand and maintain the real-time balancing of generation and load. A sophisticated control and management strategy is needed to minimize disturbance to grids yet satisfy customer needs. Operational decisions have to be made at various time scales to achieve objectives, ranging from controlling local frequencies, to controlling congestion (perhaps by using local renewable generation sources), to developing infrastructure through commercial charging stations. In the last decade, various control and management schemes for PEV charging have been proposed. The overall objectives have included (1) reducing the charging cost based on dynamic pricing (e.g.,time-of-use pricing and real-time pricing); (2) shifting the peak load and reducing the peak demand; (3) facilitating the smooth integration of intermittent renewable sources in the grid; and (4) providing ancillary services such as load following, voltage control, frequency regulation, and reactive power control.

More recently, significant research efforts have been devoted to coordinated PEV charging. Richardson et al. [88] employed a linear optimization model based on network sensitivities to maximize the total charging power that can be delivered to PEVs while operating within voltage and thermal limits. Luo et al. [89] developed a two-stage optimization model to minimize the peak load as well as the load fluctuation. Sortomme et al. [90] presented three coordinated PEV charging methods to minimize the power losses, load factor, or load variance in a distribution system. Han et al. [91] proposed an optimal V2G aggregator for frequency regulation services by using a large number of PEV batteries. Qi et al. [92] used the Lagrangian relaxation method to coordinate the charging of PEVs across multiple charging stations. Yao et al. [93] used a hierarchical decomposition approach to coordinate the charging/discharging behaviors of PEVs. Li et al. [94] presented a real-time PEV smart-charging method that not only considers currently connected PEVs but also uses a prediction of the PEVs that are expected to plug in in the future. Zhong et al. [95] presented a coordinated control strategy for large-scale PEVs, battery energy storage stations, and traditional frequency-regulation resources involved in automatic generation control (AGC). Xu et al. [96] proposed an ant-based swarm algorithm (ASA) to achieve PEV charging coordination at the transformer level, which can overcome the drawbacks of a centralized control method. Qian et al. [97] modeled and analyzed the load demand due to PEV battery charging in distribution systems. Mitra et al. [98] designed and implemented a real-time wide-area controller to improve the stability of the power system for PEVs. Su et al. [99–101] proposed a suite of computational intelligence-based approaches for managing PEV charging loads at municipal parking decks under a variety of charging scenarios. Shao et al. [102] analyzed the impact of electricity rates (based on time of use) on distribution load shapes at various levels of PEV market penetration. Su et al. [103–105] proposed control strategies for optimal charging at municipal PEV-enabled parking decks with demand response capability.

It is clear that as the number of PEV charging stations increases to more than hundreds of thousands, centralized control may not be suitable for large-scale

PEV charging. To address this challenge, one promising solution is to develop distributed control algorithms to make operating the PEV charging at parking decks more reliable, resilient, and secure. There are numerous examples of distributed control we can observe in our daily lives, such as the swarm behavior of a group of insects, a flock of birds, or a school of fish. Distributed algorithms have been studied in several research areas, including the social sciences, animal science, and computer science. However, the investigation and use of distributed algorithms in a Smart Grid environment is still at an early stage. Unlike their centralized counterparts, distributed control approaches can translate the legacy centralized management of a cluster of components into a completely distributed control architecture in which only local information is exchanged with neighbors. Hamid and Barria [106] proposed a distributed recharging rate control algorithm that combines the two objectives of regulating frequency and encouraging the use of electric generators. Liu et al. [107] proposed a decentralized vehicle-to-grid control method to provide frequency regulation service for power system operation for EVs. Ma et al. [108] used non-cooperative game theory to coordinate the charging process of PEVs. Gan et al. [109] proposed a decentralized algorithm to exploit the elasticity of EV charging loads to fill the valleys in load profiles.

Figure 3.11 illustrates the PEV ecosystem (PEV owners, PEV parking lot owners, aggregators, and distribution companies) at the distribution/retail level. As the figure shows, it is important to introduce the inter-relationship between the PEV parking lot owner and other entities. The smart meters and sensors can monitor the electric energy consumption at every single node of the power distribution system and exchange the real-time information with the grid operators at the control center through a reliable two-way communication network. The grid operators can also send back control signals to a variety of entities (e.g., local aggregators). Multiple aggregators serve as the "middleware" between the central controller and PEV charging stations. When given the real-time information from multiple

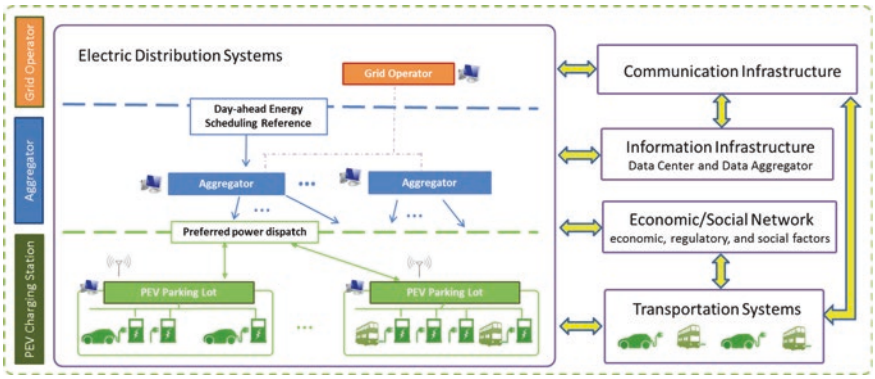

Fig. 3.11 PEV ecosystem

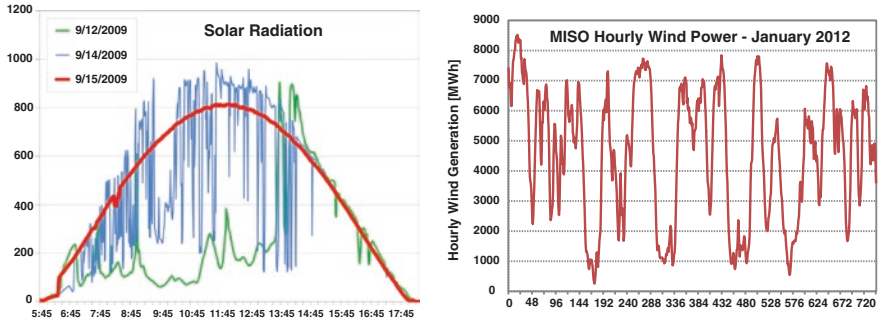

Fig. 3.12 Illustrated intermittent renewable energy power output: solar [110] and wind [111]

aggregators, the central controller does the energy scheduling and sends back control signals periodically.

Figure 3.12 illustrates the intermittent nature of solar and wind energy sources [110, 111]. These renewable resources tend to fluctuate dramatically depending on the time of day and time of year [112]. Such variability and uncertainty need to be carefully taken into account when automating the distribution of the Smart Grid.

From a power system perspective, we need to determine two-stage operational strategies for PEV parking lots: for day-ahead energy scheduling and for real-time dispatching. Here's an example. In the first stage, PEV parking deck operators need a systematic optimal price reference on electricity sale prices and parking fees for customers for tomorrow's operations. Because different types of parking decks have different traffic behaviors (e.g., arrival and departure distributions), the parking deck operators need an exclusive price reference determined according to historical traffic behaviors. In addition, traffic behaviors also vary between weekends and weekdays, summer and winter, etc. To overcome the operational challenges associated with on-site distributed renewable energy generators, stochastic programming approaches may be used to consider the forecasting errors of variable solar power output and the changing demands of customers. The first-stage problem is to find a dependable reference that parking deck operators can use as a basis for making a price decision and selecting the optimal charging scenario. One objective function is to maximize the total revenue of a PEV parking deck with several chargers (each PEV has its own charger) over 24 h. The parking deck operators have to consider the price of acquiring electricity from the grid, the initial PEV battery state of charge, charging power, parking fee, and parking fee rebate rate. The expected daily revenue comes from the total revenue of parking and the total revenue of charging. The price mechanism provides the flat electricity sale price and the parking fee for PEV owners. Using a flat fee is an efficient way to build customers' confidence about using PEV parking decks, because the price for customers is constant during a whole day. In addition, the price mechanism offers a rebate on the parking fee to customers when their PEVs are being charged.

First-stage control and management are also subject to a number of objectives. For example, every PEV needs to be fully charged before it leaves the parking deck. The charging power for each PEV at any time interval needs to be limited. A main function of first-stage scheduling is to find the marginal electricity sale price for parking deck operators to use as a reference for tomorrow's operation; this helps them determine the electricity sale price and parking fee rebate rate for customers and thus maintain enough revenues to cover operating costs. During each day's operations, the PEV parking deck needs to maintain its revenues in order to pay for the possible bank loan, repairs, and the cost of labor. The total revenue of one day needs to be higher than the cost of operations over 24 h. That means that the electricity sale price for customers has to be higher than the marginal electricity sale price; otherwise, the parking deck would be in deficit. Thus, the operators need a credible price reference for the next 24 h to ensure their profits. The marginal prices are obtained by these simulation results using different charging scenarios and several selected parking fee rebate rates. Another main function of first-stage scheduling is to help parking deck operators select the optimal charging scenario after the price decision has been made. The electricity sale price and parking fee are both flat for customers; thus, if the parking deck changes the charging scenario, the change will not compromise the customers. Thus, it is essential for parking deck operators to select a suitable charging scenario to maximize their revenues for different situations.

Given the reference determined by the first-stage day-ahead energy scheduling, the second-stage real-time power dispatching tends to maximize revenues while satisfying the real-time power balance and decreasing related uncertainties [113, 114]. In a Smart Grid environment, utilities may offer the parking deck real-time pricing (RTP). This is a dynamic price that reflects the electric energy cost on an hourly base. Instead of a flat rate, utilities charge the residential customers the real-time retail price based on the hourly whole electricity market price. Based on all the real-time information and measurements, the parking deck operators can make the best decision related to the amount of power to be allocated to each PEV, assuming that the PEV owners allow dynamic charging control in exchange for a parking fee rebate. The uncertain parameters associated with PEV charging (e.g., charging time, initial battery state of charge, starting/ending time) make it difficult to predict the day-ahead charging load. To address these challenges in the second stage, a model predictive control (MPC)-based approach for power dispatching [113] can be used to minimize the operational cost while accommodating the PEV charging uncertainty.

There are also new research trends associated with the control and management strategies. For example, a public PEV parking lot is an ideal home for major distributed renewable energy generators (e.g., roof-top photovoltaic panel, small-scale wind turbine), depending on the available space; the lot is suitable for the efficient collection of wind and solar energy. The PEV parking lot also enables greater adoption of intermittent energy sources by scheduling electrical loads to coincide with periods when the sun or wind is strong. Normally, these on-site

generators that use renewable energy resources are considered non-dispatchable units. From the point of view of long-term operations, the operational cost of renewable-energy-based distributed generators is negligible. However, the inherent intermittency and variability of these energy resources make it complicated to determine their effects on the economic operation of integrated transportation systems. One can therefore say that the targeted optimization problem is complex over time and space with a number of associated uncertainties.

According to Kempton and Dhanju [115], EV will serve the majority of needs for integrating wind energy into the power system. Markel et al. [116] proposed a variety of fleet control methods. One of the charging schemes, renewable-energy-signal charging, is based on the premise that the plug-in fleet can be charged exclusively by using renewable energy, with plug-in vehicles acting as the energy sink. This paper also highlighted the limitations and opportunities associated with using renewable energy resources to fuel PEVs in the future. Guille and Gross [117] estimated the positive effect of PEV on wind power operations. Wang et al. [118] used a new unit commitment model to simulate the interactions among PEVs, wind power, and demand response. Liu et al. [119] proposed using a stochastic unit commitment model to consider the coordination of thermal generating units and PEV charging loads as well as the penetration of large-scale wind power. The proposed model can also address ancillary services provided by vehicle-to-grid techniques. A model predictive control (MPC) approach can accommodate forecasting errors by combining the real-time observations and short-term predictions. The MPC approach determines the series of optimal control operations that should occur over a receding finite horizon. At each time step, a deterministic optimization problem is solved based on the look-ahead, finite-horizon prediction and the updated current state and measurement. But only the first step of the open-loop optimal control sequences is performed. At each time step, the initial condition over the prediction horizon is determined by the real-time measurement of the actual system. The on-line optimization process repeats until the last time step. Figure 3.13 shows the envisioned PEV parking lots with distributed renewable energy generators [120, 121].

Vehicle-to-grid (V2G) technology is a promising opportunity with regard to PEV adoption. Basically, it allows the PEV fleet to feed electricity directly back into the electric distribution systems. There has been a growing amount of literature on V2G technology in last decade. Kempton and Tomic [122] formulated mathematical equations to calculate the capacity for grid power from vehicle fleets. They evaluated the revenue and costs involved for these vehicles to supply electricity to four electric markets (baseload power, peak power, spinning reserves, and regulation). According to the authors, V2G power cannot compete with the low price of the baseload power market. However, V2G power is cost effective in the peak power market in particular cases in which the peak power is unusually high and the energy capacity of the fleet can support that power for 3–5 h. Nonetheless, the engineering rationale and economic motivation for using V2G power in spinning reserves and the regulation market are compelling. These results are based mainly on several case studies, particularly an investigation of the

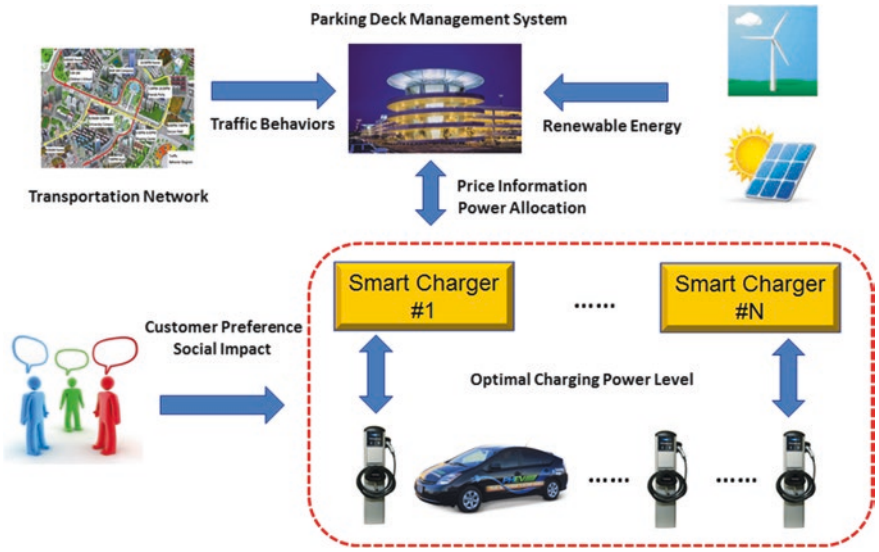

Fig. 3.13 PEV parking lot with distributed renewable energy generators [120, 121]

California electric power market reported by Kempton et al. [123]. The revenue and cost evaluation used in this study is more comprehensive and accurate than that used in the earlier methods, using the avoided costs found in Kempton and Letendre [124] and the retail time-of-use rates found in Moura and Moura [125]. The avoided cost of the utility is equal to its least-cost generation options. All the costs and revenues used for making assessments in these studies are based on the current conventions of the power market. Sovacool and Hirsh [126] investigated the idea that the obstacles to V2G transition are not merely technical but are actually related more to social and cultural values, business practices, and political interests. These socio-technical difficulties can easily be discovered by reviewing the history of other energy transitions, especially the history of renewable energy technologies [126].

The concept of V2G has been promoted for a long time, but V2G is a controversial idea. To summarize, there are two main issues that could adversely affect the real-world deployment of V2G at PEV parking lots in the near term: (1) a system infrastructure enabled by two-way communication and (2) an unproven business model and economic justification.

In March 2012, U.S. President Obama announced a series of Clean Energy Grand Challenges, including "EV Everywhere" [127], which focuses on the U.S. becoming the first nation in the world to produce PEVs for the average American family that are as affordable as today's gasoline-powered vehicles within the next 10 years. EV Everywhere sets up the battery goals for 2022: cost of $125/kWh, energy density of 400 Wh/L, specific energy of 250 Wh/kg, and specific power of 2,000 W/kg. Figure 3.14 shows the current status of PEV battery technology

Status of conventional PEV battery development				
• Initial PEV battery development contracts were completed in FY2011 • New contracts to focus on high voltage/ high capacity cathodes				
DOE energy storage targets	**PEV (10 mile AER)**		**PEV (40 mile AER)**	
	Target	Status (2011)	Target	Status (2011)
Discharge Pulse Power: 10 sec (kW)	45	~70	38	~95
Regen Pulse Power: 10 sec (kW)	30	~ 40	25	~70
Available Energy (kWh)	3.4	3.4	11.6	11.6
Calendar Life (deep cycle)	10+	8 - 10	10+	8 - 10
Cycle Life (deep cycles)	5,000	3,000 – 5,000	5,000	3,000 – 5,000
Maximum System Weight (kg)	60	~ 57	120	~ 175
Maximum System Volume (I)	40	~ 45	80	~ 100
System Production Price @ 100k units/yr	$1,700	~2600	$3,400	~ 6850

Fig. 3.14 PEV battery technology development status [128]

[128]. Even under normal operating conditions, the state-of-the-art battery technology is very far from its theoretical energy density limit. It is worth noting that two-way power flow control is the key to enabling technologies that will make V2G come true. According to the recent DOE report [127], the modeled cost of PEV batteries under development has been lowered from more than $625/kWh in 2010 to the current 2014 cost of $325/kWh of usable energy. Although the cost of PEV batteries has been significantly reduced by approximately 50 % over the past 4 years, PEV battery technology is not expected to be ready for a frequent switch between charging/discharging modes in the near term. The high opportunity cost of batteries prevents V2G from becoming a reality. To the best of our knowledge, the majority of U.S. automotive companies and battery manufactures today are against this idea, since the negative effects on battery degradation have not been fully addressed.

In addition, a reliable two-way communication network is greatly needed to enable V2G technology. DeForest et al. [23] discussed the unproven economic justification for the utilities and the customer. According to this source, it is not yet clear whether the economic incentives justify V2G from the utility's perspective; several issues (e.g., battery technology, lack of support for Smart Grid technologies, the complexity of the distribution system required) prevent the deployment of V2G. Madawala and Thrimawithana [129] proposed a bidirectional inductive power interface to facilitate V2G technology. Quinn et al. [130] compared the impact of the communication architecture on the V2G ancillary services in terms of the availability, reliability, and value of the vehicle-provided ancillary services.

However, there are three intermediary steps that can be taken before the equivalent vision of V2G comes to fruition. The potential three stages are as follows.

1. *Smart charging (grid-to-vehicle or G2V).* The vehicle charging rate is controlled locally or remotely based on grid conditions and user preferences. The benefits include, but are not limited to, these: (1) minimizes the overall charging cost by using time-of-use/real-time-price-based charging, (2) reduces the additional load at peak times (e.g., load as spinning reserve), and (3) allows

easier integration of intermittent renewable resources (like wind and solar resources) in the grid. The disadvantages of V2G technology and its application were detailed in previous sections. Many recent literature works have shown the promising results of G2V and the huge impact it could have on Smart Grid development.

2. *Vehicle-to-building (V2B) technology.* In addition to V1G, the charger would be able to feed power back to the charging facility into which it is plugged. V2B provides additional benefits: (1) provides backup power, (2) ensures there is high-quality power for buildings, and (3) supplies power to buildings when grid power is costly.
3. *V2G technology.* At the final stage, V2G allows for the vehicle to feed power back directly to the grid. Such a system would require constant bidirectional communication between the charger and the grid. As mentioned in a previous section, V2G offers the following: (1) provides grid-stabilizing ancillary services (e.g., reactive power and voltage control, loss compensation, energy imbalance; (2) allows for the easier integration of renewable resources by ensuring high-quality power from the resource [131]; and (3) supplies power to grid when economically viable.

Figure 3.15 illustrates the potential deployment of V1G, V2G and V2B technologies.

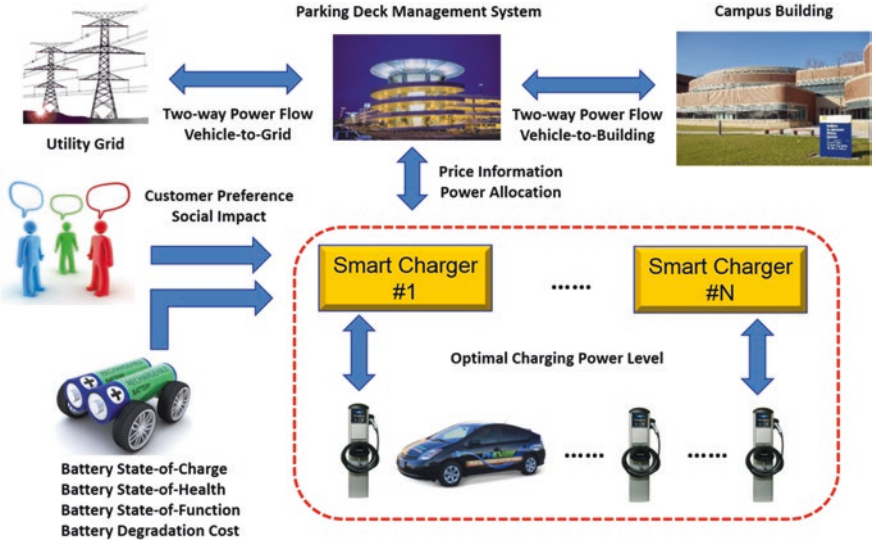

Fig. 3.15 Smart charging (G2V), vehicle-to-Grid (V2G), and vehicle-to-building (V2B) technologies

3.5 Conclusions

Smooth grid integration is critical for achieving a massive introduction of PEVs into the marketplace. Our long-term goal is to enhance the smart operations of PEV charging facilities so that they promote economic efficiency, encourage customer participation, reduce costs, maintain grid reliability, and support the integration of sustainable mobility with the multidisciplinary complexities in the grid. The PEV charging facility is the most critical component for the electrification of transportation. This chapter provides a general view of both the concepts and applications associated with the planning, control, and management strategies used for PEV parking lots. First it introduces the state-of-the-art PEV charging facility, describing its use around the world. Second, it investigates the long-term planning of PEV parking lots in terms of opportunities, challenges, and solutions. Third it describes control and management strategies for PEV parking lots. There is still a significant amount of investigation needed before the full vision of the electrification of transportation comes to fruition. Finally, this chapter discusses future research needs, covering the planning, control, and management aspects of PEV parking lots in a Smart Grid environment.

Acknowledgments This work is in part supported by the Institute for Advanced Vehicle Systems (IAVS) Research Seed Funding and the Faculty Research Initiation and Seed Grant at University of Michigan-Dearborn.

References

1. Underwood SE (2014) Disruptive innovation on the path to sustainable mobility: creating a roadmap for road transportation in the United States. In: Meyer and Beiker (eds) Lecture notes mobility in road vehicle automation, Springer, Berlin
2. Chan CC (2007) The state of the art of electric, hybrid, and fuel cell vehicles. In: Proceedings of the IEEE 95(4):704–718
3. Su W, Rahimi-Eichi H, Zeng W, Chow MY (2012) A survey on the electrification of transportation in a smart grid environment. IEEE Trans Ind Inform 8(1):1–10
4. Lopes JAP, Soares FJ, Almeida PMR (2011) Integration of electric vehicles in the electric power system. In: Proceedings of the IEEE 99(1):168–183
5. Dyke KJ, Schofield N, Barnes M (2010) The impact of transport electrification on electrical networks. IEEE Trans Ind Electron 57(12):3917–3926
6. Clement-Nyns K, Haesen E, Driesen J (2010) The impact of charging plug-in hybrid electric vehicles on a residential distribution grid. IEEE Trans Power Syst 25(1):371–380
7. Fernandez LP, Roman TGS, Cossent R, Domingo CM, Frias P (2011) Assessment of the impact of plug–in electric vehicles on distribution networks. IEEE Trans Power Syst 26(1):206–213
8. Sikes K, Gross T, Lin Z, Sullivan J, Cleary T, Ward J (2010) Plug-in hybrid electric vehicle market introduction study: final report. U.S. Department of Energy, Washington
9. Duvall M, Knipping E (2007) Environmental assessment of plug-in hybrid electric vehicles. Electric Power Research Institute, Charlotte
10. Electrification Coalition (2013) State of the plug-in electric vehicle market–EV market outlook. Washington. http://www.pwc.com/en_GX/gx/automotive/industry-publications-and-thought-leadership/assets/pwc-ec-state-of-pev-market-final.pdf

11. KPMG Insights Series (2011) China's 12th five-year plan: energy (English version). http://www.kpm-g.com/CN/en/IssuesAndInsights/ArticlesPublications/Documents/China-12th-Five-Year-Plan-Energy-201104.pdf
12. Wu QT (2009) Progress in "Ten Cities & Thousand Units" plan. New Energy Veh 1(13):15–19
13. Cobb J (2014) Top 6 plug-in adopting countries, Jan 16. http://www.hybridcars.com/top-6-plug-in-car-adopting-countries
14. Shepard S et al. (2014) Executive summary: electric vehicle geographic forecasts—plug-in electric vehicle sales forecasts for North America and select European and Asia Pacific cities by state/province, metropolitan area, city, and selected utility service territories. Navigant research report
15. Navigant Research (2014) US to remain largest national plug-in vehicle market over next 10 years, Tokyo to take metro market lead spot from LA. Green Car Congress, Apr 24. www.greencarcongress.com/2014/04/20140424-navigant.html
16. Society of Motor Manufacturers and Traders (2014) Mar 2014—EV registrations
17. Foy H (2014) Spending to encourage use of electric cars falls flat. Financial Times
18. Kane M (2014) Sweden and UK drive growth of CHAdeMO chargers in Europe to 1,117. http://www.insideEVs.com
19. Kempton W, Tomic J (2005) Vehicle-to-grid power implementation: from stabilizing the grid to supporting large-scale renewable energy. J Power Sources 144(1):280–294
20. Su W, Wang J, Zhang K, Chow M-Y (2012) Framework for investigating the impact of PHEV charging on power distribution and transportation networks. In: 38th annual conference of the IEEE Industrial Electron Society, Montreal, Canada, Oct 2012
21. Green EH, Skerlos SJ, Winebrake JJ (2014) Increasing electric vehicle policy efficiency and effectiveness by reducing mainstream market bias. Energy Policy 65:562–566
22. Bessa RJ, Matos MA (2011) Economic and technical management of an aggregation agent for electric vehicles: a literature survey. European Trans Electr Power 22(3):334–350
23. DeForest N, Funk J, Lorimer A et al (2009) Impact of widespread electric vehicle adoption on the electrical utility business-threats and opportunities. Center for Entrepreneurship and Technology, UC Berkeley
24. Farhangi H (2010) The path of the smart grid. IEEE Power Energy Mag 8(1):18–28
25. Su W, Wang J, Ton D (2013) Smart grid impact on operation and planning of electric energy systems. In: Conejo A, Yan J (ed) Handbook of clean energy systems, Wiley
26. Dimitrakopoulos G, Demestichas P (2010) Intelligent transportation systems. IEEE Veh Technol Mag 5(1):77–84
27. Behr P (2011) M.I.T. panel says a charging infrastructure may be a bigger roadblock for electric vehicles than technology. http://www.scientificamerican.com/article/mit-panel-electric-vehicles/
28. Society of Automotive Engineers (2012) SAE electric vehicle and plug in hybrid electric vehicle conductive coupler (SAE J1772)
29. Society of Automotive Engineers International (2012) SAE ground vehicle standards. http://publicaa.ansi.org/sites/apdl/Documents/Meetings%20and%20Events/EDV%20Workshop/Presentations/Pokrzywa-ANSI-EDV-0411.pdf
30. Electric Transportation Engineering Corporation (2010) Electric vehicle charging infrastructure deployment guidelines for the Oregon I-5 metro areas of Portland, Salem, Corvallis and Eugene. http://www.oregon.gov/ODOT/HWY/OIPP/docs/EVDeployGuidelines3-1.pdf
31. Battelle Energy Alliance (2008) Advanced vehicle testing activity: plug-in hybrid electric vehicle charging infrastructure review. U.S. Department of energy vehicle technologies program
32. Markel T (2010) Plug-in electric vehicle infrastructure: a foundation for electrified transportation. In: MIT transportation electrification symposium, Cambridge, MA
33. Nguyen T-D, Li S, Li W, Mi CC (2014) Feasibility study on bipolar pads for efficient wireless power chargers. In: 2014 twenty-ninth annual IEEE applied power electron conference and exposition (APEC), Fort Worth, TX, Mar 2014
34. Kurs A, Karalis A, Moffatt R, Joannopoulos JD, Fisher P, Soljacic M (2007) Wireless power transfer via strongly coupled magnetic resonances. Science 317:83–86

35. Sample AP, Meyer DA, Smith JR (2011) Analysis, experimental results, and range adaptation of magnetically coupled resonators for wireless power transfer. IEEE Trans Ind Electron 58:544–554
36. Cannon BL, Hoburg JF, Stancil DD, Goldstein SC (2009) Magnetic resonant coupling as a potential means for wireless power transfer to multiple small receivers. IEEE Trans Power Electron 24:1819–1825
37. Kurs A, Moffatt R, Soljacic M (2010) Simultaneous mid-range power transfer to multiple devices. Appl Phys Lett 96:044102–044103
38. Sanghoon C, Yong-Hae K, Kang S-Y, Myung-Lae L, Jong-Moo L, Zyung T (2011) Circuit-model-based analysis of a wireless energy-transfer system via coupled magnetic resonances. IEEE Trans Ind Electron 58:2906–2914
39. Miller JM, Scudiere MB, McKeever JW, White C (2012) Wireless power transfer. In: Oak ridge national laboratory (ORNL)'s power electron symposium. http://web.ornl.gov/adm/partnerships/events/power_electronics/presentations/T2-F-Wireless_Power_Transfer.pdf
40. Groom N (2013) Electric car maker Tesla unveils 90 second battery pack swap. http://www.reuters.com/-article/2013/06/21/us-tesla-swap-idUSBRE95K07H20130621
41. Zheng Y, Dong Z, Xu Y, Meng K, Zhao J, Qiu J (2014) Electric vehicle battery charging/swap stations in distribution systems: comparison study and optimal planning. IEEE Trans Power Syst 29(1):221–229
42. Chen L, Wu M, Xu X (2012) The development and applications of charging/battery swap technologies for EVS. In: 2012 China international conference on electricity distribution (CICED), Shanghai, Sept 2012
43. Liu Y, Hui F, Xu R, Chen T, Li J (2011) Investigation on the construction mode of the charging station and battery-exchange station. In: 2011 Asia-Pacific power and energy engineering conference (APPEEC)
44. Accenture (2011) Plug-in electric vehicles changing perceptions, hedging bets. http://www.accenture.c-om/SiteCollectionDocuments/PDF/Resources/Accenture_Plugin_Electric_Vehicle_Consumer_Perceptions.pdf
45. Dai Q, Cai T, Duan S, Zhao F (2014) Stochastic modeling and forecasting of load demand for electric bus battery-swap station. IEEE Trans Power Deliv 29(4):1909–1917
46. Zheng D, Wen F, Huang J (2012) Optimal planning of battery swap stations. In: 2012 international conference on sustainable power generation and supply (SUPERGEN 2012), Hangzhou, China
47. Sucheski P (2009) CNNMoney.com. http://money.cnn.com/galleries/2009/fortune/0904/gallery.betterplace.fortune/index.html
48. U.S. Department Energy (2010) Communication requirements for smart grid technologies. Washington, DC
49. ZigBee + HomePlug Joint Working Group (undated), Smart energy profile—Marketing requirements document. http://www.homeplug.org/tech/ZBHP_SE_MRD_ 090624.pdf
50. Sauter T, Lobashov M (2011) End-to-end communication architecture for smart grids. IEEE Trans Ind Electron 58(4):1218–1228
51. Gungor V, Sahin D, Kocak T, Ergut S, Buccella C, Cecati C, Hancke G (2011) Smart grid technologies: Communications technologies and standards. IEEE Trans Ind Inform 7(4):529–539
52. Khurana H, Hadley M, Ning L, Frincke DA (2010) Smart-grid security issues. IEEE Secur Priv Mag 8(1):81–85
53. Ericsson GN (2010) Cyber security and power system communication: Essential parts of a smart grid infrastructure. IEEE Trans Power Deliv 25(3):1501–1507
54. Alcaraz C, Lopez J (2010) A security analysis for wireless sensor mesh networks in highly critical systems. IEEE Trans Syst Man Cybern Part C Appl Rev 40(4):419–428
55. Lu Z, Lu X, Wang W, Wang C (2010) Review and evaluation of security threats on the communication networks in the smart grid. In: 2010 military communications conference, San Jose, CA, Nov 2010
56. NIST (National Institute for Standards and Technology) (2001) Advanced Encryption Standard (AES), Standard FIPS PUB 197, Gaithersburg, MD

57. Newman R, Yonge L, Gavette S, Anderson R (2007) HomePlug AV security mechanisms. In: Proceedings of 2007 IEEE international symposium on power line communication and its application, Pisa, Italy, pp 366–371
58. Soyjaudah KMS, Hosany MA, Jamaloodeen A (2004) Design and implementation of Rijndael algorithm for GSM encryption. In: Proceedings of 2004 joint IST workshop mobile future/symposium on trends in communications, pp 106–109
59. Carcano A, Coletta A, Guglielmi M, Masera M, Fovino IN, Trombetta A (2011) A multidimensional critical state analysis for detecting intrusions in SCADA systems. IEEE Trans Ind Inform 7(2):179–186
60. Maciá-Pérez F, Mora-Gimeno F, Marcos-Jorquera D, Gil-Martínez-Abarca JA, Ramos-Morillo H, Lorenzo-Fonseca I (2011) Network intrusion detection system embedded on a smart sensor. IEEE Trans Ind Electron 58(3):722–732
61. McDaniel P, McLaughlin S (2009) Security and privacy challenges in the smart grid. IEEE Secur Priv Mag 7(3):75–77
62. Liu C, Chau KT, Wu D, Gao S (2013) Opportunity and challenges of vehicle-to-home, vehicle-to-vehicle and vehicle-to-grid technologies. In: Proceedings of IEEE 101(11):2409–2427
63. Steen D, Tuan LA, Carlson O, Bertling L (2012) Assessment of electric vehicle charging scenarios based on demographical data. IEEE Trans Smart Grid 3(3):1457–1468
64. Skerlos SJ, Winebrake JJ (2009) Targeting plug-in hybrid electric vehicle policies to increase social benefits. Energy Policy 38(2):705–708
65. Ahman M (2006) Government policy and the development of electric vehicles in Japan. Energy Policy 34(4):433–443
66. Armaroli N, Balzani V (2011) Towards an electricity-powered world. Energy Environ Sci 9:3193–3222
67. Diamond D (2009) The impact of government incentives for hybrid-electric vehicles: evidence from US states. Energy Policy 37(3):972–983
68. Bahn O, Marcy M, Vaillancourt K, Waaub J (2013) Electrification of the Canadian road transportation sector: a 2050 outlook with TIMES-Canada. Energy Policy 62:593–606
69. Beresteanu A, Li S (2011) Gasoline prices, government support, and the demand for hybrid vehicles. Int Econo Rev 52(1):161–182
70. Gardner LM, Duell M, Waller ST (2013) A framework for evaluating the role of electric vehicles in transportation network infrastructure under travel demand variability. Transp Res Part A 49:76–90
71. Wu D, Aliprantis DC (2013) Modeling light-duty plug-in electric vehicles for national energy and transportation planning. Energy Policy 63:419–432
72. Tamor MA, Gearhart C, Soto C (2013) A statistical approach to estimating acceptance of electric vehicles and electrification of personal. Trans Res Part C: Emerging Technol 26:125–134
73. Su W, Zhang K (2014) Investigating the impact of plug-in electric vehicle charging on power distribution systems with the integrated modeling and simulation of transportation network. In: 2014 IEEE transportation electrification conference and expo (Asia-Pacific), Beijing, China, 31 Aug–3 Sept 2014
74. Xu S, Guo Y, Su W (2014) A proof-of-concept demonstration of transportation electrification for smart grid education. In: 2014 IEEE transportation electrification conference and expo (Asia-Pacific), Beijing, China, 31 Aug–3 Sept 2014
75. Su W, Zeng W, Chow M-Y (2012) A digital testbed for a PHEV/PEV enabled parking lot in a smart grid environment. In: The third conference on innovative smart grid technologies (ISGT), Washington, DC, 17–19 January 2012
76. He F, Yin Y, Wang J, Yang Y (2014) Optimal prices of electricity at public charging stations for plug-in electric vehicles. Network and Spatial Economics. doi:10.1007/s11067-013-9212-8
77. Zhang H, Tang W, Hu Z, Song Y, Xu Z, Wang (2014) A Method for Forecasting the Spatial and Temporal Distribution of PEV Charging Load. In: 2014 IEEE power and energy society general meeting, Washington, 27–31 July 2014

78. Taylor J, Maitra A, Alexander M, Brooks D, Duvall M (2010) Evaluations of plug-in electric vehicle distribution system impacts. In: 2010 IEEE power and energy society general meeting, Minneapolis, MN, 25–29 July 2010
79. Taylor J, Maitra A, Alexander M, Brooks D, Duvall M (2009) Evaluation of the impact of plug-in electric vehicle loading on distribution system operations. In: IEEE power & energy society general meeting, Calgary, Alberta, Canada, 26–30 July 2009
80. Darabi Z, Ferdowsi M (2011) Aggregated impact of plug-in hybrid electric vehicles on electricity demand profile. IEEE Trans Sustain Energy 2(4):501–508
81. Jayakrishnan R, Mahmassani HS, Hu T-Y (1994) An evaluation tool for advanced traffic information and management systems in urban network. Transp Res Part C 2(3):129–147
82. Zhou X, Mahmassani HS, Zhang K (2008) Dynamic micro-assignment modeling approach for integrated multimodal urban corridor management. Transp Res Part C 16:167–186
83. EV Charger Map (2014), Map of charging locations in California. http://www.evchargermaps.com/?Address=Anaheim&Want=SPI%20LPI%2-0AVC%20OC&Zoom=9
84. BlinkNet Map (2014), Map of U.S. charging locations. Car Charging Group, Inc
85. ChargePoint (2014), Station map. http://www.chargepoint.net/findstations.php
86. U.S. Department of Energy (2012), Plug-in electric vehicle handbook for public charging station hosts. DOE/GO-102012-3275. http://www.afdc.energy.gov/pdfs/51227.pdf
87. Consumers Energy (2011) Consumers energy's free plug-in electric vehicle charging stations help fulfill customers' increased interest, demand. http://www.consumersenergy.com/News.aspx?id=4760&year=-2011
88. Richardson P, Flynn D, Keane A (2012) Optimal charging of electric vehicles in low-voltage distribution systems. IEEE Trans Power Syst 27(1):268–279
89. Luo Z, Hu Z, Song Y, Xu Z, Lu H (2013) Optimal coordination of plug-in electric vehicles in power grids with cost-benefit analysis—Part I: enabling techniques. IEEE Trans Power Syst 28(4):3546–3555
90. Sortomme E, Hindi MM, Pherson S, Venkata SS (2011) Coordinated charging of plug-in hybrid electric vehicles to minimize distribution system losses. IEEE Trans Smart Grid 2(1):198–205
91. Han S, Han S, Sezaki K (2010) Development of an optimal vehicle-to-grid aggregator for frequency regulation. IEEE Trans Smart Grid 1(1):65–72
92. Qi W, Xu Z, Shen ZM, Hu Z. Song Y (2014) Hierarchical coordinated control of plug-in electric vehicles charging in multi-family dwellings. IEEE Trans Smart Grid 5(3):1465–1474
93. Yao W, Zhao J, Wen F, Xue Y, Ledwich G (2013) A hierarchical decomposition approach for coordinated dispatch of plug-in electric vehicles. IEEE Trans Power Syst 28(3):2768–2778
94. Li Z, Guo Q, Sun H, Xin S, Wang J (2014) A new real-time smart-charging method considering expected electric vehicle fleet connections. IEEE Trans Power Syst 29(6)
95. Zhong J, He L, Li C, Cao Y, Wang J, Fang B, Zeng L, Xiao G (2014) Coordinated control for large-scale EV charging facilities and energy storage devices participating in frequency regulation. Appl Energy 123:253–262
96. Xu S, Feng D, Yan Z, Zhang L, Li N, Jing L, Wang J (2014) Ant-based swarm algorithm for charging coordination of electric vehicles. Int J Distrib Sens Net
97. Qian K, Zhou C, Allan M, Yuan Y (2011) Modeling of load demand due to EV battery charging in distribution systems. IEEE Trans Power Syst 26:802–810
98. Mitra P, Venayagamoorthy GK (2010) Wide area control for improving stability of a power system with plug-in electric vehicles. IET Gener Trans Distrib 4(10):1151–1163
99. Su W, Chow M-Y (2012) Computational intelligence-based energy management for a large-scale PHEV/PEV enabled municipal parking deck. Appl Energy 96:171–182
100. Su W, Chow M-Y (2011) Investigating a large-scale PHEV/PEV parking deck in a smart grid environment. In: The 43rd North American power symposium, Boston, MA, 4–6 Aug 2011

101. Su W, Chow M-Y (2011) Performance evaluation of a PHEV parking station using particle swarm optimization. In: 2011 IEEE power and energy society general meeting, Detroit, MI, 24–29 July 2011
102. Shao S, Zhang T, Pipattanasomporn M, Saifur R (2010) Impact of TOU rates on distribution load shapes in a smart grid with PHEV penetration. In: 2010 IEEE PES transmission and distribution conference and exposition
103. Su W, Chow M-Y (2011) Sensitivity analysis on battery modeling to large-scale PHEV/PEV charging algorithms. In: 37th annual conference of the IEEE industrial electron society (IECON), Melbourne, Australia, 7–10 Nov 2011
104. Su W, Chow M-Y (2011) Evaluation on intelligent energy management system for PHEVs using monte carlo method. In: 4th international conference on electric utility deregulation and restructuring and power technologies, Weihai, China, 6–9 July 2011
105. Su W, Chow M-Y (2010) An intelligent energy management system for charging PHEVs considering demand response. In: 2010 FREEDM annual conference, Tallahassee, FL, May 2010
106. Hamid QR, Barria JA (2013) Distributed recharging rate control for energy demand management of electric vehicles. IEEE Trans Power Syst 28(3):2688–2699
107. Liu H, Hu Z, Song Y, Lin J (2013) Decentralized vehicle-to-grid control for primary frequency regulation considering charging demands. IEEE Trans Power Syst 28(3):3480–3489
108. Ma Z, Callaway D, Hiskens IA (2013) Decentralized charging control of large populations of plug-in electric vehicles. IEEE Trans Control Syst Technol 21(1):67–78
109. Gan L, Topcu U, Low SH (2012) Optimal decentralized protocol for electric vehicle charging. IEEE Trans Power Syst 28(2):940–951
110. SMUD (Sacramento Municipal Utility District) NREL (National Renewable Energy Laboratory), www.nrel.gov/midc/smud_anatolia/
111. MISO (Midwest Independent Transmission System Operator) https://www.misoenergy.org/Pages/Home.aspx
112. Su W, Yuan Z, Chow M-Y (2010) Microgrid planning and operation: solar energy and wind energy. In: 2010 IEEE power and energy society general meeting, Minneapolis, MN, July 25–29, 2010
113. Su W, Wang J, Zhang K, Huang AQ (2014) Model predictive control-based power dispatch for distribution systems considering plug-in electric vehicle uncertainty. Electr Power Syst Res 106:29–35
114. Su W, Wang J (2012) Energy management systems in microgrid operations. Electricity J 25(8):45–60
115. Kempton W, Dhanju A (2006) Electric vehicles with V2G: storage for large-scale wind power. Windtech Int, Bedford
116. Markel T, Kuss M, Denholm P (2009) Communication and control of electric drive vehicles supporting renewables. In: 2009 vehicles power propulsion conference
117. Guille C, Gross G (2010) The integration of PHEV aggregations into a power system with wind resources. In: 2010 bulk power system dynamics and control (iREP) symposium
118. Wang J, Liu C, Ton D, Zhou Y, Kim J, Vyas A (2011) Impact of plug-in hybrid electric vehicles on power systems with demand response and wind power. Energy Policy 39(7):4016–4021
119. Liu C, Wang J, Botterud A, Zhou Y, Vyas A (2012) Assessment of impacts of PHEV charging patterns on wind-thermal scheduling by stochastic unit commitment. IEEE Trans Smart Grid 3(2):675–683
120. Guo Y, Hu J, Su W (2014) Stochastic optimization for economic operation of plug-in electric vehicle charging stations at a municipal parking deck integrated with onsite renewable energy generation. In: 2014 IEEE transportation electrification conference and expo, Dearborn, MI, 15–18 June 2014

121. Guo Y, Liu X, Yan Y, Zhang N, Su W (2014) Economic analysis of plug-in electric vehicle parking deck with dynamic pricing. In: 2014 IEEE power and energy society general meeting, National Harbor, MD, 27–31 July 2014
122. Kempton W, Tomic J (2005) Vehicle-to-grid power fundamentals: calculating capacity and net revenue. J Power Sources 144:268–279
123. Kempton W, Tomic J, Letendre S, Brooks A, Lipmanet T (2001) Vehicle-to-grid power: battery, hybrid, and fuel cell vehicles as resources for distributed electric power in California CARB. CEPA (California Environmental Protection Agency), Los Angeles, CA
124. Kempton W, Letendre SE (1997) Electric vehicles as a new power source for electric utilities. Transp Res Part D Transp Environ 2:157–175
125. Moura T, Moura F (2008) Vehicle-to-grid systems for sustainable development: an integrated energy analysis. Technol Forecasting Social Change 75:1091–1108
126. Sovacool BK, Hirsh RF (2009) Beyond batteries: an examination of the benefits and barriers to plug-in hybrid electric vehicles (PHEVs) and a vehicle-to-grid (V2G) transition. Energy Policy 37:1095–1103
127. DOE (U.S. Department of Energy) (2014) EV everywhere grand challenge. http://energy.gov/sites/prod/fil-es/2014/02/f8/eveverywhere_road_to_success.pdf
128. Biancomano V (2012) Industry grappled with EV battery economics. http://powerelectronics.com/power-electronics-systems/industry-grapples-ev-battery-economics
129. Madawala UK, Thrimawithana DJ (2011) A bidirectional inductive power interface for electric vehicles in V2G systems. IEEE Trans Ind Electron 58(10):4789–4896
130. Quinn C, Zimmerle D, Bradley TH (2010) The effect of communication architecture on the availability, reliability, and economics of plug-in hybrid electric vehicle-to-grid ancillary services. J Power Sources 195:1500–1509
131. Su W, Wang J, Roh J (2013) Stochastic energy scheduling in microgrids with intermittent renewable energy resources. IEEE Trans Smart Grid 5(4):1876–1883

Chapter 4
Testbed Design and Co-simulation of PEV Coordination Schemes Over Integrated Fiber-Wireless Smart Grid Communications Infrastructures

Intissar Harrabi, Taycir Louati, Martin Lévesque and Martin Maier

Abstract It is of great importance to smart grids to build a communications network that can support the future power utility growth, customer connections, and new applications. Relying on advanced communications and broadband access technologies, power utilities are moving towards distribution grid modernization to optimize energy utilization. One significant main concern is the integration of plug-in electric vehicles (PEVs) within smart grids. This chapter provides a comprehensive performance evaluation of PEV coordination strategies over integrated Fiber-Wireless (FiWi) smart grid communications infrastructures using a scaled-down testbed and advanced co-simulator. As the coordination of PEVs was not experimentally demonstrated previously, this chapter describes a smart grid testbed based on a real-world distribution network in Denmark by scaling a 250 kVA, 0.4 kV real low-voltage distribution feeder down to 1 kVA, 0.22 kV. The architecture of the power and communications networks, the scaling-down process, and its main functionalities are described. Furthermore, a novel centralized PEV scheduling and decentralized coordination mechanism is proposed. The obtained experimental results show that the proposed hybrid centralized and decentralized control approach for PEV charging simultaneously takes into account the charging cost, network congestion, and local voltage. Moreover, the coordination between distribution management system (DMS) and sensors is realized in real-time using the developed smart grid testbed (SGT) by the synchronized exchange of power and control signals via a heterogeneous Ethernet-based mesh network. The developed SGT is a step forward to (i) identify practical problems and (ii) validate and test new smart grid mechanisms under realistic physical conditions. However, building such a testbed is time and space consuming. To evaluate large-scale smart grid systems, co- and multi-simulation experiments may be carried out instead. Therefore, the chapter next presents the co-simulation of a power distribution system combined with a

I. Harrabi · T. Louati · M. Lévesque · M. Maier (✉)
Optical Zeitgeist Laboratory, Centre Énergie, Matériaux et Télécommunications,
Institut National de la Recherche Scientifique (INRS), Montréal, QC, Canada
e-mail: maier@emt.inrs.ca

S. Rajakaruna et al. (eds.), *Plug In Electric Vehicles in Smart Grids*,
Power Systems, DOI 10.1007/978-981-287-299-9_4

smart grid communications infrastructure in order to enable real-time exchange of information between PEVs and utilities for the coordination of charging algorithms, which allow PEVs to intelligently consume or send stored power back to the grid (Vehicle-To-Grid capability). Different types of coordinated PEV charging algorithms in a multidisciplinary approach by means of co-simulation of both power and communication perspectives are implemented. A comparison of both centralized and decentralized PEV charging algorithms is drawn in terms of power and communication performance. The integration of photovoltaic solar panels to locally charge PEVs, which plays a major role in limiting the impact of PEV charging on the utility grid and thereby minimizing peak energy demand as well as effectively achieving load balancing, is also investigated.

Keywords Centralized scheduling · Decentralized scheduling · Grid-to-vehicle · Plug-in electric vehicle · Smart grid · Testbed · Vehicle-to-grid

4.1 Introduction

The deployment of plug-in electric vehicles (PEVs) plays a key role in the transformation of today's energy systems towards an emerging low-carbon society. With an electricity-based mobility model, the transportation system becomes more energy efficient compared to conventional internal combustion engines. PEVs enable zero carbon transport when coupled with renewable energy sources (RESs). Consequently, the introduction of PEVs will be integral in realizing modern mobility solutions based on the implications of the emerging Third Industrial Revolution (TIR) economy, recently officially endorsed by the European Commission as the economic growth roadmap toward a competitive low carbon society by 2050. Toward this end, emerging high-capacity fiber-wireless (FiWi) broadband access networks may not only be deployed in the telecommunications sector, but also in other relevant economic sectors, including energy and transport, in order to improve their efficiency and decrease their carbon emissions for a sustainable society.

As a PEV consumes electricity instead of fossil fuel for driving, it can be a double-edged sword because it provides environmental and economic opportunities while posing new challenges to the electric power system with regard to load demand. The increased electricity utilization causes higher demands and puts pressure on existent power grids. According to a recent Annual Energy Outlook report of the U.S. Energy Information Administration, residential electricity demand is forecasted to increase by 24 % within the following several decades and the global electricity consumption is also reported to increase continuously [1].

PEVs will have a huge impact on power systems as they present a significant factor of load growth and create a new demand, which causes problems of congestion and violation of network constraints. Nevertheless, they will play an interesting role in distribution systems as loads as well as power providers [vehicle-to

grid (V2G)], trying to improve profits for owners and system operators. Hence, the challenge is to incorporate new technologies that let us control the grid in a smart way. It's the smart grid technology. It integrates several methods of coordination between different PEVs, which in turn could help avoid network congestion. The integration of PEVs poses several challenges to the operation and management of electric power systems. The convenient charging [grid-to-vehicle (G2V)] and discharging (V2G) is essential to realize the full potential of the electric mobility concept by benefiting from electricity as an economic and clean transportation technology [2]. Furthermore, this approach helps improve voltage regulation and minimize power losses [3]. As a consequence, coordinated PEV charging is instrumental in decreasing operation risks and enhancing power system performance.

This chapter presents an experimental solution to enable the control and coordination of PEV charging via different strategies. The remainder of the chapter is structured as follows. Section 4.2 describes our developed scaled-down smart grid testbed, including its power and communications networks architecture, configuration, and PEV charging scheduling. Section 4.3 evaluates the performance of different types of coordinated PEV charging algorithms implemented over an integrated fiber-wireless smart grid communications infrastructure. Conclusions are drawn in Sect. 4.4.

4.2 Scaled-Down Smart Grid Testbed

The smart grid is a modernized electric grid that uses a communications network to collect information about the power network as well as monitor and supervise it. To investigate new network architecture designs and protocols in a lab environment, a proposed Smart Grid Testbed (SGT) has been implemented. The main objective of the developed architecture and algorithms in this testbed is to optimize the distribution of electricity and its utilization by controlling the charging of PEVs.

In this section, the smart grid testbed architecture and the developed centralized and decentralized PEV scheduling schemes are presented. Furthermore, experimental results showing the performance of the developed testbed are presented and explained.

4.2.1 Scaled-Down Smart Grid Testbed Architecture

The distribution network is composed of 13 nodes, whereby each node represents one or multiple homes. Figure 4.1 shows the details of each node and its major components.

The smart grid network is a combination of power and communication networks, as described in greater detail in the following.

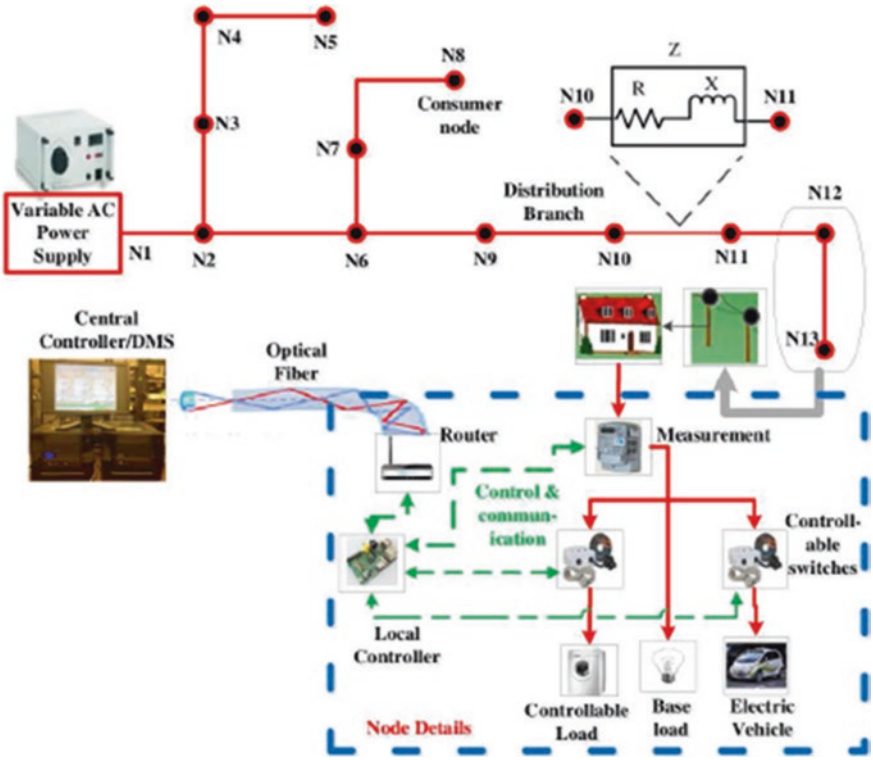

Fig. 4.1 Smart grid network

4.2.1.1 Power Network

In this testbed, two cabinets each composed of 5 stages are used. Figure 4.2a shows all 13 nodes together and Fig. 4.2b depicts the components of a single node.

The components in the power network are as follows: main power supply, batteries, battery chargers, controllable switches, dynamic and discharging loads, and converters (Fig. 4.3).

- Main power supply "Global Specialties 1515": The whole network is powered by a main power supply of type Global Specialties 1515, which is characterized by a wide operating frequency range of 47–450 Hz and a continuous current ratings of 10 and 15 A. This AC source provides an adjustable voltage as needed. In this testbed, the voltage is fixed to 120 V. This power supply is attached to the first node and then the power propagates from one node to another one.
- Battery: The main objective of the smart grid architecture is to optimize the charging and discharging of the batteries, whereby each battery represents a separate electric car. Two different battery capacities are used: 4 and 7 Ah.

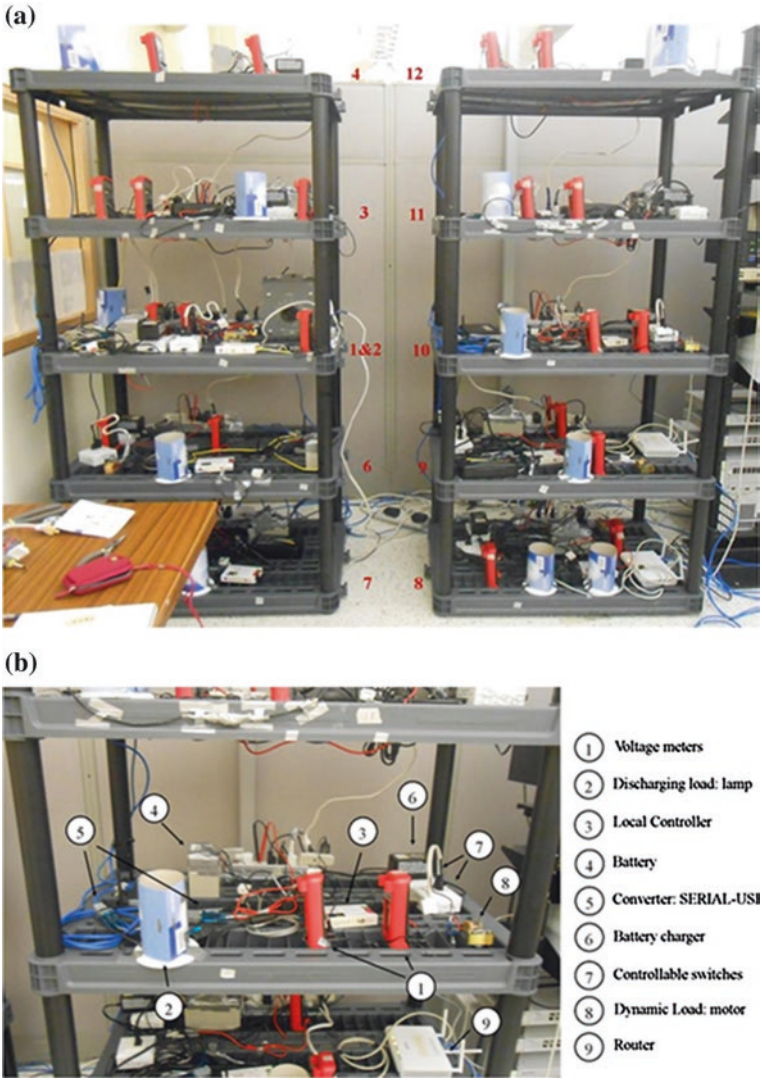

Fig. 4.2 **a** Smart grid nodes, **b** components of a single node

- Battery chargers "Enerwatt 612-900/EWC12-248": The batteries in the nodes are powered by chargers. Chargers of type Enerwatt 612-900, delivering 900 mA (current) at 6 or 12 V (voltage), are used to charge the batteries with a capacity of 4 Ah. At some nodes, a second type of charger is added to the components. We deploy the Enerwatt EWC12-248 to deliver 12 V. It allows the following three charge levels to be selected: 2, 4 and 8 A, which is used to charge batteries with a capacity of 7 Ah. The rationale behind adding the second charger is to change the speed of the charging process.

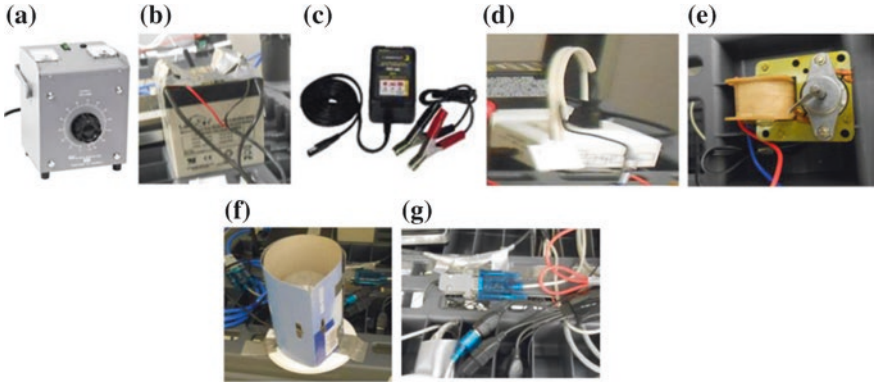

Fig. 4.3 **a** Main power supply, **b** battery, **c** battery charger, **d** controllable switch, **e** controllable load, **f** lamp, **g** converters SERIAL-USB

- Controllable switches "USB Net Power 8800 power controller": As shown in Fig. 4.1, two controllable switches are used at each node. One is used to switch the PEV charger ON/OFF and the other one is used for the motor.
- Controllable loads "0.2 A motor": The base load in the power network varies during the day depending on the consumption of the users and their habits. To account for this time-of-day variation, five controllable loads are installed. The total charge depends on the number of active loads.
- Lamps "25 W incandescent bulbs": An electric car is represented only by its battery, because it's the component which is related to the smart grid network and there is no particular interest in the car itself. To discharge the batteries and thereby emulate PEV travels, lamps are used.
- Converters SERIAL-USB: Between voltage meters and local controllers, serial to USB converters are used to transfer the signal.
- Lines: Due to space constraints in the lab, it was not possible to add real lines between nodes of the architecture. As a consequence, lines are scaled down and characterized only by their resistance and inductance. How to determine the value of these parameters will be explained shortly next.
  The real-world LV distribution feeder fed by a 10/0.4 kV LV transformer substation and owned by the Danish Distribution company SEAS-NVE, hereafter called the actual feeder, is scaled down and implemented in the laboratory. A 13-node 250 kVA, 0.4 kV low voltage distribution feeder is scaled down to 1 kVA, 0.22 kV network. The next subsections explain the scaling down process of lines between nodes and load parameters in more detail.

  – Distribution branch scaling down (SD)
    The realization of the network in the testbed has to adjust to the space limitation in the laboratory. That's why each line between two nodes is characterized by its resistance and reactance, whose values are calculated as follows:

$$R_{act,SD} = R_{PU} \cdot Z_{b,SD} \tag{4.1}$$

$$R_{act,SD} = \left(R_{act} \cdot \frac{V_b^2}{S_b} \right) \cdot \frac{V_{b,SD}^2}{S_{b,SD}} \tag{4.2}$$

where R_{act} and $R_{act,SD}$ denote the resistance value before and after the scaling down; S_b and $S_{b,SD}$ represent the base power before and after SD; V_b and $V_{b,SD}$ denote the base voltage before and after SD; and R_{PU} is the per unit resistance. The results obtained from the calculation of Z_b and $Z_{b,SD}$ are listed in Table 4.1.
Note that in Table 4.1 we have

$$Z_b = \frac{V_b^2}{S_b}. \tag{4.3}$$

– Load SD
To scale down the load at each node, we have

$$S_{i,SD} = S_i \cdot \frac{S_{b,SD}}{S_b}, \tag{4.4}$$

whereby S_i and $S_{i,SD}$ denote the total feeder power before and after SD, respectively.

4.2.1.2 Communication Network

The smart grid communication system in this testbed is based on a Passive Optical Network (PON) that can carry multiple services. The PON consists of three main parts:

- Optical Line Terminal (OLT): It is located at the service provider's central office and allocates dynamically the bandwidth to each active user.
- Optical Network Unit (ONU): It is located near the end users and provides them with a service interface.
- Optical Distribution Network (ODN): It connects the OLT and ONUs by means of optical fibers and splitters.

The PON is a point-to-multipoint optical network, where an OLT located at the central office (CO) is connected to many ONUs at remote nodes through one or multiple optical splitters. The network between the OLT and the ONU is passive,

Table 4.1 Characteristic features of SGT

	Before SD	After SD
S_b	250 kVA	1 kVA
V_b	400 V	208 V
Z_b	0.64	43.264

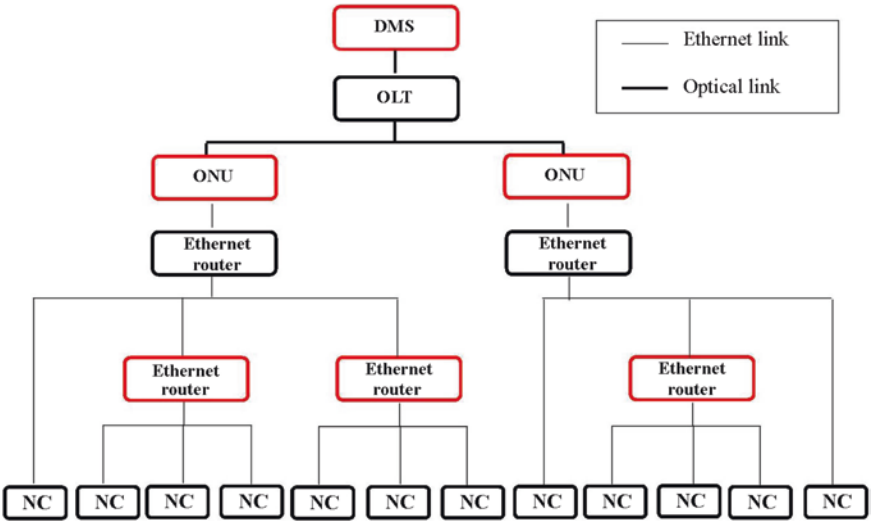

Fig. 4.4 Communication network architecture

i.e., it does not require any power supply. A PON combines the high capacity provided by optical fiber with the low installation and maintenance cost of a passive infrastructure.

In this testbed, an Ethernet PON (EPON) from Sun Telecom GE8100/GE8200 Series with 4 ONUs at a distance of 20 km from the OLT in conjunction with a wireless mesh neighborhood area network (NAN) are used to interconnect the DMS with the different nodes. The communications network architecture used in the smart grid testbed is illustrated in Fig. 4.4, where five Ethernet routers are shared by twelve nodes at different levels.

The OLT provides the interface between the central controller at the DMS and the rest of the network. The ONUs are attached to the two first routers (see Z1 and Z2 in Fig. 4.5). All routers in the architecture have IP addresses, which belong to the same subnetwork. In this testbed, the routers communicate with each other by using Ethernet connections. For illustration, Fig. 4.5 shows the equipment used for the implementation of the EPON.

Nano-computers (NCs) are in permanent connection with the DMS by sending measurements and information about the correspondent node and its state and subsequently receiving control signals. At each node, multiple devices participate in the control process. They collect different types of information and send them to the DMS. When a decision related to the charge and discharge of batteries is made, orders are sent across the communications network and the power network adheres to them.

Figure 4.6 depicts the different devices used in this communications and monitoring network:

- Voltage meters of type TP4000ZC digital meter: Voltage meters are used as sensors to measure the considered system parameters. Since these meters are

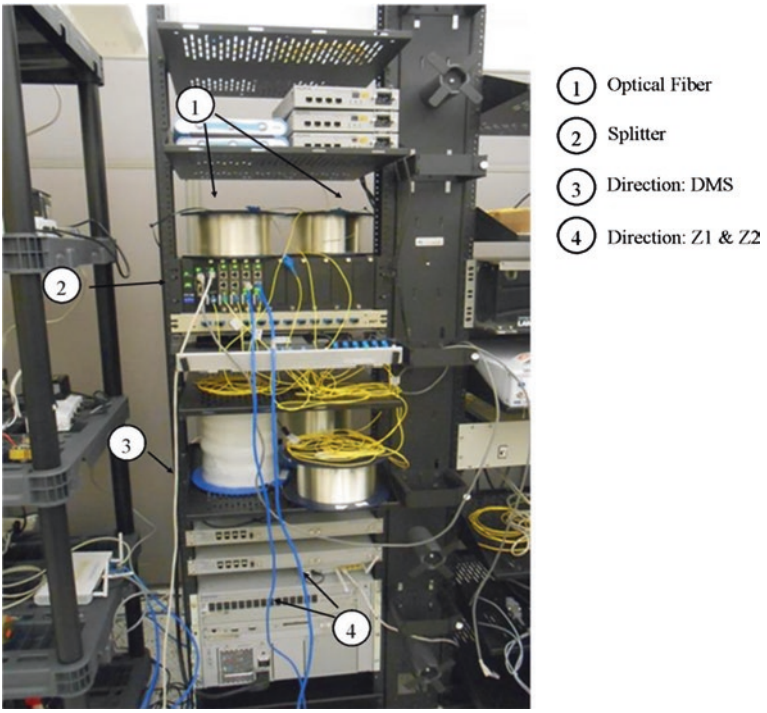

Fig. 4.5 EPON equipment

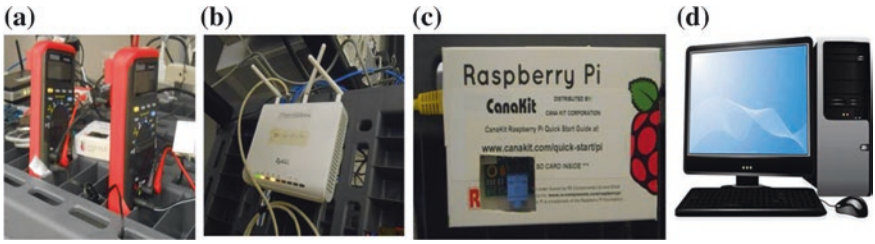

Fig. 4.6 **a** Voltage meters, **b** router, **c** local controller, **d** distribution management system (DMS)

able to measure only one parameter, it is required to use two voltage meters for current (I) and voltage (V). (I) is used to measure the current flowing from the charger to the battery. It is configured in 'AC' if it is connected to a current source like the case of the first node and in 'DC' if it is connected to the charger. (V) is used to measure the node's voltage. It is always configured in 'AC' because it is attached to the power strip.

- Routers: In the communication network, routers are used to ensure the transmission of control signals by selecting the right path. Each router has an IP address and a specific configuration.

- Local controller of type Raspberry Pi model B: It is of high importance to add a local controller to each single node. The controller collects information from the voltage meters about the state of batteries during charging and discharging. Some calculations and decisions are made in these mini PCs, though the more involved ones are made in the DMS. In doing so, local controllers behave like a link between a given node and the DMS.
- Distribution management system (DMS): In the communications network, the most important network element in charge of controlling the entire smart grid testbed is the DMS. It contains algorithms, which control the network and all its network elements. More details on these algorithms will be described shortly.

As already mentioned above, we use an EPON cascaded with a mesh NAN to interconnect the DMS with the local controllers. The data rate of information between DMS and local controllers is equal to 1 Gbps. Given that we deal with a network realized in a small laboratory space, the communication topology is limited to only 4–5 hops.

Moreover, in the communication network reliable packet transport is realized by layer-4 transmission control protocol (TCP) with a round-trip time (RTT) equal to 2 ms. RTT indicates the time required for a signal pulse or packet to travel from a specific source to a specific destination and come back again.

The relation between the NCs and the DMS is a client/server model. Both are developed in Python programming language, which is an interpreted programming language. When instructions are written, they are automatically transcribed to machine language. This language presents several advantages. It is simple to use and portable. So, we don't need to change to code instructions, when we move from one operating system to another one.

In the developed testbed, it is important to note that the DMS and NCs play a major role in control processes, as explained next.

- DMS
  The DMS is responsible for the collection of information about PEVs from NCs. To assure the interrogation, it is of high importance to synchronize this exchange. Toward this end, time is discretized into 40-s slots and the synchronization can be done in two ways. The first approach is to use time based sensors such that measurements are sent from NCs to DMS periodically. The second approach is to use coordinated sensors, where the DMS broadcasts a synchronization message to all NCs. Upon receipt of this message, NCs send their measurements to the DMS.
  Furthermore, the centralized EV scheduling is made in the DMS. The centralized PEV scheduling algorithm is implemented using Matlab. Finally, the DMS provides the user with a real-time graphical interface, showing the status of each node and monitoring the events.
- NCs
  Through the use of NCs nodes are not passive anymore. They participate via the communications network in the charging control process. More precisely, they participate in the centralized PEV scheduling process by receiving

interrogations from the DMS and sending back updated measurements. Each NC reads the two meters belonging to a given node twice per second. NCs also control the ON/OFF switches of the controllable loads.

4.2.2 Coordinated PEV Charging Algorithms

PEVs are getting more popular as a long-term vehicular technology to reduce the dependence on fossil fuel and the emission of greenhouse gases. They present several technical, environmental, and financial advantages. However, due to the high capacity of their batteries, the load in power grids may increase significantly. As a consequence, battery charging control is recommended. One way to tackle this problem is to adopt a smart grid solution that allows PEVs to communicate with the utility, which in turn coordinates their charging activities and regulate their power consumption. In addition, the negative impacts of PEVs on the power grid can be mitigated if the chosen smart grid technology implements charging algorithms.

Actually, the charging of PEVs may not have a significant impact on the power system as the integration of PEVs into the smart grid is limited. However, for PEV numbers expected to increase in the near to mid-term, the charging process may seriously affect the load of the distribution network in terms of peak load, power losses, voltage deviation, etc. Thus, shifting the peak load as well as adopting coordinated PEV charging algorithms by extracting power from both storage batteries and distribution network can solve this problem. Coordinated charging is therefore instrumental in decreasing the operation risks and enhancing the performance of power systems. Possible PEV coordination algorithms can be categorized into the following two subgroups: centralized and decentralized charging strategies.

In the proposed testbed, these two types of control algorithms were developed and combined: a centralized PEV scheduling algorithm and a decentralized local control algorithm. This choice was made to help ensure a more effective control performance. Both algorithms are explained in more detail in the following sections.

4.2.2.1 Centralized PEV Scheduling

With centralized charging strategies, a central operator coordinates the charging process of all customers. The central operator determines when each individual PEV should be charged. Decisions are based only on the system level, e.g., mitigating total losses and feeder congestion, taking into account customer preferences, such as final SOC, permissible charging interval, and charging cost. PEVs can communicate with the central operator in real time and may be charged at different charging rates. The central operator collects information from the connected PEVs while leveraging renewable energy or extra energy sources to charge each PEV by using a specific charging scheduling algorithm. The central operator determines the optimal charging patterns of PEVs by employing power flow studies [4].

The implementation of centralized algorithms requires that the central operator acquire global knowledge about all connected PEVs. As shown in Fig. 4.7, the central operator decides precisely the scheduling of each individual PEV. When a PEV is connected, it sends a G2V/V2G request message to the central operator, containing its node ID, battery SOC, and deadline by when it has to leave home or the charging station. After receiving this message, the central operator performs the coordination algorithm to schedule both the G2V (charging) and V2G (discharging) time slots. Subsequently, the central operator sends back the information containing the corresponding G2V/V2G slots to the connected PEVs. According to the information given in the G2V/V2G response, each PEV follows the specific charging and discharging schedule defined by the central operator according to given PEV requirements, load variability, and power generation.

Previous studies have shown that a centralized charging strategy is able to efficiently mitigate PEVs' detrimental impact on the power grid. In [5, 6], centralized control strategies were used to minimize power loss and load variance as well as maximize load factor and supportable penetration level of PEVs. A centralized infrastructure was required to gather information from all connected PEVs and optimize their charging profiles. However, achieving optimal results using a practical centralized charging algorithm for scenarios with large fleets of PEVs may become impossible. More precisely, centralized optimization increases in size with the number of PEVs connected to the grid and full knowledge of all these connected vehicles is required to achieve optimal results. Clearly, the limitation of a

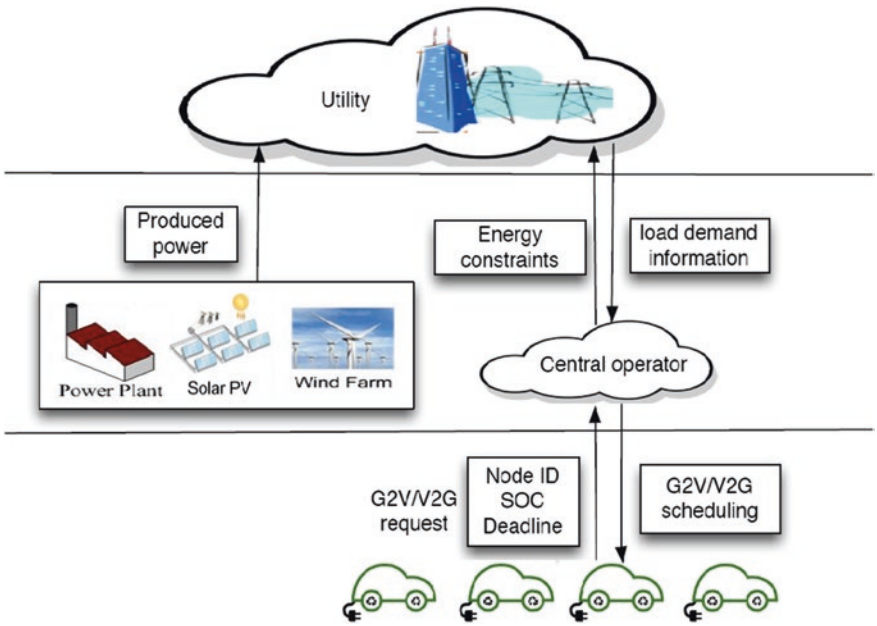

Fig. 4.7 Centralized PEV charging (G2V)/discharging (V2G) approach

centralized approach is therefore its unfeasibility for large fleets of PEVs. Besides, its implementation requires high bandwidth and extensive bidirectional communication. Thus, the implementation is computationally expensive and sometimes even intractable. To avoid this shortcoming, one needs to adopt a decentralized charging strategy to improve the performance for scenarios with high penetration of PEVs.

In the proposed case, the centralized control is realized by the DMS. The DMS collects information from nodes related to each PEV's current state and the whole network state as well. According to this information, it aims at optimally scheduling the charging and discharging of the individual PEVs.

Toward this end, the collection of information and the creation of optimized PEV charging schedules are made in every time slot. In this testbed, the 24 h per day are divided into 96 equal time slots. As the DMS has to optimize the PEV scheduling by minimizing total energy cost, it first has to determine the daily load profile in the network, as illustrated in Fig. 4.8.

To calculate the available feeder margin for each time slot, the DMS uses the following equation:

$$AM_k = FC - FL_k \quad \forall k = 1 : N_{slt}, \tag{4.5}$$

where AM_k, FC, and FL_k denote the available feeder margin, feeder capacity, and actual feeder loading for the kth time slot, given that N_{slt} is the number of time slots.

As shown in Fig. 4.8, the demand of electricity is typically not stable during the day. Since the availability of electricity is not the same, its price may vary as well. Hence, there is a certain hourly electricity price (C_h) for a given time slot price (C_k). C_k together with other variables determine the optimized PEV charging schedules.

The other variables interfering with the slot price are sent by the gird-connected PEVs. More specifically, PEVs send to the DMS information about the current state of charge (SOC_i), plug-in time ($T_{in,i}$), expected plug-out time ($T_{out,i}$), connection point to the network, battery capacity (BC_i), and charger capacity (P_i). Any of this information such as the SOC, charging power, charging current, and local voltage should be updated every single time slot in the DMS. Moreover, PEV owners should mention any unusual travel requirement during the plug-in.

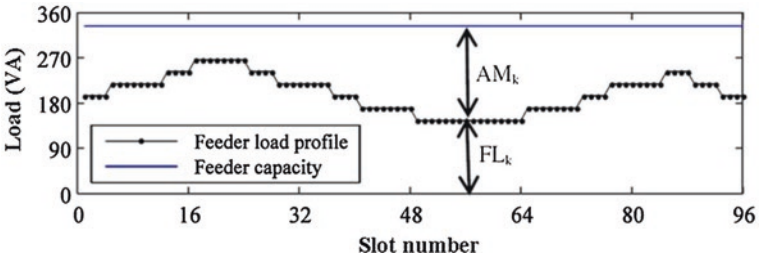

Fig. 4.8 Daily load profile

After the DMS has collected all the aforementioned information, it prepares an optimized PEV charging schedule as follows:

$$\text{Minimize} \sum_{k=Tin}^{Tout} P_{i,k}.x_k.t_k.C_k \tag{4.6}$$

$$\begin{aligned} \text{Subject to} \quad & P_{i,min} < P_i < P_{i,max} && \forall i = 1 : N_{PEV} \\ & P_{i,avg} \leq P_{i,max} && \forall i = 1 : N_{PEV} \\ & SOC_{i,Tout} = SOC_{i,max} && \forall i = 1 : N_{PEV}, \end{aligned} \tag{4.7}$$

where $P_{i,k}$, t_k, x_k, and C_k represent the charging rate, slot duration (in hour), operating state of the PEV, and electricity price for the ith PEV in the kth time slot, respectively. N_{PEV} stands for the number of PEVs. Furthermore, $P_{i,min}$ and $P_{i,max}$ denote the minimum and maximum PEV charging rate, while $P_{i,avg}$ is the average charging rate for the ith PEV to be fully charged by plug-out time T_{out}. Also, $SOC_{i,max}$ corresponds to the maximum permissible SOC of PEV i.

After the optimization in Eq. 4.6, we obtain a solution binary vector x_k, which indicates the state of the PEV. If x_k is equal to 1 the PEV is ON. Otherwise, the PEV changes to OFF.

Note that the above minimization processes operates based on the parameter values sent by each PEV and do not take into account of the overall network characteristics. Thus, it is required to consider the whole network constraints related to all PEVs in order to guarantee an optimal schedule. In this case, Eq. 4.6 is replaced by Eq. 4.8 to satisfy this optimization requirement:

$$\text{Minimize} \sum_{k=1}^{N_{slt}} \left(\sum_{i=1}^{N_{PEV}} (P_{i,k} \cdot x_{i,k}) \cdot t_k \cdot C_k \right) \tag{4.8}$$

$$\text{Subject to} \quad \sum_{i=0}^{N_{PEV}} P_{i,k} \leq AM_k \quad \forall k = 1 : N_{slt} \tag{4.9}$$

The network constraints in Eq. 4.9 help avoid problems related to network congestion. If any of these constraints are violated, the DMS reschedules the charging profile of some PEVs. More precisely, the DMS selects the PEV that has the highest value of $SOC_{F,i}$ as given below in Eq. 4.10, which assigns this PEV a higher charging priority:

$$SOC_{F,i} = \frac{SOC_{i,max} - SOC_i}{SOC_{i,max} - SOC_{i,min}}, \tag{4.10}$$

where SOC_i, $SOC_{i,min}$, and $SOC_{i,max}$ are the current, minimum, and maximum states of charge of the ith PEV, respectively.

The centralized control creates an inter-slot optimization schedule for all PEVs, but only the charging schedule for the next slot is sent to the corresponding PEVs.

Any uncertainties such as load, electricity price, and PEV arrival/departure can be compensated for by periodic optimization of PEV charging in every slot. However, any variations within a time slot (intra-slot) cannot be captured by the centralized control.

The model is solved using a two-stage dynamic programming optimization approach described shortly in Sect. 4.2.2.3.

4.2.2.2 Decentralized Local Control

With decentralized charging strategies, charging decisions are based on given customer preferences and electricity prices. PEVs are able to determine directly their own charging patterns and are allowed to individually choose their charging profile. As shown in Fig. 4.9, in a decentralized approach individual PEVs send a load request to the utility. According to the received information, each PEV defines its own G2V/V2G scheduling by using a smart charging algorithm implemented at the PEV level according to its requirement, electricity tariff, and load demand. Decentralized schemes may be implemented at the vehicle level without the need for a complicated central controller on the grid side. Another advantage is that decentralized algorithms are scalable and typically have a lower degree of

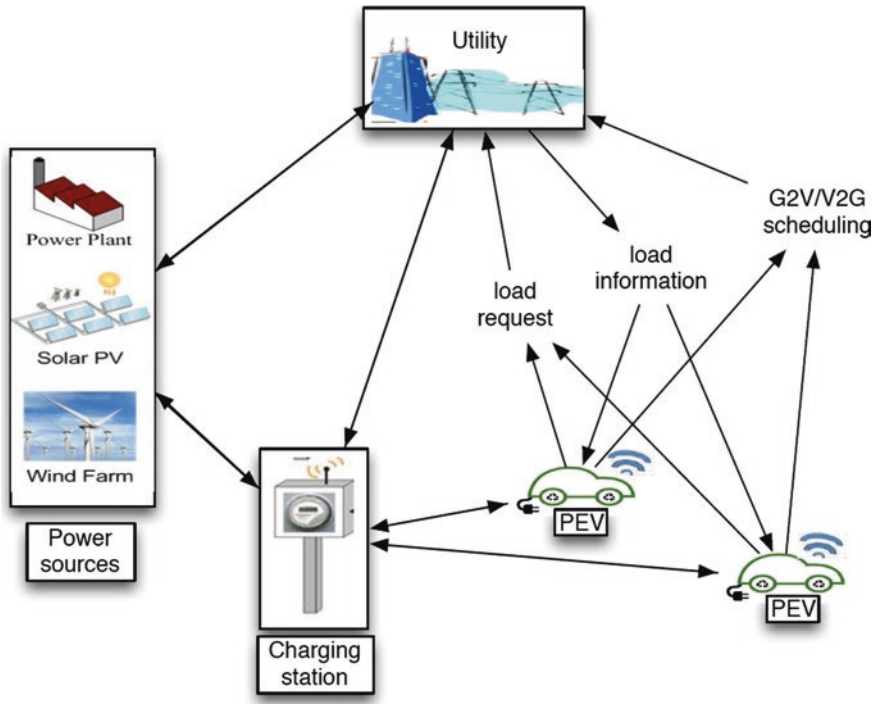

Fig. 4.9 Decentralized PEV charging (G2V)/discharging (V2G) approach

complexity and reduced communications requirements. However, the optimality of a decentralized scheme is nontrivial to achieve due to numerous challenges of the methods utilized to control local charging patterns. Therefore, a decentralized charging approach represents a challenging task and among the few studies dealing with this scheme we briefly highlight the following ones.

In [7], a decentralized algorithm was proposed to solve an optimal power flow charging problem that optimizes jointly both the operation of power grid and PEV charging activity. Each PEV determines its own charging rate following a valley level broadcast received from the utility. The suggested algorithm proved to be optimal in terms of minimizing power loss even when the PEV penetration increases. However, this work considered a time-invariant pricing scheme throughout the charging scheduling period. This is not realistic as electricity prices vary in real time especially when renewable sources are integrated. In fact, electricity prices vary throughout the day. Prices increase and decrease at different times of the day depending on load demand and availability of supply. In [8], a decentralized algorithm was proposed to determine an optimal PEV charging scheduling. According to a control signal broadcast by the utility, individual PEVs update their charging profiles and report them to the utility. The suggested decentralized algorithm proved to iteratively solve the optimal control problem using asynchronous computation. However, this work didn't exploit PEVs as distributed storage resources. Thus, a V2G concept that helps integrate fluctuating energy sources into the power system was not studied. We note that trough V2G capability, the bidirectional power flow between a PEV's battery and the electric power grid is allowed. Note that V2G is able to increase the utilization of intermittent RESs, which increases the flexibility of the electric power network. In [9], a decentralized algorithm was proposed to coordinate autonomous PEV charging based on non-cooperative game theory. The suggested procedure identifies the Nash equilibrium of charging problems for large populations of PEVs. The authors assume that PEVs are cost-minimizing and coupled to each other through a price signal. However, the paper lacks reality since it didn't consider in the sense that non-PEV load is stochastic given that renewable generation is unpredictable, which makes energy supply and demand variable. The variability and uncertainties of renewable resources should be managed carefully by accounting for the charging and discharging capabilities of mobile PEV fleets. In [10], a PEV charging selection concept was studied, which maximizes user convenience levels by selecting a specific subset of connected PEVs. The selection strategy is based on PEVs with less remaining charging time and lower initial SOC, thus giving them higher charging priority. To solve the PEV charging selection problem in a decentralized manner, the authors proposed a distributed optimization problem, where charging decisions are determined locally by each PEV. However, this paper neither considered the V2G concept nor investigated the specific uncertainties of RESs. The appropriate integration of renewables may play a major role in minimizing the peak of energy demand and load balancing as well as saving energy cost and reducing emission when interacting with PEVs. Distributed RES integration and next-generation PEV deployment with V2G capabilities are among the most important solutions to deal with carbon emission increase and energy resource depletion. Moreover, V2G

allows PEVs to help the electric power system mitigate RES variability and minimize the costs of grid operation.

As previously explained, the local control is locally implemented in each PEV. Unlike the centralized PEV scheduling, which is implemented in the DMS, the decentralized control scheme is executed by the local controller. This approach enables the network to adapt to real-time operating conditions. Each local controller decides the status (ON/OFF) of its associated PEV by considering conditions on the node voltage V_N, as given by:

$$\begin{aligned} V_N \leq 0.95 \quad then \quad PEV_{i,N} = OFF \\ V_N > 0.95 \quad then \quad PEV_{i,N} = ON. \end{aligned} \tag{4.11}$$

In this case, two possible problems might occur. The first possible problem happens when a large number of PEVs simultaneously switch ON/OFF leading to voltage oscillation. The second possible problem is that PEVs located at the far end in the feeder are facing more problems compared to the upstream PEVs.

To solve this problem, a random response time between 0 and 10 s is applied at each PEV, which allows the system to avoid simultaneous ON/OFF switching of PEVs. PEVs are also prioritized by the value of their SOC to avoid favoring upstream PEVs.

4.2.2.3 PEV Charging Coordination

Both centralized and decentralized algorithms need to be well coordinated to guarantee appropriate control without violating given limits and constraints. Figure 4.10 shows the coordination between the centralized scheduling control and the decentralized local control of PEVs. This coordination ensures an optimum PEV charging while reducing potential violations.

At the beginning of each time slot, the DMS receives the PEV input data listed in Fig. 4.10, including the SOC, plug-in and plug-out times, as well as the charger and battery capacities. From a central perspective, the DMS next performs a two-stage dynamic programming optimization technique. The first stage considers the PEV level with Eqs. 4.6–4.7. If the feeder limit is not violated, then the computed optimization results can be used to schedule the PEVs. However, if the feeder limit is violated, then the second stage is operated by rescheduling PEVs using Eqs. 4.8–4.10. Finally, once the PEVs receive their schedules and slot starts, the decentralized local control mechanism operates to maintain the voltage within the permissible values.

4.2.3 Results

4.2.3.1 Configuration

After the installation of the require equipment and the implementation of our proposed algorithms, the testbed design has to be tested to verify the performance of

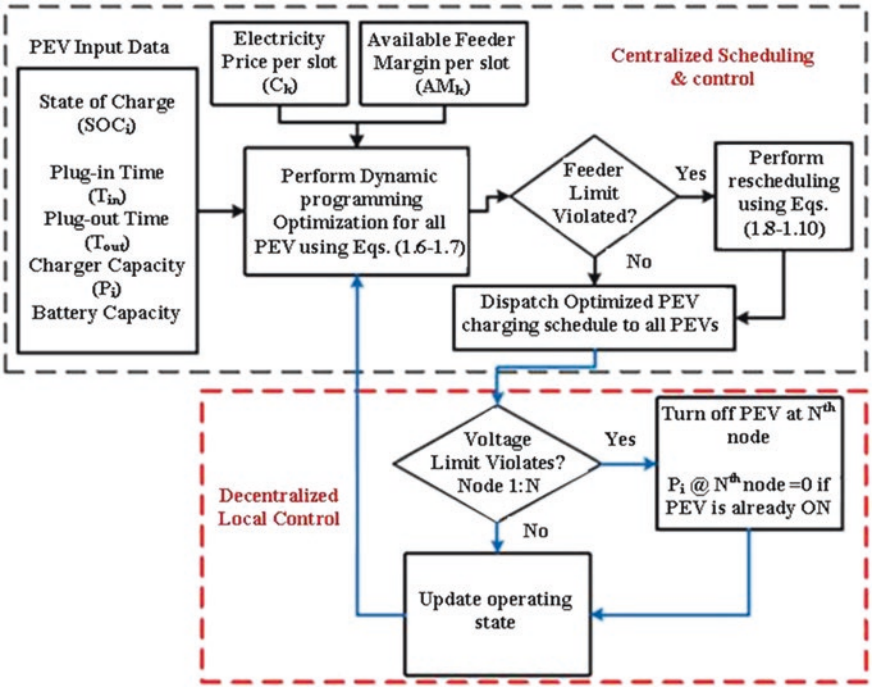

Fig. 4.10 PEV charging coordination

the configuration as well as the optimality of the PEV charging methods. Toward this end, the configuration in the testbed has been done as follows:

- The PEV charging period of 24 h is divided into 15-min time slots. The period starts at noon and lasts until noon of the next day.
- Each 15-min time period is scaled down to 40 s time slots to avoid long running times for each experiment while having sufficient long time slots to have time to save multiple measurements.
- A time factor t_f is used to adjust the parameters. Its value is set to $t_f = 15 \times 60/40 = 22.5$.
- Each PEV is assumed to be available for charging during the whole day at home or office, resulting in an unavailability of PEVs for charging in the same feeder for the whole day. Further, T_{in} and T_{out} are accepted only if the charging period is out of the office hours, as illustrated in Fig. 4.11a. To simplify the experiments, T_{in} and T_{out} are considered constant for each PEV.
- The above configuration along with the corresponding load profile in Fig. 4.8 are used throughout the simulations.
- The electricity price profile used to implement the centralized PEV scheduling is depicted in Fig. 4.11b.

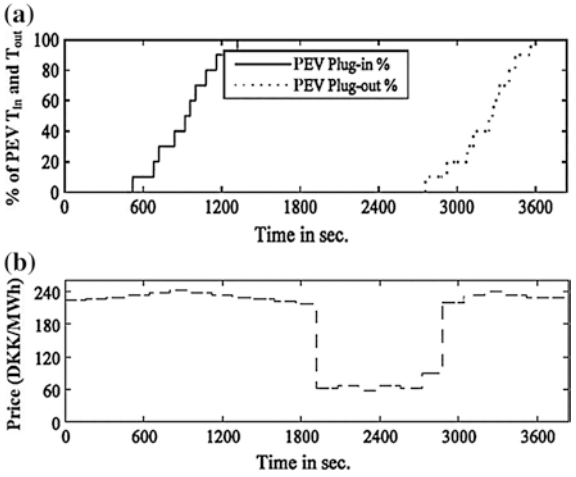

Fig. 4.11 **a** Plug-in and plug-out profile of PEVs, **b** electricity price profile

4.2.3.2 PEV Charging Optimization Results

- Price based optimization
  The electricity cost is a very important factor, which charging algorithms are based on. In this testbed it is of high importance to minimize the total cost of electricity consumption. PEVs are therefore scheduled to be charged at lower price periods. As shown in Fig. 4.12a, the power profile is high between 1,800 and 3,000 s when the electricity price is low (see Fig. 4.11b).
  One possible problem must be kept in mind, namely, the violation of network conditions when all PEVs are ON during the low electricity price period. We observe from Fig. 4.12a that almost 200 VA is demanded between 1,800 and 3,000 s, which in turn causes network congestion. To solve this problem, only small base loads of 12 W are used in the experiments.
- Optimization related to network constraints
  In the optimization, network constraints are required to avoid network congestion. The load profile in Fig. 4.8 is used with a network limit of 300 VA to avoid the violation of the feeder capacity. When the load value is lower than the feeder capacity, the PEV charging profile in Fig. 4.12b follows the electricity price profile. Conversely, when the total charging load is higher than 300 VA, the DMS detects this violation and reschedules the PEV charging in order to not only decrease the PEV charging power but also remain below the feeder capacity limit. In this case, the charging cost increases by almost 27.8 % compared to the proposed price-based optimization. This increase is due to the deviation of PEV charging schedules from the optimal ones, following the violation of network limits. Moreover, in this testbed, the charger efficiency is underestimated and the feeder losses are not considered. That's the reason that the feeder load in Fig. 4.12b is a little bit higher than 300 VA.

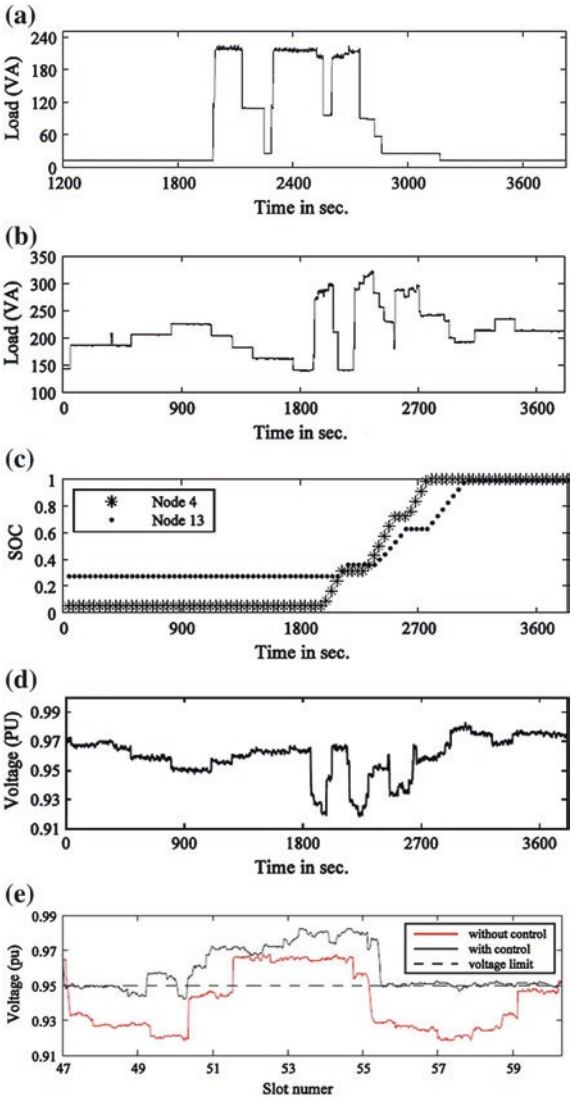

Fig. 4.12 **a** Optimized PEV charging power profile, **b** PEV charging power profile, **c** SOC of batteries at *node 4* and *13*, **d** voltage profile of *node 13*, **e** voltage profile of node with local voltage control

As already mentioned above, two types of charger with different charging speeds were used. The first charger 'Enerwatt 612-900' is slower than the second one 'Enerwatt EWC12-248'. Among others, Enerwatt 612-900 is used at node 13 while Enerwatt EWC12-248 is used at node 4. Figure 4.12c shows the SOC of PEV batteries at nodes 4 and 13, whereby SOC corresponds to the charging level; SOC = 0.5 means the battery is half charged. We notice that the PEV at node 4 is charged faster than the one at node 13. In Fig. 4.12d, we observe that the voltage of node 13 exceeds the threshold limit of 95 % during lower price periods, when most PEVs are scheduled for charging. Thus, despite the optimization and local control, it is possible to exceed the threshold limit.

- Local voltage based optimization
  To avoid the violation of the network constraints, a local voltage control was integrated in the smart grid testbed. To illustrate the impact of this control on the voltage profile, the voltage profiles at node 13 (with and without control) are depicted in Fig. 4.12e. This figure shows that the voltage control is able to minimize the violation of the limit. Hence, the local control represents an effective means to adopt real-time conditions to the voltage control.

4.2.3.3 Communication and Computation Complexity

To evaluate the performance of the optimization algorithm, we show its computation duration in Fig. 4.13a. The computation time is given by:

$$CT = |t_c - t_r|, \tag{4.12}$$

where CT, t_c, and t_r denote the computation time, the time when the optimization function is called, and the time when the optimized schedule is received, respectively.

Figure 4.13a shows that the computation duration decreases for an increasing slot number. We note that the computation time increases slightly in some time slots. This is due to the rescheduling of PEV charging in the event of network violations.

To choose the right method of synchronization, a comparative study between time based sensors and coordinated sensors is conducted. For this comparison, the average time interval between received measurements for one time slot is calculated as follows:

$$\Delta_m = \frac{1}{|M_s| \cdot (|M_s| - 1)} \cdot \sum_{i \in M_s} \sum_{j \in M_s - \{i\}} |t_i - t_j|, \tag{4.13}$$

where M_s are the measurements received by the DMS in slot s.

Figure 4.13b depicts Δm for the two different types of sensor, whereby measurements are sent every second. Note that Δ_m should be minimized in order to compare the two types of sensors. As shown in Fig. 4.13b, we note that the use of coordinated sensors yields a better performance than time-based sensors.

Next, the well-known Wireshark packet analyzer is used to measure the traffic profile. The obtained results are illustrated in Fig. 4.13c. The first small peak between 0 and 20 s indicates the connection of NCs to the DMS for the first registration. In each time slot there is a peak transmission rate of 450 Kbps, which indicates the interrogations between DMS and NCs. To decrease this peak, the transmission of one TCP message per NC can be replaced with broadcast messages.

The building of such a real-world testbed is time and space consuming. To evaluate large-scale smart grid systems, co- and multi-simulation experiments can be carried out instead. Therefore, the co-simulation of coordinated PEV charging algorithms over a smart grid communications infrastructure is studied next.

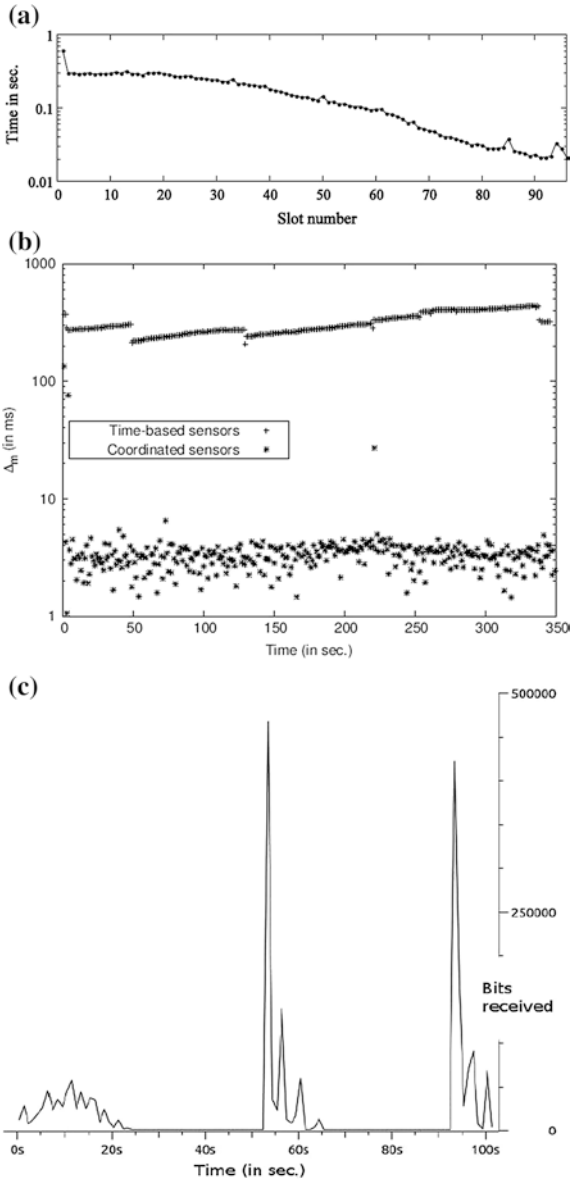

Fig. 4.13 **a** Computation duration of the optimization process, **b** synchronization performance of time-based and coordinated sensors, **c** communications traffic captured at the DMS port to/from the OLT

4.3 Co-simulation of Coordinated PEV Charging Algorithms

This section investigates different scenarios for centralized and decentralized PEV charging algorithms in a multidisciplinary manner by means of analysis and powerful co-simulation of both power and communication perspectives. Toward this

end, there is a strong need to match the requirements of a bidirectional smart grid communications infrastructure that enables the data exchange of sensor and control signals between utility and PEV operators in order to perform the simulation and implementation of centralized and decentralized charging algorithms. We use an integrated fiber-wireless (FiWi) smart grid communications infrastructure, whose architecture and operation principles have recently introduced in [11]. As shown in Fig. 4.14, the FiWi smart grid infrastructure is used to exchange information between PEVs and the DMS in order to coordinate V2G/G2V scheduling. The FiWi smart grid communications infrastructure is based on an IEEE 802.3ah Ethernet passive optical network (EPON) for urban areas with high population density and an IEEE 802.16 WiMAX for rural areas with low population density

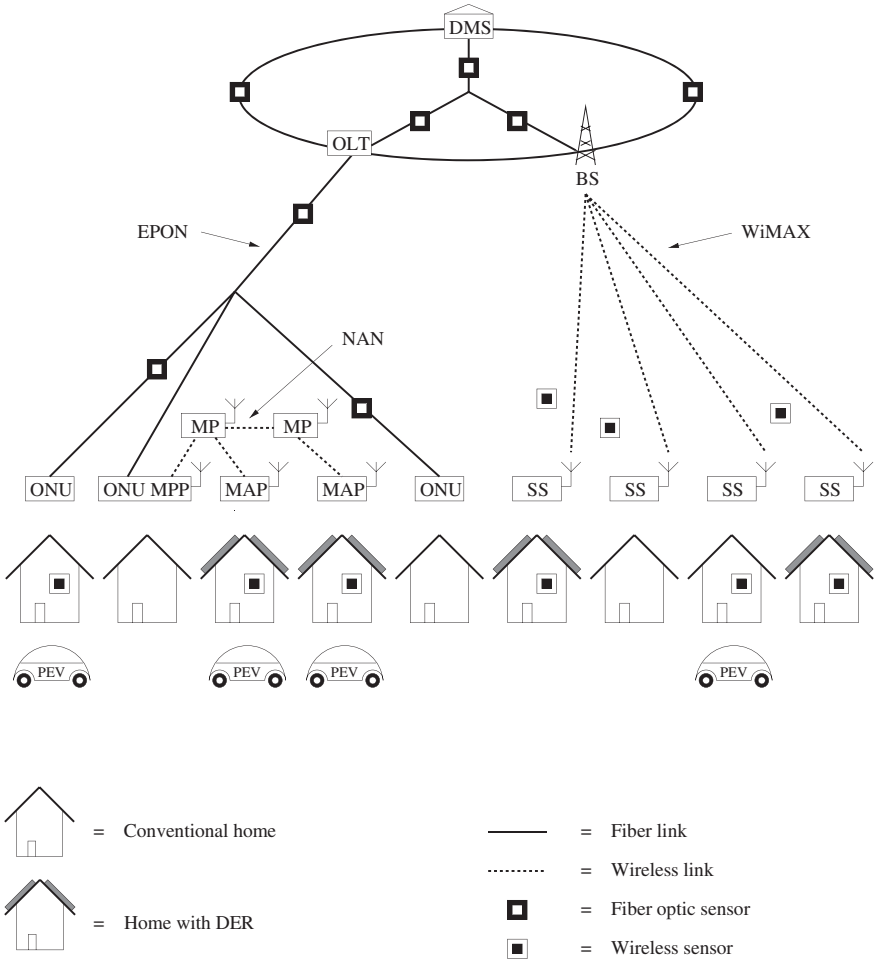

Fig. 4.14 Fiber-wireless (FiWi) smart grid communications infrastructure

Table 4.2 Parameters and default values

Variable	Value
Load profile	RELOAD database [14]
PEV	Nissan LEAF 2012 [15]
Battery full capacity	24 kWh (100 miles)
Battery used capacity	18 kWh (70 miles)
Driving efficiency	0.26 kWh/mile
Charging level	Level 1 of 1.44 kW (120 V/12 A)
Deadline/arrival time and daily trip (miles)	Distributions extracted from NHTS [16]

as a complementary solution deployed where fiber is not available. The communications from the PEV to the DMS is established as follows:

- Each PEV connects to the EPON optical line terminal (OLT) via optical network units (ONUs) and to a WiMAX base station (BS) via subscriber stations (SSs).
- The PEV and the ONU communicate via the wireless mesh network through the mesh portal point (MPP) collocated at the ONU to aggregate sensor data, mesh access points (MAPs), and mesh points (MPs) that relay packets between the MPP and MAPs.
- ONUs are distributed uniformly to cover the entire distribution network, whereby each ONU is equipped with a collocated MPP. The ONU operates at a data rate of 1 Gbps.

To implement the co-simulator from both communication and power perspectives, both the open source simulation framework OMNeT++ [12] for communications and the OpenDSS [13] for load flow analysis are used. Table 4.2 summarizes the parameters and assumptions used throughout the simulations.

4.3.1 G2V/V2G Scheduling Algorithms

The main objective of coordinated centralized and decentralized PEV charging algorithms is to flatten the aggregated demand profile by shaping the PEV load. In the following, we present the developed coordinated PEV charging algorithms implemented for different scenarios in order to improve the communication and power performance.

- Centralized integrated V2G/G2V coordination algorithm (IntVGR)
  The recent work in [17] proposed an integrated centralized charging algorithm called 'IntVGR.' The centralized IntVGR reduces the total losses while filling the valley when home G2V scheduling (PEV charging) is required. It also aims at shaving the peak of load by coordinating home V2G scheduling and aggregating PEVs to send energy back to the grid (PEV discharging). Moreover, IntVGR attempts to maximize the utilization of locally generated solar power when RES units are available at the workplace. When there is a shortage of renewable energy generation, charging of PEVs can be postponed to time slots when

renewable energy becomes available. This allows avoiding higher electricity prices and helps the overall charging profile at the parking match the RES output profile. As illustrated in Fig. 4.7, PEVs follow the charging schedule calculated by the central operator after sending a G2V/V2G request. At work, PEVs are charged during the parking period according to the intelligent IntVGR coordination scheme, which maximizes PEV charging from RESs. At home, the central operator (i.e., the DMS in our case) performs the home charging of our IntVGR algorithm to find both G2V and V2G slots. When receiving the G2V/V2G response, the connected PEV follows the specific V2G and/or G2V schedule.

- Real-time decentralized vehicle/grid coordination algorithm (RT-DVG)
  Unlike the centralized IntVGR, in the developed real-time decentralized vehicle to grid (RT-DVG) algorithm, each PEV dispatches its own schedule by exchanging information with the utility (see also Fig. 4.9). The decentralized RT-DVG aims at reducing the peak load and flattening the power-time curve. The RT-DVG algorithm is implemented at the PEV level and each PEV determines its optimal schedule according to the base load sent by the utility as well as the required charging hours. The RT-DVG coordination scheme is based on a real-time information exchange and functional optimization, whereby decisions are driven by actions according to the grid state advisory signals sent by the utility. Three types of state advisory signal are used: green signal (off-peak system, PEV charging is required), yellow signal (mid-peak system, PEV charging can be delayed), and red signal (on-peak system, V2G is required and PEV charging should be postponed if possible). In addition, a workplace charging scenario (RT-DVG/RES) is considered to maximize the usage of power generated from PV solar panels installed at the car parks and to limit the impact of PEV charging on the power grid. At the workplace, RT-DVG/RES allows PEVs to schedule charging (G2V) and discharging (V2G) slots while maximizing the usage of locally generated renewable energy, if available.

4.3.2 Power Results

Figure 4.15a–e shows the power network performance of the coordinated algorithms mentioned above (IntVGR and RT-DVG) for a summer load profile and a PEV penetration level of 40 %. We note that both centralized and decentralized algorithms lead to a flattened demand curve and a decrease of the peak of the base load. As shown in Fig. 4.15a, the centralized IntVGR shows higher peaks and deeper valleys occur more frequently compared to the decentralized algorithm RT-DVG. Thus, the decentralized RT-DVG outperforms the centralized IntVGR in terms of peak shaving during the whole day. The performance is further improved by integrating RESs to locally charge PEVs at workplaces, as depicted in Fig. 4.15b. For instance, by leveraging coordinated workplace charging from PV solar panels IntVGR/RES and RT-DVG/RES behave similarly during the time period from 6 a.m. to 2 p.m., when locally generated solar energy satisfies the PEVs' power demand. Whereas from

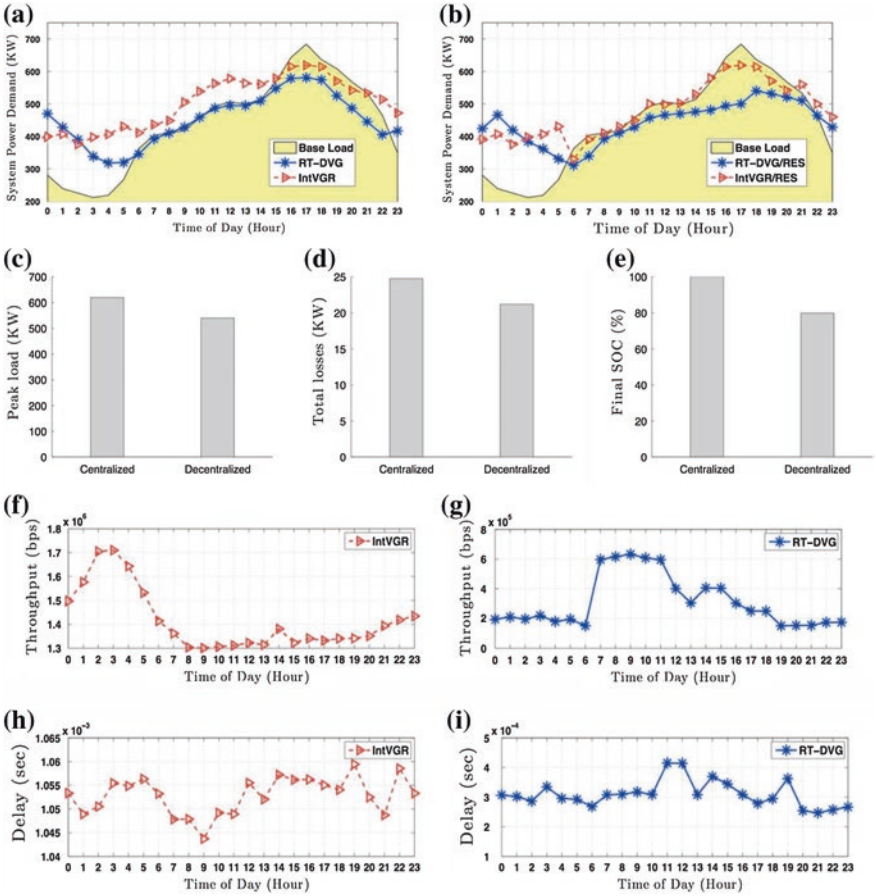

Fig. 4.15 Power and communication network performance for centralized and decentralized PEV charging algorithms

3 p.m. to 6 a.m., coordinated charging using the decentralized algorithm RT-DVG/RES yields a lower power demand than that achieved with the centralized algorithm IntVGR/RES. We also observe that peak shaving in the afternoon seems to be more efficient when considering RES at the workplace for both algorithms. We can therefore conclude that a PEV at workplace stores solar energy and returns it to the grid (V2G mode), resulting in an improved peak reduction. Furthermore, we observe from Fig. 4.15c that by using the decentralized algorithm peak shaving is more pronounced than with the centralized algorithm: RT-DVG/RES has a peak load of 540.16 versus 619.26 kW for IntVGR/RES. Moreover, the decentralized algorithm exhibits a significant improvement in minimizing total losses during peak times compared to the centralized algorithm. The total losses are reduced from 24.47 kW with IntVGR/RES to 21.22 kW with RT-DVG/RES, translating into a 13 % loss reduction, as depicted in Fig. 4.15d.

In summary, by comparing the power performance between centralized and decentralized algorithms via simulation, we observed that the decentralized algorithm is superior in terms of load flattening to the centralized algorithm. Interestingly, the decentralized algorithm leads to a lower power demand and smaller total losses as compared to the centralized algorithm, which demonstrates its effectiveness to limit the stress on the grid. However, it is important to emphasize that the centralized algorithm proves to be more efficient in terms of battery degradation by guaranteeing a satisfactory final SOC of 100 versus 80 % achieved by the decentralized algorithm (see Fig. 4.15e). We can therefore conclude that decentralized algorithms can be implemented locally and provide good power performance in terms of peak reduction and lower degree of complexity, while centralized algorithms require full knowledge to achieve optimal results and guarantee customer satisfaction. We also note that the integration of RESs throughout the smart microgrid plays a major role in limiting the impact of PEV charging on the utility grid and minimizing the peak of energy demand.

4.3.3 Communication Results

To examine the performance of the FiWi smart grid communications infrastructure of Fig. 4.14, we investigate the upstream throughput and delay for a PEV penetration level (PL) of 40 % for the developed centralized and decentralized algorithms in order to evaluate the achievable performance gain from a communication point of view. As shown in Fig. 4.15f, with the centralized algorithm (IntVGR) the throughput reaches its maximum during off-peak hours (from 9 p.m. to 7 a.m.). Afterwards, it remains nearly constant as it is the time when drivers leave home for work. With the decentralized algorithm, throughput starts increasing from 7 a.m. to 3 p.m. when PEVs arrive at work and start exchanging requests with the DMS to coordinate their scheduling G2V and V2G slots, as depicted in Fig. 4.15g. We note that the centralized algorithm requires a maximum throughput of 1.7 Mbps for a PL of 40 %, whereas the maximum throughput of the decentralized algorithm equals 0.63 Mbps. We conclude that the high bandwidth requirement of the centralized algorithm is due to the excessive exchange of packets per second. In contrast, in the decentralized scheme, information between PEVs and the DMS needs to be interchanged only once per hour.

Figure 4.15h, i illustrates the delay of packets sent between PEVs and the DMS for the decentralized and centralized algorithms. We observe that the decentralized algorithm outperforms the centralized one in terms of delay reduction. For instance, the centralized algorithm achieves a maximum delay of nearly 1 ms, whereas the decentralized algorithm is able to lower the maximum delay to 0.41 ms, translating into a 50 % decrease of end-to-end delay. This decrease in delay is a result of the reduced frequency of packet exchanges and number of packet types. In fact, packets interchanged between the PEVs and utility are different for decentralized algorithms from those of centralized algorithms and are

modified in size, content, and count. For instance, in our centralized co-simulator, 6 types of packet are used for each connected PEV, whereas in the decentralized case only 3 types of packet are needed with less encapsulated data and at lower exchange rates. More specifically, during each simulation cycle the following packets need to be exchanged:

- With centralized PEV charging algorithms:
  - Charging request packet: each connected PEV sends a packet containing its node ID, deadline, battery SOC, and travel distance.
  - Charging response packet: the central operator sends back the appropriate G2V/V2G slots to each PEV following a specific scheduling algorithm.
  - SOC notification: each PEV sends a notification packet indicating its SOC after charging according to the received schedule.
  - Node notification: a message that contains the distribution node, load, and voltage is sent periodically.
  - Substation notification: a substation has to send its node, total power load, and overall power losses to the central operator.
  - Control message: the central operator sends PEVs messages to control the distribution network.
- With decentralized PEV charging algorithm:
  - Charging request packet: when a connected PEV is ready to begin charging it sends a charging request packet to initiate the scheduling process.
  - Charging response packet: the DMS receives the charging request and sends back another packet containing the load advisory signals for the period between the PEV arrival and deadline time.
  - PEV control message packet: the DMS sends control messages to the PEVs in case of voltage deviations.

4.4 Conclusions

This chapter described a smart grid testbed realized in the Optical Zeitgeist Laboratory. The major challenge was to build a whole smart grid network similar to networks in reality in a small lab space. We described the smart grid testbed based on a real-world distribution network in Denmark by scaling a 250 kVA, 0.4 kV real low-voltage distribution feeder down to 1 kVA, 0.22 kV. The architecture of the underlying power network and its scaling down was described. Next, we explained the architecture of communications network and described its important functionalities. The details about control and coordination strategies of PEV charging were discussed in depth. A novel centralized PEV scheduling and decentralized coordination mechanisms were proposed. The obtained experimental results showed that charging cost, network congestion, and local voltage are taken into account in the centralized and decentralized control approaches for PEV

charging. Moreover, coordinated sensors were used to synchronize the exchange between the DMS and sensors.

In a next step, the performance of centralized and decentralized PEV charging algorithms from both power and communication perspectives was evaluated by combining a power distribution system with a smart grid communications infrastructure. Given that the electrification of transportation is a progressive undertaking, the obtained results suggest that the adoption of a centralized charging algorithm optimizes the charging profile based on global knowledge about all connected PEVs. Further, the adoption of a coordinated decentralized PEV charging algorithm was shown to be more effective and yield a superior communication and power performance than that obtained with a centralized scheme. Further improvement was achieved through the integration of photovoltaic solar panels to locally charge PEVs. The presented results showed a significant peak energy demand reduction, thereby limiting the impact of PEV charging on the power grid.

References

1. Erol-Kantarci M et al (2011) Wireless sensor networks for cost-efficient residential energy management in the smart grid. IEEE Trans Smart Grid 2(2):314–325
2. Akhavan-Rezai E et al (2012) Uncoordinated charging impacts of electric vehicles on electric distribution grids: normal and fast charging comparison. Paper presented at the IEEE power and energy society general meeting, San Diego, July, pp 1–7
3. Xu Z et al (2012) Coordinated charging strategy for PEVs charging stations. Paper presented at the IEEE power and energy society general meeting, San Diego, Jul 2012, pp 1–8
4. Moeini-Aghtaie M et al (2013) PHEVs centralized/decentralized charging control mechanisms: requirements and impacts. Paper presented at the IEEE North American power symposium, Manhattan, Sept 2013, pp 1–6
5. Clement K et al (2009) Coordinated charging of multiple plug-in hybrid electric vehicles in residential distribution grids. Paper presented at the IEEE/PES power systems conference and exposition, Seattle, Mar 2009, pp 1–7
6. Sortomme E et al (2011) Coordinated charging of plug-in hybrid electric vehicles to minimize distribution system losses. IEEE Trans Smart Grid 2(1):198–205
7. Chen N et al (2012) Optimal charging of electric vehicles in smart grid: characterization and valley-filling algorithms. Paper presented at the IEEE smart grid communications, Tainan, Nov 2012, pp 13–18
8. Gan L et al (2013) Optimal decentralized protocol for electric vehicle charging. IEEE Trans Power Syst 28(2):940–951
9. Ma Z et al (2013) Decentralized charging control of large populations of plug-in electric vehicles. IEEE Trans Control Syst Technol 21(1):67–78
10. Wen CK et al (2012) Decentralized plug-in electric vehicle charging selection algorithm in power systems. IEEE Trans Smart Grid 3(4):1779–1789
11. Maier M et al (2012) NG-PONs 1&2 and beyond: the dawn of the Über-FiWi network. IEEE Netw 26(2):15–21
12. OMNET++ simulator (2014) http://www.omnetpp.org/. Accessed 25 Jul 2014
13. OpenDSS power flow calculator (2014) http://sourceforge.net/projects/electricdss/, http://sourceforge.net/projects/electricdss/. Accessed 25 Jul 2014
14. RELOAD Database Documentation and Evaluation and Use in NEMS (2014) http://www.onlocationinc.com/LoadShapesReload2001.pdf. Accessed 25 Jul 2014

15. LEAF's manual (2014) http://www.nissanusa.com/leaf-electric-car. Accessed 25 Jul 2014
16. National Household Travel Survey (2014) http://nhts.ornl.gov/. Accessed 25 Jul 2014
17. Xu DQ et al (2013) Integrated V2G, G2V, and renewable energy sources coordination over a converged fiber-wireless broadband access network. IEEE Trans Smart Grid 4(3):1381–1390

Chapter 5
Cyber Security of Plug-in Electric Vehicles in Smart Grids: Application of Intrusion Detection Methods

Sajjad Abedi, Ata Arvani and Reza Jamalzadeh

Abstract With emerging penetration of Plug-in Electric Vehicles (PEVs) into smart grids, system operators face new challenges regarding the system security. The security involves all parties in the energy system, because PEVs are not only considered as loads, but also as demand response or distributed energy resources, with bidirectional power flow into the distribution network. Furthermore, due to the random time, amount and location of the PEVs utilization, their behavior is inherently uncertain. In this context, monitoring and control of PEVs utilization necessitate the real-time data communication with control centers throughout the smart grid. The security and reliability of power system will be dependent on how the PEVs data are collected and managed. Hence, assuring data confidentiality, integrity and availability are significant parts of PEV-integrated cyber-physical systems (CPS). This chapter aims at exploring the cyber security issues of PEVs in the smart grid and review some of the state-of-the-art analysis methods to detect the cyber-attacks. We study the model-based and signal-based intrusion detection methods to detect any anomalies, followed by a specific application to PEVs false data injection in the smart grid. The chi-square test and discrete wavelet transform (DWT) are used for anomaly detection.

5.1 Introduction

The PEVs fleet in the US is anticipated to grow rapidly in the near future, with the current estimates of a million or more PEVs on the road by 2016 and more than 10 million by 2030 [1]. Such large-scale deployment of PEVs introduces several technical challenges, such as imposing significant uncertain load to the distribution

S. Abedi (✉) · A. Arvani · R. Jamalzadeh
Smart Grid Energy Center, Texas Tech University, Lubbock, TX 79409, USA
e-mail: s.abedi@ieee.org

A. Arvani
e-mail: ata.arvani@ttu.edu

S. Rajakaruna et al. (eds.), *Plug In Electric Vehicles in Smart Grids*,
Power Systems, DOI 10.1007/978-981-287-299-9_5

network, reliable communication network needs, cyber security issues, as well as the quality and stability of the overall distribution system. By penetration of large, distributed, and mobile PEVs fleet, secure and trustworthy communications and control systems are required to meet the needs of many stakeholders: vehicle owners, utilities, system operators, private parties operating charging stations, and ancillary service providers.

Several studies have been conducted regarding the different technical aspects of PEVs integration and their influence on the smart grid [2]. The related works regarding consumption-side aspects focus on charging and control strategies, battery or gird interface technologies, and design of smart parks [3–6]. The utility-side aspects of PEVs integration such as energy management issues, demand response services, power losses, voltage and frequency regulation, and participation in electricity markets are also covered in some other studies [7–9]. The study in [10] explored and compared the deterministic and aggregative communication structures based on the reliability and availability of PEVs for ancillary services provisions. The study by Matta et al. [11] presented an aggregative communication architecture for PEV communications that uses an agent-based model to allow cooperation, negotiation and trading mechanisms within the PEVs network.

Although many studies such as [12–14] have been conducted on the cyber security in the wider area of smart grids, so far, the literature lacks considerable studies with the aim to address the potential cyber security problems raised with the development of PEVs. The only few available references has focused on identifying the security problems and to a lesser extent towards presenting solutions. Chaudhry et al. [15] discussed the security issues of PEVs as distributed nodes in a data communication network and reviewed some of the potential vulnerabilities in the PEVs infrastructure. Hoppe et al. [16, 17] studied the sniffing/replay attacks on controller area network (CAN) buses deployed to in-vehicle networks as well as some short-term countermeasures. The PEV security with respect to the architectural security features, intrusion detection systems (IDS), and threats and attacks particularly for the in-vehicle network have been surveyed [18].

Cyber security of PEV-integrated smart grid is an important requirement for maintaining the integrity of distribution system. False Data Injection Attack (FDIA), data manipulation, and Advanced Metering Infrastructure (AMI) tampering can cause detrimental problems. As a countermeasure to these problems, the Intrusion Detection Methods (IDM) are utilized to analyze the measurement data to detect any possible cyber-attacks on the operation of smart grid systems [19].

In general, there are two methods to detect malicious data: (i) Anomaly detection, (ii) Misuse detection [20]. Anomaly detection is used to detect any activity which significantly deviate from system normal behavior. Misuse detection can identify malicious data based on the characteristics of known attacks.

In this chapter, the model-based and signal-based IDMs are explained. The chi-square test and Discrete Wavelet Transform (DWT) are used for anomaly-based detection [21, 22]. The False Data Injection Attack (FDIA) can be detected using measurement residuals. If the measurement residual is larger than expected detection threshold, then malicious data can be identified.

The remainder of the chapter is outlined as follows: In Sect. 5.2.1, the communication infrastructure and cyber security challenges in PEV systems are discussed. Then, various types of attacks and intrusions to PEV data are described in Sect. 5.3. The IDMs applied in this study are presented in Sect. 5.4. Section 5.5 demonstrates an application of IDM to the injection of false PEV penetration level data in the Unit Commitment (UC) problem. Finally, Sect. 5.6 concludes with summary of the present work and a discussion of future works and developments in the area of PEVs cyber security.

5.2 Smart Grids with PEVs

In this section, a review of standard communication infrastructure for PEV-integrated systems as well as the potential vulnerabilities are briefly discussed.

5.2.1 Communication Infrastructure

PEVs are capable to connect and communicate to various electronic devices and interfaces throughout the smart grid via wired and wireless networks (Fig. 5.1). Generally, the communication network can comprise five levels [23, 24]:

- Wide Area Network (WAN): This communication system can establish continuous services among the substations and utility control centers in cities and different regions within a large geographical area, through which the demand response and scheduling signals can be transmitted. The WAN usually uses

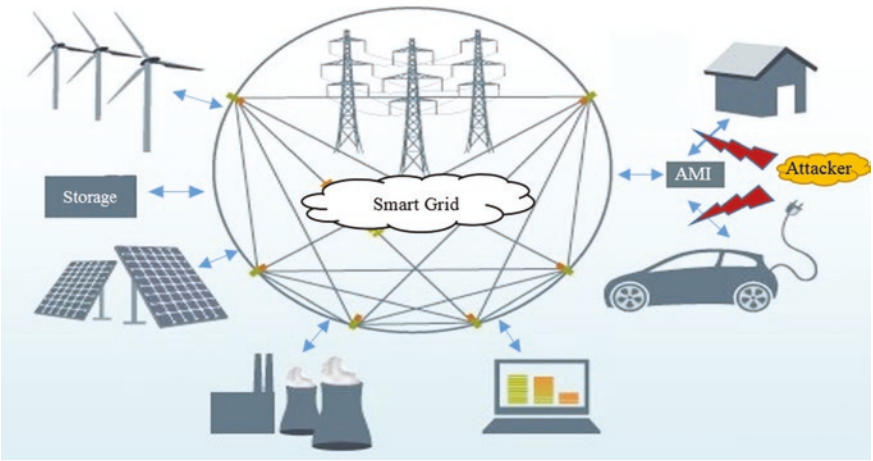

Fig. 5.1 PEV-integrated in smart grid system

either a service provider network like cellular network or over a utility network such as private WiMAX.

- Neighborhood Area Network (NAN): NAN connects smart meters and grid data collectors in distribution automation system. Smart meters in a certain area, such as a residential community, can form a neighborhood area network (NAN) through wireless mesh networks, power line communication (PLC), or Ethernet.
- Field Area Network (FAN): FAN is a combination of NANs and local devices connected to a Field Area Router (FAR), are nominated as a central component of the smart grid IT infrastructure. Monitoring and information exchange between the PEV charging stations and the control center in the distribution system are commonly performed through FAN.
- Home Area Network (HAN): HAN is a network within premises which can connect PEVs, smart meters, Energy Management System (EMS) as well as control and monitoring devices. HAN facilitates the smart grid functionalities on the customer-side like demand side management by smart meters, with the aim to monitor the electric energy exchange in real-time and apply control actions on various customer-side appliances.
- Control Area Network (CAN): CAN is the in-vehicle network designed to allow the Engine Control Unit (ECU) and any other control devices within a car. This connection can be through wire or wireless protocols such as Zigbee. In the PEV case, the PEV attributes can be read from the CAN bus and linked to the charge controller and charging station.

The overall utility/consumer/PEVs network is illustrated in Fig. 5.2. The network forms an interconnected mesh of residential/commercial charging stations and the utility. The Energy Service Interface (ESI) provides secure communication between HAN appliances and the utility for the purpose of load and distributed generation monitoring and control, the EMS enables jointly control of PEV charging and

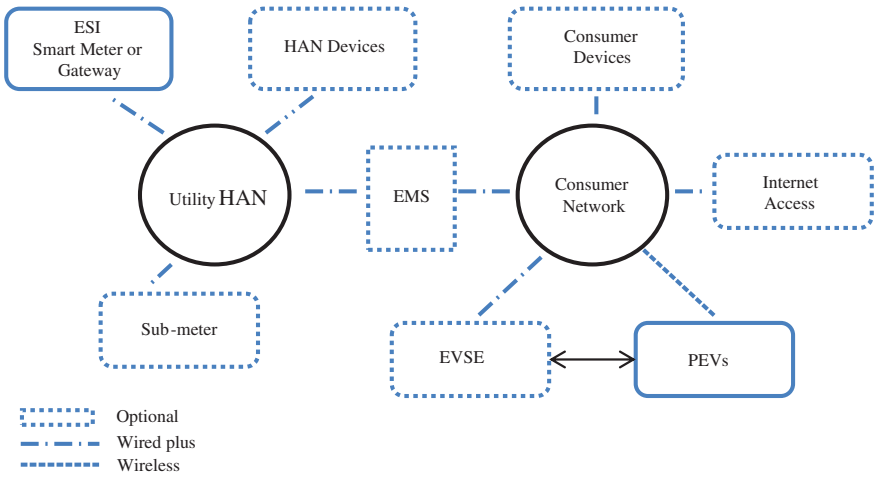

Fig. 5.2 Utility/consumer/PEVs network

distributed energy resources for both utility and consumer devices. PEVs can connect to the grid by Electric Vehicle Supply Equipment (EVSE) such as 120 V AC, and 240 V AC. Utilities have the option of communicating with the EVSE over the NAN or HAN. The NAN connectivity provides more security than HAN such as better range, peer-to-peer communication between EVSE and other smart grid appliances, and eliminating HAN repeater [15].

5.2.2 Communication Standards

The PEVs communication standards developed by the Society of Automotive Engineers (SAE) are listed in Table 5.1 [23]. SAE has also developed standards in other fields of PEV design including SAE J1772, named as the surface vehicle recommended practice standard, SAE J2293 for the off-board EVSE, as well as SAE J2894 for the power quality of charging equipment. Other communication standards include IEEE 1901–2010 [25].

Table 5.1 SAE communication standards

Standard ID	Description
J2836	General information (use cases)
	J2836/1: Utility programs
	J2836/2: Off-board charger communications
	J2836/3: Reverse energy flow (PEV as Distributed Generation)
	J2836/4: Diagnostics
	J2836/5: Customer to PEV and HAN/NAN
	J2836/6: Wireless charging/discharging
J2847	Detailed information (messages)
	Sub-categories are the same as J2836 since use cases and messages are directly related together
J2931	Protocol (requirements)
	J2931/1: General requirements
	J2931/2: In-band signaling (control pilot)
	J2931/3: NB OFDM PLC over pilot or mains
	J2931/4: BB OFDM PLC over pilot or mains
	J2931/5: Telematics
	J2931/6: DSRC/RFID (wireless charging) J2931/7: Security
J2953	Interoperability
	J2953/1: General requirements
	J2953/2: Testing and certification

HAN home area network, *NAN* neighborhood area network, *NB OFDM* narrow-band orthogonal frequency division multiplexing, *PLC* power line communication, *BB OFDM* base-band orthogonal frequency division multiplexing, *DSRC* dedicated short-range communications, *RFID* radio frequency identification

5.2.3 Cyber Security Challenges

Secure and bidirectional control and communication mechanisms for accommodation of PEVs is needed for the purposes of reliable billing, demand response arrangements for Vehicle-to-Grid (V2G) integration, reliable and stable load demand balance, and forensic analysis in case of security breaches. Thus, the confidentiality, integrity and availability (CIA) of PEV integrated system should be met. The cyber-attack on PEV-integrated system may have severe detrimental effects on both electric power and transportation infrastructures simultaneously. The security issues associated with PEVs can be categorized as follows:

- Payment security: Individuals information must be protected from third parties during and after payment transactions by means of secure authentication and data encryption technologies. Payment frauds and unauthorized transaction by a third party or attacker may expose the consumer and the utility with financial losses.
- Smart metering (AMI): AMI provides real-time access to the energy consumption for customers, and perform real-time data acquisition of the energy usage and price information for the utilities to enable smart grid functions. The energy flow in charge/discharge process of PEVs might be intentionally manipulated by the PEV owner or the energy provider for their own benefits. On the top of that, the charging station would be able to tamper the smart meters, bypass the authentication in metering protocols, overrun the buffer in the AMI firmware, as well as firmware manipulations, to cheat both the energy providers and the PEV owners. In addition to the energy flow, the intrusion might affect the system operation or control variables, such as market clearing prices (MCP), reserve allocations, distribution congestion management, and dispatch of generation units. The impact on PEVs may include the charge/discharge current rate, state of charge of the batteries, etc. Therefore, the smart meters should be well secured.
- Cyber physical critical infrastructure (CPCI): The charging station is a part of the CPI, alternatively referred to as smart parks. From the electric grid viewpoint, smart parks are networks of charging stations, operating as distributed storage and demand response resources in the load-side with limited and uncertain capacity. The security concerns from the CPI perspective can be on protecting any appliance or devices including the charging stations and the PEVs in the network against malicious cyber-attacks or firmware infections.
- Communication: Each of the aforementioned levels in the PEV communication infrastructure can be subject to cyber-attacks, especially the data transmission in wireless networks, which is inherently public. Furthermore, data concentrators coordinate a large number of PEVs data from charging stations and homes and manage the communication between them and the utility, by collecting smart meters data and transferring the utility instruction and information via WAN. The potential attacks can be middleman-attack, spoofing, etc., as depicted in Fig. 5.1. The most effective way for preventing malicious attacks across the

communication network is cryptography. For instance, HAN and Zigbee use Advanced Encryption Standard (AES) encryption [26].

- Client privacy: PEVs usually contribute data such as location, identity, the distance travelled, energy exchange patterns, as well as clients' personal information. This information should be kept confidential for user privacy.

5.3 Data Attacks and Intrusions in PEV Communications

In general, there are three main attack types in smart grids including vulnerability, intentional, and false data injection attacks. The first type of attack is associated with the failure of network devices or communication channels, and deterioration of feedback signals within control processes. Vulnerability attacks can be protected by fault diagnosis and localization methods. Intentional attacks can be caused by paralyzing a part of the network nodes if an adversary have knowledge about the network topology. False data injection attacks aims at the manipulation of smart meter measurement to affect the smart grid operations, mostly the economic variables [27]. In this chapter, we will study the false data injection attack in PEV-integrated systems.

Different types of data is communicated between the PEVs, charging station and utility over the network during the connection of PEVs to the grid. The data vulnerable to false data injection attacks can be listed as follows:

(1) Energy request
(2) Energy usage
(3) Price signal from the utility
(4) Demand response bidding from the PEV charging station
(5) Demand response needs from the utility
(6) Event messages
(7) PEV ID
(8) Premise location ID
(9) Utility ID
(10) Customer ID

The potential impacts of data attacks against PEVs can target network availability, data integrity, and information privacy. If the energy request, energy usage, price signal, and demand response parameters are subject to data attacks, it might lead to the overcharging of batteries and cause severe damage to PEVs. Overcharging constraint parameters in the PEV battery charge controllers should be secured by methods such as electrical and cyber physical tamper-proofing and tamper-resistance strategies.

The connection of PEVs to smart grids should allow the PEVs to register, and initially set up communications with the utility, or an alternative energy supplier, repeatedly reestablish communications for each charging session, provide PEVs charging and other status information to customer information channels such as

web and display devices, and correctly bill PEVs customers according to their selected rates or programs. These services include the inquiry of the PEV, premise location, utility, and customer IDs. Any attacks to these data may result in unauthorized access or modification to customer information, and the energy program the customer is registered.

5.4 Intrusion Detection Methods

In general, there are two methods to detect malicious data [16]:

(1) Anomaly detection methods: these methods are used to detect any activities which significantly deviate from system normal behavior, such as machine learning, data mining methods, and statistical models.
(2) Misuse detection methods: these methods can identify malicious data based on the characteristics of known attacks, like rule-based languages, and state transition analysis tool kit.

Any intrusions in PEV systems may be detected through the analysis of system model or the features of the signals transmitted over the network. The methods based on the system model analysis and signal analysis are referred to as model-based and signal-based intrusion detection methods, respectively. The main feature of model-based method lies in the development of dynamic models of the smart power system. On the other hand, the signal-based method exploits the statistical properties of the signals using various signal processing methods. In this chapter, a model-based intrusion detection method is illustrated using the chi-square test along with largest normalized residual to detect and identify the malicious data. In addition, a signal-based detection method presented and implemented by means of the Discrete Wavelet Transform (DWT).

5.4.1 Model-Based Method Using Chi-Square Test

Model-based intrusion detection methods can be used if the measured variables can be represented by the system state variables. For example, in a given power system, measurements like bus active/reactive power, line active/reactive power flows can be expressed as a function of system state variables, i.e. bus voltage magnitudes and phase angles.

In this section, an intrusion detection method based on the chi-square distribution test and the largest normalized residual test are presented to detect and identify the malicious data [21].

In general, the measured data which may be exposed to attack can be expressed as follows:

$$z = h(x) + e \tag{5.1}$$

where $h(x)$ is a nonlinear function relating measurements z to the state vector x and the error vector e.

The linearized model is presented in terms of the system Jacobian coefficient matrix $H_{m\times n}$ and the state variables vector, as follows:

$$\Delta z = H\Delta x + e \tag{5.2}$$

$$\Delta z = z - h(x) \tag{5.3}$$

where m and n denote the length of z and x vectors, respectively, Δz is the measured data vector representing the linearized relation between Δz and the system state variables Δx, with: $E(e) = 0$ and $Cov(e) = \sigma^2 = R$. The weighted least square (WLS) estimator of the linear state vector can be obtained as follows:

$$\Delta\widehat{x} = (H^{\mathrm{T}}R^{-1}H)^{-1}H^{\mathrm{T}}R^{-1}\Delta z \tag{5.4}$$

And the estimated value of Δz is:

$$\Delta\widehat{z} = H\Delta\widehat{x} \tag{5.5}$$

The model-based intrusion detection method comprises malicious data detection and identification of bad data. Here, the chi-squares test is used to detect the malicious data. In other words, it can recognize whether the data set is attacked or not. Then, the largest normalized residual test is used to identify the malicious data.

The malicious data detection is performed by comparing the minimum weighted residual vector $J(\widehat{x})$ with the detection confidence determined by the system operator (e.g., $p = 95$ %). $J(\widehat{x})$ is defined and computed by the following equation:

$$J(\widehat{x}) = \sum_{i=1}^{m} \frac{(z_i - h_i(\widehat{x}))^2}{\sigma_i^2} = \sum_{i=1}^{m} \frac{(\mathrm{r}_i)^2}{\sigma_i^2} \tag{5.6}$$

The residual vector can be represented by a Chi-square distribution function. The Chi-square distribution values corresponding to a detection confidence with probability p and (m – n) degrees of freedom can be obtained from the Chi-square lookup table [28].

$$p = \Pr(J(\widehat{x}) \leq \chi^2_{(m-n),p}) \tag{5.7}$$

If $J(\widehat{x}) \geq \chi^2_{(m-n),p}$, the malicious data will be detected. Then, the largest normalized residual test can be used to identify the malicious data.

A gain matrix is defined as:

$$G = H^{\mathrm{T}}R^{-1}H \tag{5.8}$$

And the hat matrix K is:

$$K = HG^{-1}H^{\mathrm{T}}R^{-1} \tag{5.9}$$

The hat matrix is used to find the residual sensitivity matrix S where I is the identity matrix:

$$S = I - K \tag{5.10}$$

S is multiplied by the error vector e to find the measurement residuals r. The measurement residual vector is divided by the square root of the residual covariance matrix, Ω, which is defined as:

$$\Omega = SR \tag{5.11}$$

Thus, the normalized value of the residual, $r_i^{(N)}$, can be obtained as follows:

$$r_i^{(N)} = \frac{|r_i|}{\sqrt{diag(\Omega)}} \tag{5.12}$$

The variable associated with the largest normalized residual will be suspected as malicious data.

5.4.2 Signal-Based Method Using Discrete Wavelet Transform

The DWT is a mathematical tool to decompose a time-series signal into several temporal scales (or frequencies), enabling to extract information in different resolution levels [29].

Wavelet transform breaks the signal into its wavelets, which are scaled and shifted versions of a base waveform known as the mother wavelet. The irregular shape and compactly-supported nature of wavelets make wavelet analysis a promising tool for analyzing signals of non-stationary nature. Their fractional nature allows them to analyze signals with discontinuities or sharp changes, while their compactly supported nature enables temporal localization of a signal's features.

A one-dimensional DWT is composed of decomposition (analysis) and reconstruction (synthesis). DWT produces two sets of constant terms as approximation and detail coefficients. The approximation coefficients are the high scale, low frequency components and the detail coefficients are the low scale, high frequency components. The signal is passed through a series of high pass and low pass filters to analyze the respective functions at each level. DWT analysis starts by selecting a basic scaling function, $\Phi(t)$, and wavelet function $\Psi(t)$. Haar wavelet is one of the most well-known basic wavelet functions. By choosing the Haar wavelet, the scaling function $\Phi(t)$ and the wavelet function $\Psi(t)$ are defined as [30]:

$$\Phi(t) = \begin{cases} 1 & 0 \le t < 1 \\ 0 & otherwise \end{cases} \tag{5.13}$$

$$\Psi(t) = \begin{cases} 1 & 0 \le t < \frac{1}{2} \\ -1 & \frac{1}{2} \le t < 1 \\ 0 & otherwise \end{cases} \tag{5.14}$$

The wavelet representation of a function $f[n]$, can be given by:

$$f[n] = \frac{1}{\sqrt{M}} \sum_{k=-\infty}^{+\infty} a_{j0,k} \Phi_{j0,k}[n] + \frac{1}{\sqrt{M}} \sum_{j=j0}^{\infty} \sum_{k=-\infty}^{+\infty} d_{j,k} \Psi_{j,k}[n] \tag{5.15}$$

where $a_{j0,k}$ and $d_{j,k}$ are the approximation and detail coefficients, respectively, and M is the number of samples. Also, $\Phi_{j0,k}[n]$, and $\Psi_{j,k}[n]$ can be calculated as follows:

$$\Phi_{j0,k}[n] = 2^{j0/2} \Phi[2^{j0} n - k] \tag{5.16}$$

$$\Psi_{j,k}[n] = 2^{j/2} \Phi[2^{j} n - k] \tag{5.17}$$

where j is the dilation parameter, and k is the position parameter. The given signal $f(t)$ is convolved with the scaling function for calculating the approximation coefficients and with the wavelet function for calculating the detail coefficients at each level.

$$a_{j0,k} = \frac{1}{\sqrt{M}} \sum_{n=0}^{M-1} f[n] \Phi_{j0,k}[n] \tag{5.18}$$

$$d_{j,k} = \frac{1}{\sqrt{M}} \sum_{n=0}^{M-1} f[n] \Psi_{j,k}[n] \tag{5.19}$$

The signal $f(t)$ is used to calculate the approximation and detail coefficients at level one. Then, the calculated approximation coefficients are utilized to obtain the approximation and detail coefficients at level two, and so on.

Anomaly detection of malicious data in smart grids consists of three steps as indicated in Fig. 5.3 [31]. The first step is to collect the measured data from the smart meters. The second step is the DWT to analyze the signal features. In the final step, the detail coefficient values are compared with predefined threshold values (confidence intervals) for the determination of the anomalies in the signal. For instance, if the data anomalies are considered as a random white noise with Gaussian distribution, for any random variable, choosing $\pm 3\sigma$ confidence interval yields to:

$$P(\mu - 3\sigma < X \leq \mu + 3\sigma) \approx 99.7\ \% \tag{5.18}$$

This interval corresponds to 99.7 % confidence level, which means that we can detect anomalies with 0.3 % error rate.

Fig. 5.3 Malicious data detection and identification using wavelet analysis

5.5 Application to the Detection of Malicious PEV Penetration Level

In this section, a case study of PEV data attack is illustrated and their impacts on the power grid operation is presented. Then, DWT-based intrusion detection method has been used to detect malicious data as described in Sect. 5.4.2. In Sect. 5.3, the potential data attacks in PEV-Integrated systems were reviewed. The available PEV charge/discharge capacity throughout the grid is collected by smart meters and transmitted to the utilities. This data may have detrimental effects on determining optimal dispatch of generation units and demand response resources to maintain the balance between generation and demand. This predictive optimization problem is generally referred to as the unit commitment (UC) problem, periodically solved in the Energy Management System (EMS) by the utility. The UC can aim at one or more of the following objectives: minimizing the system operation costs, energy usage, peak demand, and charging cost, emission cost, as well as maximizing the social welfare and system reliability. UC results have detrimental effect system operation costs on the nodal electricity prices [32]. The UC formulation can be found in [33, 34]. The UC can be modified to accommodate the penetration of PEVs [35]. As one of the most effective demand response resources, the coordinated and smart charging/discharging of PEVs can reduce the charging cost and be very helpful for load leveling and peak shaving purposes in power systems.

The contribution of PEVs to load and demand response can be reflected in the demand balance constraint in the UC problem, expressed by the following equation:

$$D(t) = \sum_{i=1}^{I} P_i(t) + \left(N_{DSCH}(t) - N_{CH}(t)\right) C_{PEV} \cdot \eta \cdot \delta \tag{5.19}$$

where $D(t)$ is the total load demand at time t, $P_i(t)$ is the total generation at time t, δ is the state of charge of PEV batteries, and C_{PEV} is the average PEVs battery capacity. Each vehicle should have a desired level state of charge (SOC) at the time of departure. η is defined as the integrated efficiency for charging/discharging controller as well as the inverter. $N_{DSCH}(t)$ and $N_{CH}(t)$ are the number of discharging and charging vehicles at hour t, respectively.

Here, it is assumed that the PEVs are charged to their desired SOC within a short time and after that, while the PEVs are connected to the grid in smart parks,

the amount of power received by vehicles from the grid is equal to the amount of power that vehicles inject to the grid. For the sake of simplicity, in this study, charging/discharging frequency is assumed to be once a day.

$$\sum_{t=1}^{T} N_{DSCH}(t) = \sum_{t=1}^{T} N_{CH}(t) \tag{5.20}$$

In order to have a reliable operation, a limited number of PEVs should be discharged or charged at the same time over the scheduling time step.

$$N_{DSCH}^{\min} \leq N_{DSCH}(t) \leq N_{DSCH}^{\max} \tag{5.21}$$

$$N_{CH}^{\min} \leq N_{CH}(t) \leq N_{CH}^{\max} \tag{5.22}$$

where $N_{CH}^{\max}$ and $N_{DSCH}^{\max}$ are the maximum number of charging and discharging vehicles at hour t, respectively. The UC problem incorporating PEVs can be formulated as a Mixed-Integer Linear Programming (MILP) problem, and solved easily by using an optimization software, such as MATLAB^{TM} Optimization Toolbox.

In this case study, a 24 h scheduling horizon with 10 generation units and maximum 100,000 PEVs are assumed for the simulation. The initial states of units, and startup coefficients can be found in [36, 37]. Also, the following assumptions are considered for PEVs: average battery capacity (C_{PEV}) = 15 kWh; charging/discharging frequency = 1 per day; departure SOC (δ) = 50 %; total efficiency (η) = 85 %, the maximum number of charging/discharging at each hour = 10 % of the total PEVs [35].

Since the exact number of PEVs connecting to the grid is indeterminate at any given time, it should be forecasted. The forecasted number of attended PEVs in smart parks in a city during the hours of a day represents the penetration level of the PEVs into the grid. This data has been resembled from a parking lot located in the city of Livermore, CA [38]. This data is considered to be under potential attack in this study. Figure 5.4 depicts the actual and malicious data.

In order to examine the effect of malicious PEV penetration level data on the UC results, the UC has been solved for both the case of using the actual data and the malicious data. Figure 5.5 depicts the total operation cost of the system without the PEVs, as well as with actual and malicious PEV penetration level. The impact of PEV penetration on the net demand is shown in Fig. 5.6. It can be seen that the malicious PEV penetration level results in the change of total system operation cost and unit schedules as well as the net demand, which also puts the power system under risk exposure for maintaining the balance and stability.

Figures 5.7 and 5.8 demonstrate the optimal number of charging/discharging PEVs based on the actual and malicious penetration level data, respectively.

For the anomaly detection, Haar wavelet is employed and the one-dimensional DWT is computed for the data in Fig. 5.4 up to two levels. In order to obtain the

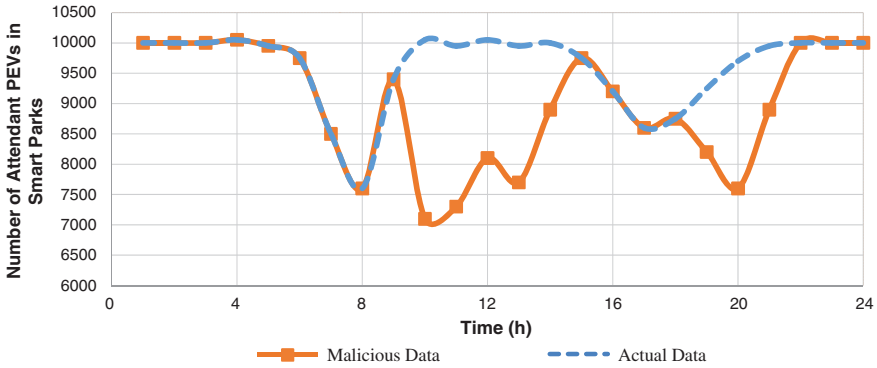

Fig. 5.4 The forecast pattern of PEVs attendance in a smart park at each hour of a day

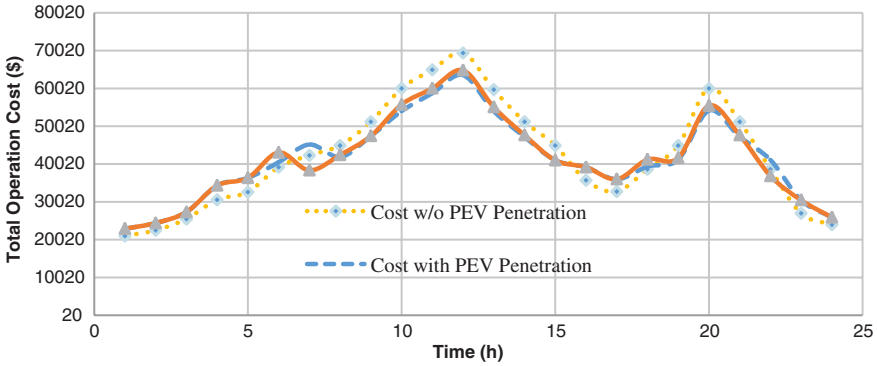

Fig. 5.5 The total operation cost without the PEVs, as well as with actual and malicious PEV penetration level

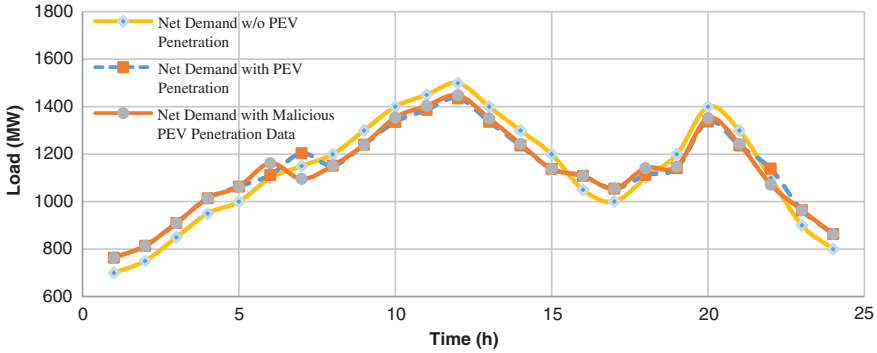

Fig. 5.6 The impact of PEV penetration on the net demand

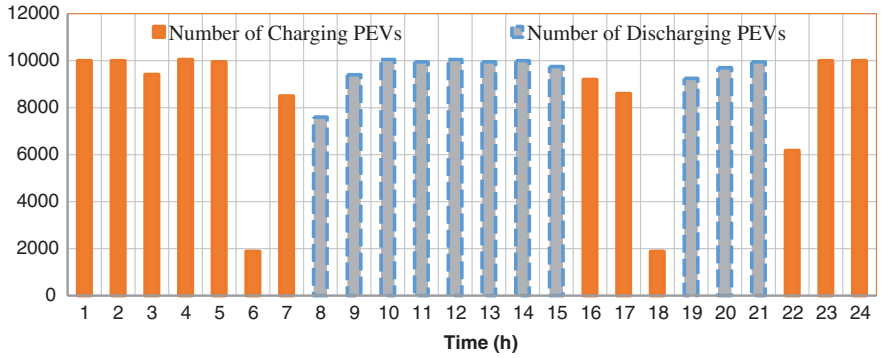

Fig. 5.7 Optimal number of charging/discharging PEVs based on the actual penetration level data

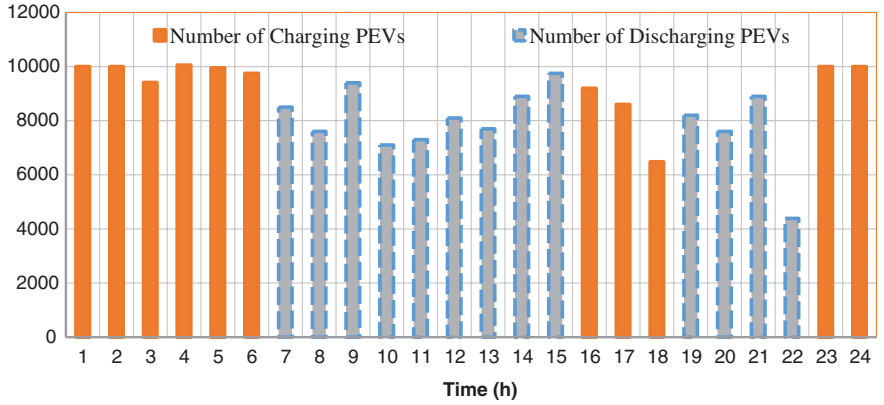

Fig. 5.8 Optimal number of charging/discharging PEVs based on the malicious penetration level data

thresholds, the distribution of the wavelet reconstructed signal without anomaly should be analyzed. Then, normality is verified by Lilliefors test for goodness of fit to the normal distribution [39]. This has a normal distribution at 5 % confidence interval. We can detect anomaly intrusion by choosing some of the levels through selective reconstruction. Table 5.2 shows statistical properties of the actual and malicious data of PEV penetration level.

In Figs. 5.9 and 5.10 the detail coefficients at level 1 and 2 for anomaly detection are plotted, respectively. These data are compared to the threshold levels to identify the places where the false data injection occurred and alert the operator regarding the presence of anomalies in the data. For example, at level one, the data between hours 10–14 and 19–22 has passed the threshold level. The data at hour 22 has been mistakenly detected which is referred to as false negative alarm [40].

Table 5.2 Statistical properties of detail coefficient and threshold for malicious data detection

Actual data			Malicious data	
Level	Standard deviation	Threshold	Level	Standard deviation
1	132.51	397.54	1	400
2	285.11	855.35	2	631.08
3	276.65	829.97	3	591.82
4	86.88	260.64	4	437.88
5	34.10	102.32	5	24.07

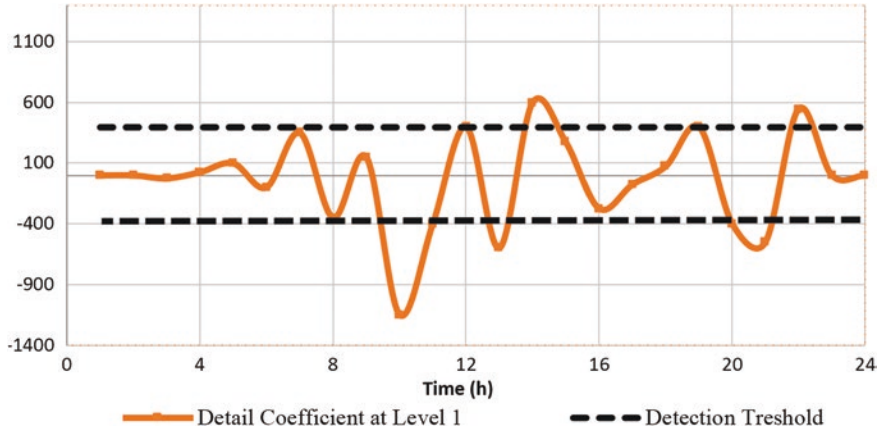

Fig. 5.9 Detail coefficient at level 1 for anomaly detection

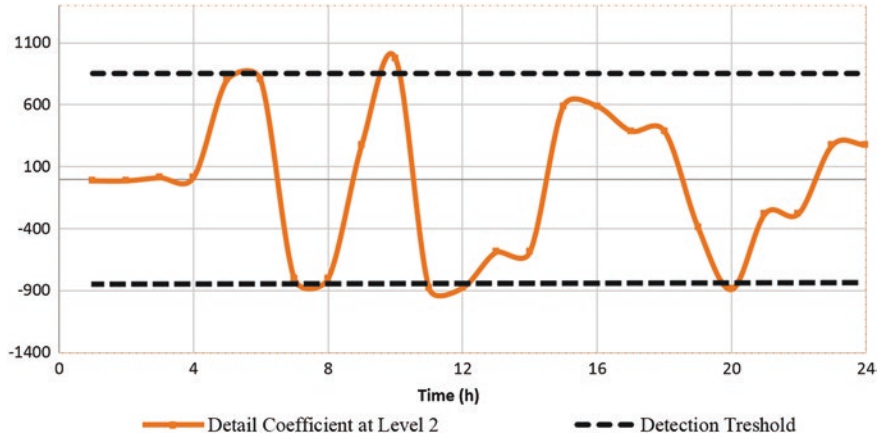

Fig. 5.10 Detail coefficient at level 2 for anomaly detection

As a result, there is no guarantee for exact identification of false data values which necessitates the further improvements in anomaly detection and identification methods in the future.

5.6 Conclusion

Assuring data confidentiality, integrity and availability are significant parts of PEV-integrated cyber-physical systems (CPS). In this chapter, cyber security challenges due to incorporation of PEVs in smart grids were probed. PEVs are not only considered as loads, but also as demand response or distributed energy resources and therefore, the security issues involves all parties in the energy system, including the consumer, charging stations, and the utility.

Various AMI data intrusions and their impacts on smart grid stability, operation, and economics were explained. Afterwards, two types of intrusion detection methods including the model-based and signal-based methods were presented for anomalies detections. Among different detection methods, the chi-square test and discrete wavelet transform (DWT) were addressed with specific application to false data injection to PEVs penetration level in the smart grid generation scheduling (Unit Commitment) problem. These attacks may have detrimental impacts on the operating costs and reliability of energy supply. Therefore, the use of intrusion detection methods should be developed to improve the protection and security of future smart grids. The future works can be accomplished to enhance preventive measures against cyber-attacks and anomaly detection methods.

References

1. http://en.wikipedia.org/wiki/Plug-in_electric_vehicles_in_the_United_States (2014). Accessed 20 June 2014
2. Hota AR, Juvvanapudi M, Bajpai P (2014) Issues and solution approaches in PHEV integration to smart grid. Renew Sustain Energy Rev 30:217–229
3. Green II, Robert C, Wang L, Alam M (2011) The impact of plug-in hybrid electric vehicles on distribution networks: a review and outlook. Renew Sustain Energy Rev 15(1):544–553
4. Tie SF, Tan CW (2013) A review of energy sources and energy management system in electric vehicles. Renew Sustain Energy Rev 20:82–102
5. Wirasingha SG, Emadi A (2011) Classification and review of control strategies for plug-in hybrid electric vehicles. IEEE Trans Veh Technol 60(1):111–122
6. Emadi A, Young JL, Rajashekara K (2008) Power electronics and motor drives in electric, hybrid electric, and plug-in hybrid electric vehicles. IEEE Trans Ind Electron 6:2237–2245
7. Peng M, Liu L, Jiang C (2012) A review on the economic dispatch and risk management of the large-scale plug-in electric vehicles (PHEVs)-penetrated power systems. Renew Sustain Energy Rev 16(3):1508–1515
8. Bessa RJ, Matos MA (2012) Economic and technical management of an aggregation agent for electric vehicles: a literature survey. Eur Trans Electr Power 22(3):334–350

9. Su W, Eichi H, Zeng W, Chow MY (2012) A survey on the electrification of transportation in a smart grid environment. IEEE Trans Ind Inf 8(1):1–10
10. Quinn C, Zimmerle D, Bradley TH (2010) The effect of communication architecture on the availability, reliability, and economics of plug-in hybrid electric vehicle-to-grid ancillary services. J Power Sources 195(5):1500–1509
11. Matta N, Rahim-Amoud R, Merghem-Boulahia L, Jrad A (2011) A cooperative aggregation-based architecture for vehicle-to-grid communications. Global information infrastructure symposium (GIIS), IEEE, pp 1–6
12. Kim TT, Poor HV (2011) Strategic protection against data injection attacks on power grids. IEEE Trans Smart Grid 2(2):326–333
13. Sridhar S, Govindarasu M (2014) Model-based attack detection and mitigation for automatic generation control. IEEE Trans Smart Grid 5(2):580–591
14. Bou-Harb E, Fachkha C, Pourzandi M, Debbabi M, Assi C (2013) Communication security for smart grid distribution networks. IEEE Commun Mag 51(1):42–49
15. Chaudhry H, Bohn T (2012) Security concerns of a plug-in vehicle. In: Innovative smart grid technologies (ISGT), 2012 IEEE PES, IEEE, pp 1–6
16. Hoppe T, Dittman J (2007) Sniffing/replay attacks on CAN buses: a simulated attack on the electric window lift classified using an adapted CERT taxonomy. In: Proceedings of the 2nd workshop on embedded systems security (WESS)
17. Hoppe T, Kiltz S, Dittmann J (2008) Security threats to automotive CAN networks–practical examples and selected short-term countermeasures. In: Computer safety, reliability, and security. Springer, Berlin, Heidelberg, pp 235–248
18. Kleberger P, Olovsson T, Jonsson E (2011) Security aspects of the in-vehicle network in the connected car. Intelligent vehicles symposium (IV), 2011, IEEE, pp 528–533
19. Arvani A, Rao VS (2014) Detection and protection against intrusions on smart grid systems. Int J Cyber Secur Digit Forensics 3(1):38–48
20. Renk R, Saganowski L, Hołubowicz W, Choraś M (2008) Intrusion detection system based on matching pursuit. Proc Intell Netw Intell Syst 213–216
21. Abur A, Exposito AG (2004) Power system state estimation: theory and implementation. CRC Press, Boca Raton
22. Kim SS, Reddy ALN, Vannucci M (2004) Detecting traffic anomalies using discrete wavelet transform. In: Information networking. Networking technologies for broadband and mobile networks, Springer, Berlin, Heidelberg, pp 951–961
23. Hybrid Committee (2010) Use cases for communication between plug-in vehicles and the utility grid. SAE international, Detroit, Michigan, standard J2836/1, Jan 2010
24. Hybrid Committee (2010) SAE electric vehicle and plug in hybrid electric vehicle conductive charge coupler. SAE international, Detroit, Michigan, standard J1772, Jan 2010
25. IEEE standard for broadband over power line networks: medium access control and physical layer specifications (2010) IEEE Std 1901–2010, pp 1–1586
26. Advanced encryption standard (AES) (2001) National Institute for Standards and Technology
27. Chen PY, Cheng SM, Chen KC (2012) Smart attacks in smart grid communication networks. Commun Mag IEEE 50(8):24–29
28. http://sites.stat.psu.edu/~mga/401/tables/Chi-square-table.pdf
29. Mallat S (1999) A wavelet tour of signal processing. Academic Press, Waltham
30. Chun-Lin L (2010) A tutorial of the wavelet transform. ed: NTUEE
31. Kim SS, AL Narasimha Reddy, Vannucci M (eds) (2004) Detecting traffic anomalies using discrete wavelet transform. In: Information networking. Networking technologies for broadband and mobile networks. Springer, Berlin, Heidelberg, pp 951–961
32. Norouzi H, Abedi S, Jamalzadeh R, Rad MG, Hosseinian SH (2014) Modeling and investigation of harmonic losses in optimal power flow and power system locational marginal pricing. Energy 68:140–147
33. Padhy NP (2004) Unit commitment-a bibliographical survey. IEEE Trans Power Syst 19(2):1196–1205

34. Abedi S, Riahy GH, Hosseinian SH, Alimardani A (2011) Risk-constrained unit commitment of power system incorporating PV and wind farms. ISRN Renew Energy 2011:8
35. Saber AY, Venayagamoorthy GK (2010) Intelligent unit commitment with vehicle-to-grid—a cost-emission optimization. J Power Sources 195:898–911
36. Damousis IG, Bakirtzis AG, Dokopoulos PS (2004) A solution to the unit-commitment problem using integer-coded genetic algorithm. IEEE Trans Power Syst 19(2):1165–1172
37. Kazarlis SA, Bakirtzis A, Petridis V (1996) A genetic algorithm solution to the unit commitment problem. IEEE Trans Power Syst 11:83–92
38. Carrión M, Arroyo JM (2006) A computationally efficient mixed-integer linear formulation for the thermal unit commitment problem. IEEE Trans Power Syst 21:1371–1378
39. City of Livermore (2006) Downtown parking study. Livermore, CA
40. Gonzalez F, Dasgupta D, Kozma R (2002) Combining negative selection and classification techniques for anomaly detection. In: CEC'02: Proceedings of the 2002 Congress on evolutionary computation, 2002, vol 1. IEEE, Piscataway, pp 705–710

Chapter 6
Impact Evaluation of Plug-in Electric Vehicles on Power System

Pol Olivella-Rosell, Roberto Villafafila-Robles and Andreas Sumper

Abstract The aim of this chapter is to expose the probabilistic Plug-in electric vehicle (PEV) charging model and to apply it in a distribution grid to evaluate the PEV impact. The model is based on agent-based techniques, has probabilistic variables, includes queuing theory, and applies Monte Carlo methodology. The PEV user's charging needs can be divided in two categories: private charging points and public charging points. Regarding private charging points, the PEV charging demand depends strongly on private user's mobility needs and it includes variables as number of trips per day, driving distance, and arrival time. Also, the user's profile can be modelled with probabilistic variables as the PEV model and the charging connection point. All these variables can be modelled with probabilistic distributions functions to obtain a probabilistic model with data from different sources. Additionally, public charging points are made available for PEV users that need to plug-in the vehicle between trips to extend the vehicle autonomy. After that, the model is applied to a case study to analyze the impact to the power network. Probabilistic grid impact includes the probability to exceed a maximum voltage drop, and transformer and current saturations. The main impact is on saturations of lines and they can be reduced controlling private points but it does not make sense to control the public points. Fast chargers present some challenges for grid integration because they are public charging points of 50 kW power rate per charger. In this chapter, a stochastic arrivals model is applied to analyze the public fast charging stations, the PEV user's charging

P. Olivella-Rosell (✉) · R. Villafafila-Robles · A. Sumper
Centre d'Innovació Tecnològica en Convertidors Estàtics i Accionaments (CITCEA-UPC), Departament d'Enginyeria Elèctrica, EU d'Enginyeria Tècnica Industrial de Barcelona, Universitat Politècnica de Catalunya-BarcelonaTech, Barcelona, Spain
e-mail: pol.olivella@citcea.upc.edu

R. Villafafila-Robles
e-mail: roberto.villafafila@citcea.upc.edu

A. Sumper
e-mail: sumper@citcea.upc.edu

S. Rajakaruna et al. (eds.), *Plug In Electric Vehicles in Smart Grids*, Power Systems, DOI 10.1007/978-981-287-299-9_6

needs and their grid impact. Fast charging stations are designed to extend the autonomy of PEV and their arrivals to the station have a certain stochastic behavior. The probabilistic arrivals for the fast charger impact evaluation are based on queuing theory and the corresponding electricity demand is evaluated. The case study analyzed includes three fast chargers installed in the same grid and they provoke saturations in lines.

Keywords Plug-in electric vehicles · Grid impact · Stochastic evaluation · Driving pattern · Distribution networks

6.1 Introduction

The deployment of Plug-in Electric Vehicles (PEV) on energy system seeks a global welfare, as reduction of energy dependency, improvement of energy efficiency, reduction of polluting emissions and greenhouse gas (GHG) emissions, and improvement the utilization of renewable energy resources [1]. Among these benefits, PEV are a promising technology for power system specifically because they can facilitate demand-side management strategies if PEV deployment is accompanied by information and communication technology, power infrastructure required, and the appropriate regulation.

Besides, power networks must be able to accommodate this new demand. This depends on the power required for charging the batteries of PEV according to the charging time desired for this process. Here, PEV conductive charging equipment standards as SAE J1772 and IEC 62196 consider 16 A as rated current for single-phase systems, that is, a power rating up to 2 kW in countries with 120 V supply, and up to 4 kW in countries with 230 V supply. This is known as slow charging because it can last up to 8 h, and corresponds to the slow domestic charging. In order to reduce this time up to 1 h, three-phase connection can be used up to 63 A, but this is expected to be performed in public parking locations due to it requires up to 44 kW that are not feasible in domestic installations. The former options are AC systems with on-board chargers. By using off-board DC charging systems it is possible to reduce the duration of the charging process up to 30 min, and make the procedure similar to fill the tank of conventional vehicles [2]. This is called fast charging and its main characteristics are described in Sect. 6.3.

The analysis to determine if current power networks could cope with this new demand is challenging when considering private PEV due to its stochastic behavior as it depends on individual mobility needs in which time and driving distance are difficult to assess in advance. On the contrary, the performance of commercial PEV is supervised and controlled anytime. Moreover, the facilities where they are charged are designed considering PEV and their charging needs.

Stochastic models are useful in problems with variability and they permit to take decisions based on the probability. In the PEV charging demand problem, the

variability depends on mobility variables and these provoke a probable power consumption range for each period of time. In this chapter, load demand ranges are applied to analyze the grid impact and its capacity to supply PEV energy demand.

Old distribution networks will present higher impacts because they usually have higher voltage drops and they are located in urban areas with higher energy consumption density. Urban networks will present capacity problems in terms of line loadings. In contrast, rural networks will present problems in terms of voltage drops because they have long lines, lower operation voltages, and dispersed consumption.

PEV charging loads are not the same as other loads with similar power rating, e.g. heat pumps, electric cookers, and electric boilers. This new demand can be controlled in function of user needs (mobility requirements) and grid constraints. Thus, the PEV control could permit to avoid a grid expansion by shifting the charging action to off-peak periods. From the point of view of distribution system operator (DSO), the objective of the control system is to minimize the grid impact, to avoid the grid expansion, and to operate it at an acceptable cost. Other objectives are the energy cost minimization for the costumer and its retailer, and the reduction of GHG emissions from the environmental point of view.

The possibility to shift the domestic battery charges in grids near its capacity will allow to minimize the network reinforcement. The scenarios included in this chapter permit to compare the differences between not-controlled charges and controlled ones. Furthermore, demand-side management techniques in other loads, combined with PEV charging management, could reduce the impact and the corresponding network expansion.

In contrast of domestic charges, it does not make sense to control the public points because the users need them to reach their destinations. Public charges can have slow or fast charging modes and both have to supply the demand at the moment when it is requested. In this chapter, both situations are considered in two case studies to compare an extended slow charging public points, and centralized public points in a fast charging station with three fast chargers of 50 kW each one.

Thus, the estimation of domestic charge of PEV is a cumbersome task but it is very important for distribution system operator in order to avoid network constraints and provide the proper quality of service. This chapter deals with calculating demand of domestic PEV and fast charging for reducing their impact on power network.

There are different models in the literature as Clement et al. [3], Huang et al. [4], Qian et al. [5] Soares et al. [6] and Acha et al. [7]. The majority of models from the literature make assumptions as: only consider PHEV, no charges between displacements, charging processes with constant power, only one type of charging strategy, or only one type of PEV user between others. Moreover, the work carried out by them do not have the objective of exposing the methodology used to get the models.

The recent studies as Leemput et al. [8] include photovoltaic generation and travel patterns but the methodology to obtain the charging model is not exposed. One of the objectives of this chapter is to propose a methodology to implement the PEV charging model, based in agents modeling, at any place with the appropriate data.

Furthermore, there are different analysis in the literature. The majority of studies analyses the voltage drop or transformer load as Valsera et al. [9, 10]. Clement et al. [3] include Joule losses and Maitra et al. [11] include overloading and unbalances. Kleiwegt et al. [12] propose a methodology to detect overloads during a whole year. Other possible impacts in power system are the economic impact. It is reviewed by Dallinger et al. [13]. The presented work includes the probabilistic calculations of voltage drop and current loadings.

According to different authors, the PEV charging demand could committee voltage stability in power networks in scenarios of 10 % of PEV [14]. There are many strategies proposed to reduce PEV impact in power networks. The objective is to manage the PEV charging demand to shift it to valley periods. Tie et al. [15] analyze supervisor control algorithms used in PEVs to reduce impact on power networks. Sheikhi et al. [16] propose an algorithm for charging scheduling considering a stochastic start time of charging. Sortomme et al. [17] apply optimization techniques to coordinate PHEV charges minimizing distribution losses. Clement et al. [18] compare 2 optimization techniques to reduce EV charging impact. The first one use quadratic functions to minimize the power losses in distribution networks with deterministic and also probabilistic EV demand models. The second one, they compare them to dynamic programming techniques which separate the problems into subproblems of 1 variable (Dynamic Programing successive approximation).

6.2 Probabilistic PEV Charging Demand

As it is exposed in the introduction, the multiple stochastic variables will determine the PEV charging demand. To estimate the reasonable demand from PEV it is necessary to model the stochastic variables and include them in a probabilistic model. Thus, it is possible to consider the interaction of all variables.

PEV charging demand model is designed according an agent-based methodology (ABM). Following there are the main strengths of ABM and its application:

- Heterogeneous individual components: PEV model and mobility pattern of each PEV owner.
- Flexible systems: to manage the charging demand of each PEV.
- Influence of location: to consider the effects of charging point location in power network.
- Representation of social interactions: different types of PEV owners could have different influences on whole system.

A set of agents has been defined, each one as an autonomous software entity with different attributes. These determine the way the agent behaves in the given scenario, and how it interacts with the environment and the other agents [19, 20]. The main reason for using this methodology, is the fact that it has been previously tested in mobility related applications [21], and it enables to test a wide range of different agents.

In this case, every agent will represent a PEV owner, with its own driving profile for every day simulated and the same type of vehicle for all the period evaluated. Figure 6.1 shows a general scheme with the stages of the model. Driving profiles are based on data obtained from travel mobility surveys, and only weekdays are taken into account. For every agent and travel the information includes: driving distance, time, average speed and travel cause, either occupational or personal. Travels are then ordered along the day considering its cause and probability functions based on real data.

During simulation, each agent goes about its daily driving profile, and the battery state of charge (SOC) is computed at the end of every travel, considering the distance travelled, and the vehicle's consumption rate. Then, the vehicle will be plugged to the network at some time during the day, in order to charge its battery. The algorithm chosen for Li-ion batteries charging considers 3.7 kW as the maximum power for all charging events. This rate is thought to become a common option for private home-charging, as it is enough to charge completely PEV batteries during

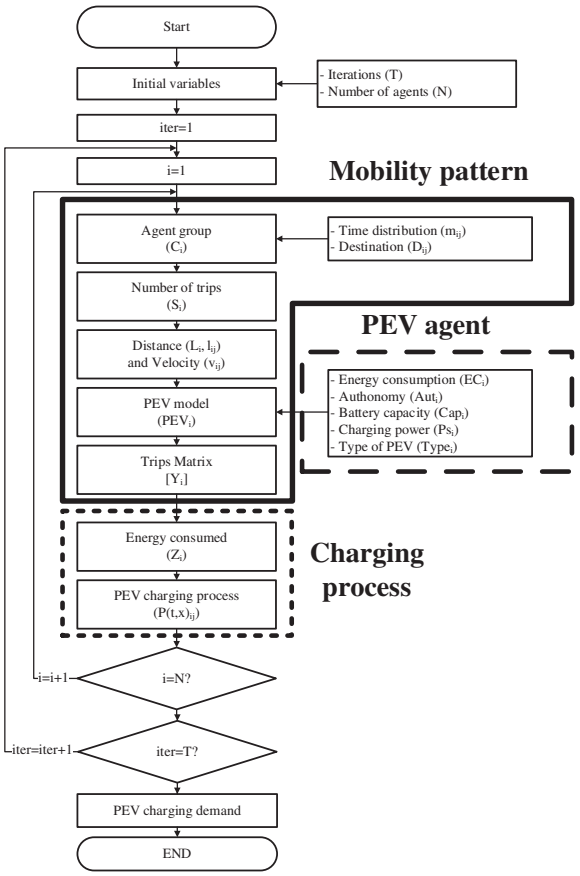

Fig. 6.1 Probabilistic PEV ABM algorithm of the model

the night. The same rate and profile is applied for public charging points. In this model, charging time will be directly dependent on battery size and SOC.

Variables

ABM diagram shown in Fig. 6.1 has three groups: PEV agent, mobility pattern, and charging process.

(a) **PEV agent**

First of all it is necessary to define PEV agents and their variables. Each PEV agent is defined in function of *PEV model* (PEV_i) considering:

- Energy consumption (EC_i)
- Average autonomy (Aut_i)
- Capacity of the battery (Cap_i)
- Maximum power supply (Ps_i)
- PEV type ($Type_i$): if it is a battery or plug-in hybrid electric vehicle

PEV_i of each agent is based on real data according automakers and their public data of year 2013. It is modeled as a probabilistic variable and the probability distribution function (PDF) applied is based on data of forecasting sales [22]. PEV models considered are listed in Appendix 6.A.

Place of residence (R_i): it depends on power network scenario and it is modelled as a constant probability, based on public data [23] and the corresponding transformer capacity. R_i is linked with charging point at home usage.

In this model it is assumed that the PHEV is fully propelled by electrical drives until the end of the energy stored in the battery, when they consume oil as hybrid electric vehicles.

(b) **Mobility variables**

Mobility variables are assigned to each PEV agent in order to model its mobility behavior. Different mobility patterns are based on mobility public data for the Barcelona City [24]. The variables considered to define a mobility pattern are defined below:

- Trips per day (S_i) are determined using a probabilistic variable which is generated through a Poisson distribution function by parameter λ of Eq. 6.1 and the average value of S_i from Barcelona is 3.53 trips/day. Equation 6.2 ensures that the minimum trips per day are two.

$$P(k, \lambda) = \frac{e^{-\lambda} \lambda^k}{k!} \tag{6.1}$$

$$\lambda = S_i - 2 \tag{6.2}$$

- Driving distance (L_i) and Driving distance per trip (l_{ij}) are determined through an exponential distribution function from public reports. In the case study analyzed,

L_i is 83 km based on public data. If $l_{ij} > 10$ km, the trip j is considered as metropolitan based on Barcelona characteristics. The relation between L_i and l_{ij} is shown in Eq. 6.3 and the l_{ij} PDF is in Eq. 6.4:

$$L_i = \sum_{j=1}^{S_i} l_{ij} \tag{6.3}$$

$$l_{ij} : P(x) = 1 - e^{\mu x} \tag{6.4}$$

- Destination (D_{ij}) is the final location of each displacement where the PEV could be plugged. The reason of displacement determines D_{ij} and the reasons considered are: personal issues, to work, and to go back home. For example, D_{ij} of a trip to go to work is the office. Furthermore, D_{ij} is strongly linked to grid node where the PEV is connected in function of social data and mobility pattern. Destination is modelled with a constant PDF according to the power network topology.
- Day of the week (d_i) corresponds to the day when the PEV will be driven.
- Time distribution (m_{ij}) are the statistical data which determines in which hour the vehicles will be driven. The majority of mobility reports have this information to analyze the pattern of drivers. m_{ij} depends on the reason of displacement to drive because the trips to work occurs at morning, and to go back home occurs in the afternoon, in function of social patterns of drivers. Variables d_i and m_{ij} are linked because the time distribution of Mondays or Sundays are completely different. This information is very useful to determine the charging demand in public points in function of the SOC.
- Velocity (v_{ij}) is modelled as a constant value in function if the trip is urban or metropolitan. Average velocities for urban and metropolitan displacements are 22.2 and 59.3 km/h respectively according to [24].
- Initial/Final time (t_0, t_1) are the instants when the PEV starts (t_0^1) and finishes (t_1^1) the first trip of the day. These variables are linked with l_{ij}, v_{ij}, and m_{ij} and they are grouped in matrix Y_i which stores mobility data of each PEV:

$$Y_i = \begin{bmatrix} t_0^1 & t_1^1 \\ \vdots & \vdots \\ t_0^{S_i} & t_1^{S_i} \end{bmatrix} \tag{6.5}$$

- Social variables as gross domestic product, population density, and the number of vehicles per person in the area are applied to determine the number of agents N. For the case study the number of agent is 805.

Mobility considered is just for weekdays because the load demand is higher than during weekends. For this reason, if the PEV charging demand compromises the grid, it will happen before during weekdays.

All these parameters can be different by groups of agents (C_i) to distinguish between all agents profiles of the case study. Therefore, segregation groups of

agents permits to analyze the specific energy consumption. In Sect. 6.2.1 agent profiles applied in the case study are exposed.

(c) **Charging variables**

The charging process considered is the slow—AC single-phase-, depending on PEV model, battery capacity, SOC, energy required to arrive to next destination, and time between displacements. Furthermore, the model includes public charging points and it is assumed that there is always a public charging point available.

All PEV models are supposed to have Li-ion batteries and the slow charging process corresponds to a typical charging curve with two periods: constant current (I), and constant voltage (II). The power rate (Ps_i) is the maximum power that the PEV charger can require in function of the grid voltage available and the current limits. Ps_i considered for charging is 3.7 kW (230 V, 16 A) because it is commonly available in residential and commercial premises in Europe [25].

Charging process depends on initial SOC and energy required (E_{req}) in the process. Figure 6.2 shows the charging process of a battery with Cap_i of 16.5 kWh fully discharged. During period I, at constant current, the power is constant until the instant *a*, when the period II begins. This period corresponds to the constant voltage period and it finishes at instant *b* [26], when the power output reaches 8 % of Ps_i, which corresponds to power *c*. Besides during period I, SOC I increases linearly until instant *a* and it decreases exponentially during period II up to the final instant *b*. In this model it is assumed that the period I requires 50 % of time for a full charge. These assumptions in the charging profile permit to reduce the computation time.

IEC 61851 defines four conductive charging modes and they are shown in Table 6.1. Charging mode 1–2 are applied for charging strategies a, b, and c, mode 3 is applied for charging strategy d, which are described in Sect. 6.2.2. From the point of view of grid impact, there are no differences between charging mode 1 and 2.

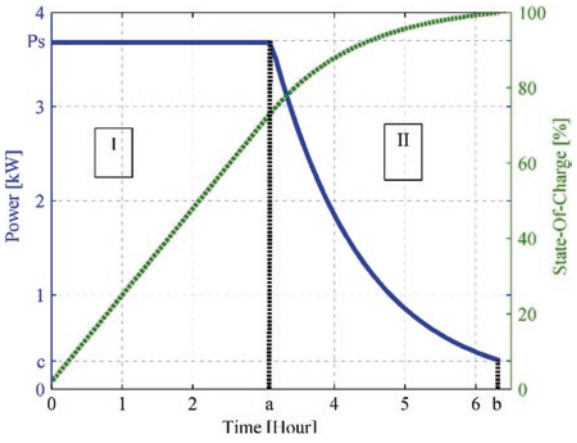

Fig. 6.2 Slow PEV charging profile of active power and the corresponding state-of-charge variation

Table 6.1 IEC 61851 conductive charging modes characteristics

Charging IEC mode	Specific connector	Charging type	Max. input current	Maximum power (kW)
1–2	No	Slow—AC	16 A—1 phase	3.7
3	Yes	Slow—AC	16 A—1 phase	3.7
4	Yes	Fast—DC	72 A per phase	50

Monte Carlo simulations

The algorithm is based on Monte Carlo methodology to combine all stochastic variables per agent and they are: R_i, S_i, L_i, l_{ij}, D_i, t_0, t_1, *and* PEV_i. For this reason, it is necessary to define the number of iterations (T). Furthermore, to start the algorithm is necessary to define the number of agents (N) that charge the PEV in the network analyzed, and the time step applied is 5 min. The algorithm defines the PEV agent profile, its mobility parameters, and the charging process of each PEV agent.

According Monte Carlo methodology, the standard deviation (*std*) of PEV power demand are evaluated to determine T needed. Considering the computing time required per iteration, the *std* begins to be stable at iteration 200. Moreover, T definition allows to avoid oversizing the problem.

6.2.1 Probabilistic Grid Impact

Given a certain level of PEV penetration, this section presents the methodology used to analyze and compare the scenarios. The analysis is focused on the maximum demand as the worst case and the objective of the analysis is to determine if any grid element does not hold up the maximum demand. It is also analyzed if some control techniques can reduce the impact and can avoid the grid expansion with its corresponding expensive solution. There are many control techniques to manage the PEV demand to minimize the energy cost or greenhouse gases emissions, but this chapter is focused on the minimum impact to the grid.

PEV demand presents new characteristics which modify the probabilistic impact analysis. Before PEV demand reaches a critical level, modelling techniques help to analyze the potential impact on the existing grids. The model applied in this case study is exposed in Sect. 6.2. As it has been seen before, PEV demand depends mainly in mobility variables as total distance travelled and time distribution but also depends on the energy consumption per vehicle. These new variables could increase the volatility in the load demand and it could cause problems in the low and medium voltage grids. For this reason the probabilistic analysis becomes more important than before. Assuming that the distribution system operators (DSO) will maintain the same reliability at the minimum cost, the objective is to avoid new grid expansions and to deliver as much energy as PEV owners will need.

The probabilistic grid impact analysis permits to determine the likelihood of a grid for supplying the extra energy needed to charge a certain number of PEV

considering their uncertainty. Therefore, for modeling PEV charge it has to be considered PEV agent, mobility, and charging variables. The probabilistic analysis permits to obtain probabilistic results of grid variables as line and transformer saturations, and voltage drops in order to assess when the grid could have problems to supply the PEV due to power line or transformer saturation, or to present a voltage below the minimum voltage allowed.

This impact analysis is also a valuable procedure to compare different PEV charging strategies because all valid proposals should not compromise the grid operation. All the charging strategies proposed are based in the fact that the PEV demand can be shifted to, for example, the valley period, the less expensive or less pollutant hours of the day, but the economical or environmental conditions should not be necessary feasible considering the grid constraints.

Network impact evaluation

The methodology proposed to estimate the PEV charging demand is applied as follows to analyze different aspects as voltage drop, line loadings, and transformers loadings.

The test system used to analyze the PEV impact is a modified 37 nodes IEEE test grid according Barcelona typical MV grids. The cable sections are sized as telescopic distribution and there are copper and also aluminum cables. The lines near to the substation have the higher sections and the farthest lines have the thinnest sections. The voltage level of this grid is 11 kV as a representative old distribution grid from Barcelona. Figure 6.3 shows the topology of the grid, the section and

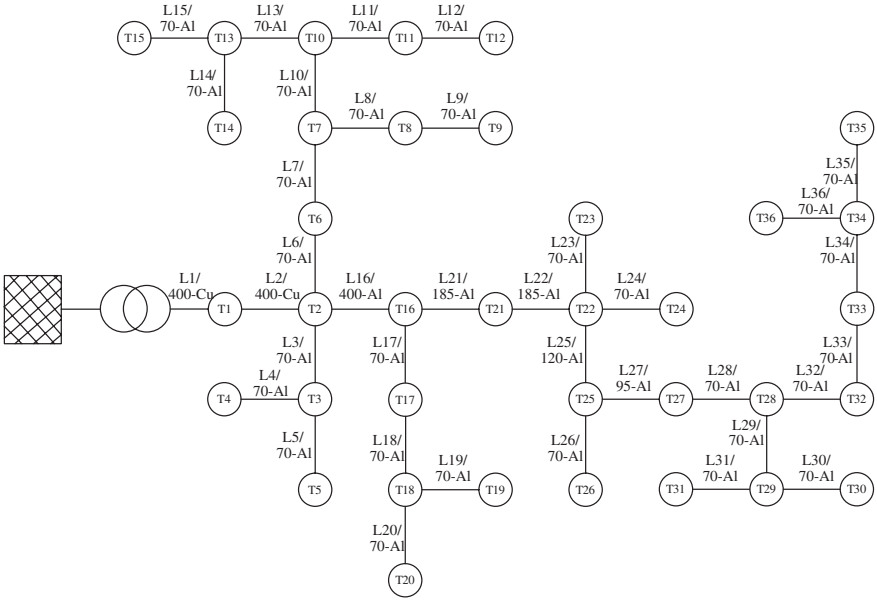

Fig. 6.3 Adapted 11 kV IEEE MV distribution test grid

material of each line of the grid. The cable characteristics and the capacity of each MV/LV transformer are listed in Appendix 6.B.

As it is explained in the following sections, the number of PEV charging stations in each grid node is a variable linked with the number households. This is because it is assumed that each PEV user will have a charging point at home or at the parking station.

Furthermore, the variable *number of households* is related to the MV/LV capacity because more households means more consumption. Number of vehicles are calculated with the following Eqs. 6.6 and 6.7 in function of Spanish electrotechnical standards for new MV/LV transformers (ITC-BT-10).

$$n_h = 21 + 2 \cdot \left(\frac{P_{trans} \cdot C_{trans} \cdot PF}{P_{contr}} - 15.3 \right) \tag{6.6}$$

$$n_{veh} = n_h \cdot \rho_{veh} \cdot \rho_{pop} \tag{6.7}$$

where

n_h	number of households
n_{veh}	number of vehicles
P_{trans}	Power of transformer in function of each node
C_{trans}	Charge of transformer: 80 %
PF	Power factor: 0.9 for residential areas
P_{contr}	Contracted power: 5.5 kW per household
ρ_{veh}	Vehicles density (veh/inhab)
ρ_{pop}	Population density (inhabitants/household)

The base case with No PEV is basically defined by the load demand and this provokes a certain voltage drop in each bus and a certain line loading.

The active load demand without PEV considered is shown in Fig. 6.4a. This demand is determined in function of MV/LV capacity and the load curve of Spain. The load curve corresponds to a winter day with the highest peak power consumption because the grid analysis has to consider the worst situation. Furthermore, it is forecasted to the next 5 years from the original data. This is because all grid planning activities has to be considered in an adequate time horizon to ensure a good quality of service. Otherwise, the grid could be saturated and a new grid expansion should be necessary in a short period of time.

Voltage drop and line loading are the parameters to analyze the grid impact. Figure 6.4b shows the lines near the maximum loading: L1, L2, L6, L21, L22, and L25. Figure 6.4c shows the maximum voltage drop during the day in the worst node T35, which is at 4.3 km from the HV/MV transformer. The maximum voltage drop is near 0.96 p.u., and it happens after the 18th hour. This voltage drop is not a considerable problem but it has to take carefully to not exceed the minimum voltage permitted of 0.93 p.u. based on European Standard EN 50160 [26]. This case is considered as a representative case of high loaded distribution grids with different possible problems that have to be considered. The N−1 contingency analysis is not considered in case of radial distribution grids because any fault in

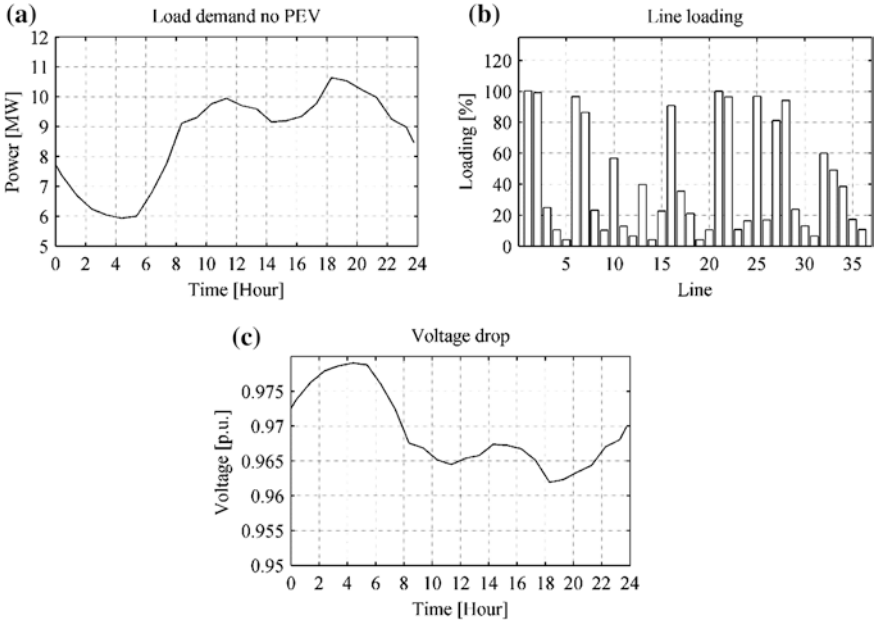

Fig. 6.4 Scenario without PEV **a** Total active power in the grid. **b** Line loadings in the grid. **c** Voltage drop in node T35

the grid could provoke the disconnection of all of users and the DSO has not an alternative line to supply them.

To include different types of PEV users that charge in the grid is necessary to analyze the profiles of drivers in the area. In Barcelona it has been identified differences between private and professional drivers, three different levels of origin areas and two types of preferences of charge are considered. Professional users drive more than 7 trips per day. Origin levels considered are: local, urban, and metropolitan, referred to users with their household in the same grid, in the same city but connected to another MV grid or in another location. This variable is linked to the driving distance and the energy consumption of PEV, and also with the charging station because it could be in public location or at household and then, users from other origins impact on the grid only at the public charging points. Table 6.2 shows the six groups included in the PEV demand and their characteristics.

6.2.2 Charging Strategies

Based on the state of the grid shown before, the grid is near to the limit and new loads could compromise the security and the safety of it. To compare the potential grid problems in different cases, the analysis includes 4 charging strategies to

Table 6.2 Social characteristic of PEV users in function of group

Group	Use of vehicle	Origin	Preferences
1	Private	Local	At-the-end
2	Private	Urban	Between disp.
3	Private	Metropolitan	Between disp.
4	Professional	Local	At-the-end
5	Professional	Urban	Between disp.
6	Professional	Metropolitan	Between disp.

Table 6.3 Charging strategies applied in the case study

Scenario	Charging strategy	Range anxiety	Electricity tariff
Intensive charge	At the end of each displacement	High	Constant
Plug-and-Play	At the end of the day	Medium	Cheaper at home
Tariff controlled	During the cheapest period	Low	TOU
Smart charging	Under aggregator control	Low	TOU

analyze the impact of each scenario to the grid. Each scenario assumes different PEV owners behavior, their mobility needs are considered, and always there are available public charging points with IEC mode 1 if they are needed. Table 6.3 resumes them and below they are explained in detail:

- Intensive charge (a): This scenario assumes a high range anxiety and private charging points at mode 1. It is also assumed a constant electricity price during the day. According to that, PEV owners plug-in the vehicle after each displacement and always try to reach the higher SOC.
- Plug-and-Play (b): In this scenario, PEV users have lower range anxiety and can wait until they arrive at home to charge the PEV if they do not need it to reach their destination. As previous scenario, private charging points are uncontrolled and they are mode 1. The electricity price considered is higher in public than in private points, for this reason, the users try to plug-in their PEV at the end of the day at home if they do not need it before.
- Tariff controlled (c): This scenario is similar to the previous one but the household tariff is different in function of the period as a time-of-use (TOU) tariff. Based on Spanish case [27], the cheapest period for PEV owners begins at 1 a.m. For this reason, private charging points have a device that allows to shift the charge to the cheapest period.
- Smart charging (d): As it is shown in following sections, the previous scenarios increase line loadings over the capacity of the grid. To mitigate this potential negative impact, this scenario analyses the possibility to include an aggregator which has the control over all PEV chargers. Electricity tariff is also a TOU tariff and it is assumed that the aggregator knows the SOC of each PEV and the moment when the PEV will leave.

The following sections show the results for all scenarios using four subfigures: PEV demand, Total demand, Voltage drop, and Line loading. The PEV demand is the sum of the load caused of all PEV charges in the analyzed grid and it is represented with the maximum, mean, and minimum demand value for the studied period (from the highest value to the lowest, respectively). In this way, the figure shows the feasible area of demand for each moment. The maximum value is useful for the grid analysis to determine contingencies. The mean value is useful from the point of view of market and generation planning to schedule the corresponding energy generation. And the minimum value shows the lower value of PEV demand and it could be also useful for the generation and retailer companies as a value similar as the base load. This discussion is more appropriated for not controlled scenarios when the volatility of demand is directly applied to the grid. In contrast, the PEV volatility in controlled scenarios is smoothed by control system.

The total demand subfigure shows the sum of all loads in the studied grid with the maximum, the minimum demand with PEV, and the No PEV demand (from the highest value to the lowest, respectively). The No PEV demand corresponds to the case of No PEV impact combined with the highest demand case. To analyze the volatility of the PEV demand, the base case has to be constant and it has to correspond to the maximum demand and the 5 year demand forecast.

Load flow calculations are executed for each demand daily curve. The results of these simulations are represented in the subfigure voltage drop. The No PEV, the minimum demand and maximum demand cases are depicted in this subfigure (from the highest value to the lowest, respectively).

The line loading subfigure shows the relationship between the loadings of the cables from the load flow results with their rated currents. The white bars correspond to the base case without PEV, the black values are the maximum saturation with the PEV maximum demand case. Each line number corresponds to the line numbers exposed in Fig. 6.3.

(a) **Intensive charge**

This section exposes the analysis of Intensive charge scenario in which all agents can plug-in the vehicle and start the charge at the end of each displacement. Figure 6.5 shows four analysis. PEV demand shows the range of uncertainty for a day caused by mobility and electric probabilistic variables. The approximated uncertainty value during the most charged hours is around 150 kW. The consumption presents three peaks. The first one is after hour 8 when PEV users arrive at the office. The second one is less pronounced at hour 14 when PEV users move for lunch. The higher peak demand occurs at 19 h when people go back home after some personal activities. Of course, the third peak occurs approximately at the same time that winter peak demand for the same reason, when people go back home. The PEV peak demand is near to 500 kW and total peak demand is 11.04 MW, 3.75 % higher than in the No PEV case. The impact on voltage profile is that minimum voltage reaches 0.96 p.u. but is far from the limit value of 0.93 p.u. About line loadings, the maximum current reached is 655.43 A and this corresponds to 104 % of saturation in L1.

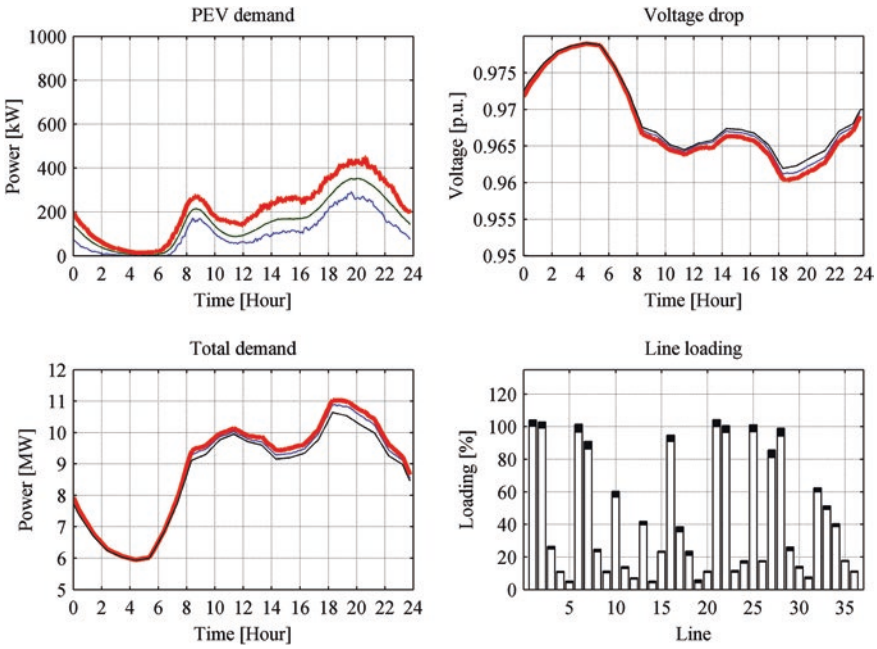

Fig. 6.5 Simulation results of the grid impact for the intensive charge scenario

(b) **Plug-and-Play**

For this and the following scenarios, the same methodology is applied as the previous one. The first and second peak demands from PEV are smoothed because the energy price in public stations is higher than at home. The SOC at the end of the initial displacements is enough to continue during the day. As it is shown in Fig. 6.6, the energy consumed at the evening is 628 kW and occurs at hour 20. As previous scenario, the peak total demand is approximately synchronized and the maximum value is 11.12 MW after 18th hour. Minimum voltage is near to 0.96 p.u., out of risk range. About line loadings, the higher saturation is 105.2 % and the maximum current is 662.66 A in L1 .

(c) **Tariff controlled**

This scenario includes a simple control system which shifts the charging process to the cheapest period at hour 1. As it is shown in Fig. 6.7—PEV demand, this system provokes a maximum peak of 1,857 kW because all charges begin at the same time. The consumption during the day is caused by users without enough SOC after the displacement by plugging-in the PEV in public charging points. This peak at hour 1 in total demand has a tiny impact because the consumption at this time is much lower than during the evening. From the point of view of generation, this could be a problem of supply to deliver the energy perfectly synchronized with the PEV demand. From the point of view of grid impact, the voltage profile is not really affected and the saturation is a bit higher, but lower in comparison with the previous scenarios.

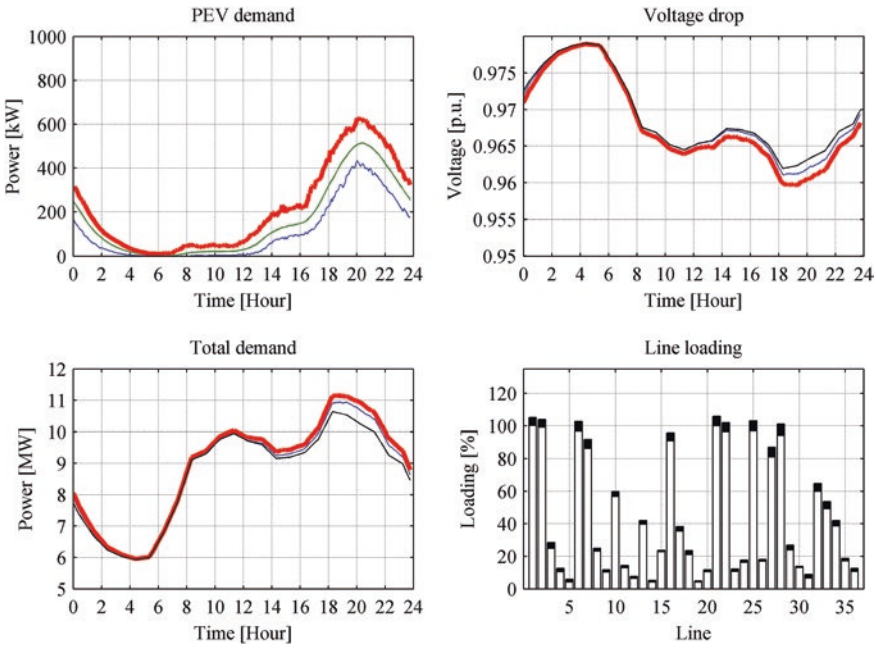

Fig. 6.6 Simulation results of the grid impact for the plug-and-play scenario

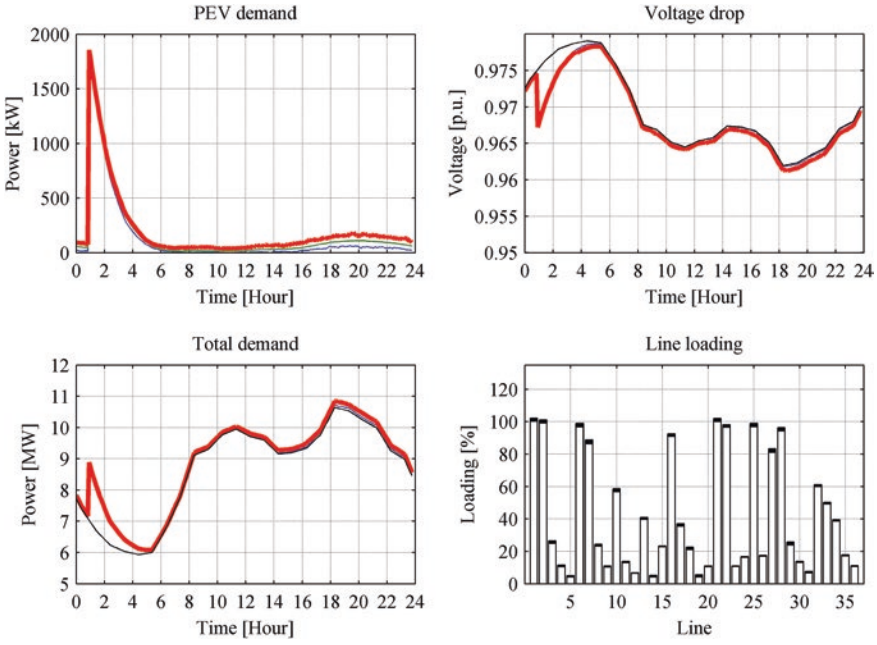

Fig. 6.7 Simulation results of the grid impact for the tariff controlled scenario

According with these results, public charging points provokes saturations in L1, L2, L21, and L25. The higher saturation is 102.3 % and the maximum current is 644.12 A in L1. For this reason, the option of installing public charging points is not considered for the next scenario.

(d) **Smart charging**

This scenario assumes a completely control on PEV charging by the aggregator, the third agent responsible to manage the charges. In this case, the objective is to fill the valley period at the minimum power with no line saturation. Furthermore, in this scenario there are no public charging points because in the previous scenario they are the cause of saturations of some lines. As it is shown in Fig. 6.8, the uncertainty in this scenario related to the energy consumption in each iteration is very tiny. From the point of view of the grid, this scenario is the best option because the voltages and line loadings keep in the same range as the base case. From the point of view of generator and retailers, it is also the best option because the consumption is really constant and predictable.

To evaluate the impact on the MV/LV transformers in the whole grid is necessary to analyze the probabilistic demand. To do that, a useful approach is to represent the consumption in boxplots and the nominal power in boxes. This type of plot is useful because they show the distribution of the data as 1st, 2nd, and 3rd quartile and also show the whiskers which indicate the values out of quartiles. All this information indicates the normal range operation of transformers and also the

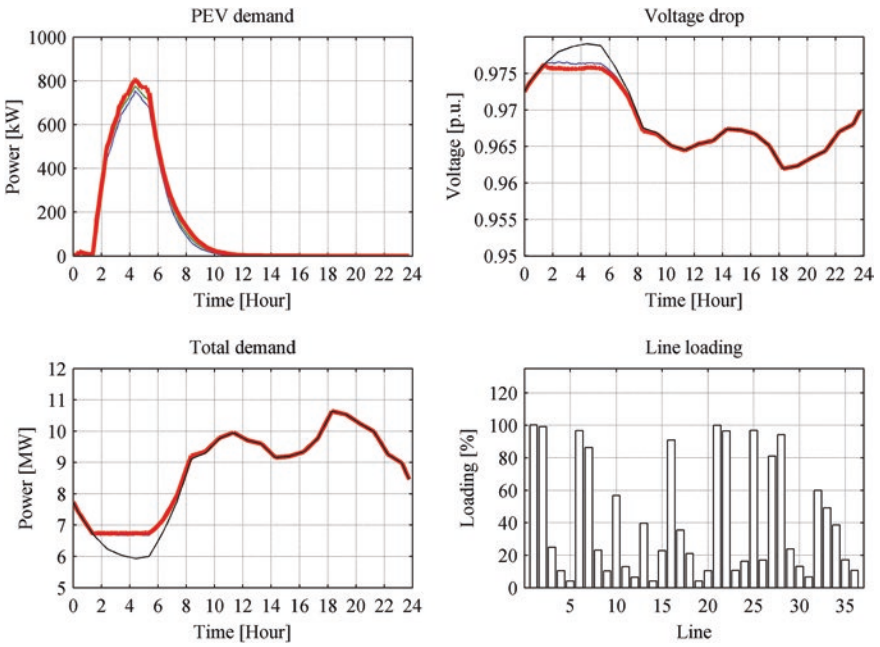

Fig. 6.8 Simulation results of the grid impact for the smart charging scenario

upper and the lower values. Furthermore, it is possible to distinguish between the transformers overloaded and the transformers with some critical situation but not an overload problem. Transformers have the capacity, under certain conditions, to deliver more power than their rated power over a short period of time without significant degradation.

This analysis can be done with saturation values as percentage, but the plot with real capacity permit to distinguish between transformers with more or less capacity. This information is useful because for the DSO is not the same to reinforce a transformer of 250 kVA than one of 630 kVA.

Figure 6.9 shows the boxplots for each transformer and each scenario. In this case three situations are shown: overcharged, near overcharged, and normal condition. A clear example of the first situation is the T7 of Fig. 6.9b with the 2nd quartile above the nominal capacity. T34 of Fig. 6.9a has the upper quartile at the range of nominal power and it is an example of near overcharged situation. And Fig. 6.9d shows that all transformers are in normal conditions with all the upper quartiles below the nominal capacity.

To contrast the probability of time to the descended power or current is useful to compare charging strategies and also to determine the time probability with higher demand or lower voltages. This information is also convenient for generators and retailers to design their acquisition or generation strategies.

Figure 6.10a shows the duration curve of total demand and it is clear that the higher demand occurs in Plug-and-Play scenario. Furthermore, near the 20 % of

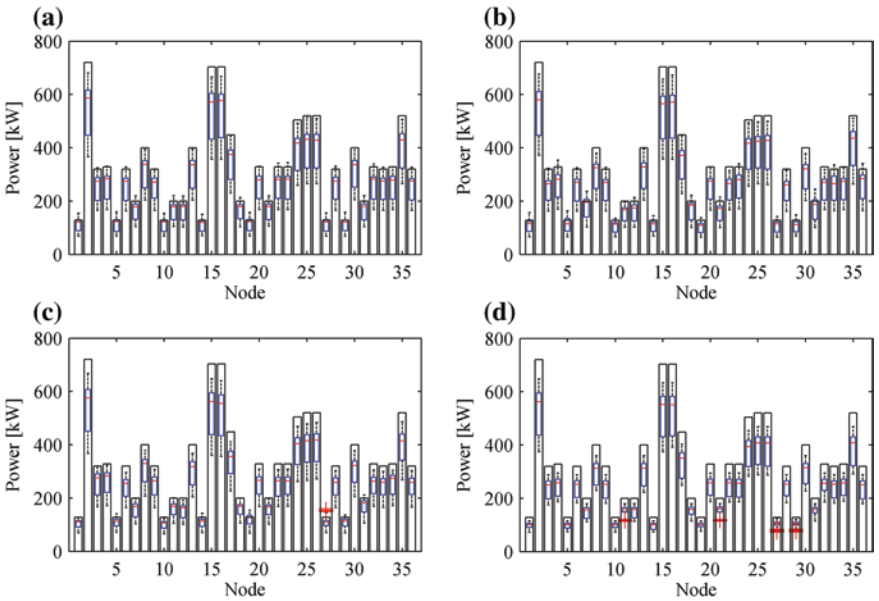

Fig. 6.9 Simulation results of total demand in MV/LV transformers for each scenario: **a** Intensive charge. **b** Plug-and-Play. **c** Tariff controlled. **d** Smart charging

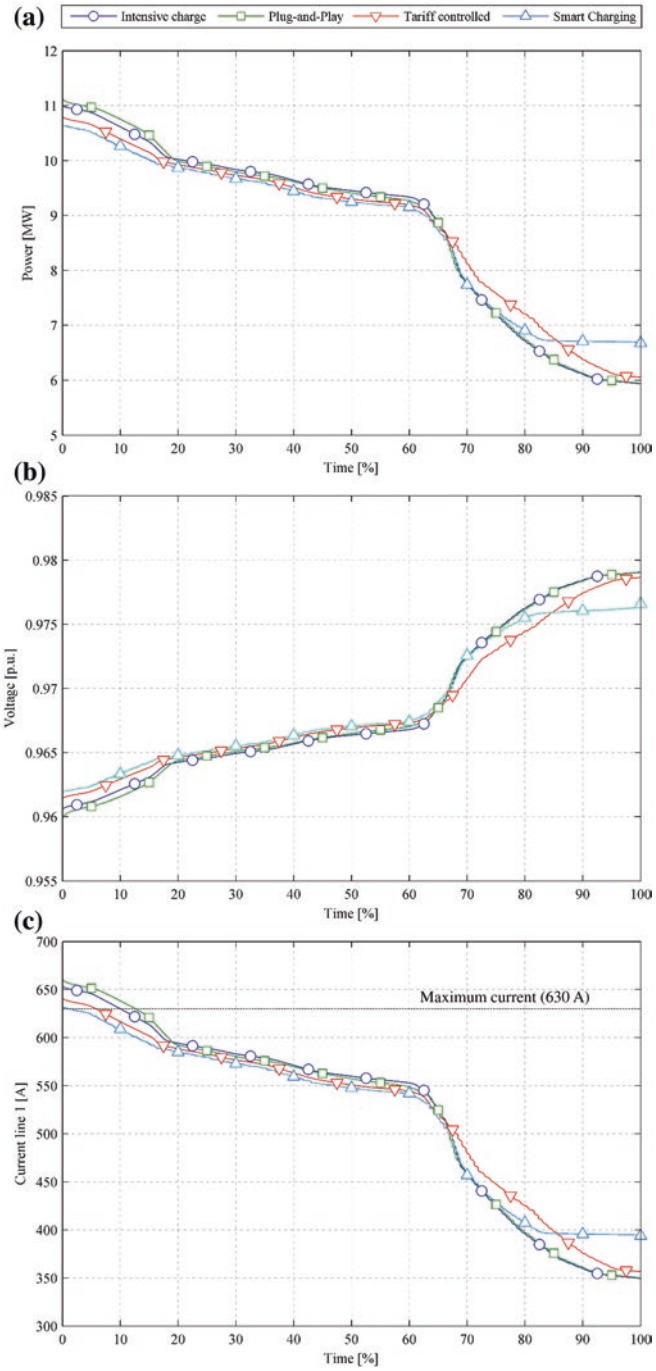

Fig. 6.10 Duration curves from simulations of each scenario of: **a** Total load demand. **b** Voltage profile in T35. **c** L1 loading

time, the demand is higher than the other scenarios. Intensive charge scenario generates the highest demand for the next 45 % of time and it is a reasonable range of power. Tariff controlled is the higher consumption for the following 20 % of time, and higher scenario of the last 15 % of time is the smart charging.

The same approach occurs for the voltage duration curve in Fig. 6.10b, and also for the current duration curve in Fig. 6.10c. These figures show the range of voltage and current of each time range.

Load curves sort the power in descend order to analyze the percentage of time that the power demand is higher than the base case. This type of plot is useful to compare different scenarios and to analyze the effects from the base case. The scenario which provokes a higher power peak increase is the Plug-and-Play. The Smart charging scenario provokes that power increases during the lower charged time. All the demand is focused in the 20 % lower charged of time.

The most saturated lines in Plug-and-Play scenario are the L1 (105.13 %) and L21 (105.83 %). The analysis is focused on L1 to be the most critical grid line but the procedure is also valid for L21.

6.3 Fast Charging Points

Slow charging process of the battery of PEV is usually expected to be carried out at private places during night hours, although it can be performed during different time at workplace, malls, and public car parks. However, in order to deal with driver's needs for long rides and keep the usual way of re-fuelled engine vehicles, fast charging is considered due to it can recover up to 80 % of SOC within 30 min. Then, fast charging is considered as a complement of slow charging since it can deal with range anxiety although it is likely to reduce electric vehicle battery life. However, it is even more difficult to predict respect to domestic charging.

Fast charging is performed with an off-board charger based in two standards: SAE J1772 [28] and IEC 61851 [29] in order to access directly in DC the battery. As traditional re-fueling stations, fast charging station for PEV may consist of several fast charging points, with individual power rating around 50 kW. Then, fast charging stations require a proper sizing in power and number of fast charging points to meet PEV fast charging demand. Therefore, the deployment of fast charging infrastructure requires a previous assessment in order to cope with its impact on distribution network due to the high power level it may require. Furthermore, power quality issues as unbalance and harmonics can appear for both slow and fast charging processes [30].

This section deals with the ability of distribution networks operator to integrate charging infrastructure without overloading power system components and it is applied to the same case study, because it is important to consider a combination of both domestic and fast charging. Moreover, the study includes the proper sizing of the fast charging stations.

6.3.1 Probabilistic Arrivals

The arrivals and service time are the main stochastic variables of a fast charging station. To size the station it is important to consider the variability of arrivals to ensure a suitable supply service. The data applied for the case study is also from Barcelona and its mobility [24]. Figure 6.11a shows the PDF to simulate the PEV arrivals to the fast charging station. This profile corresponds to the cars flow at Barcelona's entries and it is the most appropriate profile because it is linked with long trips and these PEV may need to charge to come back home. Figure 6.11b depicts the fast charging power profile of 30 min and 50 kW as the maximum power.

From the point of view of sizing the infrastructure, it is important to install the adequate number of fast charging stations to avoid queues or unused chargers. The methodology applied is based on [31] and it is a Markov chain model according to a certain level of arrivals and time service. Figure 6.12 shows the Markov chain diagram and, according Kendall notation, the model corresponds to M/M/c/N type: M arrivals distribution, M service time, c number of charging points and N capacity of the system. Furthermore, an adequate number of fast chargers can reduce the grid expansion associated and the grid impact.

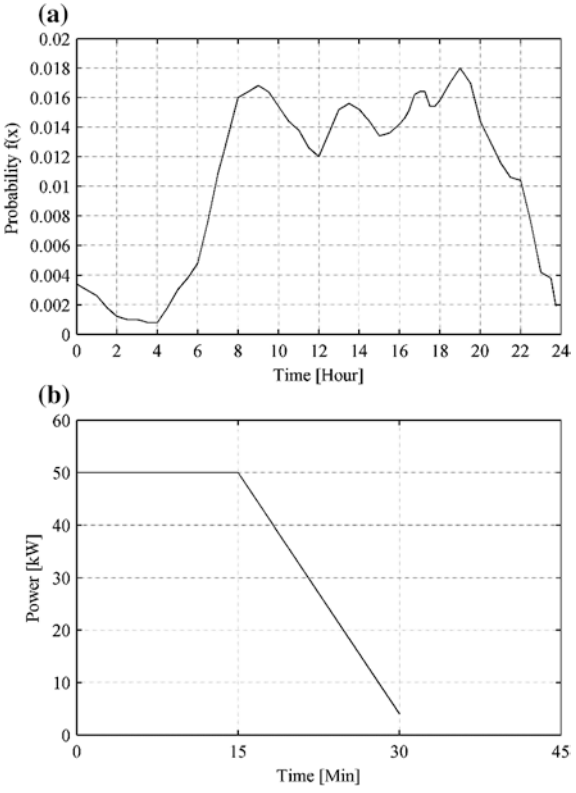

Fig. 6.11 Data implemented in the probabilistic model: **a** Arrivals probability to the fast charging station. *Source* [24]. **b** Average power consumption per fast charge

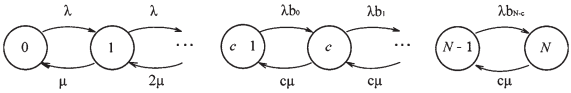

Fig. 6.12 Markov chain of the model applied M/M/c/N in the probabilistic model

Parameters used are the number of arrivals, service time, type of queue, and the waiting space.

- The arrival distribution function is based on Poisson distribution (Eq. 6.8) with average arrivals of λ(t) in function of the time. The successes k occurs randomly and it is defined as PEV arrival to the fast charging station with average λ(t) arrivals.

$$f_X = P(k = X) = \frac{e^{-\lambda}(\lambda^k)}{k!} \tag{6.8}$$

- The service time is modelled as an exponential distribution function (Eq. 6.9) and it represents the time between the arrival and the end of the service. The average time is 1/μ, and it is 30 min when the battery capacity is 24 kWh and the SOC goes from 20 to 80 %.

$$f_x = P(X \leq x) = 1 - e^{-\mu x} \tag{6.9}$$

- Service discipline applied is FIFO (First In–First Out). The first vehicle how arrives will be the first served.
- Capacity of the system is N. If the system is full the user is rejected.
- The number of chargers is called as c and it is considered more places than chargers ($N > c$) to analyze the size of waiting space. In the case of PEV is important to consider the space for the vehicles.

The probability P_n that the system has a certain number of PEV (n) is calculated according Eq. 6.10,

$$P_n = \frac{1}{c!} \cdot (c\rho)^c \cdot \rho^{n-c} \cdot P_0 \tag{6.10}$$

where P_0 is the probability that the system is empty:

$$P_0 = \left(\sum_{n=0}^{c} \frac{1}{n!} \cdot (c\rho)^n + \frac{1}{c!}(c\rho)^c \cdot \sum_{n=c+1}^{N} \rho^{n-c} \right)^{-1} \tag{6.11}$$

Average proportion of time which the charger is occupied is ρ and it must be $\rho < 1$ to have a stable queue:

$$\rho = \frac{\lambda}{c \cdot \mu} \tag{6.12}$$

And P_N is the probability that the system is full:

$$P_N = \rho^{N-c} \cdot \frac{(c\rho)^c}{c!} \cdot P_0 \tag{6.13}$$

The average waiting time W_q:

$$W_q = \frac{L_q}{\lambda(1 - P_N)} \tag{6.14}$$

where L_q is the average waiting PEV in the queue:

$$L_q = \frac{(c\rho)^c \cdot \rho}{c!(1-\rho)^2} \cdot P_0(1 - \rho^{(N-c)} - (N-c) \cdot \rho^{(N-c)} \cdot (1-\rho)) \tag{6.15}$$

And finally the average number of PEV in the system:

$$L = \sum_{n=0}^{c-1} n \cdot P_n + L_q + c \cdot (1 - \sum_{n=0}^{c-1} Pn) \tag{6.16}$$

6.3.2 Probabilistic PEV Charging Demand

The analysis of queues with PEV demand of fast charges compares the effect of the waiting space and the number of fast chargers. The analysis includes two possible cases: to install two or three fast chargers, and their corresponding waiting spaces. The decision variables considered are P_N and W_q, and the results are shown in Table 6.4. It seems clear that the option with two chargers and three waiting spaces increases the waiting time over the desired time, until near 17 min. For this reason the station has three fast chargers.

Considering the PEV charging demand, three fast chargers, and one waiting space, the probabilistic electricity demand is shown in Fig. 6.13. Boxplots show the distribution of consumption during the day and it is mainly concentrated between hour 8 and 20. The chargers during the night are exceptional.

6.3.3 Probabilistic Grid Impact of Fast Chargers

The fast charging station with three fast chargers is installed in T15. This node could present some problems because it is located at the end of the branch and the cable section is the thinner one. To avoid transformer capacity limitations, the owner of the station decides to install his own transformer of 160 kVA. Power factor of each fast charger considered is 0.96 as is described in [32].

Table 6.4 Results of queues of the fast charger station comparing to feasible options

Fast chargers c	Waiting spaces N-c	Capacity of the system N	Probability that the system is full P_N (%)	Waiting time W_q (min)
3	1	4	7.56	2.30
2	3	5	5.7	16.64

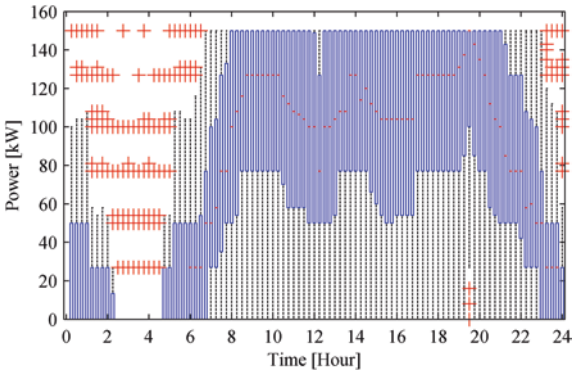

Fig. 6.13 Simulation results of total active demand in the fast charging station

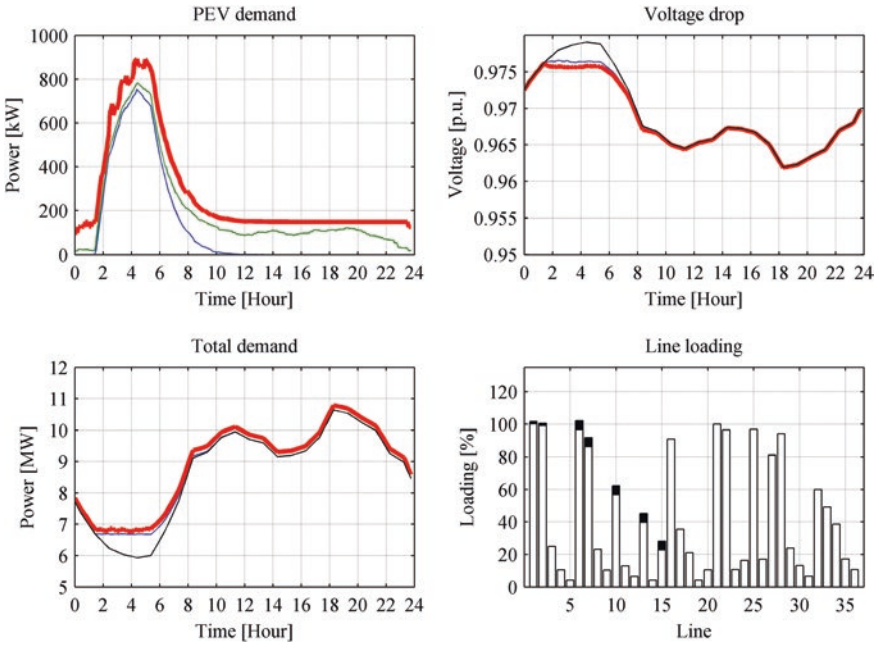

Fig. 6.14 Simulation results of the grid impact for smart charging scenario with 3 fast chargers in T15

According to Spanish regulation, all the grid elements that should be changed to connect this new load must be paid by the petitioner of the connection. The grid impact analysis has to determine if, in some cases, the grid could present some capacity limits and also to avoid to oversize the grid.

As it is shown in Fig. 6.14, the fast charging station demand provokes a cascade effect on its corresponding lines, saturating L6 with 168.54 A and 103.4 %

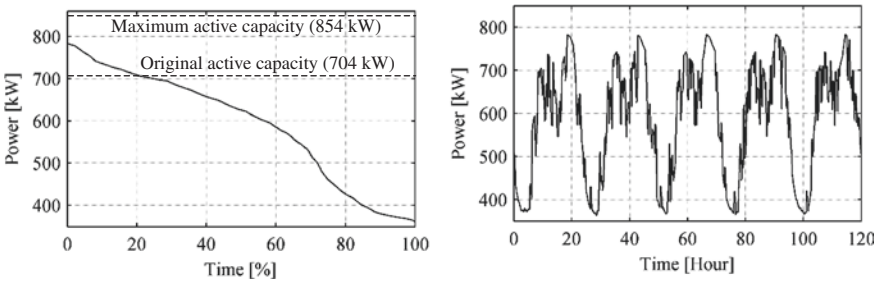

Fig. 6.15 Load demand duration curve (*left*) and five consecutive weekdays consumption in T15 (*right*)

of saturation, but no very different from the case without fast charging. From the point of view of voltage drops, there are no relevant effects in any node.

To avoid L6 saturation is not possible to shift the fast charger demand because it has to be supplied at the moment when it is required whit the minimum delay. The alternative to substitute this cable should be applying demand-side response techniques in other consumers to avoid the peak produced by the chargers.

About the energy demand, Fig. 6.15 shows the duration curve and load demand never exceeds its maximum active capacity. Furthermore, the consumption of 5 weekdays shows the load fluctuation caused by the fast chargers.

6.4 Conclusions

In this chapter, the PEV demand modeling for slow charging, the distribution grid impact analysis and the impact of fast charging stations has been presented.

Concerning PEV demand modeling, the agent-based methodology using stochastic variables allows a detailed problem formulation. The main advantage of this methodology is the flexibility to include new variables or to exclude the less significant ones. Moreover, this flexibility also permits to compare models with different variables or different case studies.

Regarding the distribution grid impact, there are three aspects to be considered: the total demand of the studied grid including PEV, the voltage drop, and the saturations of the power lines. The analyzed system represents a high charged urban 11 kV distribution network with a longest feeder of 4.3 km. This grid does not show any voltage drop above the established limits. The network shows saturations in several lines with the introduction of the PEV in the system. The most important cause of these saturations are the private-domestic PEV charges which could be controlled to reduce the grid impact.

The two control charging strategies presented in this study are the Tariff Controlled and the Smart Charging. The Tariff Controlled strategy allows to

reduce the grid impact and it could be implemented easily with a time based switch installed in the charging point. However, the power gradient caused by the charging synchronization could be not possible to supply. On the other hand, Smart Charging reduces all drawbacks from private-domestic charging. However, it requires an expensive ITC infrastructure with bidirectional information flow and control centers with an energy management system (EMS). Moreover, the public slow charging stations cannot be controlled and the grid should be reinforced for this case.

Regarding MV/LV transformers, boxplots are used to evaluate the loading of each transformer. This representation permits to analyze the probability of occurrence of overloading, as in transformers certain overloading can be admitted over a short period. Similarly, load duration curves permit to compare different charging scenarios, and to analyze the periods with the highest charging demand and also its probability.

Fast charging permits to extend the PEV range and complements the slow charging. The queueing theory is the used methodology to size the fast charging stations. Assuming a certain demand of charges, this theory permits to calculate the number of fast chargers, the average waiting time of users and the waiting spaces needed. Furthermore, this stochastic demand model allows to evaluate the corresponding grid impact. Typically, fast charging stations are not controlled; the grid should be reinforced and the connection should be designed to avoid grid saturation. In some cases, the grid elements reinforced could be numerous because of the cascade effect.

In general, it is important to highlight the benefits of including stochastic variables in the problem formulation of electric vehicle charging. For the PEV demand determination, the data needed for the analysis is based on variables linked with user profile and the electrical charging characteristics, both can have a stochastic nature. The combination of these two adds more variability and complexity to the problem. For these reasons, it is important to develop a stochastic model to take into account all different aspects that will determine the PEV charging demand.

Appendix 6.A—PEV Models

See Table 6.5.

Appendix 6.B—Grid Data

See Tables 6.6, 6.7 and 6.8.

Table 6.5 List of PEV models considered in the case study

Automaker	Model	$Type_i$	Cap_i (kWh)	Aut_i (km)	EC_i (kWh/km)
Aixam mega	Mega city	BEV	8.16	70	0.117
BMW	i8	PHEV	5	35	0.143
BMW	i3	BEV	32	160	0.200
BYD	F3DM	PHEV	16.50	60	0.275
Daimler	Smart	BEV	14.62	135	0.108
Fiat	Fiat 500	BEV	15.14	120	0.126
Fisker Automotive	Karma	PHEV	20	80	0.250
Ford	Focus BEV	BEV	23	161	0.143
Ford	Transit	BEV	28	105	0.267
GM	Ampera	PHEV	16.65	60	0.278
Hyundai	BlueOn	BEV	16.50	150	0.110
Mitsubishi	iMiEV	BEV	16.50	150	0.110
Peugeot	ePartner	BEV	27	97	0.280
Peugeot	eBoxer	BEV	56	153	0.366
Pininfarina	BluecCar	BEV	30	200	0.150
PSA	Citroen C-zero	BEV	16.50	150	0.110
PSA	Peugeot iON	BEV	16.50	150	0.110
Pure mobility AS	Buddy	BEV	14.40	90	0.160
Renault Nissan	Twizy ZE	BEV	6.10	80	0.076
Renault Nissan	ZOE ZE	BEV	22	161	0.137
Renault Nissan	Kangoo ZE	BEV	22	170	0.129
Renault Nissan	Fluence	BEV	22	185	0.119
Renault Nissan	LEAF	BEV	23.76	175	0.136
REVA	NXG	BEV	13.70	160	0.086
REVA	Li-Car	BEV	9.70	100	0.097
Tata	Indica vista	BEV	26.50	200	0.133
Tesla	Roadster	BEV	51.45	340	0.151
Th!nk	City	BEV	23	160	0.144
Toyota	RAV4	BEV	41.80	160	0.261
Toyota	Prius	PHEV	5.20	25	0.208
Volvo	C30	BEV	22.70	150	0.151
Volvo	V60 plug-in	PHEV	11.20	50	0.224
VW	Seat leon	PHEV	12	50	0.240
VW	Audi A3 e-tron	PHEV	17.50	88	0.199
VW	Up!	BEV	18	150	0.120
VW	Golf	PHEV	10	50	0.200

Active power assumed is 80 % of rated capacity for each MV/LV transformer as a conservative assumption.

Table 6.6 Cable data considered in the case study

Area (mm^2/Material)	R (Ω/km)	X_1 (Ω/km)	Imax (A)	Armor
70-Al	0.568	0.11	165	Three core
95-Al	0.411	0.105	200	Three core
120-Al	0.325	0.1	225	Three core
185-Al	0.211	0.094	290	Three core
400-Al	0.102	0.085	425	Three core
400-Cu	0.063	0.096	630	Single core

Source Nexans 6.35/11 (12) kV laid in single way ducts

Table 6.7 MV/LV transformers characteristics

Feature	Assigned value
Power	160-250-400-630 kVA
Connection type: 250-400-630 kVA	Dyn11
Voltage of the HV coupling	11 kV
No-load voltage of the LV coupling	420 V
Capacity of resisting short-cct events in the LV side	22.2 I_{nom}

Table 6.8 System data without fast chargers

CT	Number of transformers	$P_{nominal}$ (kVA)	Line	Length (km)	Area (mm^2)
T0	1	25,000	–	–	–
T1	1	160	L1	0.3	400-Cu
T2	3	250 + 250 + 400	L2	0.2	400-Cu
T3	1	400	L3	0.4	70-Al
T4	2	160 + 250	L4	0.4	70-Al
T5	1	160	L5	0.3	70-Al
T6	1	400	L6	0.2	70-Al
T7	1	250	L7	0.3	70-Al
T8	2	250 + 250	L8	0.2	70-Al
T9	1	400	L9	0.3	70-Al
T10	1	160	L10	0.2	70-Al
T11	2	250	L11	0.3	70-Al
T12	1	250	L12	0.3	70-Al
T13	2	250 + 250	L13	0.3	70-Al
T14	1	160	L14	0.3	70-Al
T15	2	250 + 630	L15	0.2	70-Al
T16	2	630 + 250	L16	0.4	400-Al
T17	2	400 + 160	L17	0.4	70-Al
T18	1	250	L18	0.2	70-Al
T19	1	160	L19	0.5	70-Al
T20	2	250 + 160	L20	0.1	70-Al

(continued)

Table 6.8 (continued)

CT	Number of transformers	$P_{nominal}$ (kVA)	Line	Length (km)	Area (mm^2)
T21	1	250	L21	0.4	185-Al
T22	2	160 + 250	L22	0.2	185-Al
T23	2	160 + 250	L23	0.3	70-Al
T24	1	630	L24	0.2	70-Al
T25	2	250 + 400	L25	0.5	120-Al
T26	2	400 + 250	L26	0.2	70-Al
T27	1	160	L27	0.3	95-Al
T28	1	400	L28	0.2	70-Al
T29	1	160	L29	0.2	70-Al
T30	2	250 + 250	L30	0.3	70-Al
T31	1	250	L31	0.2	70-Al
T32	2	160 + 250	L32	0.7	70-Al
T33	1	400	L33	0.3	70-Al
T34	2	160 + 250	L34	0.5	70-Al
T35	2	400 + 250	L35	0.3	70-Al
T36	1	400	L36	0.4	70-Al

References

1. International Energy Agency (IEA) (2013) Electric vehicle initiative global EV outlook
2. Bauer P, Zhou Y, Doppler J, Stembridge N (2010) Charging of electric vehicles and impact on the grid. Paper presented at 13th international symposium in MECHATRONIKA, Trencianske Teplice, pp 121–127, 2–4 June 2010
3. Clement-Nyns K, Haesen E, Driesen J (2010) The impact of charging plug-in hybrid electric vehicles on a residential distribution grid. IEEE Trans Power Syst 25:371–380
4. Huang S, Infield D (2009) The potential of domestic electric vehicles to contribute to power system operation through vehicle to grid technology. Paper presented at universities power engineering conference (UPEC) proceedings of the 44th international, Glasgow, 1–4 Sept 2009
5. Qian K, Zhou C, Allan M, Yuan Y (2011) Modeling of load demand due to EV battery charging in distribution systems. IEEE Trans Power Syst 26(2):802–810
6. Soares J, Canizes B, Lobo C, Vale Z, Morais H (2012) Electric vehicle scenario simulator tool for smart grid operators. Energies 5:1881–1899
7. Acha S, van Dam K, Shah N (2012) Modelling spatial and temporal agent travel patterns for optimal charging of electric vehicles in low carbon networks. Paper presented at power and energy society general meeting, 2012 IEEE, San Diego, 22–26 July 2012
8. Leemput N, Geth F, Van Roy J, Delnooz A, Buscher J, Driesen J (2014) Impact of electric vehicle on-board single-phase charging strategies on a flemish residential grid. IEEE Trans Smart Grid 5(4):1815–1822
9. Valsera-Naranjo E, Martinez-Vicente D, Sumper A, Villafafila-Robles R, Sudria-Andreu A (2011) Deterministic and probabilistic assessment of the impact of the electrical vehicles on the power grid. Paper presented at power and energy society general meeting, 2011 IEEE, San Diego, 24–29 July 2011
10. Valsera-Naranjo E, Sumper A, Villafafila-Robles R, Martinez-Vicente D (2012) Probabilistic method to assess the impact of charging of electric vehicles on distribution grids. Energies 5:1503–1531

11. Maitra A, Taylor J, Brooks D, Alexander M, Duvall M (2009) Integrating plug-in-electric vehicles with the distribution system. Paper presented at 20th international conference and exhibition on electricity distribution—Part 1, 2009. CIRED, Prague, 8–11 June 2009
12. Kleiwegt E, Lukszo Z (2012) Grid impact analysis of electric mobility on a local electricity grid. Paper presented at 9th IEEE international conference on networking, sensing and control (ICNSC), 2012, Beijing, 11–14 Apr 2012
13. Dallinger D, Wietschel M (2012) Grid integration of intermittent renewable energy sources using price-responsive plug-in electric vehicles. Renew Sustain Energy Rev 16(5):3370–3382
14. Lopes J, Soares F, Almeida P (2011) Integration of electric vehicles in the electric power system. Proc IEEE 99(1):168–183
15. Tie S, Tan C (2013) A review of energy sources and energy management system in electric vehicles. Renew Sustain Energy Rev 20:82–102
16. Sheikhi A, Bahrami S, Ranjbar A, Oraee H (2013) Strategic charging method for plugged in hybrid electric vehicles in smart grids; a game theoretic approach. Int J Electr Power Energy Syst 53:499–506
17. Sortomme E, Hindi M, MacPherson S, Venkata S (2011) Coordinated charging of plug-in hybrid electric vehicles to minimize distribution system losses. IEEE Trans Smart Grid 2:198–205
18. Clement K, Haesen E, Driesen J (2009) Stochastic analysis of the impact of plug-in hybrid electric vehicles on the distribution grid. Paper presented at the 20th international conference and exhibition on electricity distribution—Part 2, 2009 CIRED, Prague, 8–11 June 2009
19. Macal C, North M (2010) Tutorial on agent-based modelling and simulation. J Simul 4:151–162
20. Bonabeau E (2002) Agent-based modeling: methods and techniques for simulating human systems. Proc Natl Acad Sci USA 99:7280–7287
21. ElBanhawy E, Dalton R, Thompson EM, Kotter R (2012) A heuristic approach for investigating the integration of electric mobility charging infrastructure in metropolitan. Paper presented at 2nd international symposium on environment friendly energies and applications, Newcastle upon Tyne, 25–27 June 2012
22. Frost & Sullivan (2012) Executive analysis of global electric vehicle forecast
23. Department of Statistics of Barcelona Council (2006) Barcelona statistical guidelines and districts. (in Catalan)
24. Institut d'Estudis Regionals i Metropolitans de Barcelona (2006) Enquesta de mobilitat quotidiana (in Catalan)
25. Marra F, Guang Ya Yang, Traholt C, Larsen E, Rasmussen C, You S (2012) Demand profile study of battery electric vehicle under different. Paper presented at power and energy society general meeting, 2012 IEEE, San Diego, 22–26 July 2012
26. European Committee for Electrotechnical Standardisation (CENELEC) (1994) Voltage characteristics of electricity supplied by public distribution systems. European Norm EN 50160 Nov
27. BOE (Boletín oficial del Estado) (2011) Real Decreto 647/2011, de 9 de mayo, por el que se regula la actividad de gestor de cargas del sistema para la realización de servicios de recarga energética (which regulates aggregator activities (Gestor de carga) and Time-Of-Use tariff for PEV)
28. Society of Automotive Engineers (SAE) (2009) Surface vehicle recommended practice J1772 electric vehicle conductive charge coupler
29. International Electrotechnical Commission (2010) IEC 61851–1 ed2.0: Electric vehicle conductive charging system
30. Seljeseth H, Taxt H, Solvang T (2013) Measurements of network impact from electric vehicles during slow and fast charging. Paper presented at 22nd international conference and exhibition on electricity distribution 2013. CIRED, Stockholm, 10–13 June 2013
31. Farkas C, Prikler L (2012) Stochastic modelling of EV charging at charging stations. Paper presented at international conference on renewable energies and power quality. ICREPQ, Santiago de Compostela, 28–30 Mar 2012
32. ABB (2014) Terra multistandard DC charging station 23 CJ (CE) catalogue, June 2014

Chapter 7
Strategies for Plug-in Electric Vehicle-to-Grid (V2G) and Photovoltaics (PV) for Peak Demand Reduction in Urban Regions in a Smart Grid Environment

Ricardo Rüther, Luiz Carlos Pereira Junior, Alice Helena Bittencourt, Lukas Drude and Isis Portolan dos Santos

Abstract The strategy of using Plug-in Electric Vehicles (PEVs) for vehicle-to-grid (V2G) energy transfer in a smart grid environment can offer grid support to distribution utilities, and opens a new revenue opportunity for PEV owners. V2G has the potential of reducing grid operation costs in demand-constrained urban feeders where peak-electricity prices are high. Photovoltaic (PV) solar energy conversion can also assist urban distribution grids in shaving energy demand peaks when and where there is a good match between the solar irradiation resource availability and electricity demands. This is particularly relevant in urban areas, where air-conditioning is the predominant load, and on-site generation a welcome resource. Building-integrated photovoltaics (BIPV) plus short-term storage can offer additional grid support in the early evening, when solar irradiation is no longer available, but loads peak. When PEVs become a widespread technology, they will represent new electrical energy demands for generation, transmission and

R. Rüther (✉) · L.C.P. Junior · A.H. Bittencourt
Grupo de Pesquisa Estratégica em Energia Solar, Universidade Federal de Santa Catarina, Caixa Postal 476, Florianópolis, SC 88040-900, Brazil
e-mail: ricardo.ruther@ufsc.br

L.C.P. Junior
e-mail: pereira1435@gmail.com

A.H. Bittencourt
e-mail: alicehb_eel@yahoo.com.br

L. Drude
Universität Paderborn, Warburger Straße 100, 33098 Paderborn, Germany
e-mail: drude@nt.upb.de

I.P. dos Santos
Colégio Politécnico, Universidade Federal de Santa Maria, Campus UFSM, Santa Maria, RS 97105-900, Brazil
e-mail: isisporto@gmail.com

S. Rajakaruna et al. (eds.), *Plug In Electric Vehicles in Smart Grids*,
Power Systems, DOI 10.1007/978-981-287-299-9_7

distribution (GT&D) utilities. PEVs that are parked in the early evening can play the role of short-term energy storage devices for PV electricity generated earlier in the day. In a smart-grid environment, the combination of PEVs and PV can offer a good solution to assist the public grid. In this chapter, results on analyses of these strategies applied to selected urban feeders in the metropolitan area of a capital city in Brazil are presented. It is shown that, in a smart-grid environment, it should be possible to accommodate PEVs, BIPVs, V2G and the recharging of PEVs (grid-to-vehicle—G2V), and at the same time assist the urban grids and supply the new energy demands represented by the introduction of a PEV fleet, without compromising the existing grid infrastructure.

Keywords Photovoltaics · Plug-in electric vehicles · Vehicle-to-Grid (V2G) · Building-integrated photovoltaics (BIPV) · Smart buildings · Smart grids

7.1 Introduction

Among all human activities, transportation and energy generation are the two single largest contributors to greenhouse gas (GHG) emissions worldwide, and despite technological innovation leading to lower emissions per km or per kWh, total global emissions due to these activities keeps increasing every year. In this chapter the combined use of electric vehicles and on-site, building-integrated solar electricity generation in the context of smart grids are presented, in order to provide utility grid support both in terms of energy (kWh) and capacity (kW).

Plug-in Electric vehicles (PEVs) have been experiencing considerable development in recent years, and pure plug-in battery vehicles are now commercially available from a number of car manufacturers worldwide. PEVs have been proposed as a new power source for electric utilities in the US and Japan in the late nineties [1, 2]. Vehicle-to-grid power (V2G) uses electric-drive vehicles to provide power for specific electricity markets, since the electric power grid and light vehicle fleets are exceptionally complementary as systems for managing energy and power [3, 4]. A control signal from the grid operator can send a request for power to a large number of parked and plugged-in PEVs to feed energy to the grid. As information technology and battery technology evolve, the opportunities for PEVs to assist the public electricity grid in the V2G concept in a smart-grid environment become ever more real.

Electric drive vehicles (EVs) for V2G can be either hybrid, fuel cell, or pure battery vehicles (PEVs). They are all EVs in the sense that they all use an electric motor to provide all or part of the mechanical drive power. For V2G, each individual vehicle must have three required elements: (i) a connection to the grid for electrical energy flow, (ii) control or logical connection to allow for communication with the grid operator, and (iii) controls for metering on-board the vehicle. PEVs already have a grid connection to allow for charging, and the incremental costs and operational adjustments to add V2G are negligible [3, 4]. Furthermore, PEVs

have larger batteries (e.g. 24 kWh battery capacity for the Nissan Leaf[1]) than plug-in hybrids (e.g. 6–14 kWh for the DaimlerChrysler Sprinter[2]), or hybrid EVs (e.g. 1.6 kWh for the Toyota Camry[3]).

Among all renewable energy technologies, direct solar energy conversion or photovoltaics (PV) is the fastest growing segment in the energy generation industry [5]. In the last decade the PV industry annual production moved from megawatts to gigawatts, reaching the multi-gigawatt scale in the second half of the decade. The photovoltaic industry's compound annual growth rate (CAGR) from 2001 through the end of 2013 was 46 % [6]. In 2013 grid parity—when the cost of solar electricity becomes competitive with conventional, retail (including taxes and charges) grid-supplied electricity—was achieved in many places worldwide. Grid-connected PV used to be perceived as an energy technology for developed countries, whereas isolated, stand-alone PV was considered as more suited for applications in developing nations, where so many individuals still lack access to electricity. This rationale is based on the higher costs of PV, when compared with conventional, centralized electricity generation [7]. With the falling costs of PV and the increasing costs of conventional electricity, on-site PV generation became competitive with retail, end-consumer electricity prices also in many developing countries of the sunbelt.

The direct conversion of sunlight into electricity with grid-connected PV generators leads to a number of benefits to both the environment and the electricity system. The main technical advantage is the possibility of producing clean and renewable electrical power close to consumers or even at point of use, integrating PV generators on buildings or around urban areas. The peak shaving capability of distributed PV power systems reduces the strain on grid infrastructure [8–10]. A large number of distributed units for the same installed capacity allows for deferral of a bigger network investment. This favors small- to medium-sized urban PV systems [11]. The traditional utility concept relies on a relatively small number of fairly large and centralized power plants, which quite often are distant from the urban centers where energy is consumed. In large countries, transmission and distribution (T&D) infrastructure and associated losses are considerable, adding value to distributed PV power that goes beyond the value of the kilowatt-hour.

PV can contribute to a distribution utility's capacity if the demand peak occurs in the daytime period. Besides the advantage of peak demand reduction, PV systems will also contribute to a longer life of utility feeders [12]. Commercial regions with high midday air-conditioning loads have normally a demand curve in a good synchronism with the solar irradiance [9, 10, 13]. Another important factor in this analysis, is the comparison between the peak load values in summer and winter. The greater the demand in summertime in comparison with the demand in wintertime, the more closely the load is likely to match the actual solar resource.

[1] http://www.nissanusa.com/electric-cars/leaf/charging-range/battery/.

[2] http://www.epri.com/search/Pages/results.aspx?k=Plug-In%20Hybrid%20Electric%20Sprinter%20Van%20Test%20Program.

[3] http://www.toyota.com/toyota-owners-online-theme/pdf/Batteries2011-LowRes.pdf.

This is the typical picture of most capital cities in many sunny, developed and developing countries of the sunbelt, and the match between solar generation availability and power demands in urban areas is growing with the growing use of air-conditioning. Utility feeders in urban areas show distinct regions where commercial and office buildings dominate, and which present daytime peak demand curves, and residential regions where the peak demand values take place in the evening. To add value to the distributed nature of solar generated electricity, it is important to know the PV capacity of the different regions of a city when installing a PV power plant, in order to select the utility feeder with the greatest capacity credit. In this context, the concept of the Effective Load Carrying Capacity (ELCC) of PV was defined, to quantify the capacity credit of a strategically sited PV installation [8, 9, 13].

The widespread use of PEVs in urban environments will lead to considerably large new electrical energy demands, which will have to be met by new, and ideally distributed, power generation plants. Especially in large and sunny countries, solar PV conversion can meet these new electricity requirements, offering at the same time clean and renewable energy to alleviate the environmental impact of the transportation sector, and making the most of the distributed nature of the solar radiation resource in a distributed generation (DG) and smart-grid scenario. In this environment, the combination of PEVs and PV can offer a good solution to assist the public grid: (i) PEVs can offer grid support to urban feeders in the early evening through smart vehicle-to-grid (V2G) discharging strategies; (ii) BIPV can generate all the electricity needed to supply the new energy demands represented by PEVs and also offer grid support to urban feeders at daytime; and (iii) utilities can offer idle GT&D resources to recharge PEVs through smart grid-to-vehicle (G2V) recharging strategies in the early hours (00:00–06:00).

7.2 Urban Grid Electricity Demand Profiles, Electric Vehicles and Photovoltaics in a Smart Grid Scenario

In most urban centers, due to the extensive use of air-conditioners and electric resistance showerheads for water heating, energy demand peaks in the late afternoon/early evening, from 19:00 to 21:00 [14, 15]. Distribution utilities impose prohibitively high tariffs to business and industry in this period to avoid even higher power demands. These demand peaks coincide with the typical urban driver weekday habits of returning home from a working day. Figure 7.1 shows the typical load curve of a specific urban feeder in the Brazilian metropolitan area of Florianópolis-SC [16]. In this example, the local distribution utility needs to provide a costly energy supply infrastructure to cover the 5-h period from 17:30 to 22:30. This additional capacity remains idle for most of the day and represents a considerable investment from the distribution utility, which is passed on to electricity consumers as a component of the electricity tariff. While the potential contribution of PV in the peak hours shown in this example is limited, charging PEVs with solar electricity while

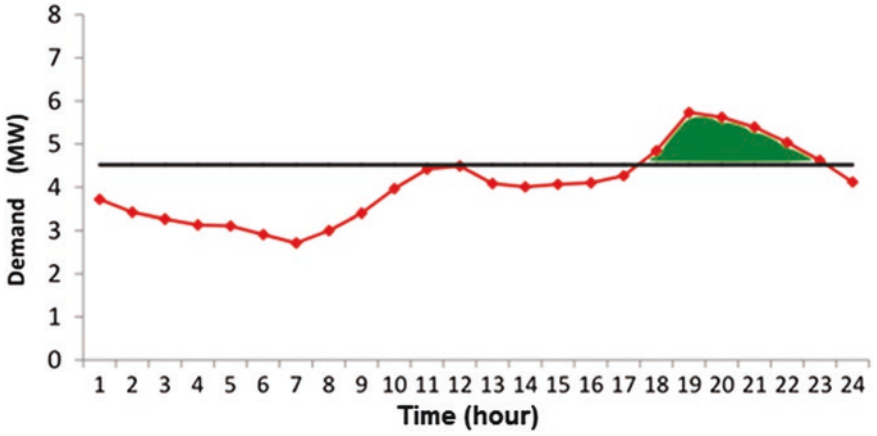

Fig. 7.1 Typical load curve of urban utility distribution feeder TDE05 in Florianopólis-SC, Brazil. With vehicle-to-grid (V2G) strategies in a smart-grid environment, a fleet of PEVs can assist the grid in reducing the evening peak (*green area*), while solar electricity generation with PV integrated on buildings can provide the additional electricity requirements resulting from the introduction of PEVs

they are parked at home or at work, and using a fraction of that electricity to feed the utility's grid and alleviate the load at peak hours has become a technically viable alternative with the advent of the smart-grid. In a smart-grid scenario, with PEVs and grid-connected PV integrated on buildings, the potential contribution of PEVs to assist in shaving the load peaks of a distribution utility feeder at peak hours can be assessed. Furthermore, the potential of PV to supply or complement the additional energy requirements represented by the incorporation of a number of PEVs to the urban fleet in a specific utility feeder area in the metropolitan region of small and large cities can also be proposed and evaluated.

The distribution utility feeder TDE05, for which Fig. 7.1 shows a load curve on a typical day, supplies energy to a mixed residential/commercial/university area. Figure 7.2 shows a color contour map with the hourly demand profile of this feeder for all the 8,784 h of the year, where a distinct peak (warmer colors) is noticeable in the early evening all over the year, from before 18:00 to after 22:00. The figure also shows that during the early hours from 00:00 to 06:00 the feeder is underutilized and therefore technically able to supply energy to recharge a considerable amount of PEVs. Furthermore, Fig. 7.2 shows that during daytime hours the feeder is able to receive large amounts of PV-generated electricity from grid-connected, building-integrated PV generators installed in the area covered by this particular feeder. In the early evening, however, when solar PV generation is no longer available, a fraction of the surplus electricity stored in the batteries of parked and plugged PEVs can be made available for grid support. Figure 7.3 shows a schematic diagram of this concept. The daily urban commute in the metropolitan area of Florianópolis is very typical and representative of many metropolitan areas around the globe, where the driver leaves home for work in the early

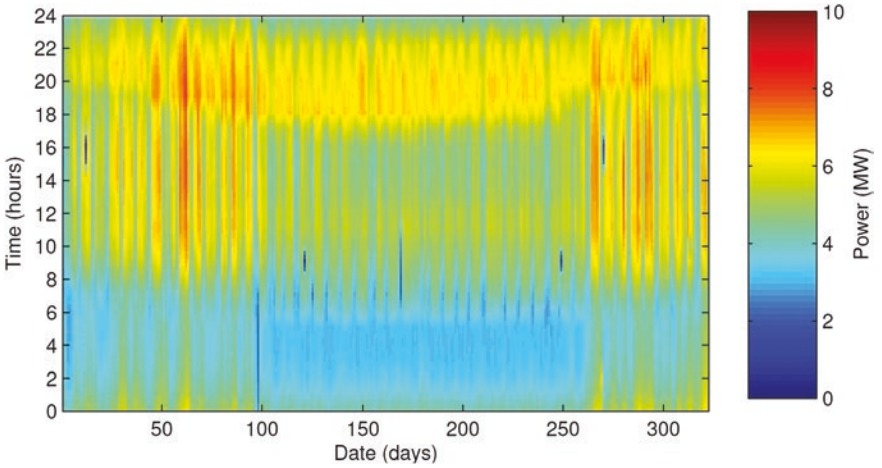

Fig. 7.2 Original energy demand profile of the urban feeder TDE05 (in MW) in Florianópolis for the 8,784 h of the year

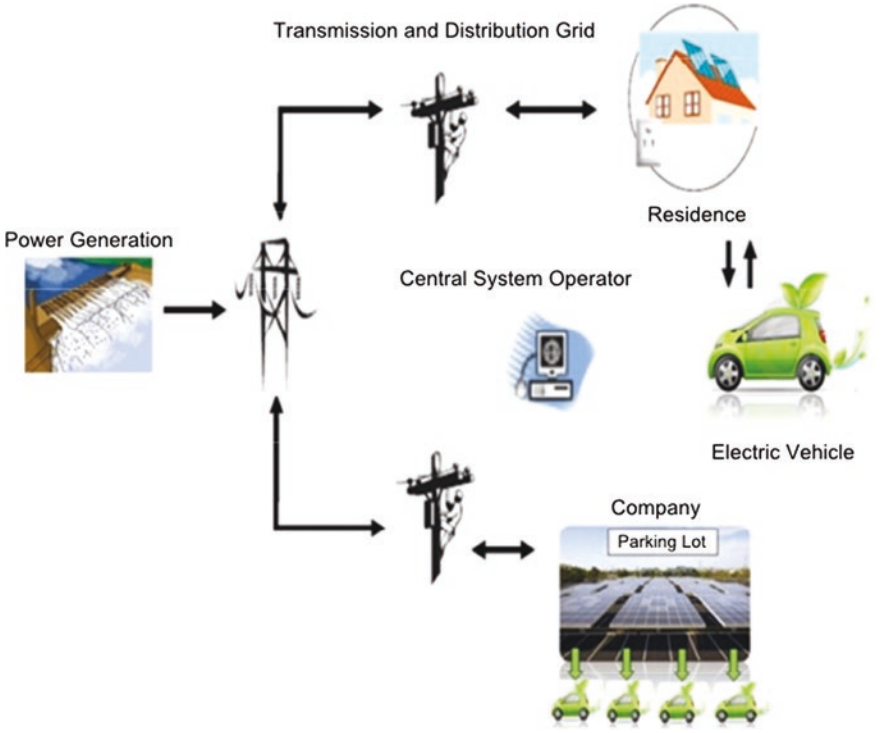

Fig. 7.3 Schematic diagram of the interaction of solar PV generators and PEVs with the public electricity grid in a smart-grid environment

morning, driving for some 20 km on average, and leaving the car parked all day long. In a smart-grid, BIPV and PEV environment, this vehicle could be parked under a PV-covered car parking lot. Distribution utility feeder characteristics and load profiles can vary depending on a number of aspects ranging from climatic and seasonal effects (heating and cooling loads), user characteristics (residential, commercial, business/public, industrial), among others, and the effects of using both building-integrated PV and the energy available in PEVs batteries to flatten the feeder's load curve are a matter of growing interest. Figure 7.4 shows a real, typical and original load curve of the previously shown distribution utility feeder on a particular day. The figure also shows the peak-shaving effect of a number of PEVs assisting this feeder at peak hours in the evening (blue triangles), the contribution of PV solar generation at day-time (green diamonds), and the recharging of the PEV fleet during the early hours (brown circles), when conventional, centralized generators operate at partial load conditions.

Figure 7.5 shows, as an example for the month of March 2008 and on a daily basis, the total maximum number of PEVs that can (top) participate in assisting the corresponding feeder with peak-shaving in the evening (V2G), and (bottom) be recharged in the early hours (G2V) without imposing the need of any upgrade in the existing urban distribution system. The number of vehicles involved in both V2G and G2V shown in these figures is considerably smaller than the existing vehicle fleet available in the corresponding area. In a smart-grid environment,

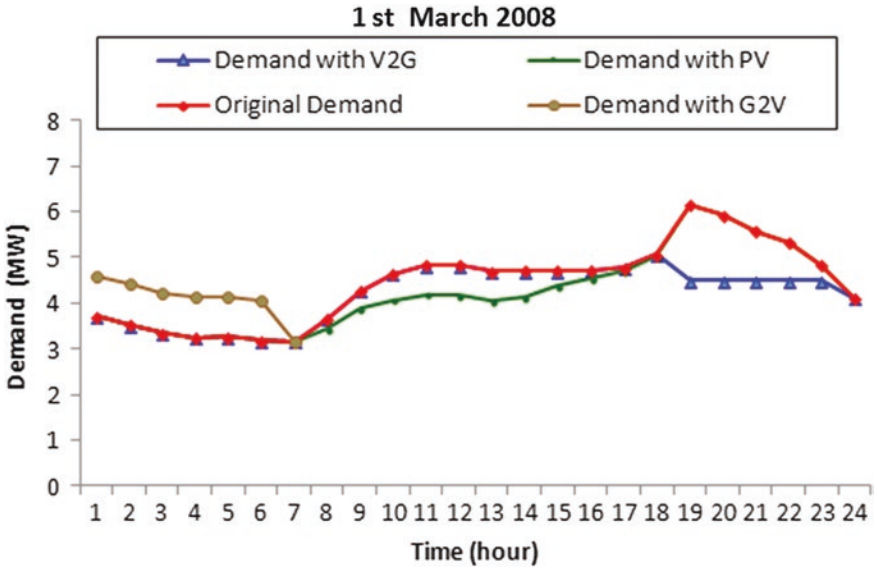

Fig. 7.4 Original demand profile for the distribution utility feeder TDE05 in Florianópolis—Brazil (*red circles*), and the potential contribution of PV (*green diamonds*) for daytime hours peak-shaving, PEVs for evening hours peak-shaving (*blue triangles*), and the corresponding load for PEV recharging in the early hours (*brown circles*)

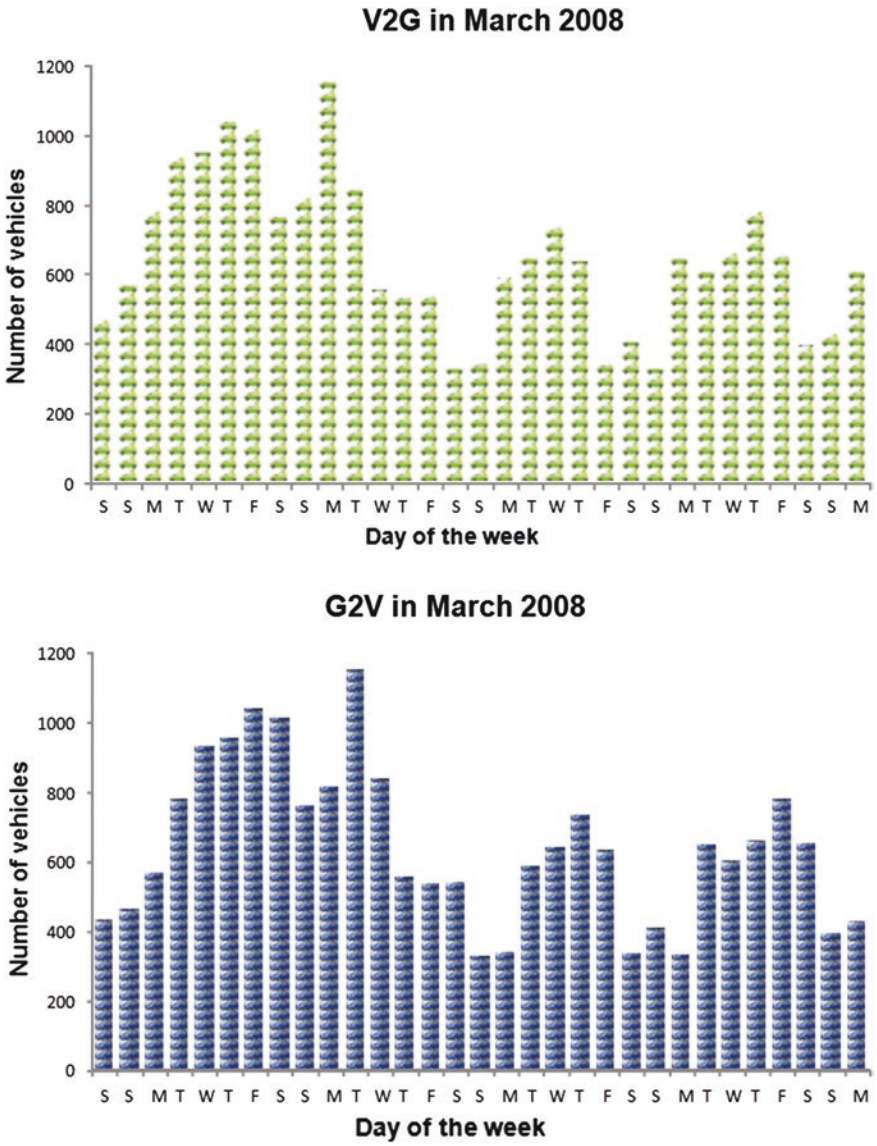

Fig. 7.5 Maximum number of PEVs that the distribution utility feeder TDE05 can take on a given day in March 2008, for evening peak-shaving V2G discharging (*top*), and early hours G2V recharging (*bottom*)

parked and plugged PEVs will participate in V2G and G2V energy transfer transactions in a first-come, first-served priority order.

Central System Operators all over the world struggle to maintain a load curve as flat and constant over the day as possible. With the advent of the smart grid, PEVs that allow for V2G, and distributed rooftop PV in residential, commercial,

industrial and public buildings are faced with both an opportunity, but also new challenges, in dispatch and control. While the conventional utility concept relies on a relatively small number (typically up to a few thousands), of fairly large and centralized generators and power plants (in the hundreds of megawatts up to the gigawatts level) that can be dispatched when needed, the decentralized generation paradigm consists of millions of dispersed and small power plants, most of which are intermittent in nature and cannot be dispatched in a controlled way. As the penetration level of these new and dispersed generation units increases, Central System Operators also need to introduce new control strategies for effectively profiting from decentralized generation.

7.3 Photovoltaics in Buildings for PEV Recharging and Grid Support

PV solar energy conversion to electricity has been the fastest growing segment of the electricity generation market in the last seven years, and in 2013, for the first time, the world added more solar PV than wind generating capacity [5]. The consistent cost reduction experimented by the PV industry as a consequence of volume markets, associated with the possibility of installing PV generators directly at the point of energy use, and the development of PV modules suited for building integration, make PV an ideal technology for deployment in the urban environment [17, 18]. Large-scale, centralized PV generation is an area-intensive technology, but dispersed, building-integrated and building-applied photovoltaics (BIPV and BAPV) constitute a most elegant way of generating considerable fractions of urban electricity, without the need of dedicating exclusive surface areas for PV plant installations. While in BIPV generators either conventional or tailor-made PV modules become an integral part of the building envelope, replacing roofing tiles or other building elements; BAPV systems are more typically used in retrofits, with off-the-shelf PV modules mounted on a separate metal support structure, superimposed on an existing building's roof. In any case, the building envelope (roofs and façades) provides the surface area for the PV plant at premium urban locations in many cases; the building's electrical installation provides the electrical interface of the PV plant to the public utility grid. Energy is generated at very close proximity to the end user, avoiding the infrastructure investments and losses related to transmitting and distributing electrical power, since in most of the cases no extra infrastructure requirements need to be provided for connecting a BIPV or a BAPV plant to the grid. There are additional benefits of scattering PV generators in the urban environment, since PV can also offer distribution utilities ancillary services such as grid support and demand peak shaving, especially when there is a good match between the solar energy resource availability and electricity loads (e.g. air-conditioning loads) [8, 10, 13, 18–23].

In order to optimize the annual output performance of PV generators on buildings, PV array orientation (azimuth) and tilt angle are a major concern, as system

design and electrical configuration must maximize sunlight exposure. A number of studies have been carried out on the performance of PV generators at various orientations and tilt angles for different latitudes [24, 25]. Ideally a PV generator should be oriented towards the equator, and at a tilt angle close to the site latitude. Low-latitude sites will be less sensitive to azimuth deviations for low tilt angles on roof-mounted PV generators, and high-latitude sites will have lower energy output losses for PV generators on vertical façades [25]. Single-family detached homes in residential suburbs can be considered the most suitable building stock for BIPV and BAPV generators, due to their typically large roof areas and small mutual shading effects, while residential and commercial multistorey buildings will often represent challenging aspects in PV system output optimization [26–30], as well as in assessing the incoming solar irradiation resource availability [31].

7.3.1 The Potential of Residential and Public Building Rooftop PV in Supplying the Additional Energy Requirements of a PEV Fleet in a Smart Grid Environment

The widespread uptake of PEVs in urban areas brings new challenges to both the electricity distribution supply and control, and the new energy requirements represented by a fleet of PEVs needs to be assessed. In this section, the potential of a stock of residential buildings with rooftop PV integration in supplying the energy needs of a defined number of PEVs is presented. The existing buildings rooftops of both the residences where the PEVs will be plugged-in during the evening and early hours, as well as large-area public buildings (the local distribution utility headquarters building and the local university theater building), which are served by the same feeder, are presented and assessed. The study was carried out for both thin-film amorphous silicon (a-Si) and traditional crystalline silicon (c-Si) PV modules [32]. On the University campus alone, the potential for integrating PV on existing, large-area rooftops is larger than 3 MWp for a-Si, and larger than 6.7 MWp for c-Si. Using a typical annual energy yield of 1,200–1,300 MWh/MWp for Florianópolis, the annual PV electricity production potential of these areas is over 3,600 MWh for a-Si and 8,040 MWh for c-Si. This is enough to supply electricity to a PEV fleet of some 1,800 cars using a-Si, and over 4,000 cars using c-Si PV modules. The next step in the assessment is to investigate (i) the effects of making hundreds (400–600) of PEVs available to assist this particular utility feeder in the urban distribution grid from 19:00 to 24:00; (ii) the effects of introducing a certain amount (e.g. 1 MWp) of grid-connected, building-integrated PV to generate enough energy to cover the new energy demands represented by the new EV fleet, and at the same time assist the utility feeder during daytime hours; and (iii) the capacity of, and the effects on, the utility feeder in recharging the PEV fleet during the early hours (00:00–06:00). A typical 4 kW PEV battery charger to recharge the Nissan Leaf 24 kWh EV battery in up to 6 h is assumed.

The first grid-connected, building-integrated PV system in Brazil was installed at the Solar Energy Laboratory at Universidade Federal de Santa Catarina in Florianópolis in 1997 [33, 34]; this PV generator includes a comprehensive data acquisition system that has been continuously logging electrical performance, ambient and PV module temperature and plane-of-array and horizontal solar irradiation data at 5-min intervals [19, 33, 34]. The annual global horizontal solar irradiation resource averages some 1,550 kWh/m^2/year, and there are a number of PV installations at various orientations and tilt angles being continuously monitored and assessed, with detailed output performance, ambient and PV module operating temperature, and irradiation data available. Two of these PV systems were used as a reference to establish the baseline for the typical output performance of traditional c-Si and thin-film a-Si PV generators with ideal orientation and tilt angle. Both PV systems are oriented towards the Equator (true North), at latitude tilt (27°), with no shading effects from dawn to sunset. The 2.25 kWp c-Si PV system operates on the roof top of the local Utility Eletrosul Energy Efficient House (Fig. 7.6), and the a-Si PV system is installed on the Universidade Federal de Santa Catarina's Theater building (Fig. 7.7). Real operational performance data (electrical output generation values at 5-min intervals) collected from these two reference PV installations have been used to calibrate the PV output simulation method used to assess the potential generation capacity, in kWh generated per kWp installed, of all PV generators presented in this chapter. Figure 7.8 shows the monthly energy generation (in kWh/kWp), of the two reference PV systems, and also the measured monthly global radiation (in kWh/m^2).

Fig. 7.6 Traditional crystalline silicon (c-Si) rooftop PV system at the Energy Efficient House, in Florianópolis, Brazil (27°S latitude). The PV generator faces true North, and is tilted at 27°

Fig. 7.7 Thin-film amorphous silicon (a-Si) rooftop PV system at the UFSC's University Theater, in Florianópolis, Brazil (27°S latitude). The PV generator faces true North, and is tilted at 27°

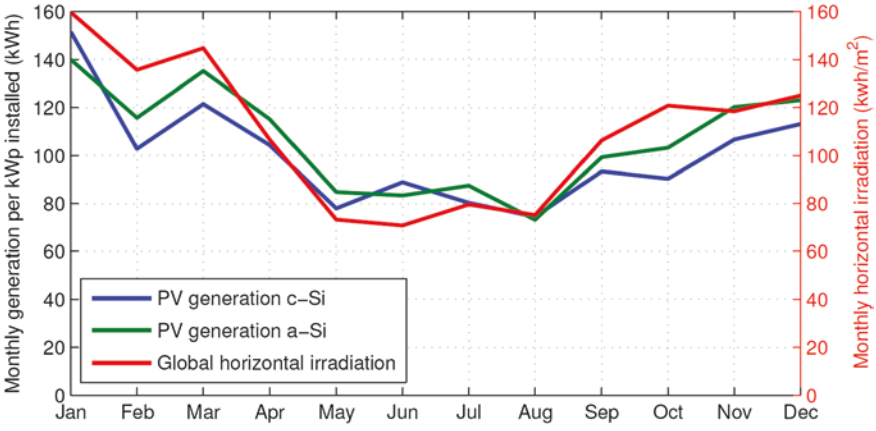

Fig. 7.8 Monthly average of the global horizontal irradiation (*green dotted line*, in kWh/m^2), PV energy generation (in kWh/kWp) of the traditional c-Si PV system (*blue solid line*), and thin-film a-Si PV system (*red dashed line*) operating in Florianópolis, Brazil (27°S latitude)

A typical urban area was selected to study the PV roof integration potential of PV kits on single-family residential houses, and the resulting energy generation potential of the proposed PV generators was established. The urban area under study is a mixed residential-commercial area, with a predominance of detached, single-family, one- or two-storey houses, with negligible mutual shading effects

on roof covers. As previously shown in Fig. 7.1, the electricity demand of the utility feeder supplying energy to this area presents two peaks, with an early evening peak around 19:00, and a second peak close to midday.

The next step consisted in analyzing the available rooftop surface area, orientation, and tilt angles of this complete building stock, in order to determine the availability of suitable areas for PV integration. The GEO map (Corporative Geoprocessing Map), supplied by the city council was used to obtain the residential sample size determination of that urban zone, which is comprised of 496 single-family houses. This information was also compared with the orthoimage of the area for the same year, in order to ascertain that the energy demand, solar irradiation availability, and land occupation characteristics all corresponded to the same period. It was assumed that the PV kits defined in this study have an area small enough to fit on the residential buildings studied, and a conservative 7.5 % error margin was adopted. The sample size determination (n) of the selected residential buildings is a function of the total number of total residential houses (N), confidence level (Z = 95 %), probability to find available area for PV kits on residential rooftops (p = 95 %, with q = 1–p), and error margin (E = 7.5 %), it was obtained from Eq. 7.1 as follows:

$$n = \frac{N \cdot Z_{\alpha/2}^2 \cdot p \cdot q}{E^2 \cdot (N-1) + Z_{\alpha/2}^2 \cdot p \cdot q} \tag{7.1}$$

$$n = \frac{496 \cdot 1,96^2 \cdot 95 \cdot 5}{7,5^2 \cdot (496-1) + 1,96^2 \cdot 95 \cdot 5}$$

With the resulting n = 30.5, the roof cover blueprints of 31 residential houses were requested and obtained from the city council's Urban and Public Services Municipal Bureau, for a more detailed roof cover area availability analysis.

Two pre-defined PV kits were designed and proposed for the integration of a-Si or c-Si PV technologies on all of the residential buildings rooftops. These BAPV generators were sized in order to be small enough to fit on the roofs considered in this study, and large enough in order to be able to supply a considerable fraction of the electricity demands in each house. It was also defined that both PV kits should have a similar total surface area, so that the aesthetic appearance of both types of installation would also be similar. The solar-to-electricity conversion efficiency of the thin-film a-Si PV technology is about half the efficiency of the more traditional c-Si PV technology. As a consequence, for a similar surface area, an a-Si PV kit will have about half the nominal power of a c-Si PV kit. Since the current price of turn key PV generators for small, residential PV installations, can be considered independent of the PV technology selected, this decision resulted in the a-Si PV kit costing about half the price of the c-Si PV kit. The a-Si PV kit considered in this study is rated at 0.5 kWp nominal DC power, uses four 5.0 × 0.4 m^2, 125 Wp PV modules, with a total surface area of 8.0 m^2. The c-Si PV kit is rated at 1 kWp nominal DC power, uses five 1.42 × 1.00 m^2, 200 Wp PV modules, and has a total

surface area of 7.1 m^2. An 8.0 m^2 area was thus defined as a minimum roof area availability requirement for PV kit integration.

Each of the 31 sample building roof cover areas was individually analyzed for the PV integration potential, taking into account the land block area and orientation, as well as the existing roof orientation and tilt, and the availability of the minimum 8.0 m^2 area required for PV kit integration, oriented as much as possible towards the Equator (true North). This analysis resulted in a number of different possibilities for PV kit roof integration on these existing roof covers, with all the 31 houses presenting an 8.0 m^2 roof cover area suitable for PV kit integration. It was then assumed that all of the 496 houses were able to accommodate either of the PV kits, and the PV generation potential was then calculated in each case, to be further compared with the energy demand profile of the corresponding area in the suburb.

The expected PV energy generation for different orientations and tilt angles was determined based on three factors: (i) the residential houses' roof area availability, orientation and tilt angles, (ii) the individual houses' solar irradiation resource availability, which was calculated in each case from the available global horizontal irradiation data for the plane-of-array of each roof orientation and tilt angle; and (iii) the output performance of the reference a-Si and c-Si PV generators operating in the same area. Electricity consumption was estimated from the values obtained from the local utility and adjusted to the 496 houses analyzed.

Equation 7.2 was then used to estimate the energy generation potential E (in kWh) of the PV kits with an installed capacity P (in kWp), when installed on all the existing roof covers (n = number of samples), based on the corresponding reference output performance for each PV technology (GerSist, in kWh/kWp), and taking into account a reduction factor due to their non-ideal orientation and tilt angles (Def = 0.942). A weighted average of all roof orientations and tilt angles was used to calculate this Def output reduction factor, which was statistically determined as further explained.

$$E = n \cdot P \cdot GerSist \cdot Def \tag{7.2}$$

In order to obtain the generation value (GerSist), the measured output power of the two reference PV generators used to calibrate the simulation of the PV generation potential were compared. Figure 7.8 shows that the thin film a-Si PV system (annual energy yield = 1,280 kWh/kWp/year) generates more energy (>6 %) on an annual basis than the c-Si PV installation (annual energy yield = 1,205 kWh/kWp/year). Figure 7.8 also shows the profile of the monthly PV generation (in kWh/kWp) of the two PV systems, together with the solar irradiation levels for the same period (in kWh/m^2). It can be clearly seen that the thin-film a-Si PV generator is a better performer overall, especially during summer months. The reasons for this behavior are related to the lower temperature coefficient on power of a-Si when compared with c-Si; to a spectral content of sunlight in summer months more suited to the spectral response of a-Si devices; and to the partial annealing of the Staebler-Wronski effect [35], and have been described in detail elsewhere [36, 37]. Also noteworthy is the fact that the energy output in

summer months is almost double of that during the winter, in accordance with the solar irradiation availability at the site.

As shown by the blue diamonds in Fig. 7.9, the 31 houses sample analyzed in this chapter present more variations in roof cover orientation than in tilt angle. Roof tilt angle is associated with roofing tile model, and in this suburb most houses use the typical red clay tiles, tilted between 15° and 35°. Roof orientation, on the other hand, varies according to the urban grid design and architectural concepts, and is therefore more prone to larger variations. In this analysis, the 31 sample roof orientations and tilts studied in detail, were extrapolated to the 496 existing houses. The various roof orientations and tilt angles of the house sample studied will lead to varying and specific output performance behaviours of PV generators installed on each of these roofs, which are represented by the "Def" parameter in Eq. 7.2. Figure 7.9 also allows for a rapid and efficient visualization of the expected PV generator performance on any particular roof orientation and tilt, with respect to the maximum theoretical performance of an ideally oriented and tilted PV generator. The graph is based on irradiation values calculated using the RADIASOL software [38]. This software calculates the incoming solar irradiation levels at any surface orientation and tilt angle, based on the local daily averages of the monthly global horizontal irradiation. In this chapter, solar irradiation vales obtained from the SWERA project [39] were used to calibrate the RADIASOL software. In Fig. 7.9, maximum (100 %) output corresponds to the performance of a rooftop PV generator with ideal roof orientation (facing true North in the Southern Hemisphere) and tilt angle (latitude tilt = 27° for the city of Florianopolis), with the corresponding output for all the other possible orientations

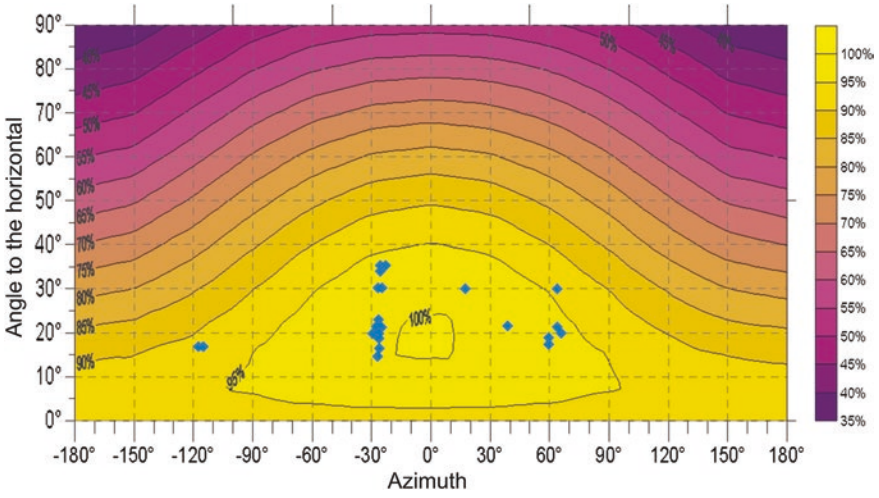

Fig. 7.9 Distribution of surface area availability for PV kit integration according to orientation (azimuth deviation) and tilt angle of the 31 residential house roof covers (*blue diamonds*), with percentage of the maximum annual PV generation potential as a function of their position in Florianópolis, Brazil (27°S latitude)

(azimuth deviations from −180° to +180° off true North), and tilts (varying from horizontal roofs = 0°, to vertical walls = 90°) being easily visualized.

Since the variance is unknown and the sample (n) is small, variances (F) in orientation and tilt angle were analyzed statistically using Eq. 7.3, to determine deviation averages, with Sx and Sy representing the sample's deviations for the small sample (n). Because most of the azimuthal deviations are statistically similar, Eq. 7.4 was used to estimate the weighted deviation (Sp) from average; Eq. 7.5 was used to determine the deviation from the difference among averages (Sw); Eq. 7.6 was used to calculate the Student's (t) distribution value; and Eq. 7.7 was used to compare t with the samples' distribution, and determine whether the averages could be considered equal at a 95 % confidence level.

$$F = \frac{Sx^2}{Sy^2} \tag{7.3}$$

$$Sp = \sqrt{\frac{(n_x - 1) \cdot Sx^2 + (n_y - 1) \cdot Sy^2}{n_x + n_y - 2}} \tag{7.4}$$

$$Sw = Sp\sqrt{\frac{1}{n_x} + \frac{1}{n_y}} \tag{7.5}$$

$$|t| = \frac{\bar{x} - \bar{y}}{Sw} \tag{7.6}$$

$$|t| = t_{\frac{\alpha}{2}}(n_x + n_y - 2) \tag{7.7}$$

The statistical analysis of the average incident solar irradiation level distribution at different azimuth angles, demonstrated that both at the ideal latitude tilt angle of 27°, and also at a more steep 45° tilt angle, deviations are similar, and there is no significant difference in average solar irradiation levels among azimuth deviations of 5°, 10°, 15°, 20°, 30°, 45° and 90°, for a 95 % confidence level.

The statistical analysis has also demonstrated that regarding tilt angles, for North-oriented (South-oriented in the Southern hemisphere) planes tilted up to 20°, there is no significant difference in averages or standard deviations at this low latitude. From tilt angles larger than 30°, averages are still similar up to 45°, but standard deviations can no longer be considered similar. For 90° tilt angles (vertical façades), both averages and standard deviations are different and cannot be compared. Since the statistical analysis did not reveal considerable differences in solar irradiation levels among the existing roof covers evaluated, a 10° step in tilt angle and a 30° step in azimuth angle variations were adopted in Fig. 7.9. The 100 % generation level in the graph corresponds to an average yearly output of 1,280 kWh/kWp for the a-Si PV technology, and 1,205 kWh/kWp for the c-Si PV technology installed in Florianopolis (GerSist, value in Eq. 7.2 corresponding to

640 and 1,205 kWh/year for the 0.5 kWp a-Si and 1.0 kWp c-Si kits respectively). For any other combination of orientation and tilt angles, *ceteris paribus*, average annual energy generation yields can be derived from Fig. 7.9. Monthly electricity demand data were obtained from the local distribution utility for the TDE05 feeder. The data obtained were peak demand measurements for each 15 min for all days of the year, from which daily demand curve averages, total consumption and also peak power demand were calculated.

After identifying the orientation and tilt angles of the 496 roof covers, and using the graph shown in Fig. 7.9 to assess their corresponding output performance, the PV kits generation potential was estimated as a fraction of the maximum potential verified for ideally oriented and tilted PV generators. Figure 7.9 also shows that 87 % of the PV kits will be able to generate at least 95 % of the maximum theoretical output for Florianópolis; about 10 % will be able to generate at least 90 % of the maximum possible; and only about 3 % of the PV kits will generate at least 85 % of their maximum potential. The averaged annual energy generation yield of the 496 PV kits proposed to be installed on these existing house roof covers, resulted in 94.2 % ("Def" parameter in Eq. 7.2) of the maximum theoretical potential. These results are significant, because they demonstrate that retrofitting PV kits to existing individual residential house roof covers which were not originally designed to integrate PV generators, leads to the majority of the BAPV installations to perform at a level which is very close to their maximum theoretical potential. From Fig. 7.9 it is clear that for low-pitched roofs (<10°) at this latitude, any roof orientation will lead to at least 90 % of the maximum theoretical energy generation potential. Figure 7.10 shows the potential electricity generation of the BAPV kits in three scenarios, namely:

- Scenario K1: All the 496 houses fitted with 1.0 kWp PV kits using the c-Si PV technology. Installed PV capacity = 496 kWp (In Eq. 7.2: n = 496; P = 1; GerSist = 1,205; Def = 0.942);
- Scenario K2: All the 496 housed fitted with 0.5 kWp PV kits using the thin-film a-Si PV technology. Installed PV capacity = 248 kWp (In Eq. 7.2: n = 496; P = 0.5; GerSist = 1,280; Def = 0.942);
- Scenario K3: Half (248) of the houses fitted with the 1.0 kWp c-Si PV kit, and the other half (248) of the houses fitted with the 0.5 kWp thin-film a-Si PV kit. Installed capacity = 372 kWp (In Eq. 7.2: n1 = 248; P1 = 1; GerSist1 = 1,205; n2 = 248; P2 = 0.5; GerSist2 = 1,280; Def = 0.942).

Following the analysis of PV kit installations in a BAPV configuration, the whole roof cover areas of the residential houses sample were evaluated in order to determine the PV generation potential in a BIPV configuration, with tailor-designed PV systems for each house. While the BAPV alternative results in economies of scale due to PV kits standardization and volume production, the BIPV option results in an optimized deployment of the existing roof cover areas, leading to net energy-positive buildings. The nearly 80,000 m^2 surface areas available on these existing roofs corresponds to a PV capacity of nearly 5 MWp for the thin-film a-Si PV technology, and over 11 MWp for the more traditional c-Si PV technology.

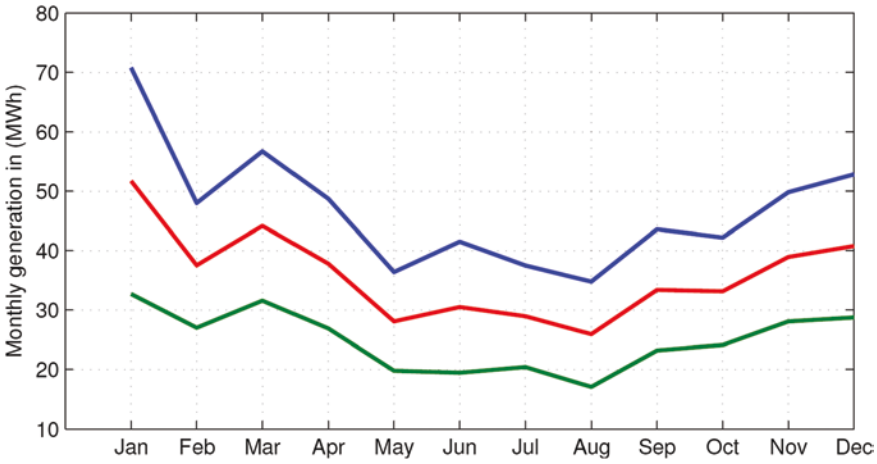

Fig. 7.10 Monthly PV energy generation potential (in kWh/month) under Scenarios K1 (496 units of the 1.0 kWp c-Si PV kit), K2 (496 units of the 0.5 kWp a-Si PV kit) and K3 (248 units of the 1.0 kWp c-Si PV kit and 248 units of the 0.5 kWp a-Si PV kit)

Assuming the average solar generation potential for the areas considered, this installed capacity translates into an annual energy generation potential of some 5,800 MWh/year for the thin-film a-Si PV technology, and around 12,300 MWh/year for the c-Si PV technology, when installed in a BIPV configuration on all of the available areas of the 496 existing houses in this suburb. This is enough to supply electricity to a PEV fleet of some 2,900 cars using a-Si, and over 6,100 cars using c-Si PV modules, which by far exceeds the total fleet of vehicles registered in this suburb.

7.3.2 The Potential of Rooftop PV and PEV Vehicle-to-Grid (V2G) Strategies in Peak Demand Reduction in Urban Areas in a Smart Grid Environment

In order to establish the potential of rooftop PV in a public building in both supplying the additional energy requirements of a PEV fleet, and in providing grid support to the local utility in a smart grid environment, the local public utility Eletrosul Headquarters building in Florianópolis was studied. Figure 7.11 shows the 1 MWp solar PV installation integrated on both the building's roof (450 kWp) as well as in the surrounding parking areas (565 kWp distributed in nine parking canopies). In order to evaluate the best energy flux strategies over a daily period, three phases were defined along the 24-h period, namely: Phase 1—daytime (solar PV feeding the Eletrosul Headquarters building + V2G from the parked PEV fleet to the Eletrosul Headquarters building); Phase 2—nighttime (V2G from the parked PEV fleet to the Eletrosul Headquarters building at peak demand hours);

Fig. 7.11 Aerial view of the Eletrosul Megawatt Solar PV plant in Florianópolis, Brazil (27° South), showing the (450 kWp) rooftop and the nine parking canopies (565 kWp), which comprise the 1 MWp solar power plant

and Phase 3—nighttime (G2V from PEV owners residence power sockets to recharge PEVs in the late night and early hours). Figure 7.12 shows a schematic diagram with these three phases distributed over the 24-h period. Phase 1 is the longest period, when sunshine is available, and when the PV generator assists the building owner (and the distribution utility) in reducing the power demand from the grid and in modulating the load curve; in case of PV generation reduction caused by unfavourable meteorological conditions, parked and plugged-in PEVs

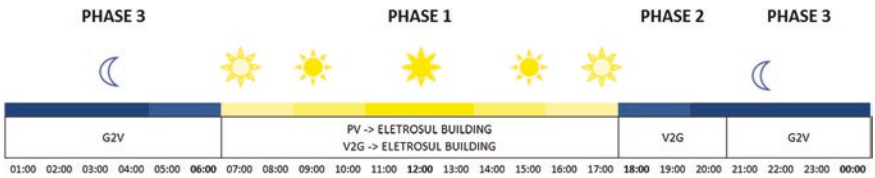

Fig. 7.12 Definition of the three phases in which different energy management strategies are applied, namely: *Phase 1*—daytime (solar PV feeding the Eletrosul Headquarters building + V2G from the parked PEV fleet to the Eletrosul Headquarters building); *Phase 2*—nighttime (V2G from the parked PEV fleet to the Eletrosul Headquarters building at peak demand hours); and *Phase 3*—nighttime (G2V from PEV owners residence power sockets to recharge PEVs)

can assist in this task with V2G, contributing to grid reliability. Phase 2 is the shortest period, and coincides with the distribution utility's load peak; this is the period in which V2G is most valuable, as end-user tariff rates can be 10 times as high as in off-peak periods. Phase 3 is also considerably long, when most of the generation, transmission and distribution assets are idling because of low power demand from the grid, and is therefore ideal for PEV recharging due to low tariff rates and abundant grid resource availability. The combination of daytime solar electricity generation and both daytime and nighttime V2G electricity injection can thus effectively assist in reducing distribution utility demand peaks. The effect of additional PEV battery cycling will affect battery lifetime, and is a function of both the depth of discharge (DOD) and the number of cycles. To analyze the impact of V2G in the urban area distribution utility feeder previously presented, a MATLAB simulation environment was implemented. This environment allows the import of measured demand data, allows the use of different charge and discharge strategies, and the analysis of the influence of the V2G-interactions on the given energy demand profiles. The simulation delivers the possibility to calculate annual costs of battery degradation, energy costs and revenue in relation to parameters like maximum DOD.

Figure 7.13 shows a bar graph of the Eletrosul Headquarters building load curve on a typical weekday, with the three phases shown in blue (Phase 1), red (Phase 2) and green (Phase 3) bars. This public building is representative of office buildings all over the world, where air-conditioning loads occurring in Phase 1 are the single largest load and dictate the curve profile. Solar electricity generation is

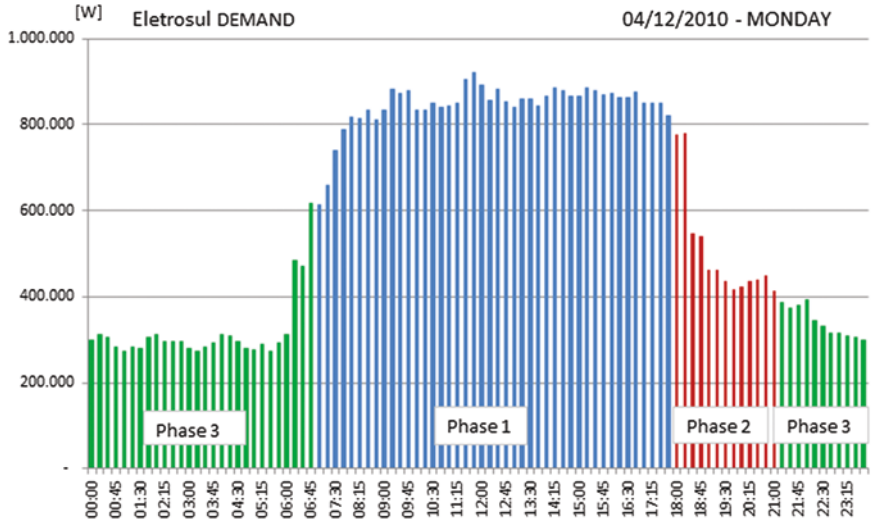

Fig. 7.13 Eletrosul Headquarter building's load curve on a typical weekday, with *Phase 1* dominated by air-conditioning loads during working hours (*blue bars*); *Phase 2*, in the early evening, when distribution utility tariff rates are as high as 10 times the off-peak tariff rates (*red bars*); and *Phase 3*, characterized by low nighttime loads (*green bars*)

reasonably well matched to such a load profile, and PV can effectively assist in shaving the daytime peak. Figure 7.14 shows the PV generation (red bars) for the same day presented in Fig. 7.13 superimposed on the load curve, and Fig. 7.15 shows the bar graph resulting from the PV contribution on the final Eletrosul Headquarter building's load curve.

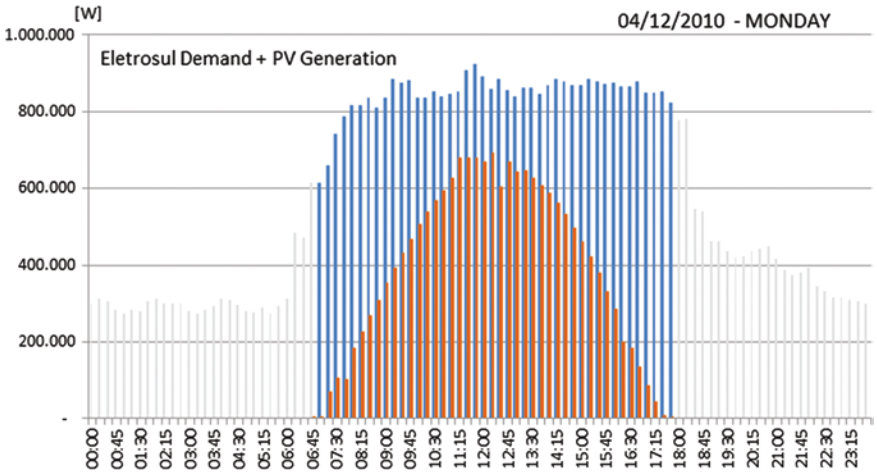

Fig. 7.14 Eletrosul Headquarter building's load curve on a typical weekday, with the one megawatt solar PV generator's contribution (*red bars*) during Phase 1

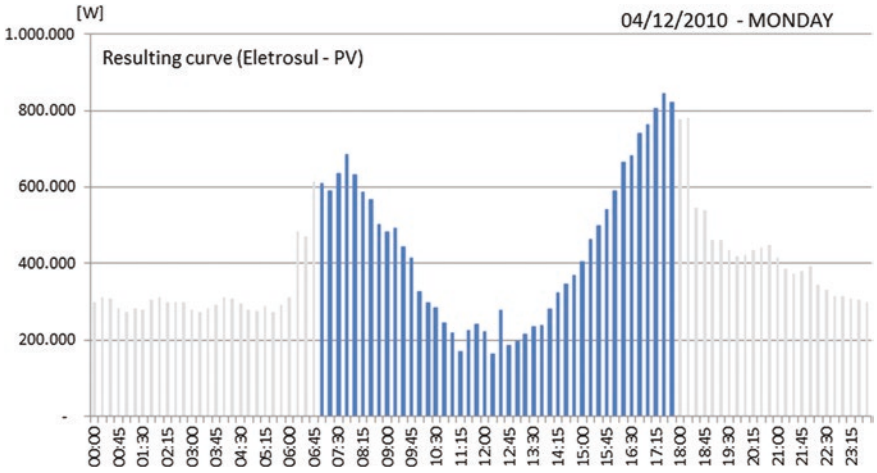

Fig. 7.15 Resulting load curve at the Eletrosul Headquarter building on a typical weekday, with the one megawatt solar PV generator's contribution during Phase 1

Based on the parked and available PEVs that can further assist in modulating this load curve, Fig. 7.16 shows the V2G contribution possible on the same date (red bars), and Fig. 7.17 shows the resulting effect on the Eletrosul Headquarter building's load curve.

In Phase 2, when a number of PEVs owners have arrived home and have plugged their vehicles in onto wall sockets for either recharging the vehicle's

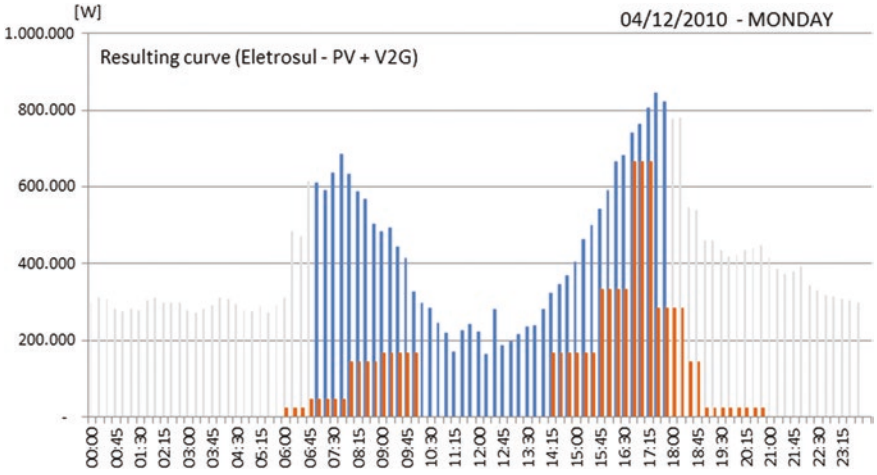

Fig. 7.16 Resulting load curve at the Eletrosul Headquarter building on a typical weekday, with the one megawatt solar PV generator's contribution during Phase 1, and the potential contribution of parked and plugged PEVs available for V2G (*red bars*)

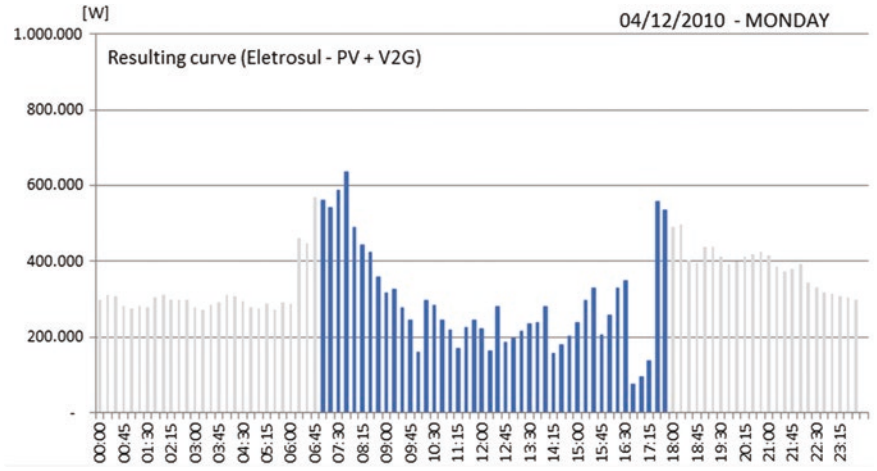

Fig. 7.17 Resulting load curve at the Eletrosul Headquarter building on a typical weekday, with the one megawatt solar PV generator's contribution during Phase 1, and the contribution of parked and plugged PEVs available for V2G

battery or supplying the remaining PEV's energy to the utility grid, a considerable amount of energy can be transferred to the grid via V2G, as the yellow bars in Fig. 7.18 show. In a smart grid environment, PEVs parked at each of these vehicles owners residences can credit the V2G injected power in favor of the Eletrosul Headquarter building. In the late night and early hours, when most of the generation, transmission and distribution assets are idling (Phase 3), the PEV fleet can be recharged with the most inexpensive electricity, as shown in Fig. 7.19.

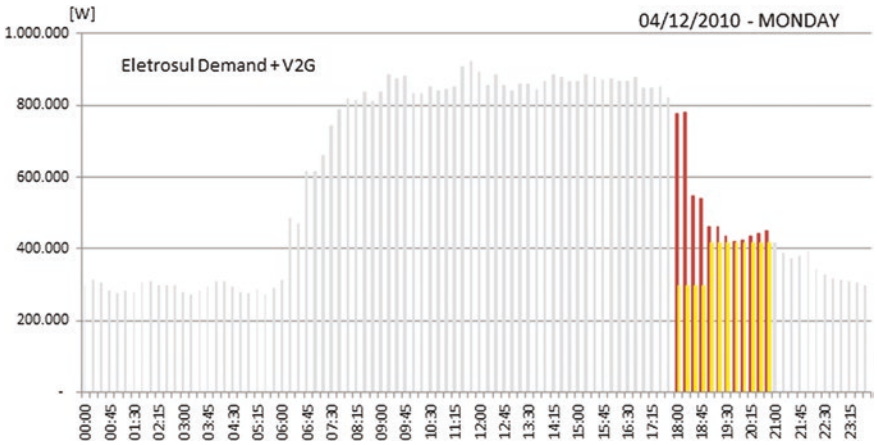

Fig. 7.18 The effect of using V2G electricity from parked and plugged-in PEVs (*yellow bars*) on the Eletrosul Headquarter building's load curve in the early evening (Phase 2) to alleviate power demands from the utility grid

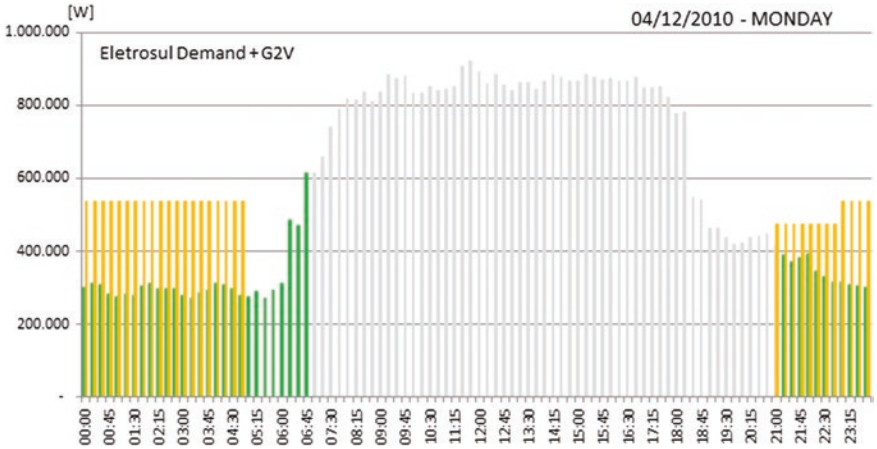

Fig. 7.19 The effect of recharging the parked and plugged-in PEV fleet in the late night and early hours (Phase 3–*yellow bars*) on the Eletrosul Headquarter building's load curve

The combined use of all these strategies can be effectively used to both alleviate the public grid and reduce power demand peaks, as well as provide all the new energy requirements represented by a fleet of PEVs.

The effects of additional charging and discharging PEV batteries in the V2G and G2V context presented previously needs to be further assessed, in order to estimate the costs involved, and a cost-benefits analysis was carried out [40]. It is assumed that PEVs are used during the day for shopping and working, and that they start becoming available for V2G as of 18:00. The shortfall in electrical energy represented by the energy needed to charge the fleet of PEVs driving a given distance per year, is supplied by BIPV and BAPV generators spread on rooftops around the corresponding #TDE05 feeder area, as previously shown. For price calculations the energy price of US$ 0.18/kWh was assumed, including taxes. The assumed car specifications were drawn from [41], as shown in Table 7.1. The battery price assumed from the international market is US$ 300/kWh [42], including taxes. The metering device (US$ 50), a communication device (US$ 50), and the additional hardware needed to allow the feeding of energy to the grid (US$ 33.33/kW) were also assumed including all taxes. All these values are summarized in Table 7.1, and are expected to decrease with technology development and scaling effects. Although the battery efficiency and lifetime both depend on the charge and discharge rate, battery efficiency is assumed at 84 % [43]. It is known that the battery suffers from deep cycling, and that a low DOD will lead to very long battery lifetimes, measured in cycles. This simulation is based on the approach of Rosenkranz and the Fraunhofer ISE's model, as shown in the following equation [41, 44]:

$$N_{\text{Cycles}} = 1331\ \text{DOD}^{-1.8248} \tag{7.8}$$

where N_{Cycles} is the expected battery lifetime in cycles as plotted in Fig. 7.20. This equation leads to an approximately linear dependence of costs per stored energy, depending on the DOD, which can be seen in Fig. 7.21.

The charging and discharging power is limited by the grid connection. In most of the countries, standard plugs allow a maximum current of 10–20 A. Thus we limit the maximum power at $P_{\text{Max}} = 4.4$ kW, based on the standard 20 A sockets, at 220 V. The DC-AC converter efficiency is assumed as $\eta_{\text{converter}} = 98\%$, since state-of-the-art, commercially available inverters for photovoltaic applications reach this efficiency [45]. The efficiencies and power limits are shown in the flow

Table 7.1 Electric vehicle assumed for the simulations in this study (data from Dallinger et al. [41]), shown in both the Brazilian currency R$, and in US$)

Description		Value
Battery capacity		25 kWh
Maximum driving range		200 km
Battery price	R$ 10,201	$ 5,481
Meter for invoicing	R$ 140	$ 75
Communication system	R$ 280	$ 150
Additional electronics	R$ 410	$ 220

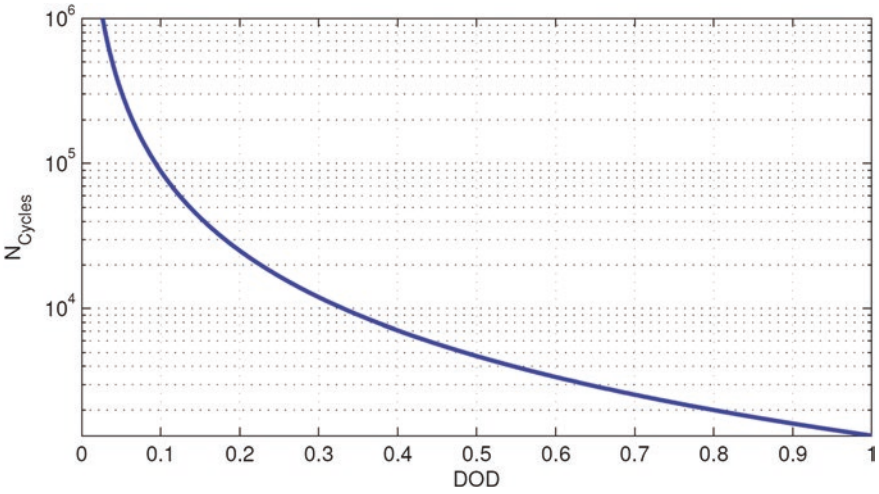

Fig. 7.20 Estimated battery lifetime in cycles, as a function of the depth of discharge-DOD

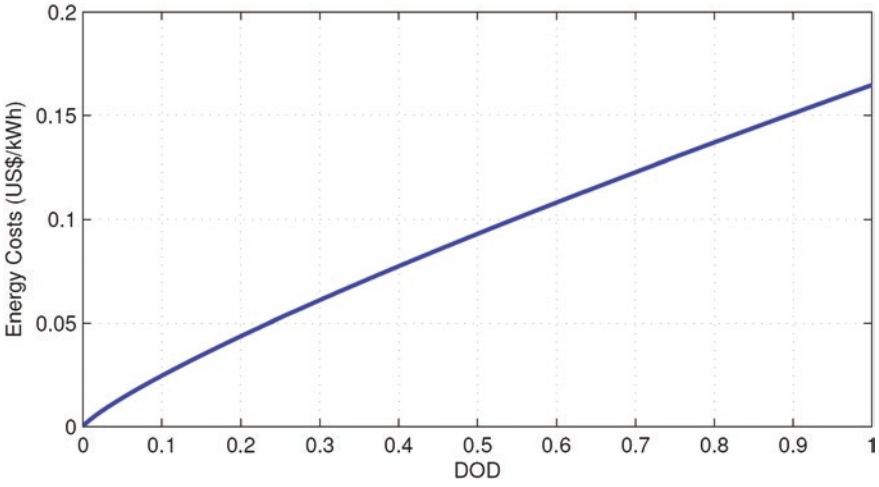

Fig. 7.21 Energy storage costs as a function of the depth of discharge-DOD

diagram in Fig. 7.22. In this figure also the points for P_{Charge} and $P_{Discharge}$ are defined, which will be further defined.

In this simulation, charging is performed between midnight and 6:00 with a charge rate as follows, where E_{SoC} is the energy stored in the battery:

$$P_{Charge}(n) = \min\left(\frac{E_{Capa} - E_{SoC}(n)}{t_{Remaining(n)}}, \eta_{Battery} P_{Max}\right) \tag{7.9}$$

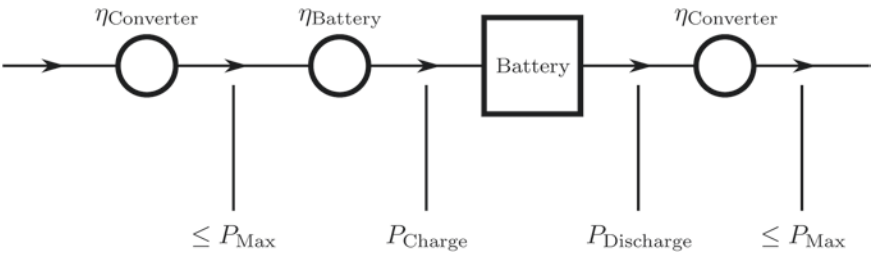

Fig. 7.22 Efficiency and power flows

where $E_{SoC}(n)$ is the energy at the given time-step, in kWh. The value E_{Capa} is the battery capacity drawn from Table 7.1. The value $t_{Remaining(n)}$ is calculated as the time difference between the current time-step and the end of the charge interval, measured in hours.

The new State of Charge (SoC) is therefore

$$E_{SoC}(n+1) = E_{SoC}(n) + P_{Charge}(n)\Delta t \tag{7.10}$$

With time-steps Δt 15 min.

The demand seen by the grid is therefore increased to

$$D_{New}(n) = D_{Old}(n) + \frac{P_{Charge}(n)}{\eta_{Battery}\eta_{Charge}} \tag{7.11}$$

where D_{New} is the resulting demand, and D_{Old} is the original demand, as measured by the distribution utility company.

Everyday, the energy for driving is discharged. With the maximum driving range given in Table 7.1 for the PEV selected for this study, the 200 km result in a driving energy $E_{Drive} = 5$ kWh for average daily driving.

$$E_{SoC}(n+1) = E_{SoC}(n) - E_{Drive} \tag{7.12}$$

While the analysis of daytime charging is outside the scope of the present analysis, in the medium term plugging in might also be possible during the day for staff driving to work every day and parking their cars in assigned parking lots in many public and private, small and large companies. This can also lead to V2G and G2V strategies to assist the public grid when cars remain parked during working hours as previously discussed.

7.3.2.1 Strategy 1: Assumptions for Profit Maximizing with Local Electricity Pricing Model

Distribution utilities around the globe are migrating to a pricing model based on time-of-use for all customers, including residential electricity consumers. To reduce peak demand, a three-level tariff is proposed for residential users. The

energy price during the peak interval from 18:30 to 21:30 is 5x higher than the off-peak price. One hour before and one hour after the peak interval, the energy price is set at 3x higher than during the off-peak period. Together with net-metering regulation for PV generation on individual consumer units, time-of-use tariffs can contribute to grid stabilization when associated with a PEV that is recharged in the early hours (G2V), and assist the utility grid during peak hours in the evenings (V2G). Power trading like proposed by Hartmann and Özdemir [46] can add additional revenue to EV car owners, but in most cases this has been analysed with spot-market prices like the European Energy Exchange (EEX). In Strategy 1, batteries are charged in the morning and energy is sold only during the peak-hours interval, even if the actual demand is already low by any reason. The power being discharged to the grid, shown in Fig. 7.22, is estimated from the available energy and the limits of power electronics:

$$\mathrm{P_{Discharge}\,(n)} = \min\left(\frac{\mathrm{E_{Soc}(n)} - (1 - \mathrm{DOD_{Max}\ E_{Capa}})}{\mathrm{t_{Remaining\ (n)}}},\ \frac{\mathrm{P_{Max}}}{\eta_{\mathrm{Converter}}}\right). \quad (7.13)$$

The parameter $\mathrm{DOD_{MAX}}$ is the maximum allowed DOD, which is going to be varied during different simulations. Here P_{Max} is divided by the converter efficiency $\eta_{\mathrm{Converter}}$, because $\mathrm{P_{Discharge}}$ is measured before the converter, as defined in Fig. 7.22.

The battery charge level is updated according to Eq. 7.14:

$$\mathrm{E_{SoC}(n+1)} = \mathrm{E_{SoC}(n)} - \mathrm{P_{Discharge}(n)} * \Delta\mathrm{t} \quad (7.14)$$

The demand values are, as a consequence, reduced to:

$$\mathrm{D_{New}(n)} = \mathrm{D_{Old}(n)} - \eta_{\mathrm{Battery}} * \mathrm{P_{Discharge}(n)} \quad (7.15)$$

7.3.2.2 Strategy 2: Assumptions for Grid Stabilization

For a fixed number of 250 EVs, as proposed in a recent study carried out in the 2,000 households mixed residential/commercial suburb supplied by feeder #TDE05 [47], a static upper power limit is introduced. These PEVs will dispatch power to the grid to avoid power demands surpassing this upper limit. Applying a merit-order strategy, the upper limit can be interpreted as the point where V2G-energy is cheaper than dispatching other reserves, including transmission and distribution costs, in a strategy designed to avoid overloads and promote grid stabilization. In this case, grid stabilization is a service provided by the car owner to the utility, and the costs for this service are estimated. Discharge power for each car is calculated with a modification of Eq. (7.9). Here Δt is used, because there is no time limitation like in the first strategy:

$$P_{\mathrm{Discharge}}(n) = \min\left(\frac{E_{\mathrm{Soc}}(n) - (1 - \mathrm{DOD_{Max}} E_{\mathrm{Capa}})}{\Delta t},\ \frac{P_{\mathrm{Max}}}{\eta_{\mathrm{Converter}}}\right) \quad (7.16)$$

As many cars as possible discharge with the highest discharge power, which is limited by the grid connection, until the new demand curve is below the upper limit, or there are no more cars available. The battery charge level is updated according to Eq. (7.10). The new demands are calculated as per Eq. (7.11).

Each day the costs for battery degradation by cycling are calculated separately with and without discharge caused by the V2G-service. At first the DOD is calculated

$$D_{New}(n) = 1 - \frac{E_{SoC}(n)}{E_{Capa}} \tag{7.17}$$

Then the number of estimated cycle lifetime N_{Cycles} with the calculated DOD is calculated using Eq. (7.8).

The costs for this discharge are then calculated with

$$Cost_{Degradation}(n) = Cost_{Degradation}(n-1) + \frac{Price_{Battery}}{N_{Cycles}} \tag{7.18}$$

where $Price_{Battery}$ is drawn from Table 7.1. The sums with and without V2G-service are stored separately to be compared afterwards.

In order to supply the new annual energy demands (MWh/year) resulting from a proposed fleet of some 250 EVs in the mixed residential/commercial suburb under study, the incorporation of rooftop PV generators on the single-family houses in the suburb was proposed. We have previously identified the potential of the roofs in that area, which resulted in some 79,000 m^2 of total roof surface, and where more than 50 % of the area are ideally oriented and tilted for receiving at least 95 % of the theoretical maximum solar irradiation daily average density of 4.74 kWh/m^2 [32]. Only areas where at least 1 kWp of PV could be integrated have been used in the simulation, resulting in more than 43,000 m^2, where 7.9 MWp of rooftop PV capacity can be incorporated.

Figure 7.2 has shown the high energy consumption profile during the day (between 8:00 and 18:00), especially during the warmer and sunnier summer months. The seasonality of demand shows a good match with the photovoltaic generation profile; the months with the largest energy demands are also the sunny summer months. Figure 7.23 shows that the integration of PV roofs on residential buildings in the region supplied by feeder #TDE05 can drastically offset the energy consumption especially during summer months. Figure 7.23 also leads to the conclusion that during daytime hours this feeder is able to accommodate these large amounts of photogenerated electricity from grid-connected, rooftop PV generators without the need of any additional distribution system upgrade. The potential of photovoltaic found for the region supplied by the #TDE05 feeder was 7.9 MWp, using high efficiency, commercially available crystalline silicon solar modules, and should be regarded as an upper limit for PV integration in that building stock. The corresponding total annual PV generation expected is just under 8 GWh/year, enough electricity to supply over 4,000 PEV units, each driving more than 12,000 km/year.

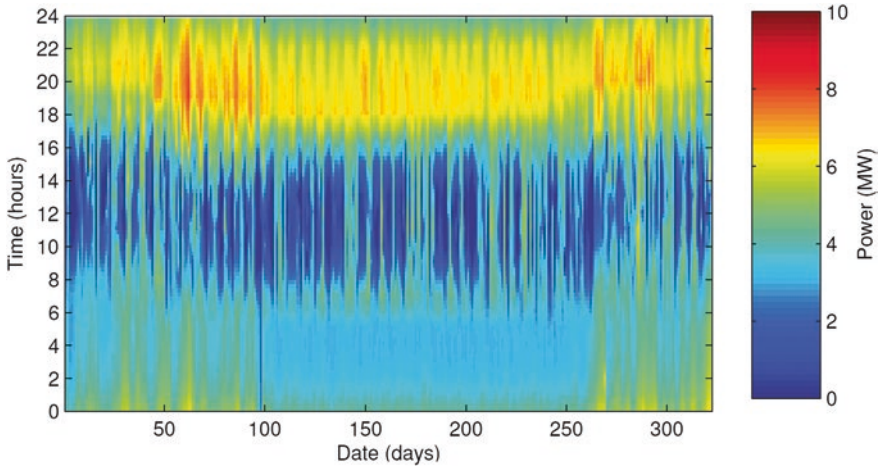

Fig. 7.23 Simulated new demand profile of the #TDE05 feeder with the solar power contribution of 7.9 MWp of PV generators spread over residential rooftops in the corresponding area. Data were calculated using the real demand profile and the corresponding solar irradiation profile for the same period

Braun and Rüther [22] have previously shown the role of grid-connected, building-integrated PV generation in commercial building energy and power loads in a warm and sunny climate. Not only can PV systems installed on residential roofs contribute strategically to alleviate urban distribution networks, shifting peak demand when there is a good correlation between loads and the solar radiation resource availability, but they can also supply all the energy requirements of a number of PEVs that is considerably larger than the number of residential households in the corresponding suburb.

7.3.2.3 Strategy 1: Results for Profit Maximizing with Local Electricity Pricing Model

The strategy of discharging cars only during peak hours in the early evening when tariffs are highest, leads to high revenues for car owners and avoided costs for the distribution utility. This leads to a new demand profile as shown in Fig. 7.24. Unfortunately, and not surprisingly, two new peaks are resulting, right before and right after dispatch, using this V2G grid-support strategy. Figure 7.25 shows the simulated hourly demand profile of the urban feeder #TDE05 resulting from both the 7.9 MWp of PV generation (daytime hours feed-in), and PEVs V2G grid-support in the early evening (during the distribution utility peak hours) for a typical day, as well as the PEVs recharging demands in the early hours (00:00–06:00). It is clear that the PEV contribution in the distribution utility's official early evening peak hours can be anticipated to 18:00 to make an optimized use of the PEVs potential, for a larger number of PEVs might be available for V2G before

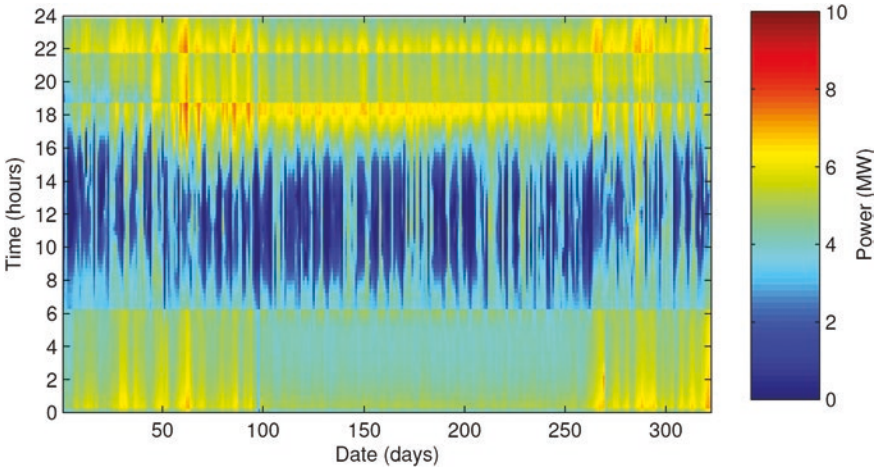

Fig. 7.24 Strategy 1: Simulated demand profile of the #TDE05 feeder, with the new demands represented by the early hours (00:00–06:00) charging of 250 EVs, the contribution of 7.9 MWp of PV generation during daytime hours, and the V2G contribution of the same 250 EV fleet to grid support in the peak hours of the early evening (19:00–21:00) at 75 % maximum DOD

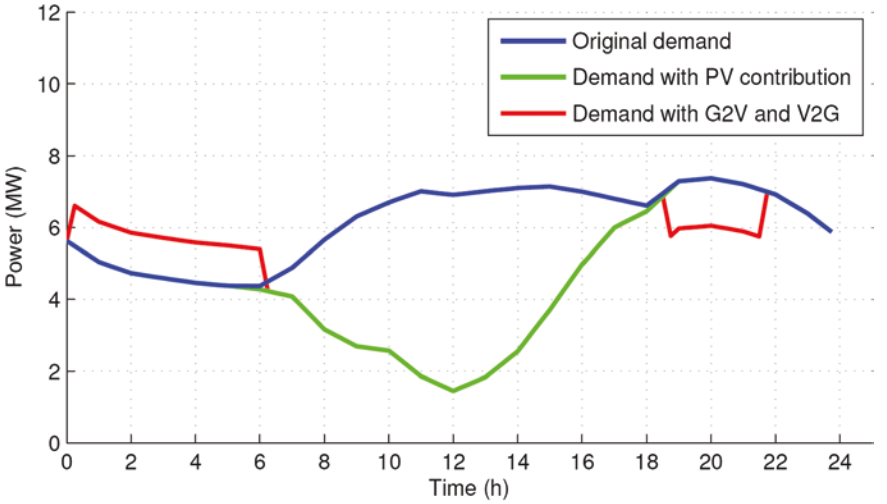

Fig. 7.25 Strategy 1: Simulation example of the new demand profile of the #TDE05 feeder on a typical day, with the new demands represented by the early hours (00:00–06:00) charging of the 250 EVs proposed fleet, the contribution of 7.9 MWp of PV generation during daytime hours, and the V2G contribution of the same 250 EV fleet to grid support in the peak hours of the early evening (19:00–21:00) at 75 % maximum DOD

18:00. The incorporation of PV to generate the new energy demands represented by the new PEV fleet is comfortably accommodated during the daytime hours. Figure 7.24 and 7.25 also show that the early hours recharging of the PEVs has to

be closely monitored to avoid overloading the grid. The new energy demands are represented for a 250 PEVs fleet, which is the optimal value for cars participating in grid stabilization as will be further shown.

The annual revenue as a function of DOD for an individual PEV is plotted in Fig. 7.26. With a DOD of 40 % the revenue already exceeds US$ 1,000 per year, where the annual revenue is calculated as the difference between the annual income and the annual costs. The income does not increase with a higher DOD after 75 %, because of the power limit P_{Max} given by the grid connection, and thus the maximum DOD cannot even be reached.

The costs are the sum of the additional hardware needed for V2G shown in Table 7.1 divided by 10 years, the price of energy recharged for G2V, and the battery degradation caused by V2G, as shown in the stacked area plot in Fig. 7.27. The cost for the grid connection does not increase with increasing the maximum DOD. The money paid for recharged G2V energy rises linearly with increasing the maximum DOD, and reaches a maximum when the power limit of the grid connection is reached. The battery degradation increases nonlinearly with the DOD, as Fig. 7.20 implies.

The time-of-use pricing model shows a large drawback. With an increasing market share of storage using the contract strategy proposed in this work, grid stability will suffer. To point out this effect, the corresponding mean squared error was calculated according to Hartmann and Özdemir [46], as shown in Eq. 7.19, where the upper limit N is the number of time-steps within a year. The mean square is a measure for the deviation between the average demand D_{av} and the current demand D(n). The optimal demand profile is a constant, thus no power margins for higher demands have to be provided. The Mean Square Error (MSE) is zero for $D(n) = D_{av} = \text{const}$.

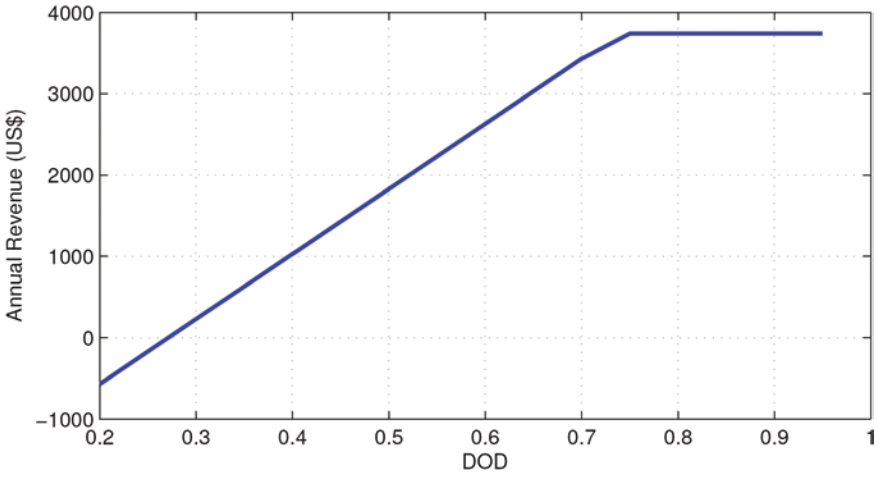

Fig. 7.26 Strategy 1: Annual revenue for one PEV as a function of the DOD with the #TDE05 feeder

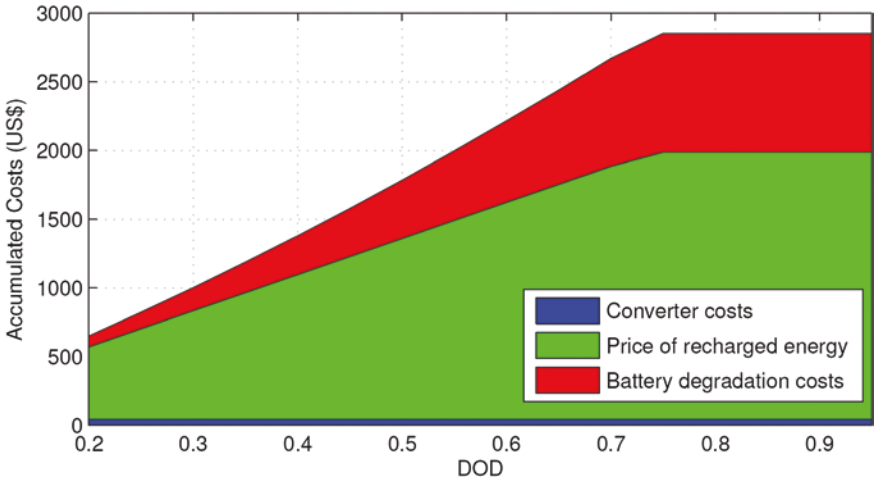

Fig. 7.27 Strategy 1: Accumulated annual costs for V2G and G2V as a function of the DOD for an individual PEV

If the demand varies a lot, a very robust grid with high power reserves has to be established yielding higher investment costs. If there is a high variation in demand, the MSE value is very high as well. Thus a high MSE value is bad for grid stability. The error was calculated for simulations with the number of PEVs varying between 0 and 1,000, and the DOD varying between 0.2 and 1.0. The maximum number of cars analyzed is 1,000, which is a rather high value when compared with the 6,949 residential and 1,099 commercial consumer units in the area.

$$\mathrm{MSE} = \sum_{n=0}^{N} (D(n) - D_{av})^2, \quad N = 30,912 \tag{7.19}$$

The MSE-values are displayed as a color map in Fig. 7.28, where the number of PEVs used is varied along the horizontal axis, and the maximum DOD is varied along the vertical axis. N = 30,912, corresponding to the 15 min time steps over the 8,760–1,032 h (excluding 43 missing days for which no data were available) of the year. The MSE without V2G-activity is calculated as 2.91 MW. Values below this reference point represent a higher grid-stability. It turns out that there is a maximum grid-stability of 2.57 MW, reached with 250 cars and a maximum DOD of 75 %. Thus, optimizing the car owners' revenue does not necessarily increase grid-stability, and these conflicting interests should be properly addressed by government-induced energy policies regarding PEVs and V2G strategies.

In Fig. 7.24 the new demand profile as a result of Strategy 1 was shown. Recharge and discharge intervals are clearly seen as horizontal stripes where the breaks are caused by time-changes because of daylight saving. The figure points out that even during times of low demand, colored in blue, energy is delivered from PEVs to the grid, which does not contribute to grid-stabilization, but generates revenue for the PEV owners.

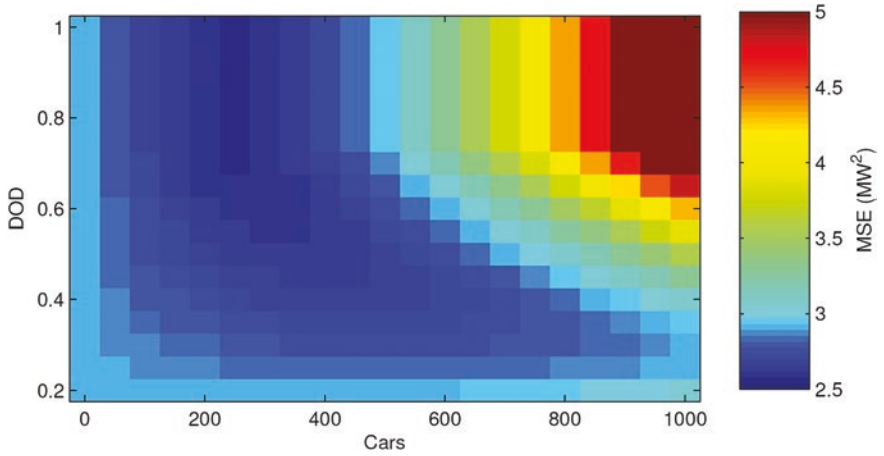

Fig. 7.28 Strategy 1: Mean squared error for different amounts of electric cars and different DOD levels

7.3.2.4 Strategy 2: Results for Grid Stabilization

In Strategy 2 the aim was to stabilize the distribution grid, making more use of the V2G approach by applying a deeper DOD level when necessary, while allowing the #TDE05 feeder to reach the maximum load limit of 6.25 MW before enabling V2G at the utility's peak-hours time. Figure 7.29 shows the resulting effect

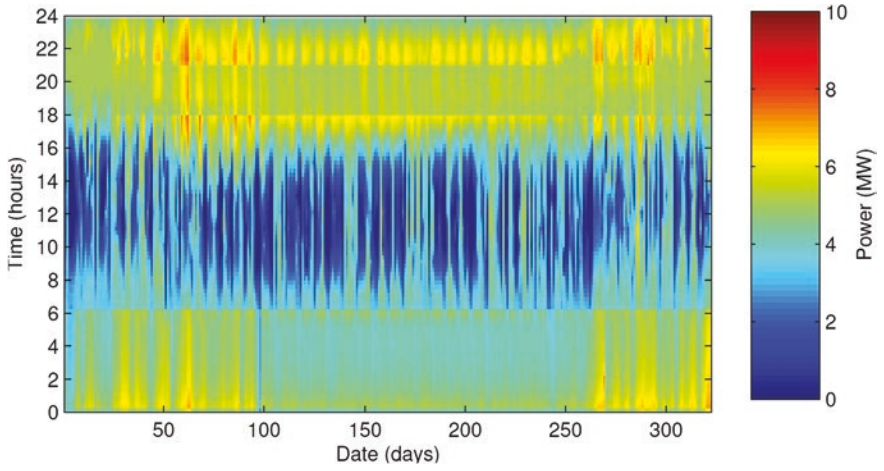

Fig. 7.29 Strategy 2: Simulated demand profile of the #TDE05 feeder with the new demands represented by the early hours (00:00–06:00) charging of 250 PEVs, the contribution of 7.9 MWp of PV generation during daytime hours, and the V2G contribution of the same 250 PEV fleet to grid support in the peak hours of the early evening (19:00–21:00) at 75 % maximum DOD, only when the distribution utility's 6.25 MW upper demand limit is reached

on the feeder's load profile. Figure 7.30 shows the same typical day as Fig. 7.25, using Strategy 2 instead. It shows that there is a lower upper limit and there are no large peaks created by G2V, as seen in Fig. 7.29. Analyzing the demand data with Strategy 2, it turns out that there are several days where the V2G service is not used at all, because the 6.25 MW utility demand limit for feeder #TDE05 is not reached. There is also a small number of days when the PEVs' battery capacity or discharge power limit are not large enough to reduce the demand to the upper limit, resulting in a remaining peak. Nevertheless this strategy will work well, if the dispatch of spinning reserves is more expensive than the dispatch of V2G services. The steep drop in the feeder #TDE05 demand curve at noon shown in Fig. 7.30 indicates a large potential for PEV recharging (G2V) at the workplace for the electric cars fleet.

In this case it also has to be noted that PEV owners' revenue is not maximized, in contrast to Strategy 1. Again the overall grid stability is measured using Eq. (7.19) to compare Strategy 2 with Strategy 1. For 250 electric cars the minimum reachable MSE value is 2.57 MW for Strategy 1, and 2.55 MW for Strategy 2, with an upper limit of 5 MW. Even if this difference is small, better knowledge of driving behavior will lead to greater improvement of MSE values for Strategy 2, but not for Strategy 1. A comparison of different upper limits and their impact on grid stability evaluated with MSE is given in Fig. 7.31, where the upper limit is varied between 4 and 8 MW. It turns out that the PEVs contribute best to grid stabilization in terms of MSE with an upper limit of 5 MW. From the grid operator's

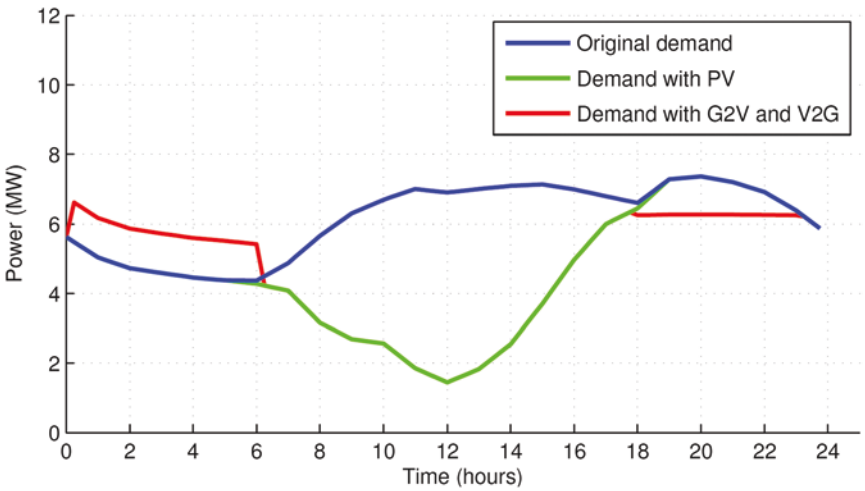

Fig. 7.30 Strategy 2: Simulation example of the new demand profile of the #TDE05 feeder on a typical day, with the new demands represented by the early hours (00:00–06:00) charging of the 250 PEVs proposed fleet, the contribution of 7.9 MWp of PV generation during daytime hours, and the V2G contribution of the same 250 PEV fleet to grid support in the peak hours of the early evening (19:00–21:00) at 75 % maximum DOD, only when the distribution utility's 6.25 MW upper demand limit is reached

perspective, the upper limit should be chosen so that the dispatch of PEVs is cheaper or equal to the dispatch of other resources. Calculating the service costs as the sum over the years of grid connection hardware, costs for efficiency losses and battery degradation divided by V2G energy delivered, leads to Fig. 7.32. It can be observed that the service cost per delivered energy is very high for a high upper limit, because the fixed costs have to be covered without selling large amounts of energy to the grid. Furthermore the service cost for low upper limits is high,

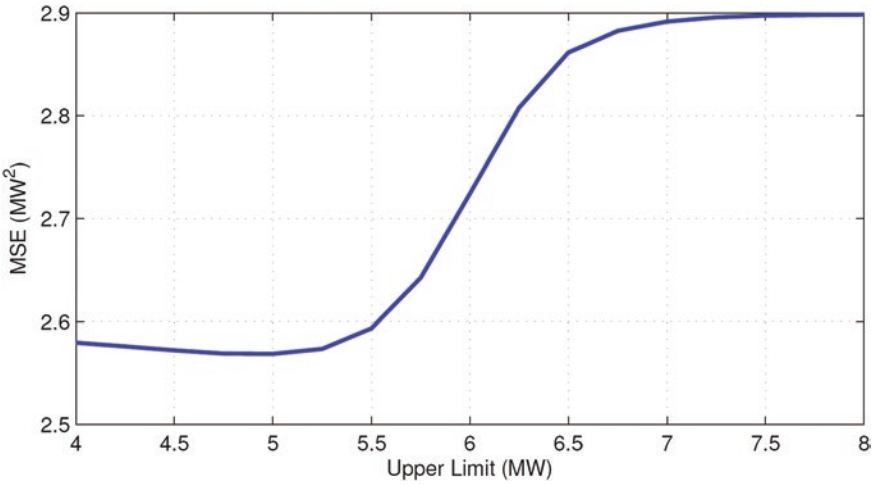

Fig. 7.31 Strategy 2: Grid stability as a function of the upper limit (in MW), where V2G is active with 250 PEVs participating in grid stabilization, and a 75 % maximum DOD level

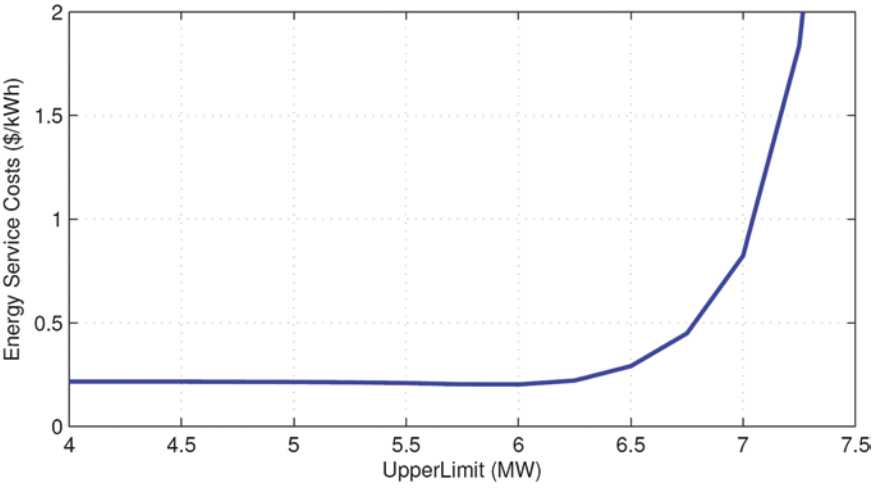

Fig. 7.32 Strategy 2: Service costs for V2G service for each PEV per energy as a function of the upper limit where V2G is active, and a 75 % maximum DOD level

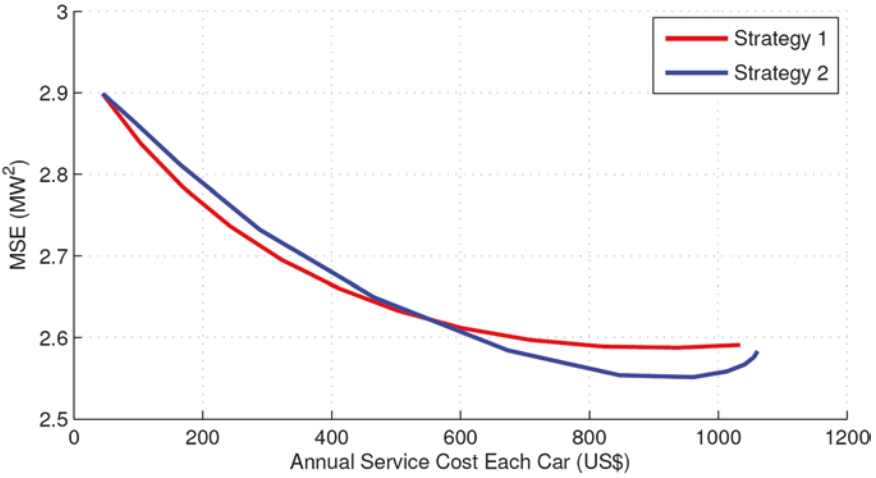

Fig. 7.33 Comparison between Strategy 1 and Strategy 2 regarding MSE, plotted as a function of annual costs per PEV including all V2G hardware, battery degradation and energy losses

because of intensive battery degradation. Comparing Figs. 7.31 and 7.32, it turns out that a reasonable compromise between costs and grid stability can be observed between 4.0 and 5.5 MW.

To compare both strategies, the MSE was plotted in Fig. 7.33 as a function of the annual service cost per PEV. It can be observed that using Strategy 2, a lower MSE, and thus a higher grid stability, can be achieved. In addition, Strategy 2 fits well in the concept of merit order, whereas Strategy 1 does not. In Fig. 7.29 new energy demands caused by Strategy 2 are exposed. During times of low demands, no energy is delivered to the grid. During times of high demands, peaks are shaved to the upper limit of 5–6 MW. In times of extraordinary high demands, battery capacity even at high DOD levels is not enough to shave peaks sufficiently, as seen during the days 61 and 62 at night in Fig. 7.29.

7.3.2.5 Energy Balance

In this section an overall energy balance is discussed. Both Tables 7.2 and 7.3 present the energy balance along the year for Strategy 1 and Strategy 2 respectively. Table 7.2 shows the energy balance considering Strategy 1, with 250 electric cars participating in grid stabilization, with a 75 % maximum DOD level, as well as the PV contribution of 7.9 MWp of rooftop generators spread all over the metropolitan region supplied by the #TDE05 feeder. Photovoltaic energy is sufficient to compensate for energy losses due to conversion and battery cycling efficiency, as well as the energy demands caused by PEV driving. As expected, PV energy generation is higher in the summer season, and thus the balanced energy is high during December and January. Over the year, Strategy 1 leads to 1,063 MWh of

Table 7.2 Energy balance for strategy 1

Months	Valid days	V2G (MWh)	G2V (MWh)	PV (MWh)	Balance (MWh)
January	29	95.7	158.6	799.7	736.9
February	28	92.4	157.1	689.0	624.4
March	29	95.7	162.7	838.5	771.6
April	29	95.7	162.7	748.6	681.6
May	31	102.3	173.9	682.8	611.1
June	18	59.4	101.0	411.3	369.8
July	16	52.8	89.7	293.8	256.8
August	24	79.2	134.6	609.7	554.3
September	27	89.1	151.4	491.3	429.0
October	30	99.0	168.3	664.6	595.3
November	30	99.0	168.3	797.1	727.9
December	31	102.3	173.9	837.2	765.6
Annual		1,062.6	1,802.2	7,863.6	7,124.0

Balance: (V2G + PV − G2V) Rows and columns may not add horizontally or vertically due to rounding

Table 7.3 Energy balance for strategy 2

Months	Valid days	V2G (MWh)	G2V (MWh)	PV (MWh)	Balance (MWh)
January	29	64.3	119.6	799.7	744.4
February	28	88.0	151.7	689.0	625.3
March	29	97.7	165.1	838.5	771.1
April	29	91.4	157.3	748.6	682.7
May	31	102.3	173.8	682.8	611.3
June	18	59.0	100.4	411.3	369.9
July	16	53.9	91.1	293.8	256.6
August	24	80.8	136.7	609.7	553.8
September	27	89.0	151.3	491.3	429.0
October	30	20.4	165.6	664.6	519.4
November	30	96.9	168.7	797.1	725.3
December	31	93.0	166.0	837.2	764.2
Annual		936.7	1,747.3	7,863.6	7,053.0

Balance: (V2G + PV − G2V) Rows and columns may not add horizontally or vertically due to rounding

electricity supplied to the grid with V2G, 1,801 MWh of electricity drawn from the grid with G2V, and 7,863 MWh of electricity generated by the 7.9 MWp of PV rooftops. There is therefore a considerably large positive annual balance of electricity fed to the public grid (V2G + PV generation − G2V) of 7,124 MWh.

In Table 7.3 the energy balance for Strategy 2 with 250 cars participating in grid stabilization, a 75 % maximum DOD level, the PV contribution of 7.9 MWp of

rooftop generators spread all over the metropolitan region supplied by the #TDE05 feeder, and an upper limit of 5 MW for the feeder demand is presented. It turns out that the overall energy gain is larger than with Strategy 1. Strategy 1 is optimized for electric car owners' revenues, and the losses are thus not necessarily minimized. With Strategy 2 fewer losses occur because the V2G option is used only to stabilize the grid, and not to maximize car owners' revenues. Over the year, Strategy 2 leads to 936 MWh of electricity supplied to the grid with V2G, 1,747 MWh of electricity drawn from the grid with G2V, and the same 7,863 MWh of electricity generated by the 7.9 MWp of PV rooftops. The positive annual balance of electricity fed to the public grid (V2G + PV generation − G2V) is in this case very similar to the one resulting from Strategy 1, totaling 7,053 MWh. In both cases, the surplus electricity generated by making use of the full PV potential of the local residential rooftops is enough to feed a PEV fleet of some 4,000 cars.

7.4 Conclusions

In this chapter the potential of using PEVs and onsite solar PV generation in a smart grid environment, to both assist peak demand reduction in urban utility grids and to supply the additional energy requirements of a PEV fleet were assessed. Real electricity demand data, and real local solar irradiation and PV generation data were used to assess the potential contribution of using both V2G and PV generation strategies to assist the distribution utility #TDE05 feeder in peak shaving in the early evening. Commercial/public building and detached, single-family residential building rooftop PV generation spread over the area supplied by this utility feeder allowed to produce electricity well in excess of the additional amounts of electricity required by a number of PEVs to be owned by a fraction of the local residents. On the basis of a simulation with time-steps of one hour using measured demand data, PV systems have shown to have the potential to reduce load fluctuations in the urban grid. The power generated correlates well with the demand data and might thus reduce the daytime demand peak. A 7.9 MWp PV system installed in the urban region shown here can compensate the consumption of air-conditioning in the commercial buildings. This analysis points out that there is a potential for PEVs to stabilize the grid in regards of peak load shaving. The introduction of time-of-use distribution utility tariffs, with higher energy prices at peak times also for residential consumers, should in fact result in reduced demand during peak time, but might also create new peaks around this time interval. As shown with Strategy 1, assumed there is a net metering contract, this policy might be exploited leading to revenues for PEV owners, but not necessarily to grid stabilization. This effect is sensitive to the number of PEVs into consideration. The second strategy, with a fixed limit, allows for the concept of merit order, and is therefore more suitable for the utility. To make use of this strategy, PEV owners would need to receive a small reward just for having the car connected to the grid. Only in rare cases, when demand exceeds a specific limit, the stored energy would be solicited by the utility.

References

1. Kempton W, Letendre SE (1997) Electric vehicles as a new power source for electric utilities. Transp Res Part D Transp Environ 2:157–175
2. Kempton W, Kubo T (2000) Electric-drive vehicles for peak power in Japan. Energy Policy 28:9–18
3. Kempton W, Tomić J (2005) Vehicle-to-grid power fundamentals: calculating capacity and net revenue. J Power Sources 144:268–279
4. Kempton W, Tomić J (2005) Vehicle-to-grid power implementation: from stabilising the grid to supporting large-scale renewable energy. J Power Sources 144:280–294
5. REN21. Renewables (2014) Global Status Report (Paris: REN21 Secretariat) 2014. Available at www.ren21.net
6. Mints P. PV Costs/ASPs/Shipments & Cost Price Delta, 2003–2014. Solar Flare, Issue 1, 2014
7. Rüther R, Zilles R (2011) Making the case for grid-connected photovoltaics in Brazil. Energy Policy 39:1027–1030
8. Perez R, Seals R, Herig C (1996) PV can add capacity for the grid. NREL Publications, Golden, USA. DOC/GO-10096-262
9. Perez R, Letendre S, Herig C (2001) PV and grid reliability: availability of PV power during capacity shortfalls. In: Proceedings of the American Solar Energy Society—ASES annual conference, Washington, DC, pp 1–4
10. Jardim CS, Rüther R, Salamoni IT, Viana TS, Rebechi SH, Knob PJ (2008) The strategic siting and the roofing area requirements of building-integrated photovoltaic solar energy generators in urban areas in Brazil. Energy Build 40:365–370
11. Méndez VH, Rivier J, de la Fuente JI, Gómez T, Arceluz J, Marín J, Madurga A (2006) Impact of distributed generation on distribution investment deferral. Electr Power Energy Syst 28:244–252
12. Jimenez H, Calleja H, González R, Huacuz J, Lagunas J (2006) The impact of photovoltaic systems on distribution transformer: a case study. Energy Convers Manag 47:311–321
13. Rüther R, Knob PJ, Jardim CS, Rebechi SH (2008) Potential of building-integrated photovoltaic solar energy generators in assisting daytime feeders in urban areas in Brazil. Energy Convers Manag 49:1074–1079
14. Naspolini HF, Militão HSG, Rüther R (2010) The role and benefits of solar water heating in the energy demands of low-income dwellings in Brazil. Energy Convers Manag 51:2835–2845
15. Naspolini HF, Rüther R (2011) The impacts of solar water heating in low-income households on the distribution utility's active, reactive and apparent power demands. Sol Energy 85:2023–2032
16. Rüther R, Pereira Junior LC, Pfitscher PH, Viana TS (2011) Assessing the potential of electric vehicles and photovoltaics in a smart-grid environment in Brazil. In: Proceedings of the 3rd European conference on smart-grids and e-mobility, pp 172–179
17. Zahedi A (2006) Solar photovoltaic (PV) energy; latest developments in the building integrated and hybrid PV systems. Renew Energy 31:711–718
18. Urbanetz J, Zomer CD, Rüther R (2011) Compromises between form and function in grid-connected, building-integrated photovoltaics (BIPV) at low-latitude sites. Build Environ 46:2107–2113
19. Ordenes M, Marinoski DL, Braun P, Rüther R (2007) The impact of building-integrated photovoltaics on the energy demand of multi-family dwellings in Brazil. Energy Build 39:629–642
20. Rüther R, Braun P (2009) Energetic contribution potential of building-integrated photovoltaics on airports in warm climates. Sol Energy 83:1923–1931
21. Heipled S, Sailor DJ (2008) Using building energy simulation and geospatial modeling techniques to determine high resolution building sector energy consumption profiles. Energy Build 40:1426–1436

22. Braun P, Rüther R (2010) The role of grid-connected, building-integrated photovoltaic generation in commercial building energy and power loads in a warm and sunny climate. Energy Convers Manag 51:2457–2466
23. Chan AT, Yeung VCH (2005) Implementing building energy codes in Hong Kong: energy savings, environmental impacts and cost. Energy Build 37:631–642
24. Brogren M, Green A (2003) Hammarby Sjostad—an interdisciplinary case study of the integration of photovoltaics in a new ecologically sustainable residential area in Stockholm. Sol Energy Mater Sol Cells 75:761–765
25. Burger B, Rüther R (2006) Inverter sizing of grid-connected photovoltaic systems in the light of local solar resource distribution characteristics and temperature. Sol Energy 80:32–45
26. Jones DL, Hattersley L, Ager R (2000) Photovoltaics in buildings BIPV projects. Energy Technology Support Unit (ETSU), Harwell (United Kingdom) Department of trade and industry. Available at www.opengrey.eu/partner/bldsc
27. Pantic S, Candanedo L, Athienitis AK (2010) Modeling of energy performance of a house with three configurations of building-integrated photovoltaic/thermal systems. Energy Build 42:1779–1789
28. Parker DS (2009) Very low energy homes in the United States: perspectives on performance from measured data. Energy Build 41:512–520
29. Penga C, Huanga Y, Wub Z (2011) Building-integrated photovoltaics (BIPV) in architectural design in China. Energy Build 43:3592–3598
30. Sun LL, Yang HX (2010) Impacts of the shading-type building-integrated photovoltaic claddings on electricity generation and cooling load component through shaded windows. Energy Build 42:455–460
31. Mardaljevic J, Rylatt M (2003) Irradiation mapping of complex urban environments: an image-based approach. Energy Build 35:27–35
32. Santos IP, Rüther R (2012) The potential od building-integrated (BIPV) and building-applied photovoltaics (BAPV) in single-family, urban residences at low latitudes in Brazil. Energy Build 50:290–297
33. Rüther R (1998) Experiences and operational results of the first grid-connected, building-integrated thin film photovoltaic installation in Brazil. In: Proceedings of the 2nd world conference and exhibition of photovoltaic solar energy convertion, Vienna, Austria, pp 2655–2658
34. Rüther R, Dacoregio MM (2000) Performance assessment of a 2kWp grid-connected, building-integrated, amorphous silicon photovoltaic installation in Brazil. Prog Photovolt Res Appl 7:257–266
35. Stabler DL, Wronski CR (1977) Reversible conductive charges in this charge produced amorphous silicon. Appl Phys Lett 31:292–294
36. Rüther R, Livingstone J (1994) Seasonal variations in amorphous silicon solar module outputs and thin film characteristics. Sol Energy Mater Sol Cells 36:29–43
37. Rüther R (1999) Demonstrating the superior performance of thin-film, amorphous silicon for building-integrated PV systems in warm climates. In: Proceedings of the international solar energy society's solar world congress. ISES, Jerusalem, Israel, pp 221–224
38. Radiasol, Laboratório de Energia Solar—GESTE—PROMEC, Porto Alegre. Available at www.solar.ufrgs.br
39. SWERA (2011) Solar and wind energy resource assessment programme, UNEP 2011. Available at http://swera.unep.net/
40. Drude L, Pereira Junior LC, Rüther R (2014) Photovoltaics and electric vehicle-to-grid (V2G) strategies for peak demand reduction in urban regions in Brazil in a smart grid environment. Renew Energy 68:443–451
41. Dallinger D, Krampe D, Wietschel M (2010) Vehicle-to-grid regulation based on a dynamic simulation of mobility behavior. Fraunhofer Institute for Systems and Innovation Research (ISI), Working Papers Sustainability and Innovation S4/2010
42. Tomić J, Kempton W (2007) Using fleets of electric-drive vehicles for grid support. J Power Sources 168:459–468

43. Biere D, Dallinger D, Wietschel M (2009) Ökonomische analyse der erstnutzer von elektrofahrzeugen. Zeitschrift für Energiewirtschaft 33:173–181
44. Rosenkranz C (2003) Deep cycle batteries for plug-in hybrid application. EVS-20 Plug-in Hybrid Workshop, Long Island-CA, United States
45. Meinhardt M (2007) Pv-systemtechnik—ein motor der kostenreduktion für die photovoltaische stromerzeugung. SMA Technologie AG, Niestetal. Available at www.fvsonnenenergie.de/fileadmin/publikationen/tmp_vortraege_jt2007/th2007_15_meinhardt.pdf2241
46. Hartmann N, Özdemir E (2011) Impact of different utilization scenarios of electric vehicles on the german grid in 2030. J Power Sources 196:2311–2318
47. Pereira Junior LC (2011) A interação entre geradores solares fotovoltaicos e veículos elétricos conectados à rede elétrica pública. Master's thesis, Universidade Federal de Santa Catarina, Florianópolis-SC

Chapter 8
PEV Load and Its Impact on Static Voltage Stability

C.H. Dharmakeerthi and N. Mithulananthan

Abstract A global resurgence of electric vehicle has taken place as a sustainable alternative to fossil fuel dependent transportation. As a result, the new plug-in electric vehicle (PEV) charging load is emerging into power networks. Even though the environmental and economic benefits of electrified transportation are very much apparent, its impacts on power systems still need to be understood. This chapter develops a mathematical model of the PEV charging load, evaluates its impact on system steady state voltage stability and suggests effective remedies to overcome the stability impacts due to PEV charging on power grids. Load characteristics profoundly influence the static voltage stability of power systems. Therefore, it is important to understand the characteristics of this emerging PEV charging load and its impact on power system voltage stability. Hence, a load model for the power electronically controlled PEV battery charging load is introduced in this chapter. The proposed PEV load model consists of a combination of a constant power load and a voltage dependent load having negative exponential characteristics. Due to the voltage dependent characteristics of PEV, the conventional power flow equations require modifications in order to accommodate the PEV load. The required modifications to the Newton Raphson power flow algorithm are described in this chapter. The system studies carried out in this chapter found that PEV charging load cause negative impact on system voltage stability, hence effective remedial measures are introduced. Further, a computationally efficient index which has good physical interpretation is introduced for identifying voltage stability considered charging infrastructure.

C.H. Dharmakeerthi · N. Mithulananthan (✉)
School of Information Technology and Electrical Engineering,
University of Queensland, Brisbane, Australia
e-mail: mithulan@itee.uq.edu.au

C.H. Dharmakeerthi
Ceylon Electricity Board, Colombo, Sri Lanka
e-mail: champa80@yahoo.com

S. Rajakaruna et al. (eds.), *Plug In Electric Vehicles in Smart Grids*,
Power Systems, DOI 10.1007/978-981-287-299-9_8

8.1 Introduction

Substantial plug-in electric vehicle (PEV) integration has resulted in the recent past owing to the distinct advantages and various incentives provided by governments. This strategic shift of the primary source of transportation energy from oil pipelines to power grids will inevitably bring numerous challenges to power grids around the world. Even though the environmental and economic benefits of the electrified transportation are very much apparent, the potential impacts of PEV integrations on the power grids are yet to be studied and well understood.

Voltage dependent loads characteristics, especially power consumption of the load with respect to terminal voltage, have profound impact on system voltage stability. This highlights the importance of accurate load representation for realistic voltage stability studies. This chapter introduces a load model for the power electronically controlled PEV battery charging load. Then, the modifications required for the conventional Newton Raphson power flow algorithm to accommodate the identified PEV charging load characteristics are described. Subsequently, impact of PEV charging on static voltage stability of power system is evaluated under different scenarios. Factors affecting the static voltage stability of power system due to PEV charging station integration and remedies which can be implemented to reduce PEV grid voltage stability impacts will also be discussed in the chapter. Once knowing the impact of PEV load on system static voltage stability, it is important to take precautions right from the planning stage of the PEV charging infrastructure. Hence, this chapter further introduces a computationally efficient index, which is having good physical interpretation, to identify a voltage stability preserved charging station planning solution.

An accurate representation of load characteristics is important in realistic system studies. Hence, load modelling is carried out first, as described in the proceeding section.

8.2 Modeling of PEV Charging Load

8.2.1 Introduction to Power System Load Characteristics

System loads can be categorized into different types depending on how they react to varying system conditions, particularly to system voltage and frequency variations. Voltage dependent load characteristics are important when consider system voltage stability and other static system studies including load flow analysis. There are three basic conventional load characteristics that describe different extent of load voltage dependencies. These are constant current,

constant impedance and constant power load characteristics. These load characteristics can be described by the general form given in Eq. (8.1), which is also known as the exponential load characteristics.

$$P = P_0\left(\frac{V}{V_0}\right)^{\alpha}; \quad Q = Q_0\left(\frac{V}{V_0}\right)^{\beta} \tag{8.1}$$

The quantities P_0 and Q_0 refers to the real and reactive power consumption of the load at voltage V_0. The conventional constant power load can be obtained by placing $\alpha = 0$ and $\beta = 0$. This load consumes constant real and reactive power despite the changes in the supply voltage. The constant current load can be derived with $\alpha = 1$ and $\beta = 1$. Its power consumption is proportional to the applied voltage. The constant impedance load can be described by $\alpha = 2$ and $\beta = 2$, where the power consumption is proportional to the square of the applied voltage. However, in reality most system loads cannot categorized purely as one of the aforesaid conventional load characteristics. Some of them show combination of above load characteristics, described by ZIP load model, as given in Eq. (8.2).

$$P = a_0 P_0\left(\frac{V}{V_0}\right)^{0} + a_1 P_0\left(\frac{V}{V_0}\right)^{1} + a_2 P_0\left(\frac{V}{V_0}\right)^{2} \tag{8.2}$$

A similar expression can be written to describe reactive power consumption as well. Parameter a_0, a_1 and a_2 describe the constant power, constant current and constant impedance proportions of the real power consumption of the load, while b_0, b_1 and b_2 are typically used to represent that of the reactive power consumption of the load. Further, many practical loads exhibit different α and β other than 0, 1 and 2 of load characteristics described in Eq. (8.1). For example, literature [1] has experimentally found load models having voltage exponents α in the range from -3.3 to 2.6 and β in the range from -4.25 to 24.17. Numerous sophisticated loads are emerging into power systems continually replacing the conventional system loads, making accurate system studies challenging than ever before.

Power electronically controlled loads are increasingly emerging into power systems. PEV is becoming one significant load among them. Many power electronic loads are having two converters. A constant dc link voltage is maintained by the first converter, despite grid voltage variations. Power factor control can also be embedded at the first converter. Required power rating and redundancy may be achieved by splitting the first converter into several parallel units. The second converter consists of one or several converters connected to one or several load units, respectively. The second converter provides the voltage/current/power requirements of the individual connected loads. If the connected loads are having "one-to-one" voltage current characteristics the power output measured at the dc link remains constant despites grid voltage variations, as long as the grid voltage variations are within the ac-dc converter designed

input voltage range. Therefore, the power electronically controlled load, when viewed at the dc link is a constant power load, as long as the connected load is having "one-to-one" voltage current characteristics [2]. However, the load voltage characteristics may be different when consider grid interface point of view, which need further investigation. The proceeding section models a PEV charging load, in the power grid point of view.

8.2.2 Modelling of the PEV Charging Load

The PEV charging load is a power electronically controlled load, which consists of a charging unit and a PEV battery. The PEV chargers can be categorized mainly into ac or dc and further according to their power demand defined by the level of charging (level 1–3) according to the SAE (Society of Automotive Engineers) charging configurations and ratings terminology [3, 4]. The level of charging increases as the charger rating increases. The well-established PEV charger configuration consists of two converters; an ac-dc converter at the front-end and a dc-dc converter at the battery-end [5–13], as shown in Fig. 8.1. The first stage perform rectification and power factor control. The second stage involves different types of resonant or Pulse Width Modulated (PWM) dc-dc converters. The dc-dc converter is required for maintaining appropriate charging current for different state of charge (SOC) conditions and cell temperatures of the battery. Furthermore, the second converter stage maintains the charging current ripples within the safe limits for the battery [6, 14].

A PEV dc fast charger, which consists of an active rectifier (controlled ac-dc converter) at the front-end and a dc-dc buck converter at the battery-end, is considered here for modelling. This charger arrangement has many desirable features including unity power factor operation and ability of connecting to a wide range of input voltages. It provides a regulated dc voltage output which is independent of the input voltage variations within the designed limits.

Load modelling for power system voltage stability studies requires identification of load demand variation with respect to the supply voltage. This power-voltage relationship is derived analytically for the charger shown in Fig. 8.1.

The equations for the first stage ac-dc converter shown in Fig. 8.2 can be derived as follow in the dq reference frame.

$$V_d = L\frac{di_d}{dt} + Ri_d - L\omega i_q + d_d V_{dc} \tag{8.3}$$

$$V_q = L\frac{di_q}{dt} + Ri_q + L\omega i_d + d_q V_{dc} \tag{8.4}$$

$$C_1\frac{dV_{dc}}{dt} = {}^{3}/_{2}\left(d_d i_d + d_q i_q\right) - i_{dc} \tag{8.5}$$

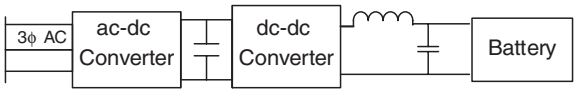

Fig. 8.1 Schematic diagram of a PEV charger

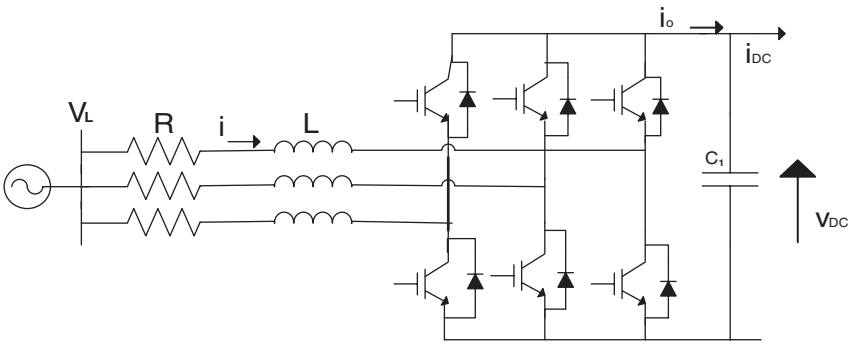

Fig. 8.2 The ac-dc converter at the grid interface

R is the total resistance of the first converter stage. The resistance R includes mainly the turn on resistances of active rectifier switches (R_s) and the parasitic resistance of the input filter (R_L). The d_d and d_q represent converter duty ratios in the dq reference frame. V_d, V_q, i_d and i_q refers to direct and quadrature axis voltages and currents, respectively.

For steady state analysis, Eqs. (8.3)–(8.5) can be rearranged as Eqs. (8.6)–(8.8).

$$V_d = Ri_d - L\omega i_q + D_d V_{dc} \tag{8.6}$$

$$\mathrm{V_q = Ri_q + L\omega i_d + D_q V_{dc}} \tag{8.7}$$

$$i_{dc} = {}^{3}/_{2}\left(D_d i_d + D_q i_q\right) \tag{8.8}$$

The D_d and D_q are the steady state direct and quadrature axis duty ratios, respectively. Real and reactive power of the PEV load in the dq reference frame are defined in Eqs. (8.9) and (8.10),

$$\mathrm{P = {}^{3}/_{2}\left(V_d i_d + V_q i_q\right)} \tag{8.9}$$

$$\mathrm{Q = {}^{3}/_{2}\left(V_d i_q - V_q i_d\right)} \tag{8.10}$$

The controller of the ac-dc converter is shown in Fig. 8.3. It regulates the dc link voltage and maintains a unity power factor operation.

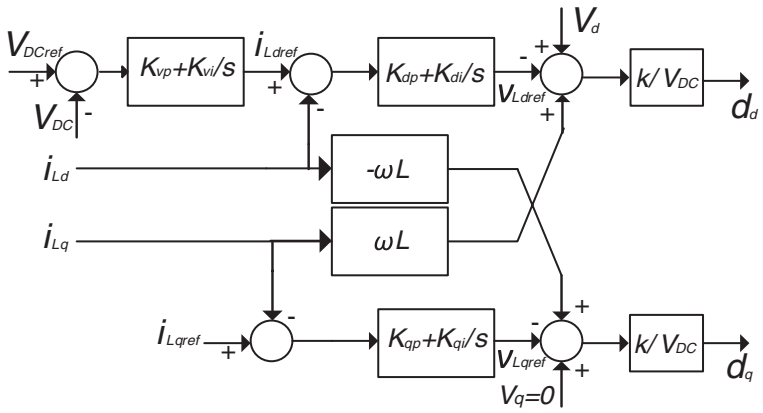

Fig. 8.3 The controller of the ac-dc converter

It is assumed that the dq frame is rotating at ω speed and the d axis is oriented along the grid voltage vector. Hence, $V_q = 0$. The i_{qref} is set to zero to achieve unity power factor operation. Hence, under steady state, $i_q = 0$. The d axis current has been used to regulate the dc link voltage. The Eqs. (8.6)–(8.9) can be reorganized as below.

$$V_d = Ri_d + D_d V_{dc} \tag{8.11}$$

$$0 = \mathrm{L}\omega \mathrm{i_d} + \mathrm{D_q V_{dc}} \tag{8.12}$$

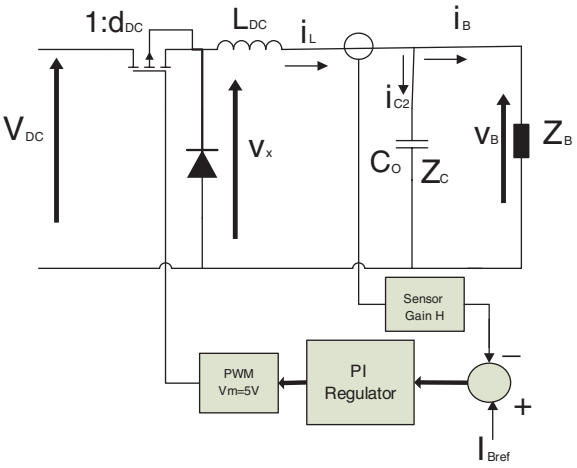

Fig. 8.4 Schematic diagram of dc-dc converter and its controller

$$i_{dc} = {}^{3}/_{2}(D_d i_d) \tag{8.13}$$

$$P = {}^{3}/_{2}(V_d i_d) \tag{8.14}$$

Considering Eqs. (8.11), (8.13) and (8.14),

$$P = V_{dc} i_{dc} + \frac{2}{3}\left(R i_{dc}^2 / D_d^2\right) \tag{8.15}$$

The second stage of the charger consists of a dc-dc buck converter. The converter and the controller are shown in Fig. 8.4.

Considering lossless switching and continuous conduction mode operation of the buck converter, the analytical expressions for the dc-dc stage can be derived as given in Eqs. (8.16)–(8.18).

$$L_{dc}\frac{di_L}{dt} = d_{DC} v_{dc} - v_B - r i_L \tag{8.16}$$

$$C_2\frac{dv_B}{dt} = i_L - i_B \tag{8.17}$$

$$i_L = \frac{i_{dc}}{d_{DC}} \tag{8.18}$$

The parameters v_B and Z_B represent Battery terminal voltage and battery impedance, respectively. The value of v_B primarily depends on battery open circuit voltage (V_{BO}) which is a function of the battery state of charge (SOC), the battery impedance and the charging current (i_B). The charging current reference is determined by the battery management system based mainly on the battery voltage, cell temperature and the SOC. The dc-dc converter controller maintains i_L at the charging current reference. The constant current-constant voltage (CC-CV) battery charging method is considered here. This method is one of the well-established battery charging methods [15, 16]. During CC-CV charging the buck converter controller maintains a constant charging current until the cell voltages reach a predetermined value, then a constantly reducing current is applied to the battery until it gets fully charged.

The modelling of the charger unit should also include modelling of the battery. A widely accepted battery model shown in Fig. 8.5 [17–20], is incorporated.

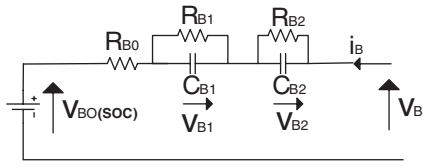

Fig. 8.5 The schematic diagram of battery

The two series connected parallel RC circuits define the transient characteristics of the battery, while R_{BO} describes charging/discharging power loss of the battery. The battery electrochemical polarization resistance and the capacitances are represented by R_{B1} and C_{B1} [19], respectively. The battery concentration polarization resistance and the capacitances are represented by R_{B2} and C_{B2} [19], respectively.

The more the number of series connected parallel RC circuits, the more accurate is the battery model. However, it has been identified that two series connected parallel RC circuits will provide reasonably accurate dynamic performance with less computational complexities [20]. The differential equations which describe the battery dynamics are shown below.

$$\frac{dv_{B1}}{dt} = \frac{1}{C_{B1}}\left(i_B - \frac{v_{B1}}{R_{B1}}\right) \tag{8.19}$$

$$\frac{dv_{B2}}{dt} = \frac{1}{C_{B2}}\left(i_B - \frac{v_{B2}}{R_{B2}}\right) \tag{8.20}$$

For steady state analysis, the battery equivalent becomes a resistor ($R_B = R_{B1} + R_{B2} + R_{B0}$) in series with a variable voltage source (V_{B0}). For steady state analysis Eqs. (8.16), (8.17), (8.19) and (8.20) can be described by Eqs. (8.21)–(8.23). The steady state duty ratio of dc-dc converter is defined by d_{DC}.

$$d_{DC}v_{dc} = v_B + ri_L \tag{8.21}$$

$$i_B = i_L \tag{8.22}$$

$$v_B = v_{BO} + i_L R_B \tag{8.23}$$

Combining Eqs. (8.15), (8.18) and (8.21)–(8.23);

$$P = \underbrace{i_L\{v_{BO} + i_L(r + R_B)\}}_{P_{cp}} + \underbrace{\frac{2Rd_{DC}^2 i_L^2}{3D_d^2}}_{P_{vd}} \tag{8.24}$$

The power consumption of the charger given in Eq. (8.24), consists of two components. Each component can be investigated carefully to identify its power and voltage relationship. The current i_L in the first term (P_{cp}) will follow the current reference of the dc-dc current controller. On the other hand, V_{BO} is a term, which is determined by the battery SOC. Hence, it is evident that P_{cp} remains constant despite supply voltage variations, hence exhibits constant power load characteristics. The second term (P_{vd}) consists of D_d, which can be obtained by solving Eqs. (8.11), (8.13) and (8.22);

$$D_d = \frac{V_d \pm \sqrt{V_d^2 - \frac{8Ri_L V_{dc} d_{DC}}{3}}}{2V_{dc}} \tag{8.25}$$

D_d can be approximated to Eq. (8.26), when assign a set of practical values to the parameter of Eq. (8.25). Hence, P_{vd} of Eq. (8.24) can be represented by Eq. (8.27).

$$D_d \approx \frac{V_d}{V_{dc}} \tag{8.26}$$

$$P_{vd} = \frac{2Rd_{DC}^2 i_L^2 V_{dc}^2}{3V_d^2} \tag{8.27}$$

It is evident from Eq. (8.27) that P_{vd} exhibits exponential load behavior with a negative alpha value, as given in Eq. (8.28).

$$\frac{P_{vd}}{P_{vdo}} == \left(\frac{V}{V_o}\right)^{-2} = \left(\frac{V}{V_o}\right)^{-\alpha} \tag{8.28}$$

The power consumption of the charger at the reference voltage (V_0) is represented by P_{vdo}. Finally, it is evident that the load model of the PEV charging load consists of constant power load component and the negative exponential load component, as given by Eq. (8.29) [21].

$$\frac{P}{P_o} = a\left(\frac{V}{V_o}\right) + b \tag{8.29}$$

Further, it is apparent that the a, b and α parameters of the PEV load model is depended on many parameters, including battery SOC, resistance values of the charging load, duty ratios of the converters and the reference voltages and currents. The influence of the R, which consist of turn on resistances of active rectifier switches (R_s) and parasitic resistance of the input filter (R_L) is evaluated numerically in the following section.

8.2.3 *Effects of Charger Resistances on Load Model Parameters*

A numerical evaluation of effects of component resistances of the charger on PEV load model parameters is carried out in this section. The turn-on resistances of the active rectifier switches (Rs) and parasitic resistance of the input filters (R_L) are taken into consideration. A 200 kW PEV dc fast charger is simulated in the MATLAB Simulink. The PEV charging load consists of an active three level ac-dc converter, a dc/dc buck converter and a 30 kWh Lithium-Ion battery. The active rectifier controllers maintain unity power factor operation and a 500 V regulated dc link voltage, while dc-dc converter maintains a battery charging current of 320 A during constant current charging phase.

The input power demand of the charger is measured for a range of terminal voltages (0.6–1.3 p.u.). All the readings are taken at 50 % SOC of the battery to ensure that the same electrical status of the battery prevails during each measurement. The power consumption of the charger is measured at the presence of different R_L (0, 0.1, 1 mΩ) and R_S (0, 0.2, 2 mΩ) values. It is observed that the input power depends on R_L and R_S. The MATLAB curve fitting function is then utilized to obtain the load models with different R_L and R_S values. It is observed that the power voltage relationship consists of a constant power component and a voltage dependent power component, confirming the analytically derived load characteristics given in Eq. (8.29). The a, α and b parameter values are given in Table 8.1 for different R_L and R_s values [22].

The characteristics of the voltage dependent power components of the charger for different R_L and R_s values are shown in Fig. 8.6. It is evident that the larger the R_L and R_S, the greater the influence of the negative α power component [22].

Table 8.1 Parameters of the PEV load model for different resistance values

Resistances	a	α	b	Load model
$R_L = 0.1$ mΩ, $R_S = 0$ mΩ	0.0036	−2.765	0.9964	LM1
$R_L = 1$ mΩ, $R_S = 0$ mΩ	0.0116	−1.777	0.9884	LM2
$R_L = 0$ mΩ, $R_S = 0.2$ mΩ	0.0144	−1.306	0.9856	LM3
$R_L = 0$ mΩ, $R_S = 2$ mΩ	0.0246	−1.842	0.9754	LM4
$R_L = 0.1$ mΩ, $R_S = 0.2$ mΩ	0.0174	−1.172	0.9826	LM5
$R_L = 1$ mΩ, $R_S = 2$ mΩ	0.0244	−2.179	0.9756	LM6

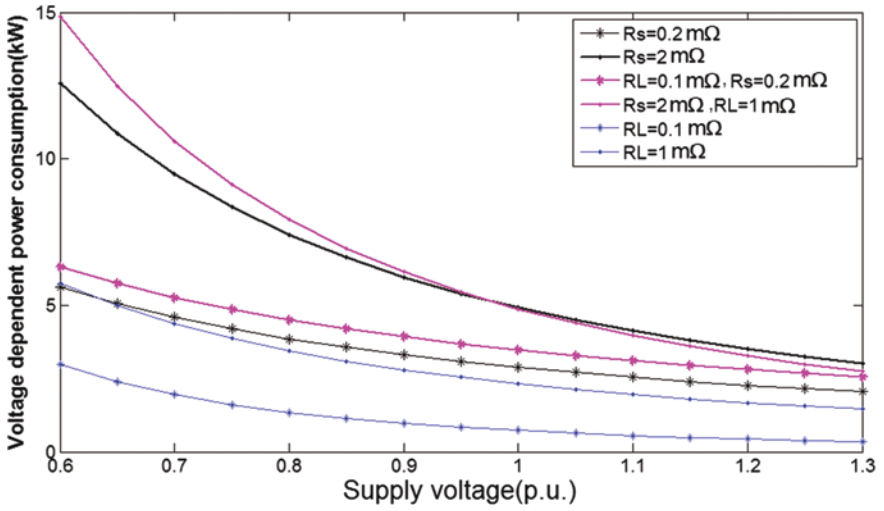

Fig. 8.6 Characteristics of the voltage dependent power component of the charger [22]

It is evident that the voltage dependent power component has increased under decreased system voltages. The constant power load consumes increasing amount of current when the load bus voltages is decreasing. Increasing input current results higher losses at the charger input resistances. Not only the R_L and R_S resistances, but also the resistance of the lead conductor will influence the power consumption of the PEV load at the point of common coupling, as identified numerically in the proceeding analysis.

Simulations are carried out to determine the combined effect of lead conductor resistance, R_L and R_S. The study considered the effect of different lead conductor resistance values (10, 20, and 30 mΩ) while keeping R_L and R_S fixed at 0.1 mΩ and 0.2 mΩ, respectively. The obtained power-voltage characteristic of the simulated charger is presented in Fig. 8.7. The derived a, α, and b parameters of Eq. (8.29) are given in Table 8.2 [22].

It is evident that an increase in lead resistance causes an increase in the voltage dependent negative exponential power component.

The derived static load models can be utilized in static voltage stability and power flow studies. However, the conventional power flow equations should be modified in order to accommodate the voltage dependent load characteristics, as described in the proceeding section.

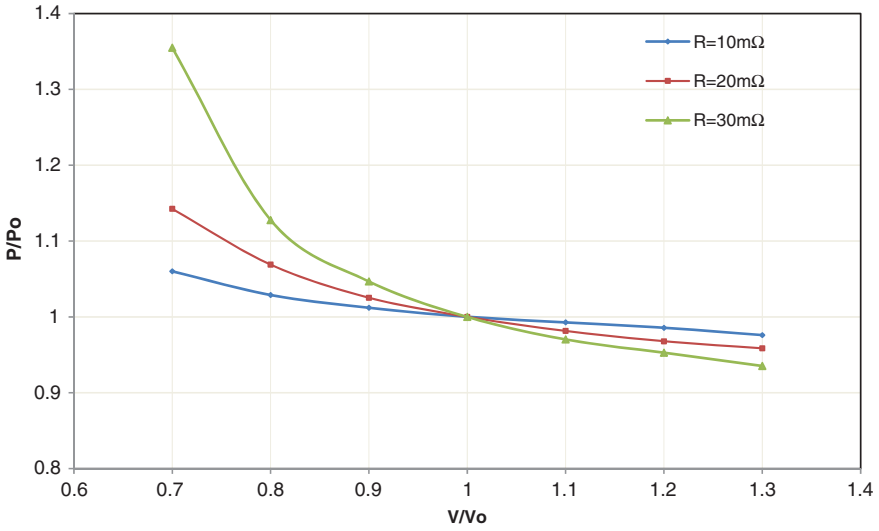

Fig. 8.7 The power voltage relationship of the PEV load at the point of common coupling [22]

Table 8.2 Parameters of the PEV load model at the point of common coupling [22]

Lead conductor resistance (Ω)	a	b	α	Load model
0.01	0.0463	0.9537	−2.324	Exp. 1
0.02	0.0721	0.9279	−3.101	Exp. 2
0.03	0.0730	0.9270	−5.228	Exp. 3

8.2.4 Newton Raphson Power Flow with PEV Load

It is identified that the PEV is having voltage dependent load characteristics. Hence, accommodating it in Newton-Raphson power flow algorithm requires certain modifications to the algorithm. The required modifications to the real and reactive power flow equations of the algorithm are shown in Eqs. (8.30) and (8.31). [23].

$$P_{Gi} - P_{Di}(v) = v_i \sum_{k=1}^{N_{B-1}} v_j \left[G_{ij} \cos \delta_{ij} + B_{ij} \sin \delta_{ij} \right] \tag{8.30}$$

$$Q_{Gi} - Q_{Di}(v) = v_i \sum_{k=1}^{N_{PQ}} v_j \left[G_{ij} \sin \delta_{ij} - B_{ij} \cos \delta_{ij} \right] \tag{8.31}$$

The bus voltage angle between buses i and j is denoted by δ_{ij}. The total number of buses and number of load buses are represented as N_B and N_{PQ}, respectively. The injected real and reactive power at bus i, are represented by, P_{Gi} and Q_{Gi}, respectively. The real and reactive power consumption of the loads at bus i are given by P_{Di} and Q_{Di}, respectively. The conductance and susceptance of feeder ij are described by G_{ij} and B_{ij}, respectively. Further, the diagonal elements of the J_2 and J_4 of standard power flow Jacobian should also be modified. The modifications required are shown by Eqs. (8.32) and (8.33). The power factor angle of the charger is represented by ϕ.

$$\frac{\partial P_i}{\partial v_i} = 2G_{ii}v_i - a\alpha P_o \left(\frac{v_i}{v_o} \right)^{-\alpha-1} + \sum\nolimits_{j \neq i} v_j (G_{ij} \cos \delta_{ij} + B_{ij} \sin \delta_{ij}) \tag{8.32}$$

$$\frac{\partial Q_i}{\partial v_i} = -2G_{ii}v_i - a\alpha P_o \left(\frac{v_i}{v_o} \right)^{-\alpha-1} * \tan(\cos^{-1} \phi) + \sum\nolimits_{j \neq i} v_j (G_{ij} \sin \delta_{ij} - B_{ij} \cos \delta_{ij}) \tag{8.33}$$

The proceeding section evaluates the impact of PEV on power system static voltage stability.

8.3 Impact of PEV Charging Load on System Static Voltage Stability

8.3.1 Background

A rapid and significant PEV load integration to the power grid is anticipated in the near future. Hence, power system engineers should be aware of potential impacts of PEV integrations to their networks. The present day power systems operate closer to

their stability limits due to various economic and environmental concerns. As a result an increasing number of instability incidents have been recorded worldwide [24–26]. The system load characteristics are found to be among the main factors that cause voltage instability. Several system voltage instability incidents which were contributed by load characteristics are documented in [27, 28]. PEV charging will result substantial load integration in near future. Hence, voltage stability will be a vital concern when considering the PEV load characteristics, which consists of a negative exponential and a constant power load behavior. During an event, which results a decrease in supply voltage, a negative exponential load increases its power consumption, while a constant power load increases its current consumption. Hence, it is evident that both load characteristics contribute to degrade system voltage stability during a voltage instability incident, which is characterised by decreasing system voltages. Therefore, evaluation of PEV charging impact on power system voltage stability is important under these circumstances and considered in the following section.

8.3.2 Voltage Stability Theory

The voltage stability of a power system is preserved if acceptable voltages are maintained in all network buses during normal operating conditions and after being subjected to a disturbance [29]. During a voltage instability event, the system voltages decline progressively and uncontrollably. This happens to a significant degree when system generation and transmission are unable to meet the system reactive power demand. Heavily loaded lines, system contingencies, increased reactive power consumption of the loads, limitations in reactive power generations and actions of voltage control devices are some of the main factors which affect voltage instabilities. A voltage collapse is characterised by unacceptably low voltages in a significant portion of a power system. Control actions for voltage instability include load shedding, secondary voltage regulations, temporary reactive power overloading of generators, switching of shunt capacitors, blocking tap changing transformers, re-dispatching of generators and rescheduling of generator and pilot bus voltages. Identification of effective remedies for voltage instabilities requires efficient system studies.

8.3.3 Static Voltage Stability Analysis

Performance indexes are important to determine proximity to voltage collapse. A widely accepted voltage stability assessment index, the static loading margin has been incorporated in this research to evaluate the impact of PEV load on voltage stability. A description of the index is given in this section.

A quasi-steady state description of a power system which applicable to voltage stability analysis can be described by a set of differential and algebraic equations as given in Eq. (8.34), which can also be represented by Eq. (8.35), alternatively.

$$\begin{aligned} \dot{x} &= f(x, y, \lambda) \\ 0 &= g(x, y, \lambda) \end{aligned} \tag{8.34}$$

$$\begin{bmatrix} \dot{x} \\ 0 \end{bmatrix} = F(x, y, \lambda) \tag{8.35}$$

The state variables are represented by x, while y represents the algebraic variables. The λ represents a parameter or set of parameters which slowly change with time. As the λ changes, system moves from one equilibrium point to another until it reaches the collapse point. An equilibrium point (x_0, y_0, λ_0) is characterized by,

$$F(x_0, y_0, \lambda_0) = 0 \tag{8.36}$$

Based on the non-singularity assumption of algebraic equations, an equilibrium point where the power flow Jacobian of Eq. (8.34) is singular, is known as a singular bifurcation point (x^*, y^*, λ^*). If the system load is taken as the parameter which varies slowly, loading margin or the static voltage stability margin (SVM) can be evaluated by Eq. (8.37). The loading parameter at current operating point is denoted by λ_0.

$$SVM = \lambda^* - \lambda_0 \tag{8.37}$$

The loading margin is the additional load increment (increased in a specific pattern) that required to drive the system towards instability from the current operating point. The pattern how the system loads are increased and how the system generators are arranged to respond to that load increments are defined by the load and the generation directions, respectively. Loading margin identifies closeness of the current operating point to the voltage collapse point. It is an accurate index that considers the system nonlinearities and limits like the generator reactive power limits and the line MVA flow limits, which are encountered during system load increments.

A static voltage stability study is carried out in this research using PSAT (Power System Analysis Toolbox). The continuation of power flow (CPF) method is incorporated to develop PV curve to determine the static loading margin. It incorporates an iterative method consists of a predictor and a corrector to generate the PV curve. The nose of the curve represents the voltage collapse point. Several other existing voltage stability indexes are reviewed in Sect. 8.4.2.1 of this chapter.

Impact of PEV load on power system voltage stability is evaluated in the next section by carrying out numerical simulations, using PSAT.

8.3.4 Impact of PEV Load on Static Voltage Stability

A numerical evaluation of the impact of PEV load on power system voltage stability is carried under different scenarios. The PEV load integrations to IEEE 14-bus test system shown in Fig. 8.8, are considered. The test system line and bus data

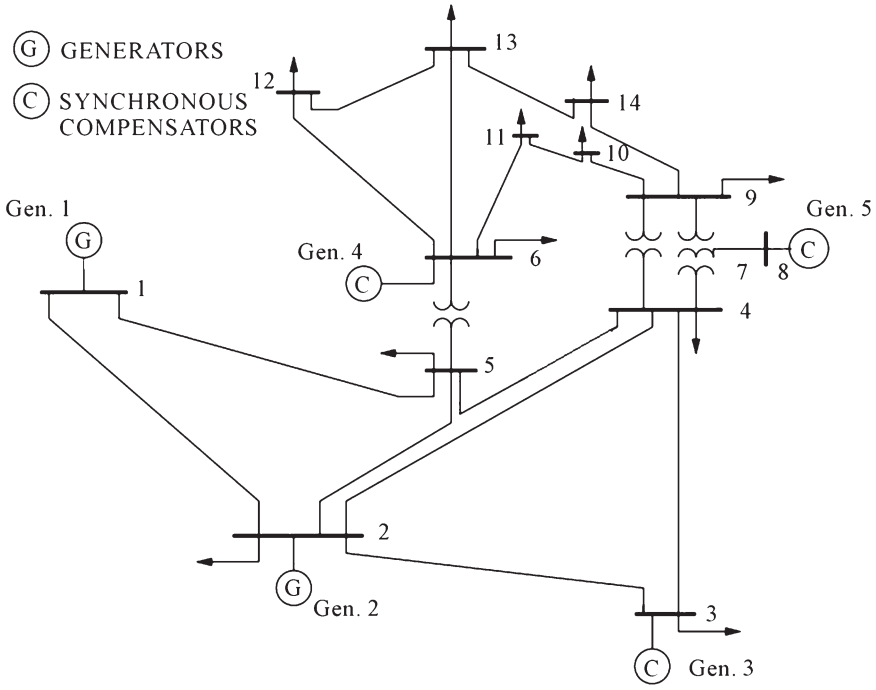

Fig. 8.8 The IEEE 14 bus test system [31]

obtained from [30], are given in Tables 8.3 and 8.4, respectively. The CPF tool in PSAT is incorporated to determine the loading margin. The generator reactive power limits are considered during the simulation.

The test system represents a typical medium and low voltage primary distribution system. There are 20 segments or branches and 14 buses with a load totalling of 259 MW and 81.4 Mvar, respectively. There are five synchronous machines, including three synchronous compensators connected to the system. There are two main system voltage levels: 69 and 13.8 kV.

The first simulation study is carried out to identify the influence of different resistance values of the active rectifier switches (Rs) and the parasitic resistance of the input filter (R_L) on system static voltage stability. The PEV load is represented by the load models LM1-LM6 shown in Table 8.1, of Sect. 8.2.3. A 5 % PEV load network integration is considered at bus 14. It is assumed that the charging load is having a power factor of 0.95, lagging. The Fig. 8.9 shows the loading margin obtained for different load models during the simulation.

A lower loading margin indicates a higher impact on system voltage stability. It is evident from the results that the impact on the system voltage stability is more when the resistances of R_L and R_S are higher.

Subsequent simulations are carried out by incorporating effect of lead conductor resistances. The PEV load is represented by the load models Exp1-Exp3

Table 8.3 IEEE 14 bus test system line data [30]

From bus	To bus	Per unit data			Tap ratio
		Resistance	Reactance	Susceptance	
2	5	0.05695	0.17388	0.034	–
6	12	0.12291	0.25581	0	–
12	13	0.22092	0.19988	0	–
6	13	0.06615	0.13027	0	–
6	11	0.09498	0.1989	0	–
11	10	0.08205	0.19207	0	–
9	10	0.03181	0.0845	0	–
9	14	0.12711	0.27038	0	–
14	13	0.17093	0.34802	0	–
7	9	0	0.11001	0	–
1	2	0.01938	0.05917	0.0528	–
3	2	0.04699	0.19797	0.0438	–
3	4	0.06701	0.17103	0.0346	–
1	5	0.05403	0.22304	0.0492	–
5	4	0.01335	0.04211	0.0128	–
2	4	0.05811	0.17632	0.0374	–
5	6	0	0.25202	0	0.932
4	9	0	0.55618	0	0.969
4	7	0	0.20912	0	0.978
8	7	0	0.17615	0	1.3043

Table 8.4 IEEE 14 bus test system bus data in 100 MVA base [30]

Bus number	Bus voltage/(kV)	Bus voltage/(p.u.)	Load real/(p.u.)	Load reactive power/(p.u.)	Generator reactive power/(p.u.)	Generator reactive power/(p.u.)	
						Max	Min
1	69	1.06	–	–	–	9.9	−9.9
2	69	1.045	0.217	0.127	0.4	0.5	−0.4
3	69	1.01	0.942	0.19	–	0.4	0
4	69	–	0.478	0.04	–	–	–
5	69	–	0.076	0.016	–	–	–
6	13.8	1.07	0.112	0.075	–	0.24	−0.06
8	18	–	–	0	–	0.24	−0.06
9	13.8	–	0.295	0.166	–	–	–
10	13.8	–	0.09	0.058	–	–	–
11	13.8	–	0.035	0.018	–	–	–
12	13.8	–	0.061	0.016	–	–	–
13	13.8	–	0.135	0.058	–	–	–
14	13.8	–	0.149	0.05	–	–	–

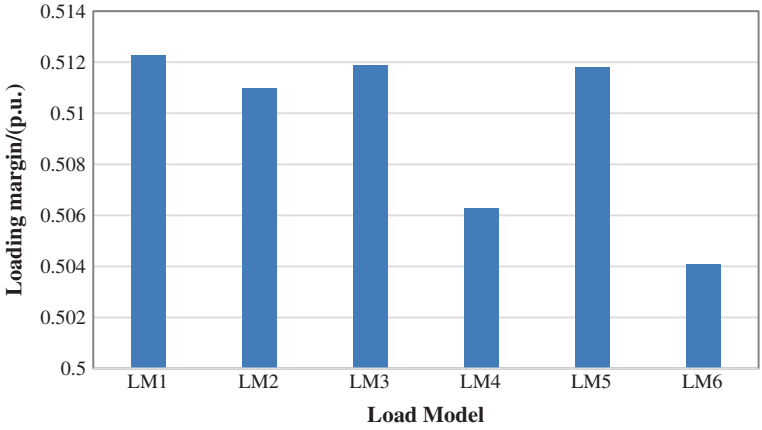

Fig. 8.9 The effect of charger parameters on voltage stability

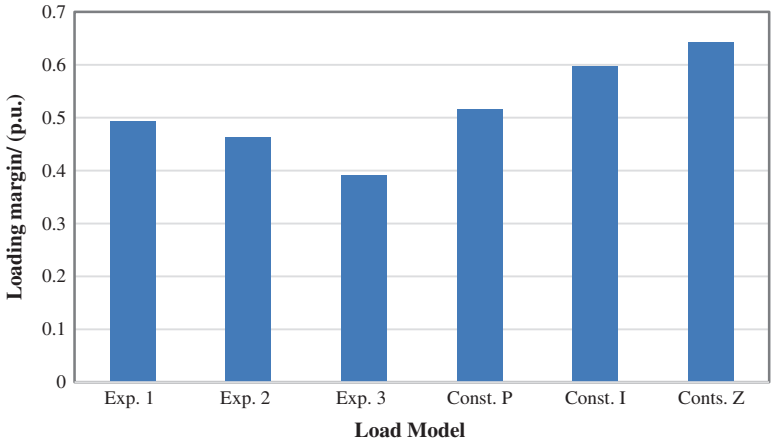

Fig. 8.10 The loading margin with different load representations

shown in Table 8.2 of Sect. 8.2.3. The results are compared with the conventional constant power, constant current and constant impedance load representations. The loading margins for different load models are evaluated with the PEV load connected at bus 14. Load is having similar magnitude and power factor as in the previous scenario. The obtained loading margins are shown in Fig. 8.10.

It is evident from the results that PEV load is having higher impact on system static voltage stability compared to conventional constant power, constant current and constant impedance loads. These results clearly explains the importance of representing the PEV load with realistic load models rather than representing with

conventional constant power, constant current and constant impedance load characteristics. Further, results confirm that higher the resistance of the lead conductor the higher the negative impact on voltage stability.

The effect of power factor (P.F.) of the PEV load on voltage stability is evaluated as indicated in Fig. 8.11, by setting the load power factor to 0.95 and 0.98 lagging, with the PEV load connected at bus 14.

It is identified that the lower the power factor the lower the voltage stability margin as indicated in Fig. 8.11. It is evident that the influence of the power factor on loading margin is noticeable on the Exp. 1, 2, 3 and constant power load modelling, compared to constant current and constant impedance load modelling.

A contingency is created in the next simulation scenario to understand the influence of EV charging on static voltage stability under a contingency condition. A contingency is created by disconnecting the line 2–4. The impact on static voltage stability is evaluated with and without the PEV load connected at buses 14. The PEV load is represented by the load model Exp. 2. The obtained loading margin during the simulations are shown is Fig. 8.12.

The loading margin of the system with no integrated charging stations is represented as the base case. It is apparent that the steady state loading margin has reduced significantly following a system contingency with the integration of PEV charging load. Further, it is interesting to note that the loading margin of the normal system (with no contingency) with PEV load integration is lower than the loading margin after the contingency for the base case.

Impacts of the PEV charging at three different network loading condition are considered in the next simulation. Three different network loading conditions (low, medium and high) are obtained by multiplying the existing network load by factors of 0.9, 1 and 1.1. Three different PEV penetration conditions (low, medium and high)

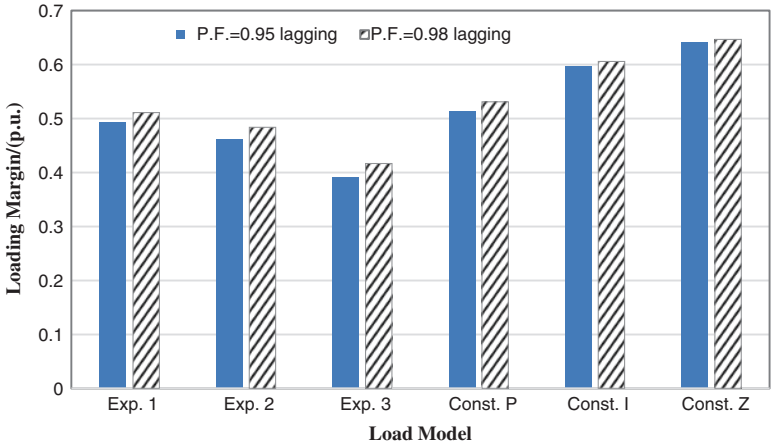

Fig. 8.11 The influence of P.F. on loading margin for different load models

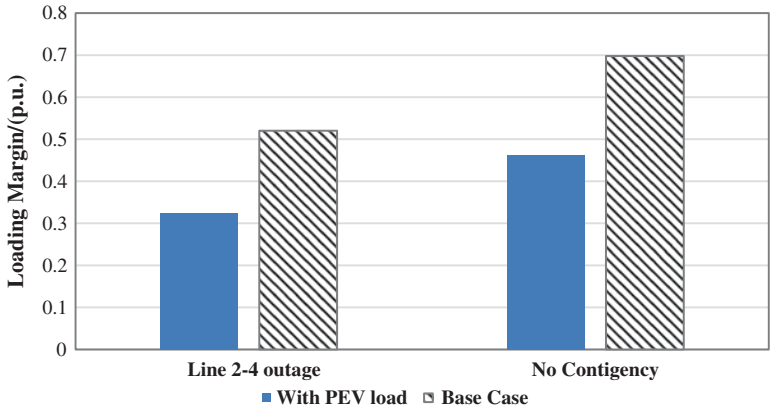

Fig. 8.12 The effect of contingency on voltage stability for different load representations

Table 8.5 A description of the three cases considered in the simulation

Case	Network loading	PEV penetration
Low	Low	Low
Medium	Medium	Medium
High	High	High

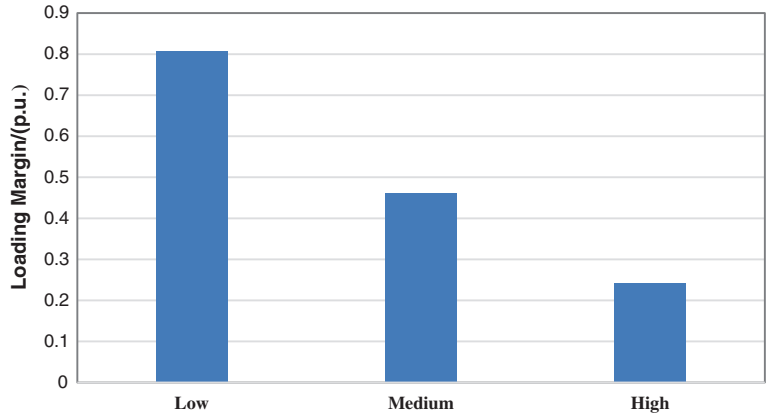

Fig. 8.13 Loading margin for the three simulation cases

are considered with 3, 5 and 8 % PEV load network integrations at bus 14. The PEV load is represented by Exp. 2 load model. It is assumed that the charging load is having a power factor of 0.95, lagging. The loading margins calculated for the three cases described in the Table 8.5, are shown in Fig. 8.13.

It is evident that high PEV penetrations at high network loading situations can significantly reduce the network loading margin.

The simulation results reveals that the PEV charging load can cause significant negative impact on the system static voltage stability. The next section introduces feasible solutions to mitigate the impact of PEV charging load on static voltage stability.

8.4 Mitigating the Impact of PEV Charging on Voltage Stability

8.4.1 Mitigating PEV Charging Impacts Through Voltage Control

The PEV charging load modelling carried out in the Sect. 8.2.2 identified that PEV is a voltage dependent load. Further, the simulation studies carried out in Sect. 8.3.4 reported that PEV charging causes considerable impact on system voltage stability. Hence, it is worth considering voltage controlling means to mitigate PEV charging impact on system voltage stability. This section experiment whether the load bus voltage controlling, by means of a tap changing transformer can alleviate the impacts of PEV charging on voltage stability.

A simulation study has been carried out in IEEE 14 bus test system, shown in Fig. 8.8. A 1 MW PEV charging load (load demand equivalent to five 200 kW PEV fast charging load) is integrated to Bus 14 via a transformer (13.8 kV/415 kV, 10 % reactance) having tap changing facility. The PEV load is represented by the proposed Exp. 2 load model derived in the Sect. 8.2.3 (with $\alpha = -3$–1, $a = 0.07$, $b = 0.93$). The network loads are reduced to 80 % of the original value to have a proper convergence for the range of transformer tap settings considered.

A CPF study has been carried out in PSAT. The evaluated loading margin, real and reactive power losses and the load bus voltages are shown in Table 8.6. The Fig. 8.14 indicates the variation of loading margin with different tap settings.

It is evident from the results that controlling load bus voltage to maintain at a higher value helps to improve system voltage stability. Further, it is interesting to see that it has resulted in lower real and reactive power losses too. Similarly, other appropriate voltage control mechanisms may also mitigate the negative impact of PEV load on system static voltage stability. Further, proper planning of charging infrastructure can also be considered to alleviate PEV charging impacts as described in the proceeding section.

Table 8.6 Simulation results

Transformer tap ratio (a = Vp/Vs)	Loading margin (p.u.)	Load bus voltage (p.u.)	Total real power losses (MW)	Total reactive power losses (Mvar)
0.96	1.1232	1.0729	8.279	6.35
0.98	1.1227	1.051	8.279	6.352
1	1.1222	1.03	8.28	6.354
1.02	1.1217	1.0098	8.28	6.356
1.04	1.1211	0.99033	8.281	6.358

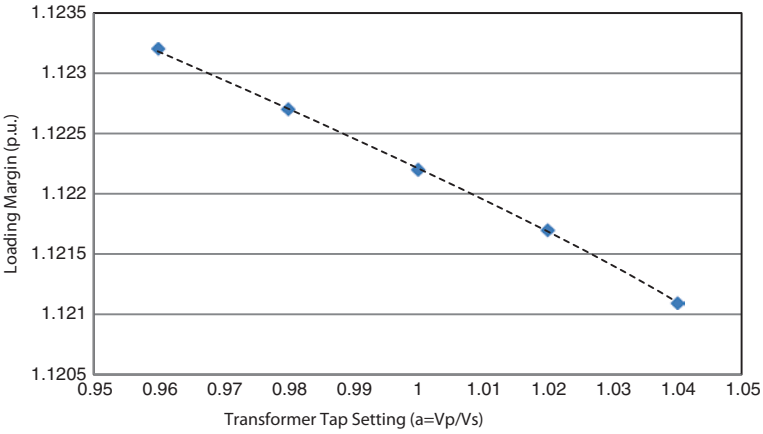

Fig. 8.14 The variation of loading margin with different tap settings

8.4.2 Mitigating PEV Charging Impacts Through Proper Planning

Proper charging infrastructure planning is a proactive measure to mitigate PEV charging caused grid impacts. The main idea behind the planning exercise is to locate and size charging infrastructure in such a way to minimize potential grid impacts while considering other concerns and limitations. PEV charging mostly takes place either during overnight at homes or day time at public charging stations. Proper planning of public PEV charging infrastructure will minimize the negative impact of PEV charging on system voltage stability. Charging day time at properly planned public charging stations will be less troublesome compared to charging at night time at homes, in voltage stability point of view, due to the following reasons.

1. During the evening peaks the network voltages are low at end distribution feeders. This will cause higher power demand and higher load current due to PEV load characteristics described by Eq. (8.29).
2. During evening peaks significantly higher system real and reactive power losses, line loadings and system reactive power demand are apparent. Hence charging at that time is unfavourable in voltage stability point of view.
3. It is much easier to implement voltage control means for a bulk charging station than for small individual charging units.
4. Proper PEV charging station placement and sizing can be done at the planning stage to minimize the negative impact of PEV load on voltage stability, proactively.

Identifying locations of charging stations and their optimum capacities, which cause least negative impact on the power grid while not violating grid constraints, is one of the most proactive ways of mitigating PEV charging caused grid impacts.

However, taking such planning decisions are not always straight forward, as planning problems are having many other objectives and constraints too. Minimization of investment cost, maximization of user convenience and investor profit are some of the planning objectives. Further, demand distributions of PEV charging load, range of PEVs, infrastructure availabilities and the distribution of existing charging station are also considered during charging station planning. In power grid point of view planning algorithms may incorporate objectives like minimising power losses and negative impact on voltage stability, while satisfying the grid constrains like regulatory limits of bus voltages, line power flow limits etc. In voltage stability point of view, it is beneficial to have an index to incorporate within a planning algorithm to identify a voltage stability preserved charging solution. The proceeding section reviews the currently available voltage stability indexes and suggests a computationally efficient index which is having good physical interpretation.

8.4.2.1 An Index for Voltage Stability Considered Planning

It has been identified that PEV charging can deteriorate the system voltage stability. Therefore, it is important to consider voltage stability within the PEV charging infrastructure planning process. This section introduces a computationally efficient index which is having good physical interpretation to compare voltage stability status of the power system between different planning options.

A review of suitability of incorporating currently available voltage stability evaluating indexes in planning algorithm is given in [23]. The popular P–V curve based loading margin is dependent on the load and generator directions [32]. It is required to assign appropriate load and generator directions to get realistic outcomes. The Q–V based indexes are lacking direct physical interpretations. The index "L" [33] is only suitable when work with constant power loads [34]. The Eigenvalues of the Jacobian matrix cannot be utilized to determine relative voltage stability. Further, indexes like voltage stability index [35], the minimum singular value of power flow Jacobian matrix and the reduced Jacobian and the line collapsed proximity index [36] exhibit sudden variations when undergoes various system limits like generator reactive power limits [37, 38], hence may not be suitable to incorporate within planning algorithms. Further, it has been identified that index L_{mn} [39] and FVSI [40] have reported pessimistic results while the line stability factor has produced conservative results in system study [36]. Therefore, the importance of an accurate and efficient index which is having good physical interpretation is highlighted, to be incorporated within planning algorithm.

Reactive power reserve (RPR) of a power system plays a major role in determining the system voltage stability [41–46]. Hence, identifying relative impacts on the system RPR is an efficient way to determine relative impact on system static voltage stability during different planning options. The above concept is incorporated in the index *QRPI* [23], defined in Eq. (8.38).

$$QRPI = \sum_{i=1}^{N_{Qr}} \left\{ W_i \frac{(Q_{R,i,base} - Q_{R,i})}{Q_{R,i,base}} \right\} \quad \forall W_i \in (0,1), \quad \sum_{i=1}^{l} W_i = 1 \tag{8.38}$$

The PRR of a source is the difference between the maximum deliverable reactive power (Q_{max}) and the reactive power supply at a certain case. The RPR of a reactive power resource *i* in the base case is given by $Q_{R,i,base}$, while the reactive power reserve of the resource at a particular planning case is given by $Q_{R,i}$. All the reactive power resources (N_{Qr}) in the particular region of the network within which they tightly coupled to provide reactive power support to the set of load buses, are considered for evaluation of *QPRI*. W_i is the weight that is assigned to resource *i* to indicate its relative importance in maintaining system voltage stability. A higher weight is assigned to the resource which is mostly contributed to maintain system voltage stability. Normalization is incorporated within the index to give more emphasis to the generators which have smaller RPR (or which are about to reach the Q_{max} limit) at the base case. Thus, placing the PEV charging station at a location having a lower *QRPI*, minimizes the risk of voltage instabilities. Validation of *QRPI* is shown in the next section.

Validation of QRPI

The validation of the proposed QRPI index is carried out in this section on the IEEE 14 bus test system, shown in Fig. 8.8, with the existing network loads are reduced by 20 %. The loading margin, reactive power reserve, the weighted reactive power reserve and the QRPI are evaluated with a 2 MW charging station connected at different network busses. The PEV load is represented by the proposed Exp. 2 load model derived in the Sect. 8.2.3 (with $\alpha = -3$–1, $a = 0.07$, $b = 0.93$).

Each reactive power resource is weighed based on the sequence they reach their reactive power limit in the base case CPF study, with no PEV connected. Higher weights are assigned to the sources which reach the reactive power limit first during the CPF study, as shown in Table 8.7. The simulation results are shown in Table 8.8. The relationship between the loading margin and the *QRPI* is illustrated in Fig. 8.15.

The charging load connected at bus 6 reports the highest loading margin, while the connected PEV loads at bus 14 indicates lowest loading margin. Hence, the bus 6 is found to be the best location for locating charging load. The relationship between the loading margin and the *QRPI* is illustrated in Fig. 8.15.

Table 8.7 The weights assigned to each reactive power source

Source connected bus	Assigned weights
1	0.1
2	0.15
3	0.2
6	0.25
8	0.3

Table 8.8 Simulation results

Charging station location (bus no.)	Loading margin (p.u.)	Reactive power reserve (Mvar)	Weighted reactive power reserve (Mvar)	*QRPI* %	Bus ranking (best to worse)
6	2.12	10.55632	1.112974	0.3005	1
9	2.1134	10.55529	1.112829	0.3135	2
10	2.1105	10.55511	1.112769	0.3189	3
14	2.0942	10.55422	1.112532	0.3401	4

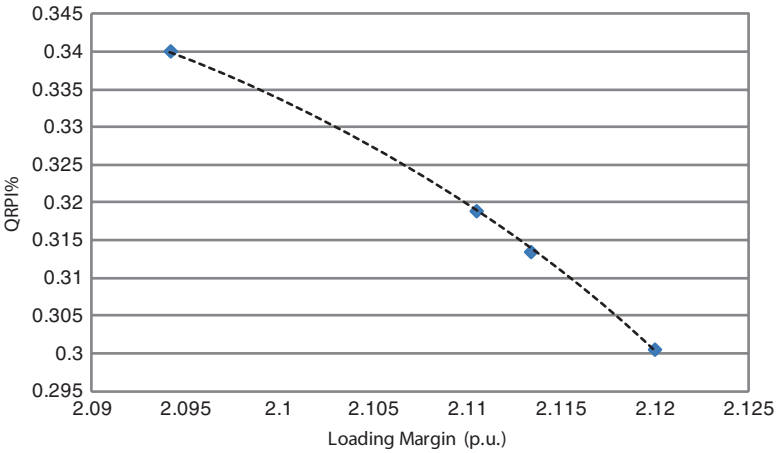

Fig. 8.15 The relationship between QRPI and loading margin

It is clear from the simulation results that there is a direct relationship between *QRPI* and loading margin. The bus ranking based on the *QRPI* is similar to the bus ranking based on loading margin. Hence, *QRPI* index which can be calculated using the load flow results can be incorporated to determine relative voltage stability between different planning solutions with less computational efforts. Hence, incorporating *QRPI* in a solution algorithm will provide an efficient way to identify a voltage stability preserved planning solution.

8.5 Conclusions

Voltage dependent characteristics of system loads are among the main factors that determine voltage stability of a power system. Most power electronic loads display constant power load characteristics when consider the power

consumption at the dc bus. The constant power loads increase their current consumption at lower supply voltages. Hence, a controlled ac-dc converter will consume increasing amount of current as the supply voltage drops, as long as the converter currents are within the designed range. In reality all ac-dc converters come with resistive loss components. The resistances present in an ac-dc converter include non-ideal component resistances of converter switches and the parasitic resistances of the input filter inductors. When there is a drop in supply voltage the current input to the ac-dc converter increases, and this cause the resistive losses to increase. If we consider the power consumption at the point of common coupling, the lead conductor losses also comes into picture. These loss components exhibits negative exponential load behaviour. Therefore, a power electronically controlled PEV charging load characteristics can be better represented by a combination of a constant power load and a negative exponential load. The constant power component is higher compared to negative exponential power component. As the load bus voltage drops, the percentage of negative exponential load component increases. The load model parameters are further dependent on battery SOC, dc bus voltage reference and charging current reference. The load model parameters vary during the charging cycle.

The loading margin of the system with the PEV load is found to be the lowest when compared with the loading margins of the system with constant power, constant current and constant impedance load models. It is important to note that the negative exponential load component of the PEV brings a considerable negative influence to the power system voltage stability even though its contribution to the total charging load is less than 10 %. Hence, it is worth to mention that representing the PEV load with conventional constant power, constant impedance or constant current load models will result in conservative outcomes in system studies. The capacity of the charging load and its power factor is found be affecting the system voltage stability. Further, if the PEV chargers are coming with universal input capability, it is possible that they remain connected to the power grid for a range of system voltages. Hence, in case of voltage collapse event characterised by declining system voltages, if the PEV load remains connected and continues to consume increasing amount of power that will evidently result in negative impact on power system voltage stability.

The load bus voltage control methods found to be helping to mitigate the voltage stability impact of PEV charging load. Further, proper PEV charging station placement and sizing which preserves system reactive power reserve will also help to proactively mitigate the impacts on steady state voltage stability. This can be achieved during charging infrastructure development. An index which is having good physical interpretations and involves less computational efforts has been introduced, to identify voltage stability prudent charging solutions. The index is based on the system reactive power reserve.

References

1. Hajagos LM, Danai B (1998) Laboratory measurements and models of modern loads and their effect on voltage stability studies. IEEE Power Syst J 13:584–592
2. Dharmakeerthi CH, Mithulananthan N (2013) A study of load and line characteristics on power system damping performance. In: Proceedings of the 8th IEEE international conference on industrial and information systems (ICIIS). University of Peradeniya, Sri Lanka, pp 6–11
3. SAE (2011) SAE charging configurations and ratings terminology, SAE hybrid committee http://www.sae.org/smartgrid/chargingspeeds.pdf. Accessed 10 Sept 2013
4. SAE (2012) SAE Charging Configurations and Ratings Terminology. http://insideevs.com/wp-content/uploads/2012/10/SAE-Combo.jpg. Accessed 30 Sept 2013
5. Miskiewicz RM, Moradewicz AJ, Kazmierkowski MP (2011) Contactless battery charger with bi-directional energy transfer for plug-in vehicles with vehicle-to-grid capability. In: Proceedings of the IEEE international symposium on industrial electronics (ISIE), pp 1969–1973
6. Bilgin B, Emadi A, Krishnamurthy M (2010) Design considerations for a universal input battery charger circuit for PHEV applications. In: Proceedings of the IEEE international symposium on industrial electronics (ISIE), pp 3407–3412
7. Gautam D, Musavi F, Edington M et al (2011) An automotive on-board 3.3 kW battery charger for PHEV application. In: Proceedings of the IEEE vehicle power and propulsion conference (VPPC), pp 1–6
8. Dusmez S, Cook A, Khaligh A (2011) Comprehensive analysis of high quality power converters for level 3 off-board chargers. In: Proceedings of the IEEE vehicle power and propulsion conference (VPPC), pp 1–10
9. Kuperman A, Levy U, Goren J et al (2010) Modeling and control of a 50 KW electric vehicle fast charger. In: Proceedings of the IEEE 26th convention of electrical and electronics engineers in Israel (IEEEI), pp 000188–000192
10. Jaganathan S, Wenzhong G (2009) Battery charging power electronics converter and control for plug-in hybrid electric vehicle. In: Proceedings of the IEEE vehicle power and propulsion conference (VPPC '09), pp 440–447
11. Young-Joo L, Khaligh A, Emadi A (2009) Advanced integrated bidirectional AC/DC and DC/DC converter for plug-in hybrid electric vehicles. IEEE Veh Technol J 58:3970–3980
12. Yan XP, Patterson DJ (1999) A high efficiency on-board battery charger with unity input power factor. Paper presented at the Australasian Universities Power Engineering Conference Darwin, 1999
13. Egan MG, O'Sullivan DL, Hayes JG et al (2007) Power-factor-corrected single-stage inductive charger for electric vehicle batteries. IEEE Ind Electron J 54:1217–1226
14. Bilgin B, Dal Santo E, Krishnamurthy M (2011) Universal input battery charger circuit for PHEV applications with simplified controller. In: Proceedings of the 26th annual IEEE applied power electronics conference and exposition (APEC), pp 815–820
15. Keun-Young K, Sang-Hoon P, Seung-Kyung L et al (2010) Battery charging system for PHEV and EV using single phase AC/DC PWM buck converter. In: Proceedings of the IEEE vehicle power and propulsion conference (VPPC), pp 1–6
16. Jingyu Y, Guoqing X, Huihuan Q et al (2010) Battery fast charging strategy based on model predictive control. In: Proceedings of the IEEE 72nd vehicular technology conference fall (VTC 2010-Fall), pp 1–8
17. Taesic K, Wei Q (2011) A hybrid battery model capable of capturing dynamic circuit characteristics and nonlinear capacity effects. IEEE Energy Convers J 26:1172–1180
18. Min C, Rincon-Mora GA (2006) Accurate electrical battery model capable of predicting runtime and I-V performance. IEEE Energy Convers J 21:504–511
19. Hongwen H, Rui X, Xiaowei Z et al (2011) State-of-charge estimation of the lithium-ion battery using an adaptive extended Kalman filter based on an improved thevenin model. IEEE Veh Technol J 60:1461–1469

20. Hanlei Z, Mo-Yuen C (2010) Comprehensive dynamic battery modeling for PHEV applications. In: Proceedings of the IEEE power and energy society general meeting, pp 1–6
21. Dharmakeerthi CH, Mithulananthan N, Saha TK (2012) Modeling and planning of EV fast charging station in power grid. In: Proceedings of the IEEE power and energy society general meeting, pp 1–8
22. Dharmakeerthi CH, Mithulananthan N, Saha TK (2014) Impact of electric vehicle fast charging on power system voltage stability. Electr Power Energy Syst J 57:241–249
23. Dharmakeerthi CH, Mithulananthan N, Saha TK (2014) A comprehensive planning framework for electric vehicle charging infrastructure deployment in the power grid with enhanced voltage stability. Electr Energy Syst J. doi:10.1002/etep.1886
24. Chendur Kumaran R, Venkatesh TG, Swarup KS (2011) Voltage stability—case study of saddle node bifurcation with stochastic load dynamics. Electr Power Energy Syst J 33:1384–1388
25. Tiwari R, Niazi KR, Gupta V (2012) Line collapse proximity index for prediction of voltage collapse in power systems. Electr Power Energy Syst J 41:105–111
26. Khani D, Sadeghi Yazdankhah A, Madadi Kojabadi H (2012) Impacts of distributed generations on power system transient and voltage stability. Electr Power Energy Syst J 43:488–500
27. Kurita A, Sakurai T (1988) The power system failure on July 23, 1987 in Tokyo. In: Proceedings of the 27th IEEE conference on decision and control, vol 3, pp 2093–2097
28. John A. Diaz de Leon II, Carson WT (2002) Understanding and solving short-term voltage stability problems. In: Proceedings of the IEEE power engineering society summer meeting, vol 2, pp 745–752
29. Kundur P (1994) Power system stability and control: McGraw-Hill
30. Milano F (2005) Power system analysis toolbox documentation for PSAT version 1.3.4., July 14, 2005
31. Heba A Hassan ZHO, El-Aziz Lasheen Abd (2014) Sizing of STATCOM to enhance voltage stability of power systems for normal and contingency cases. Smart Grid Renew Energy J 5:8–18
32. Sode-Yome A, Mithulananthan N, Lee KY (2005) Effect of realistic load direction in static voltage stability study. In: Proceedings of the IEEE/PES Asia and Pacific transmission and distribution conference and exhibition, pp 1–6
33. Kessel P, Glavitsch H (1986) Estimating the voltage stability of a power system. IEEE Power Deliv J 1:346–354
34. Hongjie J, Xiaodan Y, Yixin Y (2005) An improved voltage stability index and its application. Electrical Power Energy Syst J 27:567–574
35. Haque MH (2007) Use of local information to determine the distance to voltage collapse. In: Proceedings of international power engineering conference (IPEC 2007), pp 407–412
36. Tiwari R, Niazi KR, Gupta V (2012) Line collapse proximity index for prediction of voltage collapse in power systems. Electr Power Energy Syst J 41:105–111
37. Lof PA, Andersson G, Hill DJ (1993) Voltage stability indices for stressed power systems. IEEE Power Syst J 8:326–335
38. Canizares CA, De Souza ACZ, Quintana VH (1996) Comparison of performance indices for detection of proximity to voltage collapse. IEEE Power Syst J 11:1441–1450
39. Moghavvemi M, Omar FM (1998) Technique for contingency monitoring and voltage collapse prediction. IEE Gener Transm Distrib J 145:634–640
40. Musirin I, Rahman TKA (2002) On-line voltage stability based contingency ranking using fast voltage stability index (FVSI). In: Proceedings of the IEEE/PES Asia Pacific transmission and distribution conference and exhibition, vol 2, pp 1118–1123
41. Leonardi B, Ajjarapu V (2008) Investigation of various generator reactive power reserve (GRPR) definitions for online voltage stability/security assessment. In: Proceedings of the IEEE power and energy society general meeting—conversion and delivery of electrical energy in the 21st Century, pp 1–7
42. Ruiz PA, Sauer PW (2006) Reactive power reserve issues. In: Proceedings of the 38th North American power symposium (NAPS 2006), pp 439–445

43. Avramovic B, Fink LH (1991) Real-time reactive security monitoring. In: Proceedings of the power industry computer application conference, pp 373–378
44. Leonardi B, Ajjarapu V (2011) Development of multilinear regression models for online voltage stability margin estimation. IEEE Power Syst J 26:374–383
45. Glavic M, Van Cutsem T (2011) A short survey of methods for voltage instability detection. In: Proceedings of the IEEE power and energy society general meeting, pp 1–8
46. Lixin B, Zhenyu H, Wilsun X (2003) Online voltage stability monitoring using var reserves. IEEE Power Syst J 18:1461–1469

Chapter 9
Smart Energy Management in Microgrid with Wind Power Generators and Plug-in Electric Vehicles

Qiang Yang, Zhejing Bao, Wenjun Yan and Ting Wu

Abstract The integration of a massive number of small-scale wind turbines and plug-in electric vehicles (PEVs) brought about urgent technical challenge to power distribution network operators (DNOs) in terms of secure power supply and energy dispatching optimization. In this chapter, we exploited three coordinated wind-PEV energy dispatching approaches in the Vehicle-to-Grid (V2G) context, i.e. valley searching, interruptible and variable-rate energy dispatching, aiming to promote the user demand response through optimizing the utilization efficiency of wind power generation as well as meeting the dynamic power demands. This issue is addressed in a stochastic framework considering the uncertainties of wind power generation as well as the statistical PEV driving patterns. The performance of the proposed solutions is assessed through a comparative study through numerical simulation experiments covering sufficient system scenarios by the use of scenario generation and reduction techniques. The result demonstrates that the energy dispatch based on the latter two approaches can achieve better matching between power generation and demands as well as PEV user satisfaction. In addition, the suggested approaches can be adopted by DNOs in practice with minimal deployment hurdles to promote the energy supplies within microgrid with wind power sources and PEVs.

Keywords Microgrid · Wind power · Plug-in electric vehicles (PEVs) · Wind-PEV coordinated dispatching

Q. Yang (✉) · Z. Bao · W. Yan · T. Wu
Department of System Science and Engineering College of Electrical Engineering, Zhejiang University, Hangzhou, People's Republic of China
e-mail: qyang@zju.edu.cn

S. Rajakaruna et al. (eds.), *Plug In Electric Vehicles in Smart Grids*, Power Systems, DOI 10.1007/978-981-287-299-9_9

Nomenclature

C	Nominal battery capacity of single PEV (kWh)
CR, DR	Nominal charging and discharging rate (kW)
$cr_i(n\Delta t)$	Charging rate of PEV i during time slot n (kW)
$dr_i(n\Delta t)$	Discharging rate of PEV i during time slot n (kW)
di	Daily driving distance of PEV i (km)
$E^{\mathrm{d}}_{\max}(i)$	Maximum discharging energy of PEV i (kWh), updated in each iteration
E^{d}_i	Energy consumed by PEV i through V2G technology (kWh)
$E^{\mathrm{d}}_{\mathrm{sum}}$	Maximum total discharging energy of all PEVs (kWh), updated in each iteration
E^{c}_i	Energy required by PEV i to make it fully charged (kWh), updated in each iteration
$E^{\mathrm{c}}_{\mathrm{sum}}$	Total energy demand of all PEVs (kWh), updated in each iteration
i	Index of the PEV
n	Index of time slot
N_{pev}	Total number of PEVs
P_{load}	Baseline load profile without PEV loads (kW)
$P^{\mathrm{f}}_{\mathrm{wind}}$	Forecasted wind power generation (kW)
P^{x}_{wind}	Wind power generation in scenario x (kW)
$P_{\mathrm{gen}}(n\Delta t)$	Current power generation during $n\Delta t$ which contains P_{wind} and PEV generation (kW)
$P_{\mathrm{con}}(n\Delta t)$	Current power consumption during $n\Delta t$ which contains P_{load} and PEV loads (kW)
s	Index of the iteration
SOC^{oini}_i	Initial SOC of PEV i when it arrivals office (%)
SOC^{omin}_i	Lower bound limit of SOC of PEV i during discharging process (%)
SOC^{hini}_i	Initial SOC of PEV i when it arrivals home (%)
$\tilde{T}^i_{\mathrm{ha}}$, $\tilde{T}^i_{\mathrm{hd}}$	Home arrival and departure time of PEV i (h)
$\tilde{T}^i_{\mathrm{oa}}$, $\tilde{T}^i_{\mathrm{od}}$	Office arrival and departure time of PEV i (h)
T^{c}_i	Requested charging hours for PEV i to be fully charged (h)
$T^{\mathrm{d}}_{\mathrm{start}}(i)$, $T^{\mathrm{d}}_{\mathrm{end}}(i)$	Start and end time of discharging process of the PEV i (h)
$T^{\mathrm{c}}_{\mathrm{start}}(i)$, $T^{\mathrm{c}}_{\mathrm{end}}(i)$	Start and end time of charging process of the PEV i (h)
W	Power consumption per kilometre of each PEV (kWh/km)
x	Index for wind power generation scenarios
Δt	Time slot (h)

9.1 Introduction

Currently a massive number of distributed generators (DGs) with different forms, e.g. wind turbines and combined heat and power (CHP) plants, have been deployed near the power loads in the power distribution networks due to the quick development of distributed energy resource (DER) technology. This has greatly reshaped the energy generation and distribution with many obvious benefits, e.g. a great reduction of peak-time demand and minimization of network congestion [1–3]. Besides, the enormous efforts in the pursuit of low carbon energy consumption have led to a great boom in the utilization of plug-in electric vehicles (PEVs) due to its superiority over the conventional internal combustion engine (ICE) vehicles due to its reduction of greenhouse gas (GHG) emissions, energy cost and dependences on imported petroleum [4–6]. However, the integration of wind-based DGs, e.g. wind turbines, as well as the PEVs into the current power distribution networks can brought out technical challenges for user demand response management due to their volatile nature and dynamic behaviors, including "voltage rise, increased fault levels, altered transient stability and degradation of protection operation and coordination", which imposes an urgent technical challenge to be addressed in practical deployment [7–9].

In particular, the key issues due to the penetration of PEVs into current distribution networks are highlighted in [10] and the study showed that uncoordinated PEV charging can cause local grid problems in terms of extra power losses, voltage deviations, and power quality degradation. Based on such recognition, much research effort has been made to address the challenge from different aspects and a set of technical solutions have been proposed (e.g. [11–13]). In [11], the authors developed a coordinated dispatch method for wind power and PEVs, and presented a modeling package to assess the impact of PEV integration in a wind-thermal power system through simulation. This study confirmed that the emissions of wind-thermal power system are reduced greatly compared to the system without PEVs. The investigations made in [12] adopted a novel unit commitment model to analyze the interactive behaviors among PEVs and wind power generators to promote the user demand response (DR), and proposed four PEV charging scenarios. This study demonstrated that optimal dispatching the PEV charging loads can significantly reduce the total system operating cost. In [13], the wind-PEV complementation model in transmission grid was produced which considered the carbon emission models of the conventional and carbon capture power plants. The study concluded that the wind power energy supply efficiency of PEVs can be significantly improved based on the suggested approach. The existing studies have clearly confirmed the benefits of optimal control of energy dispatch in power networks with penetration of wind power generator and PEVs. However, it should be noted that the available solutions have not been able to consider the variability of the PEV charging behaviors as well as the distribution of the states of charge (SOC) in respect to individual vehicles, which limits the potential benefits of energy dispatch in the microgrid. Also, the uncertainties, e.g. the deviation

between the actual and forecasted wind power outputs, were not explicitly considered in these studies, which may significantly undermine the effectiveness of the solutions in practical deployments.

On the other hand, it can be envisaged that the DC-based fast charging will cover most of the public, private or commercial charging stations [14]. It is showed that the EV battery voltage is generally no larger than 400 VDC (DC bus voltage) and the charging time to fully charge the PEV its battery pack may vary depending on the battery storage capacity and charging level characteristics (voltage and current ratings). In [15], the authors proposed a day-ahead energy scheduling based on the modified particle swarm optimization approach in the context of smart grid by including the DERs and V2G into consideration. Also, the EVs are controlled to respond to the demand response and the overall operating cost can be significantly reduced with the integration of smart PEVs scheduling. In [16], a generation scheduling scheme that is coordinated with the dynamic PEV charging is investigated in the industrial microgrid (IMG).The suggested solution has considered the integration of distributed PV solar and combined heat and power generators. The dynamic optimal power flow (DOPF) approach is proposed to significantly reduce the operational cost and charging costs.

In this chapter, we follow this line of research and the key technical contributions made in this work can be summarized as follows: considering the volatility of wind power generation by stimulating possible wind power volatility scenarios, we exploited the coordinated wind-PEV energy dispatching based on the flexible control of PEV charging and discharging behaviors, and presented three energy dispatching approaches, i.e. valley searching, interruptible and variable-rate dispatching. Their performance in terms of generation-demand matching and PEV user satisfaction is assessed and compared through a set of numerical simulation experiments. The remainder of this book chapter is organized as follows: Sect. 9.2 presents the statistical model describing the PEV charging and discharging behaviors, followed by the power generation model of wind turbine generator; three coordinated wind-PEV energy dispatching methods and algorithmic solutions, i.e. the valley searching, the interruptible and the variable-rate dispatching, are presented and explained in details in Sects. 9.3; in 9.4, the suggested energy dispatching methods are assessed and compared through numerical simulation studies for a set of key performance metrics; finally, the conclusive remarks and future work are given in Sect. 9.5.

For the sake of clarity, the following notations are used through this chapter.

9.2 Wind-PEV Microgrid System Modeling

The charging and discharging behaviors of PEVs make them considered as either power loads or power supplies when connected to the power grid. Various V2G technologies have been exploited in recent years to assess the impacts and investigate the economical potentials of such PEV integration during the power network operations. It showed in [17] that statistically the idle time of PEVs is around

96 % during a day. This implies that the potential of PEVs can be investigated to optimize the energy dispatch through coordination with the distributed wind power generators in the microgrid due to the control flexibility of PEVs.

In this work, we exploit the microgrid system with a distributed wind power generator and PEVs as well as general user demands. It is assumed that the PEVs are recharged at home over night and discharged at working time in the daytime. In addition, with the recognition that the driving pattern of the PEV users is with a stochastic nature, we derive the statistical model of the PEV driving pattern (i.e. departure times, arrival times and driving distance) by using the statistics of family ICE vehicles as a reasonable reference which is obtained from National Household Travel Survey [18], and the distribution of vehicle owners' last trip ending time is depicted in Fig. 9.1

Through the normalization, maximum likelihood estimation and curve-fitting of the statistical data, the home arrival (office departure) times and the office arrival (home departure) times can both be modeled following the normal distribution with the mean time of 17:36 and 8:00 respectively and the same standard deviation of 3.4 h. The PEV daily diving distances can be approximately modeled by a logarithmic normal distribution with the mean and variance of $\mu_D = 3.20$ and $\sigma_D = 0.88$, respectively (Fig. 9.2), as shown in (9.1).

$$f_D(d) = \frac{1}{d\sigma_D\sqrt{2\pi}} \exp\left[-\frac{(\ln d - \mu_D)^2}{2\sigma_D^2}\right] \tag{9.1}$$

As a result, through a statistical random sampling of the cumulative probabilities obtained from the aforementioned normal distribution and logarithmic normal

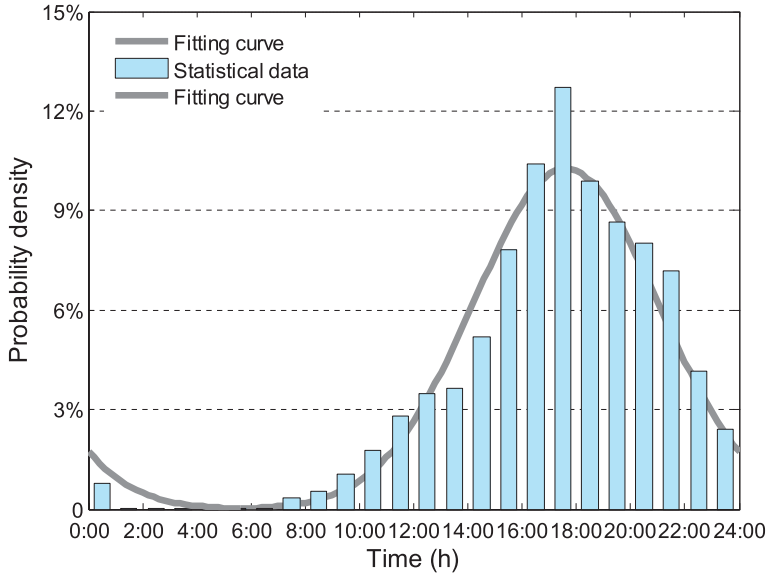

Fig. 9.1 The probability characteristics of vehicle owners' last trip ending time

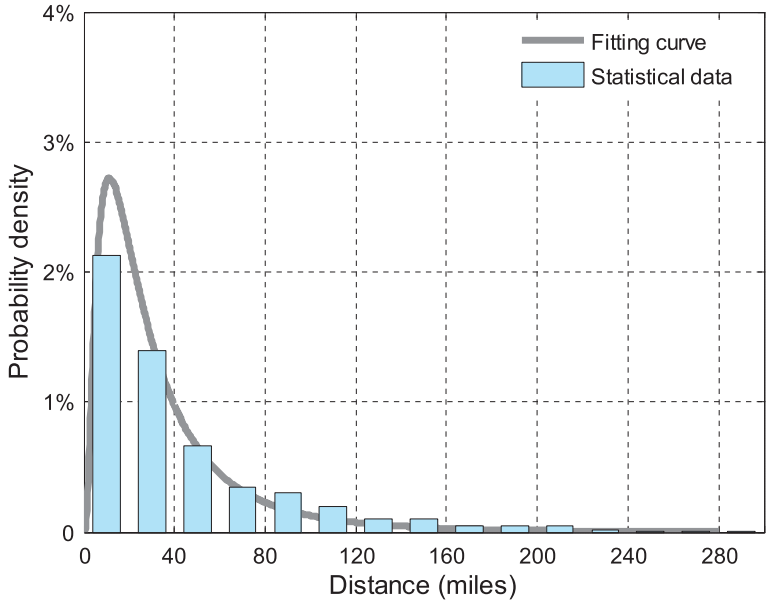

Fig. 9.2 The probability characteristics of driving distance during one day

distribution, the home arrival (office departure) time, $\tilde{T}_{\mathrm{ha}}^{i}\left(\tilde{T}_{\mathrm{od}}^{i}\right)$, home departure (office arrival) time, $\tilde{T}_{\mathrm{hd}}^{i}\left(\tilde{T}_{\mathrm{oa}}^{i}\right)$, and daily driving distance d_i of the PEV$_i$ can be derived. We take the existing concept, state of charge (SOC) [19, 20], into our work which represents the residual available energy state of the PEV. For each PEV, the SOC is assumed to be 100 % when leaving home and we consider the case that the daily driving distance is only the round trip distance between home and office, and hence the power consumption during this period equals half of the total daily driving power consumption. Thus, the initial SOC before discharging, which is determined by the daily driving distance of PEV$_i$, i.e. d_i, power consumption per kilometer, W, and nominal battery capacity, C, can be expressed as (9.2).

$$SOC_i^{\mathrm{oini}} = \left(1 - d_i W / 2C\right) \cdot 100\,\%, \quad i = 1, 2, 3, \ldots, N_{\mathrm{pev}} \tag{9.2}$$

In this work, the lower bound limit of SOC during the discharging process is set based on (9.3) to ensure that the SOC of individual PEVs is no less than 20 % at the time of arriving home. This is reasonable in practice to guarantee the safe arrivals of PEVs to the destinations.

$$SOC_i^{\mathrm{omin}} = 20\,\% + \frac{d_i W}{2C} \cdot 100\,\%, \quad i = 1, 2, 3, \ldots, N_{\mathrm{pev}} \tag{9.3}$$

The total power consumption of PEVs upon arrival at homes is the sum of the daily driving power consumption, $d_i W$, and energy consumed through V2G

technology, E_i^{d}. Thus, the initial SOC when a vehicle arrives home is described as follows:

$$SOC_i^{hini} = \left(1 - \frac{d_i W + E_i^{\mathrm{d}}}{C}\right) \cdot 100\,\%, \quad i = 1, 2, 3, \ldots, N_{\mathrm{pev}} \tag{9.4}$$

The energy required by PEV i to make it fully charged can be obtained as follows.

$$E_i^{\mathrm{c}} = E_i^{\mathrm{d}} + d_i W, \quad i = 1, 2, 3, \ldots, N_{\mathrm{pev}} \tag{9.5}$$

It is known that the forecasted generation of wind power generator $P_{\mathrm{wind}}^{\mathrm{f}}$ is determined by forecasted wind speed υ_{f} and turbine parameters, i.e. cut-in wind speed υ_{ci} , cut-out wind speed υ_{co}, nominal wind speed υ_{r} and nominal power of wind power generator P_{r}, which has been well investigated in the literature. In this work, we adopt the existing model of wind power generator from [21, 22] as given in (9.6):

$$P_{\mathrm{wind}}^{\mathrm{f}} = \begin{cases} 0, & \upsilon_{\mathrm{f}} < \upsilon_{\mathrm{ci}} \text{ or } \upsilon_{\mathrm{f}} > \upsilon_{\mathrm{co}} \\ \frac{\upsilon_{\mathrm{f}}^3 - \upsilon_{\mathrm{ci}}^3}{\upsilon_{\mathrm{r}}^3 - \upsilon_{\mathrm{ci}}^3} P_{\mathrm{r}}, & \upsilon_{\mathrm{ci}} \le \upsilon_{\mathrm{f}} < \upsilon_{\mathrm{r}} \\ P_{\mathrm{r}}, & \upsilon_{\mathrm{r}} \le \upsilon_{\mathrm{f}} \le \upsilon_{\mathrm{co}} \end{cases} \tag{9.6}$$

Due to the volatile nature of wind power generation, it cannot be forecasted with 100 % accuracy for dispatching purposes. To capture uncertainty, the wind power generation can be assumed to be subject to a normal distribution $N(\mu, \sigma^2)$ with forecasted wind power as its expected value (μ) and a percentage of μ as its volatility (σ) [23]. The Latin Hypercube Sampling (LHS) technique [23, 24] is employed for scenario generation. To decrease the computational burden caused by a large number of scenarios, the scenario reduction technique is employed to eliminate scenarios with very low probability and aggregating close scenarios based on the distance between scenarios multiplied by probability metrics [25, 26].

9.3 Coordinated Wind-PEV Energy Dispatching Methods

In this section, we present three different coordinated energy dispatching methods in the microgrid context with wind power generators and PEVs, i.e. valley searching, interruptible and variable-rate dispatching approaches. The solution aims to dynamically leverage the power generation in each scenario and the power demand by properly controlling the discharging and charging processes of PEVs in order to improve the matching performance between the power generation and consumption in the microgrid, and as a result, the power consumption from the power grid can be minimized. In the daytime, the PEVs are considered as responsive power sources by injecting power to the microgrid system to increase the power generation during the on-peak hours. On the other hand, the PEVs become responsive loads by absorbing the surplus wind power to increase the load profile

during the off-peak times at night. In this work, we are interested in exploiting the potential of PEVs to the optimal operation of the microgrid in term of the dynamic balance between power generation and demand. Thus, we do not consider the wind power energy injection to the power grid, which is also discouraged in the practical deployment for domestic environment due to many outstanding technical challenges, e.g. power quality degradation. The aforementioned coordinating dispatch methods are presented in details as follows in this section.

9.3.1 Valley Searching Dispatching Method

Firstly, we look into the valley searching dispatching method which regulates the discharging or charging process cannot be interrupted. It searches the valley of wind power/load curve in the daytime and at night respectively, and fills it through the discharging/charging process of PEVs. This approach with uninterruptible charging/discharging process is considered worth exploiting mainly due to the following facts: (1) currently some PEV battery vendors explicitly instruct to avoid interruption due to the consideration of its potential adverse impacts on the battery lifetime; (2) this charging strategy can be implemented much simpler than others and imposes less technical and engineering requirements and complexity on the PEV charging infrastructures, and hence is more deployable in the places where no advanced monitoring, control and communication infrastructures are available.

Here, the discharging rate and charging rate are set with the fixed rate, *DR* and *CR*, respectively, and the entire observation time window, T (24 h), is divided into a number of time slots with the slot duration indicated as Δt. The upper limit of discharging energy $E^{\mathrm{d}}_{\max}$ and the maximum discharging time $T^{\mathrm{d}}_{\max}$ for an arbitrary PEV i before discharging process can be derived based on the SOC_i^{oini} and SOC_i^{omin}, which can be expressed as (9.7)–(9.8).

$$E^{\mathrm{d}}_{\max}(i) = \left(SOC_i^{\mathrm{oini}} - SOC_i^{\mathrm{omin}}\right)C, \quad i = 1, 2, 3, \ldots, N_{\mathrm{pev}} \tag{9.7}$$

$$T^{\mathrm{d}}_{\max}(i) = E^{\mathrm{d}}_{\max}(i) \Big/ DR \tag{9.8}$$

For the charging process, the PEVs are expected to be charged upon arrival at homes, and the required charging hours for PEV i to be fully charged is given by (9.9).

$$T_i^{\mathrm{c}} = (1 - SOC_i^{hini})C \Big/ CR, \quad i = 1, 2, 3, \ldots, N_{\mathrm{pev}} \tag{9.9}$$

For PEV i, we search the index of the time slot, g_i^{d} and g_i^{c}, in which the current power generation, $P_{\mathrm{gen}}^{i-1}(n\Delta t)$, and consumption, $P_{\mathrm{con}}^{i-1}(n\Delta t)$, are minimized during the time interval $[\tilde{T}^i_{\mathrm{oa}}, \tilde{T}^i_{\mathrm{od}}]$ and $[\tilde{T}^i_{\mathrm{ha}}, \tilde{T}^i_{\mathrm{hd}}]$ based on (9.10) and (9.11) respectively.

$$P_{\mathrm{gen}}^{i-1}(g_i^{\mathrm{d}}\Delta t) = \min(P_{\mathrm{gen}}^{i-1}(n\Delta t)), \quad n\Delta t \in [\tilde{T}^i_{\mathrm{oa}}, \tilde{T}^i_{\mathrm{od}}] \tag{9.10}$$

$$P_{\text{con}}^{i-1}(g_i^{\text{c}}\Delta t) = \min(P_{\text{con}}^{i-1}(n\Delta t)), \quad n\Delta t \in [\tilde{T}_{\text{ha}}^i, \tilde{T}_{\text{hd}}^i] \tag{9.11}$$

Ideally, the start time of the discharging/charging process can be determined by using the searched valley as their midpoints. However, the start time of the discharging/charging process cannot be earlier than the office/home arrival time, and the end time cannot be later than the office/home departure time. Thus, the start and end time of the discharging ($T_{\text{start}}^{\text{d}}, T_{\text{end}}^{\text{d}}$) and charging process ($T_{\text{start}}^{\text{c}}, T_{\text{end}}^{\text{c}}$) for PEV, i, can be determined as (9.12)–(9.13) and (9.14)–(9.15) respectively.

$$T_{\text{start}}^{\text{d}}(i) = \begin{cases} \tilde{T}_{\text{oa}}^i, & g_i^{\text{d}}\Delta t - T_{\max}^d(i)/2 < \tilde{T}_{\text{oa}}^i \\ \tilde{T}_{\text{od}}^i - T_{\max}^d(i), & g_i^{\text{d}}\Delta t + T_{\max}^d(i)/2 > \tilde{T}_{\text{od}}^i \\ g_i^{\text{d}}\Delta t - T_{\max}^d(i)/2, & \textit{otherwise} \end{cases} \tag{9.12}$$

$$T_{\text{end}}^{\text{d}}(i) = T_{\text{start}}^{\text{d}}(i) + T_{\max}^{\text{d}}(i) \tag{9.13}$$

$$T_{\text{start}}^{\text{c}}(i) = \begin{cases} \tilde{T}_{\text{ha}}^i, & g_i^{\text{c}}\Delta t - T_i^c/2 < \tilde{T}_{\text{ha}}^i \\ \tilde{T}_{\text{hd}}^i - T_i^c, & g_i^{\text{c}}\Delta t + T_i^c/2 > \tilde{T}_{\text{hd}}^i \\ g_i^{\text{c}}\Delta t - T_i^c/2, & \textit{otherwise} \end{cases} \tag{9.14}$$

$$T_{\text{end}}^{\text{c}}(i) = T_{\text{start}}^{\text{c}}(i) + T_i^{\text{c}} \tag{9.15}$$

For each valley search iteration, the current power generation and consumption need to be updated when PEV, i, has been discharged/charged, as shown in (9.16) and (9.17) respectively.

$$\begin{aligned} P_{\text{gen}}^i(n\Delta t) &= P_{\text{gen}}^{i-1}(n\Delta t) + K_i^{\text{d}}(n\Delta t)\cdot DR, \; i = 1, 2, \ldots, N_{\text{pev}} \\ P_{\text{gen}}^0(n\Delta t) &= P_{\text{wind}}^x(n\Delta t), \quad n = 1, 2, \ldots, T/\Delta t \end{aligned} \tag{9.16}$$

$$\begin{aligned} P_{\text{con}}^i(n\Delta t) &= P_{\text{con}}^{i-1}(n\Delta t) + K_i^{\text{c}}(n\Delta t)\cdot CR, \quad i = 1, 2, \ldots, N_{\text{pev}} \\ P_{\text{con}}^0(n\Delta t) &= P_{\text{load}}(n\Delta t), \quad n = 1, 2, \ldots, T/\Delta t \end{aligned} \tag{9.17}$$

$K_i^{\text{d}}(n\Delta t)$ and $K_i^{\text{c}}(n\Delta t)$ are binary variables that equal 1 if PEV i is discharging or charging during $n\Delta t$ and 0 otherwise, shown as follows.

$$K_i^{\text{d}}(n\Delta t) = \begin{cases} 1, & n\Delta t \in [T_{\text{start}}^{\text{d}}(i), T_{\text{end}}^{\text{d}}(i)] \\ 0, & \textit{otherwise} \end{cases} \tag{9.18}$$

$$K_i^{\text{c}}(n\Delta t) = \begin{cases} 1, & n\Delta t \in [T_{\text{start}}^{\text{c}}(i), T_{\text{end}}^{\text{c}}(i)] \\ 0, & \textit{otherwise} \end{cases} \tag{9.19}$$

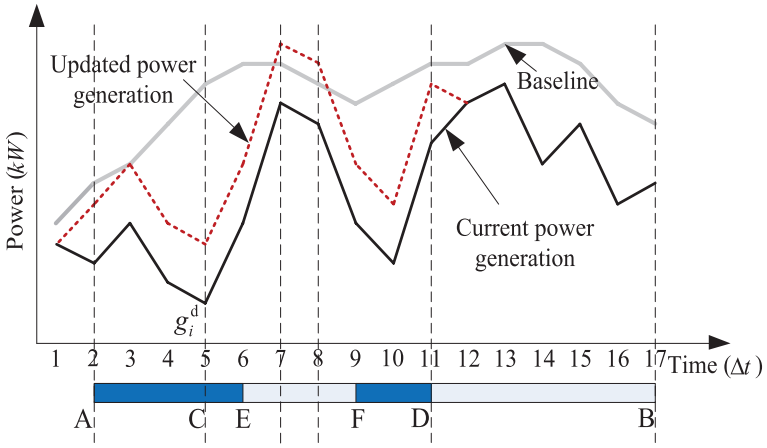

Fig. 9.3 The illustration of the valley searching method

As we assumed that the power generated from the wind turbines as well as the PEV discharging in the microgrid system cannot be injected to the local power grid, and hence the key objective of the investigation is to maximize the utilization of power generation within the microgrid, i.e. keeping the power consumption from the local grid minimal. During the PEV discharging process in the daytime, the process can be divided into several time segments at the times when the microgrid power generation instantaneously exceeds the power consumption.

This approach can be illustrated by an example, as shown in Fig. 9.3. The vehicle arrives the office at 2nd time slot (point A) and departs the office at 17th time slot (point B), which implies that the discharging process can occur within the time period. The valley of the current power generation during the time interval [A, B] is searched as g_i^{d} (point C). The maximum discharging time is 10th time slots by calculation from (9.8). Then, the start and end time of the discharging process (point A and D) can be determined by (9.12) and (9.13). It can be seen that the updated power generation (dotted line) exceeds the baseline (i.e. general user demand, e.g. lighting.) during the 7th and 8th time slots. Thus, the discharging process of this vehicle will be divided into two time segments (AE and FD). Due to the reason that the process is not interruptible, we choose the longer time period for the PEV discharging process (AE, from 2nd to the 6th time slot).

Similarly, the PEV loads are encouraged to fully utilize the surplus wind power instead of using the power from the local grid at night. The charging process can be divided into several time segments when current power consumption exceeds the wind power generation. As the charging process of PEVs cannot be interrupted, the longest time period from the divided time segments is selected for the charging process.

The detailed process of the valley searching algorithmic solution is described by the following pseudo-codes. Due to the fact that the process of

charging and discharging are symmetric, for the sake of clarity, we enclose the variables or statements of the charging process in the brackets (also applied to Algorithm 2 and 3).

Algorithm 1 Valley searching dispatching method in scenario x

Require: DR, CR, P_{load}, P_{wind}^{x}, W, Δt

1: get $\tilde{T}_{\text{ha}}, \tilde{T}_{\text{hd}}, \tilde{T}_{\text{oa}}, \tilde{T}_{\text{od}}, d$ using statistical random sampling

// note: **"content in {…}" represents the charging process**

2: **FOR** $i \leftarrow 1 \, to \, N_{pev}$ **DO**

3: calculate $T_{\max}^{\text{d}}(i)$ $\{T_i^{\text{c}}\}$ and search g_i^{d} $\{g_i^{\text{c}}\}$

// using (8) and (10) {(9) and (11)}

4: calculate $T_{\text{start}}^{\text{d}}(i)$ $\{T_{\text{start}}^{\text{c}}(i)\}$ and $T_{\text{end}}^{\text{d}}(i)$ $\{T_{\text{end}}^{\text{c}}(i)\}$

// using (12) and (13) {(14) and (15)}

5: update P_{gen}^{i} $\{P_{\text{con}}^{i}\}$ // using (16) {(17)}

6: **IF** the discharging process is divided into several time segments

7: restore $P_{\text{gen}}^{i-1} \leftarrow P_{\text{gen}}^{i} - K_i^{\text{d}} DR$ $\{P_{\text{con}}^{i-1} \leftarrow P_{\text{con}}^{i} - K_i^{\text{c}} CR\}$

8: choose the longest time segment and update $T_{\text{start}}^{\text{d}}(i)$, $T_{\text{end}}^{\text{d}}(i)$ $\{T_{\text{start}}^{\text{c}}(i), T_{\text{end}}^{\text{c}}(i)\}$

9: update K_i^{d} and P_{gen}^{i} $\{K_i^{\text{c}}$ and $P_{\text{con}}^{i}\}$

// using (18) and (16) {(19) and (17)}

10: **END IF**

11: **END FOR**

9.3.2 Interruptible Dispatching Method

The generated wind power cannot be fully utilized when using the valley searching method as the charging/discharging process is not interruptible and hence limits the flexibility of the PEV control. To solve the problem, we further look into the interruptible dispatching method, where the discharging and charging rate parameters are the same as those set in the previous method but the discharging and charging processes can be interrupted if needed. We take the concept of cut level from [27] which defines the level to which the power generation or the power consumption

need to be adjusted to identify the time slots in which the load should be met by the power generation or the surplus wind power should be absorbed by the power loads. Moreover, the cut level cannot be larger than the load profile or wind power generation at individual time slots during the discharging or charging process respectively.

Initially, the cut level is selected as the minimum wind power generation or minimum baseline load demand during the discharging or charging process, respectively. During each iteration, the cut level is incrementally increased by δ until all the PEVs are fully discharged or the iteration dominates, i.e. the number of iterations is equal to the predefined maximum iterating times during the discharging process, as shown in (9.20).

Similarly, for the charging process, the cut level is gradually lifted by δ until all the PEVs are fully charged or the iteration dominates, as shown in (9.21).

$$P^{\mathrm{d}}_{\mathrm{cut}}(s) = P^{\mathrm{d}}_{\mathrm{cut}}(s-1) + \delta,\ P^{\mathrm{d}}_{\mathrm{cut}}(0) = \min(P^{x}_{\mathrm{wind}}) \tag{9.20}$$

$$P^{\mathrm{c}}_{\mathrm{cut}}(s) = P^{\mathrm{c}}_{\mathrm{cut}}(s-1) + \delta,\ P^{\mathrm{c}}_{\mathrm{cut}}(0) = \min(P_{\mathrm{load}}) \tag{9.21}$$

The maximum iterating times of the discharging and charging process can be calculated before the iteration process by (9.22) and (9.23) respectively.

$$I^{\mathrm{d}}_{\max} = \left(\max(P_{\mathrm{load}}(n\Delta t)) - \min(P^{x}_{\mathrm{wind}}(n\Delta t))\right)\big/\,\delta \tag{9.22}$$

$$I^{\mathrm{c}}_{\max} = \left(\max(P^{x}_{\mathrm{wind}}(n\Delta t)) - \min(P_{\mathrm{load}}(n\Delta t))\right)\big/\,\delta \tag{9.23}$$

To get the criteria of judging whether the iteration stops, $E^{\mathrm{d}}_{\mathrm{sum}}$ and $E^{\mathrm{c}}_{\mathrm{sum}}$ are calculated as follows:

$$E^{\mathrm{d}}_{\mathrm{sum}} = \sum_{i=1}^{N_{\mathrm{pev}}} E^{\mathrm{d}}_{\max}(i) \tag{9.24}$$

$$E^{\mathrm{c}}_{\mathrm{sum}} = \sum_{i=1}^{N_{\mathrm{pev}}} E^{\mathrm{c}}_{i} \tag{9.25}$$

For discharging process, the cut level $P^{\mathrm{d}}_{\mathrm{cut}}(s)$ can be derived by (9.26) in the sth iteration. In the time slot n, the cut level $P^{\mathrm{d}}_{\mathrm{cut}}(s)$ is compared with the load profile to find the smaller one.

$$L_{\mathrm{d}}(n\Delta t) = \begin{cases} P^{\mathrm{d}}_{\mathrm{cut}}(s), & P^{\mathrm{d}}_{\mathrm{cut}}(s) \le P_{\mathrm{load}}(n\Delta t) \\ P_{\mathrm{load}}(n\Delta t), & P^{\mathrm{d}}_{\mathrm{cut}}(s) > P_{\mathrm{load}}(n\Delta t) \end{cases} \tag{9.26}$$

Similarly, the smaller value between cut level and wind power in scenario x during time slot n can be derived as follows.

$$L_{\mathrm{c}}(n\Delta t) = \begin{cases} P^{\mathrm{c}}_{\mathrm{cut}}(s), & P^{\mathrm{c}}_{\mathrm{cut}}(s) \le P_{\mathrm{wind}}(n\Delta t) \\ P^{x}_{\mathrm{wind}}(n\Delta t), & P^{\mathrm{c}}_{\mathrm{cut}}(s) > P^{x}_{\mathrm{wind}}(n\Delta t) \end{cases} \tag{9.27}$$

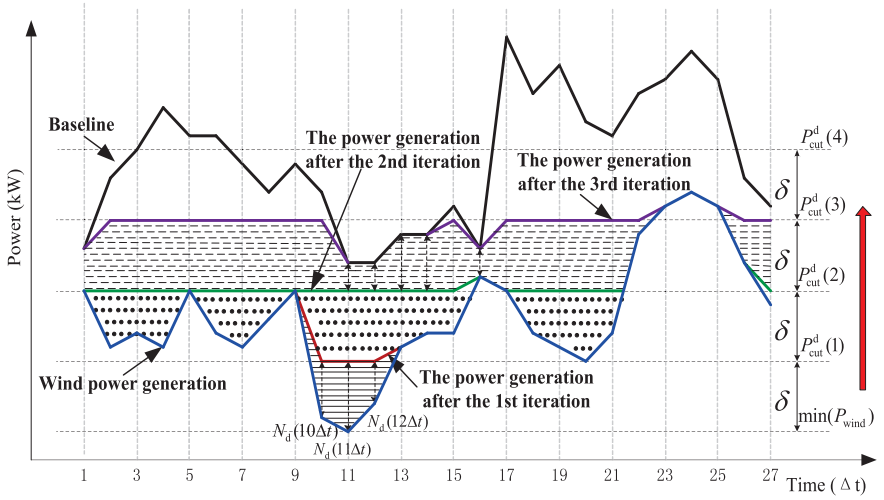

Fig. 9.4 The illustration of the interruptible discharging

Then, we compare $L_d(n\Delta t)$ with the current power generation to find the chargeable time slots where the value $L_d(n\Delta t)$ is higher than the power generation and calculate the required number (which should be rounded down) of the PEVs which can be discharged in the time slot n as follows.

$$N_d(n\Delta t) = \left\lfloor \frac{L_d(n\Delta t) - P_{gen}(n\Delta t)}{DR} \right\rfloor \tag{9.28}$$

The approach is illustrated in Fig. 9.4. In the 1st iteration there are only three time slots (i.e. 10th, 11th, 12th) where the power generation is lower than $L_d(n\Delta t)$, and then the values of $N_d(10\Delta t)$, $N_d(11\Delta t)$ and $N_d(12\Delta t)$ can be derived based on (9.28) respectively. If all the PEVs are not discharged and the iteration is smaller than I^d_{max}, we lift the cut level by δ in the next iteration based on (9.20). In the 3rd iteration, since the cut level is higher than the power consumption during the 11th, 12th,13th, 14th and 16th time slots, we choose the value of the power consumption to calculate the required number of PEVs which can be discharged during these five time slots. In Fig. 9.4, the shadowed areas marked by the solid, dotted and dashed lines represent the energy generated by the PEVs discharging in the first, second and third iterations, respectively.

Similarly, for the charging process, the required number (which should be rounded down) of charging PEVs can be calculated as follows.

$$N_c(n\Delta t) = \left\lfloor \frac{L_c(n\Delta t) - P_{con}(n\Delta t)}{CR} \right\rfloor \tag{9.29}$$

The detailed process of the interruptible dispatching method is described in pseudo-codes.

Algorithm 2 Interruptible dispatching method in scenario x

Require: DR, CR, P_{load}, P^{x}_{wind}, W, Δt

1: get $\tilde{T}_{\text{ha}}, \tilde{T}_{\text{hd}}, \tilde{T}_{\text{oa}}, \tilde{T}_{\text{od}}, d$ using statistical random sampling

// note: **"content in {…}" represents the charging process**

2: calculate $I^{\text{d}}_{\max}$ { $I^{\text{c}}_{\max}$ } // using (22) {(23)}

3: **WHILE** ($E^{\text{d}}_{\text{sum}} > 0$) **AND** ($s < I^{\text{d}}_{\max}$){($E^{\text{c}}_{\text{sum}} > CR \cdot \Delta t$) **AND** ($s < I^{\text{c}}_{\max}$)}

4: update $P^{\text{d}}_{\text{cut}}(s)$ { $P^{\text{c}}_{\text{cut}}(s)$ } // using (20) {(21)}

5: **FOR** $n \leftarrow 1 \, to \, 24/\Delta t$ **DO**

6: get $L_{\text{d}}(n\Delta t)$ { $L_{\text{c}}(n\Delta t)$ } // using (26) {(27)}

7: **IF** $P_{\text{gen}}(n\Delta t) < L_{\text{d}}(n\Delta t)$ { $P_{\text{con}}(n\Delta t) < L_{\text{c}}(n\Delta t)$ }

8: calculate $N_{\text{d}}(n\Delta t)$ { $N_{\text{c}}(n\Delta t)$ } // using (28) {(29)}

9: **END IF**

10: **FOR** $i \leftarrow 1 \, to \, N_{pev}$ **DO**

11: **IF** $(n\Delta t \in [\tilde{T}^{i}_{\text{oa}}, \tilde{T}^{i}_{\text{od}}])$ **AND** $(E^{\text{d}}_{\max}(i) \neq 0)$ **AND** $(K^{\text{d}}_{i}(n\Delta t) = 0)$

{ $(n\Delta t \in [\tilde{T}^{i}_{\text{ha}}, \tilde{T}^{i}_{\text{hd}}])$ **AND** $(E^{\text{c}}_{i} \neq 0)$ **AND** $(K^{\text{c}}_{i}(n\Delta t) = 0)$ }

12: $P_{\text{gen}}(n\Delta t) \leftarrow P_{\text{gen}}(n\Delta t) + DR$ { $P_{\text{con}}(n\Delta t) \leftarrow P_{\text{con}}(n\Delta t) + CR$ }

13: $E^{\text{d}}_{\text{sum}} \leftarrow E^{\text{d}}_{\text{sum}} - DR \cdot \Delta t$ { $E^{\text{c}}_{\text{sum}} \leftarrow E^{\text{c}}_{\text{sum}} - CR \cdot \Delta t$ }

14: $E^{\text{d}}_{\max}(i) \leftarrow E^{\text{d}}_{\max}(i) - DR \cdot \Delta t$ { $E^{\text{c}}_{i} \leftarrow E^{\text{c}}_{i} - CR \cdot \Delta t$ }

15: **END IF**

16: **END FOR**

17: **END FOR**

18: **END WHILE**

9.3.3 Variable-Rate Dispatching Method

To further the improvement in the utilization efficiency of wind power generation within the microgrid, we look into the variable-rate dispatching method. This method is similar to the interruptible dispatching method, but the discharging or

charging rate can be varied in an adaptive manner during the discharging or charging process, and the maximum discharging and charging rate are set to $DR_{\max}$ and $CR_{\max}$ respectively. In this approach, we adjust the discharging or charging rate for PEV i by comparing the $L_{\mathrm{d}}(n\Delta t)$ or $L_{\mathrm{c}}(n\Delta t)$ with the current power generation or the current power consumption in the time slot n respectively, rather than identifying the required number of PEVs which can be discharged or charged.

$$dr_i(n\Delta t) = L_{\mathrm{d}}(n\Delta t) - P_{\mathrm{gen}}(n\Delta t) \tag{9.30}$$

$$cr_i(n\Delta t) = L_{\mathrm{c}}(n\Delta t) - P_{\mathrm{con}}(n\Delta t) \tag{9.31}$$

The derived discharging rate by (9.30) should meet the following two constraints: the calculated cumulative discharging rate based on $dr_i(n\Delta t)$ cannot exceed the maximum discharging rate during any time slot (see (9.32)); and the updated maximum discharging energy of each PEV after discharging based on $dr_i(n\Delta t)$ cannot be less than zero (see (9.33)).

$$dr_i(n\Delta t) \leq DR_{\max} - CumDR_i(n\Delta t) \tag{9.32}$$

$$E^{\mathrm{d}}_{\max}(i) - dr_i(n\Delta t) \cdot \Delta t \geq 0 \tag{9.33}$$

If $dr_i(n\Delta t)$ achieved from (9.30) cannot meet these two constraints, the maximum discharging rate that need to be adopted to a corrective discharging rate during this time slot which can be calculated based on (9.34) and (9.35) respectively.

$$dr_i(n\Delta t) = DR_{\max} - CumDR_i(n\Delta t) \tag{9.34}$$

$$dr_i(n\Delta t) = E^{\mathrm{d}}_{\max}(i)/\Delta t \tag{9.35}$$

Similarly, the charging rate should also meet the following two constraints: the calculated cumulative charging rate based on $cr_i(n\Delta t)$ cannot exceed the maximum charging rate during any time slot (see (9.36)); and the calculated charging energy based on $cr_i(n\Delta t)$ cannot exceed the energy required by PEV i (see (9.37)).

$$cr_i(n\Delta t) \leq CR_{\max} - CumCR_i(n\Delta t) \tag{9.36}$$

$$E^{\mathrm{c}}_i - cr_i(n\Delta t) \cdot \Delta t \geq 0 \tag{9.37}$$

If $cr_i(n\Delta t)$ achieved from (9.31) cannot meet these two constraints, we use the following two equations to adjust the charging rate respectively.

$$cr_i(n\Delta t) = CR_{\max} - CumCR_i(n\Delta t) \tag{9.38}$$

$$cr_i(n\Delta t) = E^{\mathrm{c}}_i/\Delta t \tag{9.39}$$

The detailed process of the variable-rate dispatching method is described in the following pseudo-codes.

Algorithm 3 Variable-rate dispatching method in scenario x

Require: $DR_{\max}$, $CR_{\max}$, P_{load} , P^{x}_{wind} , W , Δt

1: get $\tilde{T}_{\text{ha}}, \tilde{T}_{\text{hd}}, \tilde{T}_{\text{oa}}, \tilde{T}_{\text{od}}, d$ using statistical random sampling

// note: **"content in {…}" represents the charging process**

2: **FOR** $i \leftarrow 1 \; to \; N_{pev}$ **DO**

3: calculate $I^{\text{d}}_{\max}$ { $I^{\text{c}}_{\max}$ } // using (22) {(23)}

4: **WHILE** ($E^{\text{d}}_{\max}(i) > 0$) **AND** ($s < I^{\text{d}}_{\max}$){($E^{\text{c}}_{i} > 0$) **AND** ($s < I^{\text{c}}_{\max}$)}

5: update $P^{\text{d}}_{\text{cut}}(s)$ { $P^{\text{c}}_{\text{cut}}(s)$ } // using (20) {(21)}

6: **FOR** $n \leftarrow \tilde{T}_{\text{oa}} \; to \; \tilde{T}_{\text{od}}$ { $n \leftarrow \tilde{T}_{\text{ha}} \; to \; \tilde{T}_{\text{hd}}$ } **DO**

7: get $L_{\text{q}}(n\Delta t)$ { $L_{\text{c}}(n\Delta t)$ } // using (26) {(27)}

8: derive $dr_i(n\Delta t)$ { $cr_i(n\Delta t)$ } // using (30) {(31)}

9: **IF** $dr_i(n\Delta t) > DR_{\max} - CumDR_i(n\Delta t)$
{ $cr_i(n\Delta t) > CR_{\max} - CumCR_i(n\Delta t)$ }

10: $dr_i(n\Delta t) \leftarrow DR_{\max} - CumDR_i(n\Delta t)$
{ $cr_i(n\Delta t) \leftarrow CR_{\max} - CumCR_i(n\Delta t)$ }

11: **END IF**

12: **IF** $E^{\text{d}}_{\max}(i) - dr_i(n\Delta t) \cdot \Delta t < 0$ { $E^{\text{c}}_{i} - cr_i(n\Delta t) \cdot \Delta t \geq 0$ }

13: $dr_i(n\Delta t) = E^{\text{d}}_{\max}(i) / \Delta t$ { $cr_i(n\Delta t) = E^{\text{c}}_{i} / \Delta t$ }

14: **END IF**

15: $P_{\text{gen}}(n\Delta t) \leftarrow P_{\text{gen}}(n\Delta t) + dr_i(n\Delta t)$
{ $P_{\text{com}}(n\Delta t) \leftarrow P_{\text{com}}(n\Delta t) + cr_i(n\Delta t)$ }

16: $E^{\text{d}}_{\max}(i) \leftarrow E^{\text{d}}_{\max}(i) - dr_i(n\Delta t) \cdot \Delta t$
{ $E^{\text{c}}_{i} \leftarrow E^{\text{c}}_{i} - cr_i(n\Delta t) \cdot \Delta t$ }

17: **END FOR**

18: **END WHILE**

19: **END FOR**

9.4 Case Study and Numerical Result

This section carries out the assessments of the proposed three coordinated energy dispatching methods in microgrid with distributed wind power generation and PEVs through numerical simulation experiments. The simulation environments are developed based on MATLAB version R2010b and the performance of the wind-PEV dispatching methods in deterministic model (i.e. forecasted wind power) and stochastic model (i.e. different scenarios obtained by the mentioned scenario generations and reduction techniques) are evaluated through a comparative study

in terms of two key metrics which are used in the literature, i.e. the matching between power generation and demand, and the PEV user satisfaction. In addition, in respect to the stochastic nature of the operational scenarios, a set of uncertainty handling tools, e.g. information gap decision theory, fuzzy method, robust optimization and related stochastic techniques [28–31] are available in the literature which can be adopted as appropriate in this chapter.

9.4.1 Case Study I

In this case study, there is no limitation on the available power from the electric utility. Three penetration degrees ($Pen \in \{10\,\%, 30\,\%, 50\,\%\}$) are considered. Two general impact categories are examined, namely the impacts of charging scenarios on the peak load and that on the flatness of overall load profile. The baseline of a residential area with 1,500 homes covers 24 h and the instantaneous power consumption is given on a 5-min time base, as shown in Fig. 9.5.

The total number of vehicles owned by the residents in this area has been estimated to be 1,500 with the different PEVs penetration degrees. All the PEVs are in the same specification and the PEV battery capacity is set as 20 kWh. The time interval between arrival and departure of each vehicle is assumed to be larger than 9 h. In addition, the rated charging rate $CR = 0.2C$ (4kW) and the maximum charging rate $CR_{\max} = 0.25C$ (5kW). For a PEV, the power consumption per 100 km is 15 kWh. Three PEVs penetration degrees ($Pen \in \{10\,\%, 30\,\%, 50\,\%\}$) are considered.

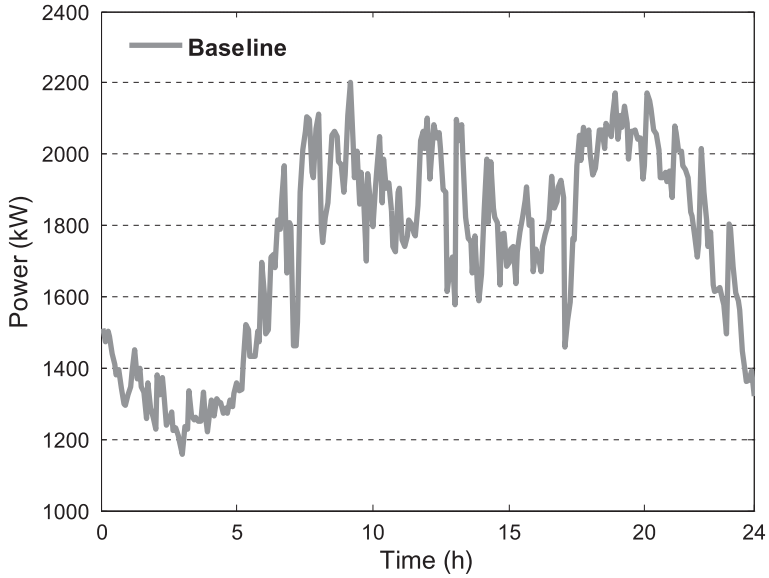

Fig. 9.5 The baseline load profile of the simulated residential area

For each PEV penetration level, the impacts of different charging patterns, with respect to the baseline, are depicted in Fig. 9.6a–c. The influence of the charging scenarios on the peak load is shown in Table 9.1. The random charging pattern has the highest peak load, which is 3.04, 10.38 and 22.20 % higher than the peak

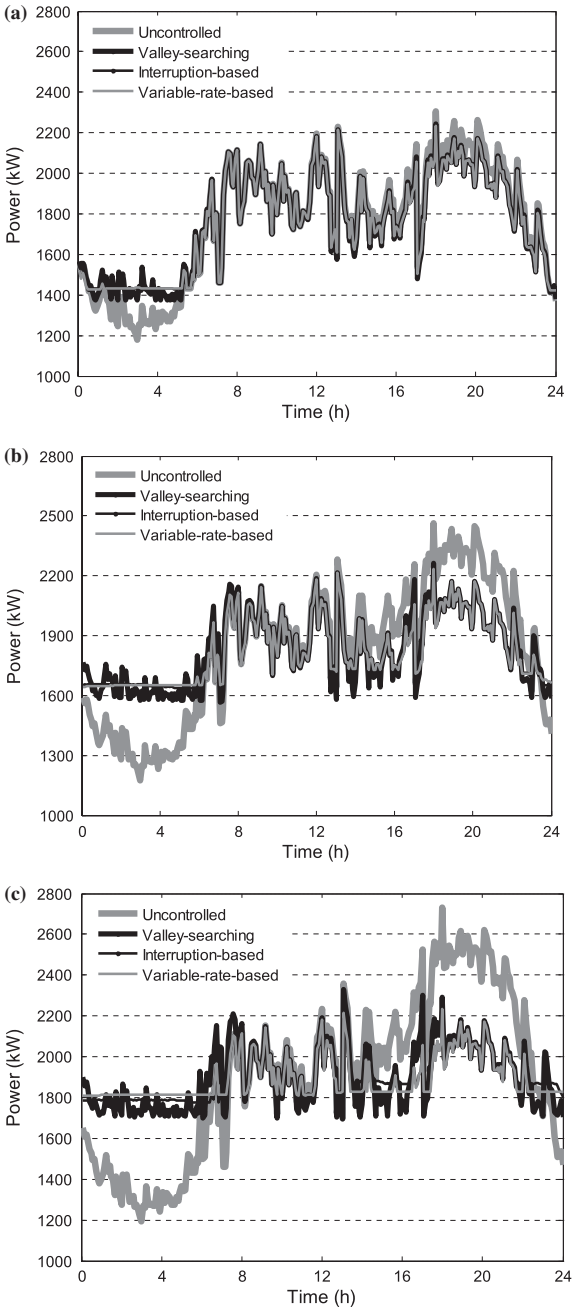

Fig. 9.6 Different charging patterns induced load profile with several PEVs penetrations: **a** 10 % PEVs penetration, **b** 30 % PEVs penetration, **c** 50 % PEVs penetration

Table 9.1 Peak load for the different charging patterns (xx % represents the PEV penetration degree)

Scenario	10 %		30 %		50 %	
	P_{max}(kW)	$P_{max}\nearrow$ (%)	P_{max}(kW)	$P_{max}\nearrow$ (%)	P_{max}(kW)	$P_{max}\nearrow$ (%)
Random charging	2,302	3.04	2,466	10.38	2,730	22.20
Valley-searching	2,242	0.36	2,262	1.25	2,329	4.25
Interruptible	2,234	0	2,234	0	2,234	0
Variable-rate	2,234	0	2,234	0	2,234	0

Table 9.2 Standard deviations of load profiles in different charging patterns

Scenario	Penetration degree (%)	s	$s\searrow$ (%)	s^2	$s^2\searrow$ (%)
No PEVs	–	282.85	–	80,005	–
Random charging	10	294.48	−4.11	86,719	−8.39
	30	337.99	−19.49	114,230	−42.78
	50	393.33	−39.06	154,710	−93.38
Valley-searching	10	244.14	13.69	59,605	25.50
	30	182.13	35.61	33,172	58.54
	50	150.98	46.62	22,795	71.51
Interruptible	10	241.26	14.70	58,206	27.25
	30	163.72	42.12	26,804	66.50
	50	110.80	60.83	12,276	84.66
Variable-rate	10	240.98	14.80	58,073	27.41
	30	163.06	42.35	26,589	66.77
	50	106.45	62.37	11,333	85.83

load of baseline respectively for the different PEV penetrations. The second highest peak load arises in the valley-searching charging pattern, being 0.36, 1.25 and 4.25 % higher than the peak of baseline with the different PEV penetrations. The interruptible charging pattern and the variable rate charging pattern avoid enlarging the peak of base load, as well as fill the valley of base load.

The flatness of overall load profiles can be evaluated by the standard deviations and variances. As shown in Table 9.2, instead of helping smooth the base load, the uncontrolled charging scenario deteriorate the fluctuation of load profile, with the standard deviation being 4.11, 19.49 and 39.06 % higher than that of the base load respectively for the different PEVs penetrations. On the contrary, all the three charging strategies in the demand dispatch scenario can improve the flatness of the load profile, and the variable-rate-based charging strategy achieves the most optimal load profile whose standard deviation is 14.80, 42.35 and 62.37 % lower than that of the base load respectively for 10, 30 and 50 % PEVs penetrations. The improvements grow with the PEVs penetration level increases, indicating PEVs are useful resources to flatten the load profile in the demand dispatch charging scenario.

9.4.2 Case Study II

With the increasing of wind power generation, part of wind power will be abandoned especially at night. In [19], it declared that the synergy between the PEVs charging and the wind power has provided a possibility of multi-resource utilization on the platform of the smart grid. In this case study, we compare and analyse the three intelligent charging patterns in the aspect of accommodating the excessive wind power during the low demand night-time period.

The baseline and the wind power generation (in July) covers 8 h (from 22:00 to 6:00) are the instantaneous power consumption is given on a 5-min time base, as shown in Fig. 9.7.

The wind power capacity is 1,200 kWh. The total number of vehicles is set as 700. The time interval between arrival and departure of each vehicle includes the 8 h. In addition, the capacity of the battery, the rated charging rate, the maximum charging rate and the power consumption per hundred kilometres are same as for the case study 1.

For different charging patterns, the PEV-wind synergistic dispatching load profiles are depicted in Fig. 9.8. The Table 9.3 shows the extra wind energy under the three intelligent charging patterns. Without PEV-wind synergistic dispatching, the extra wind energy is 3,643.2 kWh. However, the extra wind energy decrease in different degrees when applying the three intelligent charging patterns. The interruptible and the variable charging pattern have the best result in the aspect of accommodating the excessive wind power, and the extra wind energy under both charging patterns is 171.6 kWh. Compare to the other two charging pattern, the

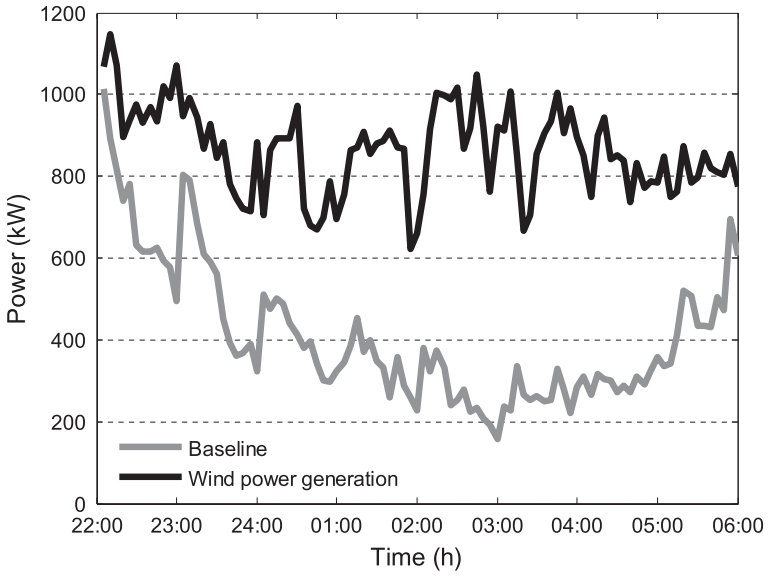

Fig. 9.7 The baseline load profile and wind power generation (from 22:00 to 6:00)

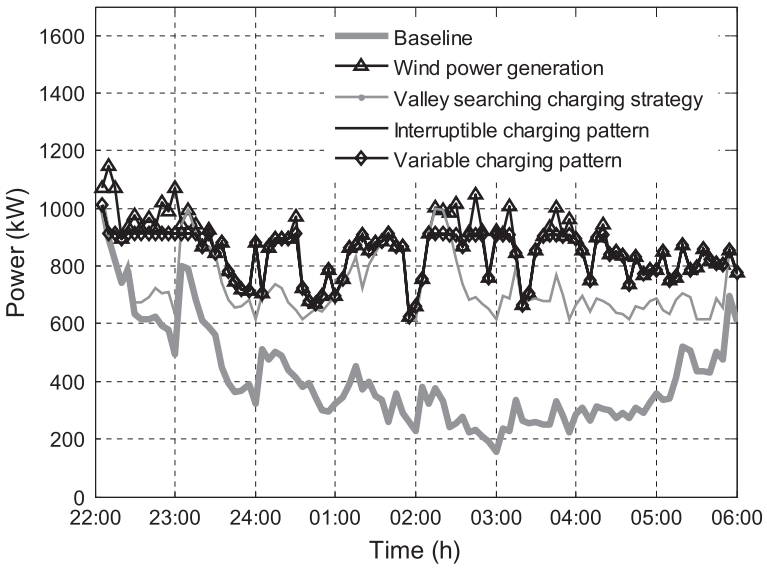

Fig. 9.8 PEV-wind synergistic dispatching load profile in different charging patterns

Table 9.3 Extra wind energy under different charging patterns

No PEVs	PEV-wind synergistic dispatching		
	Valley-searching	Interruptible charging	Variable rate charging
3,643.2 kWh	1,083.6 kWh	171.6 kWh	171.6 kWh

capacity of the valley searching charging pattern in the aspect of accommodating the excessive wind power is worse, and the extra wind energy is up to 1,083.6 kWh.

In the above two case studies, we apply a statistical load model of PEVs charging demand to simulate the driving habits of PEVs users, and then develop the controlled charging, namely demand dispatch based on smart charging of PEVs, in which three smart charging strategies are proposed, such as the valley-searching, the interruptible and the variable-rate charging strategies. Simulation results for a residential area with 1,500 homes show that, compared with the uncontrolled charging scenario, three charging strategies in the demand dispatch charging scenarios can not only reduce the peak load, as well as release the capacity of the electric utility, but also smooth the overall load profile and improve the SD of the PEV owners. The interruptible and variable rate charging strategies have better performance in the peak clipping, flatness of the load profile and high SD of the PEV owners than the valley-searching charging. However, the charging process with the interruptions and variable charging rate might have negative effects on the lifetime of PEV battery. As a future work, we will explore these negative effects result from the two charging strategies. Moreover, we also plan to research the V2G (vehicle-to-grid) capability of PEVs.

9.4.3 Case Study III

We give an overview of the simulation parameters before presenting and analyzing the simulation result. The baseline load profile of a mixed-use area (residence and office) covering the power consumption of user general demand without PEVs over 24 h on a 15-min time basis obtained from [18] is illustrated as the solid line in Fig. 9.9. The rated power of wind turbine generator is set as 1,200 kW, and other parameters, υ_{ci}, υ_r, υ_{co}, are set as 3, 10 and 20 m/s respectively. The forecasted wind speed data are collected from the National Wind Technology Center [32], Boulder, CO and shown as the dashed line in Fig. 9.9.

In our simulation evaluation, it is assumed that the total number of PEVs in the mixed-use area is 500, and all the PEVs are with the same specification where the PEV battery capacity and the power consumption per kilometer are set as 20 kWh and 0.15 kWh respectively. In addition, the rated charging or discharging rate and the maximum charging or discharging rate are $CR = DR = 0.2C$ (4 kW) and $CR_{\max} = DR_{\max} = 0.25C$ (5 kW), respectively.

Forecasted wind power, that can be derived by the forecasted wind speed using the Eq. (9.6), is assumed following a normal distribution with a standard deviation (volatility) of 20 % from the expected value (forecasted wind power generation) [23, 26]. In this work, in total 2,000 scenarios are generated using the LHS method to represent the stochastic nature of the wind power. Firstly, the cumulative distribution for each variable is divided into 2,000 equiprobable intervals. Secondly, we

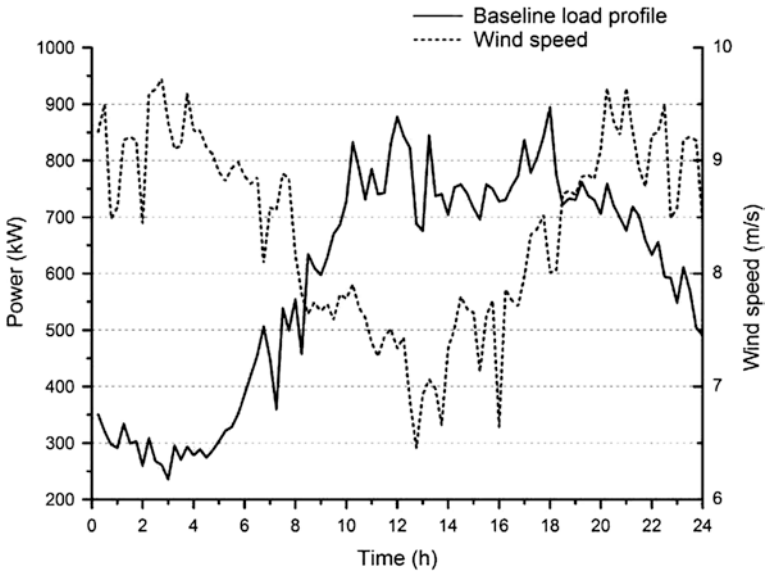

Fig. 9.9 The baseline load profile of a mixed-use area (residence and office)

select a value at each interval randomly, and the sampled cumulative probability at interval j is

$$Prob_j = (1/2,000)r_u + (j-1)/2,000 \tag{9.40}$$

where $r_u \in [0,1]$ is a uniformly distributed random number. Lastly, transform the probability values sampled into the value y using the inverse of the distribution function F^{-1}:

$$y = F^{-1}(Prob) \tag{9.41}$$

Due to the computational complexity, it is necessary to reduce the scenarios to a limited number without losing the stochastic properties of wind power generation. Scenario reduction technique determines a scenario subset and assigns new probabilities to preserved scenarios such that corresponding reduced probability Q is the closest to the original probability P in terms of a certain probability distance between P and Q. The probability distance is defined as a multiplication of the scenario probability and the distance among the scenario values [25, 33]. In this chapter, the number of scenarios is further reduced to 10 using the scenario reduction technique. The detailed data of the reduced scenarios and their probabilities can be derived.

The matching between the power generation and consumption without PEVs considering the volatile wind power is shown in Fig. 9.10a. The wind power generation/consumption within the microgrid (without PEVs) illustrated in a ring-based graph where the different rings represent different power generations/consumptions (from 0 to 1,200 kW) and applied to the rest of the chapter. It can be seen that the power consumption is higher than the power generation in the day time and the load cannot consume the surplus wind power generation at night, which indicates obvious mismatch between the forecasted power generation and power consumption over the day (00:00–24:00 h).

In each scenario x, we can get the power generation and consumption with PEVs under three different coordinated dispatching methods. Then, the final power generation, Gen, and consumption, Con, in each dispatching method considering the volatility of wind power, whose corresponding discharging and charging strategy of PEVs will be adopted in the next day, can be derived by the sum of power generation or consumption in each scenario, Gen_x or Con_x, multiplying their distribution probability of scenario x, π_x, respectively.

$$Gen = \sum_{x=1}^{10} \pi_x Gen_x \tag{9.42}$$

$$Con = \sum_{x=1}^{10} \pi_x Con_x \tag{9.43}$$

Figure 9.10b–d show the matching performance between the power generation and the power consumption with PEVs under three different coordinated dispatching methods whilst considering the uncertainties of the wind power generation.

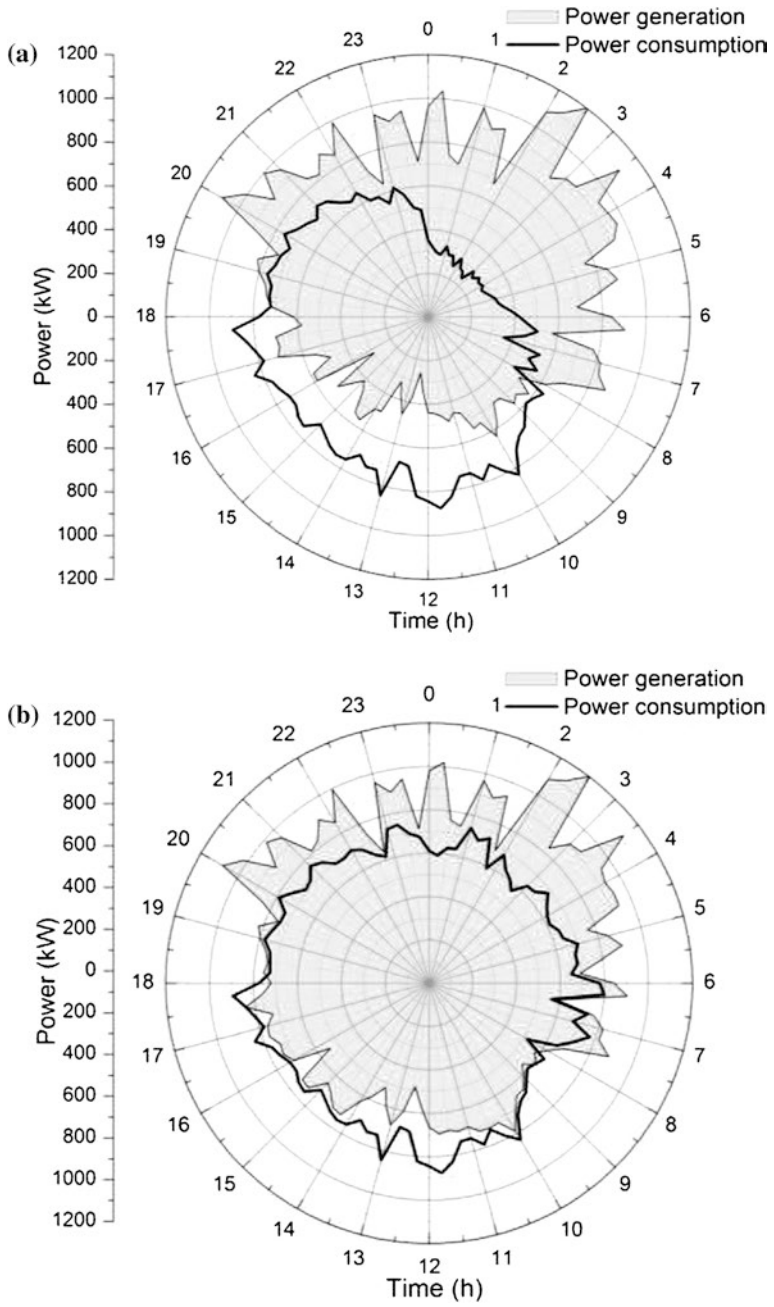

Fig. 9.10 The power generation and consumption matching performance: **a** considering volatile wind power without PEVs, **b** considering volatile wind power with valley-searching dispatching method, **c** considering volatile wind power with interruptible dispatching method, **d** considering volatile wind power with variable-rate dispatching method

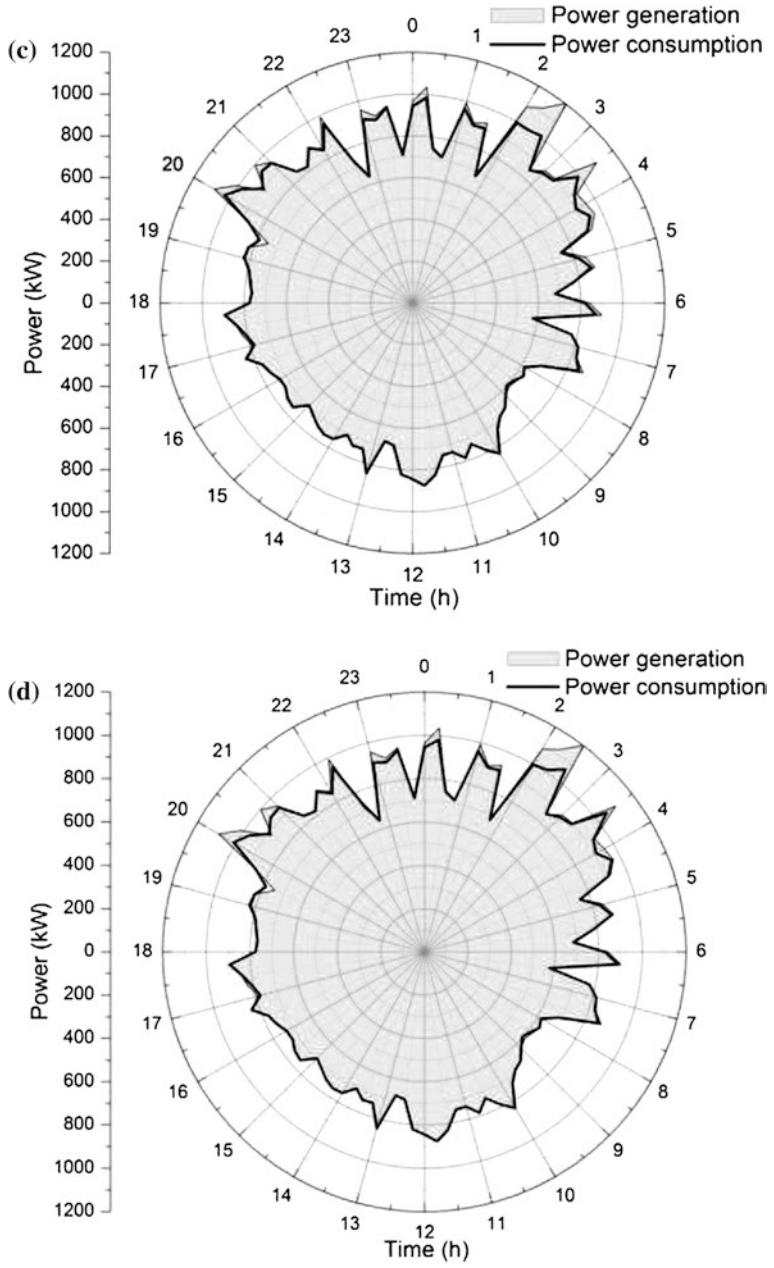

Fig. 9.10 continued

From the above results, we can see that the proposed three dispatching methods can significantly improve the matching performance between the power generation and consumption to different degree by increasing the power generation in the daytime and the power consumption at night through the discharging and charging process of PEVs respectively. Moreover, the latter two methods, the interruptible and variable-rate dispatching methods, provide an enhanced performance. This is due to the fact that the interruptions during the discharging/charging process and the variable rate can provide the PEVs with more flexibility to release energy and supply to the load in the daytime and consume the surplus wind power at night. The good matching performance between power generation and consumption of three dispatching methods indicate that PEVs can efficiently address the problems caused by the intermittent nature of wind power generator, to achieve a delicate and dynamic energy balance within the microgrid.

From another perspective, the abandoned wind energy at night and energy supplied from local grid in the daytime of deterministic (without considering uncertainties of wind power, assuming that the wind power generation can be predicted without errors) and stochastic scenario (considering uncertainties of wind power) under different dispatching methods are shown in Table 9.4. It can be seen that the case without PEVs has the highest abandoned wind energy and the highest energy supplied from grid in both deterministic and stochastic model, which indicate that there is a great waste of energy without PEVs. In the stochastic model, the abandoned wind energy and the energy supplied from grid decrease sharply by using the valley searching method, which is 53.0 and 63.4 % lower than the case without PEVs. The performances of the latter two methods are similar, and variable-rate dispatching method achieves the most optimal performance on minimizing the abandoned wind energy and the energy supplied from the power grid, which is 94.5 and 99.1 % lower than the case without PEVs. The performance result of three proposed methods confirms that PEVs can be considered as flexible units to promote the utilization efficiency of the wind power generation in microgrid. Comparing with the deterministic model, some performance indicators become worse in the stochastic model, such as the abandoned wind energy in valley-searching method sees an 18 % growth and the energy supplied from grid under three different coordinated dispatching methods increase from 665.7, 21.7, 0 kW to 760.4, 38.4 and 21.5 kW respectively. However, the stochastic solution can be feasible for all wind power scenarios in next day.

Table 9.4 Abandoned wind energy at night and energy absorbed from local grid in the daytime under different wind-PEV synergistic dispatching methods

Scenario	Abandoned wind energy		Energy supplied from grid	
	D (kWh)	S (kWh)	D (kWh)	S (kWh)
No PEVs	5,477.5	5,441.9	2,460.7	2,482.1
Valley-searching	2,168.5	2,559.8	665.7	760.4
Interruptible	345.5	319.4	21.7	38.7
Variable-rate	327.2	298.1	0	21.5

Note "D": deterministic scenario and "S": stochastic scenario

Table 9.5 The satisfaction of PEV owners under three dispatching methods

Scenario	Valley-searching		Interruptible		Variable-rate	
	D (%)	S (%)	D (%)	S (%)	D (%)	S (%)
ASD	55.35	55.21	100	99.83	100	99.92

Note "D": deterministic scenario and "S": stochastic scenario

Finally, from the PEV user's perspective, the PEV timely and fully charging is an important consideration. In this section, we adopt the satisfaction degree of PEVs owners to evaluate the proposed three dispatching methods [34]. The satisfaction degree of the *i*th PEV owner is defined as a percentage of real charged energy allocated to PEV i, E_i^{real}, over the total energy demand of this PEV, E_i^{total}, to make it fully charged.

$$SD_i = (E_i^{\text{real}} \Big/ E_i^{\text{total}}) \cdot 100\,\% \tag{9.44}$$

Table 9.5 gives the values of average satisfaction degree (ASD) among all PEVs owners of deterministic and stochastic models for different coordinated energy dispatching methods. In the deterministic model with the forecasted wind power, it can be seen that the ASD is only 55.35 % by using the valley-searching dispatch methods. However, the 100 % vehicle owners' satisfaction can be achieved when applying the latter two dispatching methods. This is due to the fact that the fixed discharging/charging rate and the continuity of the discharging/charging process limit the flexibility of PEVs' discharging/charging process. Furthermore, the ASD under all the three dispatching methods in the stochastic scenario decrease to different degrees comparing that in deterministic scenario respectively

9.5 Chapter Summary

In this chapter, we exploited the potential of flexible PEV control on its charging/discharging behavior with volatile wind power to optimize the energy dispatching within the microgrid for balancing the power generation and demand whilst meeting the PEV user requirements. By adopting the existing a statistical model of driving behaviors of PEV owners as well as scenario generation and reduction technique of volatile wind power generation, we proposed three coordinated energy dispatching methods, i.e. the valley searching, interruptible and variable-rate dispatching methods, to leverage the power generation and the power demand (including PEVs) in a microgrid environment. A set of numerical simulation experiments for a mixed-use area were carried out to evaluate the proposed dispatching algorithm solutions. The result shows that the matching performance between power generation and consumption were improved to different degrees when using three dispatching methods. Moreover, the latter two dispatch methods, in particular, the variable-rate dispatching, have better performance from the

aspects of decreasing abandoned wind energy at night, reducing the energy supplied from grid in the daytime as well as improving the satisfaction degree of PEVs owners. These suggested energy dispatching solutions can be implemented and deployed in practice with minimal technical hurdles. Although some performance indicators, such as ASD and energy supplied from grid, in the stochastic model become worse than that in the deterministic model with the forecasted wind power, the stochastic solution can be feasible for all wind power scenarios in next day. Finally, it is also worth noting that although the microgrid model exploited in this chapter only considered the scenario with distributed wind power generation and PEVs, the presented dispatching methods can be easily extended for scheduling other generation/responsive loads in microgrid.

In respect to the future work, we consider a number of technical challenges still outstanding which need further research effort. The discharging or charging process with the interruptions and variable rate may have negative effects on the lifetime of PEV battery, which needs further research and trial assessments to understand the trade-off between the technical benefits and the potential adverse impact. In addition, the dynamical electrical prices in microgrid system with distributed renewable generations is a paramount consideration which need to be studied in promoting the demand side management in. we aim to further evaluate the suggested dispatching method in the test power networks to validate its effectiveness and economical benefits.

References

1. Yang Q, Laurenson DI, Barria JA (2012) On the use of LEO satellite constellation for active network management in power distribution networks. IEEE Trans Smart Grid 3(3):1371–1381
2. Lu X, Iyer KL, Mukherjee K, Kar NC (2012) A wavelet/PSO based voltage regulation scheme and suitability analysis of copper-and aluminum-rotor induction machines for distributed wind power generation. IEEE Trans Smart Grid 3(4):1923–1934
3. Ashabani SM, Mohamed Y (2012) A flexible control strategy for grid-connected and islanded microgrids with enhanced stability using nonlinear microgrid stabilizer. IEEE Trans Smart Grid 3(3):1291–1301
4. Sundstrom O, Binding C (2012) Flexible charging optimization for electric vehicles considering distribution grid constrains. IEEE Trans Smart Grid 3(1):26–37
5. Duvall M (2008) Plug-In hybrids on the horizon-building a business case. Electr Power Res Inst (EPRI), 6–15
6. Sortomme E, El-Sharkawi MA (2011) Optimal charging strategies for unidirectional vehicle-to-Grid. IEEE Trans Smart Grid 3(1):131–138
7. Karki R, Thapa S, Billinton RB (2012) A simplified risk-based method for short-term wind power commitment. IEEE Trans Smart Grid 3(3):498–505
8. Mohod SW, Aware MV (2012) Micro wind power generator with battery energy storage for critical load. IEEE Syst J 6(1):118–125
9. Ekman CK (2010) On the synergy between large electric vehicle fleet and high wind penetration- an analysis of the Danish case. J Renew Energy 32(2):546–553
10. Clement-Nyns K, Haesen E, Driesen J (2011) The impact of vehicle-to-grid on the distribution grid. J Electr Power Syst Res 81(1):185–192
11. Göransson L, Karlsson S, Johnsson F (2010) Integration of plug-in hybrid electric vehicles in a regional wind-thermal power system. J Energy Policy 38(10):5482–5492

12. Wang JH, Liu C, Ton D et al (2011) Impact of plug-in hybrid electric vehicles on power systems with demand response and wind power. J Energy Policy 39(7):5482–5492
13. Li ZS, Sun HB, Guo QL, Wang X (2011) Study on wind-EV complementation on the transmission grid side considering carbon emission. J Proc CSEE 32(10):41–48
14. Yilmaz M, Krein PT (2013) Review of battery charger to topologies, charging power levels, and infrastructure for plug-in electric and hybrid vehicles. IEEE Trans Power Electron 28(5):2151–2169
15. Soares J, Morais H, Sousa T, Vale Z, Faria P (2013) Day-ahead scheduling including demand response for electric vehicles. IEEE Trans Smart Grid 4(1):596–605
16. Derakhshandeh SY et al (2013) Coordination of generation scheduling with PEVs charging in industrial microgrids. IEEE Trans Power Syst 28(3):3451–3461
17. Kempton W, Tomic J (2005) Vehicle-to-grid power fundamentals: calculating capacity and net revenue. J Power Sources 144(1):268–279
18. Tian LT, Shi SL (2010) A statistical model for charging power demand of electric vehicles. J Power Syst Technol 34(11):126–130
19. Cao YJ, Tang SW, Li CB et al (2012) An optimized EV charging model considering TOU price and SOC curve. IEEE Trans Smart Grid 3(1):388–393
20. Liu C, Wang JH, Botterud A et al (2012) Assessment of impacts of PHEV charging patterns on wind-thermal scheduling by stochastic unit commitment. IEEE Trans Smart Grid 3(2):388–393
21. Chedid R, Akiki H, Rahman S (1998) A decision support technique for the design of hybrid solar-wind power systems. IEEE Trans Energy Convers 13(1):76–83
22. Wang MQ, Gooi HB (2011) Spinning reserve estimation in microgrids. IEEE Trans Power Syst 26(3):1164–1174
23. Wang JH, Shahidehpour M, Li ZY (2008) Security-constrained unit commitment with volatile wind power generation. IEEE Trans Power Syst 23(3):1319–1327
24. Wyss GD, Jorgensen KH (2008) A user's guide to LHS: sandia's latin hypercube sampling software, technical report SAND98-0210. Sandia National Laboratories, Albuquerque
25. Dupacova J, Growe-Kuska N, Romisch W (2003) Scenario reduction in stochastic programming: an approach using probability metrics. Math Prog B 95(3):493–511
26. Xu LZ, Yang GY, Xu Z, Dong ZY et al (2011) Combined scheduling of electricity and heat in a microgrid with volatile wind power. Autom Electr Power Syst 35(9):53–60
27. Lassila J, Haakana J, Tikka V, Partanen J (2012) Methodology to analyze the economic effects of electric cars as energy storages. IEEE Tran Smart Grid 3(1):506–516
28. Soroudi A, Caire R, Hadjsaid N, Ehsan M (2011) Probabilistic dynamic multi-objective model for renewable and non-renewable distributed generation planning. IET Gener Transm Distrib 5(11):1173–1182
29. Soroudi A, Ehsan M, Caire R, Hadjsaid N (2011) Possibilistic evaluation of distributed generations impacts on distribution networks. IEEE Trans Power Syst 26(4):2293–2301
30. Soroudi A, Ehsan M (2013) IGDT based robust decision making tool for DNOs in load procurement under severe uncertainty. IEEE Trans Smart Grid 4(2):886–895
31. Soroudi A, Amraee T (2013) Decision making under uncertainty in energy systems: state of the art. Renew Sustain Energy Rev 28:376–384
32. National Renewable Energy Laboratory (NREL) National Wind Technology Center (NWTC), Boulder, CO. http://www.nrel.gov/midc/nwtc_m2/
33. Growe-Kuska N, Heitsch H, Romisch W (2003) Scenario reduction and scenario tree construction for power management problems. In: Proceedings of IEEE power technology. Italy, pp 23–26
34. Francesco A, Gregorio C (2011) Impact of charging efficiency variations on the effectiveness of variable-rate-based charging strategies for electric vehicles. J Power Sources 196(22):9574–9578

Chapter 10
Effects of PEV Penetration on Voltage Unbalance

Ahmed M.A. Haidar and Kashem M. Muttaqi

Abstract Balancing loads in low voltage networks is a challenging task due to a continuous fluctuation in the power demand. Voltage unbalance is a condition in which the voltage phasors differ in amplitude and/or do not have its normal 120° phase relationship. This has a potential to introduce technical issues that lead to a costly phenomenon for power distribution system due to the high penetration of Plug-in Electric Vehicles (PEVs). Voltage unbalance study is essential as the propagation of zero sequence component in the distribution system is limited by transformer winding connections and network grounding. Indeed, single phase loads are not affected by unbalance unless the unbalance causes over or under voltages which exceed the acceptable limits. However, the large numbers of PEVs charging from single phase residential feeders of distribution networks may exceed the statutory limits. This chapter presents theoretical discussion with analytical framework for modeling the effects of voltage unbalances due to PEV penetration. A PEV charging profile of a conventional PEV battery has been employed with the daily load demand to synthesize the dynamic effect of PEV penetration. A distribution network topology has been used with unbalanced allocation of single-phase loads and PEVs connected in four-wire, three phase network to investigate the effects of PEV charging on the feeders subject to voltage unbalance. Furthermore, the chapter explores the application of PEV load balancing strategy in the context of smart grid to mitigate the effects of unbalanced allocation of PEVs.

Keywords Plug-in electric vehicle · Voltage unbalance factor · PEV load balancing · Low voltage distribution

A.M.A. Haidar (✉) · K.M. Muttaqi
Australian Power Quality and Reliability Centre, School of Electrical, Computer and Telecommunications Engineering, University of Wollongong, Wollongong, NSW 2522, Australia
e-mail: ahaidar@uow.edu.au

K.M. Muttaqi
e-mail: kashem@uow.edu.au

S. Rajakaruna et al. (eds.), *Plug In Electric Vehicles in Smart Grids*, Power Systems, DOI 10.1007/978-981-287-299-9_10

10.1 Introduction

Integration of PEVs is increasing in the residential Low Voltage (LV) distribution systems. The growth of PEVs is driven by global greenhouse gas abatement efforts and oil prices due to the higher consumption of petrol and diesel in the transportation sector. The charging of PEV is often referred to Grid to Vehicle (G2V). Voltage unbalance in low voltage distribution networks can be increased due to the unbalanced allocation of customer loads, unplanned and random charging of PEVs in the networks, and lack of prior information of their normal capacity and the time of their charging. Therefore, it is a high interest to investigate the unbalance of voltage caused by the PEV integration in power grids. In general, voltage unbalance is more common in low voltage due to the phase load unbalance, and it can be severe if large single-phase power loads are used [1]. The most vulnerable loads to unbalance are three phase motors. These motors will experience increased heating, noise, vibration and a loss of efficiency. Although voltages are well balanced at the source point, the voltages at the end users can become unbalanced due to the unequal distribution of the single-phase loads, and asymmetry in line impedances or single wire earth return (SWER) systems [2, 3].

PEVs significantly increase the load on the grids, much more than the load seen in a typical distribution feeder. The level of their impact depends on their degree of penetration, charging capacity and the time in the day they are charged or discharged. Any deviation due to uncoordinated EV charging can impose more burden in the form of unbalance voltage which is regarded as a power quality problem, transformer overloading, power losses and damage to electrical network equipment leading to a financial penalty for the power grid utilities. An excessive level of voltage unbalance presents a potential problem to power distribution networks and can have serious impacts on mains connected induction motors such as overheating and de-rating of the all induction motor types of loads [4, 5]. Voltage unbalance can also affect the AC variable speed drive systems and an increase in its level will cause network problems such as mal-operation of protection relays and voltage regulation equipment. Moreover, the unbalance voltage can result in generation of non-characteristic harmonics from power electronic loads, especially in low voltage customer loads due to the phase load unbalance [4].

In addition to the legacy of load and network unbalance, a high penetration of single phase PEVs, can worsen the classical neutral current and voltage problems. PEVs could therefore have a disruptive impact on low voltage power grids if not integrated carefully, and this impact depends on their market penetration. PEV characteristics require an expansion or modification to network structure, policies, control and protection. Hence, there is a need to determine whether the current grid meets the standard energy requirements of PEVs in order to evaluate the grid capability of handling a massive PEV penetration. With an increase in the level of single phase PEV penetration, phase domain analysis is essential for examining the load unbalance and network asymmetries, and to assess the impacts of single-phase on board PEV chargers that charge the PEV battery directly from

three-phase distribution networks. Thus, analysis of network behavior under PEV penetration is essential for understanding the impacts on voltage unbalance mainly when a large number of single-phase residential solar photovoltaic (PV) are integrated in the low voltage distribution systems [6].

The conventional trial and error practical approach is not effective for phase arrangement aiming to balance the load in each feeder section of the networks. Therefore, an effective algorithm is needed to improve the unbalance and optimal operation of the networks. The optimization of the phase arrangement in distribution transformers has been introduced in [7–9] for system unbalance improvement and loss reduction. A genetic algorithm-based approach was proposed to solve a multi-objective optimization problem that provides balancing the phase loads, improving the phase voltage unbalances and reducing the neutral current for a radial-type distribution feeder [7]. The statistical estimation of the source and level of voltage unbalance in distribution networks have been investigated in [8]. A framework developed by authors in [8] for performing three-phase state estimation on a network where the measurement information is incomplete. In this approach, the level, location and effect of unbalance on a typical distribution network have been estimated. Unbalance voltage has been considered in the development of three phase optimal power-flow solution [9]. The proposed method in [9] uses the primal-dual interior point method as an optimization tool in association with the three-phase current injection method in rectangular coordinates where a set of nonlinear equations was solved by applying the Newton-Raphson method. A matrix-based methodology was used to evaluate the influence of line asymmetries on the global emission and its dependency on various load types [10]. However, the assessment presented in [10] has only addressed the global voltage unbalance based on the IEC/TR 61000-3-13 guidelines in medium voltage power systems arising as a result of line asymmetries.

Voltage unbalance, which can be associated with negative and zero sequence components, lead to increased longitudinal losses of active power and energy in power grid, and therefore lower efficiency of distribution systems [1]. Some practical techniques are used to reduce the limit of voltage unbalances as listed in [1], such as balanced repartition of single-phase loads, connecting unbalanced loads into higher voltage lines, balancing circuits through single-phase transformers or reactive power compensation balanced controllers developed based on self-commutated converters technology (e.g. Static Compensator or STATCOM). However some of these approaches may not be practically achievable and would be highly capital intensive, as it would incur additional materials and construction costs over multiple locations in a distribution feeder. As the problem of voltage unbalance is unavoidable and became a critical issue mainly with the integrating process of small size distributed generation in low voltage networks, several traditional methods have been proposed for the load unbalance mitigation of neutral current and voltage problems caused by rooftop PV as reported in [11]. The authors in [11] analyzed the limitations of the traditional methods for mitigating load unbalance caused by rooftop PV and developed a method based on the application of energy storage to balance the power injections into the grid and the power

imports from the grid, by controlling the storage charging and discharging operations. A phase identification system was designed in [12] to incorporate a fuzzy microprocessor based controller for phase measurement of transformers to support three-phase load balance of distribution feeders. Authors of [13–16] have studied the effect of PEV penetration on power quality in terms of harmonics, voltage profile and overloading. Nevertheless, a specific study about the effect of PEV on voltage unbalance mitigation considering the realistic characteristic of PEV loads with its connection time has not been received any attention yet. Though in [17, 18] the voltage unbalance impacts of PEV penetration in residential networks was analyzed, however, the authors did not address the PEV characteristics and the behavior of battery chargers used in PEVs. In this study, the above research gaps have been addressed and methodologies proposed to analyze and mitigate the PEV effects on voltage unbalance in the distribution networks.

10.2 Theoretical Aspects of Voltage Unbalance and Impacts of PEV Penetration

It is well known that voltages at high voltage connection points between transmission and distribution systems are generally regulated to have a balanced system. However, the major source of unbalance in the network is typically at lower level of distribution voltages. Though the distribution systems are not fully transposed, due to short line lengths, the small unbalanced impedances do not introduce a significant unbalance in such systems [19]. Recently, PEVs have been gaining worldwide interest as a promising potential for long-term solution to sustainable personal mobility caused by high fuel prices, increased greenhouse gas emissions, and social awareness of environmental threats. Thus, it is expected that large number of EV loads connected to distribution network whose characteristic and connection status varies with time causing to the changes in load demand in different phases of the LV feeders that may results in severe unbalance problem in distribution networks. Therefore an asymmetrical allocation of PEVs and increase of their penetration in low voltage systems will form the major source of unbalance that may propagate to the whole power system.

In a balanced sinusoidal supply system, the three-phase (line-neutral) voltages are equal in magnitude and are phase displaced from each other by 120° as seen in Fig. 10.1. Owing to unpredictable charging activities of PEVs in the three phase (line-neutral) voltages, the differences will exist in the three voltage magnitudes and/or a shift in the phase separation from 120° especially when the level of PEV penetration is high and this gives rise to an unbalanced supply as seen from Fig. 10.2. An example of a three-phase system containing m number of buses in which the base load connected with PEV loads is shown in Fig. 10.3a and the neutral voltage produced by the combined effect of the base load and PEV is shown in Fig. 10.3b. To quantify the effect of a high PEV penetration, the sizes of the PEVs are assumed to be distributed randomly as seen in Fig. 10.3a. As a result, the sum

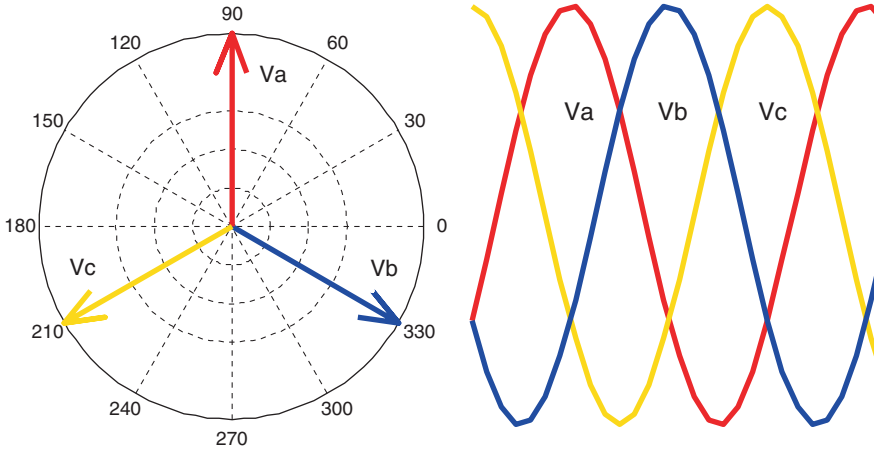

Fig. 10.1 Phasors and waveforms of a balanced three phase system

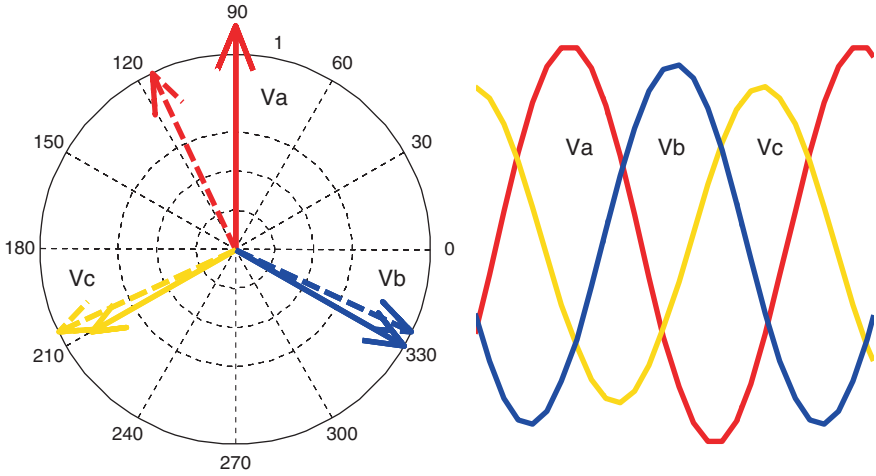

Fig. 10.2 Phasors and waveforms of an unbalanced three phase system

of the household loads including PEV loads at different phases will become unbalanced. Therefore, a neutral voltage "V_n^N" as given in Eq. (10.1) will be produced due to unbalanced PEV charging loads combined (com) with the base load especially during peak load demand.

$$V_n^N = V_a^{com} + V_b^{com} + V_c^{com} \tag{10.1}$$

As the definitions of unbalanced three-phase currents are analogs to those of unbalanced three-phase voltage, V_n^N can be expressed in terms of neutral current I_n^N for the base load and PEV load, as given by,

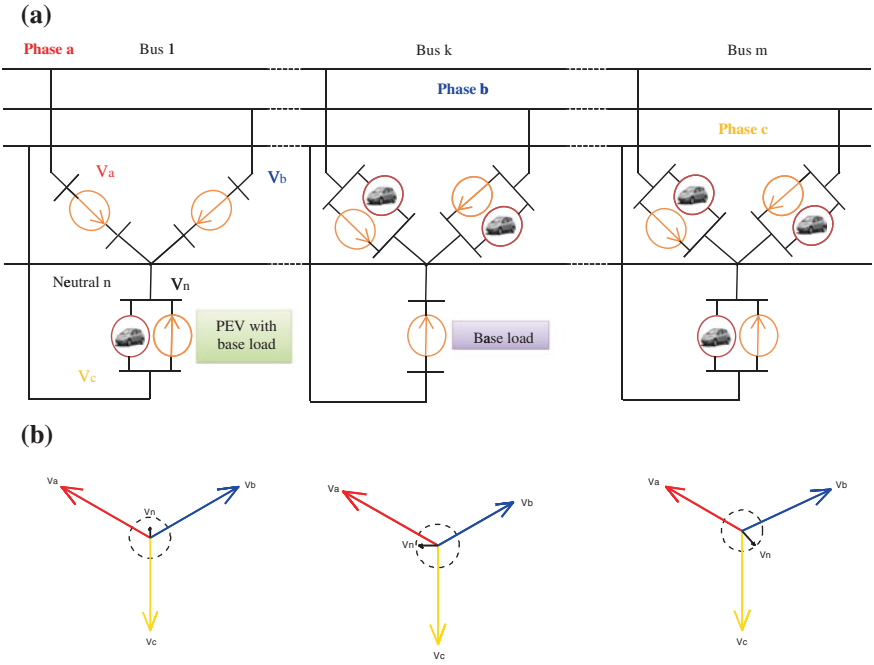

Fig. 10.3 **a** Customer voltages at three phase LV distribution system where the base loads are combined with PEV loads, **b** the voltage phasor diagram of the combined loads

$$I_n^N = I_n^{BL} + I_n^{EV} \tag{10.2}$$

where,

$$\left\{ \begin{array}{l} I_n^{BL} = I_a^{BL} + I_b^{BL} + I_c^{BL} \\ I_n^{EV} = I_a^{EV} + I_b^{EV} + I_c^{EV} \end{array} \right\} \tag{10.3}$$

Here, I_a^{BL}, I_b^{BL}, I_c^{BL} are the current of the base load at phase a, b and c respectively; I_a^{EVL}, I_b^{EVL}, I_c^{EVL} are the current of the PEV load at phase a, b and c respectively. Depending on the level of unbalance due to PEV plugged anywhere along the feeders and phases, the magnitudes and angles of the neutral current "I_n^N" will vary, thereby, varying in the neutral voltage "V_n^N". Figure 10.3b shows that the resultant neutral voltage obtained from vector addition can be lower or higher depending on their magnitudes and angular difference.

The voltage phasor diagram of the system in Fig. 10.3a is shown in Fig. 10.4 for unbalance system caused by PEVs (dot line), while the balance system (before PEVs connected into the system) is given in solid line. It is seen from this figure that the phase voltages of a balanced system are equally displaced from each other with 120°. On the other hand, the voltages become unbalanced with a phase shifting when PEVs are randomly allocated and penetrated in the distribution system. It is important to take

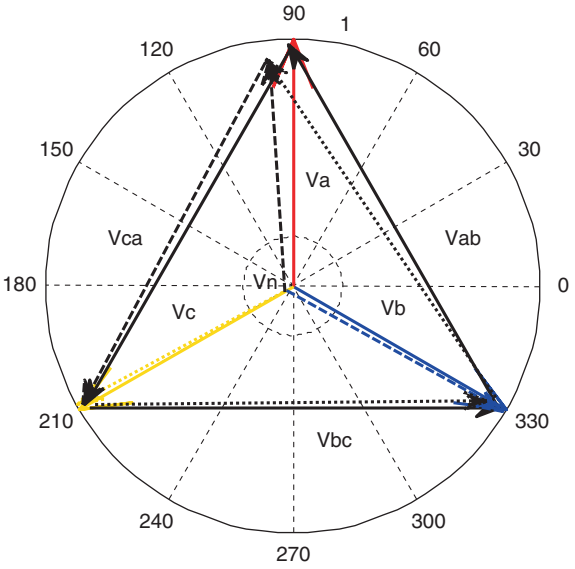

Fig. 10.4 A three-phase voltage phasor diagram of balanced and unbalanced systems

into account that connecting a poly-phase induction motor into an unbalanced three phase system will result in unbalanced current in the stator winding. This will lead to a reduction in motor efficiency while reducing the insulation life caused by overheating. Clearly in such situations, the induction motor will be noisy in its operation caused by torque and speed pulsations [4]. While it is difficult to provide a perfectly balanced system due to the unpredictable PEV loads, every attempt has to be taken to minimize the voltage unbalance to reduce its effects on the whole system. Thus, this chapter will suggest for using a PEV load balancing strategy in this purpose. The strategy assumes that PEVs are charged from its nominal charging rate. According to this strategy, it is required that the distribution of the PEVs across the low voltage three phase feeder should not be a cause of higher voltage unbalance and therefore the PEV charging should be de-rated depending on the level of unbalance. For instance, for the home charging level "1", if the unbalance is higher than the acceptable limit, the PEVs that have been already charged above 80 % state of charge (SOC) on the loaded feeders should be disconnected and reconnected as the level of voltage unbalance factor (VUF) is decreased. In other words, vehicles having a lower SOC should have a higher chance of charging from the grid than the vehicles with a higher SOC.

10.3 Theoretical Models for the Analysis of Unbalanced Voltage

To date, four methods (which are National Electrical Manufacturers Association "NEMA", Institute of Electrical and Electronics Engineering "IEEE", International Electrotechnical Commission "IEC" and International Council for Large Electric

Systems "CIGRE") have been developed by the power community for quantifying voltage unbalances. However, the accurate method that is best reflecting the configuration of the system is the symmetrical components method (IEC) which relies on the Fortescue theorem [20–22]. The four methods with their definitions are discussed in this section.

According to the symmetrical components method, the theoretical basis for the analysis of unbalance in a three-phase system follows from the transformation of phase-domain components to sequence-domain components [23]. Considering an unbalanced system, the Fortescue method of symmetrical components represents the relationship between the initial system and the symmetrical sequence systems for a set of line to neutral voltage is given in Eq. (10.4) and shown in Fig. 10.5.

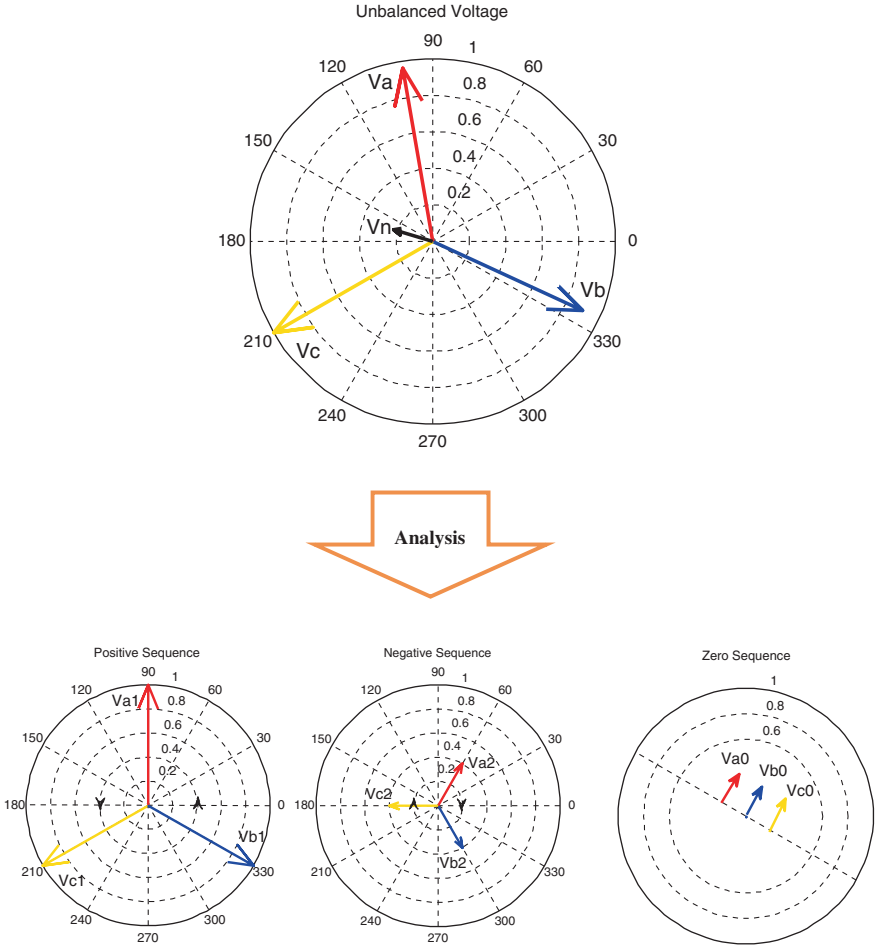

Fig. 10.5 Decomposition of an unbalanced voltage system in three balance phasor domain

$$\begin{bmatrix} V_a \\ V_b \\ V_c \end{bmatrix} = \begin{bmatrix} 1 & 1 & 1 \\ 1 & a^2 & a \\ 1 & a & a^2 \end{bmatrix} . \begin{bmatrix} V_0 \\ V_1 \\ V_2 \end{bmatrix} \tag{10.4}$$

The reverse relationship of Eq. (10.4) can be written as follows:

$$\begin{bmatrix} V_0 \\ V_1 \\ V_2 \end{bmatrix} = {}^1\!/_3 \begin{bmatrix} 1 & 1 & 1 \\ 1 & a & a^2 \\ 1 & a^2 & a \end{bmatrix} \cdot \begin{bmatrix} V_a \\ V_b \\ V_c \end{bmatrix} \tag{10.5}$$

where, the rotation operator (Fortescue operator "a") is given by $a = e^{j120^\circ}$ ($a = 1 \angle 120$); V_a, V_b and V_c are the line to neutral voltage phasors with their zero (V_0), positive (V_1) and negative (V_2) sequence voltage phasors respectively. The negative and zero sequence systems would be absent in a balanced system. The sequence systems as detailed above are not only theoretical but also correspond to the reality. The physical interpretation of these sequences (an example for motor) show that the direction of rotation of a three-phase induction motor is opposite when applied with a negative sequence set, while it will not rotate when applied with a zero sequence set as there is no displacement between the three voltages and therefore there will be no rotating magnetic field [4, 5, 24]. Equation (10.4) can be applied for line voltages in a similar way, however, having no zero sequence in the line voltages, the line voltages can be obtained from the positive and negative sequence systems by,

$$\begin{bmatrix} V_{ab} \\ V_{bc} \\ V_{ca} \end{bmatrix} = \begin{bmatrix} 1 & 1 \\ a^2 & a \\ a & a^2 \end{bmatrix} \cdot \begin{bmatrix} V_1 \\ V_2 \end{bmatrix} \tag{10.6}$$

Knowledge of how and to what extent voltage unbalance influences the steady-state performance of distribution system has been discussed in many studies [4, 5, 20, 22, 24–26]. The commonly used definitions to specify the level of voltage unbalance as detailed by NEMA, IEEE, IEC and CIGRE [20] provide different ways to calculate the voltage unbalance. The NEMA and the IEEE definitions for voltage unbalance are approximations and avoid the use of complex algebra. Generally speaking, the calculation of voltage unbalance using NEMA and IEEE definitions are convenient to use with field measurements as these methods involve only the measurement of voltage magnitudes [25]. They were created based on the fact that the available electricity meters were not able to measure the angular differences between each phase. On the other hand, the disadvantage of using these definitions is the loss of phase angle information, which could result in a high error under extreme conditions of the measured system. The CIGRE definition employs simple algebra and only needs the magnitudes of the voltages between phases and its results are more accurate compared to NEMA and IEEE definitions [26, 27]. The IEC is the most accurate, because it uses the ratio of negative sequence to positive sequence voltage. The respective differences for each definition are illustrated below [4, 20, 22].

10.3.1 NEMA Definition

The NEMA definition is known as line voltage unbalance rate (LVUR) which is an approximate expression as given by,

$$LVUR\,(\%) = \frac{\Delta V_{line-line}^{\max}}{V_{line-line}^{avg}} \times 100 \tag{10.7}$$

where, $\Delta V_{line-line}^{\max}$ is the maximum voltage deviation from the average line voltage magnitude; and $\Delta V_{line-line}^{avg}$ is the average line voltage magnitude.

10.3.2 IEEE Definition

The IEEE definition is known as phase voltage unbalance rate (PVUR) that is given by,

$$PVUR\,(\%) = \frac{\Delta V_{phase}^{\max}}{V_{phase}^{avg}} \times 100 \tag{10.8}$$

where, $\Delta V_{phase}^{\max}$ is the maximum voltage deviation from the average phase voltage magnitude; ΔV_{phase}^{avg} is the average phase voltage magnitude. IEEE definition for PVUR approximation is simpler for everyday application because it applies line to line voltage measurement only. It is not different to the NEMA definition except for the use of the phase voltages instead of line voltage.

10.3.3 IEC Definition

The IEC definition is widely used in European standards and known as the VUF. In this definition, the symmetrical components are generally employed in which, the voltage unbalance can be decomposed into three balanced systems which are called positive sequence, negative and zero sequence as detailed earlier in this section and represented in Eq. (10.5). The IEC definition is given by,

$$VUF\,(\%) = \frac{V_2}{V_1} \times 100 \tag{10.9}$$

The positive sequence can also be found by (10.10) and negative sequence by (10.11)

$$V_1 = \frac{V_{ab} + aV_{bc} + a^2V_{ca}}{3} \tag{10.10}$$

$$V_2 = \frac{V_{ab} + a^2V_{bc} + aV_{ca}}{3} \tag{10.11}$$

where, V_{ab}, V_{bc} and V_{ca} are the three line voltages.

The advantage of using the VUF as an index for analysing the effects of voltage unbalance is explained in [5]. Usually, positive-sequence component of three-phase voltages is very close to rated value, if expressed the component of sequences in per-unit (pu) quantities, the positive-sequence voltage will be very close to 1.0 pu, and the corresponding negative-sequence voltage will be very close to the VUF. Therefore, the negative-sequence component in per-unit can be considered as the VUF. Since VUF is considered as an accurate index, this index will be used in this chapter to quantify the effect of PEV penetration on voltage unbalance.

10.3.4 CIGRA Definition

The CIGRA definition employs a simple algebra but results in a better approximation. It is also known as the VUF and can be expressed in a more user-friendly form as given by,

$$VUF\ (\%) = \sqrt{\frac{1 - \sqrt{3 - 6\alpha}}{1 - \sqrt{3 - 6\alpha}}} \times 100 \tag{10.12}$$

where,

$$\alpha = \frac{V_{ab}^4 + V_{bc}^4 + V_{ca}^4}{(V_{ab}^2 + V_{bc}^2 + V_{ca}^2)^2} \tag{10.13}$$

10.4 PEV Charging Specific to Single-Phase Applications

The simple conceptual diagram of PEV charging system is shown in Fig. 10.6, where the first stage is AC to DC converter connected into power grid and the next stage is DC to DC converter connected with the battery pack terminal. The battery will be plugged into the battery charger for charging, and PEV batteries are quite different from those used in small electronic devices. These PEV batteries are required to

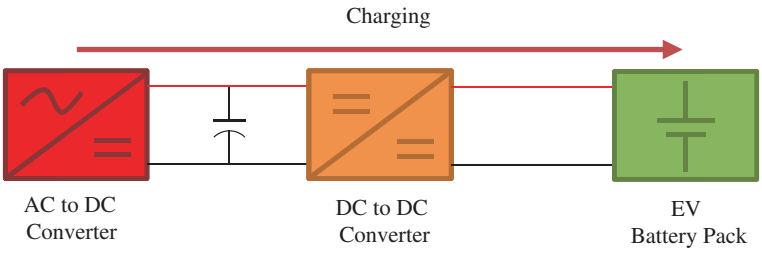

Fig. 10.6 A simple conceptual diagram of PEV charging system

handle high power and high energy capacity (up to tens of kWh) [28, 29]. The charging of PEVs from single-phase supplies, such as households (which is feed from three phase low voltage networks), can result in voltage unbalance. The effects on the phase unbalance could be significant when many PEVs are charging randomly because PEVs are acting as changeable and moveable loads and this may cause a higher level of voltage unbalance outside the limit [17]. Therefore, special attention should be given to the modeling of charging process of PEV by considering the true behavior of different types of batteries, their charging profile and their technologies.

Lithium batteries have many features that may make them attractive for PEV than other types of batteries because they are rated for much higher charge and discharge powers, allowing them to meet sudden power demands [30]. Battery SOC is the gauge that is used to understand the amount of charge that can propel the vehicle with electric power. In many designs and studies related to PEV battery chargers, the PEV battery loads are considered as a static load and the realistic system behavior of the batteries during charging process have been ignored. Indeed, the energy consumption by a PEV is a function not only of the terminal voltage but also of other variables governed by the battery SOC due to the changes in charging rate [31]. Furthermore, the voltage dependency of the charging is a function of SOC and this can cause different load characteristics for different SOC levels and the input current can vary depending on the capacity of the battery, charger parameters and the level of SOC as seen from Fig. 10.7 [28, 29].

The charging profile in Fig. 10.7 indicates without hesitation that a high penetration of uncoordinated PEVs with deferent charging characteristic would result in an increase in voltage unbalance particularly at peak hours and can cause problems such as extra power losses, voltage deviations and overloading of transformer

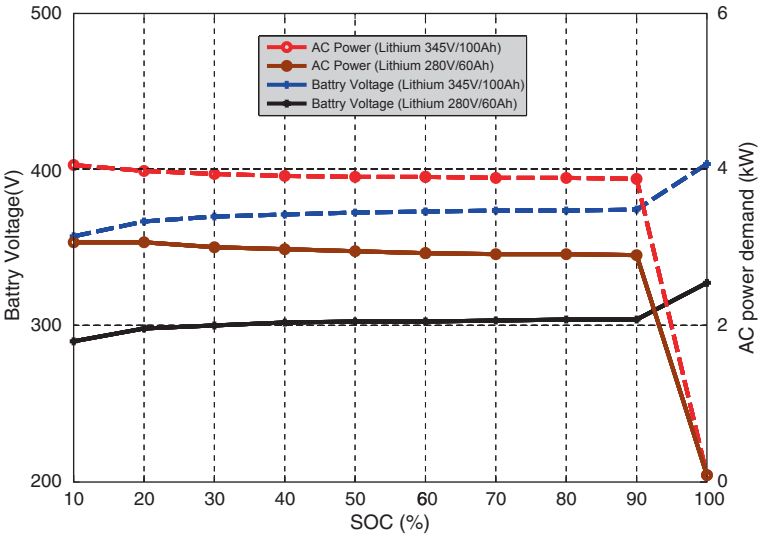

Fig. 10.7 Battery voltage and AC power demand of lithium battery as a function of SOC

winding which can become a serious issue when a number of PEVs with different SOCs and battery types are connected to a distribution transformer [32]. To deal with such problems, one approach is to upgrade the distribution transformers in the substations. However, upgrading these distribution transformers will require new resources and investments. Instead of installing additional transformer capacity, another possible approach is to perform demand management, which can be accomplished by direct load control program (curtailment actions on the demand side) or real-time smart load management. The demand management approach can be built upon the existing infrastructures of distribution system and it is mainly a software-based solution which is more cost effective than upgrading distribution transformer. However, the biggest concern is how to convince the owners that charging should be 100 % at the whim of electricity utilities. Therefore, time of use electricity rate structure should be adopted to reflect the existence and possible introduction of new policies to encourage PEV owners to recharge vehicles during the off-peak time so that PEV owners can accept that the charging control of their PEVs can be scheduled automatically. This is only the way to reduce the voltage unbalance to the acceptable level and such approach can only be achieved in the smart grid context with the application of PEV load balancing strategy as proposed in this chapter.

10.5 The Proposed Strategy for PEV Load Balancing

During steady state operation (where PEVs were not integrated) of a three phase low voltage distribution system (LVDS), the voltage balance is always depending on the distribution of the loads on the three phases. Let us to consider that before PEVs are connected into the LVDS for charging, the voltages of the three phase system were in a balancing state. However, such a balance of voltage may be disturbed by a large number of PEVs penetrated randomly for charging from different phases (i.e. phase-a, phase-b, and phase-c). In this case, the system becomes unbalanced as in Eq. (10.2). If at any stage, it is found that the VUF given by Eq. (10.9) is above the acceptable limit (2 %) [33, 34], then fast corrective actions need to be taken so as to decrease the VUF. This action is called "PEV load balancing strategy" as explained in this section.

Initially, the difference in system loss between the balanced and unbalanced systems due to charging process is defined for each phase by,

$$\Delta P_{La} = P_{La,b} - P_{La,PEV} \tag{10.14}$$

$$\Delta P_{Lb} = P_{Lb,b} - P_{Lb,PEV} \tag{10.15}$$

$$\Delta P_{Lc} = P_{Lc,b} - P_{Lc,PEV} \tag{10.16}$$

where, $P_{La,b}$, $P_{Lb,b}$ and $P_{Lc,b}$ are the power losses of phase a, b and c respectively at the base case (before charging of PEVs); $P_{La,PEV}$, $P_{Lb,PEV}$ and $P_{Lc,PEV}$ are the power losses of phase a, b and c respectively during charging of PEVs.

The amount of power loss defined by Eqs. (10.14)–(10.16) due to high VUF at a period of time t_{PEV}, will give the amount of PEV charging loads ($P_{a,Ch}$, $P_{b,Ch}$, $P_{c,Ch}$) that should be managed to maintain a minimum level of VUF by rearranging the start time of charging, or in a sequence alter the charging period of each PEV. This statement implies that

$$\Delta P_{La} = P_{a,Ch};\ \Delta P_{Lb} = P_{b,Ch};\ \Delta P_{Lc} = P_{c,Ch} \tag{10.17}$$

The justification of the proposed balancing strategy can be explained as such that, if the system given in Fig. 10.8 is a balanced system or having an acceptable level of VUF, the phase voltages at the source side can be written as,

$$V_{AN} = V_{rms}\angle 0° \tag{10.18}$$

$$V_{BN} = V_{rms}\angle -120° \tag{10.19}$$

$$V_{CN} = V_{rms}\angle 120° \tag{10.20}$$

Let us analyze phase-a; the line current can be found as,

$$I_{Aa} = \frac{V_{AN}}{Z_{line,a} + Z_{load,a}} \tag{10.21}$$

where $Z_{load,a}$ is the base load without PEV loads, the voltage of phase-a can be calculated as in Eq. (10.22) and similarly for phases (b and c).

$$V_{an} = I_{Aa} Z_{load,a} \tag{10.22}$$

With PEV loads "$Z_{EV,a}$" connected in phase-a, Eq. (10.22) will be modified as,

$$V_{an,LE} = \left(\frac{V_{AN}}{Z_{line,a} + Z_{LE,a}}\right) \times Z_{LE,a} \tag{10.23}$$

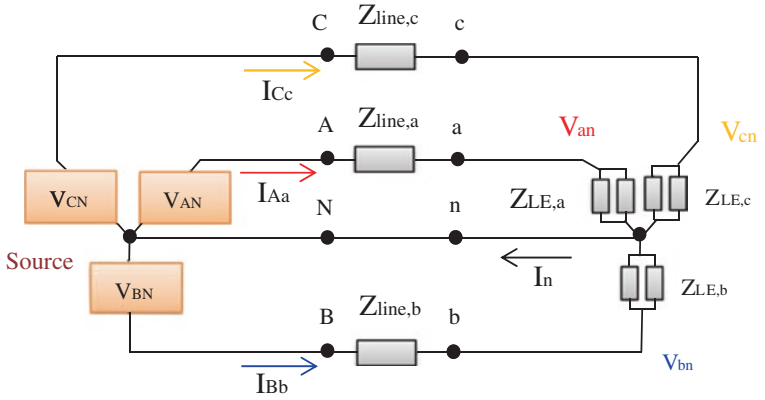

Fig. 10.8 Three phase low voltage balanced system

where,

$$Z_{LE,a} = \frac{1}{(1/Z_{load,a}) + (1/Z_{EV,a})} \tag{10.24}$$

Equation (10.23) shows that the additional load will lead to additional loss (ΔP_{La}) and voltage drop as given below,

$$\Delta V_{an} = V_{an} - V_{an,LE} \tag{10.25}$$

Thus, for decreasing the VUF, the additional power loss due to PEVs in a system as represented by ΔP_{La} should be controlled so that the load balancing can be achieved. The above mentioned strategy will result in improving the voltage unbalance profile, thereby limiting the VUF within acceptable level. It is envisaged that the PEV charging process is accomplished by the involvement of PEV aggregators and the PEV charging control within each aggregating area installed in each distribution substation. The deployment of the proposed strategy can be only achieved in the context of a smart grid infrastructure where such information exchange facility would be available. It is expected that many smart meters will be installed in the future power grids. Thus, policies of electricity utilities supporting the development of distributed generation must be revised in order to accelerate the diffusion of smarter technologies in power grids.

10.6 System Modeling and Simulation

This section presents details of analytical framework to evaluate the effects of high penetration of PEVs on voltage unbalance in residential distribution system. The work begins with the modeling of three-phase low voltage distribution networks. The basic structure of low voltage networks can be represented by four wires three phase low voltage with a three phase medium voltage (MV) distribution system. The MV is connected with the LV through a distribution transformer as shown in Fig. 10.9.

A three-phase, three-wire MV lines integrated with the delta connected primary and four-wire LV distribution lines with the grounded wye of a distribution transformer as shown in Fig. 10.9 results in a 4×4 impedance matrix given below,

$$\begin{bmatrix} V_4^a \\ V_4^b \\ V_4^c \\ V_4^n \end{bmatrix} = \begin{bmatrix} V_3^a \\ V_3^b \\ V_3^c \\ V_3^n \end{bmatrix} - \begin{bmatrix} Z_{34}^{aa} & Z_{34}^{ab} & Z_{34}^{ac} & Z_{34}^{an} \\ Z_{34}^{ba} & Z_{34}^{bb} & Z_{34}^{bc} & Z_{34}^{bn} \\ Z_{34}^{ca} & Z_{34}^{cb} & Z_{34}^{cc} & Z_{34}^{cn} \\ Z_{34}^{na} & Z_{34}^{nb} & Z_{34}^{nc} & Z_{34}^{nn} \end{bmatrix} \cdot \begin{bmatrix} I_{34}^a \\ I_{34}^b \\ I_{34}^c \\ I_{34}^n \end{bmatrix} \tag{10.26}$$

It can also be represented in a short matrix form as,

$$\begin{bmatrix} V_4^{abc} \\ V_4^n \end{bmatrix} = \begin{bmatrix} V_3^{abc} \\ V_3^n \end{bmatrix} - \begin{bmatrix} Z_{34}^{abc} & Z_{34}^{abcn} \\ Z_{34}^{nabc} & Z_{34}^{nn} \end{bmatrix} \begin{bmatrix} I_{34}^{abc} \\ I_{34}^n \end{bmatrix} \tag{10.27}$$

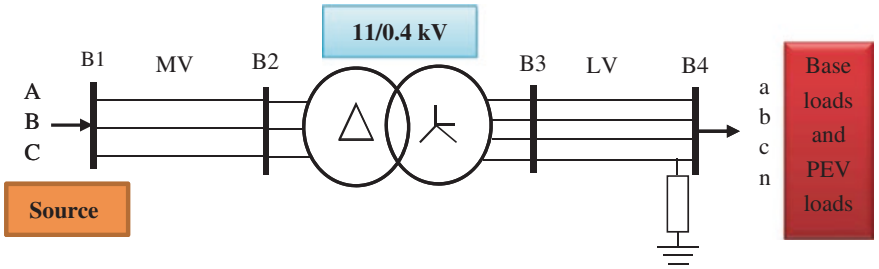

Fig. 10.9 The basic equivalent circuit of medium and low voltage distribution systems

For quantifying voltage unbalance in the network due to PEV penetration, a three phase load flow analysis can be used and the power flow solutions can be obtained by Newton Raphson method [35]. Three-phase load flow employs line impedances, voltage magnitudes and voltage angles to derive the power flows in the network. The significant difference between single-phase and three phase power flows is that all three phases impact the power flowing in any one phase [36]. Suppose a network consists of n buses, the three-phase load flow equations for powers injected at bus k in phase p are as follows,

$$P_i^p = V_i^p \sum_{k=1\ldots n} \sum_{m=a,b,c} V_k^m \left[G_{ik}^{pm} \cos(\theta_{ik}^{pm}) + B_{ik}^{pm} \sin(\theta_{ik}^{pm}) \right] \tag{10.28}$$

$$Q_i^p = V_i^p \sum_{k=1\ldots n} \sum_{m=a,b,c} V_k^m \left[G_{ik}^{pm} \sin(\theta_{ik}^{pm}) - B_{ik}^{pm} \cos(\theta_{ik}^{pm}) \right] \tag{10.29}$$

where, $Y = G + jB$ denotes the line admittance matrix between each two phases as in Eq. (10.26); θ is the admittance angle.

Referring to Fig. 10.9, the transferred power from the LV side of transformer on each phase can be derived as,

$$P_{Trafo}^{abc,\Delta t} = P_{Load}^{abc,\Delta t} + P_{Loss}^{abc,\Delta t} \tag{10.30}$$

where, $P_{Load}^{abc,\Delta t}$: total power load of each phase at time Δt; $P_{Loss}^{abc,\Delta t}$: total power loss of each phase on the LVDS at time Δt.

For a system containing n buses, the expression representing the power balance in each phase for bus k at time Δt can be written by,

$$P_{Load,k}^{abc,\Delta t} = P_{grid,k}^{abc,\Delta t} - P_{Loss}^{abc,\Delta t} \tag{10.31}$$

where $P_{grid,k}^{abc,\Delta t}$ is the injected power into bus k at time Δt. The expression given in Eq. (10.31) is for the base load, while in terms of PEV penetration, Eq. (10.31) will be modified as follows,

$$P_{Load,Int,k}^{abc,\Delta t} = P_{grid,\text{int},k}^{abc,\Delta t} - P_{Loss,Int,k}^{abc,\Delta t} \tag{10.32}$$

where,

$$P_{Loss,Int,k}^{abc,\Delta t} = P_{Loss}^{abc,\Delta t} + \Delta P_{EV,k}^{abc,\Delta t} \tag{10.33}$$

where, $\Delta P_{EV,k}^{abc,\Delta t}$ is the additional power loss of each phase due to PEV charging in bus k at time Δt (at the kth customer point connected to the PEV); $P_{grid,\text{int},k}^{abc,\Delta t}$ is the injected power into bus k at time Δt due to PEV connected in bus k at time Δt.

To demonstrate the modeling approach for the whole distribution networks, a 19-bus radial sub-distribution system as depicted in Fig. 10.10 was chosen to investigate the impacts on the networks caused by PEV mobility. This unbalance system represents a true status of one of the utility distribution feeders in Australia. The system incorporates 400 V three-phase LV main feeders starting from the point of common coupling (PCC) supplying loads in residential area. The individual sub-distribution grids are not interconnected and the LV grids are fed by distribution transformer connected to the 11 kV distribution system. The simplicity of this system allows an easier analysis of how PEVs impact the voltage unbalance in distribution system.

The time and the limit of energy required per day to charge the PEVs were defined based on true recordings of a distribution transformer load profile over a 24 h period (96 intervals) as shown in Fig. 10.11. The power demand profile of a PEV lithium-ion battery shown in Fig. 10.12 [37] was added at various households to measure the severity of system stresses in terms of power losses and voltage unbalance. The SOC for a PEV energy storage charged from a phase of the three-phase system in a given bus "k" at time $\Delta t + 1$ is determined based on the previous charged energy of the time Δt as,

$$E_{st,soc,k}^{abc,\Delta t+1} = E_{st,soc,k}^{abc,\Delta t} + \Delta E_{EV,k}^{abc,\Delta t} \tag{10.34}$$

where, $\Delta E_{EV,k}^{abc,\Delta t}$ is the change in the SOC for the charged energy of each phase in node k at time Δt; $E_{st,soc,k}^{abc,\Delta t}$ is the SOC of PEV energy for each phase in node k at time Δt. The limits of charge energy in each phase in node k at time Δt are expressed by,

$$E_{EV,ch,k}^{abc,\Delta t} = H_{G2V} \cdot E_{G2V,k}^{abc,\Delta t} \tag{10.35}$$

where, H_{G2V}: number of charging hours from power grid; $E_{G2V,k}^{abc,\Delta t}$: G2 V power flow of each phase in node k at time Δt.

Finally, symmetrical components are used to decompose the three-phase voltages derived from three-phase load flow into positive, negative and zero sequences. The transformation from the phase domain to the sequence domain at time Δt is achieved using Eq. (10.5). Finding symmetrical components is essential to calculate the VUF using Eq. (10.9) which is needed to measure the level of VUF in order to apply the proposed balancing strategy (Sect. 10.5) as the propagation of the unbalance through the network could lead to significant financial loss to network operator and end users. The flowchart in Fig. 10.13 summarizes the computation algorithm implemented in this work.

10.7 Verification and Simulation Studies

The influence of single phase PEV is investigated using low voltage unbalanced residential distribution network in a radial layout as depicted in Fig. 10.10. This system consists of a number of low voltage feeders connected into the PCC at the main or backbone feeder where each feeder may include a number of sub-feeders and the PEV can be plugged anywhere along the feeder or its sub-feeders. To analyze the

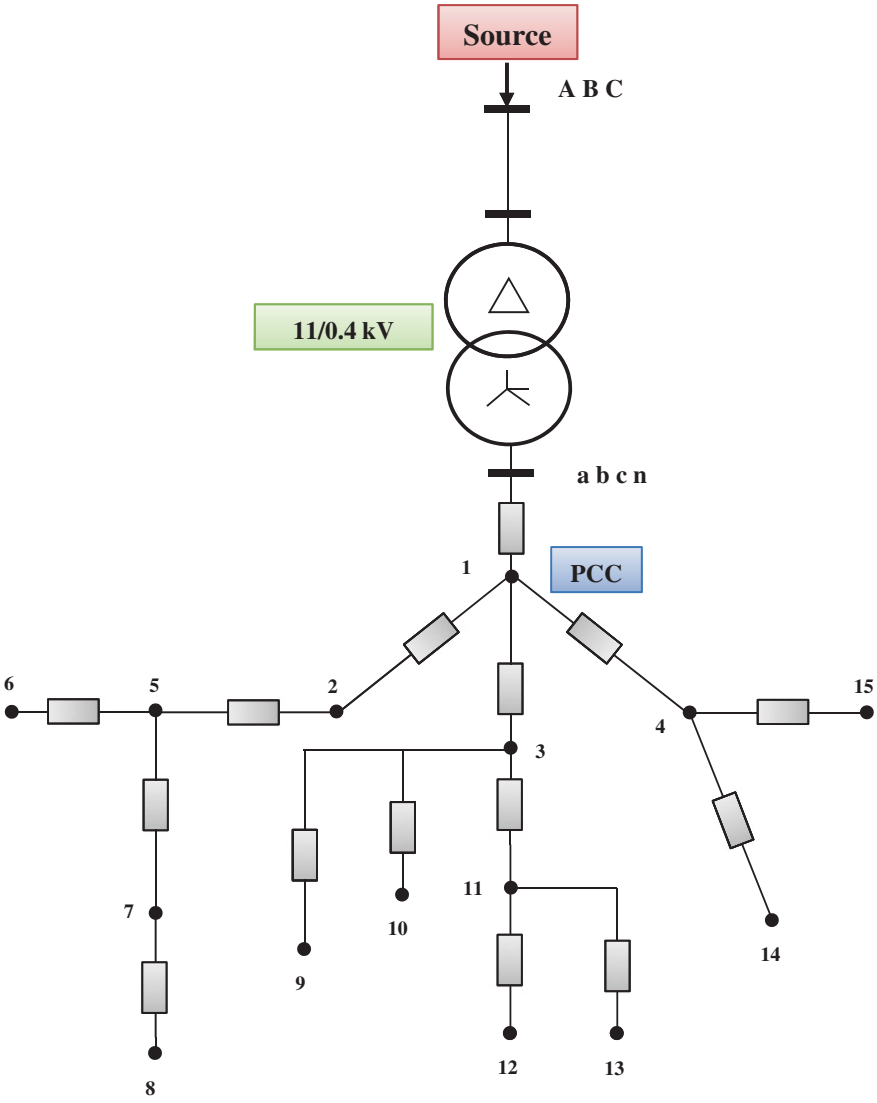

Fig. 10.10 Low voltage residential distribution system

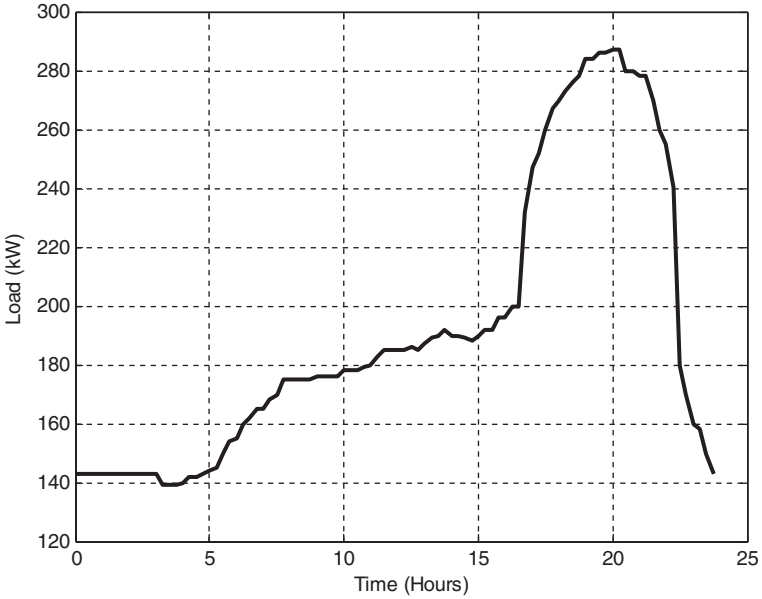

Fig. 10.11 The 15 min-interval load demand of consumers in one of the three-phases (single phase load profile)

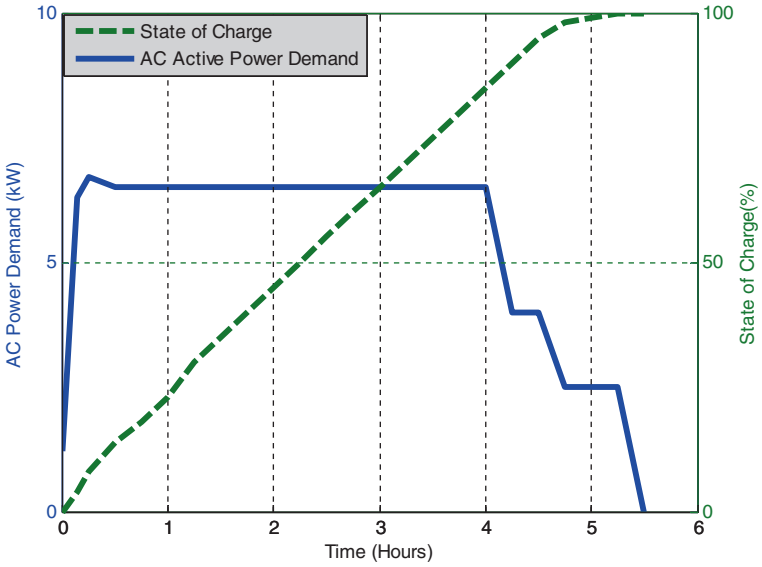

Fig. 10.12 SOC and AC power demand profile of a PEV lithium-ion battery

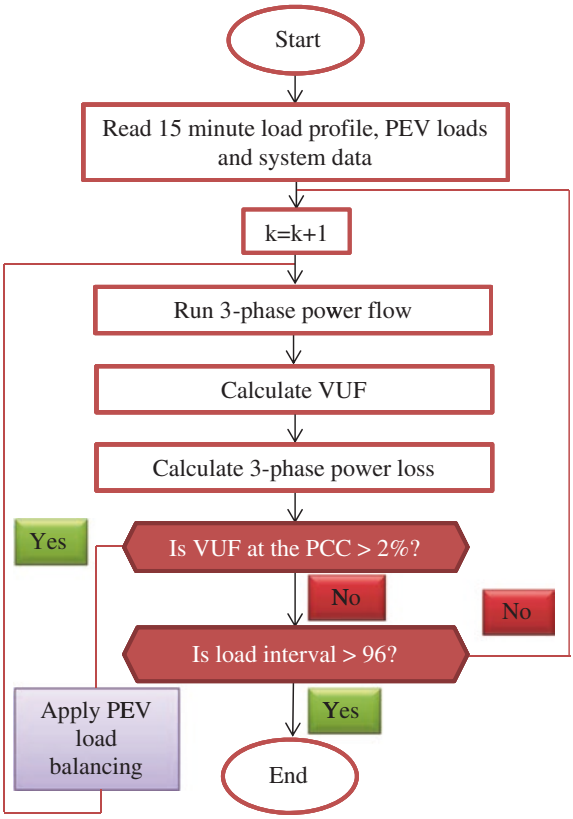

Fig. 10.13 Flowchart of the computational algorithm

impact of PEVs on the distribution system, it is important to know how the PEV load demand varies during the day in order to accommodate high penetrations of PEVs. Thus, the system in Fig. 10.10 is employed with the individual consumer load profile as shown in Fig. 10.11. In this load profile, the day is divided into 96 periods which translate into load demands at 15 min interval. The PEVs used in the simulations are lithium-ion battery charging with 220 V (Level 1) [36]. Each PEV lithium-ion battery needs to be charged roughly at initial SOC of 40–60 %. The highest penetration level is 100 %, meaning each house connected to each phase has a plugged-in PEV.

To measure the level of voltage unbalance at the base case, initially, the system was simulated without PEVs (i.e. for base case) which is considered as a reference case. As seen from Fig. 10.14, the VUF has increased during the peak period (4.5 PM–11.5 PM), however the level of unbalance in the system is still within the limit (VUF < 2 %). In order to show the realistic effects of PEV penetration on voltage unbalance, the worst case scenario is used as demonstrated in Table 10.1. The penetration level of PEVs on one of the three phases is 100 % (i.e. each house connected in first phase, "phase-a" has a PEV and all PEVs of these houses are in the state of plugged in for charging); while the penetration level in the second phase, "phase-b"

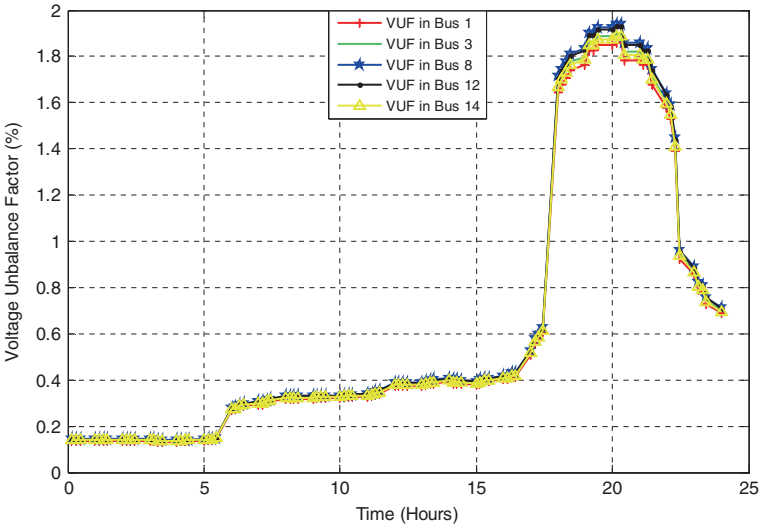

Fig. 10.14 VUF of a residential distribution network without PEVs

Table 10.1 PEV plugged-in for slow charging from different phases of 3 phase low voltage distribution system

PEV plugged (unit)	Penetration level (%)	Charging period (hours)
Phase a	100	6 PM–6 AM
Phase b	50	6 PM–6 AM
Phase c	25	6 PM–6 AM

is 50 %; as for the third phase, "phase-c", only 25 % of PEVs are plugged in. In this scenario, it is observed that results are different in terms of power losses and voltage unbalance between the system without PEVs and the system when PEVs are plugged in. The simulation is run over a 24 h period with PEVs plugged in between 6 PM and 12 PM. This is the expected period in the residential networks when PEV owners arrived home from work (6 PM) and immediately plug-in their vehicles for charging. To differentiate the starting time of charging on each phase, from the charging profile given in Fig. 10.12, two other profiles were generated by time shifting of ± 2 h. It can be seen from Figs. 10.15 and 10.16 that the power losses and VUF are higher when PEVs are plugged during the time between 6 PM and 10.30 PM. Figure 10.17 shows the VUF for some selected buses (1, 3, 8, 12, 14) that were chosen based on their configuration in the system. In other words, the penetration of PEVs in this condition can deteriorate voltage unbalance to the network.

The second scenario uses the proposed load balancing strategy which is activated when PEVs start charging from power grid. The load balancing signals to the PEVs are computed using the load balancing strategy as given in Sect. 10.5.

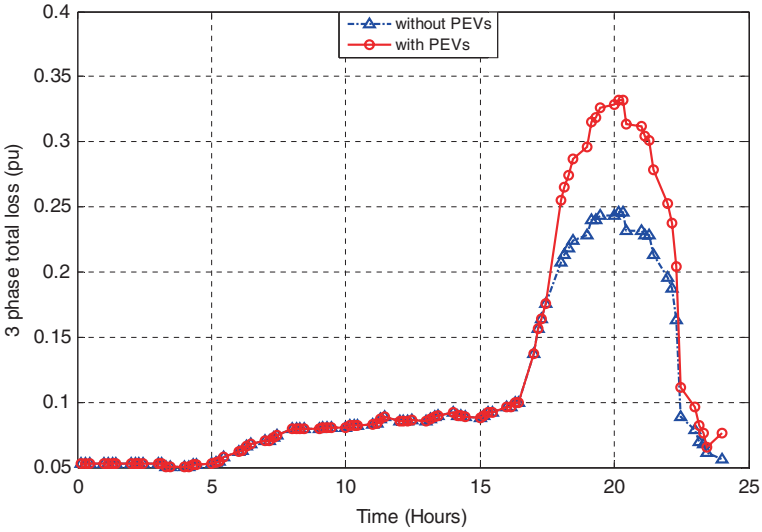

Fig. 10.15 Total power losses with and without PEVs

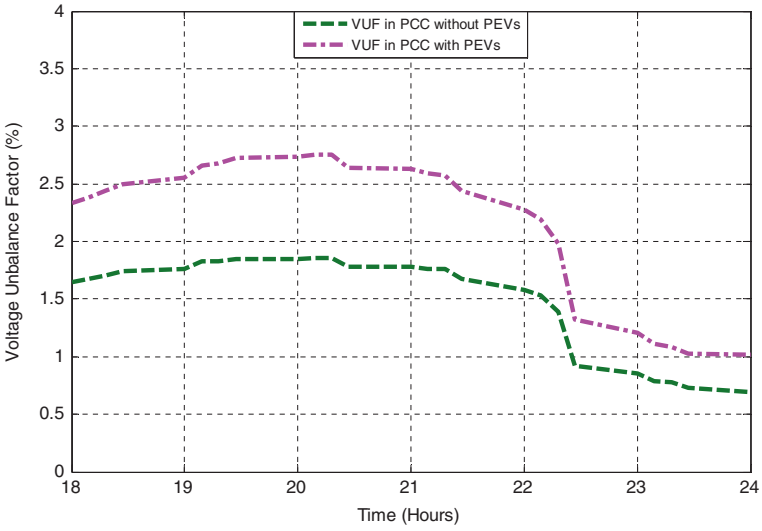

Fig. 10.16 VUF at PCC with and without PEVs

An example of the reference balancing signals is shown in Fig. 10.18. The PEVs receive the balancing signals which are then used as new balancing power for that period. The results of this scenario are shown in Figs. 10.19, 10.20, 10.21, 10.22 and the corresponding vector diagram of three phase voltages and neutral voltage are given in Fig. 10.23. As can be seen from Fig. 10.19, the power loss decreases after load balancing with the decrement of load demand as depicted in Fig. 10.20.

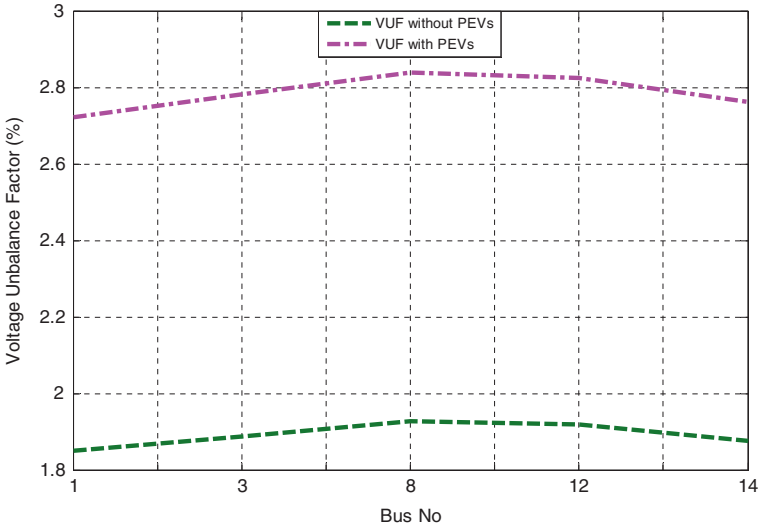

Fig. 10.17 VUF of some selected buses with and without PEVs

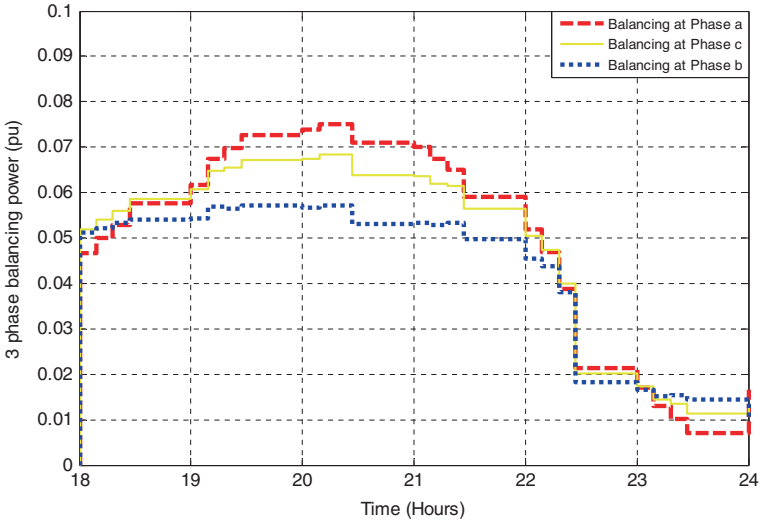

Fig. 10.18 The load balancing signals to the PEVs

With the application of PEV load balancing, the performance of the system has been improved due to the decrease in the level of VUF in the whole system as noted from Figs. 10.21 and 10.22. The results in Fig. 10.23 show that the neutral voltage can be effectively reduced by applying PEV load balancing strategy. It is also important to mention that the balancing strategy results in a slightly lower

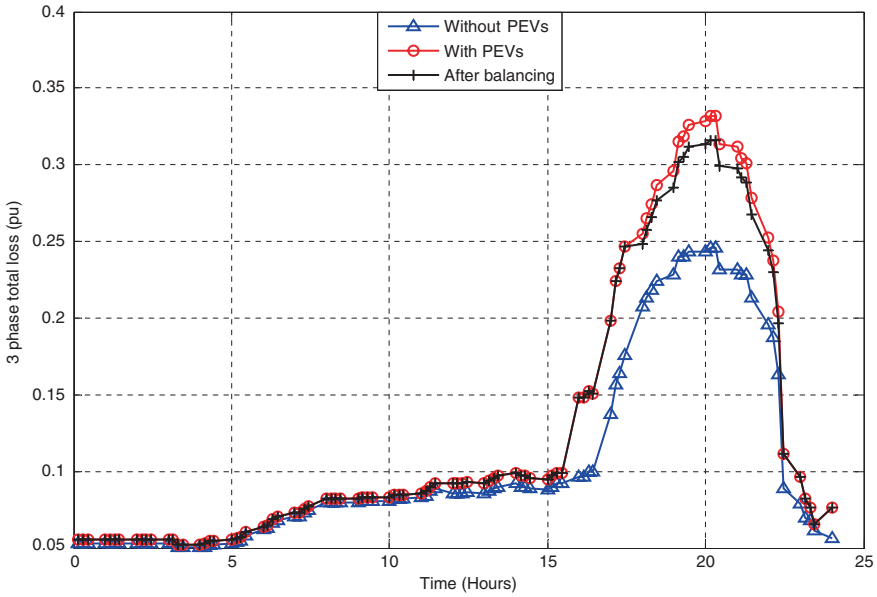

Fig. 10.19 Total power losses after PEV load balancing

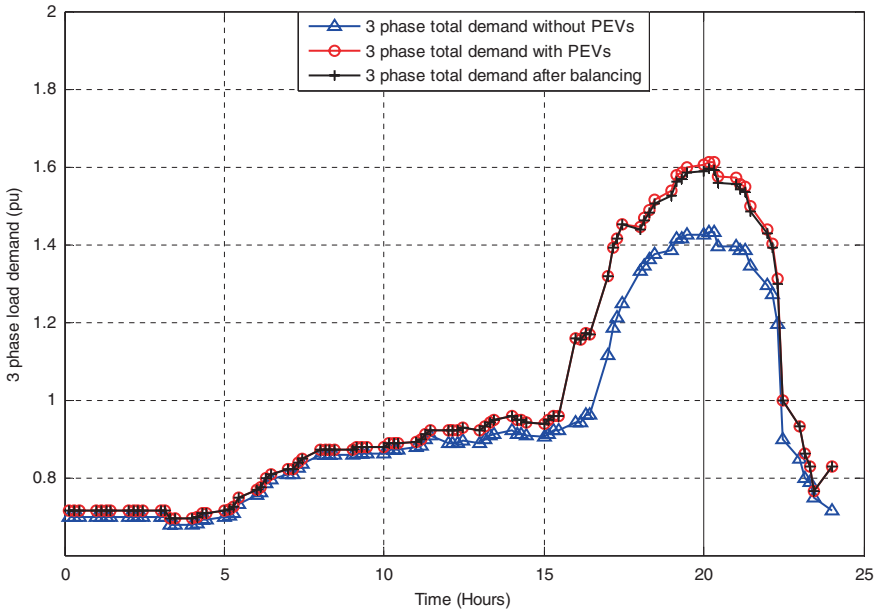

Fig. 10.20 Total load demand after PEV load balancing

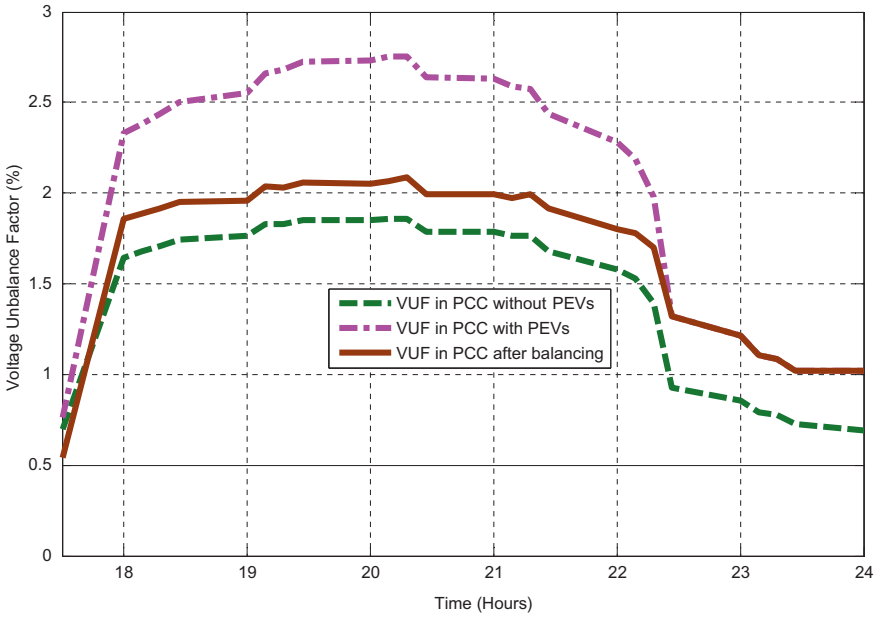

Fig. 10.21 VUF at PCC before and after PEV load balancing

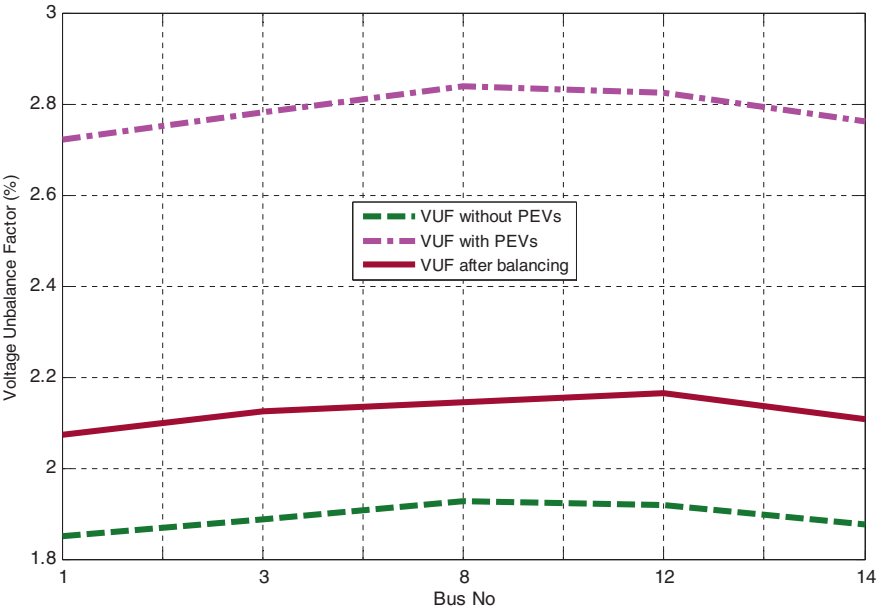

Fig. 10.22 VUF at some selected buses before and after PEV load balancing

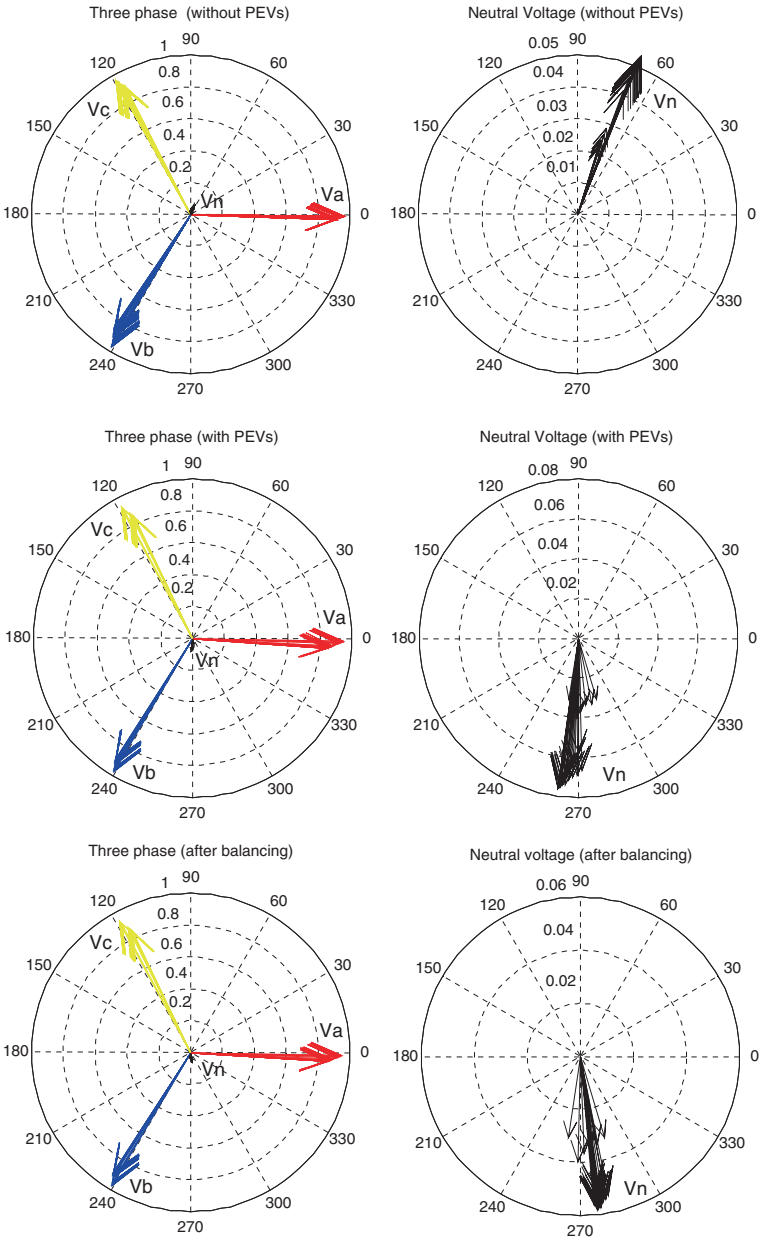

Fig. 10.23 The phasor diagrams of 3 phase voltage and neutral voltage during the time between 6 PM and 12 PM

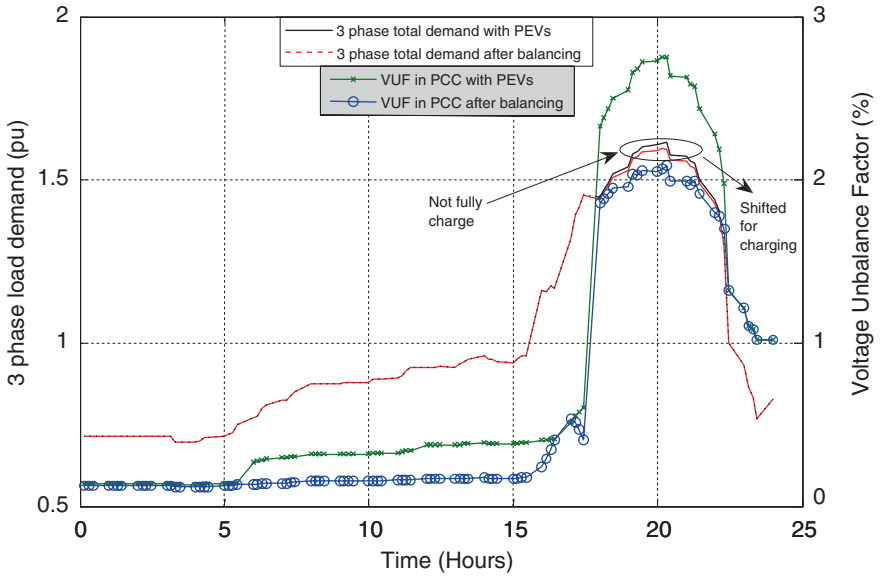

Fig. 10.24 VUF and total load demand before and after PEV load balancing

load profile in the peak hours and this can be seen from Fig. 10.24. This is due to the fact that some of PEVs connected to a highly loaded phases could not reach the highest SOC because of the disconnections applied by balancing strategy in order to maintain a lower level of VUF. As a result, some of PEVs do not fully charge during the peak period (6 PM–10.30 PM) and they may receive less than desired level of charge. However, this is not a significant issue as long as these PEVs can be shifted for charging when the levels of VUF become less than 2 % (off-peak time, in the night hours). In addition, majority of the PEV owners are not using their PEVs at night time which means that the PEV balancing strategy will not affect much the PEV users.

10.8 Conclusion

This chapter has detailed the impacts that PEVs have on the voltage unbalance. An effective balancing strategy is proposed that can be applied to balance the PEV loads in a real time system in the context of smart grids. The results presented are about home charging of a PEV connected to unbalance distribution systems. Case studies were carried out in unbalanced distribution networks varying the penetration of PEV units and their charging scenarios. Results of the case studies show that PEV charging may lead to a variety of undesired effects such as excessively VUF and asset overloading if PEV load balancing strategy is not employed. It is worth to note that the main challenge in this strategy is to keep the level of VUF as

much as low with a minimum number of disconnections of PEVs during charging process. Therefore, with the implementation of the developed PEV load balancing strategy, it is expected that the existing grid infrastructure will be able to cope with a large number of PEVs.

References

1. Adrian P (2011) Active load balancing in a three-phase network by reactive power compensation. In: Ahmed Z (ed) Power quality monitoring, analysis and enhancement, InTech, Europe, pp 219–254
2. Hosseinzadeh N et al (2004) A proposal to investigate the problems of three-phase distribution feeders supplying power to SWER systems. In: Australasian universities power engineering conference (AUPEC), pp 1–7
3. Kashem M, Ledwich G (2004) Distributed generation as voltage support for single wire earth return systems. IEEE Trans Power Deliv 19(3):1002–1011
4. Vic G, Sarath P, Vic S (2002) Voltage unbalance. Technical note, Australian Power Quality and Reliability Centre, pp 1–7
5. Yaw-Juen W (2001) Analysis of effects of three-phase voltage unbalance on induction motors with emphasis on the angle of the complex voltage unbalance factor. IEEE Trans Energy Convers 16(3):270–275
6. Jan-E-Alam Md, Kashem M, Danny S (2014) An approach for online assessment of rooftop solar PV impacts on low-voltage distribution networks. IEEE Trans Sustain Energy 5(2):663–672
7. Tsai-Hsiang C, Jeng-Tyan C (2000) Optimal phase arrangement of distribution transformers connected to a primary feeder for system unbalance improvement and loss reduction using a genetic algorithm. IEEE Trans Power Syst 15(3):994–1000
8. Woolley N, Milanovic J (2012) Statistical estimation of the source and level of voltage unbalance in distribution networks. IEEE Trans Power Deliv 27(3):1450–1460
9. Araujo L, Penido D, Carneiro S Jr, Pereira J (2013) A three-phase optimal power-flow algorithm to mitigate voltage unbalance. IEEE Trans Power Deliv 28(4):2394–2402
10. Paranavithana P, Perera S, Koch R, Emin Z (2009) Global voltage unbalance in MV networks due to line asymmetries. IEEE Trans Power Deliv 24(4):2353–2360
11. Md Jan-E-Alam, Kashem M, Danny S (2013) Effectiveness of traditional mitigation strategies for neutral current and voltage problems under high penetration of rooftop PV. In: IEEE power and energy society general meeting (PES), pp 1–5
12. Chen C, Ku T, Lin C (2011) Design of phase identification system to support three-phase loading balance of distribution feeders. In: IEEE conference on industrial and commercial power systems technical, pp 1–8
13. Moses P, Deilami S, Masoum A, Masoum M (2010) Power quality of smart grids with plug-in electric vehicles considering battery charging profile. In: IEEE PES innovative smart grid technologies, pp 1–7
14. Gomez J, Morcos M (2003) Impact of EV battery chargers on the power quality of distribution systems. IEEE Trans Power Deliv 18(3):975–981
15. Tanaka T et al (2013) Smart charger for electric vehicles with power-quality compensator on single-phase three-wire distribution feeders. IEEE Trans Ind Appl 49(6):2628–2635
16. Sortomme E, Hindi M, James S, Venkata S (2011) Coordinated charging of plug-in hybrid electric vehicles to minimize distribution system losses. IEEE Trans Smart Grid 2(1):198–205
17. Putrus G et al (2009) Impact of electric vehicles on power distribution networks. In: IEEE conference on vehicle power and propulsion, pp 827–831

18. Shahnia F, Ghosh A, Ledwich G, Zare F (2013) Predicting voltage unbalance impacts of plug-in electric vehicles penetration in residential low-voltage distribution networks. Electr Power Compon Syst 41(16):1594–1616
19. Liu Z, Milanovic J (2013) Probabilistic estimation of voltage unbalance in distribution networks with asymmetrical loads. In: 22nd international conference on electricity distribution, pp 1–5
20. Singh A, Singh G, Mitra R (2007) Some observations on definitions of voltage unbalance. In: IEEE conference on power symposium, pp 473–479
21. Pillay P, Manyage M (2001) Definitions of voltage unbalance. IEEE Power Eng Rev Mag 21(5):50–51
22. Garcia D et al (2009) Voltage unbalance numerical evaluation and minimization. Electr Power Syst Res 79(10):1441–1445
23. John J, William D (1994) Power system analysis. McGraw-Hill, New York
24. Chindriş M et al (2007) Propagation of unbalance in electric power systems. In 9th IEEE international conference on electrical power quality and utilization, pp 1–5
25. Jong-Gyeum K, Eun-Woong L, Dong-Ju L, Jong-Han L (2005) Comparison of voltage unbalance factor by line and phase voltage. In: IEEE conference on electrical machines and systems, pp 1998–2001
26. Seiphetlho T, Rens A (2010) On the assessment of voltage unbalance. In: 14th IEEE international conference on harmonics and quality of power, pp 1–6
27. IEEE recommended practice for electric power distribution for industrial plants, ANSI/IEEE Standard (December 1993)
28. Ahmed M A Haidar, Kashem M (2014) Behavioral characterization of electric vehicle charging loads in a distribution power grid through modeling of battery chargers. In: The 49th IEEE IAS annual meeting, pp 1–8 (to be presented)
29. Kwo Y, Caisheng W, Le Y, Kai S (2013) Electric vehicle battery technologies. In: Garcia-Valle R, Pecas J (eds) Electric vehicle integration into modern power network. Springer, New York, pp 15–56
30. Krieger E, Cannarella J, Arnold C (2013) A comparison of lead-acid and lithium-based battery behavior and capacity fade in off-grid renewable charging applications. Energy 60:492–500
31. Sundstro O, Binding C (2010) Planning electric-drive vehicle charging under constrained grid conditions. In: The international conference on power system technology, pp 1–7
32. Ahmed MA, Haidar Al-Dabbagh M (2013) The influences of T-joint core design on the no load losses in transformers. IEEE Potentials Mag 32(3):40–48
33. Woolley N, Milanovic J (2012) Statistical estimation of the source and level of voltage unbalance in distribution networks. IEEE Trans Power Deliv 27(3):1450–1460
34. Vic G, Sarath P, Vic S (2002) Power quality monitoring plant investigation. Technical note, Australian Power Quality and Reliability Centre, pp 1–7
35. Jan-E-Alam Md, Kashem M, Danny S (2013) A three-phase power flow approach for integrated 3-wire mv and 4-wire multigrounded LV networks with rooftop solar PV. IEEE Trans Power Syst 28(2):1728–1737
36. Hansen C, Debs A (1995) Power system state estimation using three phase models. IEEE Trans Power Syst 10(2):818–824
37. Haidar AMA, Kashem M, Danny S (2014) Technical challenges for electric power industries due to grid-integrated electric vehicles in low voltage distributions: a review. Energy Convers Manag 86:689–700

Chapter 11
Using Plug-in Electric Vehicles to Implement Ancillary Services in Smart Distribution Grids

Enrique Romero-Cadaval, Fermín Barrero-González, Eva González-Romera and María-Isabel Milanés-Montero

Abstract Plug-in Electric Vehicles (PEVs) will remain connected to the grid a high percentage of their life-time. During these connections, idle-time will be considerably longer than battery charging time. This fact turns PEV idle-time into a suitable candidate to help in the distribution grid management by implementing active distribution grid functions, leading to the future Smart Grids. In this chapter, conventional ancillary services for distribution grids are presented, including their development in the new context of Distributed Energy Resources (DER), micro grids, smart grid and either in connected or isolated modes. Later, the coordination of the previously discussed services with PEVs is analyzed, mainly considering them as Energy Storage Systems. Then, the optimization problem is presented, empathizing the indexes and constriction that could be taken into account. From the optimization procedure, reference operation setpoints are generated for each individual PEV. Then, the coordination of charger operations for maximizing global impact on the whole distribution grid is developed. Control strategies are presented and analyzed in terms of their operation setpoints in normal and abnormal grid states, when they are expected to control active, reactive and harmonic power. Finally, some examples on how the described strategies can be used for controlling active, reactive and harmonic power using a PEV charger, when the PEV is following the given operation references, are discussed.

Keywords PEVs · Ancillary services · V2G · G2V

E. Romero-Cadaval (✉) · F. Barrero-González · E. González-Romera · M.-I. Milanés-Montero
Power Electrical and Electronic Systems R+D Group, Department of Electrical, Electronic and Control Engineering, University of Extremadura, Badajoz, Spain
e-mail: eromero@unex.es
URL: http://peandes.unex.es

S. Rajakaruna et al. (eds.), *Plug In Electric Vehicles in Smart Grids*, Power Systems, DOI 10.1007/978-981-287-299-9_11

11.1 Ancillary Services

Controlling frequency and voltage has always been an essential part of power system operation. However, since the liberalization of the electricity supply industry, the resources required to achieve this control have been treated as services that the system operator has to obtain from other industry participants.

As illustrated in [1], because this liberalization has proceeded independently in different parts of the world and because of the structural differences in the underlying power systems, the technical definitions of these services and the properties of control reserves can vary significantly from country to country. Therefore, the common guidelines for the Continental Europe system (ENTSO-E CE, former UCTE area) set forth in [2, 3] are used here as a basis.

The so called entity Transmission System Operator (TSO) is responsible for the secure, reliable operation of each control area pertaining to transmission system and for connections to the transmission systems of foreign operators. To this end, TSO coordinates operation of the systems with neighboring transmission system operators and supervises its control area, for which purpose it needs ancillary services. System services in the electricity supply area are defined as essential services for system operation. Such services are delivered by grid operators to customers in addition to the transmission and distribution of electricity and hence determine the quality of the electricity supply. Ancillary services include:

- (Active power) control reserve
  - Primary control
  - Secondary control
  - Tertiary control
- Voltage support
- Compensation of active power losses
- Black start and island operation capability
- System coordination
- Operational measurement

TSO are responsible to purchase system services in accordance with a transparent, non-discriminatory and market-based procedure. The contract scenario envisages signing a framework agreement with service providers following a technical and operational appraisal (prequalification) of providers and their power stations. On this basis, providers are then eligible to bid for the ancillary service in question.

Nowadays, in the majority of countries only active power control reserve and voltage support ancillary services are remunerated by competitive market-driven mechanisms on the operation market, being these ancillary services permanently required for a safe and reliable operation of the electric power system. Remaining complementary ancillary services are provided by bilateral arrangements, being required only in some critical events. This section is only focused on active power control and voltage support ancillary services, regarding the expected potential to be provided by PEV.

The following overview describes the individual ancillary services and summarizes the intended procurement processes and procedures.

11.1.1 Active Power Control Reserve

Electric energy (electricity) cannot be stored in large quantities by conventional means. For this reason, at any given point in time, the amount of electricity produced must correspond precisely to the amount being used. This balance guarantees the secure operation of the electric grid at a constant frequency of 50 Hz (Hertz). Unforeseen fluctuations between the feed-in and/or feed-out of electrical energy in the network must be balanced out at short notice by rapidly increasing or reducing the power plant output of the suppliers of the so-called control reserve.

Technically, this is achieved within a synchronous electricity grid by a three-stage control procedure (primary, secondary and tertiary control). The following example is of a power station failure in France (Fig. 11.1). In the entire Continental Europe synchronous region, primary control is activated directly. After 30 s,

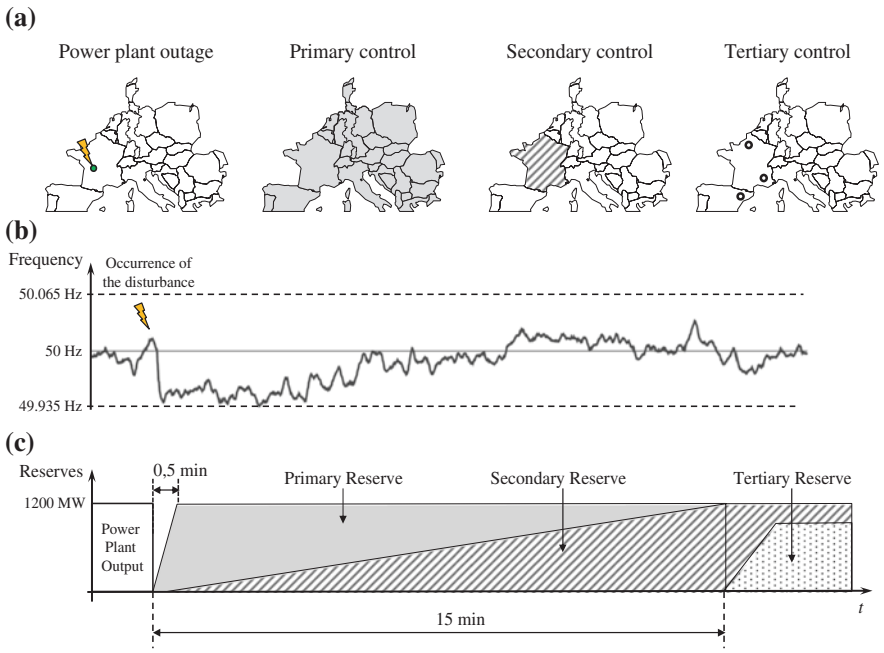

Fig. 11.1 Frequency disturbance and recovery in the Central Europe system after power plant outage in France. **a** Areas that contributes to each stage of control. **b** Frequency evolution with time. **c** Approximate time scales of frequency control-reserve activation (exact timing may vary)

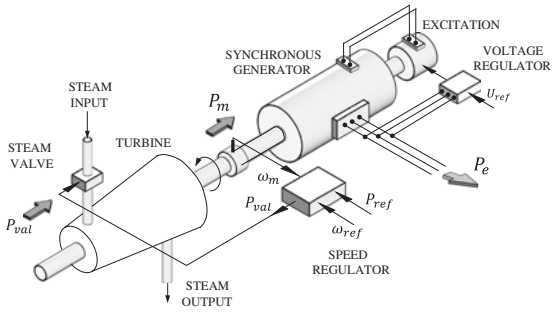

Fig. 11.2 Load-frequency and voltage control equipment on a turbine-generator set

secondary control power is automatically called up in France, and replaced after 15 min by tertiary control. For technical and/or economical reason, the power for tertiary control would be provided in part from power plants outside the control area where the generation outage was produced. In this example the necessary power is provided by power stations in France and Spain.

The fundamental component to exert power-frequency control is the synchronous generator. Control devices in each generating unit (Fig. 11.2) regulate firstly the terminal voltage of the generator and, secondly, the active power (via the throttle). Assume an initial state of operation in a given turbine-generator set, corresponding to the active power to generate assigned as a result of the electricity market. In equilibrium, the angular velocity ω_m is constant and is related to the frequency by the expression $\omega_m = 2\pi f/p$, where p is the number of pole pairs of the generator. It is assumed that the voltage control keeps it at a constant value, which is equivalent to assume that the control and power supply are totally separated. As mentioned above, in reaction to a change in power demand, the control system performs its power-frequency function with a multi-loop structure: the primary control, secondary control and the tertiary control. The following sections will address each of these controls.

11.1.1.1 Primary Control

Primary control restores the balance between power generation and consumption within seconds of the deviation occurring. During this operation, the frequency is stabilized within the permissible limit values. Activation takes place directly in the power stations by means of turbine regulators (see Fig. 11.2). In this stage, the network frequency is monitored and, in the event of deviations, the primary control power needed is activated.

In general, a power system will comprise zones or control areas, in each of which it can be assumed that generators that comprise form a coherent group, that is, they rotate in unison and, therefore, in each area frequency is uniform at all times.

Primary control is implemented on a purely local level (there is no coordination between the different units) by a simple proportional feedback loop between the electric frequency and the turbine governor. The simplicity of this mechanism

assures that participating generators in all areas work together without competing, and shares the increase in demand in proportion to their respective nominal powers.

A control area normally coincides with the area of responsibility of a TSO, a country or geographical area. Physically it is demarcated by points where the corresponding devices are installed to measure the interchanged power, enabling the establishment of contracts of sale of energy. Several interconnected control areas forming an assembly which, in turn, has interconnections with other areas, are a *synchronous area*. Within an area synchronous frequency is uniform only in steady state.

As an example, the European electricity systems whose coordinated management is assigned to the ENTSO-E [4] entity are grouped into five synchronous areas: Continental Europe (CE), Nordic, Baltic, Britain and Ireland. The Spanish power system is integrated within the CE area, which includes almost all the countries of Western Europe, connected systems of France, Portugal and Morocco.

In documents [2, 3], the primary control requirements for CE synchronous area are indicated. The so-called "reference incident" is defined as the loss of 3,000 MW generation (anywhere in the CE area). For this incident, the maximum deviation from system frequency must not exceed ±200 mHz range.

On the other hand, for a turbine-generator set, the power level from a given operation point to the full power, wherein the speed controller can act automatically, is what is known as the primary control reserve of the generating unit. In [2, 3], for the synchronous area CE, the primary control reserve is set to 3,000 MW, equal to the reference incident power value. The responsibility to provide a fraction of that reserve roughly according to their share of the total power production in the interconnection is assigned to each area (in Spain this is approximately 325 MW with a frequency deviation of ±200 MHz).

A TSO can acquire ancillary services through four procurement methods: compulsory provision, bilateral contracts, tendering, and spot market. Table 11.1, from [5] summarizes the procurement methods chosen for the different types of ancillary services (secondary and voltage control will be treated later) in various power systems: Australia (AU), France (FR), Germany (DE), Great Britain (GB), New Zealand (NZ), Pennsylvania-New Jersey-Maryland Interconnection (PJM), Spain (ES), Sweden (SE). The services used for tertiary control not related to

Table 11.1 Procurement methods used for the main ancillary service in various power systems [5]

	Compulsory provision	Bilateral contracts	Tendering process	Spot market
Primary frequency control	ES, PJM	AU, FR, NZ	DE,GB,NZ SE	AU, NZ
Secondary frequency control	–	FR	DE, NZ	AU, ES, PJM
Basic voltage control	AU, ES, DE, FR, GB, NZ, PJM, SE	FR, NZ	GB	–
Enhanced voltage control	–	FR, DE	AU, ES, GB	–

the balancing mechanism are numerous and differ significantly from system to system. Useful comparisons are therefore not possible, so these ancillary services have not been included in Table 11.1.

Primary frequency control is the ancillary service for which the widest choice of procurement methods exists. A compulsory provision for this service has the advantage of fulfilling an intrinsically homogeneous geographical repartition.

11.1.1.2 Secondary Control

The primary control prevents any disturbance to result in large frequency deviations, but it does not restore the frequency to the set-point value (50 Hz), leading this first control approach to a sustainable frequency deviation. The main purpose of the secondary control is to restore the system frequency to its set-point and the tie-lines power flow, between adjacent control areas, to their scheduled values, ensuring that activated primary control reserve within adjacent control areas is restored.

In contrast to primary control action, where all control areas contribute with mutual support, the secondary control action should only be carried out by the control area affected by the unbalance, which consequently should activate the required secondary control reserve from its resources.

If each generator had its own secondary control, they would compete with each other to achieve the reference frequency and the control system would be unstable. So the action of secondary control must be exercised in a coordinated manner. In Fig. 11.3 the classical scheme implementation of secondary control

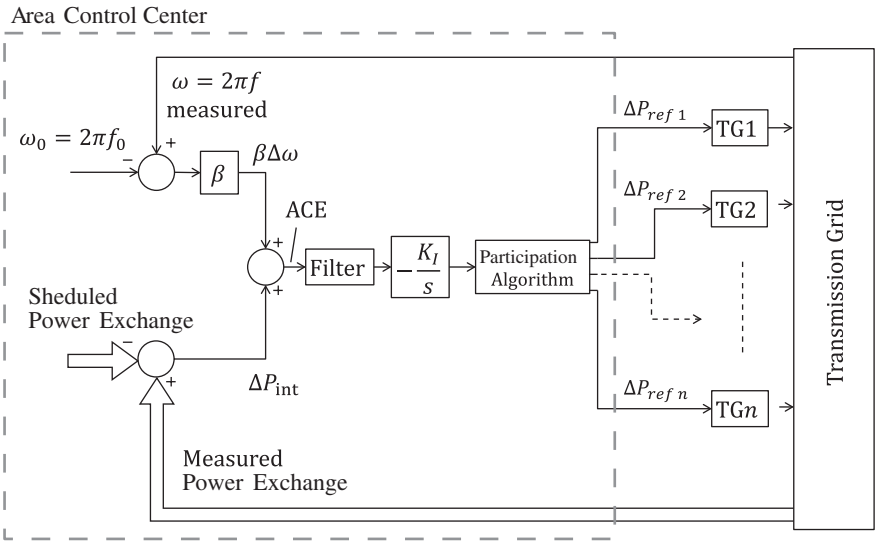

Fig. 11.3 Load-frequency control implementation

is shown. It is a unique control loop, which will be located in the area control center. Its inputs are the measurement of the area angular pulsation ($\omega = 2\pi f$) and the area power exchange. These signals are compared, respectively, with the rated angular pulsation ($\omega_0 = 2\pi f_0$) and the scheduled power exchange, yielding the $\Delta\omega$ e ΔP_{int} errors. With these values, the area control error (ACE) is calculated:

$$ACE = \Delta P_{int} + \beta \Delta\omega, \tag{11.1}$$

where β is the so called "*power-frequency characteristic*" of the area. The filtered signal ACE takes as input the integrator signal generated in the global control of the area, multiplied by the assigned participation factor is sent to each turbine-generator set. That is, for an area with n_G generators and participation factors FPi ($\sum_{i=1}^{n_G} \text{FP}_i = 1;\ i = 1, 2, \ldots, n_G$):

$$\Delta P_{ref,i} = FP_i \cdot \left[-K_I \int (ACE) \mathrm{d}t \right]. \tag{11.2}$$

Thus, the power of each turbine-generator set is varied, until the ACE is canceled. Thus ensuring that, after completion of the secondary control action, there is no frequency deviation or exchange power with respect to the scheduled and only generators pertaining to the area where the incident occurred will take over the eventually increase in demand [6]. The time horizon implementation is much slower than the primary, so that should take effect after the primary action has completed.

The reference documents [2, 3] indicate that the secondary control of each area has to start its performance no more than 30 s after a disturbance occurs, and should reduce to zero the ACE in 15 min. To achieve this, a value setting of the integrator time constant in the range of 50–200 s is recommended.

In order that the secondary control can operate, a variation margin in P_{ref} up and down from the point of operation for participating generators is required. The margin from the operating point to the maximum power of the turbine-generator set is named as the secondary control reserve positive part. And the margin from the operating point to the technical minimum is named secondary control reserve negative part. Secondary control reserve is the complementary ancillary service associated to the secondary control action.

Within the ENTSO-E, secondary frequency control is also called load-frequency control (LFC), while the term automatic generation control (AGC) is preferred in North America. However, within the ENTSO-E, the term AGC designates the combination of dispatching and secondary frequency control.

As it is shown in Table 11.1, secondary control reserve is never compulsory, and only France uses bilateral contracts. Other countries rely on more competitive procurement methods, such as tendering process or spot market; is the case of Spain, Portugal or Germany.

11.1.1.3 Tertiary Control

As a consequence of the demand increase, the performance of the secondary control changes the P_{ref} of turbine-generator sets and leads to operating points closer to its maximum capacity, reducing the reserve for secondary control. Tertiary Control aims to restore the reservation by varying the power setpoint for generators in service, by connecting standby generators (typically those that start fast as gas turbines) or by modifying programs exchange with other areas. In general, the performance of the tertiary control is sufficiently slow (10–15 min) to allow manual control.

The power connected automatically or manually under tertiary control action, in order to provide or restore an adequate secondary control reserve corresponds to the tertiary control reserve or 15 min reserve.

Tertiary control reserve is the complementary ancillary service associated to the tertiary control action. This service is often remunerated under market-driven mechanisms.

11.1.2 Voltage Support

The problem of maintaining voltages within the required limits is complicated by the fact that power system supplies power to a vast number of loads and is fed from many generating units. As loads vary, the reactive power requirements of the transmission systems vary. Since reactive power cannot be transmitted over long distances, voltage control has to be effected by using special devices dispersed throughout the system. This is in contrast to the control of frequency, which depends on the overall system active power balance. The proper selection and coordination of equipment for controlling reactive power and voltage are among the major challenges of power system engineering.

From a system perspective, the overall task of regulating the voltage is sometimes organized into a three-level hierarchy. Primary voltage control is a local automatic control that maintains the voltage at a given bus (at the stator in the case of a generating unit) at its set point. Automatic voltage regulators (AVRs) fulfill this task for generating units. Other controllable devices, such as static voltage compensators, can also participate in this primary control. Secondary voltage control is a centralized automatic control that coordinates the actions of local regulators in order to manage the injection of reactive power within a regional voltage zone. This uncommon technology is used in France and Italy. Tertiary voltage control refers to the manual optimization of the reactive power flows across the power system.

From the perspective of providers of voltage control services, it is convenient to divide the production of reactive power into a basic and an enhanced reactive power service.

- The basic or compulsory reactive power service encompasses the requirements that generating units must fulfill to be connected to the network.
- The enhanced reactive power service is a non-compulsory service that is provided on top of the basic requirements.

By definition, the basic voltage control service is always compulsory. Bilateral contracts and tendering are the preferred trading methods for enhanced voltage control. No spot market for basic or enhanced voltage control has been put in place yet because these services are very local (see Table 11.1).

In future smart grids, these services should be provided also by distribution grids (more over in isolated modes) and other ancillary service providers have to appear in the electrical energy system. In this chapter, it will be discusses how a PEV aggregator could deliver this services.

11.2 PEV Charger Optimization. Generation of Individual Operation Setpoints

11.2.1 PEVs As Energy Storage Systems

A discussion about benefits of Energy Storage Systems (ESS) in power systems, both in bulk power systems and in distribution networks, is not needed. Among other advantages, the following ones are worth mentioning:

- Demand Side Management: some loads are considered dynamical, i.e. they can be shifted with the aim of levelizing the load daily curve.
- Smoothing of RES injection of energy: less reserve capacity is needed to overcome inaccuracy in RES generation forecasting.
- Opportunity for providing ancillary services both in the grid-connected case and in micro grids and even for improving power quality in the PCC.

The benefits of ESS for a future smart grid at the distribution level are described in [7] (or for a micro grid in [8]). They can be applied in the following areas:

- Voltage control: support a heavily loaded feeder, provide power factor correction, reduce the need to constrain distributed generation energy sources (DGES), minimize on-load tap changer (OLTC) operations, and mitigate flicker, sags and swells.
- Power flow management: redirect power flows, delay network reinforcement, reduce reverse power flows, and minimize losses.
- Restoration: assist voltage control and power flow management in a post-fault reconfigured network.
- Energy market: participate in balancing market, reduce DGES variability, increase DGES yield from non-firm connections, and replace spinning reserve.
- Commercial/regulatory: assist in compliance with energy security standard (ERP2/6), reduce customer interruptions, and reduce generator curtailment.
- Network management: assist islanded networks, support black starts, switch ESS between alternative feeders at a normally open point.

In spite of that, in some authors' opinion, dedicated electricity storage is not economically viable to certain purposes, like accommodating wind power forecast errors, while more flexible storage systems, like PEVs, could be more economical [9].

In future scenarios, with a higher penetration of PEVs, thousands or even hundreds of thousands low-capacity batteries could be simultaneously connected to the grid, constituting a potential resource to face up some of the smart grid challenges. However, to use batteries in PEVs as Energy Storage Systems (Vehicle to Grid concept, V2G), new restrictions must be considered [10]:

- Charging and discharging processes must meet the vehicles' energy needs for daily trips.
- Battery state-of-charge (SOC) in each hour: this constraint keeps track of the SOC of each PEV in each hour by subtracting from the SOC of the previous hour the energy discharged into the grid or the energy used in transport (the battery SOC cannot be under 10 or over 90 % of the battery energy capacity).
- Maximum power that a PEV type can charge and discharge for a certain state is limited by the maximum charge and discharge of the individual battery times the number of PEVs in that state. It is also taken into account by the model that a PEV cannot charge and discharge at the same hour.
- Maximum power that each PEV can charge/discharge during 1 h is constrained by the amount of energy stored in the battery.
- Values must be bounded on hourly charging and discharging ramps.

PEVs could play an important role in Energy Management Systems in local environments, like houses, because they can contribute to coordinate generation and storage, smooth the consuming curve or even control the energy consumption depending on its price-by-hour. For purposes different from this local application, there is a general agreement in literature about the importance of managing aggregations of many PEVs to impact the grid in other meaningful manner [11, 12].

The influence of PEV aggregations can be summarized as follows:

- Demand Side Management: generation capacity needed to supply batteries in a high PEV penetration scenario is an important factor to be considered. Charging PEVs in valley hours could contribute to smooth demand curve so reducing the necessity of new generation capacity. Anyway, the "shiftable" nature of this kind of load constitutes a useful tool to perform Demand Side Management policies, mainly when many PEVs are simultaneously controlled.
- Centralized energy purchase: the great amount of energy needed to charge many PEV batteries permits to reduce cost either strategically bidding in the market or by obtaining economic advantages from energy supply providers.
- Possible participation in ancillary systems: for these services to be provided with a meaningful weight, a power level of MW is needed. Common range of battery power is quite lower, so aggregating them is needed for this purpose.
- As the state-of-charge (SOC) of batteries is a key issue to use the stored energy for V2G purposes, great aggregation of batteries permits to manage the charging/discharging orders to each individual PEV depending on its battery SOC, reducing degradation of batteries.

Several works have been published about the aggregator role and its interaction with both the PEV owners and the energy or grid companies [11–13].

In [11] a conceptual framework for the V2G implementation is proposed. An aggregator is presented as a new agent whose objective is to collect a great amount of batteries from PEVs by attracting and retaining owners so that a sufficient MW capacity can be managed to impact the grid and obtain benefits. The PEV aggregation may function as a controllable load or as a resource. In the first case, a load levelization objective may be reached so reducing charging costs for the PEVs as well as reducing the down regulation requests for generators. As a storage resource, the aggregation of PEVs can perform both up and down regulation tasks depending of the SOC of the individual batteries. At least the ability of absorbing energy fluctuations due to loads or intermittent RES is assured. In [11] the aggregator gets the clients motivated by providing them with park services, advantageous battery purchase and maintenance and discounts in energy price. On their behalf, PEVs put their batteries at the service of the V2G tasks programmed by the aggregator according to the information received by system operator or energy providers and to the number of PEVs available in each moment and their SOC. An important challenge in improving communication systems and incentive programs appears in this scenario. Figure 11.4 shows the flow of energy, communications and money involved in the proposed framework.

Incentives for PEV owners to participate in V2G tasks are still an unsolved issue. They may consist of providing them with some attractive services in compensation or designing a different-price scheme for charging/discharging, even

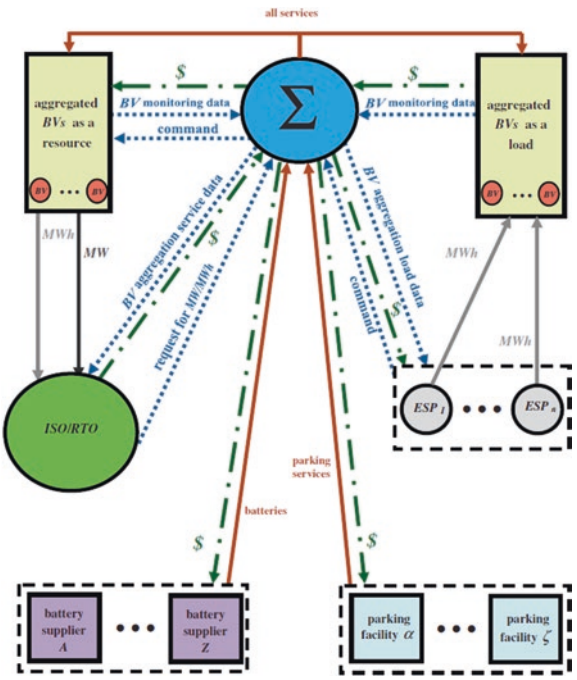

Fig. 11.4 The proposed V2G implementation framework in [11]

depending on the battery SOC. According to the kind of incentive selected, two types of control can be defined [14]:

- Direct control implies that a service provider can order the charging/discharging rate of the PEV batteries connected in a certain time period directly. The advantages of such direct control are prompt and predictable reactions to control signals. However this kind of control could cause rejection from the PEV owners, since mobility is their primary purpose of use. In addition, communication and optimization needs are very important to control a great amount of PEVs.
- Indirect control consists of sending price signals to PEV owners for them to decide to either reduce or shift the charging load when the price is high, or pay the higher price. This control is meaningful when PEV owner is considered as a consumer and the objective is to apply a Demand Side Management strategy. In this case, consumer acceptance should be higher than is the case for direct control. Disadvantages arise from the necessity to predict the reaction of consumers to different price signals. Different discharging prices depending of SOC may be programmed [13].

Regardless of the kind of control and incentive used, PEVs may perform different tasks related to smart grid concept. Some of them are discussed above.

11.2.2 PEVs As Manageable Loads

Many authors consider that the "shiftable" nature of PEV battery charging load is its most interesting and economically profitable feature [14]. The objective of the optimization algorithms designed to allocate charging rate among different connected PEVs is to minimize the cost of the energy required by the PEV owner or the aggregator. In [14] the grid resources are managed by a Virtual Power Player (VPP) that establishes contracts with resource owners, including PEV users. The problem formulation considers several PEV discharge price steps, according to the actual battery level, in order to guarantee fair discharge remuneration preventing unnecessary battery deterioration. Aggregation of PEVs with a common cost-optimization objective presents additional advantages by strategically bidding in the market (Fig. 11.5).

The coordinated control among charging PEVs managed by a common aggregator is a challenge present in the most recent literature [15–17]. It must be planned considering the changing price along the hours of the day, the peak-demand constraint imposed by the distribution company, total feeder losses, etc.

11.2.3 PEVs in Smoothing of RES Injection of Energy

One of the most promising benefits of PEVs as manageable loads is their contribution to improve the integration of intermittent Renewable Energy Resources (RES) into the grid. Through an adequate program of incentives, PEVs can be motivated

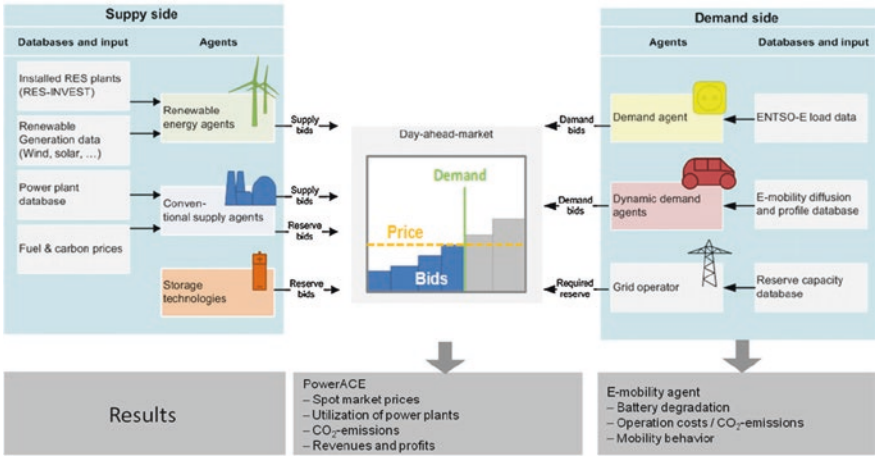

Fig. 11.5 Structure of the PowerACE model presented in [14]

to charge their batteries when RES production is high, thus smoothing the injection of energy coming from RES. In the case of wind power, one of the most powerful and widespread installed RES, its contribution may be high during the night, when demand is low. Including a storage system with a charging price scheme related to market prices may contribute to absorb this unpredictable energy production and so to reduce energy spillage in low-load hours.

11.2.4 PEVs as a Provider of Ancillary Services

In [18], a discussion about the criteria to consider an ancillary service appropriate to be performed by PEVs is presented. According to it, four criteria must be considered with that purpose:

- Supply duration: this is the period of time for which the service is called on at every instance. Depending on the service, it ranges from a few minutes to more than ten hours. Supply durations ranging from a few minutes to a few hours are suitable for PEVs.
- Directional shifts: some ancillary services require ramps up and down, both in demand and supply cases. Some services are extremely volatile, undergoing shifts in both directions rapidly (multiple times within a minute). Other services ramp in only a single direction for prolonged periods of time (few hours). The last ones produce higher degradation in batteries, so that they are not particularly adequate to be provided by PEVs.
- Response rate: this is the time within which the resource providing the ancillary service needs to initiate service. Depending on the nature of the event, response times for various ancillary services range from less than one minute up to one

hour. The advantage that PEVs provides is that it can ramp up or down rapidly at reduced costs compared to idling power plants.
- Service duty: it refers to the nature of consumption of the ancillary services, intermittent or continuous. The first ones enable the PEV to be charged while it is not providing the service.

According to [18], all the ancillary services are not particularly suitable to be provided by PEVs. Table 11.2 summarizes them.

Voltage control, as an ancillary service, as it was pointed out in the previous section, is more suitable to be performed locally, i.e close to where the voltage support is needed. Taking this into account, aggregation of PEVs connected in the same place (a park station, for example) could act as a voltage-control equipment, in spite of the conclusion shown in Table 11.2, from [18]. The allocation of the required reactive power among PEVs and the priority scheme among active- and reactive-power setpoints (P_{ref} and Q_{1ref}, respectively) must be carefully studied.

All the ancillary services considered suitable to be provided by PEVs in Table 11.2 consist of a power capacity or an amount of energy to be demanded/supplied in a fixed time period, i.e. they use active power as a reference value for the PEV aggregator. It must allocate this active power signal among the different PEVs available to provide the ancillary service en each moment.

Optimization algorithms have been developed in literature to allocate a regulation signal among available PEVs of an aggregation. In [19], authors present a very complete algorithm that improves previous works by taking into account factors

Table 11.2 Ancillary services PEV compatibility matrix according to [18]

Service	Supply duration	Directional shifts	Response rate	Service duty	Suitable for PEVs
Frequency regulation	10–15 min	High	<1 min	Continuous	Yes
Spinning reserves	10 min–2 h	Low	<10 min	Intermittent	Yes
Supplemental reserves	10 min–2 h	Low	<10 min	Intermittent	Yes
Replacement reserves	2 h	Low	<30 min	Intermittent	Yes
Voltage control	–	–	–	–	No
Load following	1–10 h	Medium	<1 h	Intermittent	No
System control	NA	NA	NA	Continuous	No
Real power loss replacement	1–10 h	Low	<10 min	Continuous	No

like uncertainty of signals and prices, dynamics of signals and availability of PEVs for regulation, costs of battery degradation and energy purchases when regulation capacity is not enough, etc. The real time optimization algorithm proposed in [19] can be summarized as follows:

Equal and short time intervals of length Δt are considered to apply the algorithm. At the beginning of each time interval, the aggregator receives a regulation signal, G_t, which has a positive value when regulation down is required and a negative value for regulation up. This regulation requirement must be allocated among the number of PEVs that are available for regulation in that time interval. PEVs available for regulation services are those that are plugged-in and they are not out of the system for personal reasons or for self-charging/discharging purpose. Assuming that all plugged-in PEVs coordinated by the aggregator can communicate bi-directionally with it, a vector $1_t = [1_{1,t}, \ldots, 1_{N,t}]$ represents the dynamics of all the N vehicles coordinated by the aggregator. Each element of 1_t has the value 1 if the corresponding PEV is available for regulation services and 0 in other case. The amount of regulation that will be assigned to an available PEV i in the time interval Δt is called $x_{i,t}$ and it can be either regulation down or up. Some restrictions must be considered to calculate each $x_{i,t}$:

- the charging/discharging rate of the ith-PEV battery is a maximum value for $x_{i,t}$;
- the state of charge of the battery at the beginning as well as at the end of the time interval Δt should lie in the preferred energy range recommended by the battery manufacturer (usually 10–90 % of the battery capacity);
- provided a degradation cost function of each battery dependent of $x_{i,t}$, the total degradation cost related to the ith PEV in a long time period must be bounded under a maximum value provided by the PEV owner.

Additionally, the sum of all PEV values of $x_{i,t}$ could be insufficient to complete the regulation requirement G_t. In this case, an energy surplus or deficit appears that must be cleared and the aggregator has to use external energy sources with it corresponding cost.

The objective of the algorithm proposed in [19] is to maximize the so-called long-term social welfare of the aggregator-PEVs system, i.es, the aggregator aims to fairly allocate the regulation amount among PEVs and to reduce the cost for the expensive external energy sources, taking into account the constraints on each PEV's regulation amount and degradation cost. As the result of the algorithm is an amount of energy to be charged or discharged by each PEV in a known time interval, it can be considered an active power setpoint P_{ref}.

The impact of including PEVs with V2G capabilities in power system is studied in [10], particularized for the Spanish case. The interest of this case study lies in the significant penetration of intermittent generation in that country. In [10] simulation of unit commitment problem in Spanish power system is performed in different scenarios of penetration of RES as well as PEVs around the target values proposed by Spanish government for the next few years. The objective is

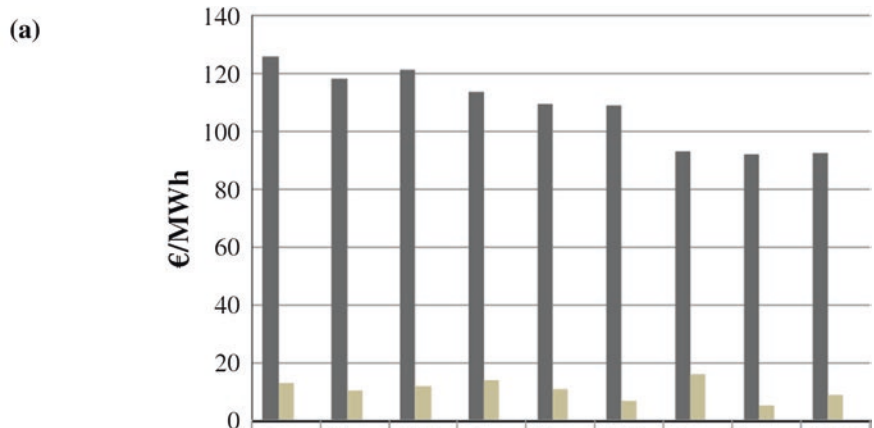

	Low RES			PANER			High RES		
	Low EV	Target EV	High EV	Low EV	Target EV	High EV	Low EV	Target EV	High EV
System marginal cost	126	118	122	114	110	109	93	92	93
Up reserve marginal cost	13	10	12	14	11	7	16	5	9
Down reserve marginal cost	0	0	0	0	0	0	0	0	0

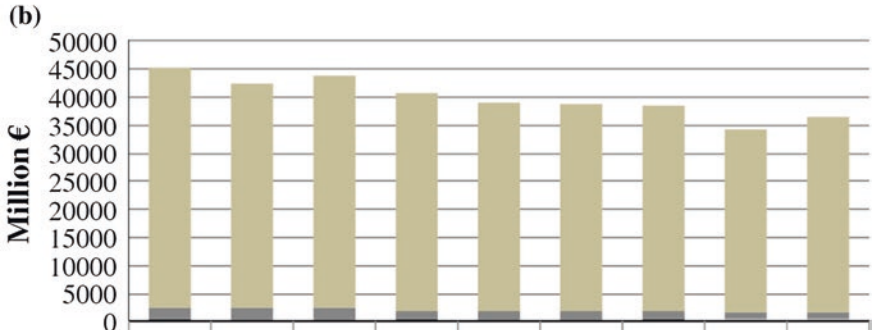

	Low RES			PANER			High RES		
	Low EV	Target EV	High EV	Low EV	Target EV	High EV	Low EV	Target EV	High EV
Generation	42560	39922	41225	38634	37112	36850	36496	32572	34710
Emissions	2122	2134	2150	1549	1560	1569	1297	1305	1317
Spillage	0	0	0	37	31	26	144	142	139
Reserve	405	287	356	404	310	212	500	319	285

Fig. 11.6 **a** Average system marginal cost and average reserves marginal cost (PANER is the target scenario for RES integration in the next years in Spanish energy policy). **b** Total system operation costs [10]

to minimize fixed and variable costs of thermal units (peaking power plants), penalty for shortcoming of up and down reserve and non-supplied energy costs. Some interesting conclusions are reached in the mentioned paper:

- Pumping storage generation can be reduced due to charging-discharging process of PEVs. This process can reach an efficiency of 90 % while pumping units have an efficiency of typically 70 %. In scenarios of high RES penetration, a higher availability of pumped storage will contribute to integrate more RES generation.
- The increment in consumption caused by PEVs charging during valley hours and hours with high intermittent generation contributes to reduce energy spillage, and, consequently, to a more efficient RES integration.
- Down reserve is always available when PEVs are integrated into the grid. With certain constraints, up reserve also increases with the deployment of PEVs.
- On the other hand, the advantages provided by the use of PEVs could turn into disadvantages if mobility patterns do not allow PEVs to be charged during valley hours. In this case system marginal cost may increase when intermittent RES generation is low. This will increase the use of more expensive generators output and up reserve, and CO_2 emissions.

Figure 11.6 shows the average marginal cost of system and reserve and the total operation costs according to simulations performed in [10] for different scenarios. The fact that marginal and total costs decrease as penetration of RES increases is not a new conclusion. On the other hand, the proliferation of PEVs with V2G capabilities seems to contribute to a marginal cost reduction, mainly with an average level of penetration.

Although it is not considered as an ancillary service in literature, an additional feature can be added to PEV batteries when they are connected to the grid and extra capacity is available after participating in ancillary systems: power quality correction. Since battery chargers are power converters connected in parallel to the grid, they may provide an active filtering service both under an aggregator setpoint or based on local measurements. This feature will be detailed later.

11.3 Control Strategies for PEVs to Follow the Individual Operation Values

The primary function of PEVs is to provide the mobility service expected by their users. However, by virtue of being equipped with a battery, if a layer of communication exists between the TSO and the PEVs, usually via an aggregator, the PEVs are potentially capable of having their electricity requirements being served according to a pre-established schedule, and even of injecting energy back into the grid [20]. The ancillary services PEVs can perform by controlling their on-board batteries have been explained previously in this chapter. This section is devoted to

analyze control strategies to provide these services from the setpoints sent by the aggregator to each individual PEV. Tree functions are discussed:

- active power interchange between the PEV and the grid, called as *P* function,
- fundamental reactive power for voltage control, *Q* function and
- reduction of harmonic components in the load-side to improve power quality, *H* function.

After proposing control strategies for each function, simulation tests are conducted to compare the strategies and show their performance. The charger specifications selected for these tests are: 16 A, 230 V single-phase, 3,700 W, according to mode 1 or preferable mode 2 in IEC 61851-1 [21]. These modes are suitable for residential customers, since normal household plugs and sockets can be used.

Regarding power quality, the impact of PEVs on the future smart grid has been assessed by the Society of Automotive Engineers (SAE) in the standard SAE J2894 [22]. This standard collects the power quality and charger efficiency requirements recommending an efficiency ratio over 90 %, Total Harmonic Distortion (THD) of the charger current lower than 10 %, and Power Factor (PF) over 95 %. It will be analyzed if the reference currents proposed in each control strategy comply with this standard and with the limits for harmonic current emissions in case of equipments with input current $\leq$16 A per phase established in IEC 61000-3-2 [23].

11.3.1 Active Power. P Function

According to what is previously defined in the market negotiations and validated by the TSO, the aggregator will manage the PEVs under its domain, by sending an active power setpoint to each individual PEV. Two operation modes can be identified [24]:

- PEVs charging: PEVs are plugged to the grid and are extracting active power to charge their batteries. This operation mode will be identified as grid-to-vehicle mode, with active power interchange (G2V-P mode).
- PEVs discharging: PEVs are injecting active power from their batteries into the grid. This operation mode will be identified as vehicle-to-grid mode, with active power interchange (V2G-P mode).

The sign criterion for the setpoint is consistent with the treatment of the charger as a generator, from the aggregator point of view. It means that the reference value provided by the aggregator is positive in the V2G-P mode ($P_{ref} > 0$), while the sign is negative in the G2V-P mode ($P_{ref} < 0$).

The power setpoint given by the aggregator has to be transformed into a reference current for the charger. In this way, two main control strategies can be applied in the P-function: Unity Power Factor (UPF) and Sinusoidal Source Current (SSC).

11.3.1.1 Unity Power Factor (UPF)

The Unity Power Factor (UPF) control strategy [25] has the objective that the charger behaves as a resistance (positive or negative depending on the charging mode). It means that the charger current has to be in phase with the source voltage, ensuring unity power factor, *PF*, so

$$i_{ch} = Ku_S, \tag{11.3}$$

where K is a constant value representing the equivalent conductance of the charging equipment.

By multiplying the instantaneous single-phase source voltage by the instantaneous charger current, and applying Eq. 11.3, the instantaneous power in the AC side of the charger, p_{AC}, can be obtained:

$$p_{AC} = u_S i_{ch} = Ku_S^2. \tag{11.4}$$

The conductance K can be determined with the criterion that the power delivered or absorbed by the charger equals the constant active power setpoint value provided by the PEVs aggregator, P_{ref}, so:

$$K = \frac{P_{ref}}{\left(u_S^2\right)_{dc}} = \frac{P_{ref}}{U_S^2}, \tag{11.5}$$

where the subscript 'dc' is to be understood as the mean value of the expression within parentheses, and U_S is the RMS value of the source voltage (the equivalent dc value).

By substituting Eq. 11.5 into Eq. 11.3, the reference charger current can be finally calculated as

$$i_{ch} = \frac{P_{ref}}{U_S^2} u_S. \tag{11.6}$$

11.3.1.2 Sinusoidal Source Current (SSC)

The Sinusoidal Source Current (SSC) control strategy [26] assures that the current demanded or injected into the grid by the charging equipment will have no harmonic content and unity displacement power factor, *dPF*.

The instantaneous power in the AC side of the charger, p_{AC}, can be calculated as the product of the instantaneous phase-to-neutral source voltage by the instantaneous charger current, as:

$$p_{AC} = u_S i_{ch}. \tag{11.7}$$

The active or constant power in the AC side of the charger has to be equal to the active power setpoint value provided by the PEVs aggregator, P_{ref}. Taking into

account the SSC objectives, the charger current will be sinusoidal and in phase with the fundamental source voltage, so:

$$P_{ref} = U_{S1} I_{ch} \tag{11.8}$$

where U_{S1} is the RMS value of the fundamental source voltage and I_{ch} the RMS value of the charger current.

Applying the SSC control strategy, the reference charger current, $i_{ch,ref}$, has to be in phase with the fundamental phase-to-neutral source voltage, so the instantaneous value is calculated multiplying the RMS value by a unity vector of the direction of the fundamental source voltage, $\overline{u}_{S1d}$:

$$i_{ch,ref} = I_{ch} \overline{u}_{S1d}. \tag{11.9}$$

Obtaining the unity vector dividing the instantaneous value by the modulus of the vector (the RMS value):

$$\overline{u}_{S1d} = \frac{u_{S1d}}{U_{S1}} \tag{11.10}$$

and applying Eqs. 11.8 and 11.10 to Eq. 11.9, the reference charger current is obtained as:

$$i_{ch,ref} = \frac{P_{ref}}{U_{S1}^2} u_{S1d}. \tag{11.11}$$

11.3.1.3 Simulation Results

In order to compare both control strategies, simulation tests have been conducted under sinusoidal and distorted source voltages. In all the tests the power setpoint is 3,680 W, what means that the charger demand or inject current into the grid at 100 % capacity (16 A).

First, the operation of the V2G-P mode in case of sinusoidal source voltage is displayed in Fig. 11.7a for UPF strategy and Fig. 11.7b using the SSC one. One can notice that in both strategies the reference charger current has the same waveform and frequency spectrum. It is easy to anticipate these results since if the source voltage has only fundamental component, $u_S = u_{S1d}$, so Eqs. 11.6 and 11.11 provide the same reference charger current. Regarding energy efficiency ratios, again both methods offer identical results, summarized in Table 11.3, where N is the non-active power defined in Std IEEE-1459 [27]. The charger current complies with the limits in IEC 61000-3-2 and Std SAE J2894.

However, when the source voltage is distorted, but complying with the limits for individual and total harmonic distortion indexes proposed in EN-50160 [28] and IEC-61000-2-2 [29], the results are not equivalent. The source voltage proposed in this test has 6 % of 5th harmonic and 5 % of 7th harmonic, so THD is 7.8 % (below 8 %) and the RMS source voltage is 230.7 V (voltage variation below 10 %). In this case, the reference current for the charger when applying the UPF strategy and SSC strategy are shown in Fig. 11.8a, b, respectively. The THD

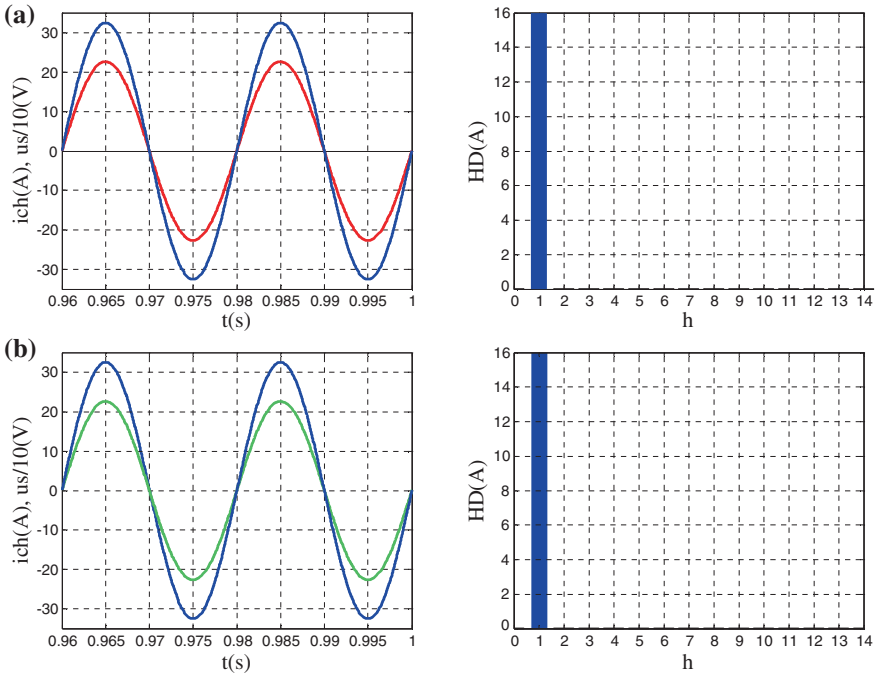

Fig. 11.7 Simulation results of V2G-P in case of sinusoidal source voltage (in *blue* u_s/10, in *red* or *green* $i_{ch,\ ref}$): **a** UPF strategy, **b** SSC strategy

Table 11.3 Comparison of simulation results in V2G-P mode under sinusoidal source voltage

Control strategy	I_{ch} (W)	$THDi_{ch}$ (%)	P (W)	S (VA)	N (VA)	PF	dPF
UPF	16	0	3,680	3,680	0	1	1
SSC	16	0	3,680	3,680	0	1	1

of the reference current is 7.8 % when applying UPF strategy, while is null in case of using SSC strategy. However, the RMS current is lower in case of UPF strategy compared to SSC strategy. It means that electrical power losses would be smaller applying UPF strategy. Information regarding charger current and power ratios are collected in Table 11.4. The charger current complies with the limits in Std SAE J2894 but the RMS of the 7th harmonic is 0.79 A, which is over the limit established in IEC 61000-3-2 (class A).

In conclusion, from the power quality point of view, SSC strategy achieves a current with no harmonic content, however, from the energy efficiency point of view, UPF strategy attains lower power losses and unity power factor. Depending on the frequency spectrum of the source voltage, the current charger could not comply with the current regulations and standards.

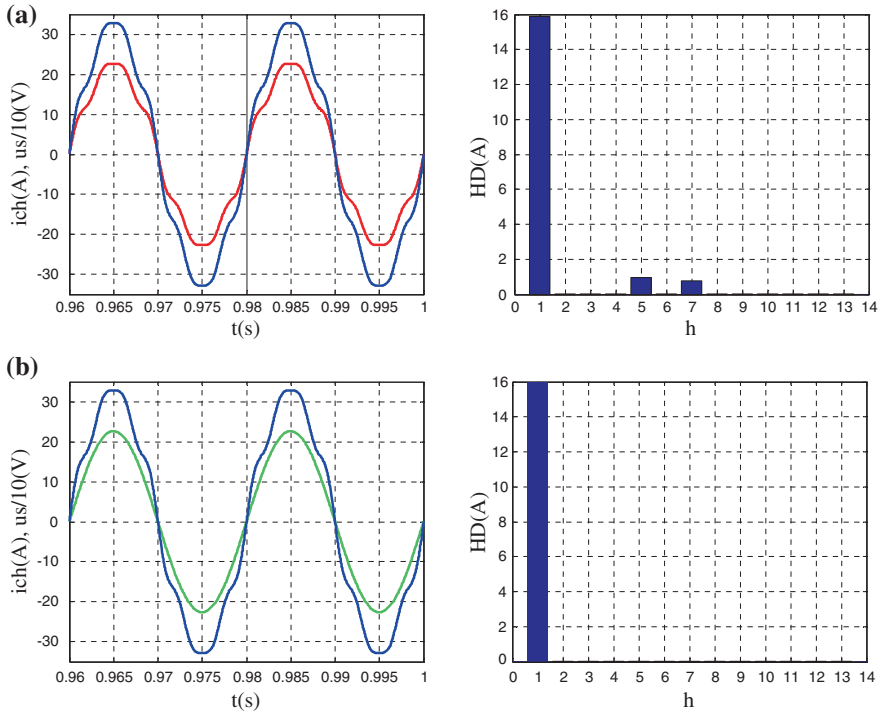

Fig. 11.8 Simulation results of V2G-P in case of distorted source voltage (in *blue* u_s/10, in *red* or *green* $i_{ch,\ ref}$): **a** UPF strategy, **b** SSC strategy

Table 11.4 Comparison of simulation results in V2G-P mode under distorted source voltage

Control strategy	I_{ch} (W)	$THDi_{ch}$ (%)	P (W)	S (VA)	N (VA)	PF	dPF
UPF	15.9514	7.81	3,680	3,680	0	1	1
SSC	16	0	3,680	3,691	284.75	0.9969	1

Finally, a simulation to test the G2V-P mode has been conducted in case of distorted source voltage. The results are similar to those concerning the V2G-P mode, but the charger current lags the source voltage by 180°. The results are displayed in Fig. 11.9a for UPF strategy and Fig. 11.9b for SSC strategy.

11.3.2 Fundamental Reactive Power. Q Function

PEVs can be used as distributed storage resources to contribute to voltage control as an ancillary service for the system. The aggregator, acting as an interface with TSO and energy service providers, can provide distributed reactive power sources.

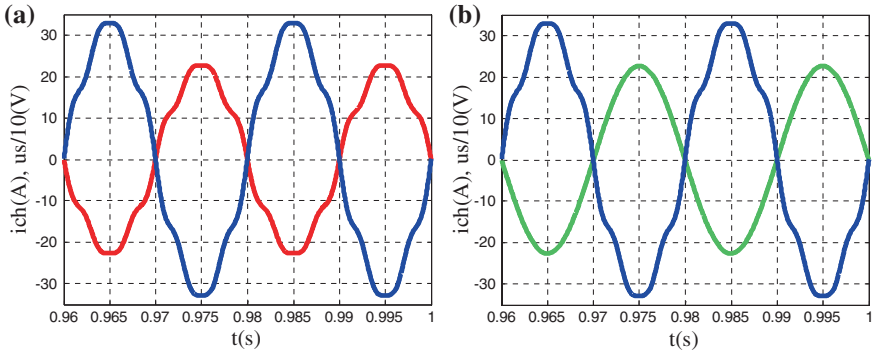

Fig. 11.9 Simulation results of G2V-P in case of distorted source voltage (in *blue* u_s/10, in *red* or *green* $i_{ch,\,ref}$): **a** UPF strategy, **b** SSC strategy

These sources can supply or consume reactive power, so that fundamental voltages at delivery points can be controlled to be within defined levels. In this way, the aggregator is in charge of calculating a fundamental reactive power setpoint, Q_{1ref}, for each individual PEV.

Again, two operation modes can be identified, depending on the consumption or injection of fundamental reactive power:

- G2V-Q mode—Grid-to-vehicle, with reactive power interchange: PEVs are absorbing fundamental reactive power from the grid, acting as controlled inductors ($Q_{1ref} < 0$).
- V2G-Q mode—Vehicle-to-grid, with reactive power interchange: PEVs are injecting fundamental reactive power into the grid, behaving as controlled capacitors ($Q_{1ref} < 0$).

Since voltage control is related to fundamental component, only one control strategy is proposed, equivalent to the SSC strategy in the *P* function, called Sinusoidal Quadrature Source Current (SQSC) control strategy. This strategy assures that the current demanded or injected into the grid by the charging equipment will have no harmonic content, and will be in quadrature with the fundamental source voltage, attaining a null *dPF*.

The fundamental reactive power in the AC side of the charger, Q_{1AC}, can be calculated as:

$$Q_{1AC} = U_{S1} I_{ch1} \sin \varphi_1, \tag{11.12}$$

where I_{ch1} is the RMS value of the fundamental charger current and φ_1 is the angle formed by the fundamental source voltage and fundamental charger current.

Applying the SQSC control strategy, the reference charger current, $i_{ch,ref}$, has only fundamental component, in quadrature with the fundamental single-phase source voltage. It means that $I_{ch} = I_{ch1}$ and $\varphi_1 = 90^{\circ}$ (considering the charger as a generator with $Q_{1ref} > 0$). The instantaneous charger current is then calculated by

multiplying the RMS charger current value by a unity vector leading the fundamental source voltage by 90°, $\overline{u}_{S1q}$:

$$i_{ch,ref} = I_{ch}\overline{u}_{S1q}. \tag{11.13}$$

This unity vector is obtained dividing the instantaneous value of the fundamental source voltage, being +90º phase shifted, by the modulus of the vector (the RMS value):

$$\overline{u}_{S1q} = \frac{u_{S1q}}{U_{S1}}. \tag{11.14}$$

Considering the above equations and taking into account that Q_{1AC} has to be equal to the fundamental reactive power setpoint value provided by the PEVs aggregator, finally the reference charger current is obtained as:

$$i_{ch,ref} = \frac{Q_{1ref}}{U_{S1}^2}u_{S1q}. \tag{11.15}$$

When a consumption of fundamental reactive power is requested from the aggregator, the charger current has to lag the source voltage, but Eq. 11.15 is also valid since in this situation $Q_{1ref} < 0$.

Simulation tests have been conducted under distorted source voltages. *P*-*Q* functions have been simultaneously validated in V2G-P-Q and G2V-P-Q modes. The active power setpoint is $P_{ref} = \pm$ 3,000 W, and the fundamental reactive power setpoint has been proposed so that the charger current demanded or injected into the grid will be at 100 % capacity (16 A), that is $Q_{1ref} = \pm$2,131 VAr.

The operation of the V2G-P-Q mode in case of distorted source voltage using SSC and SQSC control strategies is displayed in Fig. 11.10. They are also shown the $i_{ch\text{-}P}$ component, responsible for the *P* function, in phase with the fundamental source voltage (Fig. 11.10b) and $i_{ch\text{-}Q}$ component, in charge of the *Q* function, 90º leading the fundamental source voltage (Fig. 11.10c). The frequency spectrum of the charger current has only fundamental component, so the THDi_{ch} is null. On the other hand, results in case of G2V-P-Q mode under the same source voltage are displayed in Fig. 11.11. The $i_{ch\text{-}P}$ component is 180º out of phase with the

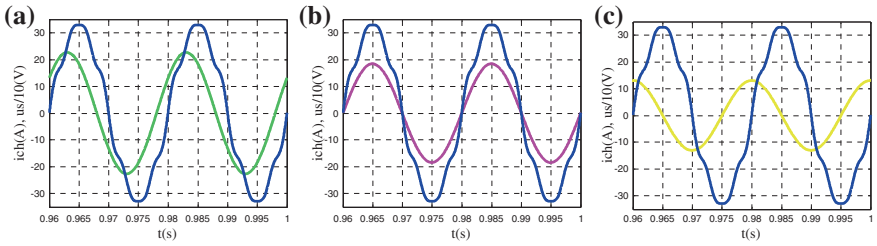

Fig. 11.10 Simulation results of V2G-P-Q in case of distorted source voltage (in *blue* u_s/10): **a** i_{ch}, **b** $i_{ch\text{-}P}$, **c** $i_{ch\text{-}Q}$

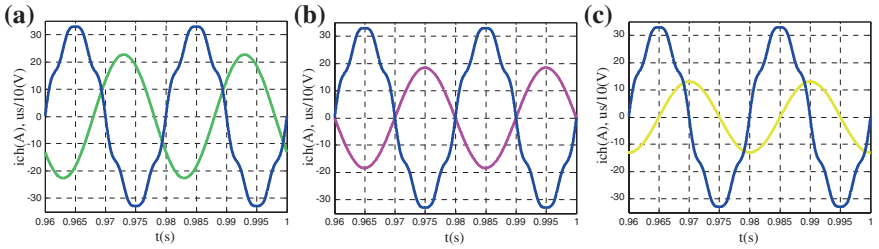

Fig. 11.11 Simulation results of G2V-P-Q in case of distorted source voltage (in *blue* u_s/10): **a** i_{ch}, **b** $i_{ch\text{-}P}$, **c** $i_{ch\text{-}Q}$

Table 11.5 Simulation results using SSC and SQSC control strategies, under distorted source voltage

Operation mode	I_{ch} (A)	$THDi_{ch}$ (%)	$I_{ch\text{-}P}$ (A)	$I_{ch\text{-}Q}$ (A)	P (W)	S (VA)	N (VA)	Q (VAr)	PF	dPF
V2G-P-Q	16	0	13.04	9.265	3,000	3,691	2,151	2,131	0.8127	0.8153

fundamental source voltage (Fig. 11.11b) and $i_{ch\text{-}Q}$ component is 90º lagging the fundamental source voltage (Fig. 11.11c). Tests results are collected in Table 11.5 for V2G-P-Q mode. In G2V-P-Q mode the results are the same, except the negative sign of *P* and *Q*.

11.3.3 Power Quality. H Function

If the capacity of a charging device is below 100 %, the PEV can contribute with an additional task concerning the improvement of the power quality at certain delivery points. This function can be carried out following a setpoint provided by the aggregator, corresponding to the harmonic content that has to be injected into the grid. In this case, the aggregator offers an additional service to reduce the harmonic distortion in the voltage at a point of common coupling, operating as an active filter connected in parallel to that point. Another option is that the controller of the charger has a specific function implemented for this purpose. In case the charger has got available capacity, while satisfying the aggregator requirements, it is used to inject the harmonic current components demanded by the household circuitry where the PEV is plugged in. This function has been referred in the literature as vehicle-to-home (V2H) mode [30, 31]. In this section the second option will be considered.

In the *H* function only one operation mode is identified, since the reference harmonic current will always be injected from the charger to the grid (V2G-H mode). However, two different control strategies can be employed, to compensate harmonic currents in terms of bandwidth [32]: overall harmonic compensation (OHC) or selective harmonic compensation (SHC). In both cases it is always necessary to check that the charger capacity is not exceeded. If the harmonic reference current

added to the current for P and Q functions exceeds the rated or nominal current of the charger, $I_{ch,n}$, the harmonic reference current has to be saturated so that the charger capacity is less than or equal to 100 %.

The maximum RMS harmonic charger current, $I_{ch\text{-}H,\max}$ is calculated as:

$$I_{ch-H,\max} = \sqrt{I_{ch,n}^2 - I_{ch-P}^2 - I_{ch-Q}^2}, \tag{11.16}$$

where $I_{ch\text{-}P}$ is the RMS charger current responsible for the P function and $I_{ch\text{-}Q}$ is the RMS charger current responsible for the Q function. This equation is valid in case of using SSC strategy in the P function, since $I_{ch\text{-}P}$ has only fundamental direct component. As $I_{ch\text{-}Q}$ has only fundamental quadrature component, and $I_{ch\text{-}H}$ contains harmonic components, the global RMS charger current is calculated as the square root of the sum of the squared components. Using UPF strategy $I_{ch\text{-}P}$ is lower, so Eq. 11.4 can also be used, with confidence that the current rating will not be exceeded.

11.3.3.1 Overall Harmonic Compensation

The Overall Harmonic Compensation (OHC) aims to provide as harmonic reference current the entire harmonic spectrum present in the load current, except the fundamental frequency, which is to be supplied by the grid. The OHC is usually applied for loads with wider or unknown harmonic spectrum, where harmonics of unpredicted orders may appear [32]. One advantage of this method is that it is only necessary to employ one harmonic extractor [33] to separate the fundamental current from the load current.

The reference harmonic charger current, $i_{ch\text{-}H,ref}$ can be calculated as

$$i_{ch-H,ref} = i_L - i_{L1}, \tag{11.17}$$

where i_L is the load current demanded by the household consumption and i_{L1} its fundamental component.

To avoid charger overload, this reference current has to be limited to the maximum RMS harmonic charger current, $I_{ch\text{-}H,\max}$, so finally the reference harmonic charger current after saturation, $i_{ch-H,ref}^{sat}$, will be

$$\begin{aligned} i_{ch-H,ref}^{sat} &= i_{ch-H,ref} && \text{if} \quad I_{ch-H,ref} \le I_{ch-H,\max} \\ i_{ch-H,ref}^{sat} &= \frac{i_{ch-H,ref}}{I_{ch-H,ref}} I_{ch-H,\max} && \text{if} \quad I_{ch-H,ref} > I_{ch-H,\max} \end{aligned}, \tag{11.18}$$

where, $I_{ch\text{-}H,ref}$ is the RMS value of the reference harmonic charger current.

11.3.3.2 Selective Harmonic Compensation

The objective of the Selective Harmonic Compensation (SHC) method is to provide in the harmonic reference current only several selected harmonic orders. The bandwidth of the compensated harmonic current is, therefore, limited to those

orders [34, 35]. This selectivity can be implicitly provided through the selected algorithm or by user's choice. For example, it could be useful to eliminate the dominant harmonics in the load current, or certain harmonic orders, as the triplen harmonic components, which are responsible for additional losses in the neutral conductor and are limited more restrictively by current regulations [28, 29]. Another option is to eliminate harmonic components in the load current which predictably could cause series or parallel resonance between installed passive filters or capacitor banks and the grid impedance.

The SHC is typically applied to loads designed to work in specified operating conditions, where harmonics of known orders appear. A disadvantage of this method, regarding control algorithms, is that it is necessary to employ as many harmonic extractors as intended harmonic components to eliminate [33].

The reference harmonic charger current, $i_{ch\text{-}H,ref}$ can be calculated as

$$i_{ch-H,ref} = \sum_{sh} i_{Lsh}, \tag{11.19}$$

where i_{Lsh} are the selected harmonic components in the load current to be compensated. Again, to avoid charger overload, Eq. 11.18 has to be applied to obtain $i^{sat}_{ch-H,ref}$.

11.3.3.3 Simulation Results

Simulation tests have been conducted under sinusoidal source voltages. *P-Q-H* functions have been simultaneously validated in V2G-P-Q-H mode.

First, the aggregator setpoints have been fixed to $P_{ref} = 1{,}850$ W and $Q_{1ref} = 1{,}850$ VAr. In this situation, $I_{ch\text{-}H,\max} = 11.25$ A. It has been proposed a typical profile of harmonics in the demand of a residential customer: $I_{L3} = 2.63$ A, $I_{L5} = 1.05$ A, $I_{L7} = 0.394$ A, $I_{L9} = 0.4037$ A, so $I_{Lh} = 2.887$ A (waveform and frequency spectrum shown in Fig. 11.12a). It means that no saturation is needed in this test, since the charger current is below its capacity (16 A) because $I_{Lh} < I_{ch\text{-}H,\max}$.

The operation by using SSC, SQSC and OHC control strategies is displayed in Fig. 11.12b and Table 11.6. One can notice that the harmonic spectrum of i_{ch} (without considering the fundamental order) is identical to harmonic spectrum of i_L, validating the proper operation of the OHC strategy.

The algorithm selected in case of using SHC strategy aims to eliminate the triplen harmonic components in the load current. In the proposed test, it means that the selected harmonics to compensate are the 3rd and 9th. Results when using SSC, SQSC and SHC control strategy, with selected harmonics to compensate 3rd and 9th, are shown in Fig. 11.13a and Table 11.6. The harmonic spectrum of i_{ch} (without considering the fundamental order) has the selected harmonics of i_L (3rd and 9th), while the uncompensated current, $i_{L,nc}$, shown in Fig. 11.13b, has the non-selected harmonics of i_L (5th and 7th), confirming the correct operation of the proposed SHC control strategy.

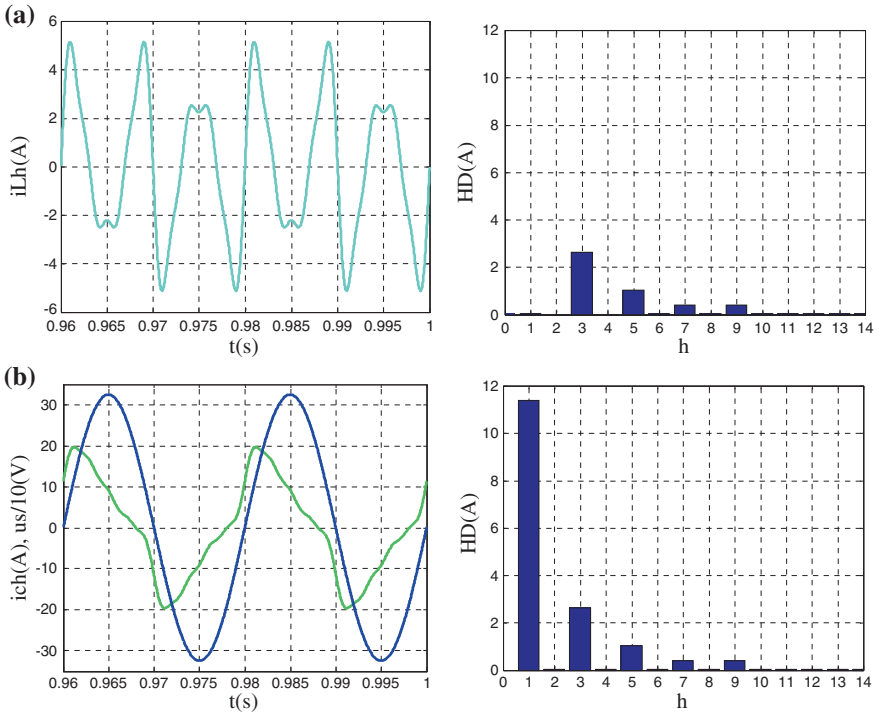

Fig. 11.12 Simulation results of V2G-P-Q-H in case of sinusoidal source voltage with OHC: **a** i_L (waveform and spectrum), **b** in *blue* u_s/10, in *green* i_{ch} (waveform and spectrum)

Table 11.6 Simulation results of V2G-P-Q-H mode under sinusoidal source voltage without saturation in *H* function

Control strategy	I_{ch} (A)	$THDi_{ch}$ (%)	$I_{ch\text{-}P}$ (A)	$I_{ch\text{-}Q}$ (A)	$I_{ch\text{-}H}$ (A)	P (W)	S (VA)	N (VA)	Q (VAr)	PF	dPF
OHC	11.74	25.257	8.043	8.043	2.887	1,850	2,700	1,966	1,850	0.6853	0.7071
SHC	11.69	23.255	8.043	8.043	2.812	1,850	2,688	1,950	1,850	0.6882	0.7071

Finally, to validate the saturation action in the *H* function, the aggregator set-points have been fixed to $P_{ref} = 3{,}000$ W and $Q_{1ref} = 2{,}100$ VAr. The load current profile is the same as in the previous tests. In this case, $I_{ch\text{-}H,\max} = 1.613$ A while $I_{Lh} = 2.887$ A (see Fig. 11.12a), so saturation is needed to prevent charger overloading.

The operation by using OHC control strategy is shown in Fig. 11.14. The harmonic load current is in part injected by the charger, but the uncompensated current, $i_{L,nc}$, has all the harmonics present in i_L, although reduced due to the saturated overall operation.

On the other hand, to test the performance of SHC strategy, instead of proposing certain harmonics to compensate, another algorithm has been validated:

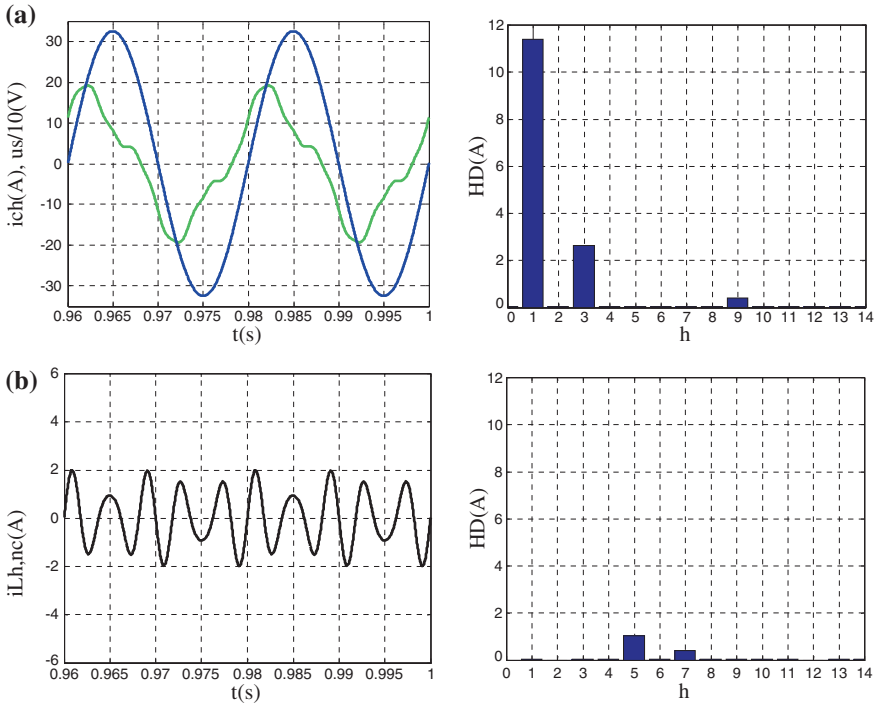

Fig. 11.13 Simulation results of V2G-P-Q-H in case of sinusoidal source voltage with SHC: **a** in *blue* u_s/10, in *green* i_{ch} (waveform and spectrum), **b** $i_{L,nc}$ (waveform and spectrum)

Table 11.7 Simulation results of V2G-P-Q-H mode under sinusoidal source voltage with saturation in *H* function

Control strategy	I_{ch} (A)	$THDi_{ch}$ (%)	$I_{ch\text{-}P}$ (A)	$I_{ch\text{-}Q}$ (A)	$I_{ch\text{-}H}$ (A)	P (W)	S (VA)	N (VA)	Q (VAr)	PF	dPF
OHC	16	9.732	13.04	9.13	1.61	3,000	3,680	2,132	2,100	0.8152	0.8192
SHC	16	9.724	13.04	9.13	1.61	3,000	3,680	2,132	2,100	0.8152	0.8192

reducing the harmonics from higher content to lower, saturating when the charger attains 100 % capacity. Thus, taking into account that in the proposed test the 3rd harmonic in the load current, $I_{L3} = 2.63$ A > $I_{ch\text{-}H,\max}$, the charger provides part of the 3th harmonic (see Fig. 11.15a), and the uncompensated current, $i_{L,nc}$ contains the rest of the 3th harmonic and the other harmonics present in the load current (see Fig. 11.15b). These results confirm the correct operation of SHC with saturation, when using the proposed SHC control algorithm.

Test results for both control strategies are summarized in Table 11.7. Since the P and Q setpoints is both tests are equal and the H setpoint has been fixed to the maximum RMS harmonic charger current, $I_{ch\text{-}H,\max} = 1.613$ A, one can notice that all the ratios in Table 11.7 are equal, except the harmonic distortion in the charger current, $THDi_{ch}$.

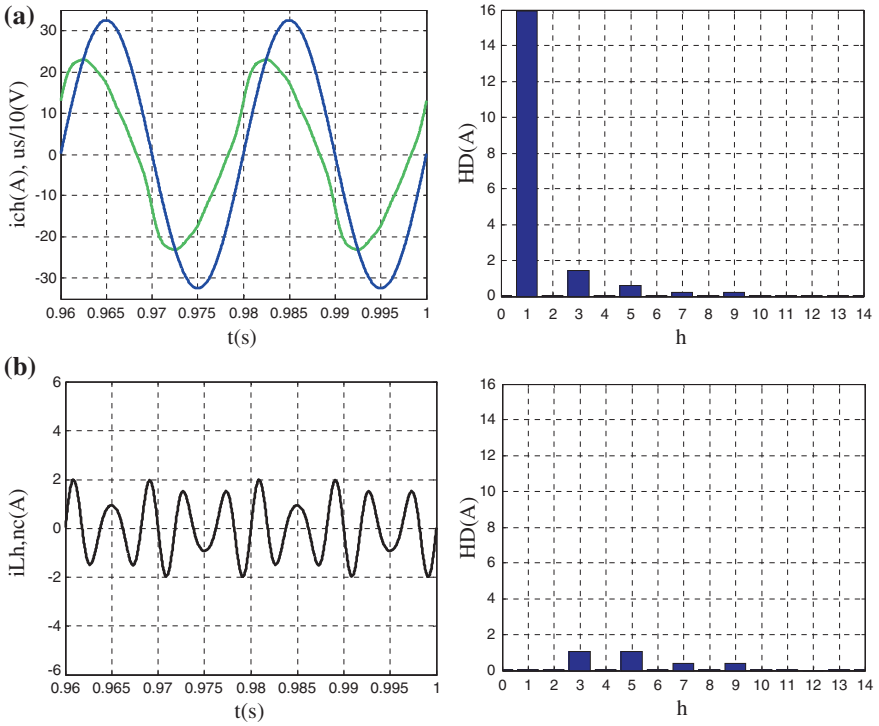

Fig. 11.14 Simulation results of V2G-P-Q-H with saturated OHC: **a** in *blue* $u_s/10$, in *green* i_{ch} (waveform and spectrum), **b** $i_{L,nc}$ (waveform and spectrum)

11.4 Systems and Control Algorithm for Smart PEV Chargers

Once determined which ancillary services can be provided by PEVs and how they can be implemented in a distributed system composed by various independent users or groups of users (Fig. 11.16), the attention should be put in which new devices or updates in current PEV electric systems are needed. These changes in the electric system mainly affect the charging systems that could be embedded in PEVs or could be an independent charging station that feeds the energy storage system.

The availability of the PEV charger to provide ancillary services depends on the nominal power of the charger and the topology of the implemented electronic converter. In this section we will classified the PEVs chargers into two main groups, single and three-phase chargers. At the actual development state of PEVs the more common chargers are single-phase chargers with a nominal power in the range from 3 to 5 kW. This situation can change in the future with the presence of not-embedded fast chargers that could have powers from 20 to 100 kW. For the examples shown in this section, a 3 kW single-phase charger will be considered.

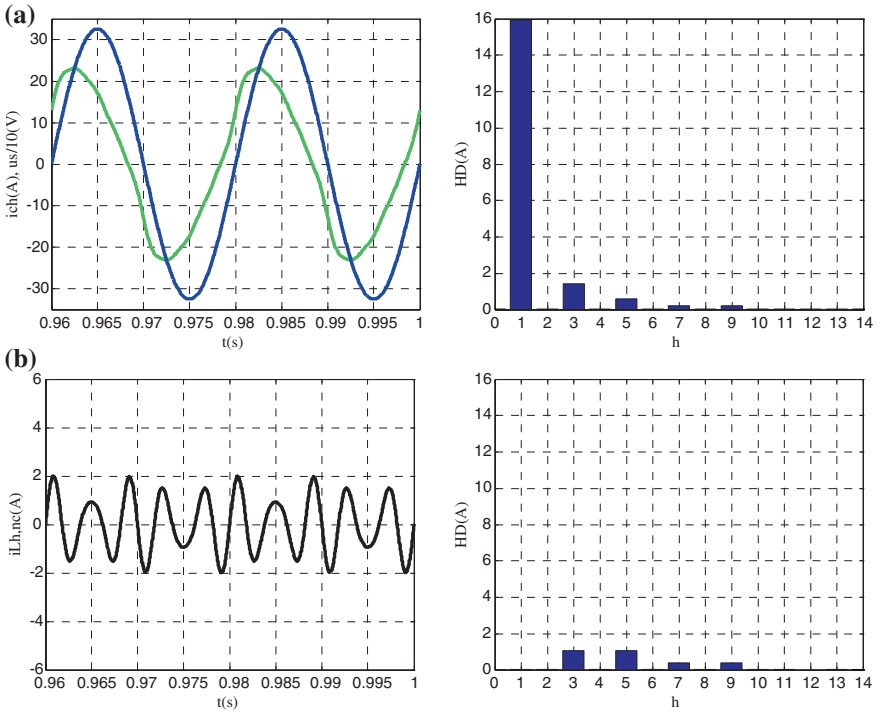

Fig. 11.15 Simulation results of V2G-P-Q-H with saturated SHC: **a** in *blue* u_s/10, in *green* i_{ch} (waveform and spectrum), **b** $i_{L,nc}$ (waveform and spectrum)

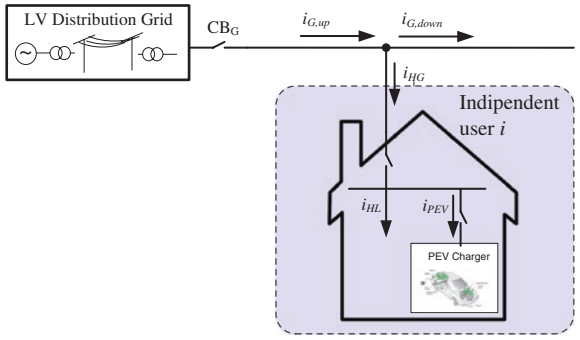

Fig. 11.16 Schematic diagram of an independent user with grid-connected PEV

As it has been said before, the topology of the electronic converter determines which service or services the PEV chargers can contribute to provide. In literature, several converter topologies can be found to charge PEVs that can be classified according to different criteria: number of phases, energy flow direction: unidirectional or bidirectional (energy to and from PEVs), harmonic emission (low or high frequency converters), electric isolation (with or without electric transformer).

11.4.1 Controlling the Fundamental Reactive Power

In order to provide any ancillary service, the PEV charger should have a bi-direction inverter topology. This inverter can be controlled in order to inject not only active power, but also fundamental reactive power. In these terms the energy storage systems embedded in PEV can contribute to produce a predefined value of reactive power or to control the voltage of the Point of Common Coupling (PCC), increasing or decreasing its RMS (root mean squared) value by controlling the reactive power that flows in or out the PEV charger. The topology used to implement these functions can be similar to the one shown in Fig. 11.17, composed by a traditional inverter that interconnects the ESS in PEV with the grid by using a first order filter (mainly compose by an inductor).

The basic control scheme of the algorithm used for the charger is depicted in Fig. 11.18. In Fig. 11.18a is supposed that a Q_{1ref} value is given to the charger that will use it for generating the reactive current component. As the nominal current RMS value should not to be over passed, saturation limits (maximum and minimum) are applied to this component according to Fig. 11.18c, resulting the following equation:

$$I_{r,\max} = -I_{r,\min} = \sqrt{I_N^2 - I_{a,ref}^2}, \tag{11.20}$$

where $I_{a,ref}$ is the active current component that must be supplied by the grid in order to obtain the required $I_{ESS,ref}$ value needed to charge the ESS or batteries of PEV.

The control described in Fig. 11.18a also includes an inner block to compensate the charger losses and to guarantee that the required charging current is achieved. The main part of the proposed block is the synchronization block, able to obtain two unitary RMS waveforms, one in phase the grid voltage and other in quadrature

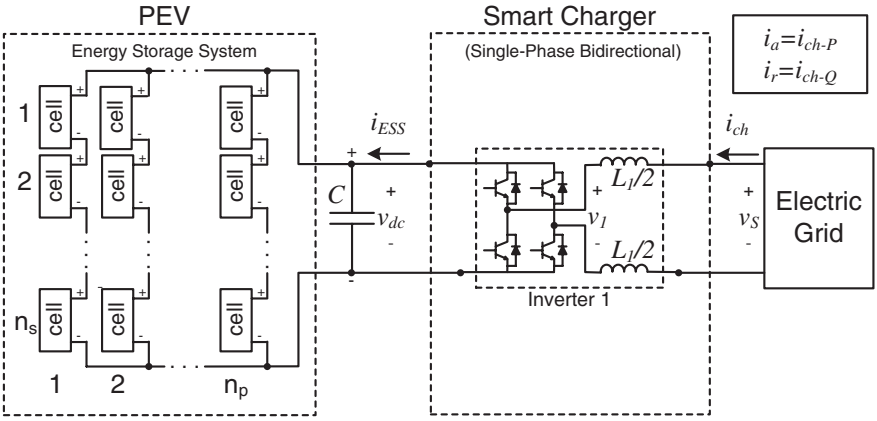

Fig. 11.17 Charger topology that can control the reactive power

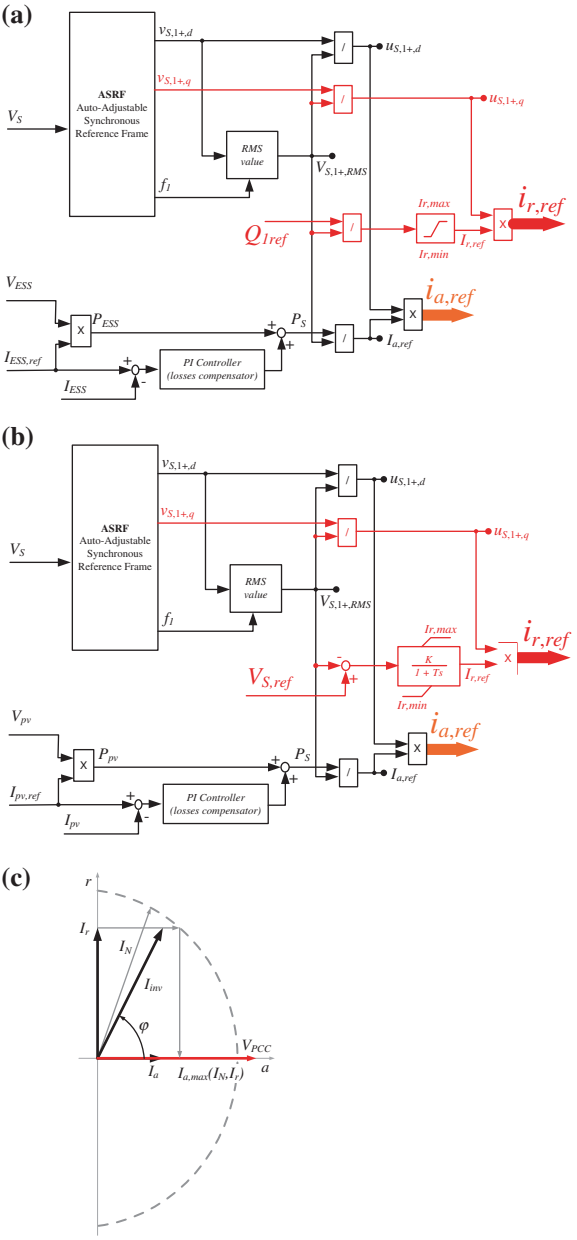

Fig. 11.18 Reactive control schemes. **a** To follow a reactive power reference value. **b** To guarantee a reference RMS voltage reference. **c** Scheme of maximum operation values for active and reactive current components

(displaced 90º), in this way the block calculates the quantity of current to inject divided in two terms: I_a, one in phase with the grid voltage to control the active power, and I_r, disphased 90º, to control the reactive power. Both values are multiplied by the grid synchronized unitary waveforms provided by a phase locked loop (PLL) [36] to generate the instantaneous reference currents.

In the second control scheme shown in Fig. 11.18b, a reference value is given for the RMS value of the PCC voltage, $V_{S,ref}$, and the reactive current component is regulated by a current controller to guarantee that this value is achieved. Saturation limits are also applied as in the previous cases for preventing the RMS value of the current over passes the nominal value. If saturation levels are applied the central system should be informed to know that the required valued, Q_{1ref} or $V_{S,ref}$, have not been achieved because these values are out of the PEV control possibilities.

Both reactive control possibilities can be jointed in a single control algorithm as the one shown in Fig. 11.19a that has different operation modes that could be applied according to the grid state as shown in Fig. 11.19b. In normal states, the active component, used for charging the PEV ESS, has priority over reactive current, controlled for providing the required ancillary services, and if the charger is over its current limits, this second component will be limited. In the opposite, in abnormal states (when the grid state is not healthy) the reactive component gets more priority than active one, in order to help the grid to recover its normal state, even if during this non-normal state it not possible to charge PEVs.

The *MODE* variable, included in the control system scheme, is used to provide three operation modes:

- MODE 1. In the top of the scheme the active power mode is solved. A balance of power between the energy flowing in or out of the PEV and grid P_s is calculated to generate a general reference current $I_{a,ref}$. A saturation block avoids a power injection higher than the power limit of the inverter P_N through the limit current I_N (taking into account the limitations shown in Fig. 11.18). If some reactive power is required the algorithm injects it up to the limit, giving priority to the active power. The loop below compensates the losses of the system by adjusting the PEV charging current I_{PEV}. The variable $I_{PEV,ref}$ comes from the charging algorithm that takes into account the user requirements and the SOC of the PEV ESS. With this mode only active current I_a is controlled.
- MODE 2. The middle of the scheme solves the reactive power reference Q_{1ref} mode. The reference reactive current $I_{r,ref}$ is obtained to be compared with the limit I_N in order to not only inject the reactive, but also the maximum active power possible. When the reactive reference is higher than the PEV power can provide, the reactive current will be managed from the grid and, if it is greater than the limit I_N, it will be saturated. This mode gives the highest priority to the reactive power through the reactive reference current I_r.
- MODE 3. The bottom adds the operation mode to adjust the voltage of the PCC V_s to a reference V_{ref} when a sag is revealed. In this case the $I_{r,ref}$ is generated through a PI controller, and then the same logic as the previous case is applied.

To illustrate the operation of the proposed control algorithm, some experimental tests have been done and their results are shown in Figs. 11.20 and 11.21 [37], with normal grid operation and with grid sag, respectively.

Figure 11.20a presents the waveforms with active power mode and only active power injected. However, Fig. 11.20b shows the results is in reactive power mode,

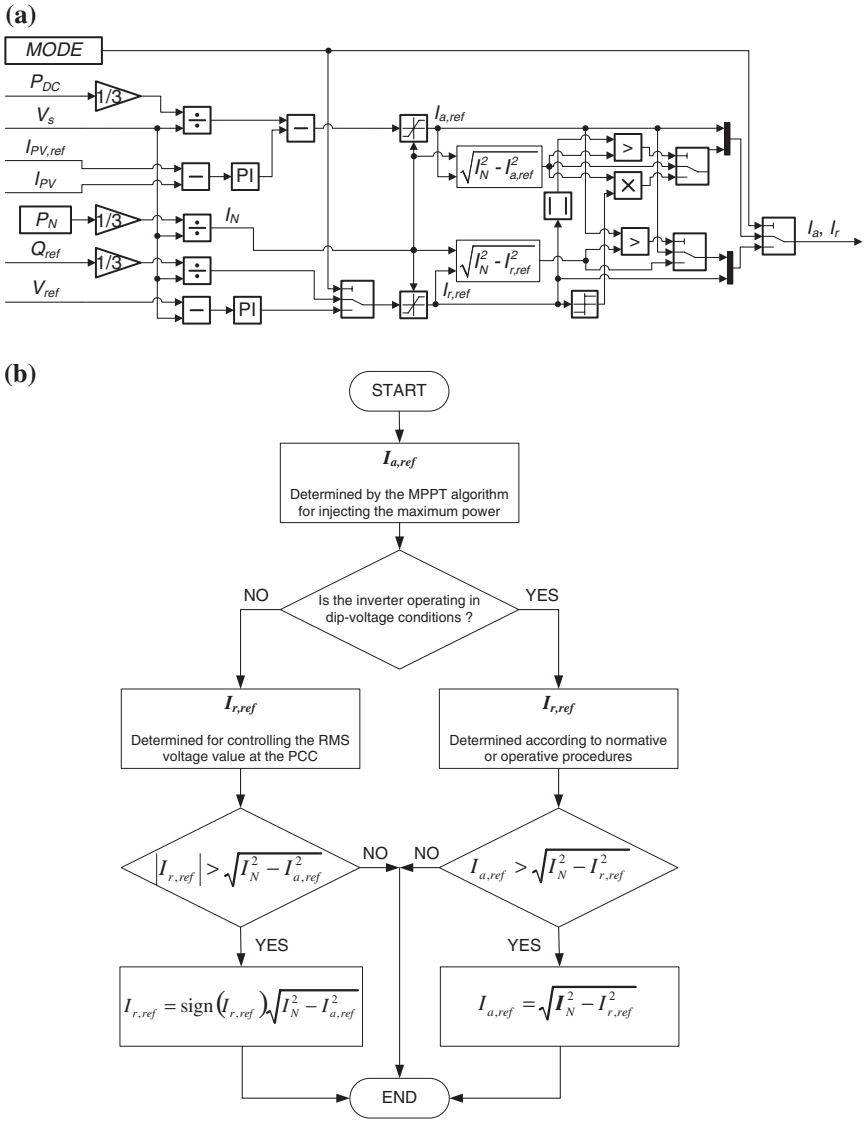

Fig. 11.19 **a** Unified reactive control scheme. **b** Operation algorithm for limiting current components during normal and non-normal grid states

injecting active and reactive power at the same time, so the voltage at the PCC is increased.

Figure 11.21a shows the only active power mode when a sag happens in the grid and the *MODE* variable keeps selecting the active power mode. One can see how the balance of power increases the injected current. Figure 11.21b

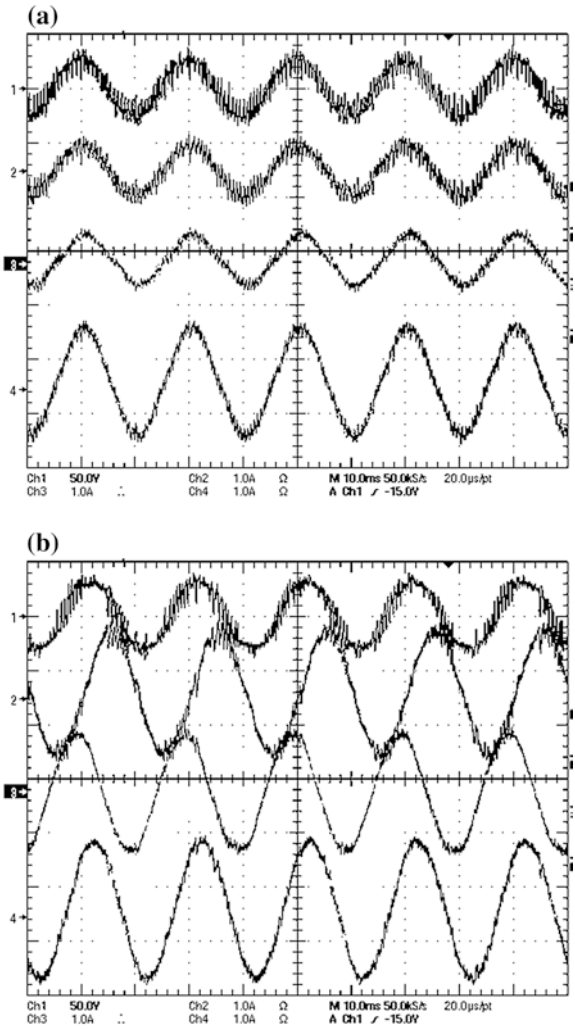

Fig. 11.20 Experimental results with reactive power reference: **a** active power mode, and **b** reactive power mode. Channels: (*1*) phase a PCC voltage, (*2*) phase a grid current, (*3*) phase a inverter current and (*4*) phase a load current [37]

presents the same case (a sag happens) but this time the *MODE* variable changes, causing that reactive power is controlled in order to maintain the PCC voltage RMS value.

11.4.2 Avoiding the Harmonic Propagation Within the Grid

In this section the analysis of how PEV charger could cancel the harmonics produced by a nonlinear load [38] which is connected to the same PCC (Fig. 11.22a) is carried out by simulation. The nonlinear load is a non-controlled single-phase rectifier with an inductive load (which produces the current displayed in Fig. 11.22b).

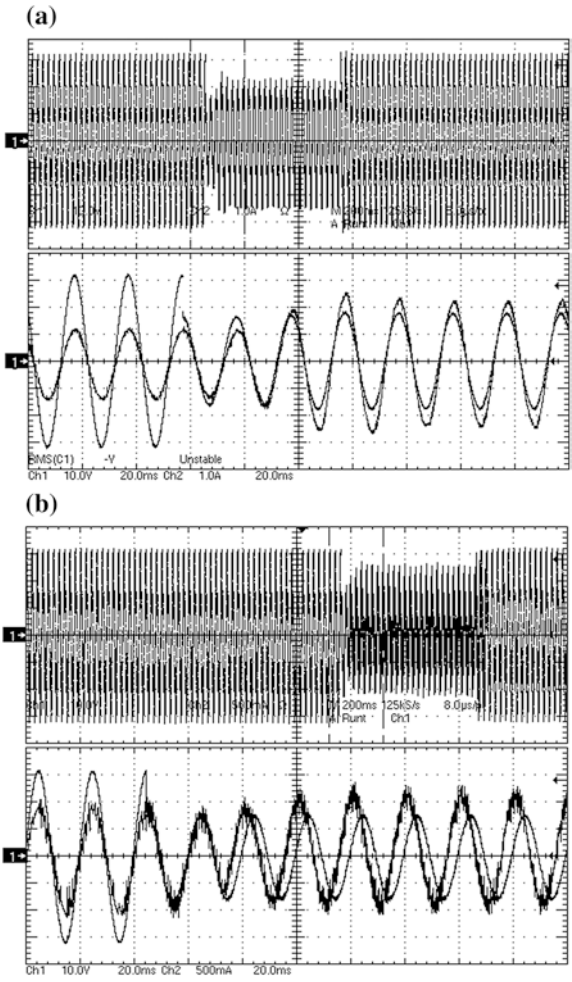

Fig. 11.21 Experimental results with sag: **a** active power mode and **b** sag mode. Channels: (*1*) Phase a PCC voltage and (*2*) phase a current [37]

There are two possibilities of operation. The first one is the usual operation (Fig. 11.23), in which the current consumed or injected by the PEV into the PCC (i_{ch}) is sinusoidal (Fig. 11.23a), and in phase with the supply voltage fundamental component. In this case, the current that flows from the grid to the PCC (i_S) is distorted (Fig. 11.23b, c) as a result of the presence of the nonlinear load.

The other possibility to operate the proposed PEV charger (Fig. 11.24) in such a way that works as an active filter and corrects the current demanded by the nonlinear load, achieving that the current that flows from the electric grid (i_S) is sinusoidal (Fig. 11.24b, c). This second operation mode could be done only by changing the current sensor position; to measure the current i_S instead of the previously measured current i_{ch}.

One can notice how the nonlinear current correction is done by the PEV charger which operates in this second case as an active filter for the non-linear

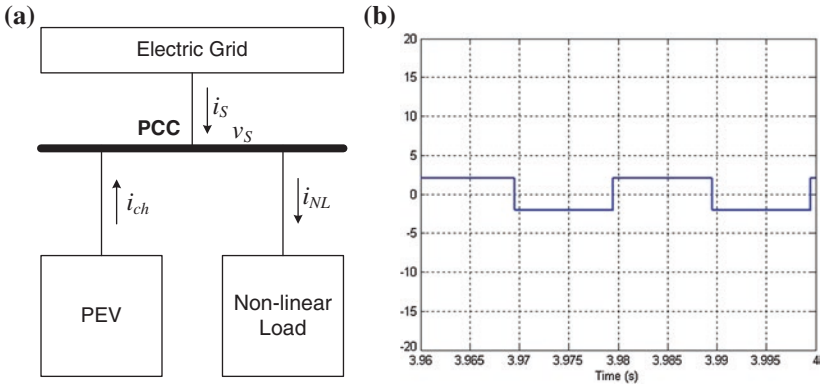

Fig. 11.22 **a** Block diagram of the system analyzed (assuming the case where the PEV is supplying energy to the grid) [38]. **b** Current demanded by the non-linear load

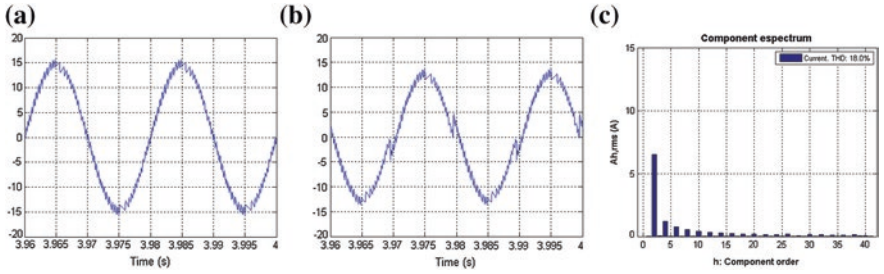

Fig. 11.23 Conventional operation. **a** Current demanded by the charger (i_{ch}). **b** Grid current (i_S). **c** Spectrum and THD of grid current (i_S)

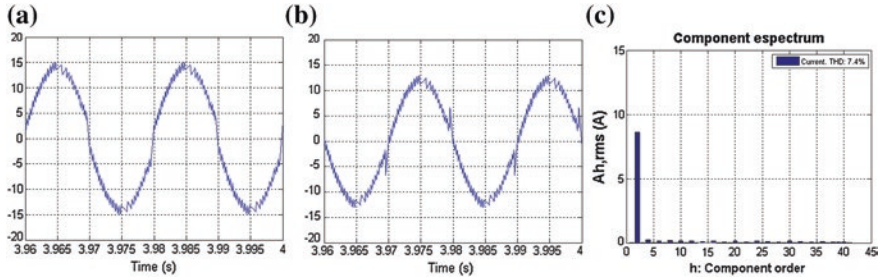

Fig. 11.24 Operating for Harmonic attenuation. **a** Current demanded by the charger (i_{ch}). **b** Grid current (i_S). (**c**) Spectrum and THD of grid current (i_S)

load. It can also be observed that, obviously, the PEV charger current is more significant in the second operation mode than in the first one. In this second operation mode the current consumed or injected by the PEV into the PCC (i_{ch}) is not sinusoidal (Fig. 11.24a).

The system performance for charging the PEV ESS from the grid is as good as in the first case. Finally, the PCC current (i_S) spectrum is shown in Figs. 11.23c and 11.24c for both operation modes. It can be seen how the second operation produces a current with THD = 7.4 % that is lower than the value produced when using the first operation mode, THD = 18 %.

11.5 Conclusions

In this chapter it has been discussed how PEV can be used for providing ancillary services, solving the problem that has appeared in electric systems that include distributed energy resources and that could operate in isolated modes. Mainly three types of regulations have been described, related to active (or real) power, reactive power and harmonic mitigation. These functions can provide ancillary services locally and could have a greater impact if a new electric agent exists, called aggregator.

References

1. Rebours Y, Kirschen D, Trotignon M et al (2007) A survey of frequency and voltage control ancillary services—part I: technical features. IEEE Trans Power Syst 22(1):350–357
2. UCTE (2009) UCTE operation handbook policy 1: load-frequency control and performance. UCTE OpHB-Team. https://www.entsoe.eu/fileadmin/user_upload/_library/publications/entsoe/Operation_Handbook/Policy_1_final.pdf
3. UCTE (2004) UCTE operation handbook appendix 1: load-frequency control and performance. UCTE OpHB-Team. https://www.entsoe.eu/fileadmin/user_upload/_library/publications/entsoe/Operation_Handbook/Policy_1_Appendix%20_final.pdf
4. ENTSO-E (2013) ENTSO-e research and development roadmap 2013–2022. https://www.entsoe.eu/publications/rd-reports/rd-roadmap
5. Rebours Y, Kirschen D, Trotignon M et al (2007) A survey of frequency and voltage control ancillary services—part II: economic features. IEEE Trans Power Syst 22(1):358–366
6. Kundur P (1994) Power system stability and control. McGraw-Hill, New York
7. DOE [US Department of Energy] (2006) Benefits of demand response in electricity markets and recommendations for achieving them—a report to the United States congress pursuant to Section 1252 of the Energy Policy Act of 2005
8. Castillo-Cagigal M, Gutiérrez A, Monasterio-Huelin F, Caamaño-Martín E, Masa D, Jimenéz-Leube J (2011) A semi-distributed electric demand-side management system with PV generation for self-consumption enhancement. Energy Convers Manag 52:2659–2666
9. Kiviluoma J, Meibom P (2010) Influence of wind power, plug-in electric vehicles, and heat storages on power system investments. Energy 35:1244–1255. doi:10.1016/j.energy.2009.11.004
10. Fernandes C, Frías P, Latorre JM (2012) Impact of vehicle-to-grid on power system operation costs: the Spanish case study. Appl Energy 96:194–202
11. Guille C, Gross G (2009) A conceptual framework for the vehicle-to-grid (V2G) implementation. Energy Policy 37:4379–4390. doi:10.1016/j.enpol.2009.05.053
12. Bessa R, Matos M (2012) Economic and technical management of an aggregation agent for electric vehicles: a literature survey. Eur Trans Elect Power 22:334–350. doi:10.1002/etep.565

13. Sousa T, Morais H, Soares J, Vale Z (2012) Day-ahead resource scheduling in smart grids considering vehicle-to-grid and network constraints. Appl Energy 96:183–193
14. Dallinger D, Wietschel M (2012) Grid integration of intermittent renewable energy sources using price-responsive plug-in electric vehicles. Renew Sustain Energy Rev 16:3370–3382
15. Sharma I, Cañizares C, Bhattacharya K (2014) Smart charging of PEVs penetrating into residential distribution systems. IEEE Trans Smart Grids 5(3):1196–1209. doi:10.1109/TSG.2014.2303173
16. Xi X, Sioshansi R (2014) Using price-based signals to control plug-in electric vehicle fleet charging. IEEE Trans Smart Grids 5(3):1451–1464. doi:10.1109/TSG.2014.2301931
17. Qi W, Xu Z, Max Shen Z-J, Hu Z, Song Y (2014) Hierarchical coordinated control of plug-in electric vehicles charging in multifamily dwellings. IEEE Trans Smart Grids 5(3):1465–1474. doi:10.1109/TSG.2014.2308217
18. Leo M, Kavi K, Anders H, Moss B (2011) Ancillary service revenue opportunities from electric vehicles via demand response. Better Place Master's Project Team. Master of Science from the School of Natural Resources and Environment, University of Michigan
19. Sun M, Dong M, Liang B (2014) Real-time welfare-maximizing regulation allocation in dynamic aggregator-EVs system. IEEE Trans Smart Grids 5(3):1397–1409. doi:10.1109/TSG.2014.2300040
20. Ortega-Vazquez MA, Bouffard F, Silva V (2013) Electric vehicle aggregator/system operator coordination for charging scheduling and services procurement. IEEE Trans Power Syst 28(2):1806–1815. doi:10.1109/TPWRS.2012.2221750
21. IEC Technical Committee 69 (2010) IEC 61851-1:2010 Electric vehicle conductive charging system-part 1: general requirements
22. Society of Automotive Engineers (SAE) (2011) SAE standard J2894: power quality requirements for plug in vehicle chargers, Warrendale
23. IEC Technical Committee 77A (2014) IEC 61000-3-2:2014 Electromagnetic compatibility (EMC)—Part 3-2: limits—limits for harmonic current emissions (equipment input current $\leq$ 16 A per phase)
24. Milanés-Montero MI, Gallardo-Lozano J, Romero-Cadaval E, González-Romera E (2011) Hall-effect based semi-fast AC on-board charging equipment for electric vehicles. Sensors (Basel) 11(10):9313–9326. doi:10.3390/s111009313
25. Milanés-Montero MI, Romero-Cadaval E, Barrero-González F (2007) Comparison of control strategies for shunt active power filters in three-phase four-wire systems. IEEE Trans Power Electron 22(1):229–236. doi:10.1109/TPEL.2006.886616
26. Gallardo-Lozano J, Milanés-Montero MI, Romero-Cadaval E, Guerrero-Martínez MA (2012) Non disturbing bidirectional charger for PHEVs and EVs. Przeglad Elektrotechniczny 12:111–116
27. Standard IEEE 1459-2010 (2010) IEEE standard definitions for the measurement of electric power quantities under sinusoidal, nonsinusoidal, balanced, or unbalanced conditions
28. EN 50160:2010 (2010) Voltage characteristics of electricity supplied by public electricity networks
29. IEC Technical Committee 77A (2002) IEC 61000-2-2:2002. Electromagnetic compatibility (EMC)—Part 2-2: environment—compatibility levels for low-frequency conducted disturbances and signalling in public low-voltage power supply systems
30. Zhou X, Wang G, Lukic S, Bhattacharya S, Huang A (2009) Multi-function bi-directional battery charger for plug-in hybrid electric vehicle application. In: Proceedings of the IEEE energy conversion congress and exposition (ECCE), San Jose
31. Bojrup M, Karlsson P, Alakula M, Simonsson B (1998) A dual purpose battery charger for electric vehicles. In: Proceedings of the 29th annual power electronics specialists conference (PESC), Fukuoka
32. Asiminoaei L, Kalaschnikow S, Hansen S (2009) Overall and selective compensation of harmonic currents in active filter applications. Paper presented at the 6th conference-workshop compatibility and power electronics (CPE), Badajoz

33. Milanés-Montero MI, Romero-Cadaval E, Barrero-González F (2011) Hybrid multiconverter conditioner topology for high-power applications. IEEE Trans Ind Electron 58(6):2283–2292. doi:10.1109/TIE.2010.2062478
34. Lascu C, Asiminoaei L, Boldea I, Blaabjerg F (2009) Frequency response analysis of current controllers for selective harmonic compensation in active power filters. IEEE Trans Ind Electron 56(2):337–347. doi:10.1109/TIE.2008.2006953
35. Miret J, Castilla M, Matas J, Guerrero JM, Vasquez JC (2009) Selective harmonic-compensation control for single-phase active power filter with high harmonic rejection. IEEE Trans Ind Electron 56(8):3117–3127. doi:10.1109/TIE.2009.2024662
36. Milanes-Montero MI, Romero-Cadaval E, Rico de Marcos A, Minambres-Marcos VM, Barrero-Gonzalez F (2007) Novel method for synchronization to disturbed three-phase and single-phase systems. Paper presented at the IEEE international symposium on industrial electronics (ISIE 2007), Vigo
37. Romero-Cadaval E, Minambres-Marcos VM, Moreno-Munoz A, Real-Calvo RJ, de la Rosa JJG, Sierra-Fernandez JM (2013) Active functions implementation in smart inverters for distributed energy resources. Paper presented at the 8th conference-workshop compatibility and power electronics (CPE), Ljubljana
38. Pinto JG, Monteiro V, Goncalves H, Exposto B, Pedrosa D, Couto C, Afonso JL (2013) Bidirectional battery charger with grid-to-vehicle, vehicle-to-grid and vehicle-to-home technologies. Paper presented at the 39th annual conference of the IEEE industrial electronics society (IECON), Vienna